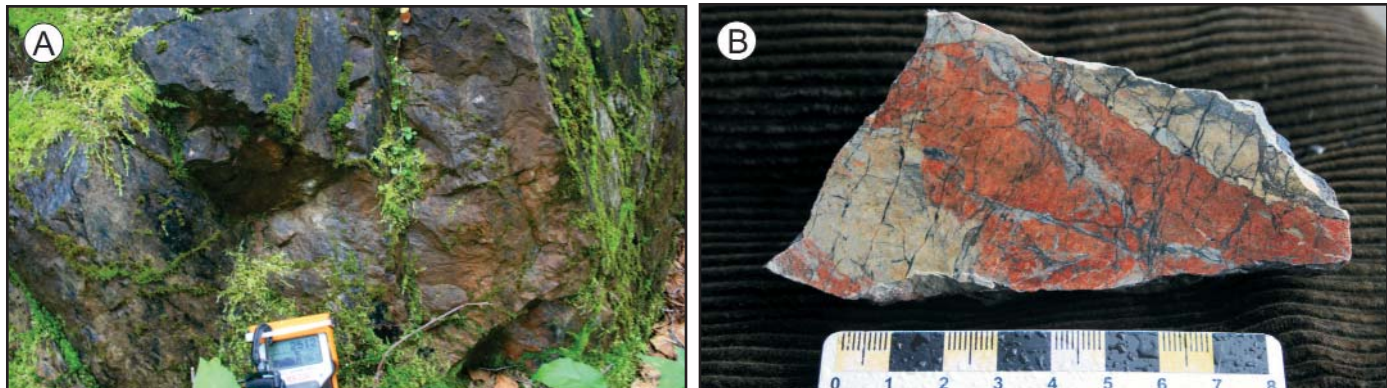




Natural Resources

Mines

# URANIUM MINERALIZATION WITHIN THE CENTRAL MINERAL BELT OF LABRADOR: A SUMMARY OF THE DIVERSE STYLES, SETTINGS AND TIMING OF MINERALIZATION



G.W. Sparkes

Open File LAB/1684

St. John's, Newfoundland  
January, 2017

### **Cover Captions**

*A. Uraniferous, leucogabbroic dyke displaying distinct brownish-orange weathering due to the pervasive Fe-carbonate alteration that accompanies uranium mineralization (~750 m northeast of main B Zone prospect).*

*B. Brecciated hematite and Fe-carbonate alteration overprinted by later dark-purple specularite-filled fractures, B Zone prospect. Sample contains 14.01 wt.% CaO, 4.39 wt.% Na<sub>2</sub>O and 127 ppm U.*



Natural Resources

Mines

# URANIUM MINERALIZATION WITHIN THE CENTRAL MINERAL BELT OF LABRADOR: A SUMMARY OF THE DIVERSE STYLES, SETTINGS AND TIMING OF MINERALIZATION

G.W. Sparkes

Open File LAB/1684



St. John's, Newfoundland  
2017

## **NOTE**

The purchaser agrees not to provide a digital reproduction or copy of this product to a third party. Derivative products should acknowledge the source of the data.

## **DISCLAIMER**

The Geological Survey, a division of the Department of Natural Resources (the “authors and publishers”), retains the sole right to the original data and information found in any product produced. The authors and publishers assume no legal liability or responsibility for any alterations, changes or misrepresentations made by third parties with respect to these products or the original data. Furthermore, the Geological Survey assumes no liability with respect to digital reproductions or copies of original products or for derivative products made by third parties. Please consult with the Geological Survey in order to ensure originality and correctness of data and/or products.

*Recommended citation:*

Sparkes, G.W.

2017: Uranium mineralization within the Central Mineral Belt of Labrador: A summary of the diverse styles, settings and timing of mineralization. Government of Newfoundland and Labrador, Department of Natural Resources, Geological Survey, St. John’s, Open File LAB/1684, 198 pages.

## CONTENTS

	Page
<b>ABSTRACT</b> .....	xxi
<b>INTRODUCTION</b> .....	1
PURPOSE AND SCOPE .....	1
METHODS .....	1
REGIONAL GEOLOGICAL SETTING .....	1
<b>URANIUM MINERALIZATION WITHIN ARCHEAN BASEMENT ROCKS</b> .....	6
INTRODUCTION .....	6
REGIONAL GEOLOGY .....	6
EXPLORATION HISTORY .....	7
ANOMALY NOS. 7, 7A AND 17; FISH HAWK LAKE SOUTH, FISH HAWK LAKE NORTH AND NEAR MISS PROSPECTS .....	12
Local Geology .....	12
Mineralization and Associated Alteration .....	13
Petrography .....	17
TWO-TIME DEPOSIT AND THE SNEGAMOOK PROSPECT .....	18
Local Geology .....	18
Mineralization and Associated Alteration .....	21
Petrography .....	24
OTHER MINOR URANIUM OCCURRENCES .....	26
Dandy and Related Prospects .....	26
GEOCHRONOLOGICAL CONSTRAINTS .....	26
GEOCHEMISTRY .....	27
SUMMARY AND DISCUSSION .....	29
<b>URANIUM MINERALIZATION WITHIN THE MORAN LAKE GROUP</b> .....	31
INTRODUCTION .....	31
REGIONAL GEOLOGY .....	33
EXPLORATION HISTORY .....	33
THE MORAN LAKE UPPER C ZONE AND TROUT POND DEPOSITS .....	34
Overview .....	34
Previous Work .....	36
Local Geology .....	36
Mineralization and Associated Alteration .....	38
Petrography .....	42
ARMSTRONG DEPOSIT .....	45
Local Geology .....	45
Mineralization and Associated Alteration .....	45
Petrography .....	47
OTHER URANIUM OCCURRENCES .....	47
Croteau Lake Prospect .....	47
Fish Hawk Lake North and Whiskey Jack Prospects .....	49
Area 51 Prospect .....	52
Canico Anomaly Nos. 15 and 16 Prospects .....	52
Boiteau Lake Prospect .....	53
GEOCHRONOLOGICAL CONSTRAINTS .....	54
GEOCHEMISTRY .....	55
SUMMARY AND DISCUSSION .....	57

	Page
<b>URANIUM MINERALIZATION WITHIN THE POST HILL GROUP .....</b>	<b>58</b>
INTRODUCTION .....	58
REGIONAL GEOLOGY .....	60
EXPLORATION HISTORY .....	61
KITTS DEPOSIT .....	63
Previous Work .....	63
Local Geology .....	65
Mineralization and Associated Alteration .....	67
Petrography .....	68
GEAR, INDA AND NASH DEPOSITS .....	71
Previous Work .....	71
Local Geology .....	71
Mineralization and Associated Alteration .....	75
ANNA LAKE DEPOSIT .....	77
Previous Work .....	77
Local Geology .....	78
Mineralization and Associated Alteration .....	79
Petrography .....	80
OTHER URANIUM OCCURRENCES .....	80
GEOCHRONOLOGICAL CONSTRAINTS .....	80
GEOCHEMISTRY .....	83
SUMMARY AND DISCUSSION .....	84
<b>URANIUM MINERALIZATION WITHIN THE AILLIK GROUP .....</b>	<b>87</b>
INTRODUCTION .....	87
REGIONAL GEOLOGY .....	90
EXPLORATION HISTORY .....	90
MICHELIN DEPOSIT .....	91
Previous Work .....	91
Local Geology .....	93
Mineralization and Associated Alteration .....	94
Petrography .....	98
JACQUES LAKE DEPOSIT .....	99
Previous Work .....	99
Local Geology .....	99
Mineralization and Associated Alteration .....	103
Petrography .....	104
OTHER URANIUM OCCURRENCES .....	109
Mustang Lake Prospect .....	109
Gayle, Burnt Brook and Aurora River Prospects .....	112
White Bear and Otter Lake Prospects .....	113
BENEDICT MOUNTAINS REGION .....	115
Local Geology .....	115
Mineralization and Associated Alteration .....	116
GEOCHRONOLOGICAL CONSTRAINTS .....	116
GEOCHEMISTRY .....	119
SUMMARY AND DISCUSSION .....	123
<b>URANIUM MINERALIZATION WITHIN THE BRUCE RIVER GROUP .....</b>	<b>124</b>
INTRODUCTION .....	124
REGIONAL GEOLOGY .....	125
EXPLORATION HISTORY .....	127

	Page
MORAN LAKE LOWER C ZONE DEPOSIT .....	127
Previous Work .....	127
Local Geology .....	127
Mineralization and Associated Alteration .....	128
Petrography .....	128
MORAN HEIGHTS PROSPECT .....	129
Previous Work .....	129
Local Geology .....	129
Mineralization and Associated Alteration .....	131
Petrography .....	131
Other Minor Uranium Occurrences .....	131
MORAN LAKE B ZONE PROSPECT .....	131
Previous Work .....	131
Local Geology .....	133
Mineralization and Associated Alteration .....	133
Petrography .....	136
OTHER URANIUM OCCURRENCES .....	138
Moran Lake A Zone Prospect .....	138
CVG Prospect .....	138
Madsen Prospect .....	138
Sylvia Lake Prospect .....	140
Minisinakwa Prospect .....	141
Stormy Lake Prospect .....	141
GEOCHRONOLOGICAL CONSTRAINTS .....	142
GEOCHEMISTRY .....	144
SUMMARY AND DISCUSSION .....	144
 URANIUM MINERALIZATION WITHIN INTRUSIVE ROCKS OF UNDETERMINED AGE .....	145
MELODY HILL PROSPECT .....	145
Previous Work .....	145
Local Geology .....	145
Mineralization and Associated Alteration .....	145
AT 649 AND SUPER 7 PROSPECTS .....	146
Previous Work .....	146
Local Geology .....	148
Mineralization and Associated Alteration .....	148
NOSEMAN PROSPECT .....	149
GEOCHEMISTRY .....	149
SUMMARY AND DISCUSSION .....	149
 DISCUSSION AND CONCLUSION .....	150
SUBDIVISION AND CLASSIFICATION OF URANIUM MINERALIZATION .....	150
Magmatic Related Mineralization .....	150
Metamorphic–Metasomatic Related Mineralization .....	151
Sediment-hosted Mineralization .....	152
CONCLUSIONS .....	152
 ACKNOWLEDGMENTS .....	152
REFERENCES .....	153

	Page
<b>APPENDIX A:</b> A summary of the procedure used in the generation of CR-39 autoradiographs .....	166
<b>APPENDIX B:</b> A summary of the geochronological techniques utilized and corresponding procedures .....	167
<b>APPENDIX C:</b> Compilation table of U–Pb data for analyses conducted at Memorial University; UTM’s for each sample are provided in NAD 27, Zone 21 coordinates .....	168
<b>APPENDIX D:</b> U–Pb SHRIMP analytical data for sample number GS-07-298; Quartz-feldspar porphyry, Kitts deposit, Labrador (z9537); from Sparkes <i>et al.</i> (2010) .....	170
<b>APPENDIX E:</b> U–Pb ID-TIMS analytical data for sample number GS-08-288; crystal lapilli tuff, Powe prospect, Benedict Mountains region; from Sparkes and Davis, 2013. ....	171
<b>APPENDIX F:</b> Summary table outlining the location and main host rock for prospects visited as part of this study, along with the corresponding classification of the style of mineralization. Note UTM’s are provided in NAD 27, Zone 21 coordinates .....	172

## FIGURES

Page

Figure 1.	A. Location map, B. Outlines of the regional subdivisions of the CMB of Labrador; (modified from Hinckley and LaFlamme, 2009), C. Regional geology encompassing the CMB; (geological base map modified from Wardle <i>et al.</i> , 1997). BFZ–Benedict fault zone, KBSZ–Kaipokok Bay shear zone, KSZ–Kanairiktok shear zone, ABFZ–Adlavik Brook fault zone . . . . .	2
Figure 2.	Schematic stratigraphic chart for the CMB showing the settings of various examples of uranium mineralization. (Note that the ages implied for these occurrences are those of the host rocks and are not necessarily the age of the mineralization, which may be much younger). . . . .	4
Figure 3.	Uranium occurrences of the CMB and surrounding region. (Geological base map modified from Wardle <i>et al.</i> , 1997.) KSZ – Kanairiktok shear zone. Occurrences highlighted in yellow contain defined NI 43-101 resource estimates . . . . .	8
Figure 4.	Regional map outlining the distribution of historic and recently discovered uranium occurrences within Archean basement rocks in the northwestern CMB. (Map modified from Wardle <i>et al.</i> , 1997.) Lake-sediment data compiled from government and industry sources . . . . .	10
Figure 5.	Map outlining the distribution of the main geological units and locations of uranium occurrences, including the Two-Time deposit and Fish Hawk Lake prospects, as compiled from company websites and press releases. (Map exert from 1:250 000 geological map of . . . . . Ermanovics, 1992.) . . . . .	11
Figure 6.	Drill log of hole 51543 from the Anomaly No. 7 prospect, outlining the distribution of fracturing and accompanying hematite alteration in association with uranium mineralization; uranium values are listed in % $U_3O_8$ (data from Perry, 1979). Note the local development of high-grade mineralization immediately adjacent to the intrusion of the mafic dyke, A. Relatively fresh, unaltered quartz monzodiorite–tonalite, B. Strongly hematized quartz monzodiorite–tonalite; minimal uranium enrichment, C. Hematized and fractured host rock and associated . . . . . uranium mineralization . . . . .	14
Figure 7.	Drill log of hole FHLS-07-03 from the Fish Hawk Lake South prospect, outlining the distribution of fracturing and accompanying hematite alteration in association with uranium mineralization; uranium values are listed in % $U_3O_8$ (data from Willett <i>et al.</i> , 2008). A. Variably chlorite altered quartz monzodiorite–tonalite, B. Strongly hematized quartz monzodiorite–tonalite and associated uranium enrichment, C. Unseparated quartz monzodiorite–tonalite and . . . . . pegmatitic intrusions . . . . .	15
Figure 8.	Schematic east-northeast–west-southwest section outlining the distribution of rock units, alteration and uranium mineralization within the Two-Time deposit; uranium values are listed in % $U_3O_8$ (data from MacGillivray <i>et al.</i> , 2008c). . . . .	23
Figure 9.	Concordia diagram of zircon (red) and monazite U–Pb results from sample GS-09-44, a quartz monzodiorite–tonalite intrusion. Error ellipses are at the $2\sigma$ level (modified from . . . . . Sparkes and Dunning, 2015) . . . . .	27
Figure 10.	Select major-element composition diagrams for the quartz monzodiorite–tonalite unit from various Archean basement-hosted uranium prospects within the western CMB. A. Alumina saturation diagram of Maniar and Piccoli (1989), showing limits of metaluminous, peraluminous, and peralkaline fields, B. $TiO_2$ vs. $SiO_2$ diagram displaying the higher Si values of the host rock in the area of the Two-Time deposit relative to those near Fish Hawk Lake, C. AFM . . . . . diagram showing calc-alkaline and tholeiitic fields of Irvine and Baragar (1971). . . . .	28
Figure 11.	Primitive mantle normalized trace-element plot showing patterns for the quartz monzodiorite–tonalite unit from various Archean basement-hosted uranium prospects within the western CMB (normalizing values of Sun and McDonough, 1989) . . . . .	29
Figure 12.	Primitive mantle normalized trace-element plot displaying the geochemical similarities between the quartz monzodiorite–tonalite unit and Maggo Gneiss (normalizing values of Sun . . . . . and McDonough, 1989) . . . . .	29
Figure 13.	Plots of uranium <i>versus</i> other elements of interest (refer to text) in relation to the development of hematite breccias within the Archean basement rocks. Note some samples of quartz monzodiorite–tonalite contain elevated uranium mineralization; these samples are fractured and	

hematized but primary texture is still evident, thus separating them from the hematite breccias. Some samples do not appear in all plots as not all samples contain a complete geochemical analysis.....	30
Figure 14. Primitive mantle normalized trace-element patterns of mafic dykes crosscutting Archean basement rocks within the western CMB (normalizing values of Sun and McDonough, 1989). The chemical trend of the younger dykes (Group 1) is highlighted in orange and older dykes (Group 2) in yellow.....	30
Figure 15. Regional geology map outlining the distribution of uranium occurrences within the Moran Lake Group (geological base map modified from Wardle <i>et al.</i> , 1997).....	31
Figure 16. Plan map outlining the distribution of geological units as well as the surface projection of mineralization and related alteration in the area of the Moran Lake Upper C Zone and Trout Pond deposits; (geology base map modified from Ryan, 1984 and Gillies <i>et al.</i> , 2009). Schematic cross-section A–B illustrated in Figure 17 .....	32
Figure 17. Schematic cross-section through the Moran Lake C Zone deposit showing the locations of the Upper and Lower C zones, along with the intervening C Zone thrust fault. (For location of schematic cross-section A–B refer to Figure 16.) Plan map above the section outlines the trace of the drillhole collars overlain on the first vertical derivative of the Crosshair airborne magnetic data .....	35
Figure 18. Drill log for drillhole ML-55 from the Upper C Zone, outlining the distribution of brecciation and accompanying alteration in association with uranium, vanadium and copper mineralization; all values are listed in weight percent (data from Morgan <i>et al.</i> , 2007). A. Hematitic breccia hosting anomalous V and Cu, without associated U enrichment, B. Uranium-bearing, siliceous chert interbedded with mafic volcanic rocks, C. Uraniferous breccia vein (dark-purple vein) crosscutting earlier albite–carbonate alteration .....	37
Figure 19. Drill log for hole ML-AR-09 from the Armstrong deposit, outlining the distribution of uranium, vanadium and copper mineralization in association with Fe–carbonate–albite–altered shear zones within the metasedimentary rocks; all values are listed in weight percent (data from Gillies <i>et al.</i> , 2009). A. Relatively barren unaltered, argillite, B. Discrete mineralized zone of albitic alteration overprinted by hematite-rich brecciation, C. Uraniferous Fe–carbonate–albite alteration zone .....	39
Figure 20. Schematic cross-section outlining the location of anomalous uranium values within rocks of the Moran Lake Group, which are juxtaposed with Archean basement rocks in the region of the Fish Hawk Lake North prospect (assay data from Willett <i>et al.</i> , 2008) .....	46
Figure 21. A. Discrimination diagram of Winchester and Floyd (1977), displaying the subalkaline basaltic nature of the host rocks to the mineralization within the Moran Lake C Zone–Anomaly No. 15 area, B. Discrimination diagram of Pearce and Cann (1973) displaying the dominant MORB-like signature of the basaltic host rocks. MORB – Mid-Ocean-Ridge Basalt, IAT – Island-Arc Tholeiites.....	52
Figure 22. Geochemical plots displaying the increase in CaO (A), Na <sub>2</sub> O (B) and MgO (C), as well as the corresponding decrease in Fe <sub>2</sub> O <sub>3</sub> (D) within the hematite-rich breccias of the Upper C Zone in comparison to the host Joe Pond basalt. Also shown are the relative enrichment of V (E) and Cu (F) relative to U within the hematite-rich breccias.....	55
Figure 23. Extended trace-element diagrams for various metasedimentary units within the Moran Lake Group. (Normalizing values are from Quinby-Hunt <i>et al.</i> , 1989, except for Cu, Ni, Pb, Ag and Mo, which are taken from Vine and Tourtelot, 1970.) A. Moran Lake Upper C Zone deposit, B. Armstrong deposit, C. Croteau Lake prospect, D. Fish Hawk Lake North area, E. Area 51 prospect .....	56
Figure 24. Primitive mantle normalized trace-element patterns for the two groups of dykes observed locally crosscutting rocks of the Moran Lake Group (normalizing values of Sun and McDonough, 1989). The shaded areas outline the trends defined for dykes within the Archean basement rocks shown in Figure 14 .....	58

Figure 25.	Regional map outlining the distribution of uranium occurrences hosted within the Post Hill Group (geological base map modified from Wardle <i>et al.</i> , 1997). The area indicated within the black outline is detailed in Figure 26 .....	59
Figure 26.	Geological map of the Kitts–Post Hill Belt, showing the location of significant uranium occurrences and the distribution of known geochronological data. Solid diamonds (amphibole) and circles (muscovite) represent Ar–Ar determinations; the solid squares represent U–Pb data. Age sources: 1) Culshaw <i>et al.</i> , 2002; 2) Ketchum <i>et al.</i> , 2001b; 3) Ketchum <i>et al.</i> , 1997; 4) Schärer <i>et al.</i> , 1988. Abbreviations KBSZ–Kaipokok Bay Shear Zone, NSZ–Nakit Shear Zone. (Modified after Marten, 1977, Gower <i>et al.</i> , 1982 and Culshaw <i>et al.</i> , 2002.) Red box shows location of Figure 27 .....	62
Figure 27.	Simplified geological map of the area surrounding the Kitts deposit and the location of the A, B and C zones (modified after Marten, 1977). Schematic cross-section A-A' illustrated in Figure 29 .....	64
Figure 28.	Schematic stratigraphic section of the representative rock units within the Kitts deposit (modified after Evans, 1980) .....	65
Figure 29.	Schematic cross section through the Kitts deposit (looking southeast) displaying the distribution of the main rock units in association with uranium mineralization (modified from Evans, 1980). Note hole K74-8 is located 30 m northwest of the section and is projected onto the current plane. For location of schematic cross-section A-A', refer to Figure 27 .....	66
Figure 30.	Partial drill log for hole K74-8 from the Kitts deposit, outlining the distribution of uranium mineralization and collection site of the geochronology sample from the quartz-feldspar porphyry dyke; values are listed in weight percent (data from Davidson <i>et al.</i> , 1978). A. Dated quartz-feldspar porphyry dyke, B. Barren sulphidic argillite above mineralized zone, C. Sulphidic argillite unit hosting discrete vein-hosted uranium mineralization (note labels on the drillcore denote counts per second). .....	69
Figure 31.	Regional geology map outlining the main distribution of units within the area of the Gear, Inda and Nash deposits (geological base map modified from Gower <i>et al.</i> , 1982) .....	72
Figure 32.	Simplified cross-section through the Gear deposit, looking southwest (modified from Cunningham-Dunlop and Lee, 2008) .....	73
Figure 33.	Simplified cross-section of the Inda deposit, looking southwest (modified from Srivastava, 1976) .....	74
Figure 34.	Simplified cross-section of the Nash deposit, looking southwest (modified from Cunningham-Dunlop and Lee, 2008) .....	75
Figure 35.	Geology map of the Anna Lake area (modified from Fraser and Giroux, 2009). For the regional location of the deposit refer to Figure 25 .....	79
Figure 36.	Concordia diagrams for U–Pb zircon data (A and B) as well as titanite data (C) for units sampled within the Kitts deposit. A. Kitts Metagabbro, B. Quartz-feldspar porphyry dyke, C) Diorite dyke. (Error ellipses are at the $2\sigma$ level; modified from Sparkes <i>et al.</i> , 2010) .....	84
Figure 37.	Discrimination diagrams for magmatic rocks examined in relation to uranium mineralization within the Kitts–Post Hill Belt; most samples are from the Kitts deposit, A. Discrimination diagram of Winchester and Floyd (1977) outlining the main compositions of the magmatic rocks sampled as part of this study, B. Discrimination diagram of Pearce and Cann (1973) displaying the MORB-like signature of Kitts Pillow Lava Formation and the Kitts Metagabbro; MORB–Mid-Ocean-Ridge basalt, IAT–Island-Arc Tholeiites, C. Discrimination diagram of Pearce and Cann ( <i>op. cit.</i> ) displaying predominant ocean-floor signature of the Kitts Pillow Lava Formation, D. AFM diagram illustrating the overall tholeiitic trend of the Kitts Pillow Lava Formation and Kitts Metagabbro in relation to the more calc-alkaline diorite and quartz-feldspar porphyry dykes. ....	85
Figure 38.	Chondrite normalized trace-element diagrams for magmatic rocks examined in relation to uranium mineralization within the Kitts–Post Hill Belt; most samples are from the Kitts deposit, A. Samples of the Kitts Pillow Lava Formation and Kitts Metagabbro; Kitts deposit, B. Samples of the quartz-feldspar porphyry and late-stage diorite dykes; the quartz-feldspar porphyry and diorite dykes include samples from Kitts, Gear and Nash West Extension occurrences. Normalizing values are from Sun and McDonough (1989) .....	86

Figure 39.	Extended trace-element diagrams for the metasedimentary and volcaniclastic units within the Post Hill Group. Normalizing values are from Quinby-Hunt <i>et al.</i> (1989) except for Cu, Ni, Pb, Ag and Mo, which are taken from Vine and Tourtelot (1970). A. Kitts deposit, B. Gear and Inda deposits; note the argillite sample containing elevated U represents mineralized argillite from the Inda deposit; all other samples are from the Gear deposit, C. Nash deposit and Nash West Extension prospect, D. Present Lake prospect. ....	87
Figure 40.	Regional geology map outlining the distribution of known uranium occurrences hosted within in the Aillik Group; geological base map modified from Wardle <i>et al.</i> (1997). Area outlined in black box detailed in Figure 41. ....	89
Figure 41.	Regional geology map outlining the distribution of uranium occurrences within the White Bear Mountain–Walker Lake area (geological base map modified from Gower <i>et al.</i> , 1982, and Ryan, 1984). ....	92
Figure 42.	Local geology map outlining the distribution of the main rock units and surface projection of uranium mineralization in the area of the Michelin deposit (modified from Barrett and Ash, 2009). Cross-section A–B illustrated as Figure 43 ....	95
Figure 43.	Schematic cross-section through the Michelin deposit outlining the distribution of the main rock units and uranium mineralization (modified from Cunningham-Dunlop and Lee, 2008). Location of cross-section refer to Figure 42 ....	96
Figure 44.	Drill log for hole M06-11 from the Michelin deposit, outlining the distribution of uranium mineralization and main rock units; uranium values are listed in ppm (data from Cunningham-Dunlop <i>et al.</i> , 2007b). A. Photograph displaying localized development of hematite alteration without associated uranium mineralization or sodium metasomatism; host rock contains approximately 4.45 wt.% Na <sub>2</sub> O and 5.9 ppm U, B. Photograph displaying hematization and albitization with anomalous uranium enrichment; host rock contains approximately 6.12 wt.% Na <sub>2</sub> O and 308 ppm U, C. Photograph showing a post-mineralization mafic dyke crosscutting the mineralized metavolcanic host rock (dyke contains 2.6 ppm U, whilst adjacent metavolcanic rock is host to approximately 905 ppm U) ....	97
Figure 45.	Local geology map outlining the distribution of the main rock units and diamond-drill holes in the area of the Jacques Lake deposit (modified from Cunningham-Dunlop and Lee, 2008). Cross-section A–B illustrated as Figure 46 ....	102
Figure 46.	Schematic cross-section through the Jacques Lake deposit outlining the distribution of the main rock units and uranium mineralization (modified from Hertel <i>et al.</i> , 2009). Location of the cross-section refer to Figure 45. Also shown are the results from U–Pb geochronological studies carried out on samples from the deposit (refer to text). ....	103
Figure 47.	Drill log for hole JL-07-060 from the Jacques Lake deposit, outlining the distribution of uranium mineralization and main rock units; uranium values are listed in ppm (data from Cunningham-Dunlop <i>et al.</i> , 2008b). Abbreviations: Act—actinolite, Mag—magnetite, Cb—carbonate. A. Photograph illustrating zones of intermittent hematization associated with uranium mineralization (note labels on core denote counts per second (cps) as determined by a hand-held scintillometer; a sample from this zone returned up to 6.23 wt.% Na <sub>2</sub> O and 1470 ppm U), B. Quartz–feldspar–porphyry dyke containing a pseudorapakivi texture; note the zoned feldspar crystals of similar composition to those within the feldspar-rich core also occur within the marginal mafic-dominated material (dyke contains background uranium values of 10.1 ppm U), C. Zone of pervasive hematization containing significant uranium enrichment (note labels on core denote cps); a sample from this zone returned up to 3.95 wt.% Na <sub>2</sub> O and 2620 ppm U) ....	105
Figure 48.	Regional geology map of the western belt of supracrustal rocks in the Benedict Mountains region (geological base map from Gower, 2010) ....	117
Figure 49.	Concordia diagrams for U–Pb data from Aillik Group rocks. Red ellipses denote zircon analyses, blue ellipses are titanite analyses. A. Metavolcanic host rock hosting uranium mineralization, Michelin deposit, B. Footwall granodiorite intrusion, Michelin deposit, C. Quartz–feldspar porphyry, Jacques Lake deposit, D. Footwall granodiorite, Jacques Lake deposit,	

Figure 50.	E. Metavolcanic host rock to uranium mineralization, Jacques Lake deposit; F. Felsic volcanic host rock to uranium mineralization, Powe prospect. Note error ellipses are at the $2\sigma$ level . . . . .	118
Figure 51.	Rock classification diagrams after Pearce (1996), outlining the classification of major units at select occurrences. A. Michelin deposit, B. Jacques Lake deposit, C. Mustang Lake prospect, D. Benedict Mountains region . . . . .	120
Figure 52.	Primitive mantle normalized spider diagrams (values from Sun and McDonough, 1989) outlining the trace-element characteristics of major units within the Michelin deposit. A. Sub- and coarsely porphyritic metavolcanic host rocks, B. Felsic-dominated intrusive units, C. Mafic-dominated intrusive units. Note the yellow highlighted field denotes the older foliated dykes contained within the sequence . . . . .	121
Figure 53.	Primitive mantle normalized spider diagrams (values from Sun and McDonough, 1989) outlining the trace-element characteristics of major units within the Jacques Lake deposit. A. Felsic and intermediate metavolcanic host rocks, B. Felsic-dominated intrusive units, C. Mafic-dominated intrusive units. Note the shaded yellow area outlines the profile of the foliated dykes from the Michelin deposit for comparison . . . . .	121
Figure 54.	Primitive mantle normalized spider diagram (values from Sun and McDonough, 1989) outlining the trace-element characteristics of major units within the Mustang Lake prospect. A. Felsic and intermediate metavolcanic host rocks, B. Mafic-dominated intrusive units. Note the shaded yellow area outlines the profile of the foliated dykes from the Michelin deposit for comparison . . . . .	122
Figure 55.	A. Relationship of U and $\text{Na}_2\text{O}$ for the metavolcanic host rocks of the Aillik Group, B. Relationship of U and $\text{CaO}$ for the metavolcanic host rocks of the Aillik Group, C. Relationship of U and $\text{Fe}_2\text{O}_3(\text{T})$ for the metavolcanic host rocks of the Aillik Group, D. Relationship of $\text{Na}_2\text{O}$ , $\text{CaO}$ and $\text{K}_2\text{O}$ within unmineralized (<50 ppm U) metavolcanic rocks . . . . .	123
Figure 56.	Regional geology map outlining the distribution of uranium occurrences within the Bruce River Group (geological base map modified from Wardle <i>et al.</i> , 1997) . . . . .	126
Figure 57.	Plan map outlining the distribution of drillholes at the Moran Heights prospect as well as the distribution of geological units (modified from Morgan <i>et al.</i> , 2007). Note grid coordinates are in NAD 27, Zone 21 . . . . .	132
Figure 58.	Plan map outlining the distribution of drillholes and the main geological units at the Moran Lake B Zone prospect. Note grid coordinates are in NAD 27, Zone 21 . . . . .	135
Figure 59.	Concordia diagrams for U–Pb zircon data from rocks within the Bruce River Group. A. Tuff from the basal Heggart Lake Formation, Lower C Zone deposit, B. Granite intrusion, B Zone prospect, C. Tuff from the basal Brown Lake Formation, Croteau Lake prospect, D. Crystal tuff, Minisinakwa prospect. Note error ellipses are at the $2\sigma$ level . . . . .	143
Figure 60.	Extended trace-element diagrams for sandstone-hosted uranium mineralization within the Bruce River Group. A. Lower C Zone deposit, B. Moran Heights prospect, C. Moran A Zone prospect, D. Moran B Zone prospect. Barren samples contain less than 100 ppm U. Normalizing values are from Quinby-Hunt <i>et al.</i> (1989) except for Cu, Ni, Pb, Ag and Mo, which are taken from Vine and Tourtelot (1970) . . . . .	144
Figure 61.	Regional geology map outlining the distribution of uranium occurrences within miscellaneous intrusive rocks within the CMB (geological base map modified from Wardle <i>et al.</i> , 1997) . . . . .	146

## PLATES

Page

	Page
Plate 1. Mafic dyke (outlined by white dashed line) crosscutting hematized uraniferous quartz monzodiorite-tonalite, Anomaly No. 7 prospect. The mafic dyke is interpreted to postdate the uranium mineralization and associated alteration .....	12
Plate 2. Centimetre-scale, strongly hematized, shear zone (top center of photograph) separating mineralized quartz monzodiorite-tonalite (left) from unmineralized pegmatite (right); Fish Hawk Lake South prospect; DDH FHLS-07-06, ~90 m depth .....	13
Plate 3. A similar style contact to that shown in Plate 2 exposed at surface, whereby a fault trending approximately 80°, separates hematized quartz monzodiorite-tonalite (right) from relatively unaltered and barren equivalent rocks (left); Anomaly No. 7 prospect .....	13
Plate 4. Variable degrees of hematite alteration developed within the host quartz monzodiorite-tonalite. Initial chlorite alteration (1) is progressively replaced by hematite (2) until all primary textural features are obscured in regions of intense hematite alteration (3); Fish Hawk Lake South prospect .....	16
Plate 5. Initial hematization of feldspars within the host quartz monzodiorite-tonalite proximal to a mineralized fracture zone; Anomaly No. 7 prospect .....	16
Plate 6. A. Sample displaying regional chlorite alteration overprinted by mineralized, hematite-bearing fractures, B. Accompanying autoradiograph showing the preferential concentration of the radioactivity (yellow, minus the outline of the sample) in association with the distribution of the fracturing shown in (A); Fish Hawk Lake North prospect .....	16
Plate 7. A. Sample displaying intense brick-red hematite alteration developed within fine-grained quartz monzodiorite-tonalite, crosscut by a later dark-purple specularite-rich vein, B. Accompanying autoradiograph showing the distribution of the radioactivity (yellow, minus the outline of the sample) within the sample; Near Miss prospect .....	17
Plate 8. Cataclasite hosting uranium-bearing hematized quartz monzodiorite-tonalite fragments within a chlorite-rich breccia matrix; note that the breccia is crosscut by later carbonate veins (Anomaly No. 7 prospect; DDH 51544, ~45 m depth) .....	17
Plate 9. A. Sample displaying brittle fracturing within mineralized pegmatite; note the initial brick-red hematite alteration is relatively unmineralized, and is subsequently overprinted by a second stage of dark-purple specularite, associated with the majority of radioactivity within the sample, B. Accompanying autoradiograph of the sample showing the distribution of radioactivity (yellow, minus the outline of the sample); Fish Hawk Lake South prospect .....	18
Plate 10. Rare, late-stage chalcopyrite (green arrow) infilling fractures crosscutting hematized quartz monzodiorite-tonalite; Fish Hawk Lake South prospect .....	18
Plate 11. Photomicrographs of mineralized samples showing the distribution of radioactivity in relation to the Fe-Ti-oxides in thin section. A. Initial chlorite alteration overprinted by later uranium-bearing Fe-Ti-oxides within tectonically brecciated quartz monzodiorite-tonalite, PPL, B. Autoradiograph outlining the distribution of radioactivity (yellow) in the field shown in (A), C. Mineralized, finely disseminated Fe-Ti-oxides, PPL, D. Reflected light image of (C) showing the distribution of apatite (Ap), chalcopyrite (Cpy), hematite (Hem) and possible uraninite (U), E. Highly fractured host rock showing local development of cataclastic brecciation accompanied by hematite alteration and uranium mineralization, PPL, F. Cross-polarized view of (E) .....	19
Plate 12. A. Second-stage chlorite alteration overprinting the development of mineralized Fe-Ti-oxide minerals and associated carbonate alteration, PPL, B. Autoradiograph outlining areas of high radioactivity (yellow) in (A) .....	20
Plate 13. Well-developed banding in the Maggo Gneiss displaying local folding of the gneissic banding, crosscut by a late pegmatite dyke; Two-Time deposit, DDH CMB-07-21, ~440 m depth .....	20
Plate 14. Fine-grained tonalite intruding weakly banded, chlorite-rich, gneiss. Note the well-developed fracturing and associated brecciation within the tonalite unit; Two-Time deposit, DDH CMB-07-14, ~160 m depth .....	20

Plate 15	Feldspar-rich pegmatite overprinted by chlorite-rich brecciation; Two-Time deposit, DDH CMB-07-21, ~380 m depth .....	21
Plate 16.	Moderately foliated, carbonate-altered, fine-grained mafic dyke hosting enclaves of hematite–carbonate-altered tonalite; Two-Time deposit, DDH CMB-07-11, ~280 m depth .....	21
Plate 17.	Fresh, fine-grained mafic dyke displaying a well-developed chilled contact with the adjacent gneissic host rock; Two-Time deposit, DDH CMB-07-21, ~475 m depth .....	21
Plate 18.	Relatively barren protocataclasite developed within hematite–carbonate-altered quartz monzodiorite–tonalite; Two-Time deposit, DDH CMB-07-11, ~250 m depth .....	22
Plate 19.	Mineralized cataclastic breccia; note highest concentrations of radioactivity (labelled in counts per second) are associated with the development of intense hematite alteration of the breccia; Two-Time deposit, DDH CMB-07-14, ~280 m depth .....	22
Plate 20.	Development of the chlorite-rich ‘mega breccia’ within Maggo Gneiss marginal to the main mineralized zone; Two-Time deposit, DDH CMB-07-14, ~205 m depth .....	22
Plate 21.	Small-scale example of the crush protobreccia developed marginal to unmineralized cataclasite; Two-Time deposit, DDH CMB-07-14, ~220 m depth .....	22
Plate 22.	Early pinkish-red hematite (Early Hem) alteration crosscut by chlorite (Chl. Rich Bx)-rich brecciation overprinted by later hematite alteration (Late Hem); all phases are barren with respect to uranium mineralization; Two-Time deposit, DDH CMB-07-07, ~200 m depth .....	24
Plate 23.	Mineralized cataclastic breccia (A), and an accompanying autoradiograph outlining the distribution of radioactivity (yellow, minus the outline of the sample) within the sample (B). Note the initial pale-pink hematitic alteration occurring as fragments is overprinted by later, uranium-bearing, dark-purple, specularite-rich alteration .....	24
Plate 24.	Hand sample displaying ‘vuggy’ textured zone, infilled with a pale-cream clay mineral (yellow circle) identified as phengitic illite on the basis of VIRS analysis .....	24
Plate 25.	A. PPL image of relatively unaltered quartz monzodiorite–tonalite displaying early chlorite alteration along grain boundaries in association with minor Fe–Ti-oxide minerals, B. XPL image of (A), C. Early, barren, chlorite-rich cataclasite, D. XPL image of (C), E. PPL image of early chlorite-rich breccia crosscut by mineralized fracture hosting Fe–Ti-oxide minerals, F. Autoradiograph outlining regions of radioactivity (yellow) in the field shown in (E) .....	25
Plate 26.	Hematite–albite–carbonate alteration (stubby yellow arrow) developed within metres of the overlying conglomerate of the Heggart Lake Formation. Note the sharp structural contact separating the two units ( <i>see</i> inset). Moran Lake C Zone, DDH ML-56, ~50 m depth .....	36
Plate 27.	Early pinkish-orange hematite–albite alteration (Phase 1A) overprinted by white Fe-carbonate–quartz–albite alteration (Phase 1B), which is, in turn, crosscut by dark-purple hematite-rich fracturing (Phase 2) and associated brecciation. Note pale-green patches of relatively unaltered mafic volcanic are still locally preserved. Moran Lake C Zone, DDH ML-3, ~55 m depth .....	38
Plate 28.	Hematite-rich breccia associated with Phase 2 alteration, containing fragments of the earlier, Phase 1, pale-orange hematite–albite–carbonate alteration. This breccia is barren with respect to uranium mineralization, but is enriched in vanadium. Moran Lake C Zone, DDH ML-3, ~105 m depth .....	40
Plate 29.	Pervasive Fe-carbonate alteration replacing the dark-purple hematite-rich matrix of a finely milled breccia associated with Phase 2 alteration. Note the presence of remnant millimetre-scale hematite altered fragments ‘floating’ in the Fe-carbonate alteration. Moran Lake C Zone, DDH ML-4, ~80 m depth .....	40
Plate 30.	A. Uranium-bearing, dark-purple, specularite-rich breccia vein (Phase 2) crosscutting earlier hematite–albite–carbonate (Phase 1) alteration, B. Autoradiograph of (A) outlining the distribution of radioactivity (yellow) within the sample .....	40
Plate 31.	A. Hematite-altered jasperoidal chert overprinted by fracturing and brecciation infilled with specularite. This is, in turn, crosscut by a second mm-scale specularite-filled fracture (yellow arrow), B. Autoradiograph of (A) outlining the distribution of radioactivity (yellow) within the sample. Note the highlighted specularite-filled fracture is devoid of any significant radioactivity .....	41

Plate 32.	Pervasive Fe-carbonate alteration hosting localized zones of uranium mineralization within the Lower Shear Zone. Note the development of the intense fabric giving the zone a mylonitic appearance, as well as the late crosscutting quartz-carbonate veins. Moran Lake C Zone, DDH ML-56, ~150 m depth .....	41
Plate 33.	A. Pervasive Fe-carbonate alteration hosting anomalous uranium mineralization associated with dark-red hematite-rich bands, B. Autoradiograph of (A) outlining the distribution of radioactivity within the sample (yellow; minus the outline of the sample) .....	41
Plate 34.	Brecciated and mineralized conglomerate of the Heggart Lake Formation. Moran Lake C Zone, DDH ML-82, ~115 m depth .....	41
Plate 35.	A. Pervasive hematite alteration accompanied by specularite-rich brecciation within conglomerate of the Heggart Lake Formation, B. Autoradiograph of (A) outlining the distribution of radioactivity within the sample (yellow; minus the outline of the sample) .....	42
Plate 36.	A. Sample of early 'jig-saw' brecciation of Phase 1 alteration, crosscut by late-stage quartz-carbonate veins, B. XPL image from a portion of the brecciation shown in (A), displaying the early fragmentation of the altered mafic volcanic rock characterized by abundant plagioclase displaying albite twining, C. Sample of milled breccia displaying subrounded matrix-supported clasts of Phase 1 alteration in a specularite–carbonate-dominated matrix, D. PPL image from a portion of (C) displaying the local alignment of fragments within the hydrothermal breccia, E. XPL image of (D); note carbonate occurring as both fragments and matrix material, F. PPL image highlighting the 'ragged' margins of the fragments within the hydrothermal breccia .....	42
Plate 37.	A. PPL photomicrograph displaying an uraniferous fracture infilled with magnetite and specularite followed by carbonate and rutile, B. Reflected light image of (A) displaying the distribution of magnetite subsequently replaced by the specularite, C. Close-up reflected-light image displaying the replacement of the magnetite by the bladed specularite, D. Reflected-light image displaying the rare occurrence of well-formed uraninite hosted within a magnetite–hematite-filled fracture, E. PPL image of a fracture lined with uraninite and subsequently infilled with carbonate and euhedral pyrite, F. Close-up view showing euhedral pyrite overgrowing uraninite. Abbreviations: Cb–carbonate, Hem–specularite, Mag–magnetite, Py–pyrite, Rt–rutile, U–uraninite .....	43
Plate 38.	A. Reflected-light image of mineralized, specularite (Hem)-rich breccia containing millimetre-scale fragments of carbonate (Cb) along with subhedral pyrite (Py), B. Autoradiograph of the region shown in (A) showing the association of the radioactivity (yellow) with the development of the specularite .....	45
Plate 39.	Pinkish-red hematite–carbonate–albite alteration flanked by pale-beige Fe-carbonate–albite alteration within altered argillite; note the highly disrupted nature of the host rock due to the structural control of the mineralization. Armstrong deposit, DDH MLAR-04, ~280 m depth .....	47
Plate 40.	A. PPL photomicrograph of mineralized Fe-carbonate–albite alteration containing finely disseminated Fe–Ti oxide minerals throughout, B. Autoradiograph of (A) outlining the distribution of radioactivity (yellow), C. Hematite–albite alteration crosscut by mineralized fractures containing specularite, and trace chalcopyrite, D. Autoradiograph outlining the distribution of radioactivity (yellow) in (C), E. PPL photomicrograph of area containing anomalous radioactivity in association with the development of Fe–Ti oxide minerals (field of view approximately 2.5 mm in width), F. SEM image outlining the distribution of Fe within (E), G. SEM image outlining the distribution of Ti within (E), H. SEM image outlining the distribution of U within (E) .....	48
Plate 41.	A. Mineralized boulder from the Croteau Lake prospect containing 0.07% $U_3O_8$ , B. Corresponding autoradiograph highlighting the distribution of radioactivity within the sample (yellow) .....	48
Plate 42.	Pale-beige siltstone of the Warren Creek Formation displaying an influx of hematite and magnetite along brittle network-style fractures; Croteau Lake prospect .....	49

Plate 43.	Highly disrupted chert and interbedded iron formation crosscut by barren hematite–magnetite-filled fractures, highlighting the mobilization of iron-rich fluids; Croteau Lake prospect. ....	49
Plate 44.	A. PPL photomicrograph from the sample in Plate 41, displaying the development of finely disseminated Fe–Ti oxide minerals in association with carbonate alteration that overprints the magnetite–chlorite assemblage, B. Accompanying autoradiograph outlining the distribution of the radioactivity (yellow) in association to the Fe–Ti oxide alteration ....	49
Plate 45.	A. PPL photomicrograph displaying the finely disseminated Fe–Ti oxides associated with the anomalous radioactivity, B. Reflected-light image of (A) displaying the finely disseminated Fe–Ti oxides enveloping primary magnetite (Mag) along with minor chalcopyrite (Ccp), C. Reflected-light image of hematite associated with uranium mineralization locally displaying a colloform texture (lower right corner), cored by an earlier pyrite phase, D. Magnified view of colloform hematite growth shown in (C) ....	50
Plate 46.	A. Hand sample of highly fractured chert containing 0.08% $U_3O_8$ and 964 ppm Cu, crosscut by network-style fractures infilled with iron-carbonate and chlorite, B. Autoradiograph of the hand sample shown in (A) displaying fracture-hosted radioactivity (yellow), C. Hand sample of pale-green siltstone containing 0.22% $U_3O_8$ , 2.25% Cu and 162 ppb Au; note siliceous material similar to that in (A) in upper left hand corner of the sample, D. Autoradiograph of (C) displaying finely disseminated radioactivity within the pyriteiferous siltstone; note siliceous material in upper left corner is devoid of any significant radioactivity. ....	51
Plate 47.	Mineralized and locally brecciated dolostone immediately overlain by sulphidic black shale hosting abundant quartz-carbonate veining; note mineralization is confined to the disrupted portions of the dolostone unit. Area 51 prospect, DDH MLA51-03, ~20 m depth ....	53
Plate 48.	A. Sample GS-08-05; variably altered hand sample of Joe Pond basalt taken from a mineralized interval assaying up to 0.32% $U_3O_8$ . Sample displays the complex nature of the Fe-carbonate–albite and hematite–albite alteration, B. Autoradiograph of (A) displaying the distribution of radioactivity within the sample (yellow) ....	53
Plate 49.	A. Hand sample displaying pervasive Fe-carbonate alteration developed within a siltstone unit subsequently overprinted by barren, white carbonate alteration and chlorite–pyrite-filled fractures; sample contains 0.31% $U_3O_8$ , B. Autoradiograph of (A) outlining distribution of radioactivity (yellow) ....	54
Plate 50.	A. Hand sample containing 0.17% $U_3O_8$ associated with extensive brittle fracturing, infilled with pyrite and minor quartz, B. Autoradiograph outlining the fracture-hosted radioactivity (yellow) in (A) ....	54
Plate 51.	Mineralized metasedimentary rock (left) containing up to 0.09% $U_3O_8$ as well as 0.3% Mo and 1.31 ppm Re, crosscut by a quartz-feldspar porphyry dyke (right) containing up to 0.04% $U_3O_8$ associated with fractures; Kitts deposit ....	67
Plate 52.	Undeformed, fine- to medium-grained amphibole-rich diorite dyke. DDH B-11, ~25 m depth; Kitts deposit ....	67
Plate 53.	A. Hand sample of vein-hosted uranium mineralization, B. Corresponding autoradiograph of the uranium mineralization (yellow, minus the outline of the sample) within the hand sample. DDH K-74-18, Kitts deposit, ~118 m depth ....	68
Plate 54.	Mineralized sample shown in Plate 53 from the Kitts deposit. A. Uranium mineralization hosted with amphibole and rimmed by the development of brownish haloes, PPL, B. Autoradiograph of the thin section shown in (A) outlining the distribution of radioactivity (yellow); note the region of the second generation of amphibole (dark areas) is devoid of any significant radioactivity (refer to text), C. Reflected-light photomicrograph of the mineralized area shown in (A) illustrating the finely disseminated nature of the uraninite (U) in association with minor pyrite (Py) and trace chalcopyrite (Ccp), D. PPL photomicrograph of an uraniferous fracture crosscutting the quartz-feldspar porphyry unit, E. Reflected-light photomicrograph of (D), outlining the distribution of pyrite (Py), uraninite (U) and allanite (Aln) within the sample, F. PPL photomicrograph of titanite (Ttn) occurring within late-stage quartz-rich segregations in the diorite unit ....	70

Plate 55.	Garnetiferous metasedimentary rocks overlying amphibolite; DDH G-68-132, ~37 m depth; Gear deposit .....	73
Plate 56.	Intercalated mafic and felsic tuffaceous beds within the ‘Transition Zone’ of Evans (1980). This unit is locally intruded by fine-grained pink aplite dykes, which are, in turn, deformed with the host rock; DDH G-68-142, ~20 m depth; Gear deposit .....	74
Plate 57.	Deformed pillow basalt of the Kitts Pillow Lava Formation immediately adjacent to, and structurally below, mineralized tuffaceous rocks at the Nash deposit .....	75
Plate 58.	A. Predominantly mafic tuffaceous rocks of the Post Hill Group displaying a strong foliation and localized folding within the footwall of the Nash deposit, B. Interbedded pink felsic tuff with associated tuffaceous sandstone of the Aillik Group in the hangingwall of the Nash deposit .....	76
Plate 59.	A. Hydrothermally altered metasedimentary rocks hosting anomalous radioactivity; DDH G-68-142, ~83 m depth; Gear deposit, B. Mineralized drillcore showing a late, light-green, alteration assemblage overprinting earlier uranium mineralization, C. Corresponding autoradiograph for the sample shown in (B) outlining the uranium mineralization (yellow, minus the outline of the sample) within the hand sample .....	76
Plate 60.	Sulphidic argillite, similar to that seen at the Kitts deposit, containing syn-sedimentary sulphides and minor porphyroblasts of garnet. DDH G-68-131, ~80 m depth; Gear deposit .....	76
Plate 61.	A. Uraniferous metasedimentary rocks with minor mafic tuff, Inda deposit, B. Mineralized metasedimentary rock displaying a strong foliation developed parallel to compositional layering within the sample, C. Autoradiograph of (B) outlining the roughly stratiform uranium mineralization (shown in yellow) within the sample .....	77
Plate 62.	Contrasting styles of uranium mineralization developed within the area of the Nash deposit. A. Metavolcanic/metasedimentary host rock displaying foliation-parallel uranium mineralization as indicated by the accompanying autoradiograph. DDH NW-77-04, ~43 m; Nash West Extension prospect, B. Autoradiograph of the uranium mineralization (yellow, minus the outline of the sample) within the sample; note the tight isoclinal fold displayed by the uranium mineralization indicating that the mineralization has been deformed, C. Brittle fracture-hosted mineralization associated with hematization of surrounding wallrock within felsic metavolcanic rocks of the Aillik Group. DDH NW-77-02, ~14 m; Nash West Extension prospect, D. Accompanying autoradiograph of (C) outlining the association of the radioactivity (yellow, minus the outline of the sample) with the hematite alteration .....	78
Plate 63.	Mineralized samples from the Anna Lake deposit displaying the effects of post-mineral deformation. A. Amphibole–biotite schist displaying a crenulation cleavage. DDH AL-07-01, ~21 m, B. Autoradiograph of (A) outlining the distribution of radioactivity within the sample (yellow minus the outline of the sample); note the effect of the crenulation cleavage overprints the distribution of the radioactive material within the sample, C. Similar metasedimentary unit as in (A) displaying tight, cm-scale folding. DDH AL-07-01, ~117 m, D. Autoradiograph of (C) outlining the distribution of radioactivity within the sample (yellow minus the outline of the sample); note the effect of the folding on the distribution of the radioactive material within the sample .....	80
Plate 64.	A. Uraniferous opaque minerals incorporated within amphibole crystals in metasedimentary rocks of the Anna Lake deposit, B. Corresponding autoradiograph of (A) outlining the areas of radioactivity (yellow), C. Complex intergrowth of magnetite–hematite–pyrrhotite within opaque minerals associated with radioactivity; shown in (A) .....	81
Plate 65.	A. SEM image of mineralized material from the Anna Lake deposit, showing the distribution of finely disseminated uraninite (bright white). The coloured plates are element specific and include, B. uranium, C. lead, D. molybdenum, E. titanium, F. iron. Note, the field of view in each image is approximately 0.2 mm .....	82
Plate 66.	A. Interlayered amphibole-rich and epidote-rich bands within mineralized metasedimentary rocks of the Anna Lake deposit, B. Corresponding autoradiograph of (A) outlining the areas	82

of elevated radioactivity shown in yellow, C. Reflected light image of (A) outlining the abundance of pyrrhotite in the non-radioactive portion of the thin section. The radioactive portion is dominated by magnetite, hematite and finely disseminated uraninite along with lesser pyrrhotite .....	83
Plate 67. Coarse-grained, pegmatitic patches within the Kitts Metagabbro, sampled for U–Pb geochronology .....	83
Plate 68. Metavolcanic host rock of the Michelin deposit illustrating the variably porphyritic nature of the unit. Note the inset of the stained sample outlining the primary potassic minerals within the metavolcanic rock prior to being overprinted by the sodic alteration associated with the uranium mineralization; DDH M-06-11, ~140 m depth .....	93
Plate 69. A. Photograph of the complex dyke of Piloski (1976) displaying a sharp upper contact between the adjacent metavolcanic rock and the fine-grained amphibolite margin of the dyke, which, in turn, transitions into a coarsely porphyritic felsic core; Michelin deposit, DDH M-07-75A, 792 m, B. Similar dyke as shown in (A), located approximately 900 m to the northeast; DDH M-06-11, 227 m .....	94
Plate 70. Typical features of mineralized core from the Michelin deposit illustrating the light-coloured (albitized) and red (hematized) metavolcanic host rock. A. Sub-porphyritic metavolcanic host rock; M-06-13, 400 m, B. Coarsely porphyritic metavolcanic host rock, is the primary host to the mineralized zones; M-06-13, 408 m .....	96
Plate 71. A. Representative sample of mineralized, coarsely porphyritic, metavolcanic rock obtained from material excavated during construction of the adit; note the pervasive hematite alteration and a moderate to strong penetrative fabric, B. Corresponding autoradiograph of (A) outlining the location of radioactivity (yellow, minus the outline of the sample); note the fine-grained disseminated radioactivity throughout the host rock as well as localized increases in radioactivity within more strongly foliated portions of the sample .....	98
Plate 72. A. Pervasive hematization within a coarsely porphyritic sample of mineralized metavolcanic rock displaying a strong penetrative fabric affected by local crenulation (white arrows); DDH M-07-072, 554 m, B. Corresponding autoradiograph of (A) outlining the location of radioactivity (yellow, minus the outline of the sample); note the lack of influence on the disseminated uranium mineralization relative to the development of the crenulation .....	98
Plate 73. A. Representative sample from the Michelin deposit (DDH M-06-11 at 64 m depth) stained for potassium-bearing minerals (yellow colouration). The sample consists of a K-feldsparphyric, fine-grained, quartz-rich metavolcanic rock illustrating the potassic nature of the metavolcanic host rock, distal to uranium mineralization, B. PPL photomicrograph showing the distribution of potassium (yellow) throughout the groundmass of the volcanic protolith. Also note the presence of fine-grained disseminated opaque minerals (primarily consisting of magnetite) enveloped by titanite rims within the groundmass; minor biotite is also distributed throughout, C. XPL photomicrograph showing the same view as in (B) .....	99
Plate 74. Representative sample of mineralized drillcore (Michelin deposit; DDH M-06-11, 380 m). A. Photograph of a mineralized thin section; note the inset box displays the location of (C), B. Corresponding autoradiograph of the mineralized thin section outlining the distribution of radioactivity within the sample (yellow, minus the outline of the sample), C. PPL photomicrograph covering an area of intense radioactivity. The sample contains finely disseminated magnetite throughout, but the area associated with the most intense radioactivity also contains finely disseminated hematite and Fe–Ti-oxides; note the inset box in (C) outlines the area of (E), D. XPL image of (C); note that the coarser grained quartz–albite lacks any significant radioactivity, E. PPL photomicrograph outlining the distribution of the turbid, finely disseminated Fe-oxide minerals along discrete fractures within the thin section; this area is associated with the highest radioactivity within the sample, F. Reflected light image of (E) showing the distribution of magnetite and hematite as well as highlighting the finely fractured nature of the host rock within the zone of elevated radioactivity .....	100

Plate 75.	Photomicrographs of the complex dyke unit from the Michelin deposit. A. PPL image of a large feldspar crystal displaying relic compositional zoning of a more K-feldspar-rich core and albite-rich rim; the crystal is supported by a groundmass of fine-grained quartz and feldspar along with abundant blue-green amphibole and lesser biotite, pyroxene, opaque minerals and titanite; DDH M-06-11, 228 m depth, B. XPL image of (A), C. PPL image of a large feldspar phenocryst displaying a relic compositional zonation within a finer grained quartz-feldspar-biotite-rich groundmass; note how the foliation in the upper right hand corner of the image wraps around the feldspar phenocryst; DDH M-06-11, 230 m depth, D. XPL image of (C), E. Fine-grained, quartz-feldspar-biotite-rich groundmass, hosting disseminated magnetite rimmed by titanite; DDH M-06-11, 230 m depth, F. XPL image of (E) .....	101
Plate 76.	Strongly foliated intermediate metavolcanic host rock displaying a typical upper-greenschist-to lower-amphibolite-facies metamorphic assemblage consisting of chlorite, actinolite, biotite and epidote; Jacques Lake deposit, DDH JL-06-10, 142 m .....	102
Plate 77.	Quartz-feldspar porphyry dyke displaying a distinctive pseudorapakivi texture; Jacques Lake deposit, DDH JL-06-10, 365 m .....	104
Plate 78.	Feldspar crystals from the adjacent quartz-feldspar porphyry dyke hosted within a more mafic-dominated phase that intrudes along the margin of the porphyry unit; DDH JL-07-60, 205 m .....	104
Plate 79.	A. Representative sample of mineralized metavolcanic host rock from the Jacques Lake deposit displaying hematization in association with uranium mineralization. Note the most intense radioactivity within the sample is developed within a hematitic fracture, roughly sub-parallel to the actinolite–magnetite–carbonate ± biotite ± pyrite veining; DDH JL-07-60, 132 m, B. Corresponding autoradiograph of (A) outlining the location of radioactivity (yellow, minus the outline of the sample), C. Grab sample from moderately to strongly foliated outcropping mineralization proximal to the high-strain zone within the Jacques Lake deposit, D. Corresponding autoradiograph of (C) outlining the location of radioactivity (yellow, minus the outline of the sample); note the radioactivity is strongest within the pinkish hematized metavolcanic marginal to the actinolite veining, which is subsequently overprinted by later carbonate veining containing notably less radioactivity .....	106
Plate 80.	Representative sample of mineralized drillcore from the Jacques Lake deposit (DDH JL-07-60, 132 m). A. Photograph of the mineralized thin section. (The large inset box, near the centre of the section, displays the location of (C), whilst the smaller inset box to the lower left displays the location of (E)), B. Corresponding autoradiograph of the mineralized thin section outlining the distribution of radioactivity within the sample ( yellow, minus the outline of the sample); note the highest concentration of radioactivity within the sample is associated with a discrete hematitic fracture, C. PPL photomicrograph showing the fine-grained metavolcanic host rock containing abundant disseminated magnetite, crosscut by actinolite–magnetite–carbonate ± biotite ± pyrite veining containing at least two generations of actinolite, D. XPL image of (C), E. PPL image of the highly radioactive hematitic fracture outlining the abundance of Fe-oxide minerals within the zone; F. Reflected light image of (E) highlighting the fractured nature of the host rock in the area of most intense radioactivity; note magnetite is more strongly altered to hematite within this zone .....	107
Plate 81.	Representative sample of mineralized drillcore from the Jacques Lake deposit (DDH JL-07-60, 216 m). A. Photograph of the mineralized thin section. (The large inset box to the left of centre displays the location of (C), whilst the smaller inset box to the right displays the location of (F)), B. Corresponding autoradiograph of the mineralized thin section outlining the distribution of radioactivity within the sample (yellow, minus the outline of the sample); note the absence of radioactivity within the metavolcanic host rock in the lower left section, away from the vein margin, C. PPL image of the actinolite–magnetite–carbonate ± biotite ± pyrite vein. The actinolite at the margins of the vein is devoid of any significant radioactivity, but some irregularly distributed radioactivity is developed within the centre of the vein. (The small inset box outlines the location of (E)), D. XPL image of (C), E. Actinolite within the	

core of the vein shown in (C) hosting minor uraninite surrounded by the characteristic brown halos, F. PPL image outlining two generations of actinolite, the first forms along the vein margins and occurs as 'inclusions' within the second phase, which is accompanied by carbonate and is barren with respect to any significant radioactivity .....	108
Plate 82. A representative sample of mineralized drillcore from the Jacques Lake deposit (DDH JL-07-60, 245 m). A. Photograph of the mineralized thin section. (The inset box to the lower right displays the location of (C), whilst the box to the left displays the location of (D); the small inset box near the centre at the top displays the location of (E)), B. Corresponding autoradiograph of the mineralized thin section outlining the distribution of radioactivity within the sample (yellow, minus the outline of the sample); note the radioactivity within the sample is entirely confined to the actinolite-rich portion of the section, C. PPL image showing the sharp contact between the metavolcanic host rock (lower right) and the uraniferous actinolite (upper left), D. PPL image of uraniferous actinolite (top) and relatively barren actinolite (bottom), E. PPL image of actinolite hosting finely disseminated uraninite throughout, F. Reflected light image of (E) showing the fine-grained nature of the uraninite.....	108
Plate 83. A. Representative sample of the quartz–feldspar–porphyry dyke stained for potassium-bearing minerals (yellow colouration; Jacques Lake deposit, DDH JL-06-10, 360 m), B. PPL image of a zoned feldspar phenocryst within a quartz–feldspar bearing groundmass, C. XPL image of (B) outlining the zonation within the feldspar phenocryst, D. PPL image of the groundmass of the porphyry unit, displaying the spatial association of magnetite and titanite that often occurs as rims around the oxide minerals, E. XPL image of (D).....	110
Plate 84. Photograph displaying a portion of the mineralized intersection in hole SP-06-10, which returned 0.12% $U_3O_8$ over 9.11 m; Mustang Lake area. The most significant zones of mineralization are associated with intense magnetite–hematite alteration (white numerics denote cps as determined using a handheld scintillometer); mineralization is also locally crosscut by post-mineralization mafic dykes .....	111
Plate 85. A. Sample of mineralized drillcore displaying strong magnetite–hematite alteration from an interval containing 1700 ppm U over 0.5 m; DDH SP-06-10, 169.5 m; Mustang Lake area, B. Corresponding autoradiograph of (A) outlining the location of radioactivity (yellow, minus the outline of the sample); note the strong foliation and local crenulation developed within the uranium mineralization indicating post-mineral deformation.....	112
Plate 86. A. Sample of mineralized intermediate metavolcanic host rock from drillcore displaying localized hematization and biotite–magnetite–amphibole alteration in association with uranium mineralization; DDH SP-06-10, 172.5 m: Mustang Lake area, B. Corresponding autoradiograph of (A) outlining the location of radioactivity (yellow, minus the outline of the sample); note the predominant fracture-hosted nature of the mineralization .....	112
Plate 87. Intermediate metavolcanic host rock displaying patchy hematization and chlorite–magnetite–actinolite–calcite veining within the mineralized zone at the Gayle prospect.....	113
Plate 88. A. Sample of mineralized material collected from trenching at the Gayle prospect displaying hematization and chlorite–magnetite–actinolite–calcite veining in association with uranium mineralization, B. Corresponding autoradiograph of (A) outlining the location of radioactivity (yellow, minus the outline of the sample); note zones of highest radioactivity are associated with the dark-red hematized zones that appear to be overprinted by later chlorite–magnetite–actinolite–calcite veining, C. Representative hand specimen of mineralized metasedimentary rock exposed at the Burnt Brook prospect, D. Corresponding autoradiograph of (C) outlining the location of radioactivity (yellow, minus the outline of the sample); note the highest zones of radioactivity are associated with patchy hematization of the host rock, E. Highly sheared mineralized metavolcanic host rock from the Aurora River prospect, F. Corresponding autoradiograph of (E) outlining the location of radioactivity (yellow, minus the outline of the sample); note the highest levels of radioactivity within the sample are associated with hematite alteration which appears to predate the development of the mafic mineral assemblage associated with shearing.....	114

Plate 89.	A. Representative sample of mineralized material from the White Bear prospect; sample contains 1300 ppm U, B. Corresponding autoradiograph of (A) outlining the location of radioactivity (yellow, minus the outline of the sample); note the fracture-hosted radioactivity as well as the aggregates of mafic minerals (white arrow) associated with elevated radioactivity within the groundmass, C. Mineralized sample from the Otter Lake prospect displaying an amphibole-rich vein in addition to abundant hairline fractures hosting hematite alteration, D. Corresponding autoradiograph of (C) outlining the location of radioactivity (yellow, minus the outline of the sample); note the association between the hematitic fractures and the areas of highest radioactivity within the sample. The amphibole-rich vein is also associated with weak radioactivity, but much less than the marginal hematitic fractures .....	115
Plate 90.	Photograph displaying the unconformable contact between basalt and overlying sandstone, Lower C Zone deposit (DDH ML-44, 340 m). The sandstone in the immediate vicinity of the contact and extending 4–5 m up-section is reduced and hosts uranium mineralization, which, in turn, grades upwards into oxidized sandstone.....	128
Plate 91.	Oxidized sandstone overprinted by fractures displaying an influx of reduced fluids immediately above the mineralized zone of the Lower C Zone deposit (DDH ML-34, ~310 m depth).....	128
Plate 92.	Photograph displaying the patchy distribution of disseminated uranium mineralization within reduced sandstone of the Lower C Zone deposit (DDH ML-44, ~345 m depth); the labels denote counts per second.....	129
Plate 93.	A. Sample of reduced sandstone overprinted by hematite–carbonate alteration, Lower C Zone deposit (DDH ML-55, ~330 m depth), B. Accompanying autoradiograph of (A), outlining the distribution of radioactivity within the sample (yellow; minus the outline of the sample) .....	129
Plate 94.	A. PPL photomicrograph of two areas of anomalous radioactivity associated with opaque minerals, developed in association with pervasive chlorite–carbonate alteration within reduced sandstone of the Lower C Zone (DDH ML-38, ~295 m depth), B. XPL view of (A), C. Magnified view of (A) illustrating the intergrowth of the opaque oxide minerals with the chlorite alteration, D. Reflected light magnified view of (C) showing the formation of the Fe–Ti oxide minerals along with chalcopyrite, both of which locally envelope an earlier pyrite phase, E. PPL photomicrograph of the radioactive area shown in Plate 93B (DDH ML-55, ~330 m depth); also shown is the area of the SEM image shown in (G and H), F. XPL view of (E), G. SEM image outlining the distribution of uranium (red), H. SEM image outlining the distribution of titanium (green) .....	130
Plate 95.	Photograph illustrating a zone of uranium mineralization developed at the transition zone between the reduced and oxidized siliciclastic sedimentary rocks of the Moran Heights prospect (DDH ML-MH-04, ~40 m depth); white labels denote counts per second .....	133
Plate 96.	Uraniferous hematite–carbonate veins crosscutting reduced sandstone, Moran Heights prospect (DDH ML-MH-13, 36.5 m depth); white labels denote counts per second.....	133
Plate 97.	A. XPL view of the reduced sandstone containing euhedral disseminated pyrite and uraniferous Fe–Ti oxide minerals; inset outlines magnified view shown in (C), B. Reflected light view of (A) illustrating abundant coarse-grained euhedral pyrite within the sample, C. Magnified view of pyrite and point source of radioactivity as outlined by an autoradiograph of the thin section, D. SEM image outlining the distribution of uranium (shown in red); note the local presence of a uranium-rich phase enveloping pyrite, E. SEM image outlining the distribution of titanium (green), F. SEM image outlining the distribution of copper (shown in magenta); note local spatial association of uranium and copper mineralization .....	134
Plate 98.	Uraniferous, leucogabbroic dyke displaying distinct brownish-orange weathering due to the pervasive Fe–carbonate alteration that accompanies uranium mineralization (~750 m northeast of main B Zone prospect).....	136
Plate 99.	Brecciated hematite and Fe–carbonate alteration overprinted by later dark-purple specularite-filled fractures, B Zone prospect. Sample contains 14.01 wt.% CaO, 4.39 wt.% Na <sub>2</sub> O and 127 ppm U .....	136

Plate 100.	Fine- to medium-grained leucogabbroic dyke intruding red sandstone, and where minor fracture-hosted uranium mineralization is developed along the margin of the dyke; core of dyke contains background levels of radioactivity whilst the contact zone measures up to 300 cps (DDH ML-BZ-02, ~73 m depth); white label denotes counts per second .....	136
Plate 101.	Uranium-bearing breccia located along the intrusive margin of a leucogabbroic dyke; B Zone prospect. A sample from this interval returned 0.34% $U_3O_8$ , 0.12% $V_2O_5$ , 0.25% Cu and 14.3 g/t Ag over 0.5 m (Sample #90838; Morgan <i>et al.</i> , 2007; DDH ML-BZ-04, ~43 m depth); white labels denote counts per second .....	136
Plate 102.	A. Scanned thin section of the mineralized breccia shown in Plate 101; inset shows location of (C), B. Accompanying autoradiograph outlining the distribution of radioactivity (yellow) within (A), C. PPL photomicrograph illustrating the plagioclase-rich nature of the dyke fragments within the breccia; inset shows the location of (D), D. Reflected light image of opaque oxide minerals showing magnetite and Fe-Ti oxide minerals that host uranium mineralization; inset shows the location of (E), E. Backscattered SEM image of an uraniferous zone as outlined by the autoradiograph; note finely disseminated bright spots are inferred to be uraninite, F. SEM view of (E) outlining the distribution of uranium (red), G. SEM view of (E) outlining the distribution of iron (orange), H. SEM view of (E) outlining the distribution of titanium (green). .....	137
Plate 103.	A. Reflected light image of opaque oxide minerals developed within the breccia matrix. B. Backscattered SEM image of uraniferous zone as outlined by the autoradiograph, illustrating the close spatial association of uranium mineralization and magnetite within the breccia matrix; field of view is approximately 2 mm, C. SEM view of (B) outlining the distribution of uranium (red), D. SEM view of (B) outlining the distribution of titanium (green), E. SEM view of (B) outlining the distribution of iron (shown in orange) .....	139
Plate 104.	Rusty-weathering, highly sheared, uraniferous pebble conglomerate, Moran Lake A Zone prospect .....	140
Plate 105.	A. Uraniferous sample of pebble conglomerate from the Moran Lake A Zone prospect; sample assayed 0.15% $U_3O_8$ , B. Corresponding autoradiograph of (A) outlining the distribution of radioactivity within the sample (yellow, minus the outline of the sample) .....	140
Plate 106.	Large gabbroic dyke intruding siliciclastic sedimentary rocks of the Heggart Lake Formation, CVG prospect .....	140
Plate 107.	Uraniferous hematite and related Fe-carbonate alteration overprinting a gabbroic dyke intruding sedimentary rocks of the Heggart Lake Formation, CVG prospect .....	140
Plate 108.	Anomalous radioactivity developed within brittle fractures in felsic volcanic rocks of the Sylvia Lake Formation, Madsen Lake Zone 4B prospect (DDH ML-MA-02, 20 m depth); white labels denote counts per second .....	141
Plate 109.	A. Uraniferous sample of a felsic volcanic rock from the Sylvia Lake prospect; sample assayed 0.69% $U_3O_8$ , B. Corresponding autoradiograph of (A) outlining the distribution of radioactivity within the sample (yellow minus the outline of the sample); note the brittle fracture-hosted nature of the mineralization .....	141
Plate 110.	Quartz- and feldspar-phyric felsic metavolcanic rock displaying fracture-hosted magnetite alteration, Minisinakwa prospect .....	142
Plate 111.	A. Uraniferous boulder of felsic metavolcanic rock from the Minisinakwa prospect; sample assayed 0.35% $U_3O_8$ , B. Corresponding autoradiograph of (A) outlining the distribution of radioactivity within the sample (yellow, minus the outline of the sample); note spatial association between the magnetite alteration and distribution of radioactivity within the sample .....	142
Plate 112.	Highly sheared, metavolcanic rocks of the Sylvia Lake Formation, hosting anomalous U, Cu, Au, Ag and local fluorite, Stormy Lake prospect .....	143
Plate 113.	Highly fractured and hematite-altered granite juxtaposed against highly fractured, relatively unaltered granite; Melody Hill prospect .....	148

	Page
Plate 114. Strongly foliated hematite–magnetite alteration developed within outcrop exposures of the Melody Hill Granite; Melody Hill prospect .....	148
Plate 115. A. Hematite–magnetite-altered granodiorite containing 0.61% $U_3O_8$ , B. Autoradiograph of (A) outlining the distribution of radioactivity within the sample (yellow, minus the outline of the sample); AT 649 prospect .....	149
Plate 116. Weakly mineralized, variably foliated, locally hematite altered intrusive unit; Super 7 prospect (DDH MBS7-08-05, ~50 m depth); white labels denote counts per second .....	149
Plate 117. A. Cataclastic breccia developed within granodiorite, displaying moderate hematization, B. Autoradiograph of (A) outlining the distribution of radioactivity within the sample (yellow, minus the outline of the sample); Noseman prospect .....	150

## TABLES

Table 1. NI 43-101 compliant resource estimates for mineralization within the Archean basement rocks.....	6
Table 2. Summary of the various stages of alteration and the associated mineralogy in the Anomaly No. 7–Fish Hawk Lake area; based on field mapping and petrography.....	13
Table 3. Summary of the various stages of alteration and associated mineralogy in the Two-Time–Snegamook area; based on field mapping and petrography .....	24
Table 4. NI 43-101 compliant resource estimates for mineralization within the Moran Lake Group .....	31
Table 5. Summary of the stages of alteration and associated mineralogy for the Moran Lake Upper C Zone deposit; based on field mapping and petrography .....	38
Table 6. Summary of the alteration and associated mineralogy for the Armstrong deposit; based on field mapping and petrography .....	45
Table 7. NI 43-101 compliant resource estimates for mineralization within the Post Hill Group.....	60
Table 8. NI 43-101 compliant resource estimates for mineralization within the Aillik Group .....	88
Table 9. NI 43-101 compliant resource estimates for mineralization within the Bruce River Group .....	127

## ABSTRACT

*The Central Mineral Belt (CMB) of Labrador is a diverse geological environment and is host to widespread uranium mineralization. It contains a variety of different styles of uranium mineralization that are developed within a number of different rock units. This study classifies the main uranium occurrences within the CMB, which have been subdivided on the basis of host rock, alteration and textural characteristics, displayed by the uranium mineralization. Based on these attributes, the uranium mineralization, within the CMB, has been interpreted to have formed in three different mineralizing environments; namely magmatic, metamorphic–metasomatic and sedimentary environments.*

*Magmatic-related mineralization includes syngenetic mineralization occurring as pegmatite- and aplite-hosted occurrences, and volcanic-hosted mineralization occurring in relatively unaltered and undeformed volcanic rocks, as well as magmatic–hydrothermal mineralization of an epigenetic affinity. The latter is associated with alkali (Ca, Na) metasomatism in association with the development of iron-rich breccias displaying V, Cu and Ag enrichment (e.g., Moran Lake Upper C Zone deposit) and may represent so-called iron-oxide-copper-gold (IOCG) mineralization within the region.*

*Metamorphic–metasomatic styles of mineralization are primarily hosted within felsic metavolcanic and pelitic metasedimentary rocks and commonly display a fundamental structural control. Within the CMB, this style of mineralization is currently the most economically significant with respect to the associated uranium resource and includes the high-grade Kitts deposit, as well as the lower grade, larger tonnage, Michelin and Jacques Lake deposits. The largest deposit in the region, the Michelin deposit, is associated with the development of strong sodium metasomatism and may be related to the so-called ‘metasomatite’ or ‘albite’ style of uranium mineralization.*

*Sedimentary-hosted mineralization primarily occurs within terrestrial sedimentary rocks; here uranium mineralization is associated with localized reduced zones within an otherwise oxidized sedimentary sequence. This style of mineralization has several affinities to sandstone-hosted mineralization, known mostly from Phanerozoic sequences, or to some mineralization associated with Proterozoic unconformity-style deposits.*

*U–Pb geochronological data from the region is used to bracket the timing of the various styles of uranium mineralization into four main mineralizing events. Uranium mineralization within the eastern CMB is primarily bracketed between 2030–1880 and 1860–1800 Ma. In more western parts of the region, uranium mineralization is bracketed between 1860–1660, and later than 1650 Ma. There is some overlap in the timing of mineralization between the eastern and western CMB, and the possibility exists for a common mineralizing event between these two regions; however, further study is required to investigate such a relationship. U–Pb geochronological results from titanite and monazite also provide additional data for several deformational events that are syn- to post-development of uranium mineralization. Data obtained as part of this study highlight the Makkovikian (1900–1710 Ma), Labradorian (1710–1620 Ma) and Grenvillian (ca. 1000 Ma) orogenies, as locally playing a role in the formation and/or local remobilization of uranium mineralization in the region.*

## INTRODUCTION

### PURPOSE AND SCOPE

The Central Mineral Belt (CMB) of Labrador has long been recognized for its uranium potential and has been the focus of intermittent uranium exploration, since the first prospect was discovered in the late 1950s. Early exploration continued up until the mid-1980s, when a decline in demand in world uranium markets marked an end to exploration in the region. In the mid-2000s, renewed market interest in uranium once again sparked exploration in the CMB, which resulted in the generation of large amounts of industry data including modern geophysical and geochemical surveys, along with significant amounts of diamond drilling. A number of summary reports on the geology and metallogeny of the CMB include sections on uranium mineralization (e.g., Gower *et al.*, 1982; Ryan, 1984; Kerr, 1994; Wilton, 1996); however a report, solely focused on the development and genesis of uranium mineralization in the region, was lacking.

In 2007, the Geological Survey of Newfoundland and Labrador commenced a metallogenic study aimed at documenting the style and setting of the numerous uranium occurrences throughout the CMB. The overall goal of this project was to provide regional context for the various styles of mineralization, in addition to providing insight into the timing and nature of uranium mineralization. This work was greatly aided by the large industry presence in the area between 2007 and 2009, most notably from the diamond drilling and trenching that was carried out during this peak period of exploration activity. Preliminary results have already been presented (e.g., Sparkes and Kerr, 2008; Sparkes and Dunning, 2009, 2015; Sparkes *et al.*, 2010, 2016; Sparkes and Davis, 2013). This report represents a detailed synthesis, in addition to presenting new information. Significant outputs of this study include:

1. A proposed classification scheme for the various styles of uranium mineralization developed within the CMB.
2. Documentation and classification of significant uranium occurrences throughout the region.
3. Detailed imaging of select styles of uranium mineralization through the use of autoradiograph techniques, and
4. Geochronological data enabling the uranium mineralization within the CMB to be subdivided into discrete metallogenic events.

### METHODS

Most of the data presented here were gathered from the examination of diamond drillcore from select uranium occurrences, generated during the most recent period of exploration

activity within the CMB (*ca.* 2005–2009). This data, combined with field mapping and the compilation of available industry data (from assessment files), were used to develop a regional synthesis, regarding the nature and timing of uranium mineralization within the CMB.

As part of this study, select mineralized samples were imaged utilizing an autoradiograph technique first outlined by Basham (1981); a summary of this technique is given in Appendix A. The resultant autoradiographs were then used to select specific areas of mineralized samples for more detailed investigations, such as petrography or scanning-electron-microscope (SEM) imaging.

Numerous samples were collected for geochronological and geochemical studies. The bulk of geochronology analyses were conducted at Memorial University of Newfoundland, but several samples were analyzed at the Geological Survey of Canada laboratories; a summary of the geochronological techniques used at both facilities is provided in Appendix B. Various geochemical techniques and analytical packages from several different commercial labs were utilized over the course of the study; a summary of these techniques and related procedures along with the geochemical data will be released in a later report (~March, 2017). For this report, those samples assaying greater than 1%  $U_3O_8$  are considered ‘high-grade’, while those containing less than 1%  $U_3O_8$  are referred to as ‘low-grade’.

### REGIONAL GEOLOGICAL SETTING

The CMB of Labrador spans several different structural provinces including parts of the Archean Nain Province, the Paleoproterozoic Makkovik and Churchill provinces, and the Mesoproterozoic Grenville Province (Figure 1). The CMB has no firm geographic boundaries, but rather is defined by the distribution of the various mineral occurrences throughout the region. It is host to most of the uranium mineralization known within Labrador, and is also well-known for Cu, Mo and REE mineralization. The regional geology of the CMB (and parts thereof) is summarized by Gower *et al.* (1982), Ryan (1984), Ermanovics (1993), Kerr, (1994), Kerr *et al.* (1996), Wilton (1996), Hinckley (2007), and Hinckley and LaFlamme (2009); the following overview is largely derived from these sources. A summary diagram, which outlines a simplified stratigraphy of the region, is illustrated in Figure 2, which highlights the temporal context of the main examples of uranium mineralization. It should be noted that this figure illustrates only the ages of the host rocks to specific occurrences, and the actual ages of mineralization may be significantly younger in some cases.

Rocks within the Archean Nain Province, and their reworked equivalents, represent the oldest units, and form the

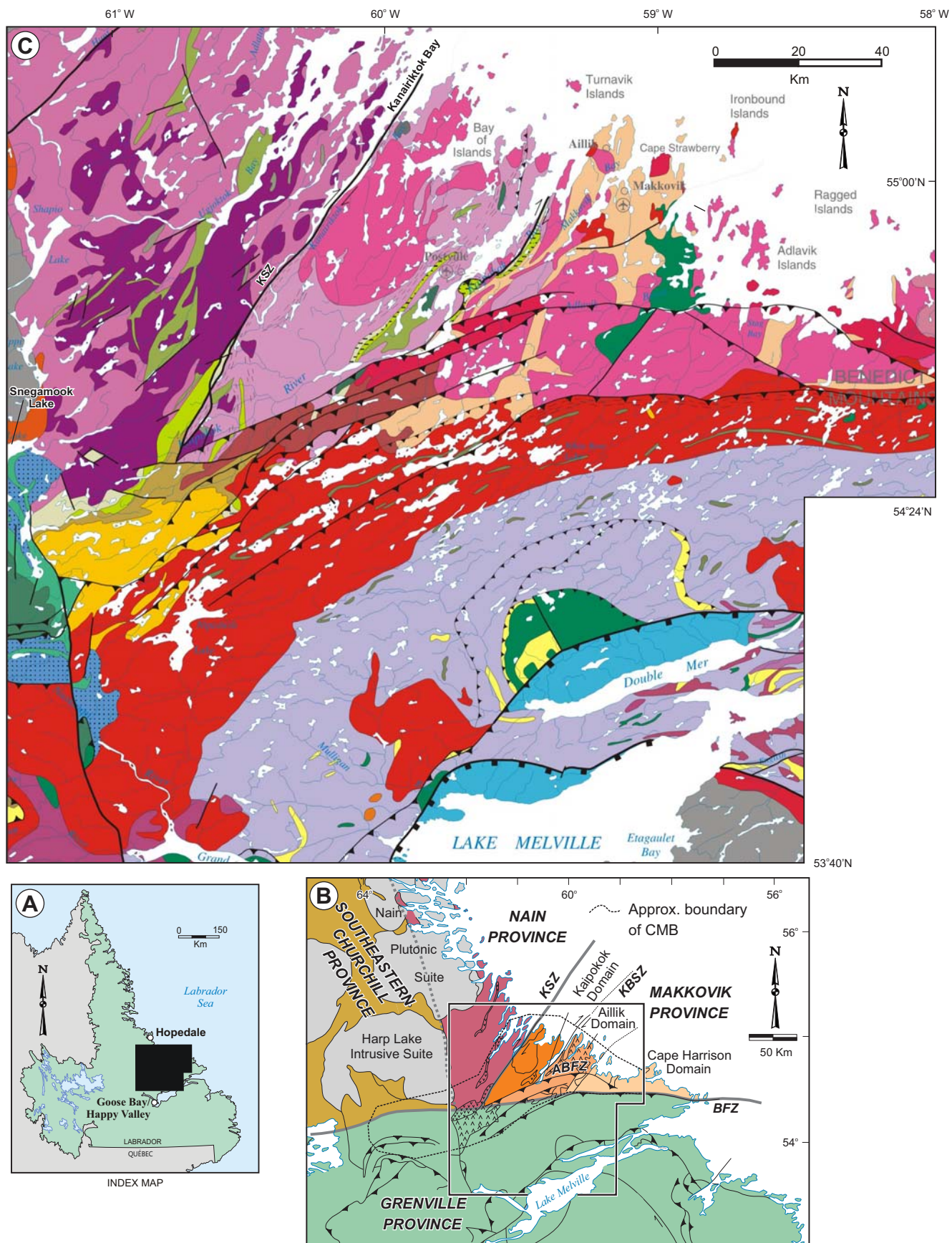


Figure 1.

## LEGEND

### NEOPROTEROZOIC

Arkose and conglomerate

### MESOPROTEROZOIC

Gabbro sills (ca. 1250 to 1224)

Subaerial basalt flows

Arkose, grading south into quartzite

Granite plutons (ca. 1296 Ma)

Olivine gabbro and metamorphic equivalents

Granitoid rocks (1500 to 1420 Ma)

Anorthosite and other, locally layered, mafic rocks

Quartz diorite

### PALEOPROTEROZOIC

Rhyolitic to andesitic volcanic rocks including ash-flow tuff and agglomerate (ca. 1650 Ma)

Volcaniclastic sandstone, arkose and conglomerate

Granite, quartz monzonite, granodiorite, syenite and minor quartz diorite (ca. 1650)

Granitoid rocks (1645 to 1626 Ma; including some ca. 1780 to 1720 Ma rocks)

Anorthosite and other, locally layered, mafic components (1645 to 1625 Ma)

Mafic intrusive suites (gabbronorite, lesser diorite), some metamorphosed as amphibolite to granulite facies

Granodioritic orthogneiss (lesser quartz diorite and granitic orthogneiss (s. l.); may include Mesoproterozoic rocks)

Mafic gneiss, probably of supracrustal origin, mainly at granulite facies

Quartz diorite to granodiorite plutons

K-feldspar megacrystic granite and other granitoid plutonic rocks

Pelitic, migmatitic metasedimentary gneiss and minor psammitic gneiss at amphibolite to granulite facies

High-level, locally flourite-bearing granites (1776 to 1719 Ma)

Rhyolite, ash-flow tuff, breccia and hypabyssal rhyolite intrusions; volcaniclastic siltstone and sandstone; minor basalt (ca. 1860 to 1807 Ma)

Granite and granodiorite (1840 to 1795 Ma)

Tonalite, granodiorite and monzogranite gneiss; minor amphibolite, calc-silicate and felsic (metavolcanic ?) gneiss

Gabbro and leucogabbro sills (ca. 1884 to 1874 Ma)

Pillow basalt, basaltic pyroclastic rocks; minor siltstone and greywacke

Schistose amphibolite derived from mafic volcanic rocks (Moran Lake and Post Hill groups)

Granite plutons (ca. 2134 Ma, locally 2032 Ma in the Nain Province; 1973 to 1891 Ma in the Makkovik Province)

Shale and sandstone of shallow- to deep-water origin

Pelitic schist

### ARCHEAN AND/OR PALEOPROTEROZOIC

Anorthosite, leucogabbro, leuconorite and derived gneiss

### ARCHEAN

Tonalitic and other gneisses reworked and retrograded during Makkovikian orogenesis

Mafic volcanic and volcaniclastic rocks, lesser sedimentary and felsic volcanic rocks, and mafic-ultramafic sills; at greenschist to amphibolite facies

Granodiorite, tonalite and minor granite (Kanairiktok Intrusive Suite, ca. 2850 to 2830 Ma)

Tonalitic to granodioritic migmatitic orthogneiss containing abundant mafic to ultramafic inclusions and relict mafic dykes

Mafic gneisses including rocks of intrusive and extrusive origin

### SYMBOLS

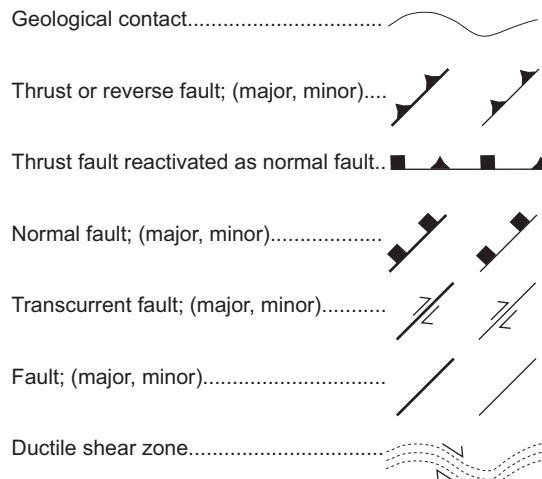


**Figure 1 (opposite).** A. Location map, B. Outlines of the regional subdivisions of the CMB of Labrador; (modified from Hinchey and LaFlamme, 2009), C. Regional geology encompassing the CMB; (geological base map modified from Wardle et al., 1997). BFZ–Benedict fault zone, KBSZ–Kaipokok Bay shear zone, KSZ–Kanairiktok shear zone, ABFZ–Adlavit Brook fault zone.

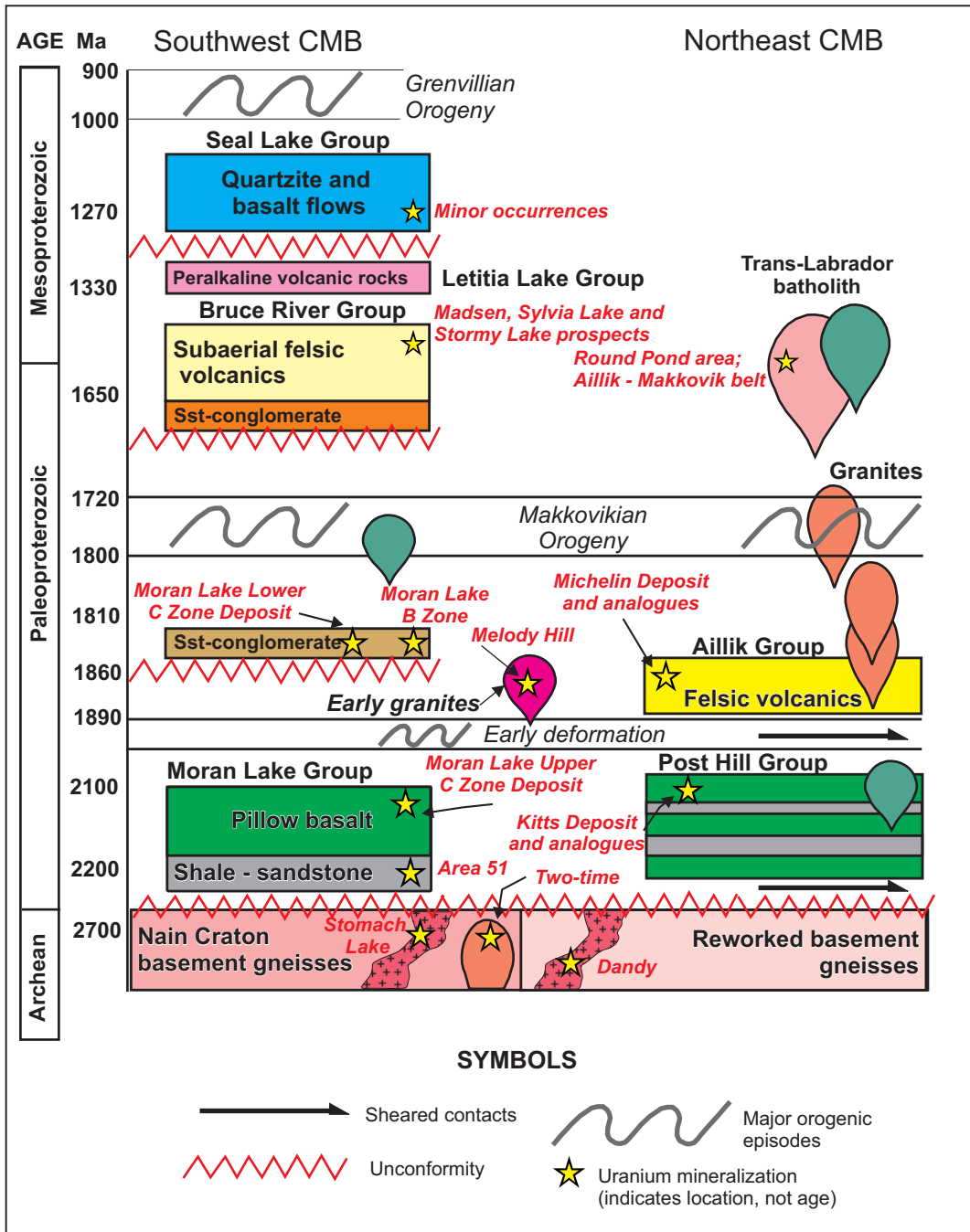


**Figure 2.** Schematic stratigraphic chart for the CMB showing the settings of various examples of uranium mineralization. (Note that the ages implied for these occurrences are those of the host rocks and are not necessarily the age of the mineralization, which may be much younger.)

basement rocks to the Proterozoic supracrustal sequences (Ryan, 1984; Ermanovics, 1993; Kerr *et al.*, 1996). Rocks of the Nain Province consist of orthogneiss and lesser remnants of an older supracrustal sequence. The orthogneiss is intruded by rocks of the Kanairiktok Intrusive Suite (KIS), which consist of massive to strongly foliated tonalite, granodiorite and granite. Both the orthogneiss and KIS are crosscut by a se-

quence of mafic dykes, known as the Kikkertavak dykes that have been dated at  $2235 \pm 2$  Ma (Cadman *et al.*, 1993). These dykes do not crosscut the overlying supracrustal sequences of the CMB and therefore provide a maximum age constraint for the deposition of the overlying Moran Lake and Post Hill groups (*cf.* Ermanovics, 1993; Wilton, 1996).

The boundary between the Nain and Makkovik provinces is marked by a prominent northeast-trending shear zone known as the Kanairiktok shear zone (Figure 1). This shear zone has a long and complex history of deformation and syntectonic magmatism, and contains multiple sheets of leucocratic and pegmatitic granite, locally dated at  $1870 \pm 2$  Ma (Culshaw *et al.*, 2000; Ketchum *et al.*, 2001b). The northwestern Makkovik Province contains the same units as the Nain Province, but here they have undergone Paleoproterozoic deformation and metamorphism, and are intruded by complex plutonic rocks ranging from *ca.* 1900 to *ca.* 1720 Ma (Ermanovics, 1993; Ketchum *et al.*, 2001b). The *ca.* 2235 Ma Kikkertavak dykes are transformed into folded amphibolites within the Makkovik Province, but locally retain their original discordance with Archean host rocks (Ryan *et al.*, 1983). Deformed and metamorphosed supracrustal rocks, likely equivalent to the Post Hill Group (see below) also occur within this region (Marten, 1977; Ryan *et al.*, 1983).

The oldest supracrustal sequences in the CMB are the Moran Lake and Post Hill groups (Figure 2). The Post Hill Group was previously known as the Lower Aillik Group, prior to redefinition of the terminology by Ketchum *et al.* (2002). The Moran Lake and Post Hill groups both consist of siliciclastic sedimentary rocks and mafic volcanic rocks, and have long been correlated on the basis of their similar stratigraphy and lithologies (e.g., Marten, 1977; Wardle and Bailey, 1981). U–Pb geochronological data from the Post Hill Group demonstrate that mafic metavolcanic rocks in its lowermost part were deposited *ca.* 2178 Ma ago, but that sedimentary rocks higher in the sequence were deposited after *ca.* 2013 Ma, suggesting that there are some unresolved stratigraphic complexities (Ketchum *et al.*, 2001b). The Moran Lake Group remains undated, but is unconformably overlain by *ca.* 1850 Ma siliciclastic sedimentary rocks (Sparkes *et al.*, 2016; see Section, Uranium Mineralization within the Bruce River Group); it sits unconformably upon Archean basement rocks, but the more strongly deformed and metamorphosed Post Hill Group is in tectonic contact with these older rocks. The Post Hill Group is strongly deformed and disrupted by shear zones, and displays amphibolite-facies metamorphism, which locally led to partial melting. In contrast, the Moran Lake Group displays only greenschist-facies metamorphism. However, regional relationships, and the presence of deformed clasts of typical Moran Lake Group rock types in the basal part of the *ca.* 1650 Ma Bruce River Group (Smyth *et al.*, 1978), indicate pre-1650 Ma deformation of the Moran Lake Group.

Younger supracrustal sequences in the eastern part of the CMB are very different in character from the Moran Lake and Post Hill groups, as they are dominated by shallow-water to terrestrial sedimentary rocks and subaerial felsic volcanic rocks of the Aillik Group. These rocks were previously known as the Upper Aillik Group, prior to the redefinition of

terminology by Ketchum *et al.* (2002). The Aillik Group includes a lower sequence of mixed sedimentary rocks and volcanic rocks of both mafic and felsic composition, which is overlain by a thick sequence of felsic volcanic, pyroclastic and volcaniclastic rocks. The metavolcanic rocks within this group range in age from 1883 to 1856 Ma (Schärer *et al.*, 1988; Hinckley and Rayner, 2008), but their primary features are obscured by metamorphism, recrystallization and locally intense deformation. The contact between the Aillik Group and the older Post Hill Group has been the focus of much debate, but is generally interpreted to be largely tectonic (Marten, 1977; Gower *et al.*, 1982; Kerr *et al.*, 1996; Ketchum *et al.*, 2002). The Aillik Group is the single most important host to uranium mineralization within the CMB.

In the southwestern part of the western CMB, the Bruce River Group sits unconformably upon the Moran Lake Group. The Bruce River Group is described, in detail, by Ryan (1984), and consists of a lower terrestrial sedimentary sequence dominated by conglomerates, arkoses and sandstones, which are, in turn, overlain by a thick sequence of mostly felsic volcanic rocks, dated *ca.* 1650 Ma (Schärer *et al.*, 1988; Sparkes *et al.*, 2016). However, as part of this study, U–Pb dating of tuff layers interbedded with basal sandstone units within the lower Bruce River Group produced an age of *ca.* 1850 Ma (Sparkes *et al.*, 2016; see Section, Uranium Mineralization within the Bruce River Group), indicating the presence of unrecognized complexities within the stratigraphy of the Bruce River Group.

Large areas of the CMB are underlain by plutonic rocks of broadly granitoid composition, particularly in the southern and eastern parts. These plutonic rocks were formed in at least four main episodes: 1895 to 1870 Ma, 1815 to 1790 Ma, 1720 to 1715 Ma, and 1650 to 1640 Ma (Kerr *et al.*, 1992; Kerr, 1994; Ketchum *et al.*, 2001b, 2002). Thus, they both predate and postdate development of the supracrustal sequences of the Aillik and Bruce River groups. The oldest plutonic rocks locally display intense deformation, and the 1815–1790 Ma suites include both syntectonic and posttectonic suites that are temporally linked to the Makkovik Orogeny. Evidence exists for the presence of earlier deformational events within the northwestern portion of the Makkovik Province, as indicated by the initial metamorphic recrystallization of Kikkertavak dykes, dated at *ca.* 1900 Ma (Ketchum *et al.*, 1997); however, the true extent of this event is difficult to resolve accurately (Schärer *et al.*, 1988; Kerr *et al.*, 1992; Ketchum *et al.*, 1997). The younger (*ca.* 1650 Ma) plutonic suites are undeformed within the Makkovik Province, but are affected by the *ca.* 1000 Ma Grenvillian Orogeny in the southern portion of the CMB. In the central part of the Makkovik Province, plutonic suites of *ca.* 1720 and *ca.* 1650 Ma form small, isolated plutons cutting the Aillik Group, suggesting that the erosion surface coincides with the roof zone(s) of

larger batholiths at depth (Kerr, 1994). Some of these plutonic suites are associated with hydrothermal mineralization of granophyre character, which locally includes uranium, in addition to Cu, Mo and F (Wilton and Wardle, 1987; Kerr, 1994; Wilton, 1996).

The youngest supracrustal sequences in the CMB are the Letitia Lake and the Seal Lake groups. The Letitia Lake Group, dated at *ca.* 1330 Ma (Thomas, 1981; Gandhi *et al.*, 1988), is dominated by alkaline volcanic rocks and is not represented in Figure 1. It is known primarily for its REE occurrences, and is not discussed here further. The Seal Lake Group consists of terrestrial sedimentary rocks and minor mafic volcanic rocks, both of which are intruded by mafic sills (Brummer and Mann, 1961; Ryan, 1984; van Nostrand and Lowe, 2010). The sedimentary rocks are undated, but unconformably overlie the Letitia Lake Group, indicating deposition after *ca.* 1330 Ma. U–Pb ages from the mafic sills of *ca.* 1250 and *ca.* 1225 Ma (Romer *et al.*, 1995) provide a minimum age for deposition of the sequence. The Seal Lake Group occurs on the western edge of the area illustrated in Figure 1, where it sits unconformably upon a number of different units, including several plutonic suites and the felsic volcanic rocks of the Bruce River Group. The Seal Lake Group is best-known for copper mineralization (Gandhi and Brown, 1975; Wilton, 1996) but is also reported to host minor uranium occurrences, only one of which was evaluated during this study (see Section, Uranium Mineralization within the Bruce River Group).

## URANIUM MINERALIZATION WITHIN ARCHEAN BASEMENT ROCKS

### INTRODUCTION

Prior to the resurgence in uranium exploration within the CMB during the mid-2000s, only three occurrences of uranium mineralization were known to be hosted by Archean basement rocks in the region; these include the Anomaly No. 7, No. 7A and No. 17 prospects, located in the northwestern extent of the CMB (Figures 3 and 4). The renewed uranium exploration brought about the discovery of additional prospects within the Archean basement rocks, the most notable of which is the Two-Time deposit (Figure 3). These new

occurrences include previously known styles of uranium mineralization such as the structurally controlled mineralization developed akin to the Anomaly No. 7 prospect, and newly identified syn-magmatic (pegmatite-hosted) styles of uranium mineralization (*e.g.*, Soggy Bog prospect; Figure 4). The Archean basement rocks, which were previously perceived to be relatively barren with respect to significant uranium mineralization, are now known to host some 30 uranium occurrences, one of which, the Two-Time deposit, has a NI 43-101 compliant resource estimate of approximately six million pounds of  $U_3O_8$  (see Table 1).

### REGIONAL GEOLOGY

Archean rocks in the CMB form the southern portion of the Hopedale block as defined by Ermanovics (1993). To the south, the Archean sequence is unconformably overlain by siliciclastic sedimentary rocks and associated mafic volcanic rocks of the Moran Lake Group (*cf.* Ryan, 1984, and see references therein). The area of the Archean basement that has been the focus of uranium exploration extends from Snegamook Lake in the west, to Kanairiktok Bay in the east (Figure 3). This region predominantly consists of medium- to coarse-grained, variably foliated intrusive rocks of the KIS (Kanairiktok Plutonic Suite of Ermanovics, 1993) and derived granitoid gneiss (Ryan, 1984). The KIS locally intrudes older amphibolite-facies banded gneiss, known as Maggo Gneiss, which is, in turn, host to enclaves of amphibolite, known as Weekes Amphibolite. Enclaves of the Weekes Amphibolite are reported to range from fifty to several hundred metres in length, and form concordant bands and lenses within the Maggo Gneiss (Ermanovics, 1993).

The Weekes Amphibolite consists primarily of hornblende and lesser garnet, clinopyroxene, biotite, sulphides, and Fe-oxides. This unit contains a greenschist-facies retrograde mineral assemblage of actinolite, amphibole, epidote, chlorite, and carbonate (Ermanovics, 1993). These enclaves are characterized by the presence of zoned and recrystallized plagioclase, abundant sphene, and relatively large zircon contained within hornblende and zoned plagioclase. Such criteria were used by Ermanovics (1993) to classify a roughly 2.5 km-long northeast-trending belt of amphibolite, located to the immediate northeast of the Two-Time deposit (Figure 5), as Weekes Amphibolite.

**Table 1.** NI 43-101 compliant resource estimate for mineralization within the Archean basement rocks

Deposit	Resource Classification	Cut-off (% $U_3O_8$ )	Grade (% $U_3O_8$ )	Tonnage (tonnes > cut-off)	Contained Resource (lbs. $U_3O_8$ )	Source
Two-Time	Indicated	0.03%	0.059%	1,760,000	2,287,000	Ross, 2009
	Inferred	0.03%	0.056%	2,973,000	3,669,000	Ross, 2009

The Maggo Gneiss is a migmatized quartzofeldspathic orthogneiss, which ranges from tonalite to granodiorite in composition, and dominantly consists of hornblende, clinopyroxene, perthite and biotite. It is distinguished from the locally deformed intrusive rocks of the KIS by the presence of discordant granoblastic amphibolites, termed the 'Hopedale dykes' (Ermanovics, 1993). Several phases of deformation are recorded within the Maggo Gneiss, including both refolded folds and deformed mafic dykes that crosscut earlier metamorphic layering. Geochronological study of the gneissic unit has identified a complex history, from which Loveridge *et al.* (1987) determined an age of  $3105 +6/-9$  Ma; he interpreted this age as a tentative emplacement age for the precursor rocks of the gneissic unit.

The KIS consists of biotite–hornblende-bearing grey to pink tonalite, granodiorite and lesser pink granite of a calc-alkaline composition. These rocks occur as irregular lenticular and elongate intrusions (Ermanovics, 1993; Ryan, 1984). A U–Pb zircon age from a sample collected near the coast of Labrador gave an upper intercept age of  $2858 +4/-3$  Ma (Loveridge *et al.*, 1987) and provides the only known age constraint for this unit prior to this study, albeit far removed from the current study area. Within the CMB, the area of the KIS that hosts most of the uranium prospects occurs to the west and north of Moran Lake (Figure 4). In this region, rocks of the KIS are only weakly deformed and are dominated by medium- to coarse-grained tonalitic rocks consisting of oligoclase, andesine, quartz, biotite, hornblende and low-grade metamorphic mineral assemblages (chlorite, epidote, calcite, biotite and muscovite; Ermanovics, 1993).

Two major periods of deformation are recognized within the Archean basement rocks (Ermanovics, 1993). The older deformation predates the intrusion of the KIS and is associated with northwesterly trending structures and upper amphibolite-facies metamorphism (Ermanovics, 1993); however, the presence of local northwesterly trending structures cross-cutting the KIS in some areas is inferred to represent evidence for the local reactivation of these structures during subsequent deformation (see below). The younger of the two deformational events affects the KIS and is associated with northeasterly trending structures and greenschist-facies metamorphism (Ermanovics, 1993). A brittle to ductile transition is noted within the rocks of the KIS from the southwest to the northeast, which is also associated with increasing metamorphic grade toward the northeast (Ermanovics, 1993). The brittle deformation is locally accompanied by the development of cataclastic fabrics within shear zones in the area south of the Kanairiktok River and northwest of Moran Lake (Figure 4).

## EXPLORATION HISTORY

The Anomaly No. 7 prospect was discovered by Brinex in 1978, during follow-up prospecting of an airborne radio-

metric survey and was the first occurrence of uranium mineralization noted within Archean rocks in the area. The occurrence was drilled the same year, and produced favourable results including intersections of up to  $0.25\% \text{ U}_3\text{O}_8$  over 9.68 m, within a broader interval averaging  $0.13\% \text{ U}_3\text{O}_8$  over 23.38 m (drillhole 51543; Perry, 1979). Subsequent drilling tested the down-dip extension of the mineralization and locally intersected high grades with assays of up to  $4.36\% \text{ U}_3\text{O}_8$  over 0.15 m (drillhole 51557; Perry, 1980a); however, the mineralization is very sporadic. Perry (1979) noted that hematite alteration within the host granodiorite was spatially associated with uranium mineralization and that the mineralized fracture network was developed close to prominent topographic lineaments trending approximately  $55^\circ$ .

The main mineralized zone at the Anomaly No. 7 prospect is approximately 250 m in length and locally attains widths of up to 30 m (Perry, 1979). Early drilling noted that the mineralized fracture system was localized, and that sharp transitions occurred between unaltered and altered rocks, with no significant uranium mineralization occurring within the unaltered, unfractured granodiorite. Further exploration in the region during 1980 identified a second zone of mineralization along the same structural lineament approximately 1.5 km west of Anomaly No. 7; an area referred to as Anomaly No. 7A (Perry, 1979, 1980a; Figure 5). Mineralization within this area was reported to be similar to that of the Anomaly No. 7 prospect; however, no follow-up drilling was ever carried out.

The Anomaly No. 17 prospect was also discovered during initial prospecting in 1978. Alteration and mineralization at the prospect was reported to be similar to the Anomaly No. 7 prospect, with localized uranophane and malachite staining noted along discrete fracture zones, but the alteration was generally less intense (Perry, 1979). Mineralized boulders were subsequently discovered approximately 2 km north-northwest of the Anomaly No. 17 prospect in an area termed the Anomaly No. 17 North prospect (Perry, 1980b); this is the general area of the Near Miss prospect of Silver Spruce Resources (Figure 4; *see* below). The mineralized boulders were eventually traced to their source, which consisted of large outcrops of variably hematized granodiorite containing fracture-hosted uranium mineralization; however, no follow-up work was conducted in the area.

In 2005, the area surrounding the Anomaly No. 7 prospect was staked by Santoy Resources, and limited exploration drilling confirmed previous results, and extended the mineralization down-dip to an approximate vertical depth of 150 m (Willett *et al.*, 2006a). Mineralization was found to have a limited strike extent and a variable dip, ranging from steeply north to steeply south, along the host structure. In 2006, Santoy discovered the Fish Hawk Lake South and Fish Hawk Lake North prospects, approximately 2.5 and 4.0 km northeast of the Anomaly No. 7 prospect, respectively (Figure

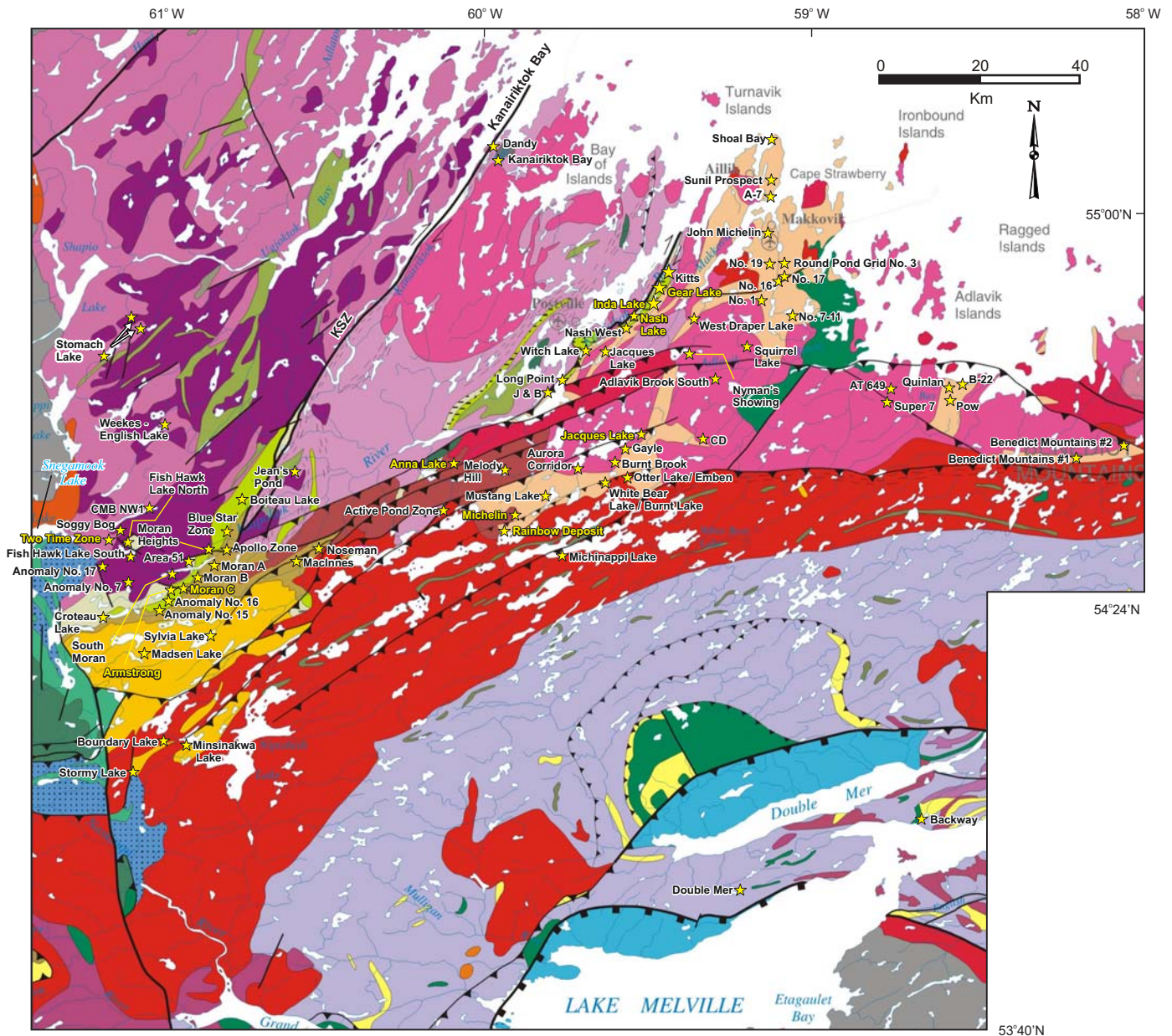


**Figure 3.** Uranium occurrences of the CMB and surrounding region. (Geological base map modified from Wardle *et al.*, 1997.) KSZ – Kanairiktok shear zone. Occurrences highlighted in yellow contain defined NI 43-101 resource estimates.

5). These new zones of mineralization, which are also associated with extensive hematite alteration hosted within granodiorite, were the focus of subsequent trenching and diamond-drilling programs between 2006 and 2008. Surface samples from Fish Hawk Lake North produced assay values up to 0.15%  $U_3O_8$  in outcrop, with angular float in the same area locally assaying up to 5.09%  $U_3O_8$  (Willett *et al.*, 2007b). Grab samples collected along the Fish Hawk Lake South zone locally assayed up to 1.49%  $U_3O_8$ , and channel sampling of trenches produced up to 0.09%  $U_3O_8$  over 6.0 m (Willett *et al.*, 2007b).

Drilling at the Fish Hawk Lake South prospect outlined a region of mineralization extending up to 250 m along strike and to a vertical depth of approximately 120 m. The best intersection from this area included two separate zones of mineralization assaying 0.18%  $U_3O_8$  over 4.50 m and 0.11%  $U_3O_8$  over 9.92 m (drillhole FHLS-07-03; Willett *et al.*, 2008). This drilling demonstrated the steep northerly to subvertical dip of the fracture-hosted uranium mineralization, which pinches out at depth. Additional prospecting conducted by Santoy Resources also identified a number of other smaller radioactive occurrences associated with uraniferous pegmatitic intrusions

## LEGEND

### NEOPROTEROZOIC

 Arkose and conglomerate

### MESOPROTEROZOIC

 Gabbro sills (ca. 1250 to 1224)

 Subaerial basalt flows

 Arkose, grading south into quartzite

 Granite plutons (ca. 1296 Ma)

 Olivine gabbro and metamorphic equivalents

 Granitoid rocks (1500 to 1420 Ma)

 Anorthosite and other, locally layered, mafic rocks

 Quartz diorite

### PALEOPROTEROZOIC

 Rhyolitic to andesitic volcanic rocks including ash-flow tuff and agglomerate (ca. 1650 Ma)

 Volcaniclastic sandstone, arkose and conglomerate

 Granite, quartz monzonite, granodiorite, syenite and minor quartz diorite (ca. 1650)

 Granitoid rocks (1645 to 1626 Ma; including some ca. 1780 to 1720 Ma rocks)

 Anorthosite and other, locally layered, mafic components (1645 to 1625 Ma)

 Mafic intrusive suites (gabbronorite, lesser diorite), some metamorphosed as amphibolite to granulite facies

 Granodioritic orthogneiss (lesser quartz diorite and granitic orthogneiss (s. l.); may include Mesoproterozoic rocks

 Mafic gneiss, probably of supracrustal origin, mainly at granulite facies

 Quartz diorite to granodiorite plutons

 K-feldspar megacrystic granite and other granitoid plutonic rocks

 Pelitic, migmatitic metasedimentary gneiss and minor psammitic gneiss at amphibolite to granulite facies

 High-level, locally flourite-bearing granites (1776 to 1719 Ma)

 Rhyolite, ash-flow tuff, breccia and hypabyssal rhyolite intrusions; volcaniclastic siltstone and sandstone; minor basalt (ca. 1860 to 1807 Ma)

 Granite and granodiorite (1840 to 1795 Ma)

 Tonalite, granodiorite and monzogranite gneiss; minor amphibolite, calc-silicate and felsic (metavolcanic ?) gneiss

 Gabbro and leucogabbro sills (ca. 1884 to 1874 Ma)

 Pillow basalt, basaltic pyroclastic rocks; minor siltstone and greywacke

 Schistose amphibolite derived from mafic volcanic rocks (Moran Lake and Post Hill groups)

 Granite plutons (ca. 2134 Ma, locally 2032 Ma in the Nain Province; 1973 to 1891 Ma in the Makkovik Province)

 Shale and sandstone of shallow- to deep-water origin

 Pelitic schist

### ARCHEAN AND/OR PALEOPROTEROZOIC

 Anorthosite, leucogabbro, leuconorite and derived gneiss

### ARCHEAN

 Tonalitic and other gneisses reworked and retrograded during Makkovikian orogenesis

 Mafic volcanic and volcaniclastic rocks, lesser sedimentary and felsic volcanic rocks, and mafic-ultramafic sills; at greenschist to amphibolite facies

 Granodiorite, tonalite and minor granite (Kanairiktok Intrusive Suite, ca. 2850 to 2830 Ma)

 Tonalitic to granodioritic migmatitic orthogneiss containing abundant mafic to ultramafic inclusions and relict mafic dykes

 Mafic gneisses including rocks of intrusive and extrusive origin

### SYMBOLS

Geological contact.....



Thrust or reverse fault; (major, minor)....



Thrust fault reactivated as normal fault..



Normal fault; (major, minor).....



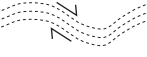
Transcurrent fault; (major, minor).....



Fault; (major, minor).....



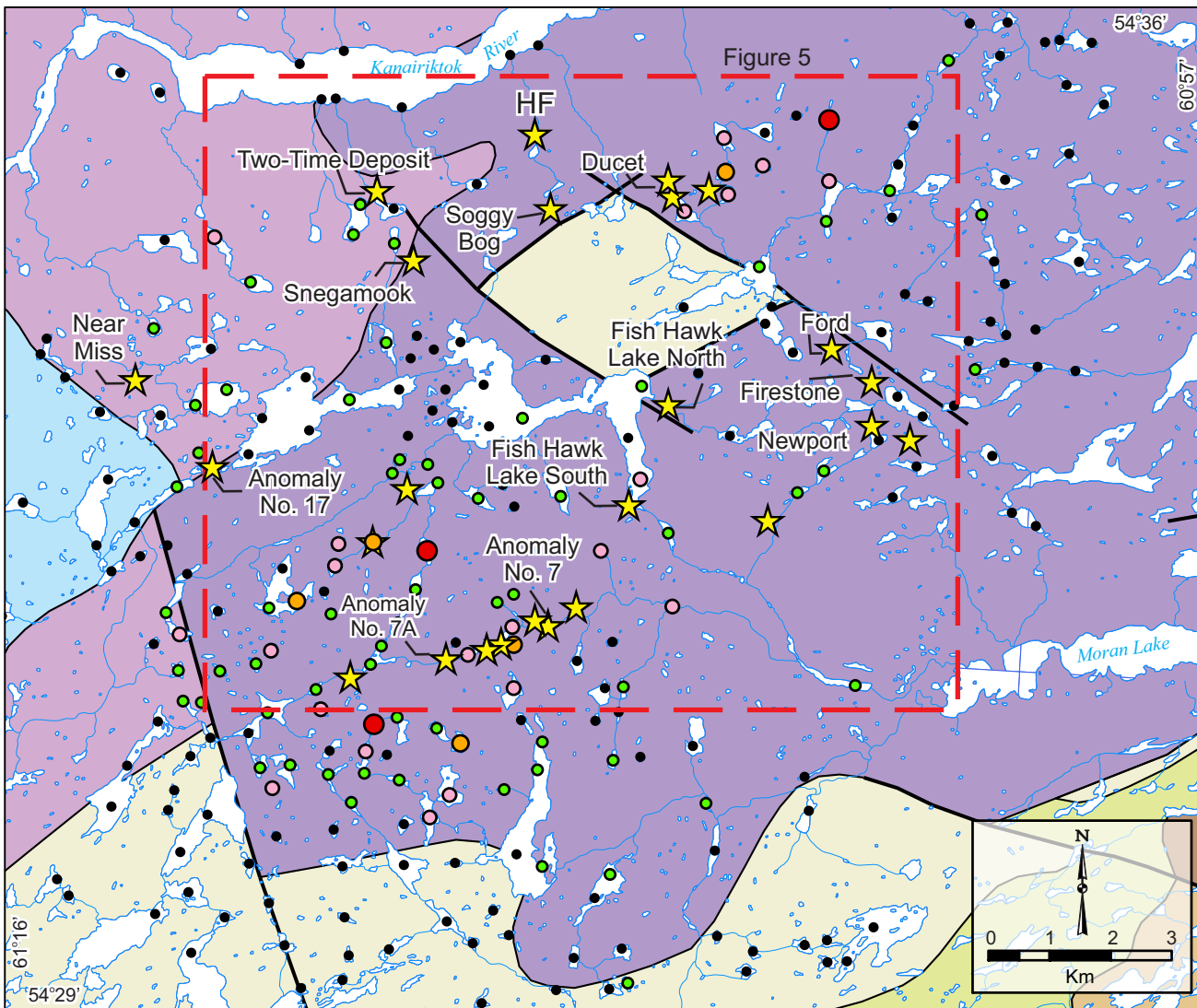
Ductile shear zone.....



Uranium Occurrence.....



Figure 3. Legend for Figure 3 (opposite).



## LEGEND

### Seal Lake Group

Arkose, grading south into quartzite

### Bruce River Group

Brown Lake Formation - Conglomerate and volcaniclastic sandstone

Heggart Lake Formation - Volcaniclastic sandstone, arkose and conglomerate; minor mafic flows and sills

### Moran Lake Group

Pillow basalt, basaltic pyroclastic rocks; minor siltstone and greywacke

Shale and sandstone, shallow- to deep-water origin

### Archean Basement Rocks

Kanairiktok Intrusive Suite - Granodiorite, tonalite and minor granite

Tonalitic to granodioritic migmatitic orthogneiss containing abundant mafic to ultramafic inclusions and relict mafic dykes

## SYMBOLS

Lake sediment values compiled from government and industry data (values in ppm)

0.7 - 20.3



20.4 - 70.0



70.1 - 175.0



175.1 - 275.0



275.1 - 375.0



Fault



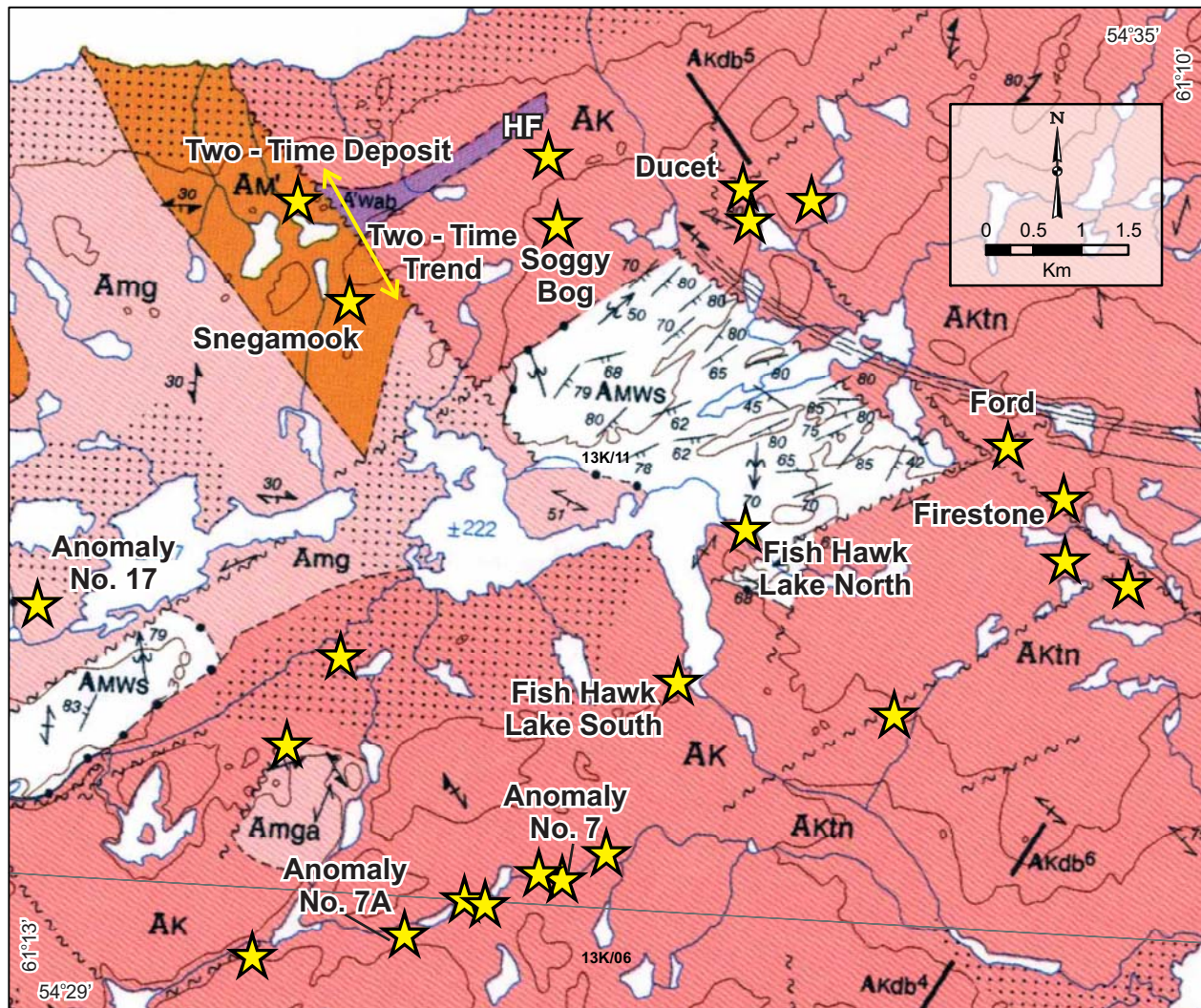
Geological contact



Uranium occurrence



**Figure 4.** Regional map outlining the distribution of historic and recently discovered uranium occurrences within Archean basement rocks in the northwestern CMB. (Map modified from Wardle et al., 1997.) Lake-sediment data compiled from government and industry sources.



### LEGEND

Unconsolidated deposits; gravel, stratified sand and silt; minor clay

#### PALEOPROTEROZOIC

##### Moran Lake Group

AMWs Warren Creek Formation: grey to black mudstone, slate, siltstone, sandstone, minor limestone, dolostone and chert

##### Kikkertavak Diabase

A'wab Kikkertavak diabase: width indicated in superscript

#### LATE ARCHEAN

AMg Migmatite: felsic, gneissic, undivided metapluemonic rocks derived from Middle Archean rocks

AMga Mobilite derived during amphibolite-facies metamorphism of polymetamorphic metapluemonic rocks

#### Kanairiktok Intrusive Suite

AK Tonalitic, granodiorite, and rare granite containing 10-15% biotite or hornblende, or both; medium to coarse grained, foliated to gneissic and locally schlieric

AKtn Tonalitic rocks

#### Middle Archean Modified Gneiss

AM' Tonalitic gneiss: compositionally well preserved Maggo Gneiss, Weeks Amphibolite and transposed Hopedale dykes

#### Weekes Amphibolite

A'wab Amphibolite: commonly associated with ultramafics and rare laminae and layers of ferruginous or aluminous metasediments

#### SYMBOL

Uranium occurrence

**Figure 5.** Map outlining the distribution of the main geological units and locations of uranium occurrences, including the Two-Time deposit and Fish Hawk Lake prospects, as compiled from company websites and press releases. (Map exert from 1:250 000 geological map of Ermanovics, 1992.)

in the immediate area, but these are of limited extent (Willett *et al.*, 2008).

The most significant zone of uranium mineralization within the Archean basement rocks is the Two-Time deposit, discovered in 2006 within the western CMB (Figure 4). Silver Spruce Resources initially identified the potential of the area based on anomalous uranium values in regional lake-sediment samples; the actual deposit was subsequently discovered in 2006 during ground follow-up of an airborne radiometric survey. Since that time, extensive trenching and diamond drilling have been conducted, with up to 40 drillholes completed as of April, 2008 (Ross, 2009). This work has outlined a small, low-grade uranium resource that is hosted within brecciated quartz monzodiorite-tonalite of the KIS. Drilling in the area has returned up to 0.05%  $U_3O_8$  over 107 m, which includes 0.11%  $U_3O_8$  over 30 m, and 0.03%  $U_3O_8$  over 199 m (MacGillivray *et al.*, 2008c). A NI 43-101 compliant resources estimate was completed in 2008 for the Two-Time deposit, which defined an indicated resource of 2.33 million lbs and an inferred resource of 3.73 million lbs with an average grade of 0.06%  $U_3O_8$  (Ross, 2009; Table 1).

The discovery of the Two-Time deposit provided an incentive for further prospecting and mapping of the Archean rocks in the area, which resulted in the discovery of several other uranium occurrences; these include the Near Miss, Snegamook, Firestone and Soggy Bog prospects (Figure 4). The main focus of drilling has been along the structural trend between the Two-Time deposit and the Snegamook prospect, located approximately 1.5 km to the south-southeast (Figure 5). The Snegamook prospect contains a similar style of uranium mineralization to the Two-Time deposit, with low-grade uranium mineralization distributed over wide intervals. Minor exploratory drilling was also completed at the Near Miss and Firestone prospects, but produced only minimal results (*cf.* MacGillivray *et al.*, 2008b; Fox and Wallis, 2012).

## ANOMALY NOS. 7, 7A, 17, FISH HAWK LAKE SOUTH, FISH HAWK LAKE NORTH AND NEAR MISS PROSPECTS

### Local Geology

Uranium mineralization at the Anomaly Nos. 7 and 7A as well as the Fish Hawk Lake South and North prospects is hosted within a variably foliated, locally porphyritic, fine-to medium-grained quartz monzodiorite-tonalite phase of the KIS (Ryan, 1984; Wilton, 1996). This unit is crosscut by variably oriented fine-grained mafic dykes and pegmatitic intrusions. The pegmatite intrusions in the area remain undated, but are potentially coeval with *ca.* 1870 Ma pegmatitic dykes identified farther to the east along the coast (see below), which are also locally associated with the develop-

ment of anomalous uranium mineralization. The quartz monzodiorite-tonalite consists of plagioclase, and lesser interstitial quartz and mafic minerals, which have been replaced by chlorite and minor epidote due to regional metamorphism. The pegmatitic intrusions are generally feldspar-rich, have lesser quartz, and range from several 10s of centimetres to several metres in width. At least two generations of mafic dykes are present within the region, some of which locally contain mm-scale plagioclase phenocrysts. The inferred ‘older’ dykes are amphibolitized and have undergone deformation, whereas the ‘younger’ dykes are characterized by an overall fresh appearance and display well-developed chilled margins. Most of the mafic dykes are observed to postdate both the development of the pegmatite dykes and the uranium mineralization; this is supported by the absence of any significant hematite alteration or uranium mineralization within the mafic dykes observed at surface (Plate 1). However, rare narrow high-grade intersections locally assaying up to 2.57%  $U_3O_8$  have been reported from veins hosted within mafic dykes in drillcore from the area (Willett *et al.*, 2006a); but this may also represent later remobilized uranium mineralization into fractures during subsequent post-mineral deformation.

Evidence for both dextral and sinistral structural offset of mafic and pegmatite dykes are locally observed within outcrop exposures at the Anomaly No. 7 prospect, which is the best exposed prospect. This deformation affects the post-mineralization mafic dykes and therefore must overprint the uranium mineralization. The very sharp transition between altered and unaltered rocks within drillcore from the Fish Hawk Lake South prospect is also indicative of post-mineralization deformation (Plate 2). The local juxtaposition of mineralized and unmineralized quartz monzodiorite-tonalite also occurs along faults that are developed subparallel to the



**Plate 1.** Mafic dyke (outlined by white dashed line) crosscutting hematized uraniferous quartz monzodiorite-tonalite, Anomaly No. 7 prospect. The mafic dyke is interpreted to postdate the uranium mineralization and associated alteration.



**Plate 2.** Centimetre-scale, strongly hematized, shear zone (top center of photograph) separating mineralized quartz monzodiorite-tonalite (left) from unmineralized pegmatite (right); Fish Hawk Lake South prospect; DDH FHLS-07-06, ~90 m depth.

mineralized fractures at the Anomaly No. 7 prospect. This may imply reactivation of earlier mineralized structures during latter post-mineralization deformation, or may just represent the local structural juxtapositioning of mineralized and non-mineralized rocks (Plate 3). Much of the fracturing and faulting within the area is observed to have two predominant orientations, both of which are locally mineralized. One orientation trends between 70 and 80°, whilst the second trends between 125 and 145°, suggesting the presence of a conjugate fault system within the Archean basement rocks. The same structural trends are also visible as topographic lineaments on a regional scale, many of which host minor uranium occurrences.

At the Anomaly No. 17 and Near Miss prospects, uranium mineralization is hosted within a fine- to medium-grained quartz monzodiorite-tonalite, similar to that seen elsewhere within the region. At these prospects, localized zones of uranium mineralization are again linked with the de-



**Plate 3.** A similar style contact to that shown in Plate 2 exposed at surface, whereby a fault trending approximately 80° separates hematized quartz monzodiorite-tonalite (right) from relatively unaltered and barren equivalent rocks (left); Anomaly No. 7 prospect.

velopment of hematized faults; however, at these localities the mineralized structures have no obvious preferred orientation.

### Mineralization and Associated Alteration

The uranium mineralization occurring within this area is structurally controlled and is developed close to topographic lineaments. Along these lineaments the granitoid rocks are locally affected by fracturing and/or brecciation and associated hematite alteration (Perry, 1979, 1980a, b). The host quartz monzodiorite-tonalite contains background (<5 ppm) uranium values outside of areas affected by this brittle deformation. Hematite alteration is generally restricted to narrow zones, except in regions of intense fracturing and/or brecciation, where pervasive hematite alteration of the host rock is present (Figure 6). Within mineralized zones, high-grade uranium mineralization is locally developed, with the best intersection returning 4.36%  $U_3O_8$  over 0.15 m (Anomaly No. 7; drillhole #51557; Perry, 1980a). A summary of the various alteration stages developed within these prospects as determined from field and petrographic observations is outlined in Table 2.

**Table 2.** Summary of the various stages of alteration and the associated mineralogy in the Anomaly No. 7–Fish Hawk Lake area; based on field mapping and petrography

Associated Alteration Minerals	
Stage 1	Chlorite ± epidote
Stage 2	Hematite ± carbonate
Stage 3	Hematite ± Fe–Ti oxides ± uranium mineralization ± chalcopyrite ± carbonate
Stage 4	Chlorite ± pyrite ± chalcopyrite
Stage 5	Carbonate

At the Fish Hawk Lake South prospect the host quartz monzodiorite-tonalite is more pervasively chloritized when compared to the host rock at the Anomaly No. 7 prospect (Figure 7). The chlorite alteration (Stage 1) is variably developed and is interpreted to be related to regional metamorphism, as it is widely developed throughout the area. This alteration is inferred to predate the development of the uranium mineralization and restricts the development of the brittle fracture network within the quartz monzodiorite-tonalite. In areas where the quartz monzodiorite-tonalite contains extensive chlorite alteration, the brittle fracturing is better developed within the less altered pegmatite dykes; however, this may also be the result of grain-size competency contrasts between the quartz monzodiorite-tonalite and the pegmatite dykes. In general, uranium mineralization in the pegmatite dykes is most prevalent where chloritic alteration is extensively developed within the host quartz monzodiorite-tonalite. Thus, the degree of chlorite alteration is inferred to

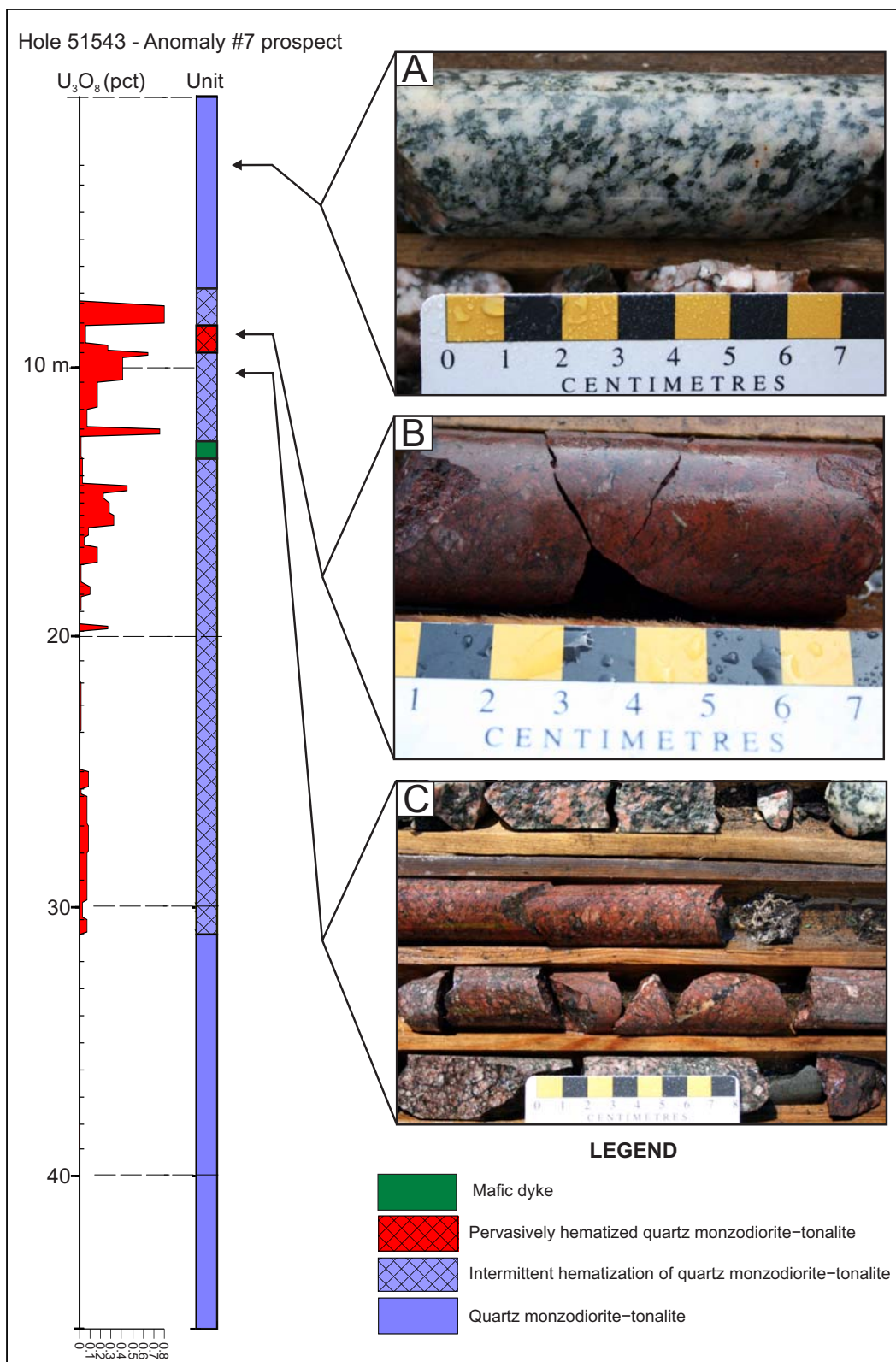


**Figure 6.** Drill log of hole 51543 from the Anomaly No. 7 prospect, outlining the distribution of fracturing and accompanying hematite alteration in association with uranium mineralization; uranium values are listed in % U<sub>3</sub>O<sub>8</sub> (data from Perry, 1979). Note the local development of high-grade mineralization immediately adjacent to the intrusion of the mafic dyke, A. Relatively fresh, unaltered quartz monzodiorite-tonalite, B. Strongly hematized quartz monzodiorite-tonalite; minimal uranium enrichment, C. Hematized and fractured host rock and associated uranium mineralization.

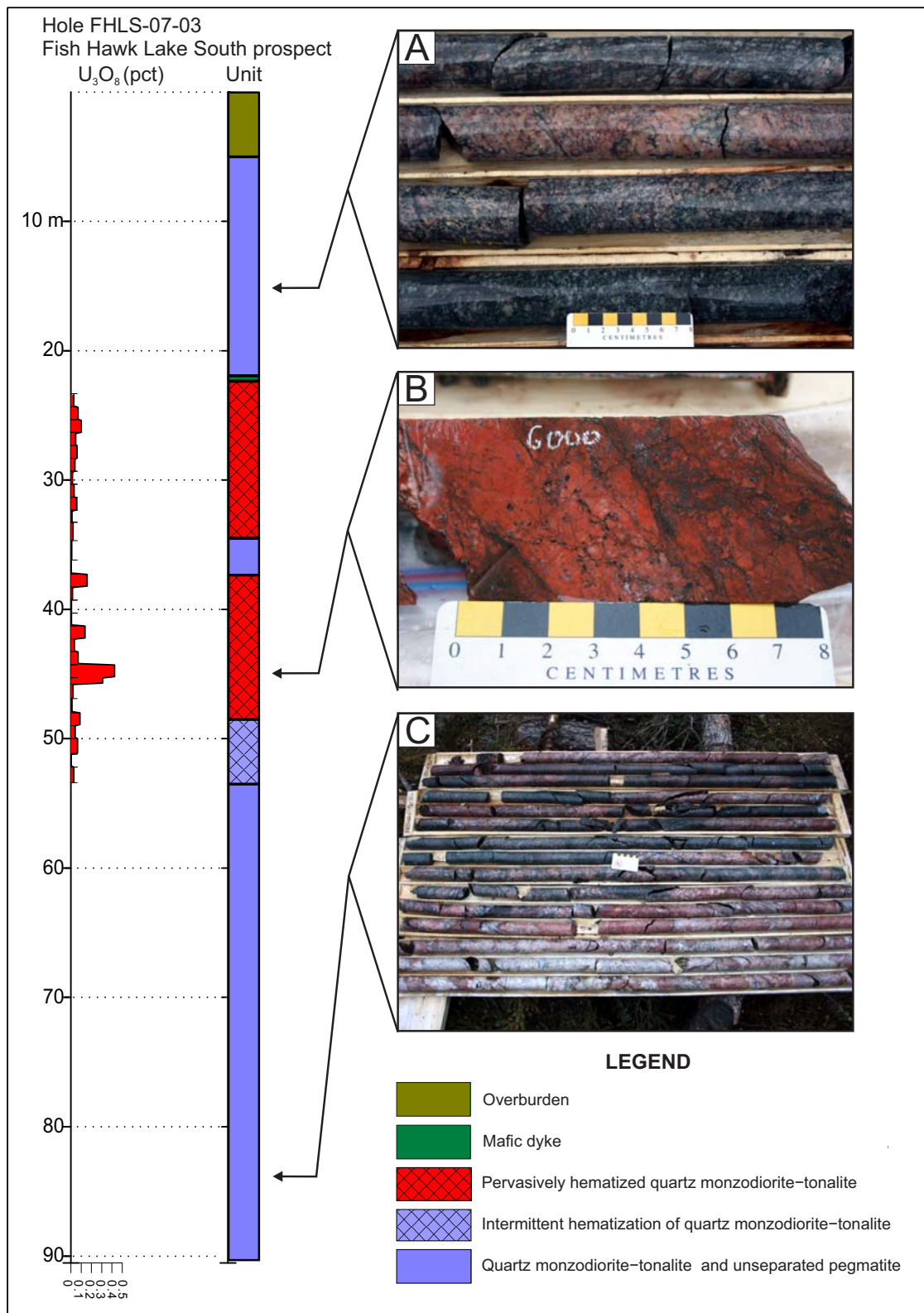


**Figure 7.** Drill log of hole FHLS-07-03 from the Fish Hawk Lake South prospect, outlining the distribution of fracturing and accompanying hematite alteration in association with uranium mineralization; uranium values are listed in % U<sub>3</sub>O<sub>8</sub> (data from Willett et al., 2008). A. Variably chlorite altered quartz monzodiorite-tonalite, B. Strongly hematized quartz monzodiorite-tonalite and associated uranium enrichment, C. Unseparated quartz monzodiorite-tonalite and pegmatitic intrusions.

affect the ability of the quartz monzodiorite–tonalite to host the brittle fracture networks, which is a prerequisite for the subsequent development of uranium mineralization.

The mineralized fracture network developed at the Fish Hawk Lake South prospect generally consists of millimetre- to centimetre-scale brittle fractures that locally coalesce to form intense zones of brecciation and hematization (Plate 4). Alteration surrounding the mineralized fractures is very limited, but can be recognized by the reddening of the plagioclase feldspar within several metres of the hematized fractures; a small-scale example of this is visible in Plate 5. This hematite alteration overprints a regionally extensive, variably developed, chlorite–epidote (Stage 1) assemblage within the groundmass of the host quartz monzodiorite–tonalite. However, not all hematized rocks are mineralized and at least two stages of hematite alteration can be recognized. The initial hematization (Stage 2) is generally barren,

and locally intensifies to give the quartz monzodiorite–tonalite a distinctive brick-red colouration. This initial hematite alteration is overprinted by dark-purple hematite-rich fractures, containing variable amounts of specularite and uranium mineralization (Stage 3; Plates 6 and 7). From the accompanying autoradiographs in Plates 6 and 7, the fracture-hosted nature of the uranium mineralization is clearly shown. The hematite alteration and associated mineralization are subsequently overprinted by a second stage of chloritic alteration (Stage 4), which is, in turn, locally overprinted by carbonate-filled fractures (Stage 5; Plate 8). The development of the carbonate veining displays a close spatial association with the mineralized fractures and presumably exploits the same permeable zones as the mineralizing fluids.

Pegmatitic dykes display variably developed fracture-hosted mineralization throughout the region, which locally results in a ‘shattered’ appearance. These dykes initially develop a brick-red hematite alteration (Stage 2) of the feldspar followed by dark-purple specularite-bearing fractures and accompanying uranium mineralization (Stage 3; Plate 9). Both the quartz monzodiorite–tonalite and the pegmatitic dykes are crosscut by mafic dykes that postdate mineralization and hematite alteration. However, the presence of rare uranium-bearing mafic dykes hosting veins of specularite–calcite–chalcopyrite is locally noted (*cf.* Willett *et al.*, 2006a). These dykes either represent older, pre-mineralization intrusions, or alternatively, the mineralized veins represent remobilization of the primary uranium mineralization during the emplacement of the dykes or during subsequent deformation, which postdates the dyke emplacement.

Uranium is the predominant economic mineral associated with the mineralizing system in the area, but anomalous



**Plate 4.** Variable degrees of hematite alteration developed within the host quartz monzodiorite–tonalite. Initial chlorite alteration (1) is progressively replaced by hematite (2) until all primary textural features are obscured in regions of intense hematite alteration (3); Fish Hawk Lake South prospect.



**Plate 5.** Initial hematization of feldspars within the host quartz monzodiorite–tonalite proximal to a mineralized fracture zone; Anomaly No. 7 prospect.

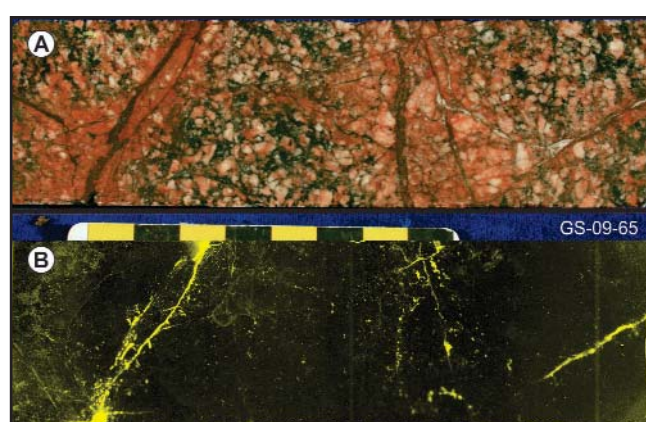


**Plate 6.** *A.* Sample displaying regional chlorite alteration overprinted by mineralized, hematite-bearing fractures. *B.* Accompanying autoradiograph showing the preferential concentration of the radioactivity (yellow, minus the outline of the sample) in association with the distribution of the fracturing shown in (A); Fish Hawk North prospect.

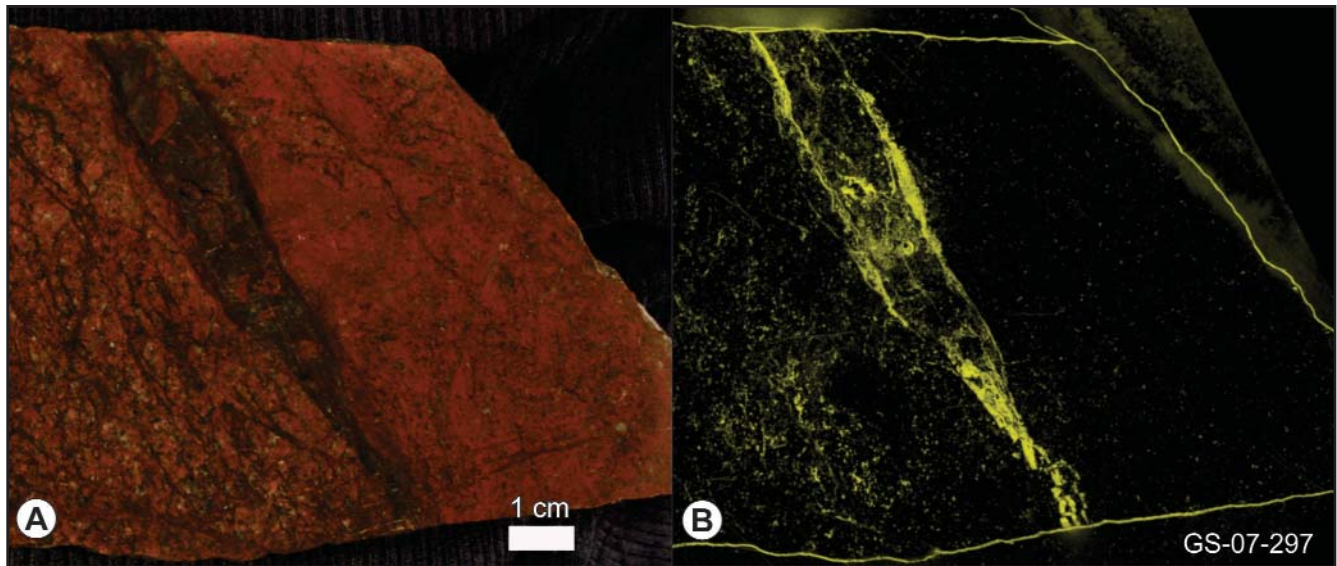


**Plate 7.** *A. Sample displaying intense brick-red hematite alteration developed within fine-grained quartz monzodiorite–tonalite, crosscut by a later dark-purple specularite-rich vein. B. Accompanying autoradiograph showing the distribution of the radioactivity (yellow, minus the outline of the sample) within the sample; Near Miss prospect.*



**Plate 8.** *Cataclasite hosting uranium-bearing hematized quartz monzodiorite–tonalite fragments within a chlorite-rich breccia matrix; note that the breccia is crosscut by later carbonate veins (Anomaly No. 7 prospect; DDH 51544, ~45 m depth).*

copper concentrations are also locally reported. Chalcopyrite was noted close to the Anomaly No. 7 prospect, and at both the Fish Hawk Lake prospects (Perry, 1980a; Willett *et al.*, 2008). The chalcopyrite generally postdates the uranium mineralization and related alteration, locally occurring as coarse ‘clots’ enveloping altered fragments of the quartz monzodiorite–tonalite unit (Plate 10). The development of copper mineralization appears to be spatially associated with the presence of the overlying Moran Lake Group, with the highest copper values recorded within the basal sedimentary rocks of that group where it occurs immediately adjacent to the quartz monzodiorite–tonalite at the Fish Hawk Lake North prospect. Here local assays of up to 0.06%  $U_3O_8$  and 1% Cu over 3 m have been reported (Willett *et al.*, 2008).

Visible-infrared reflectance spectroscopy (VIRS) was used to investigate the hematite alteration developed within the quartz monzodiorite–tonalite. Spectral analyses of both barren and mineralized hematite-bearing fractures as well as the brick-red and dark-purple forms of hematite alteration display similar spectra. Both are dominated by hematite, and some contain late carbonate minerals.

### Petrography

All of the prospects described within this section display similar petrographic features and characteristics. The host quartz monzodiorite–tonalite unit contains variable amounts of feldspar, mainly plagioclase, and lesser finer grained interstitial quartz distributed throughout the groundmass. The groundmass contains variable chlorite alteration that propagates along grain boundaries, and is locally associated with minor epidote. This chlorite alteration is subsequently overprinted, in mineralized fracture zones, by the introduction of hematite and abundant Fe–Ti-oxide minerals in the form of mm-scale fracture-filling material and fine-grained disseminations developed throughout the groundmass (Plate 11A).

As shown by the autoradiograph in Plate 11B, the radioactivity is associated with the fine-grained Fe–Ti-oxide minerals. These patchy zones of radioactivity consist of a complex intergrowth of hematite and bladed specularite along with apatite, rutile, titanite and trace amounts of pyrite and rare chalcopyrite; uranium-bearing phases are commonly too finely disseminated to be visible, but rare coarser grained material, believed to be uraninite, are locally observed along the

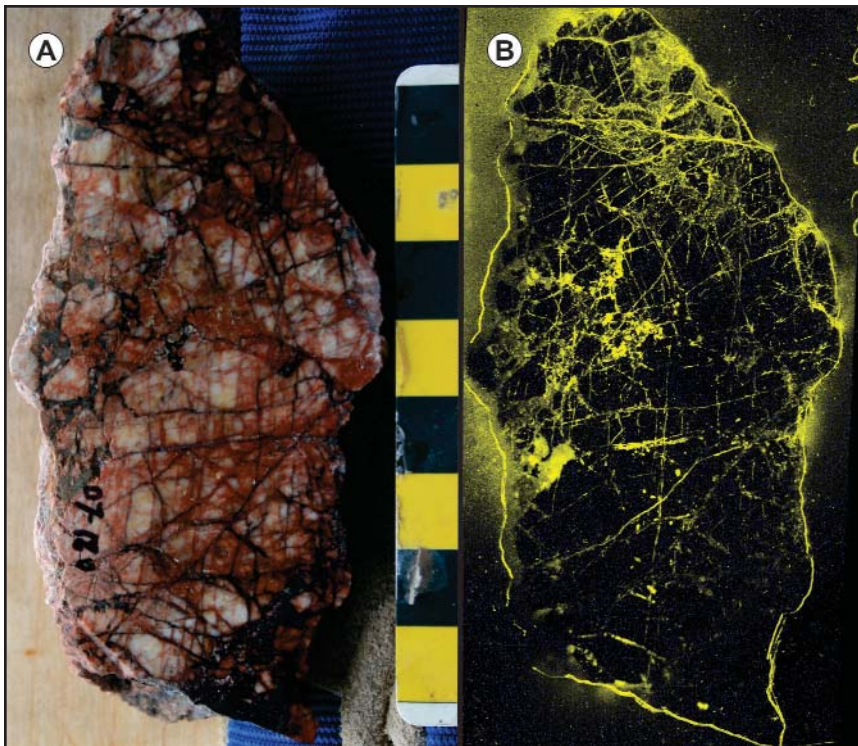


**Plate 9.** *A. Sample displaying brittle fracturing within mineralized pegmatite; note the initial brick-red hematite alteration is relatively unmineralized, and is subsequently overprinted by a second stage of dark-purple specularite, associated with the majority of radioactivity within the sample. B. Accompanying autoradiograph of the sample showing the distribution of radioactivity (yellow, minus the outline of the sample); Fish Hawk Lake South prospect.*



**Plate 10.** *Rare, late-stage chalcopyrite (green arrow) infilling fractures crosscutting hematized quartz monzodiorite-tonalite; Fish Hawk Lake South prospect.*

margins of the oxide minerals (Plate 11C, D). In areas surrounding the mineralization, the quartz monzodiorite-tonalite displays evidence of brittle deformation in the form of microscopic brittle fracturing and associated cataclasis (Plate 11E, F). These zones of increased permeability are exploited by the mineralizing fluids, but not all zones of brecciation and

hematite alteration carry uranium mineralization. Locally, fractures filled with chlorite and minor pyrite crosscut the mineralized hematite-filled fractures and associated brecciation, demonstrating the presence of a second stage of chlorite alteration within the region (Plate 12A, B).

## TWO-TIME DEPOSIT AND THE SNEGAMOOK PROSPECT

### Local Geology

The Two-Time deposit is located approximately 6.5 km east of Snegamook Lake and 7 km northwest of the Fish Hawk Lake-Anomaly No. 7 area (Figure 3). Within this area, uranium mineralization is primarily hosted within brecciated quartz monzodiorite-tonalite assigned to the *ca.* 3000 Ma KIS. The linear belt between the Two-Time deposit and the Snegamook prospect, which is located approximately 1.3 km along strike to the southeast of Two-Time, is referred to as the Two-Time Trend (Figure 5). In contrast to the Fish Hawk Lake-Anomaly No. 7 area, uranium mineralization along the Two-Time Trend is associated with intense brecciation within a more leucocratic host rock. This trend is roughly parallel to a northwest-southeast-trending fault separating Maggo Gneiss to the west from the KIS to the east (Figure 5). However, the faulted contact is assumed to be developed close to an original intrusive contact, as intrusive relationships between the KIS and the Maggo Gneiss are locally preserved.

The Maggo Gneiss has well-developed centimetre- to decimetre-scale banding, and is typically a pale grey-green to pink, tonalite to quartz diorite gneiss (Plate 13). The melanocratic bands are dominated by dark-green chlorite and minor epidote, and the more leucocratic bands by pale-pink plagioclase feldspar and quartz. Local migmatization is developed close to contacts with the KIS (Ryan, 1984), and the gneiss is commonly crosscut by numerous undeformed, centimetre- to metre-scale pegmatite dykes. Metre-scale folding of the gneissic banding observed in drillcore is interpreted to predate the intrusion of the KIS due to the lack of any significant penetrative fabric within the KIS in the immediate area. The Maggo Gneiss and adjacent quartz monzodiorite-tonalite of the KIS are compositionally similar, and they can be difficult to separate when overprinted by intense fracturing and brecciation in areas of brittle deformation. The presence of banding and foliation is the main criterion for separating the

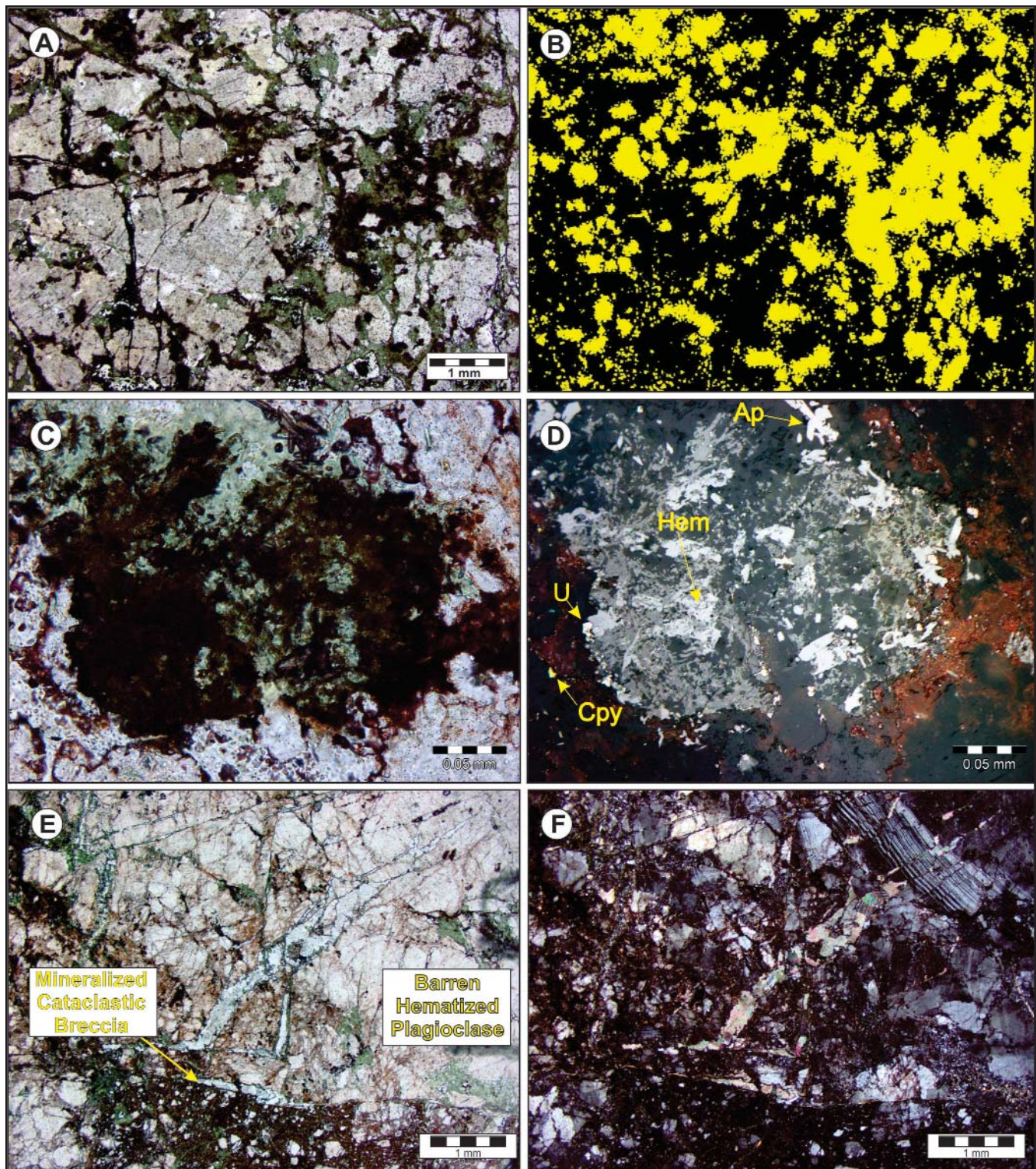


**Plate 11.** Photomicrographs of mineralized samples showing the distribution of radioactivity in relation to the Fe-Ti-oxides in thin section. A. Initial chlorite alteration overprinted by later uranium-bearing Fe-Ti-oxides within tectonically brecciated quartz monzodiorite-tonalite, PPL. B. Autoradiograph outlining the distribution of radioactivity (yellow) in the field shown in (A). C. Mineralized, finely disseminated Fe-Ti-oxides, PPL. D. Reflected light image of (C) showing the distribution of apatite (Ap), chalcopyrite (Cpy), hematite (Hem) and possible uraninite (U). E. Highly fractured host rock showing local development of cataclastic brecciation accompanied by hematite alteration and uranium mineralization, PPL. F. Cross-polarized view of (E).

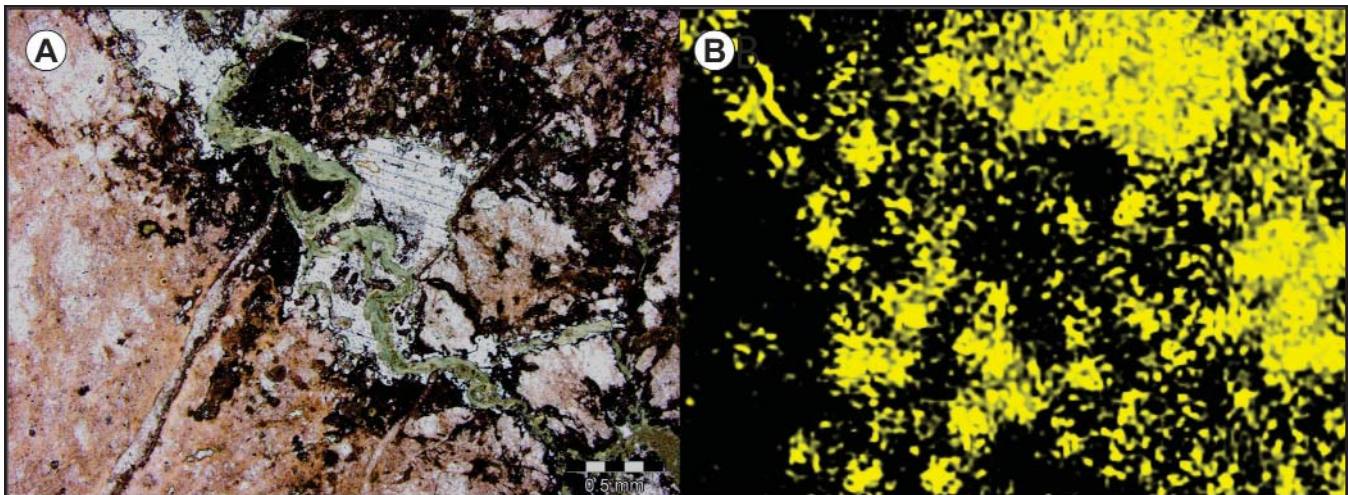


**Plate 12.** *A. Second-stage chlorite alteration overprinting the development of mineralized Fe–Ti-oxide minerals and associated carbonate alteration, PPL. B. Autoradiograph outlining areas of high radioactivity (yellow) in (A).*



**Plate 13.** *Well-developed banding in the Maggo Gneiss displaying local folding of the gneissic banding, crosscut by a late pegmatite dyke; Two-Time deposit, DDH CMB-07-21, ~440 m depth.*

Mago Gneiss from rocks of the KIS in the area of the Two-Time Trend. In rare instances, original intrusive contacts between the Maggo Gneiss and the KIS are preserved (Plate 14). Marginal to the main intrusion of the KIS, rare metre-scale dykes consisting of fine-grained equivalent rocks are also observed to crosscut the Maggo Gneiss.

The quartz monzodiorite–tonalite phase of the KIS is predominantly medium to coarse grained, green-grey to pale-pink, and contains moderate to strong chlorite alteration. Fine-grained rocks of similar composition occur locally, along with lesser amounts of pink granite. The quartz monzodiorite–tonalite is locally weakly foliated, but this early fabric is overprinted by brittle, millimetre- to centimetre-scale fracturing with associated cataclasite. Brittle deformation, cataclasis and uranium mineralization are best developed in



**Plate 14.** *Fine-grained tonalite intruding weakly banded, chlorite-rich, gneiss. Note the well-developed fracturing and associated brecciation within the tonalite unit; Two-Time deposit, DDH CMB-07-14, ~160 m depth.*

the quartz monzodiorite–tonalite suggesting that competency contrasts between it and the Maggo Gneiss played a fundamental role in the development of the brittle deformation, as noted in the Fish Hawk Lake area. Away from mineralized zones, the quartz monzodiorite–tonalite is generally massive and relatively undeformed.

The Maggo Gneiss and the KIS are both crosscut by feldspar-rich pegmatite dykes of varying widths. These dykes are similar to those seen farther south in the area of Fish Hawk Lake, but are much less abundant; no contact relationships between the uranium mineralization and the pegmatite dykes were observed. Pegmatites within the quartz monzodiorite–tonalite are barren with respect to uranium, although pegmatite hosted within the adjacent Maggo Gneiss is locally overprinted by chlorite-rich brecciation that may be a precursor to the main mineralizing event (see below; Plate 15). Uraniferous pegmatite dykes have been reported outside of



**Plate 15.** Feldspar-rich pegmatite overprinted by chlorite-rich brecciation; Two-Time deposit, DDH CMB-07-21, ~380 m depth.

the main Two-Time Trend, but these dykes appear undeformed and have a random distribution (Ross, 2008). These mineralized dykes are interpreted to represent a less significant, syn-magmatic style of mineralization that is locally noted elsewhere within the Archean basement rocks farther to the east (*cf.* Sparkes and Kerr, 2008).

At least two generations of mafic dykes are present along the Two-Time Trend. Those inferred to be oldest are amphibolitized and are crosscut by mm-scale veins of light-green epidote and minor carbonate, are variably foliated, and their contacts with adjacent rocks are sheared. These dykes are inferred to predate uranium mineralization (Ross, 2008); however, no clear evidence of mineralization hosted within mafic dykes was observed by the author. To the contrary, weakly foliated versions of the mafic dykes locally host enclaves of hematite–carbonate-altered material, suggesting that the dykes may, in fact, postdate the uranium mineralization (Plate 16). Local enrichment of uranium mineralization near the contacts of mafic dykes was locally observed, and is interpreted to represent remobilization of pre-existing mineraliza-



**Plate 16.** Moderately foliated, carbonate-altered, fine-grained mafic dyke hosting enclaves of hematite–carbonate-altered tonalite; Two-Time deposit, DDH CMB-07-11, ~280 m depth.

tion in response to the emplacement of mafic dykes. Similar features were noted in the Fish Hawk Lake area. This is further supported by elevated uranium values within dykes that crosscut uranium mineralization.

A second generation of mafic dykes has a very fresh appearance and display well-developed chilled margins (Plate 17). The mafic dykes vary in width from several decimetres to in excess of twenty metres (Ross, 2008), and are more abundant within the main zones of brecciation and the adjacent footwall region. As with the Fish Hawk Lake area, these mafic intrusions are inferred to represent the youngest intrusive rocks within the region. The dykes are locally carbonate-rich, containing disseminated carbonate throughout the groundmass, and are also crosscut by network-style white carbonate veinlets, suggesting that carbonate alteration was most likely synchronous with their emplacement.

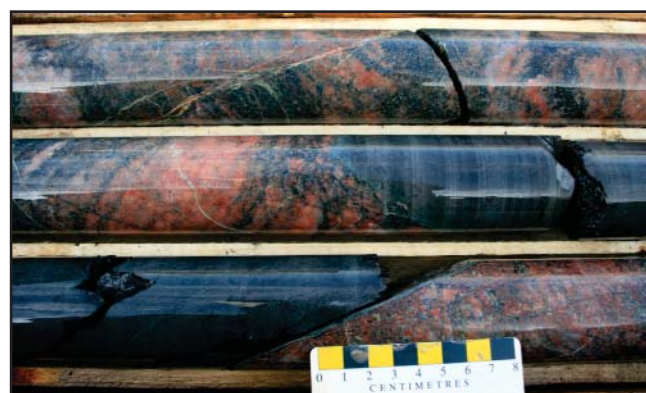


**Plate 17.** Fresh, fine-grained mafic dyke displaying a well-developed chilled contact with the adjacent gneissic host rock; Two-Time deposit, DDH CMB-07-21, ~475 m depth.

### Mineralization and Associated Alteration

Uranium mineralization along the Two-Time Trend is generally associated with brittle deformation in the form of highly variable centimetre- to metre-scale, network-style fracturing and cataclasis. This brittle deformation appears to be preferentially developed along the contact margin between the Maggo Gneiss and the quartz monzodiorite–tonalite of the KIS (Figure 5). The breccias have many similarities to ‘tuffisite’ brecciation associated with high-level intrusions, and they were originally thought to be of hydrothermal origin (Sparkes and Kerr, 2008). However, further petrographic examination of the mineralization (*see* below), coupled with the linear trend of the breccia development and its close spatial association with a major regional fault (Figure 5) suggests that the breccia is actually structural and represents an *in situ* fault breccia. The degree of brecciation within the structural corridor is highly variable and ranges from crush breccia (Plate 18) to well-developed cataclasite (Plate 19) as outlined by Sibson (1977).

Mineralization at the Two-Time deposit has been traced intermittently along strike for up to 500 m and has been intersected down-dip at up to 500 m depth; this zone remains open at depth and along strike to the south. Within this zone, several mineralized lenses have been defined, varying in thickness from 4 to 30 m, with the main ore zone having a predominant strike of 345° and a plunge between 30 and 40° to the south (Ross, 2008). Most of the uranium mineralization occurs at the hanging-wall and footwall contacts of a well-defined, steep southwesterly dipping, structural zone that measures approximately 60–75 m in width (Ross, 2008). The concentration of uranium mineralization along the upper and lower contacts of this zone may reflect regions of higher permeability within the overall structural corridor or some sort of mineralogical contrast highlighted by the preferential precipitation of the uranium mineralization (Figure 8). Similar styles of brecciation and intermittent mineralization have been intersected along the length of the Two-Time Trend, which has an approximate strike length of 1.3 km.



**Plate 18.** Relatively barren protocataclasite developed within hematite–carbonate-altered quartz monzodiorite–tonalite; Two-Time deposit, DDH CMB-07-11, ~250 m depth.



**Plate 19.** Mineralized cataclastic breccia; note highest concentrations of radioactivity (labelled in counts per second) are associated with the development of intense hematite alteration of the breccia; Two-Time deposit, DDH CMB-07-14, ~280 m depth.

The main zone of mineralization is surrounded by a much more aerilly extensive halo of mm-scale, network-style fracturing termed the ‘mega breccia’ (Ross, 2008). This zone contains fractures infilled with dark-green chlorite, possibly representing a crush protobreccia or crush breccia developed marginal to the main structural zone (Plate 20). This style of brecciation is locally observed up to 70 m from the mineralized zone and is generally barren with respect to uranium mineralization. A small-scale example of the overall larger scale process within the structural corridor is shown in Plate 21, which illustrates the overall progression from crush protobreccia to well-developed cataclasite over several metres. The initial development of this cataclasite predates the introduction of uranium, as much of the mineralization is associated with intense hematite alteration that overprints the cataclasite. As noted above, the host rocks within the region are affected by a regional chlorite–epidote metamorphic assemblage; the marginal crush protobreccia and early cataclasite zones are also dominated by chlorite alteration.

A summary of the various alteration stages is presented in Table 3; these alteration stages display many similarities



**Plate 20.** Development of the chlorite-rich ‘mega breccia’ within Maggo Gneiss marginal to the main mineralized zone; Two-Time deposit, DDH CMB-07-14, ~205 m depth.



**Plate 21.** Small-scale example of the crush protobreccia developed marginal to unmineralized cataclasite; Two-Time deposit, DDH CMB-07-14, ~220 m depth.

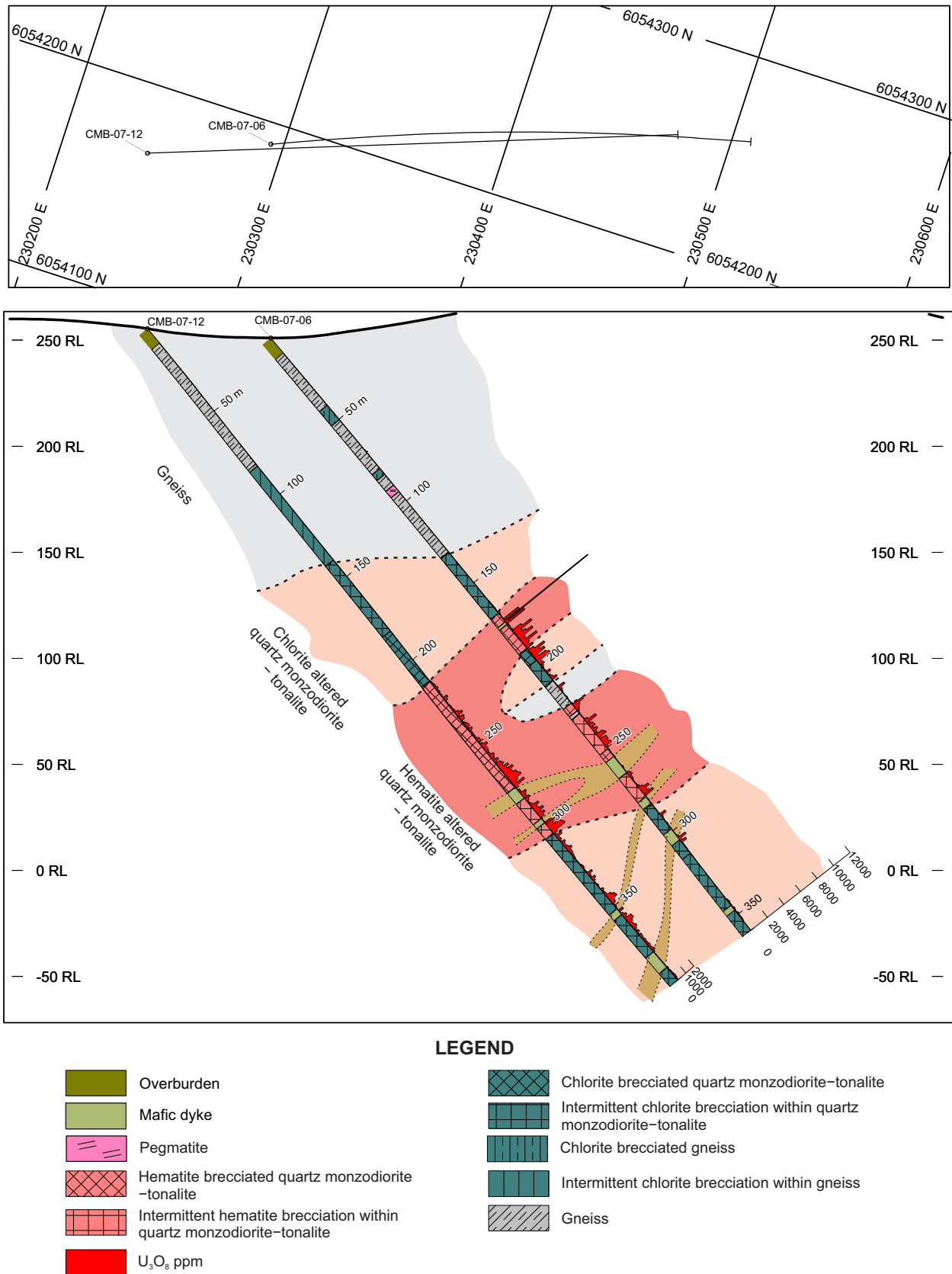


**Figure 8.** Schematic east-northeast–west-southwest section outlining the distribution of rock units, alteration and uranium mineralization within the Two-Time deposit; uranium values are listed in % U<sub>3</sub>O<sub>8</sub> (data from MacGillivray et al., 2008c).

**Table 3.** Summary of the various stages of alteration and the associated mineralogy in the Two-Time–Snegamook area; based on field mapping and petrography

Associated Alteration Minerals	
Stage 1	Chlorite ± epidote
Stage 2	Hematite ± carbonate
Stage 3	Chlorite
Stage 4	Hematite ± Fe–Ti oxides ± uranium mineralization ± carbonate
Stage 5	Chlorite
Stage 6	Carbonate

to those identified within the area of Fish Hawk Lake. Two distinct phases of hematite alteration are discerned within mineralized samples. The first phase of hematite alteration is generally more pervasive and results in a pale-pink to light-red colouration of the host rock, or as a brick-red fracture-filling material, and is locally associated with carbonate alteration (Plate 22). This phase of the hematite alteration predates the development of the chlorite-rich brecciation as hematized fragments are locally hosted within chlorite-rich breccia. The second phase of hematite alteration is dark-purple, specularite-rich, and is locally accompanied by uranium mineralization. This phase overprints the initial chlorite-rich brecciation, however it must be noted that it is not everywhere mineralized (Plate 23). As seen in the Fish Hawk Lake area, there is local evidence for a second stage of chlorite alteration within the hematized zones, which overprints the dark-purple specularite-bearing alteration. In rare instances metre-scale, pale-grey to white, vuggy textured zones are developed within the breccia. Such features appear to be late stage and are locally infilled with a white to pale-yellow clay mineral, which has been identified as phengitic illite on the basis of VIRS analysis (Plate 24).



**Plate 22.** Early pinkish-red hematite (Early Hem) alteration crosscut by chlorite (Chl. Rich Bx)-rich brecciation overprinted by later hematite alteration (Late Hem); all phases are barren with respect to uranium mineralization; Two-Time deposit, DDH CMB-07-07, ~200 m depth.

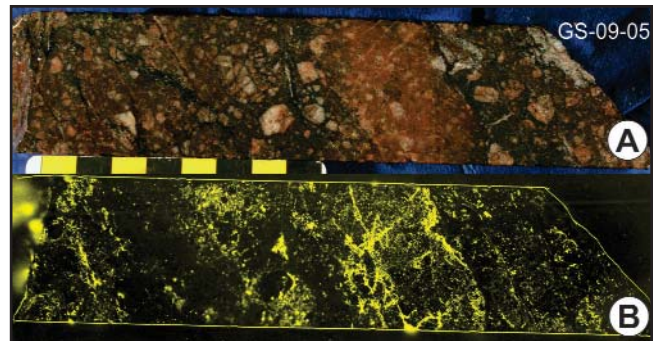


**Plate 23.** Mineralized cataclastic breccia (A), and an accompanying autoradiograph outlining the distribution of radioactivity (yellow, minus the outline of the sample) within the sample (B). Note the initial pale-pink hematitic alteration occurring as fragments is overprinted by later, uranium-bearing, dark-purple, specularite-rich alteration.



**Plate 24.** Hand sample displaying 'vuggy' textured zone, infilled with a pale-cream clay mineral (yellow circle) identified as phengitic illite on the basis of VIRS analysis.

The highest grade mineralization is developed within the breccia zones, notably in association with post-mineralization mafic dykes that appear to have remobilized earlier uranium mineralization. An example of such includes assay values of up to 1.01%  $U_3O_8$  over 0.40 m, which has been reported marginal to the intrusion of a mafic dyke (MacGillivray *et al.*, 2008c).

### Petrography

The quartz monzodiorite–tonalite is dominated by variably sericitized plagioclase and minor quartz. Unmineralized and relatively unaltered samples display a well-developed hypidiomorphic-granular texture with interlocking plagioclase and quartz crystals. Early chlorite–epidote alteration occurs along grain boundaries and is associated with minor carbonate alteration and the dissemination of Fe–Ti-oxide minerals (Plate 25A, B). The development of the cataclastic breccia is associated with a chlorite-rich matrix, as shown in Plate

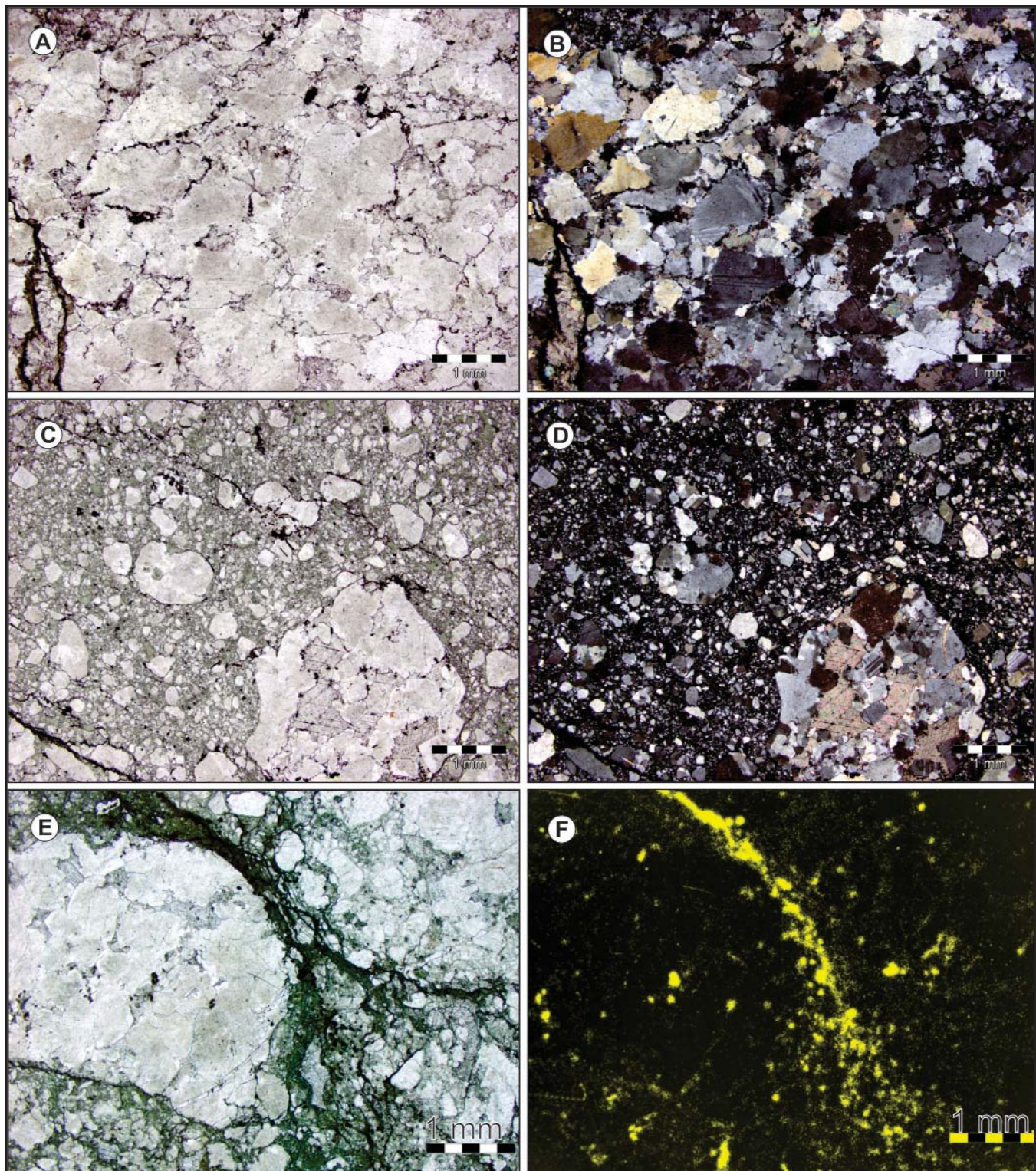


**Plate 25.** A. PPL image of relatively unaltered quartz monzonodiorite-tonalite displaying early chlorite alteration along grain boundaries in association with minor Fe-Ti-oxide minerals, B. XPL image of (A), C. Early, barren, chlorite-rich cataclasite, D. XPL image of (C), E. PPL image of early chlorite-rich breccia crosscut by mineralized fracture hosting Fe-Ti-oxide minerals, F. Autoradiograph outlining regions of radioactivity (yellow) in the field shown in (E).

25C, D. These breccias are monolithic, poorly sorted, and contain rounded to subangular fragments of feldspar and lesser quartz. Within the mineralized breccias, the chlorite-rich matrix is subsequently overprinted by hematite alteration, accompanied by very finely disseminated Fe–Ti-oxide minerals. Plate 25E displays early chlorite-rich brecciation overprinted by hairline fractures hosting Fe–Ti-oxide minerals; the accompanying autoradiograph shows that the latter is host to most of the radioactivity within the sample (Plate 25F). This relationship is common throughout the deposit and most uranium mineralization occurs as very fine-grained disseminations associated with finely bladed specularite and Fe–Ti-oxide minerals. The mineral associations within mineralized samples have been confirmed through SEM imagining, but these mineral intergrowths are relatively obscure even at high magnifications.

## OTHER MINOR URANIUM OCCURRENCES

Several other examples of structurally controlled mineralization have been identified along lineaments to the east of Fish Hawk Lake, including the Firestone and Ford prospects (Figure 4). Here, similar styles of hematite alteration, in association with brittle deformation and uranium mineralization, are hosted within quartz monzodiorite–tonalite. These prospects are associated with pronounced topographic lineaments, which are coincident with anomalous lake-sediment values, suggesting that there is potential for the discovery of additional structurally controlled uranium mineralization within the area. One distinguishing characteristic of the Firestone prospect, which separates it from others in the region, is the elevated thorium that accompanies uranium mineralization suggesting it may be related to a different mineralization event. Boulders representing similar styles of mineralization to the Two-Time Trend have been observed as far east as the region of Boiteau Lake (Figure 3), suggesting the possible presence of yet undiscovered mineralization within eastern portions of the Archean assemblage.

In the area of the Fish Hawk Lake–Anomaly No. 7 prospects, uraniferous pegmatitic intrusions have been identified crosscutting rocks of the KIS. These dykes appear to postdate the development of the ductile deformation, but predate the brittle deformation and accompanying hematite alteration and associated uranium mineralization. Similar features are also described from areas around the Two-Time Trend farther to the north (MacGillivray *et al.*, 2008c), as well as from areas farther east, near Kanairiktok Bay (Sparkes and Kerr, 2008). Both altered and unaltered versions of radioactive pegmatite were observed. The altered examples display many similarities to the brittle style, fracture-hosted, hematite alteration and associated uranium mineralization as seen elsewhere within the region of the Fish Hawk Lake–Anomaly No. 7 prospects. Unaltered pegmatites locally appear to host primary, magmatic, uranium mineralization, and are observed

intermittently throughout the Archean basement rocks extending from the area of Fish Hawk Lake and the Two-Time Trend, northeast to Kanairiktok Bay, where they are best exemplified by the Dandy prospect.

## Dandy and Related Prospects

Exploration of the Archean basement rocks immediately adjacent to the supracrustal sequences of the CMB has resulted in the discovery of numerous, variably radioactive, pegmatitic intrusions ranging from several metres to several tens of metres in width. These pegmatite dykes are predominantly hosted within the KIS (*e.g.*, Dandy, Kanairiktok, Stomach Lake, Fish Hawk Lake North and Soggy Bog prospects; Figure 3) and are inferred by Ermanovics (1993) to be related to the Proterozoic intrusions in the CMB farther south.

Although the pegmatite intrusions generally have no preferred orientation, some swarms are developed within large-scale regional shear zones and related structures, resulting in multiple sheet-like zones. In these zones, anomalous radioactivity occurs over considerable widths. At the Dandy prospect (Figure 3), pegmatite dykes occur within a zone of anomalous radioactivity spanning some 600 m in width, and can be traced intermittently along strike for up to 1.5 km. Grab samples from within this zone have assayed up to 0.18%  $U_3O_8$  (Fraser *et al.*, 2008) and represent a prospective exploration target. The mineralization, however, is sporadically distributed in the pegmatite dykes and is generally concentrated in biotite-rich shear bands within individual dykes (Sparkes and Kerr, 2008). Drilling carried out by Bayswater Uranium Corp. in the area of the Dandy prospect provided a best intersection of 0.04%  $U_3O_8$  over 5.0 m (Fraser *et al.*, 2008). Less-deformed pegmatite dykes have also been identified in the region of Stomach Lake (Figure 3), where sporadic radioactivity is developed within 2–3-m-wide intrusions, locally assaying up to 0.46%  $U_3O_8$  (Fraser *et al.*, 2008).

## GEOCHRONOLOGICAL CONSTRAINTS

Very few geochronological constraints exist for the uranium occurrences hosted in Archean basement rocks in the CMB. The quartz monzodiorite–tonalite, which hosts the uranium mineralization at the Snegamook prospect, was sampled for U–Pb geochronology, and was processed and analyzed at Memorial University (*see* Appendix B and D for a description of techniques and accompanying U–Pb data tables). The sample produced an abundant population of both zircon and monazite, the zircon displaying well-developed igneous growth zoning. Both mineral phases were analyzed by thermal ionization mass spectrometry (TIMS) and three analyses of single zircon fractions produced a weighted average  $^{207}Pb/^{206}Pb$  age of  $3043 \pm 2.5$  Ma (95% confidence interval, MSWD = 0.18; (Figure 9); Sparkes and Dunning, 2015). This age is interpreted as the igneous age of the host rock and provides a

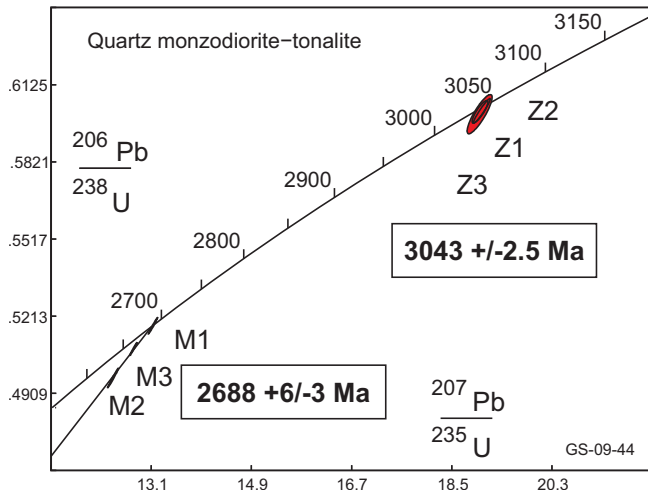


**Figure 9.** Concordia diagram of zircon (red) and monazite U–Pb results from sample GS-09-44, a quartz monzodiorite–tonalite intrusion. Error ellipses are at the  $2\sigma$  level (modified from Sparkes and Dunning, 2015).

maximum age constraint on the development of the uranium mineralization. Three separate analyses of monazite collected from the same sample produce a discordia line with an upper intercept age of  $2688 +6/-3$  Ma (Figure 9); Sparkes and Dunning, 2015); the latter age possibly represents a younger metamorphic overprint.

The only other age determination in the western portion of the CMB, relative to uranium mineralization, comes from uraninite that was collected from the Anomaly No. 7 prospect. The uraninite produced a  $^{206}\text{Pb}/^{207}\text{Pb}$  age of  $1774 \pm 9$  Ma (Wilton and Longerich, 1993). Whether this age represents the primary age of mineralization or has been reset by later deformational events is unknown, but elsewhere within the CMB it has been shown that most  $^{206}\text{Pb}/^{207}\text{Pb}$  ages from uraninite in the region have been reset and do not reflect the primary age of the uranium mineralization (e.g., Sparkes *et al.*, 2010).

Farther to the east at the Dandy prospect (Figure 3), pegmatite dykes similar to those hosting uranium mineralization have been dated at  $1870 \pm 2$  Ma (Ketchum *et al.*, 2001b), but the mineralized dykes have yet to be dated directly. Pegmatite intrusions are also common throughout the area around Fish Hawk Lake; however the relationship between these dykes and those dated along the coast has yet to be determined.

## GEOCHEMISTRY

Geochemical investigations suggest that the quartz monzodiorite–tonalite hosting most of the uranium occurrences is broadly similar throughout the region. This unit straddles

the boundary between the metaluminous and peraluminous fields on the alumina saturation diagram (Figure 10A); altered and mineralized samples plotting well within the metaluminous fields due to the introduction of carbonate in association with breccia development. The quartz monzodiorite–tonalite along the Two-Time Trend has a more evolved chemical composition compared to similar rocks from the area of Fish Hawk Lake (Figure 10B, C). However, the trace-element data exhibits less variability and displays a similar pattern for the unit in all areas (Figure 11). Similarly, a comparison of the Maggo Gneiss and the quartz monzodiorite–tonalite illustrates the geochemical similarities between the two units, which further complicate their separation (Figure 12).

Uranium enrichment in the mineralized zones does not display any significant association with any other elements, aside from a minor correlation with increased Mn (Figure 13). Wilton (1996) noted elevated  $\text{TiO}_2$ ,  $\text{Al}_2\text{O}_3$ ,  $\text{CaO}$ ,  $\text{Na}_2\text{O}$ , LOI, Pb and Zn, at the Anomaly No. 7 prospect, relative to unmineralized samples. Despite the association of uranium mineralization with the development of hematite-filled fractures in the region, there is no appreciable difference in the overall total-iron content of mineralized and unmineralized samples. The one sample that does show elevated iron levels in Figure 13 is from a hematite breccia developed marginal to a mafic dyke, and may have included some dyke material, which would account for the higher iron content of the sample.

Background uranium values within both the gneiss (avg. 2.6 ppm U;  $n=5$ ) and the quartz monzodiorite–tonalite (avg. 2.7 ppm U;  $n=14$ ) display no significant enrichment outside of mineralized zones. Thus, these units do not represent plausible source rocks for the uranium mineralization. In addition thorium values within the mineralized zones are low, with thorium/uranium ratios of mineralized samples generally being less than 0.5. One exception is the Firestone prospect, which contains elevated thorium/uranium ratios (up to 1.5) and has some of the highest thorium values obtained within the region (up to 231 ppm).

Most of the mafic dykes present within the Archean basement rocks display similar geochemical trends with respect to one another, aside from one anomalous group (Group 1) that displays a very distinctive trend (Figure 14). The anomalous trend is highlighted in two separate dykes, one from Fish Hawk Lake South and the other from the Two-Time deposit. These dykes display a similar geochemical pattern as described for the Harp Lake and Kikkertavak dykes of Cadman *et al.* (1993), the most notable of which are elevated Ba in association with an arched Nb–La–Ce–Sr pattern; these dykes also plot in the within-plate basalt field of Pearce and Cann (1973). Both the Harp Lake and Kikkertavak dykes are precisely dated at 1273 and 2235 Ma, respectively (Cadman *et al.*, 1993); however, as noted by Cadman *et al.* (*op. cit.*),

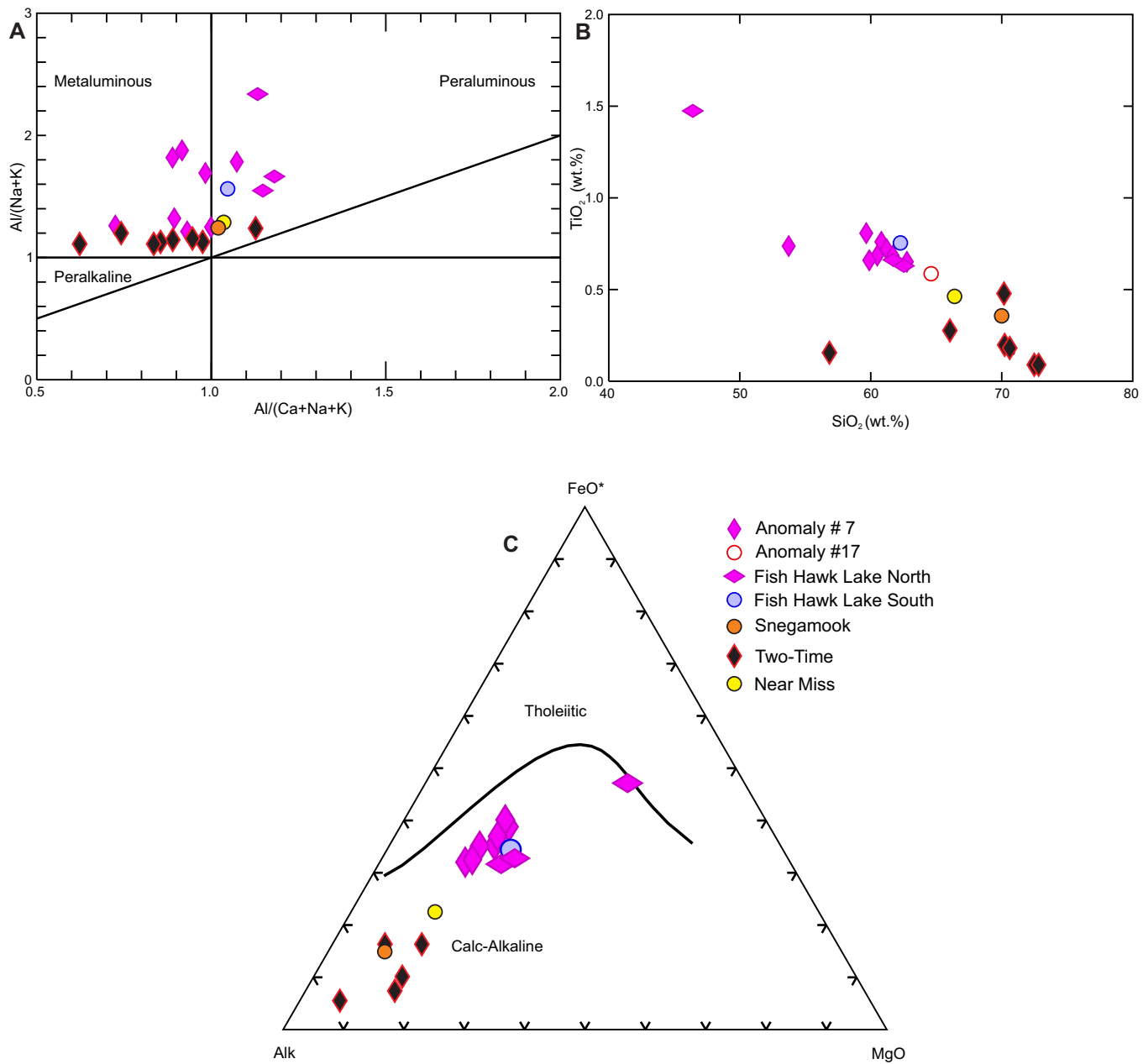


**Figure 10.** Select major-element composition diagrams for the quartz monzodiorite–tonalite unit from various Archean basement-hosted uranium prospects within the western CMB. A. Alumina saturation diagram of Maniar and Piccoli (1989), showing limits of metaluminous, peraluminous, and peralkaline fields, B.  $TiO_2$  vs.  $SiO_2$  diagram displaying the higher Si values of the host rock in the area of the Two-Time deposit relative to those near Fish Hawk Lake, C. AFM diagram showing calc-alkaline and tholeiitic fields of Irvine and Baragar (1971).

these dykes cannot be separated on the basis of geochemistry alone. In drillcore, the anomalous dykes display well-developed chilled margins, plagioclase-phyric texture, and are undeformed (Plate 17). These dykes were not observed in direct contact with mineralized units, but they do appear to postdate the development of the marginal hematite alteration and associated brecciation.

Mineralized rocks are crosscut by frequent mafic dykes. These dykes (Group 2) display a common geochemical pattern, distinct from those mentioned above (Figure 14). This pattern displays an overall depleted concentration in element abundances and primitive mantle normalized samples display a negative Nb/La ratio. Dykes contained within this group plot within the ocean-floor basalt field of Pearce and Cann (1973).

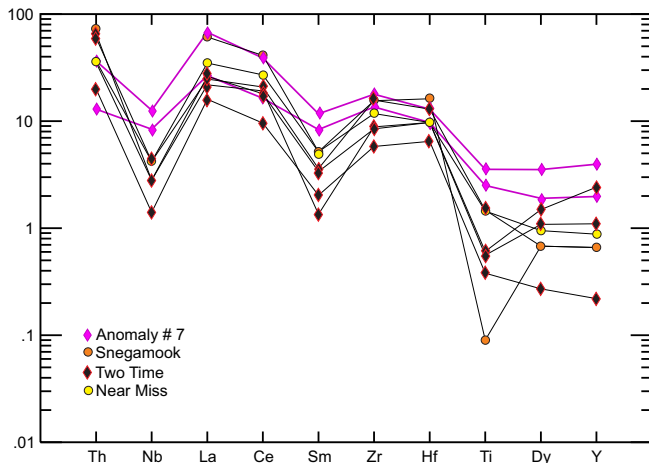


**Figure 11.** Primitive mantle normalized trace-element plot showing patterns for the quartz monzodiorite-tonalite unit from various Archean basement-hosted uranium prospects within the western CMB (normalizing values of Sun and McDonough, 1989).

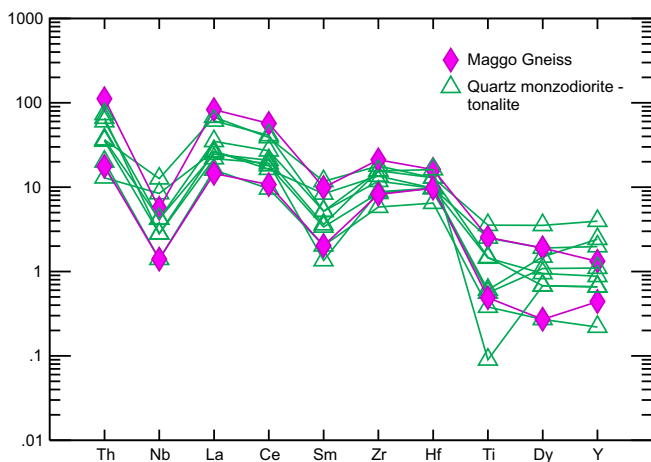


**Figure 12.** Primitive mantle normalized trace-element plot displaying the geochemical similarities between the quartz monzodiorite-tonalite unit and Maggo Gneiss (normalizing values of Sun and McDonough, 1989).

## SUMMARY AND DISCUSSION

The presence of structurally controlled uranium mineralization within the Archean basement rocks in the western portion of the CMB has been known since the late 1970s. Exploration since 2005 has led to the identification of low-grade uranium mineralization of economic significance, suggesting that there is unrecognized potential for further exploration in the area. The Two-Time deposit is the most significant discovery to date, and is associated with a zone of brecciation interpreted to be the result of brittle deformation within a fault structure. A similar style of mineralization is also developed

in several other smaller prospects in the area of Fish Hawk Lake—Anomaly No. 7, the majority of which are hosted by the KIS.

Outside of the intensely brecciated zones, lesser structurally controlled uranium mineralization consists of network-style fracturing, which is generally sporadic and diminishes at depth, based on diamond-drilling results. Both forms of mineralization are characterized by several stages of alteration, which can be subdivided into an early hematite alteration that is followed by the development of specularite, Fe–Ti-oxides and uranium mineralization. Early stages of the hematite alteration are generally weakly developed, and are barren with respect to the development of uranium mineralization. The overall iron content of both mineralized and unmineralized samples is similar, which indicates that there is no significant addition of iron in relation to mineralization. The uranium enrichment is generally not accompanied by any other minerals of economic interest, aside from a local, weak association with anomalous copper.

Mineralization within the Archean basement rocks is crosscut by mafic dykes, locally resulting in elevated uranium values along their margins. Field observations, as well as geochemical data, suggest the presence of multiple dykes within the region, some of which may be correlative with the dated Harp Lake or Kikkertavak dykes (Cadman *et al.*, 1993). These dykes represent potential targets for future geochronological study, as they could possibly provide a minimum age for the development of the brittle deformation within the basement rocks.

The identification of locally uraniferous pegmatite dykes in the area surrounding the Two-Time Trend, and farther east along the coast, greatly increases the aerial extent of known mineralized pegmatite intrusions as first identified by Wilton (1996). Although significant widths have yet to be identified in association with this style of mineralization, the exploration for such, within the Archean basement rocks, has been limited.

Historical models for the uranium mineralization in the Archean basement rocks interpreted the mineralized structures as the eroded remnants of sub-unconformity type uranium deposits, associated with the overlying supracrustal rocks of the Moran Lake Group (Perry, 1979). This style of mineralization is herein grouped with the metamorphic–metasomatic style of mineralization resulting from structurally controlled uraniferous fluids; the origins and timing of which are yet unknown. The local occurrence of uranium mineralization within outliers of the overlying metasedimentary rocks of the Moran Lake Group (see Section, Uranium Mineralization within the Moran lake Group), combined with the development of structurally controlled mineralization along faults

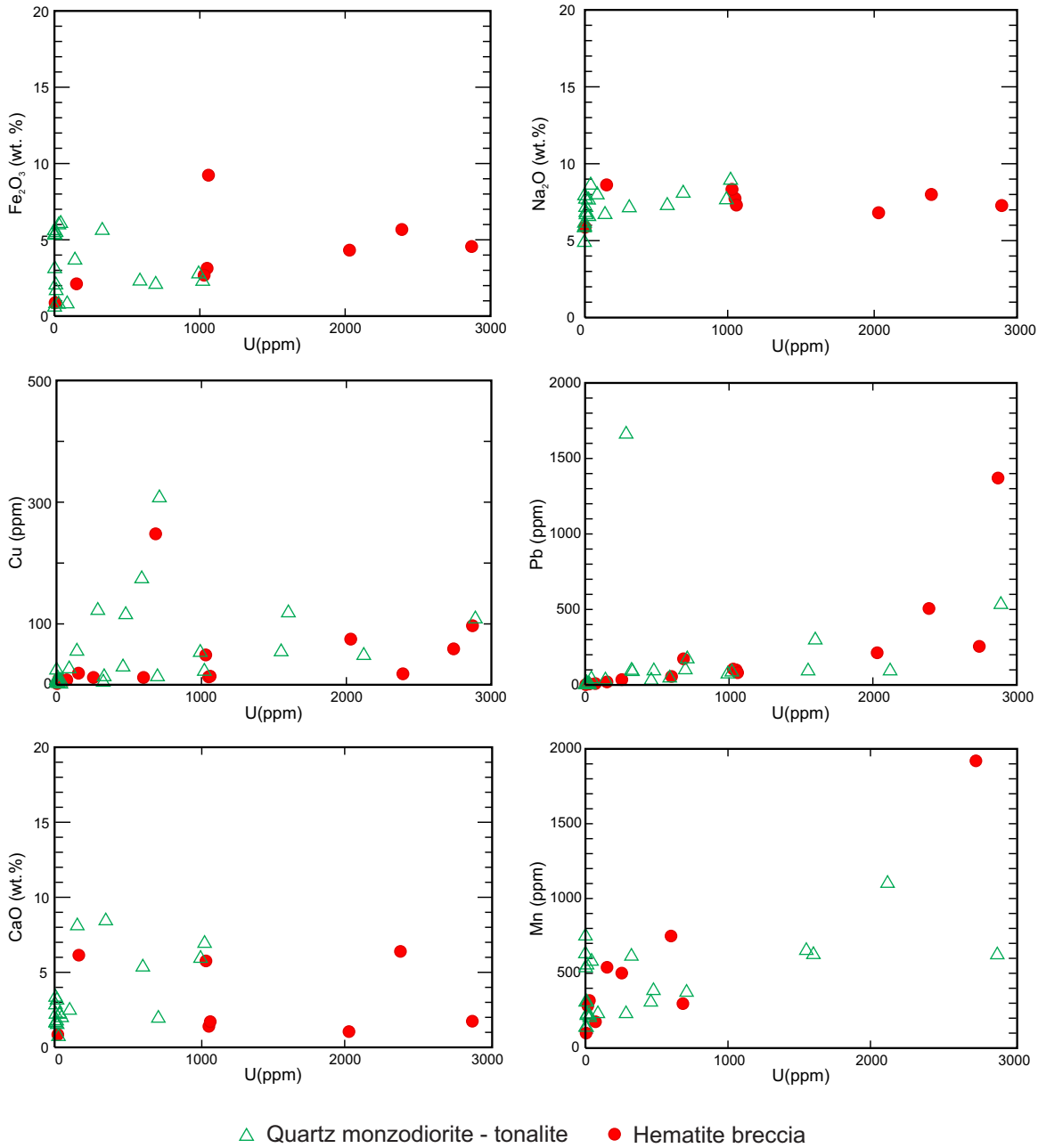


**Figure 13.** Plots of uranium versus other elements of interest (refer to text) in relation to the development of hematite breccias within the Archean basement rocks. Note some samples of quartz monzodiorite-tonalite contain elevated uranium mineralization; these samples are fractured and hematized but primary texture is still evident, thus separating them from the hematite breccias. Some samples do not appear in all plots as not all samples contain a complete geochemical analysis.

locally affecting those same metasedimentary units, suggests a Paleoproterozoic or younger age for the mineralization. The lack of uranium-enriched source rocks within the basement terrane, aside from minor occurrences of uranium-enriched pegmatite dykes, provides supporting evidence that an external source for the uranium is required.

The host quartz monzodiorite-tonalite appears to be lithologically and geochemically similar throughout the area encompassing the Two-Time Trend and the Fish Hawk Lake-Anomaly No. 7 occurrences. Significant fault structures, and areas of structural intersections, represent the best target areas for further exploration. The association of ele-

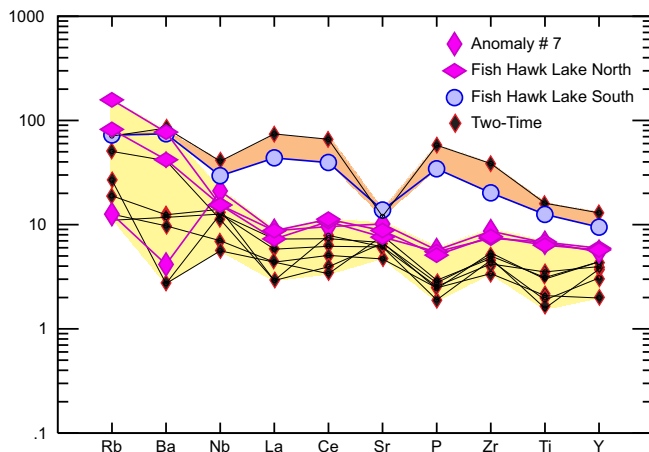


**Figure 14.** Primitive mantle normalized trace-element patterns of mafic dykes crosscutting Archean basement rocks within the western CMB (normalizing values of Sun and McDonough, 1989). The chemical trend of the younger dykes (Group 1) is highlighted in orange and older dykes (Group 2) in yellow.

vated uranium mineralization within zones of intense brecciation and fracturing highlight the overall permeability control on the mineralizing fluids. This requires detailed structural mapping in order to identify possible fault intersections or flexures along potential mineralized structures, which could provide zones of increased permeability favourable for the development of uranium mineralization.

## URANIUM MINERALIZATION WITHIN THE MORAN LAKE GROUP

### INTRODUCTION

The Moran Lake Group hosts some of the most significant uranium occurrences in the western portion of the CMB, the most notable of which is the Moran Lake C Zone deposit. This deposit is divided into the Upper and Lower C zones, which consist of distinctly different styles of uranium mineralization (*cf.* Sparkes and Kerr, 2008). The Upper C Zone is described here, whereas the Lower C Zone is discussed later

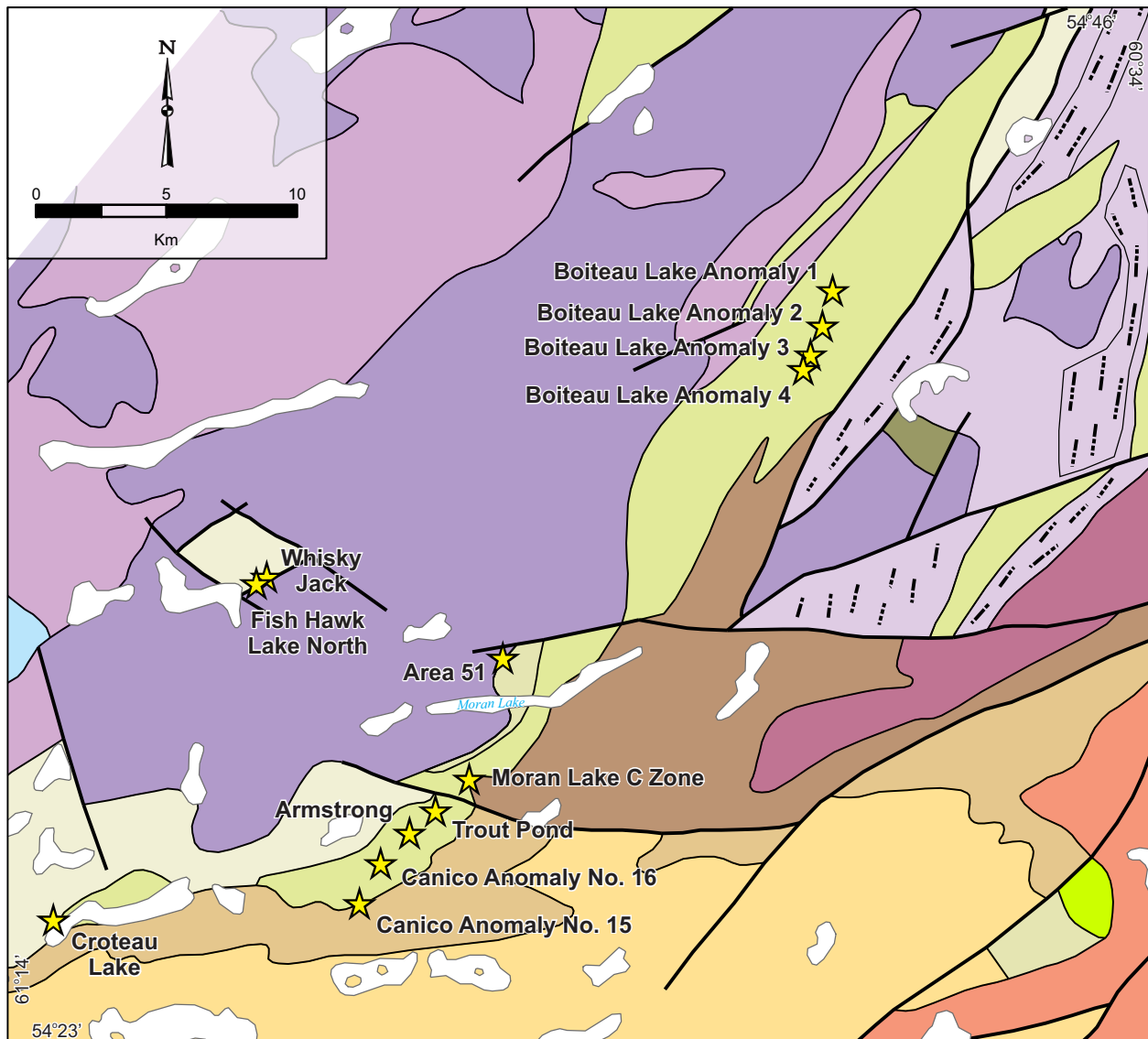
(see Section, Uranium Mineralization within the Bruce River Group).

Mineralization was first discovered in the western CMB in the late 1950s, and was subsequently the focus of two main periods of uranium exploration, the first in the late 1950s and the second in the late 1970s. This area became the focus of renewed exploration in the early 2000s, which was sparked by interest in the extensive hematitic breccias hosting elevated copper values; such features were thought to represent potential Iron-Oxide–Copper–Gold (IOCG) mineralization. By the mid-2000s, renewed market interest in uranium shifted attention in the area toward re-evaluating and expanding known uranium occurrences; this resulted in the definition of several NI 43-101 resource estimates for occurrences hosted within the Moran Lake Group (Table 4). Uranium mineralization within the Moran Lake Group displays some similarities with mineralization in the Archean basement rocks, such as the association of uranium enrichment within zones of hematite-rich brecciation (*e.g.*, Moran Lake Upper C Zone). However, as discussed below, despite being visually similar to the Archean-hosted mineralization, breccia development within the Moran Lake Group is inferred to be the result of a distinctly different process. The Moran Lake Group is also host to other styles of uranium mineralization, such as that associated with brecciated iron formation (*e.g.*, Croteau Lake prospect) and occurrences within dolomitic sedimentary host rocks (*e.g.*, Area 51 prospect).

Renewed exploration in the region has resulted in the discovery of several new zones of mineralization, such as the Boiteau Lake and Croteau Lake prospects, but most occurrences within the area were discovered during the early periods of exploration. The Moran Lake Group remains an attractive target for future exploration, in part due to the large number of occurrences identified to date (Figure 15), but also because it is interpreted to be correlative with the Post Hill Group, located farther to the northeast within the CMB (Marten, 1977; Wardle and Bailey, 1981). Although high-grade uranium mineralization similar to that hosted within argillic rocks of the Post Hill Group is rare within the Moran Lake Group, the rocks have not been subjected to the same

**Table 4.** NI 43-101 compliant resource estimates for mineralization within the Moran Lake Group

Deposit	Resource Classification	Cut-off (% U <sub>3</sub> O <sub>8</sub> )	Grade (% U <sub>3</sub> O <sub>8</sub> )	Tonnage (tonnes > cut-off)	Contained Resource (lbs. U <sub>3</sub> O <sub>8</sub> )	Source
Upper C Zone	Indicated	0.015%	0.034%	6,920,000	5,190,000	Morgan and Giroux, 2008
	Inferred	0.015%	0.024%	5,320,000	2,840,000	Morgan and Giroux, 2008
Trout Pond	Inferred	0.015%	0.055%	399,014	480,000	Morgan and Giroux, 2008
Armstrong	Inferred	0.015%	0.041%	1,000,000	900,000	Morgan and Giroux, 2008



#### Seal Lake Group

Arkose, quartzite

#### Bruce River Group

Sylvia Lake Formation - Rhyolite, dacite, andesite ash-flow tuff, agglomerate  
 Brown Lake Formation - Conglomerate and volcaniclastic sandstone  
 Heggart Lake Formation - Volcaniclastic sandstone, arkose and conglomerate; minor mafic flows and sills

#### Moran Lake Group

Joe Pond Formation - Pillow basalt, basaltic pyroclastic rocks; minor siltstone and greywacke  
 Warren Creek Formation - Shale and sandstone of shallow- to deep-water origin; minor unseparated dolostone

#### Intrusive Rocks

Granite; ca. 1650 Ma  
 Granite; ca. 1973 to 1891 Ma

#### LEGEND

##### Archean Basement Rocks

Tonalite gneiss, granitoid gneiss  
 Granodiorite, tonalite and minor granite (Kanairiktok Intrusive Suite)  
 Tonalitic to granodioritic migmatitic orthogneiss containing abundant mafic to ultramafic inclusions and relict mafic dykes  
 Amphibolite gneiss, mafic granulite gneiss

#### SYMBOLS

- Geological contact.....
- Zone of ductile deformation.....
- Fault.....
- Uranium occurrence.....

**Figure 15.** Regional geology map outlining the distribution of uranium occurrences within the Moran Lake Group (geological base map modified from Wardle et al., 1997).

intensity of exploration. In addition, the Moran Lake Group is also obscured by more significant vegetation and Quaternary cover when compared to the Post Hill Group, which further hampers exploration in the area.

## REGIONAL GEOLOGY

The Moran Lake Group is divided into two main formations, the Warren Creek Formation and the overlying Joe Pond Formation, both of which have undergone polyphase deformation. A brief summary of these units is presented herein, and a more detailed description can be found in Ryan (1984) and references therein. Siliciclastic sedimentary rocks of the Warren Creek Formation unconformably overlie the Archean basement rocks and represent a shallow, nearshore to shallow-marine shelf depositional environment (Smyth *et al.*, 1978; Wardle and Bailey, 1981; Ryan, 1984). The Joe Pond Formation consists of basaltic rocks, including pillow basalt and associated volcaniclastic and shallow intrusive rocks. Progressively younger stratigraphic units are noted to onlap the Archean basement rocks from southwest to northeast, indicating a northerly transgression of the units (Smyth *et al.*, 1978; Wardle and Bailey, 1981). Rocks of the Moran Lake Group are subsequently unconformably overlain by siliciclastic sedimentary rocks of the Bruce River Group toward the southeast (Ryan, 1984; *see* Section, Uranium Mineralization within the Bruce River Group).

Rocks of the Warren Creek Formation are divided into four subunits; in ascending stratigraphic order they are: 1) a basal grey feldspathic quartz arenite, 2) a dominantly shale (slate)–arkosic siltstone with minor iron formation, 3) brown dolostone, and 4) a dominantly shale (slate)–greywacke. To the southwest, moderately sorted grey to white sandstone and quartzite of the Moran Lake Group are observed to overlie the Archean basement rocks. These units are, in turn, overlain by black shale, arkosic siltstone and minor chert–oxide iron formation; the latter is locally host to uranium mineralization at the Croteau Lake prospect (Figure 15). In the area north of Moran Lake, dolostone and associated calcareous siltstones are developed proximal to the contact with the underlying Archean basement rocks and locally hosts low-grade uranium mineralization (*e.g.*, Area 51 prospect; Figure 15). Black shale within the upper portion of the Warren Creek Formation contains syn-sedimentary pyrite and lesser pyrrhotite, chalcopyrite and sphalerite, and have historically been targeted for their potential to host base-metal mineralization (*e.g.*, Hansuld, 1958; North and Wilton, 1988; Wilton, 1996).

The Joe Pond Formation consists of an extensive sequence of tholeiitic pillow basalt and lesser interbedded shale, dolostone, chert and mafic tuff (Ryan, 1984). The mafic volcanic rocks host most of the uranium prospects within the

Moran Lake Group, including the most significant deposit, the Moran Lake Upper C Zone.

## EXPLORATION HISTORY

Uranium mineralization was first discovered in the western CMB in 1957 by A. Montague and L. Montague whilst conducting regional prospecting for Brinex. One of the first occurrences discovered was in the vicinity of the Moran Lake C Zone (Figure 15; this was originally termed the Montague No. 2 showing). This discovery was followed up with geological and geophysical surveys along with trenching, stripping, and blasting of mineralized outcrops (Mann, 1957; Corriveau, 1958; Ellingwood, 1958). The best results obtained from the initial exploration at the Moran Lake C Zone were 0.13%  $U_3O_8$  over 0.60 m; although broader intervals were also identified (*e.g.*, 0.11%  $U_3O_8$  over 2.75 m; Corriveau, 1958). At the time, uranium mineralization within the Moran Lake C Zone was interpreted to be hosted by a volcanic breccia unit, which was affected by variable hematitic alteration. Work in the area was discontinued in 1958 due to the relatively low grade of the mineralization.

In 1964, Mokta Canada Ltd. acquired the licences for the Moran Lake area and carried out geological mapping and scintillometer surveys around the Moran Lake C Zone. The scintillometer survey identified 64 radiometric anomalies, which expanded the extent of the mineralization within the immediate vicinity of the Moran Lake C Zone. The company conducted extensive trenching in the area (Bernazeud, 1965), but allowed the licenses to expire in 1969. In 1976, Commodore Mining Ltd. acquired the ground and optioned it to Shell Canada Resources. Shell briefly evaluated the historical trenching at the Moran Lake C Zone in 1976 (McKenzie, 1976), and followed up with additional trenching, geological mapping and scintillometer surveys in 1977. During the same year, Shell carried out the first diamond-drilling program on the Moran Lake C Zone deposit. This drilling yielded localized zones of higher grade mineralization, assaying up to 0.20%  $U_3O_8$  over 3.34 m, which sparked an intense exploration program on the property (McKenzie, 1977a). Additional drilling demonstrated that the high-grade mineralization was of a limited extent, but also identified several zones of what was termed ‘quartzite-hosted’ uranium mineralization (McKenzie, 1978a). Follow-up drilling resulted in the discovery of low-grade, sandstone-hosted uranium mineralization proximal to the unconformity between the Moran Lake Group and the overlying Bruce River Group (McKenzie, 1978b; now known as the Lower C Zone deposit; *see* Section, Uranium Mineralization within the Bruce River Group). The discovery of this new style of mineralization resulted in further drilling, which tested the extent of the mineralization along 1200 m of strike length, and confirmed the presence of vari-

able low-grade uranium mineralization which generally produced drill intersections averaging 0.027%  $U_3O_8$  over 2.60 m (Gordanier, 1979). No further work was carried out and the extended licence expired in 1982.

In the late 1970s, Brinex and Canico explored parts of the CMB, which resulted in the discovery of the Canico Anomaly Nos. 15 and 16 (Figure 15). These occurrences were discovered as a result of an airborne survey carried out by Canico in the summer of 1978, which was followed up with prospecting and limited drilling. Initial drill results from Canico Anomaly No. 15 produced assays of up to 0.16%  $U_3O_8$  over 3.72 m (Perry, 1979). Follow-up investigations including geological and geophysical surveys, and trenching of mineralized occurrences indicated that the mineralization was of limited extent and the concessions were allowed to lapse in 1980.

The western CMB remained relatively inactive with respect to uranium exploration until the early 2000s. Highlights of this renewed exploration included expanding the known extent of previously identified occurrences, as well as the discovery of several new zones of mineralization. As part of this renewed exploration, more sensitive airborne radiometric surveys were conducted throughout the region, which identified several new areas of anomalous radioactivity. During follow-up prospecting of one such anomaly in the extreme western portion of the Moran Lake Group, Crosshair Exploration and Mining identified a zone of mineralized boulders consisting of iron formation believed to be derived from the Warren Creek Formation (e.g., Croteau Lake prospect; Froude *et al.*, 2006; Morgan *et al.*, 2007). This prospect represents the most western occurrence of uranium mineralization within the Moran Lake Group.

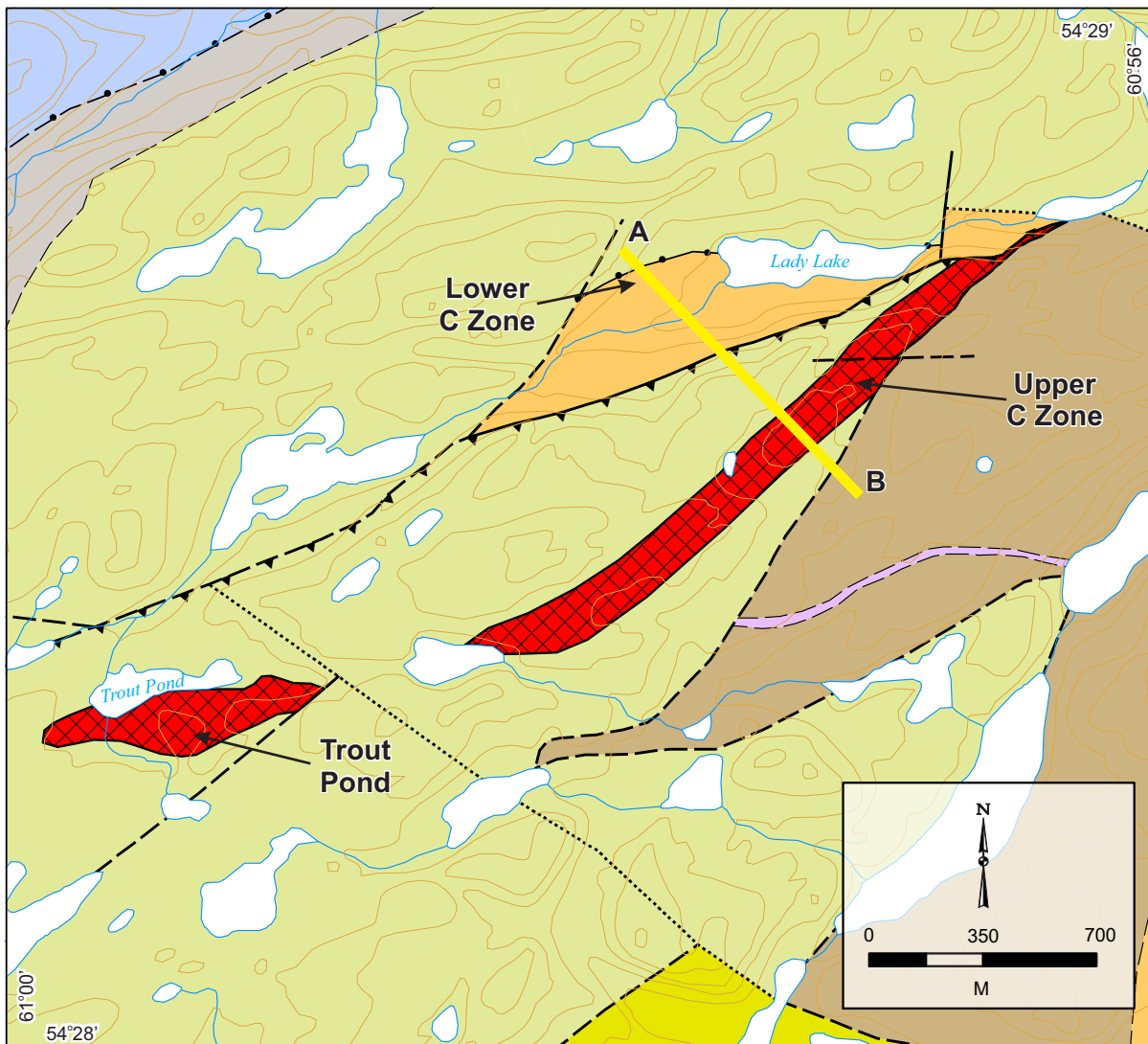
Crosshair also identified intermittent uranium mineralization along a strike length of approximately 2.5 km extending southwest from the Moran Lake C Zone deposit (Figure 15); subsequent work by the company within this area defined the Trout Pond and Armstrong deposits. These deposits have NI 43-101 compliant resource estimates of 480 000 and 900 000 lbs of  $U_3O_8$ , respectively (Table 4; Morgan and Giroux, 2008). Renewed drilling by Crosshair at the Moran Lake C Zone expanded the zone of known mineralization along strike for some 1.3 km and at depth; the mineralized zone remains open along strike to the southwest as well as down-dip (Morgan and Giroux, 2008). From this work, a NI 43-101 compliant resource estimate was generated, which consists of 8.03 million lbs  $U_3O_8$  at a cut-off grade of 0.015% for the Upper C Zone and 1.60 million lbs at a cut-off grade of 0.035% for the Lower C Zone (Morgan and Giroux, 2008). In addition, the company has also outlined a significant vanadium resource of approximately 134 million lbs of  $V_2O_5$  within the Upper C Zone of the deposit (Wallis *et al.*, 2011).

Uranium exploration within the western CMB during the late 2000s identified several new occurrences north of the Moran Lake area. One such occurrence was the Area 51 prospect (Figure 15; Morgan *et al.*, 2007), which was found in 2005 by Crosshair during ground follow-up of a large airborne radiometric anomaly. Drilling in the area revealed broad, low-grade intersections of uranium mineralization within basal units of the Warren Creek Formation, immediately above the unconformity with underlying Archean basement rocks. In 2008, Bayswater Uranium discovered several occurrences along strike to the northeast of the Area 51 prospect consisting of structurally controlled mineralization predominantly hosted within pillow basalt of the Joe Pond Formation (e.g., Boiteau Lake prospects 1-4; Figure 15; Fraser *et al.*, 2009). This mineralization occurs in association with interbedded and/or structurally interleaved sediments of the Warren Creek Formation and represents the northeastern limit of known uranium mineralization within the Moran Lake Group. Minor uranium mineralization has also been identified within an outlier of the Moran Lake Group by Santoy Resources, which consists of uraniferous metasedimentary rocks of the Warren Creek Formation (e.g., Fish Hawk Lake North and Whiskey Jack prospects; Figure 15; Willett *et al.*, 2008).

## THE MORAN LAKE UPPER C ZONE AND TROUT POND DEPOSITS

### Overview

Earlier reports summarizing the Moran Lake C Zone deposit, interpreted the mineralization to be hosted by the Bruce River Group (e.g., Ryan, 1984; Wilton, 1996). This is because the host rocks to the mineralization, interpreted to be volcanic in origin, were considered to form part of the basal Bruce River Group (*i.e.*, Heggart Lake Formation). However, recent work suggests that the area is structurally complex, and that there are two distinct styles of mineralization hosted by different geological units. The Upper C Zone consists of uranium mineralization within strongly brecciated and altered mafic volcanic rocks and lesser Fe-carbonate-altered shear zones, collectively hosted by the Joe Pond Formation of the Moran Lake Group. The mineralized mafic volcanic rocks are structurally overlain to the southeast by conglomerate and sandstone of the Heggart Lake Formation and here are rarely mineralized. The mineralized mafic volcanic rocks of the Upper C Zone are thrust to the northwest over younger, fluvial sedimentary rocks of the Heggart Lake Formation. Here, sandstone and associated conglomerate within the footwall of the thrust, host uranium mineralization proximal to the original unconformity with the underlying mafic volcanic rocks of the Joe Pond Formation (e.g., Lower C Zone, *see* Section, Uranium Mineralization within the Bruce River Group; Figure 16).



#### LEGEND

	Hematitic breccia
	Mafic/intermediate intrusive rocks
<b>Bruce River Gp. - Brown Lake Fm</b>	
	Volcaniclastic sandstone
<b>Bruce River Gp. - Heggart Lake Fm</b>	
	Conglomerate
	Sandstone
<b>Moran Lake Group</b>	
	Pillow Basalt
	Siltstone
<b>Kanairiktok Intrusive Suite</b>	
	Granodiorite/tonalite

#### SYMBOLS

Unconformity (defined, approximate).....	
Contact (approximate, assumed).....	
Fault (defined, approximate, assumed).....	
Thrust (defined, approximate).....	

**Figure 16.** Plan map outlining the distribution of geological units as well as the surface projection of mineralization and related alteration in the area of the Moran Lake Upper C Zone and Trout Pond deposits; (geology base map modified from Ryan, 1984 and Gillies et al., 2009). Schematic cross-section A–B illustrated in Figure 17.

The Trout Pond deposit (Figure 16) is located approximately 1 km to the southwest of the Upper C Zone deposit. This area of anomalous radioactivity was first noted in 1978 and was originally referred to as Anomaly No. 5 (Perry, 1979). Uranium mineralization at the Trout Pond deposit has many similarities with that of the Upper C Zone (Morgan and Giroux, 2008), but it has not been studied in as much detail during this project.

### Previous Work

The identity of the host rock to uranium mineralization within the Upper C Zone has been a matter of much debate. Smyth and Ryan (1977) highlighted the structural complexity within the vicinity of the C Zone deposit, and noted the presence of a reverse fault that locally resulted in the structural repetition of the stratigraphic sequence. Smyth and Ryan (1977) interpreted the mineralization to be hosted within an explosive breccia related to the emplacement of a gabbroic intrusion into the sedimentary rocks of the Bruce River Group. Kontak (1978) concluded that the Upper C Zone mineralization was hosted within extrusive volcanic rocks, which he assigned to the Heggart Lake Formation of the Bruce River Group. He interpreted the breccia formation to be syn-volcanic, and proposed that uraniferous fluids later ascended along localized fault zones within the stratigraphy.

A re-evaluation of the geology and uranium mineralization at the Upper C Zone was conducted by Cook (1980). Cook subdivided the alteration assemblages within the deposit into several stages, and noted seven different settings for uranium mineralization, only two of which were deemed to be of economic interest. He suggested that the original host was a synvolcanic intrusive rock that was affected by a complex alteration system involving multiple episodes of both hematite and carbonate alteration. Ryan (1984) carried out regional mapping in the vicinity of Moran Lake, including the area surrounding the C Zone deposit. He attributed the brecciation associated with the uranium mineralization to multistage emplacement of  $\text{CO}_2$ -rich fluids within a mafic sill, in which flow alignment of the fragments are locally observed. He favoured an epigenetic model for the uranium mineralization in association with hydrothermal brecciation along structures within the area. Wilton (1996) collected several samples of uranium mineralization from the Moran Lake C Zone during regional sampling of the CMB. These mineralized samples were noted to have elevated  $\text{CaO}$  and  $\text{LOI}$

contents along with distinct flat rare-earth element patterns in comparison to other prospects within the region.

### Local Geology

Exploration since the mid-2000s in the area of the Moran Lake C Zone deposit has led to the reinterpretation of key stratigraphic relationships, in part due to new information gathered from the extensive drilling conducted by Crosshair Exploration (Figures 16 and 17). Uranium mineralization in the Upper C Zone is now interpreted to be hosted by strongly altered and brecciated mafic volcanic rocks of the Joe Pond Formation (Morgan and Giroux, 2008; Sparkes and Kerr, 2008). These variably altered and brecciated mafic volcanic rocks are structurally overlain by poorly sorted pebble to cobble conglomerate of the Heggart Lake Formation; which strike northeast–southwest and dip moderately toward the southeast (Plate 26, Figure 17). The extensive hematite–albite–carbonate alteration and brecciation developed within the mafic volcanic rocks decrease markedly at the contact with the structurally overlying Heggart Lake Formation, with similar styles of brecciation only observed in one or two rare instances within the overlying sedimentary rocks.

The variably mineralized mafic volcanic rocks structurally overlie a thick sequence of chlorite–sericite-altered, pale-green basalt, locally displaying relic pillow selvages; these rocks are assigned to the Joe Pond Formation. The mineralized volcanic rocks are separated from the underlying barren, and relatively unaltered volcanic sequence by the Lower Shear Zone (Figure 17; Morgan and Giroux, 2008), which is generally the locus of the strongest Fe-carbonate alteration. Sporadic uranium mineralization is also found within the Joe



**Plate 26.** Hematite–albite–carbonate alteration (stubby yellow arrow) developed within metres of the overlying conglomerate of the Heggart Lake Formation. Note the sharp structural contact separating the two units (see inset). Moran Lake C Zone, DDH ML-56, ~50 m depth.

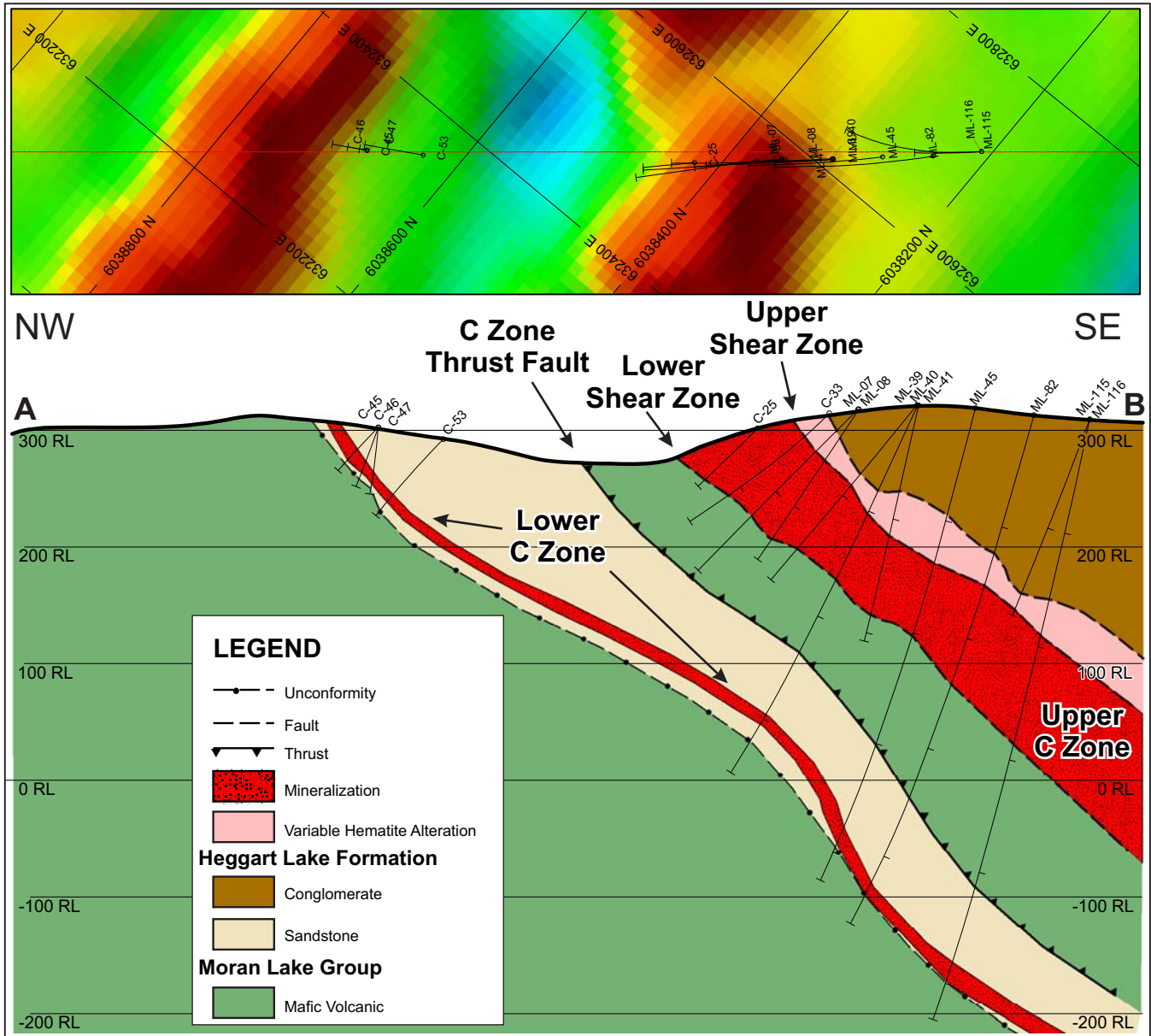


**Figure 17.** Schematic cross-section through the Moran Lake C Zone deposit showing the locations of the Upper and Lower C zones, along with the intervening C Zone thrust fault. (For location of schematic cross-section A–B refer to Figure 16.) Plan map above the section outlines the trace of the drillhole collars overlain on the first vertical derivative of the Crosshair airborne magnetic data.

Pond formation north of Lady Lake, below the unconformity (Figure 16); however this mineralization is generally in the form of discrete fracture filling material in white carbonate veins hosted by sheared basalt, and is not associated with any significant brecciation or hematite alteration (Bernazeud, 1965; Smyth and Ryan, 1977; Ryan, 1984). Several generations of mafic dykes are observed within the deposit and cut both the mineralization and the siliciclastic sedimentary rocks of the Heggart Lake Formation.

The Moran Lake Group underwent polyphase deformation prior to the deposition of the Bruce River Group, including the development of a widespread slaty cleavage and northwest to northeast trending open and closed steeply plunging folds (Smyth *et al.*, 1978). Metre-scale folding is locally observed within sulphidic black shale exposed in trenches to the immediate south of the Upper C Zone deposit. These exposures either represent interbedded sedimentary units, or sedimentary units that have been tectonically interleaved with the

mafic volcanic rocks of the Joe Pond Formation, and potentially represent examples of this earlier deformation. The main structural features noted in the immediate vicinity of the deposit consist of northeast-trending high-angle reverse faults, presumed to be synchronous with Grenvillian deformation, and northwest-southeast-trending normal faults; the latter locally displace the mineralized breccia unit (Smyth and Ryan, 1977). Based upon a detailed study of the mineralization at the Upper C Zone by Crosshair, several distinct settings for uranium mineralization were identified, which are: 1) broad zones of mineralization in association with hematite alteration and hematite-cemented breccias, 2) localized, high-grade mineralization associated with jasperoidal chert lenses, 3) rare, narrow specularite- and sulphide-cemented breccias, and 4) Fe-carbonate-flooded mylonite zones and cataclasites (Eaton *et al.*, 2008). Structural studies noted that the Upper C Zone is constrained by two gently to moderately southeast-dipping, subparallel shear zones, with the lower most shear zone roughly coinciding with the limit of mineralization and alteration within the Upper C Zone deposit (Figure 17).

### Mineralization and Associated Alteration

The mafic volcanic rocks of the Joe Pond Formation locally contain rare lenses of chert and lesser siltstone and sulphidic black shale (Figure 18). Between the Upper and Lower C Zone deposits, the mafic rocks are generally unaltered, and similar rocks are locally preserved as relict zones within the Upper C Zone alteration. Less-altered mafic rocks have dark-green chlorite and brownish-beige sericite alteration that are interpreted as regional metamorphic assemblages. Marginal to the main zone of mineralization, the mafic volcanic rocks are cut by numerous white quartz-carbonate veins that postdate the development of the hematite alteration and associated brecciation. A brief summary of the alteration events observed within the area are presented here, primarily based on observations from the Upper C Zone deposit.

The stages of alteration as determined through detailed drillcore and petrographic examinations are summarized in Table 5. During the first phase of alteration, the mafic volcanic rocks are altered to pale pink, orange, and maroon as a result of hematite-albite alteration. This alteration permeates outward from network-style fractures, resulting in a pervasive ‘reddening’ of the host rock (Phase 1A; Plate 27). This alteration is locally intergrown with, but more commonly overprinted and brecciated by white Fe-carbonate-quartz ± albite alter-

ation (Phase 1B; Plate 27). Phase 1 alteration is overprinted by extensive brittle, network-style fracturing and associated brecciation (Phase 2). The fractures and breccia matrix associated with Phase 2 alteration are dominated by dark-purple hematite (specularite), and contain variable amounts of carbonate (Plate 27). Staining of carbonate minerals (Kontak, 1980) indicated that the dominant carbonate phases (within the deposit) are ankerite and ferroan dolomite. Staining for potassium feldspar in select mineralized samples has not revealed the presence of any significant potassiac alteration within the deposit.

The breccias are typically poorly sorted, and contain angular to subrounded fragments of Phase 1 alteration within a dark-purple hematitic matrix (Plate 28). Locally, elongated fragments within the breccia are noted to display alignment

**Table 5.** Summary of the stages of alteration and associated mineralogy for the Moran Lake Upper C Zone deposit; based on field mapping and petrography

Associated Alteration Minerals	
Phase 1A	Pale-pink to orange to maroon hematite-albite alteration
Phase 1B	White Fe-carbonate-quartz-albite alteration
Phase 2	Dark-purple hematite-filled fractures and brecciation ± uranium
Phase 3	Fe-carbonate alteration
Phase 4	White carbonate-quartz veining



**Plate 27.** Early pinkish-orange hematite-albite alteration (Phase 1A) overprinted by white Fe-carbonate-quartz-albite alteration (Phase 1B), which is, in turn, cross-cut by dark-purple hematite-rich fracturing (Phase 2) and associated brecciation. Note pale-green patches of relatively unaltered mafic volcanic are still locally preserved. Moran Lake C Zone, DDH ML-3, ~55 m depth.

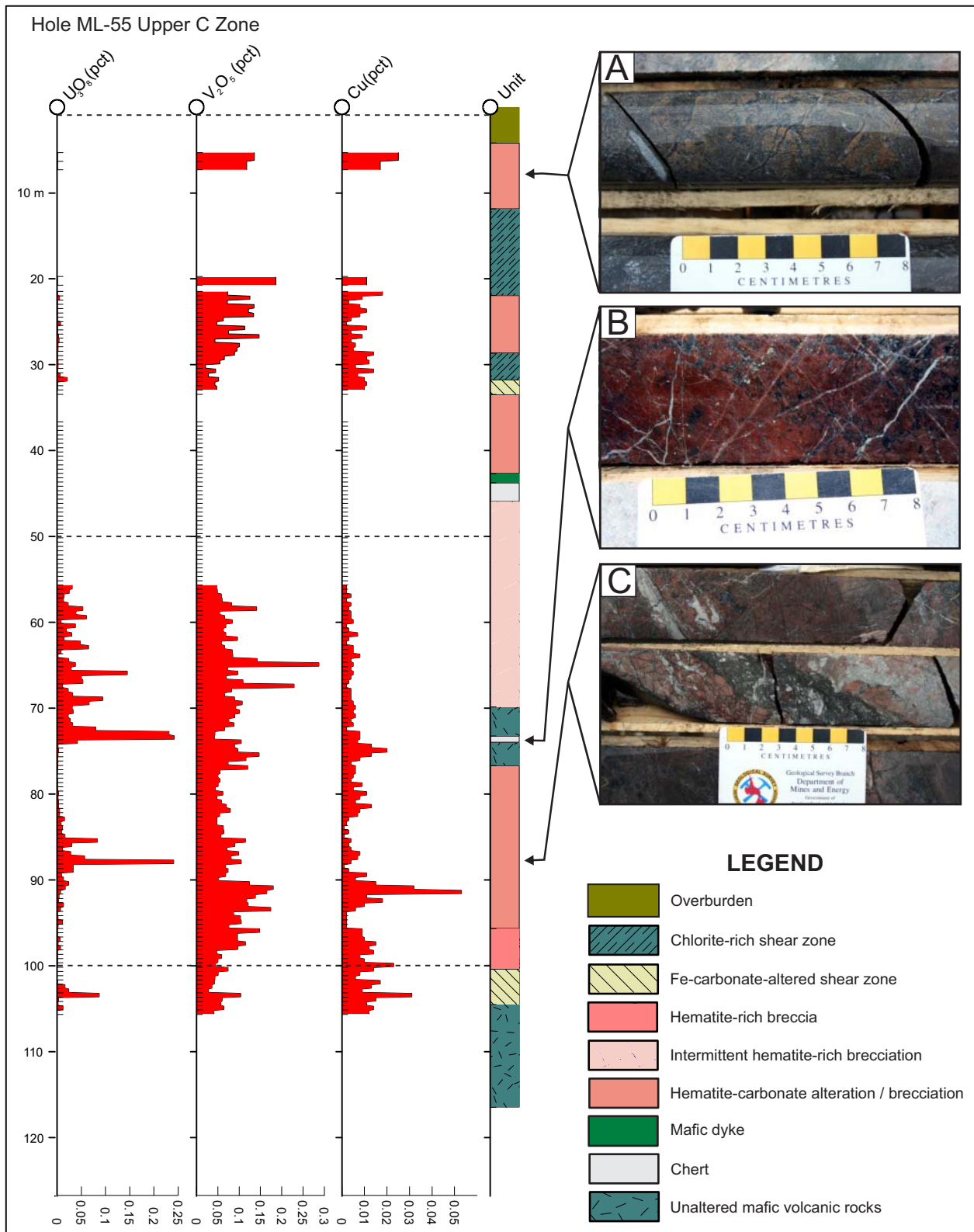


**Figure 18.** Drill log for drillhole ML-55 from the Upper C Zone, outlining the distribution of brecciation and accompanying alteration in association with uranium, vanadium and copper mineralization; all values are listed in weight percent (data from Morgan et al., 2007). A. Hematitic breccia hosting anomalous V and Cu, without associated U enrichment, B. Uranium-bearing, siliceous chert interbedded with mafic volcanic rocks, C. Uraniferous breccia vein (dark-purple vein) crosscutting earlier albite–carbonate alteration.



**Plate 28.** Hematite-rich breccia associated with Phase 2 alteration, containing fragments of the earlier, Phase 1, pale-orange hematite–albite–carbonate alteration. This breccia is barren with respect to uranium mineralization, but is enriched in vanadium. Moran Lake C Zone, DDH ML-3, ~105 m depth.

indicating possible fluidization of the breccia (Ryan, 1984). Breccia development is interpreted to be hydrothermal (Cook, 1980; Ryan, 1984). Although the alteration and brecciation form the most characteristic features associated with the Upper C Zone mineralization, the breccias are not everywhere uranium-bearing. Geochemical data indicate that the breccias are consistently associated with elevated vanadium, but elevated uranium values are generally associated with crosscutting fractures or intersections of mineralized chert (Figure 18). Whether or not the uranium and vanadium are linked to a single mineralizing event has yet to be determined. The lower stratigraphic limit for the hematite alteration and brecciation is commonly defined by the Lower Shear Zone (Figure 17), which is the site of pervasive Fe-carbonate alteration (Phase 3). Locally, this Fe-carbonate alteration overprints the dark-purple hematite-rich matrix of breccias correlated with Phase 2, and therefore postdates the development of that alteration (Plate 29). All of the above are crosscut by centimetre-scale, white carbonate–quartz veins (Phase 4) representing one of the youngest alteration events within the deposit.

The uranium mineralization is primarily located in 4 main settings within the Upper C Zone (e.g., Eaton *et al.*, 2008). The most widespread mineralization occurs in close spatial association with the hematitic alteration and associated brecciation. Within this zone, ura-



**Plate 29.** Pervasive Fe-carbonate alteration replacing the dark-purple hematite-rich matrix of a finely milled breccia associated with Phase 2 alteration. Note the presence of remnant millimetre-scale hematite altered fragments ‘floating’ in the Fe-carbonate alteration. Moran Lake C Zone, DDH ML-4, ~80 m depth.

nium generally occurs as fracture-hosted mineralization in association with the hematite-rich alteration; this is interpreted to be related with Phase 2 (Plate 30). This style of uranium mineralization is generally characterized by broad, relatively low-grade, intersections in drillcore. Mineralization is also locally associated with the development of brecciated quartz–carbonate veins, in association with minor pyrite and chalcopyrite (Morgan and Giroux, 2008).

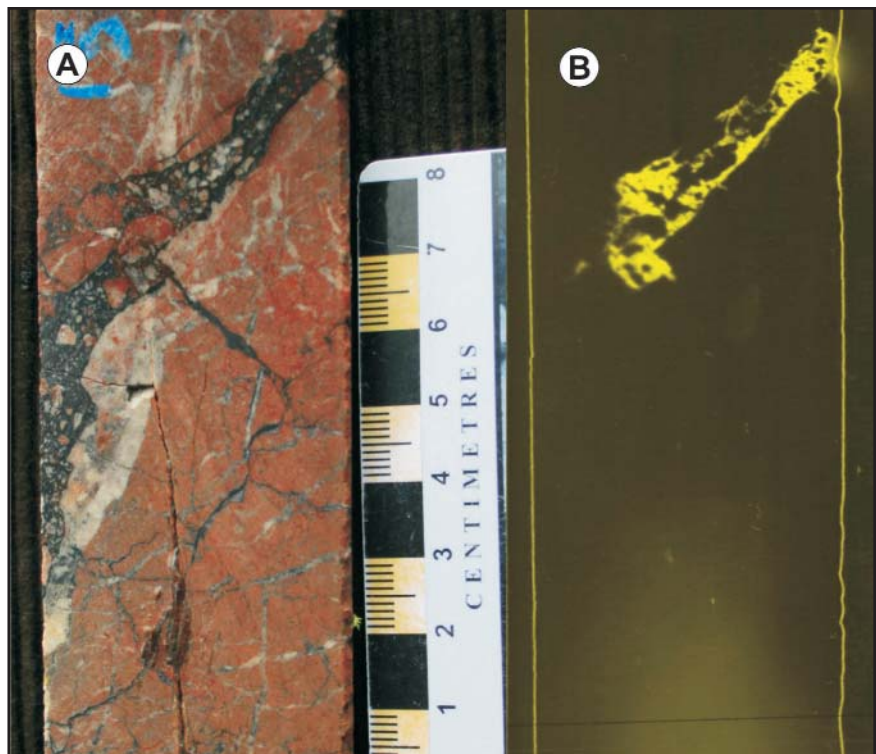


**Plate 30.** A. Uranium-bearing, dark-purple, specularite-rich breccia vein (Phase 2) crosscutting earlier hematite–albite–carbonate (Phase 1) alteration, B. Autoradiograph of (A) outlining the distribution of radioactivity (yellow) within the sample.

Higher grade uranium mineralization within the deposit is associated with discontinuous chert lenses that are interpreted to represent a primary unit within the volcanic sequence (Eaton *et al.*, 2008). These rocks are strongly magnetic and contain disseminated pyrite and lesser magnetite throughout. The mineralized chert is generally affected by a pervasive hematite alteration, resulting in a distinctive brick-red colouration. This alteration is interpreted as part of the earlier Phase 1 alteration, as it is subsequently overprinted by extensive specularite and/or white Fe-carbonate fracturing and brecciation (Plate 31). As shown by the autoradiograph in Plate 31, the uranium mineralization is predominantly confined to the dark-red specularite-filled fractures and related breccia; however, rare occurrences of barren, dark-grey, specularite-filled fractures locally overprint the mineralization indicating the presence of two phases of specularite (Plate 31). The chert unit is not everywhere developed, but where present, is often associated with narrow, high-grade intersections. In rare instances, the mineralized chert is crosscut by zones of specularite–pyrite–chlorite-cemented breccia that are also associated with high-grade uranium mineralization (*e.g.*, 1.76%  $U_3O_8$  over 2.40 m; DDH ML-122, Morgan and Giroux, 2008).

Within the Upper C Zone deposit, uranium mineralization is also developed within Fe-carbonate-altered shear

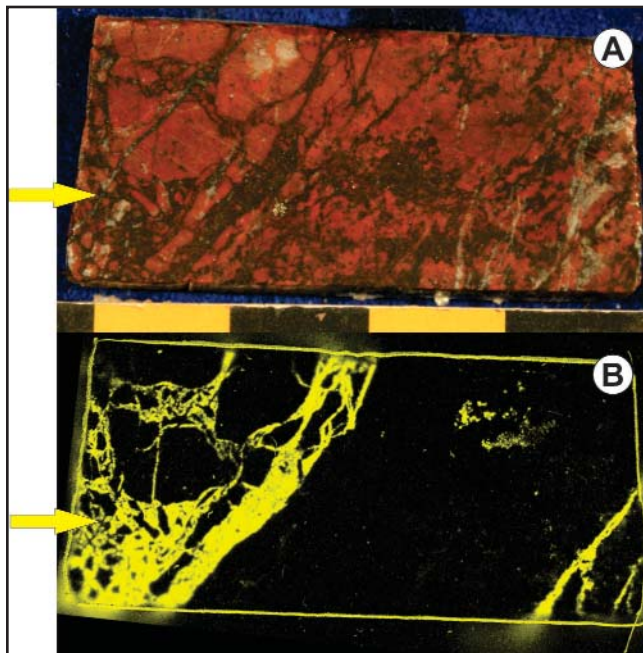


**Plate 31.** A. Hematite-altered jasperoidal chert overprinted by fracturing and brecciation infilled with specularite. This is, in turn, crosscut by a second mm-scale specularite-filled fracture (yellow arrow). B. Autoradiograph of (A) outlining the distribution of radioactivity (yellow) within the sample. Note the highlighted specularite-filled fracture is devoid of any significant radioactivity.

zones. These zones are interpreted as altered mylonites and cataclasites (Eaton *et al.*, 2008). The most significant of these shear zones is the Lower Shear Zone (Plate 32), which is generally less than 10 m wide, and is host to anomalous radioactivity with localized, higher grade, hematitic bands (Plate 33). The Fe-carbonate alteration, locally overprints and replaces earlier hematite alteration, and occurs as metre-scale zones having an intense penetrative fabric. In rare instances, discrete



**Plate 32.** Pervasive Fe-carbonate alteration hosting localized zones of uranium mineralization within the Lower Shear Zone. Note the development of the intense fabric giving the zone a mylonitic appearance, as well as the late crosscutting quartz-carbonate veins. Moran Lake C Zone, DDH ML-56, ~150 m depth.

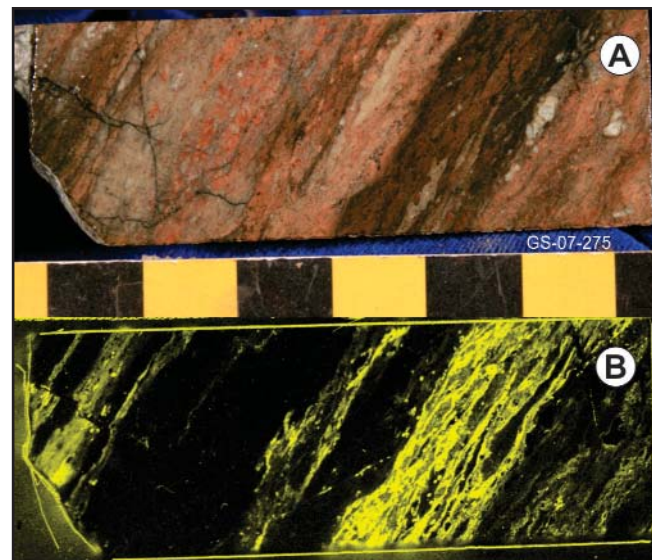


**Plate 33.** A. Pervasive Fe-carbonate alteration hosting anomalous uranium mineralization associated with dark-red hematite-rich bands. B. Autoradiograph of (A) outlining the distribution of radioactivity within the sample (yellow; minus the outline of the sample).

zones of brecciation are observed within the Fe-carbonate alteration and are interpreted to represent the incomplete replacement of earlier brecciation rather than a later breccia event that overprinted the Fe-carbonate alteration. The Fe-carbonate alteration is similar to that seen in the area of the Armstrong deposit (see below; Figure 15), which may represent the strike extension of this style of mineralization to the southwest.

Drilling within the easternmost portions of the Upper C Zone has intersected rare zones of hematite-rich brecciation within conglomerate of the Heggart Lake Formation. This style of mineralization closely resembles the dark-purple, specularite-rich brecciation associated with Phase 2 alteration and mineralization in the underlying Moran Lake Group (Plate 34), and implies that this phase of alteration postdates the deposition of the Heggart Lake Formation. At the core of this mineralized zone, strong hematite alteration obscures the original nature of the host rock but the transition into less altered conglomerate, along the margin of the zone, allows the identification of the original protolith. This mineralization is intruded by a relatively unaltered fine-grained mafic dyke. An autoradiograph from the mineralized zone demonstrates the matrix-hosted nature of the radioactivity (Plate 35). Such examples provide rare evidence that at least portions of the Upper C Zone mineralization postdate the deposition of the structurally overlying sedimentary sequence.

### Petrography

Petrographic examination of select samples from the Upper C Zone further demonstrates the complexity and intergrowth of the various alteration phases in the deposit. Within zones of intense brecciation, little remains in the way of primary textures of the original host rock. Fragments of pale-pink, to orange, to maroon hematite-altered rock observed within the hematitic breccias, contain laths of plagioclase dominated by albite twinning. Such features are interpreted to represent albitic alteration associated with the initial calcium–sodium metasomatism related to early phases of the alteration. The progression from early ‘jig-saw’ brecciation (Plate 36A, B), to well-developed ‘milled’ breccias containing subrounded fragments displaying local alignment (Plate 36C–E), demonstrate the intensity and duration of hydrothermal activity within the system. This is further supported by the local presence of fragments of pre-brecciated material, indicating multiple episodes of



**Plate 34.** Brecciated and mineralized conglomerate of the Heggart Lake Formation. Moran Lake C Zone, DDH ML-82, ~115 m depth.

brecciation within the deposit. The fragments contained within the breccias are generally subangular to subrounded, but ‘milled’ breccias contain rounded fragments <1 cm in diameter, suggesting some mechanical erosion. In addition, some fragments locally show embayed or corroded margins indicative of dissolution by the hydrothermal fluids (Plate 36D, F).

Detailed petrography of the strongly mineralized chert indicates that iron-rich fluids first precipitated magnetite, which was subsequently replaced by specularite (Plate 37). Most of the radioactivity occurs in association with finely disseminated Fe–Ti-oxide minerals and specularite; however, rare uraninite is locally observed along discrete fractures within samples of the hematized chert (Plate 37D). Fractures containing uraninite along their margins are later infilled with carbonate and secondary pyrite, indicating the overall fluid

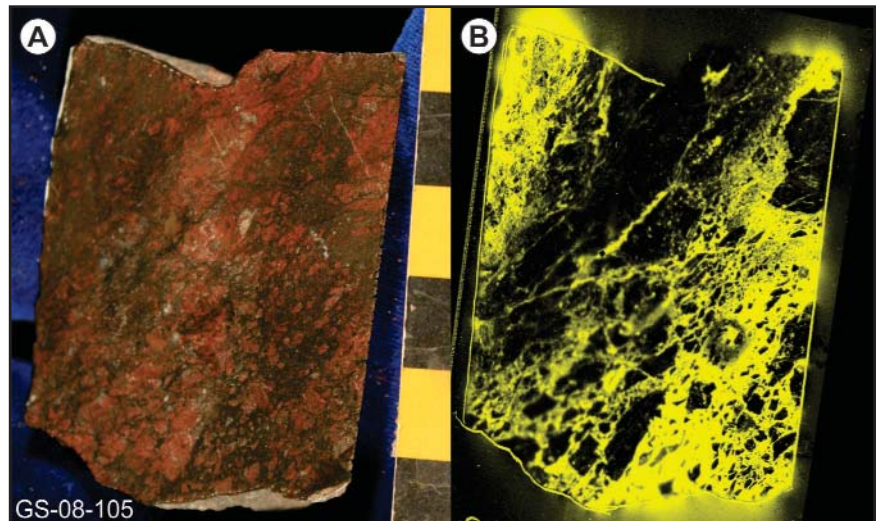


**Plate 35.** A. Pervasive hematite alteration accompanied by specularite-rich brecciation within conglomerate of the Heggart Lake Formation, B. Autoradiograph of (A) outlining the distribution of radioactivity within the sample (yellow; minus the outline of the sample).

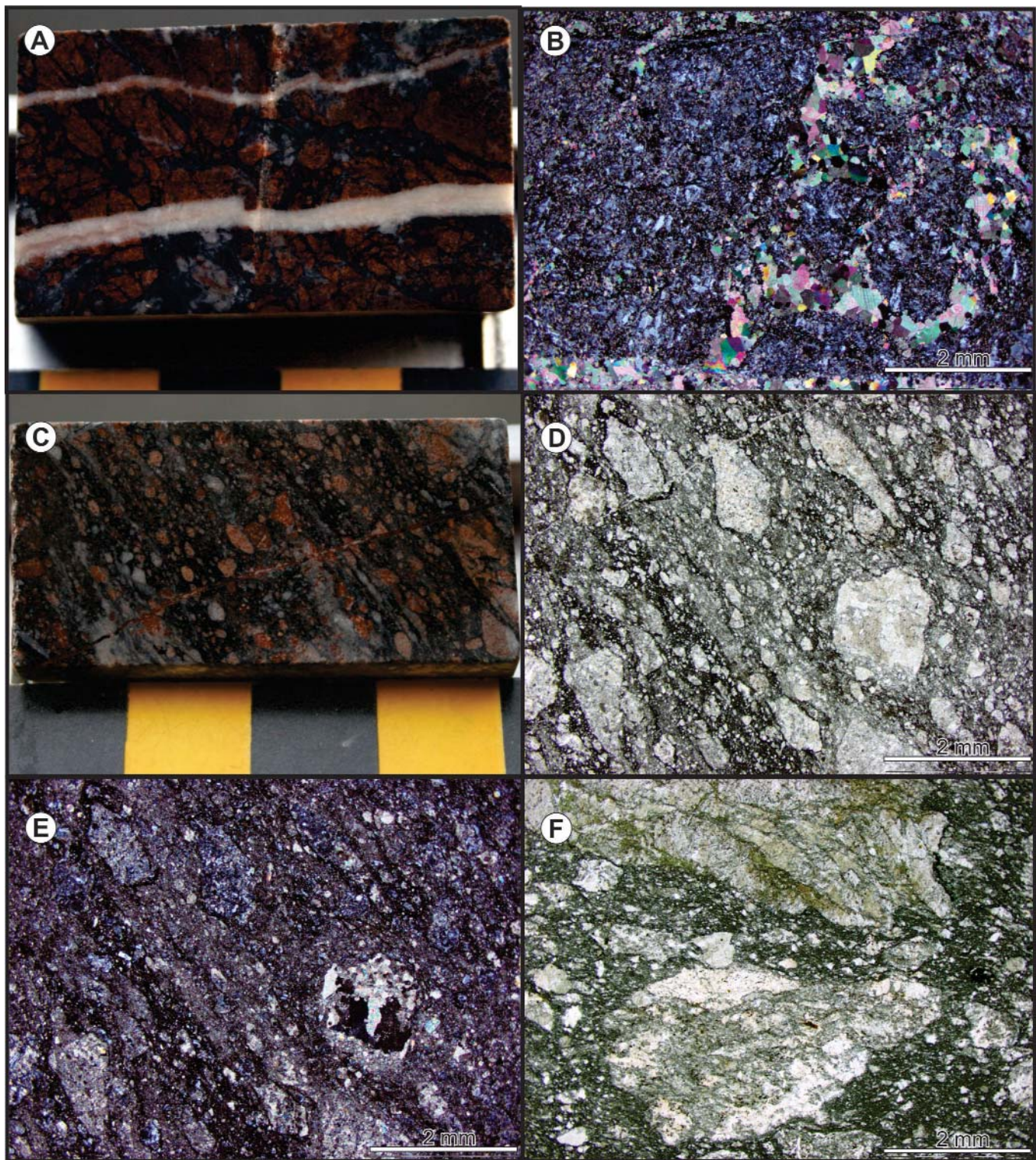


**Plate 36.** *A.* Sample of early 'jig-saw' brecciation of Phase 1 alteration, crosscut by late-stage quartz–carbonate veins, *B.* XPL image from a portion of the brecciation shown in (A), displaying the early fragmentation of the altered mafic volcanic rock characterized by abundant plagioclase displaying albite twining, *C.* Sample of milled breccia displaying subrounded matrix-supported clasts of Phase 1 alteration in a specularite–carbonate-dominated matrix, *D.* PPL image from a portion of (C) displaying the local alignment of fragments within the hydrothermal breccia, *E.* XPL image of (D); note carbonate occurring as both fragments and matrix material, *F.* PPL image highlighting the 'ragged' margins of the fragments within the hydrothermal breccia.

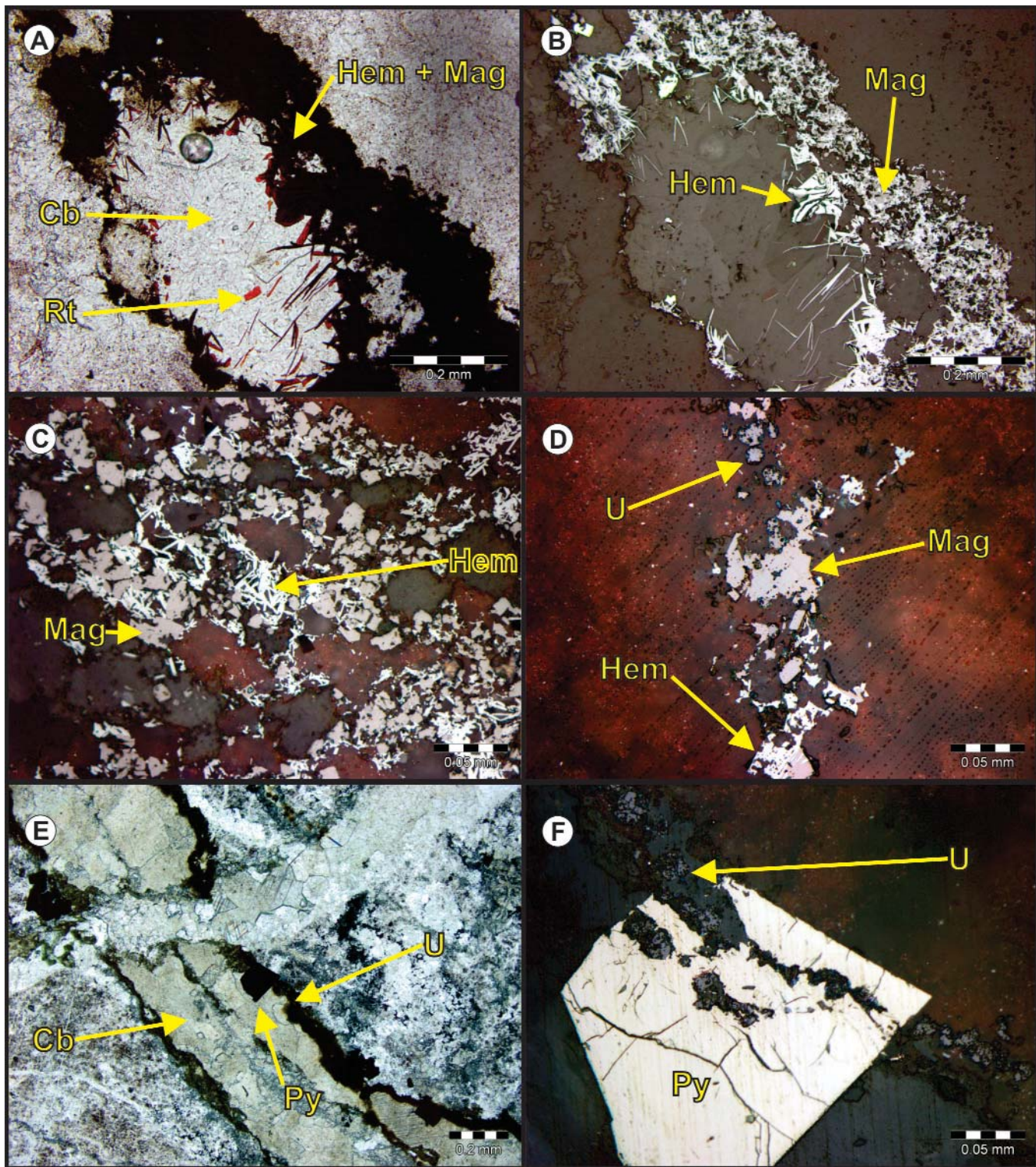


**Plate 37.** A. PPL photomicrograph displaying an uraniferous fracture infilled with magnetite and specularite followed by carbonate and rutile, B. Reflected light image of (A) displaying the distribution of magnetite subsequently replaced by the specularite, C. Close-up reflected-light image displaying the replacement of the magnetite by the bladed specularite, D. Reflected-light image displaying the rare occurrence of well-formed uraninite hosted within a magnetite–hematite-filled fracture, E. PPL image of a fracture lined with uraninite and subsequently infilled with carbonate and euhedral pyrite, F. Close-up view showing euhedral pyrite overgrowing uraninite. Abbreviations: Cb—carbonate, Hem—specularite, Mag—magnetite, Py—pyrite, Rt—rutile, U—uraninite.

evolution within the hydrothermal system (Plate 37E, F). Uranium mineralization is also developed within rare zones of specularite–pyrite–chlorite-cemented breccias, which locally overprint the hematized chert (Plate 38). As with other styles of mineralization, the uranium is developed in association with abundant specularite, but in this instance it lacks development of any significant magnetite.

## ARMSTRONG DEPOSIT

### Local Geology

The Armstrong deposit is located approximately 3.5 km southwest of the Moran Lake C Zone (Figure 15), and was discovered by Crosshair Exploration and Mining in 2006. Initial prospecting and trenching at the deposit identified a north- to northeast-trending shear zone hosting several anastomosing uraniferous fractures within variably altered pillow basalt of the Joe Pond Formation (Morgan *et al.*, 2007). The mafic volcanic rocks consist mostly of interlayered volcanic flows, cut by several mafic dykes. The pillow basalt is interbedded with, or structurally juxtaposed against, black, locally sulphidic, argillite and lesser grey siltstone and chert, which resembles rocks of the underlying Warren Creek Formation. The argillite unit is bound on both sides by mafic volcanic rocks, and is variably strained. The entire sequence is cut by numerous chloritic shear zones, which are preferentially developed within the argillite unit or along its contact with adjacent pillow basalt. Within the mafic volcanic rocks these shear zones are characterized by the presence of disrupted quartz–carbonate vein fragments hosted within a chlorite–sericite-rich matrix.

Diamond drilling at the Armstrong prospect targeted a northeast-trending electromagnetic conductor that is situated to the immediate west of the initial showing under an adjacent

pond. This drilling intersected zones of strong mineralization within altered graphitic argillite and lesser chert close to their contact with the underlying mafic volcanic rocks. Both the pillow basalt and argillite units display similar hematite and associated Fe-carbonate–albite alteration. The alteration within the argillite is generally more extensive, and this unit hosts most of the uranium mineralization within the deposit. The best drill results from the mineralized zone include 0.20%  $U_3O_8$  over 9.45 m within a zone that has a defined strike length of 300 m (Morgan and Giroux, 2008). The deposit remains open both along strike and at depth, and more work is required to better define the extent of mineralization within this area.

### Mineralization and Associated Alteration

The metasedimentary and mafic volcanic rocks display variably developed hematite, Fe-carbonate and albite alteration, which overprints an existing chlorite–sericite assemblage (Figure 19). As in the C Zone, this alteration can be divided into several phases summarized in Table 6. The development of a pale-beige Fe-carbonate–albite alteration, along with the associated pinkish-red hematite alteration and accompanying uranium mineralization, appear to have an

**Table 6.** Summary of the alteration and associated mineralogy for the Armstrong deposit; based on field mapping and petrography

Associated Alteration Minerals	
Phase 1	Hematite $\pm$ Fe–Ti oxides $\pm$ uranium mineralization $\pm$ Fe-carbonate–albite
Phase 2	Chlorite
Phase 3	White carbonate veining

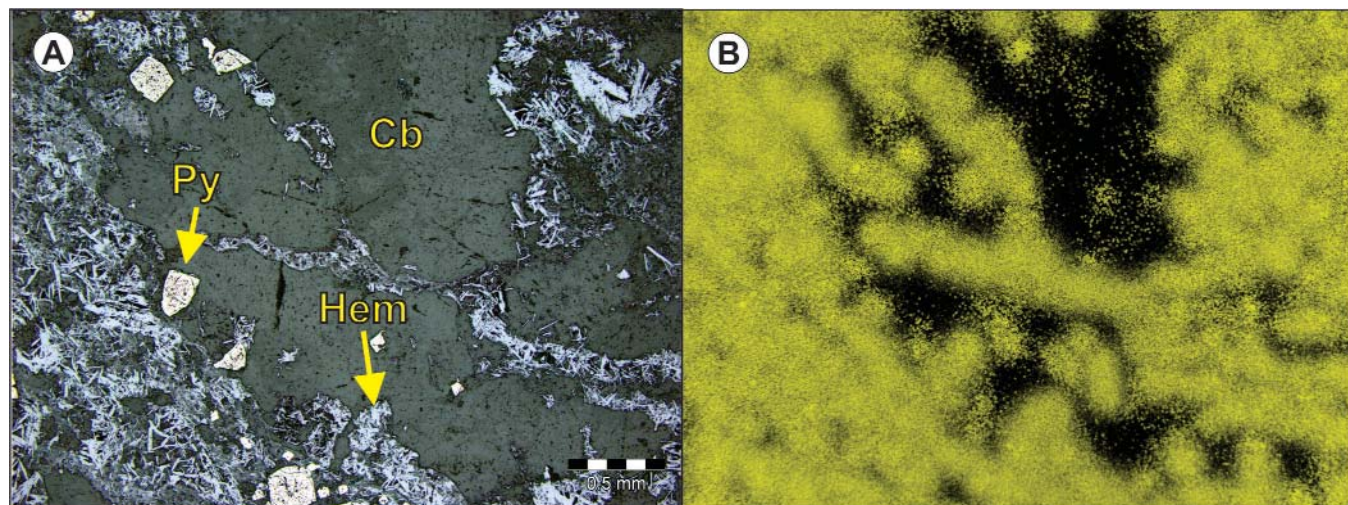


**Plate 38.** A. Reflected-light image of mineralized, specularite (Hem)-rich breccia containing millimetre-scale fragments of carbonate (Cb) along with subhedral pyrite (Py). B. Autoradiograph of the region shown in (A) showing the association of the radioactivity (yellow) with the development of the specularite.

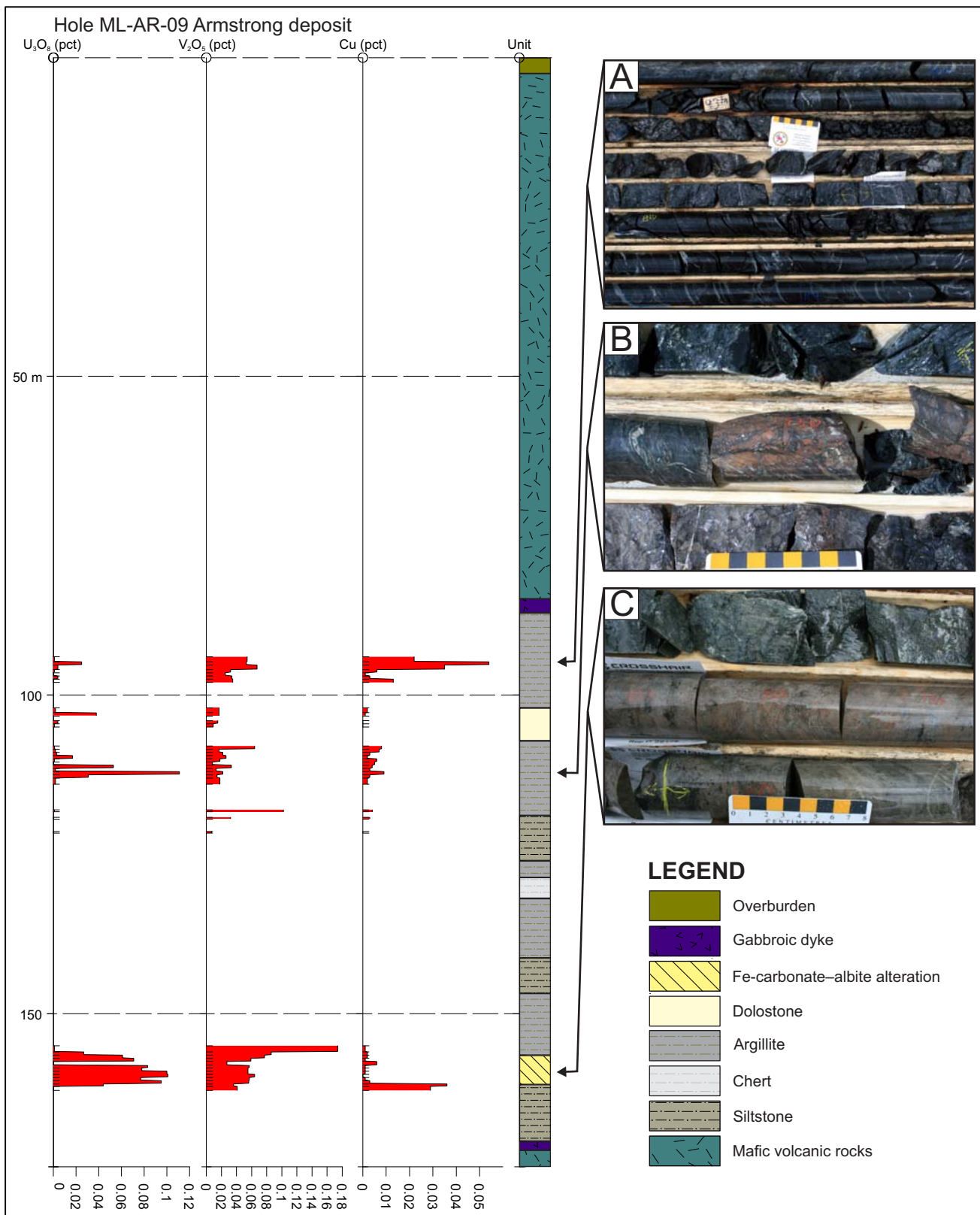


**Figure 19.** Drill log for hole ML-AR-09 from the Armstrong deposit, outlining the distribution of uranium, vanadium and copper mineralization in association with Fe-carbonate–albite-altered shear zones within the metasedimentary rocks; all values are listed in weight percent (data from Gillies et al., 2009). A. Relatively barren unaltered, argillite, B. Discrete mineralized zone of albitic alteration overprinted by hematite-rich brecciation, C. Uraniferous Fe-carbonate–albite alteration zone.

overriding structural control. The hematitic alteration is generally surrounded by a broader halo of pale-beige Fe-carbonate–albite alteration, as seen in Plate 39; however these alteration zones are not always associated with uranium mineralization. The Armstrong deposit contains a similar style of Fe-carbonate–albite alteration to that seen in the Upper C Zone, but lacks the development of extensive zones of hematite-rich brecciation. Mineralized intervals within the deposit are locally reported to contain elevated V, Ag and Cu in association with the uranium mineralization (e.g., drillhole ML-AR-27: 0.14%  $U_3O_8$ , 0.26% V, 15.2 g/t Ag and 0.45% Cu over 3.6 m; Gillies *et al.*, 2009).



**Plate 39.** Pinkish-red hematite–carbonate–albite alteration flanked by pale-beige Fe-carbonate–albite alteration within altered argillite; note the highly disrupted nature of the host rock due to the structural control of the mineralization. Armstrong deposit, DDH MLAR-04, ~280 m depth.

Although the host rocks surrounding the uranium mineralization display a strong penetrative fabric, autoradiographs of the mineralization suggest the mineralization is not affected by the same degree of deformation. However, local 0.5- to 1.0-m-wide, strongly foliated, shear zones separating the pillow basalt from adjacent argillite host fragments of the Fe-carbonate–albite alteration. This suggests that the alteration is at least locally overprinted by post-mineralization deformation. Mineralized Fe-carbonate–albite alteration is crosscut by dark-green chloritic fractures, implying that more than one generation of chlorite alteration is also present. The final stage of alteration is marked by the development of white carbonate veining, similar to that seen along strike in the Upper C Zone deposit. Locally, mafic dykes cut the entire sequence and these appear to postdate the development of the foliation within the mafic volcanic rocks, but are locally affected by the development of network-style white carbonate veins.

### Petrography

Autoradiographs of mineralized samples suggest that the uranium mineralization occurring in association with the Fe-carbonate–albite alteration is primarily developed as fine-

grained disseminations throughout the alteration (Plate 40A, B). In contrast, the more strongly mineralized zones associated with the brick-red hematite–albite alteration contain fracture-hosted mineralization, which occurs in association with specularite, pyrite and trace chalcopyrite (Plate 40C, D). Within the zones of Fe-carbonate–albite alteration, uranium mineralization is commonly associated with finely disseminated Fe–Ti-oxide minerals (Plate 40E–H), which are also associated with anomalous values of V, Cu and Pb, based on SEM imagining. The contrast in the styles of mineralization between the Fe-carbonate–albite and the hematite–albite alteration may be related to rheology contrasts between the two different assemblages. The latter is more competent and capable of sustaining fracture-hosted mineralization.

## OTHER URANIUM OCCURRENCES

### Croteau Lake Prospect

The Croteau Lake prospect consists of numerous mineralized boulders defining two discrete boulder trains of brecciated iron formation, along with rare occurrences of anomalous radioactivity, in outcrop near the western end of Croteau Lake (Figure 15; Morgan *et al.*, 2007). This area currently represents the western extent of known uranium mineralization within the Moran Lake Group. The mineralization identified in outcrop is hosted within the Warren Creek Formation, dominated by black shale, slate, and grey to pale-green siltstone along with minor chert and iron formation. As noted by North and Wilton (1988), the development of iron formation is generally concentrated within the upper portions of the Warren Creek Formation, and occurs close to its unconformable contact with the overlying Bruce River Group. The mineralized boulders resemble the iron formation of the Warren Creek Formation and are believed to be of local derivation.

The mineralized boulders are located close to the unconformable contact between the Moran Lake and Bruce River groups, but the high-grade uranium mineralization is restricted to rocks that resemble those of the Moran Lake Group. Anomalous radioactivity (<250 cps) has locally been observed along metre-scale shear zones crosscutting basal conglomerate of the Bruce River Group, but this is limited in its distribution and may represent secondary remobilization of earlier uranium mineralization. The highest grade boulders in the area consist of intensely brecciated magnetite-bearing iron formation, which have locally returned grab sample values of up to 2.09%  $U_3O_8$ , along with elevated values of V, Cu, Ag and Au (Morgan *et al.*, 2007). Polished thin sections and associated autoradiographs from mineralized boulders of iron formation indicate that the uranium occurs proximal to zones of magnetite within the broader hematitic alteration (Plate 41). Although the Warren Creek Formation is associated with abundant syn-sedimentary sulphides, none of the outcropping

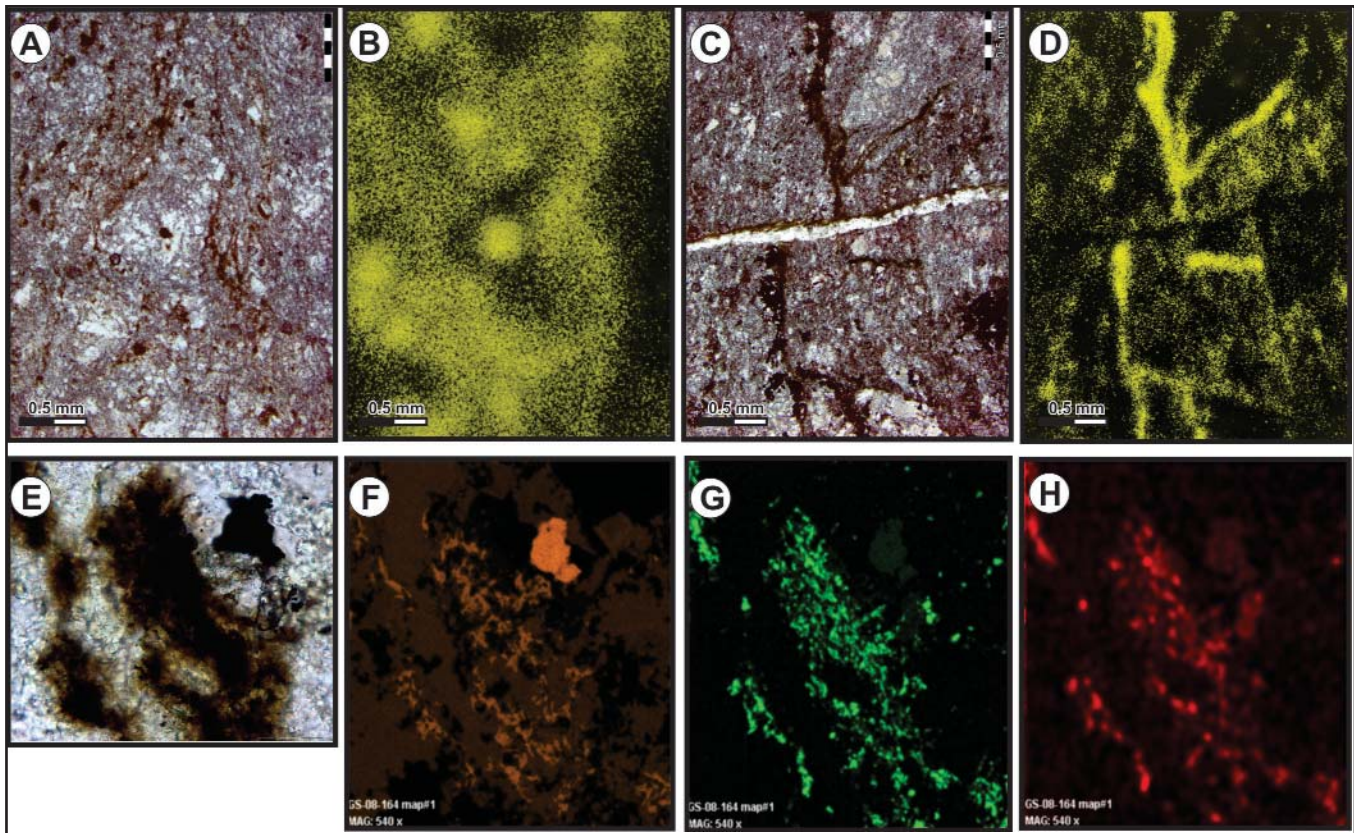


**Plate 40.** *A.* PPL photomicrograph of mineralized Fe-carbonate–albite alteration containing finely disseminated Fe–Ti oxide minerals throughout. *B.* Autoradiograph of (A) outlining the distribution of radioactivity (yellow). *C.* Hematite–albite alteration crosscut by mineralized fractures containing specularite, and trace chalcopyrite. *D.* Autoradiograph outlining the distribution of radioactivity (yellow) in (C). *E.* PPL photomicrograph of area containing anomalous radioactivity in association with the development of Fe–Ti oxide minerals (field of view approximately 2.5 mm in width). *F.* SEM image outlining the distribution of Fe within (E). *G.* SEM image outlining the distribution of Ti within (E). *H.* SEM image outlining the distribution of U within (E).

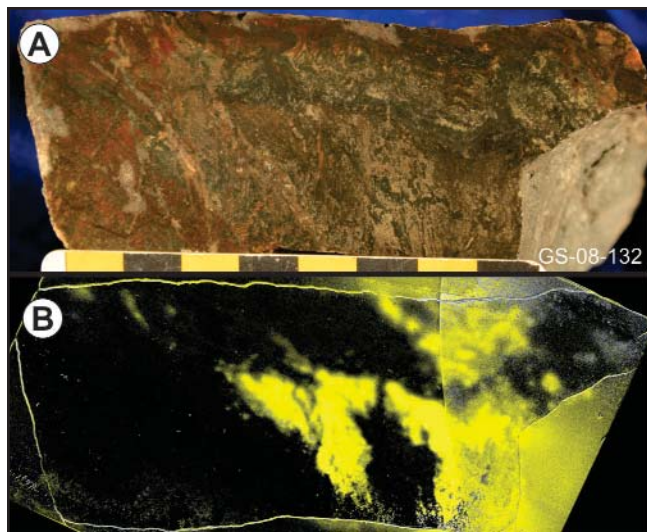


**Plate 41.** *A.* Mineralized boulder from the Croteau Lake prospect containing 0.07%  $U_3O_8$ . *B.* Corresponding autoradiograph highlighting the distribution of radioactivity within the sample (yellow).

gossan zones within the area are known to host any significant radioactivity. Limited drilling carried out on the prospect in 2008 by Crosshair Exploration intersected iron formation in a number of holes but failed to identify the source of the radioactive boulders (Eaton *et al.*, 2008).

In anomalously radioactive outcrops of the Warren Creek Formation, the iron formation is locally interbedded with pale-grey–green siltstone. Local evidence exists for the influx of iron-rich fluids along network-style fractures crosscutting the sedimentary units; these fractures are predominantly hematite-rich and also contain patchy magnetite, but lack associated uranium mineralization (Plate 42). Similarly, barren hematite–magnetite-filled fractures are observed crosscutting outcrops of brecciated chert and associated iron formation (Plate 43). The occurrence of both mineralized and barren hematite–magnetite-brecciated iron formation imply that there are multiple iron formation units within the stratigraphy, only some of which are mineralized, or alternatively the uranium mineralization is confined to structures within areas yet to be identified.



**Plate 42.** Pale-beige siltstone of the Warren Creek Formation displaying an influx of hematite and magnetite along brittle network-style fractures; Croteau Lake prospect.

Petrographic work shows that the uranium mineralization occurs as very fine-grained disseminations in association with the Fe–Ti oxide minerals, which are also accompanied by carbonate alteration. This alteration overprints a magnetite–chlorite assemblage within the original iron formation (Plate 44). Plate 45 displays hematite and accompanying Fe–Ti oxide minerals, which are associated with radioactivity as indicated by autoradiographs, along with rare relict magnetite preserved within the alteration (Plate 45B). Colloform textures displayed by the hematite alteration enveloping an earlier pyrite phase along with other minerals further demonstrates the complex alteration present within these systems (Plate 45C, D).

#### Fish Hawk Lake North and Whiskey Jack Prospects

Work carried out by Santoy Resources identified localized uranium mineralization within an outlier of the Moran



**Plate 43.** Highly disrupted chert and interbedded iron formation crosscut by barren hematite–magnetite-filled fractures, highlighting the mobilization of iron-rich fluids; Croteau Lake prospect.

Lake Group, located in the area east of Fish Hawk Lake (Figure 15). In this area, mineralization occurs near the faulted contact between Archean basement rocks in the southeast, and siltstone, shale and minor chert of the Moran Lake Group to the northwest. The uranium mineralization is hosted within metasedimentary rocks of the Warren Creek Formation. This mineralization occurs as both fracture-filling material in siliceous units, as well as fine-grained disseminations within more permeable siltstone (Plate 46). There is no evidence of any elevated radioactivity at the contact between the Archean basement rocks and the Moran Lake Group in the limited drillcore from the area, although the underlying basement rocks locally host mineralization elsewhere (see Section, Uranium Mineralization within Archean Basement Rocks). However, a trench immediately uphill from one of the drillhole collars does contain mineralization within the Moran Lake

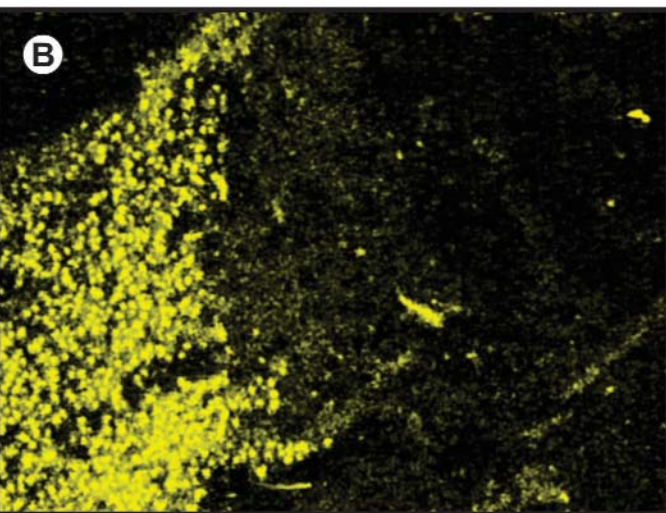
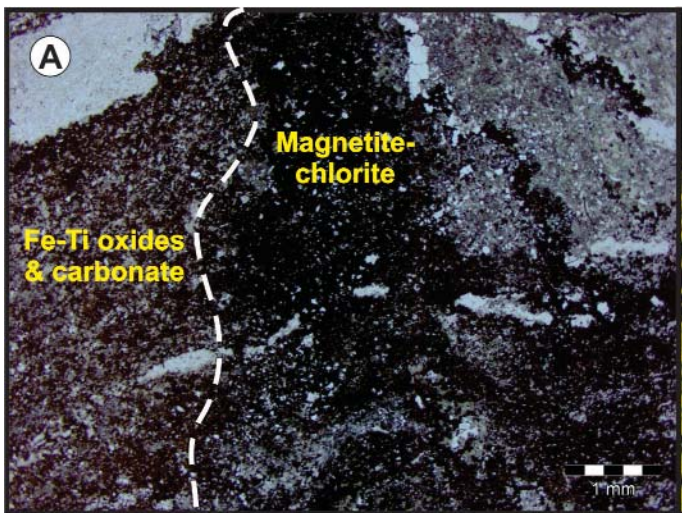


**Plate 44.** A. PPL photomicrograph from the sample in Plate 41, displaying the development of finely disseminated Fe–Ti oxide minerals in association with carbonate alteration that overprints the magnetite–chlorite assemblage, B. Accompanying autoradiograph outlining the distribution of the radioactivity (yellow) in association to the Fe–Ti oxide alteration.

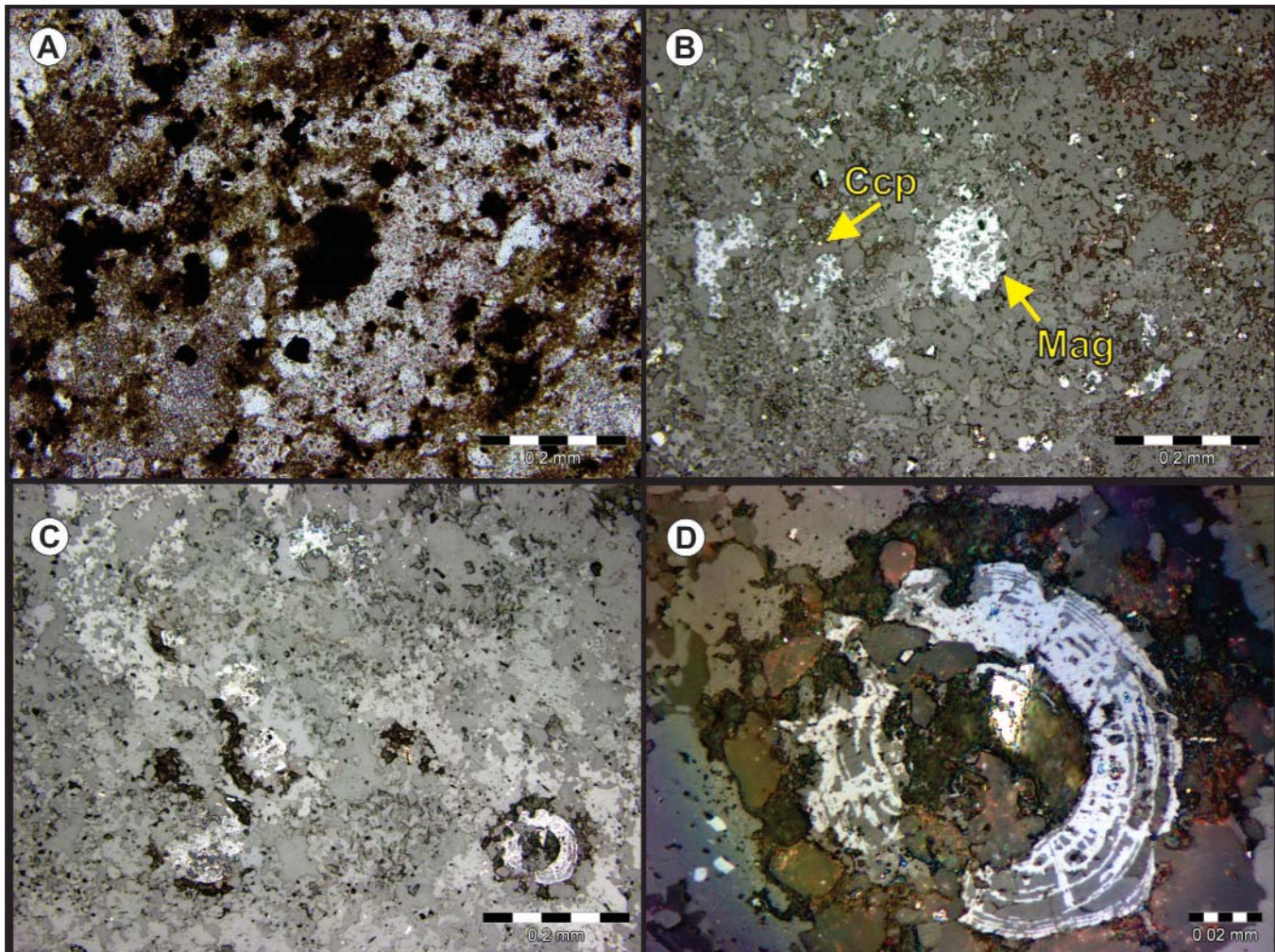


**Plate 45.** *A.* PPL photomicrograph displaying the finely disseminated Fe–Ti oxides associated with the anomalous radioactivity, *B.* Reflected-light image of (A) displaying the finely disseminated Fe–Ti oxides enveloping primary magnetite (Mag) along with minor chalcopyrite (Ccp), *C.* Reflected-light image of hematite associated with uranium mineralization locally displaying a colloform texture (lower right corner), cored by an earlier pyrite phase, *D.* Magnified view of colloform hematite growth shown in (C).

Group. Channel sampling of the trench produced up to 0.04%  $U_3O_8$  and 0.49% Cu over 14 m (Willett *et al.*, 2008), whereas individual grab samples have assayed up to 0.22%  $U_3O_8$ , 2.25% Cu and 162 ppb Au. These rocks are inferred to be immediately adjacent to the structural contact with the underlying Archean basement rocks (Figure 20).

Prospecting in the immediate area has identified mineralization farther to the north at the Whiskey Jack prospect (Figure 15). This occurrence is located some 650 m from the inferred structural contact with underlying basement rocks, and is also hosted by metasedimentary rocks of the Moran Lake Group. Here, the uranium mineralization, which locally produced assays up to 0.06%  $U_3O_8$ , is suggested to be devel-

oped within the hinge of a regional fold structure based on bedding attitudes within the area (Willett *et al.*, 2008).

Uranium mineralization hosted by the Moran Lake Group in the Fish Hawk Lake area is locally accompanied by anomalous Cu, Ag and Au values, which is not observed in association with uranium mineralization in the underlying Archean basement rocks. The mineralization within the Moran Lake Group is not associated with any obvious alteration aside from the intense chlorite–pyrite alteration typical of the Warren Creek Formation on a regional scale. Although this mineralization is sporadic it demonstrates the potential of the Warren Creek Formation on a regional scale to host uranium mineralization.

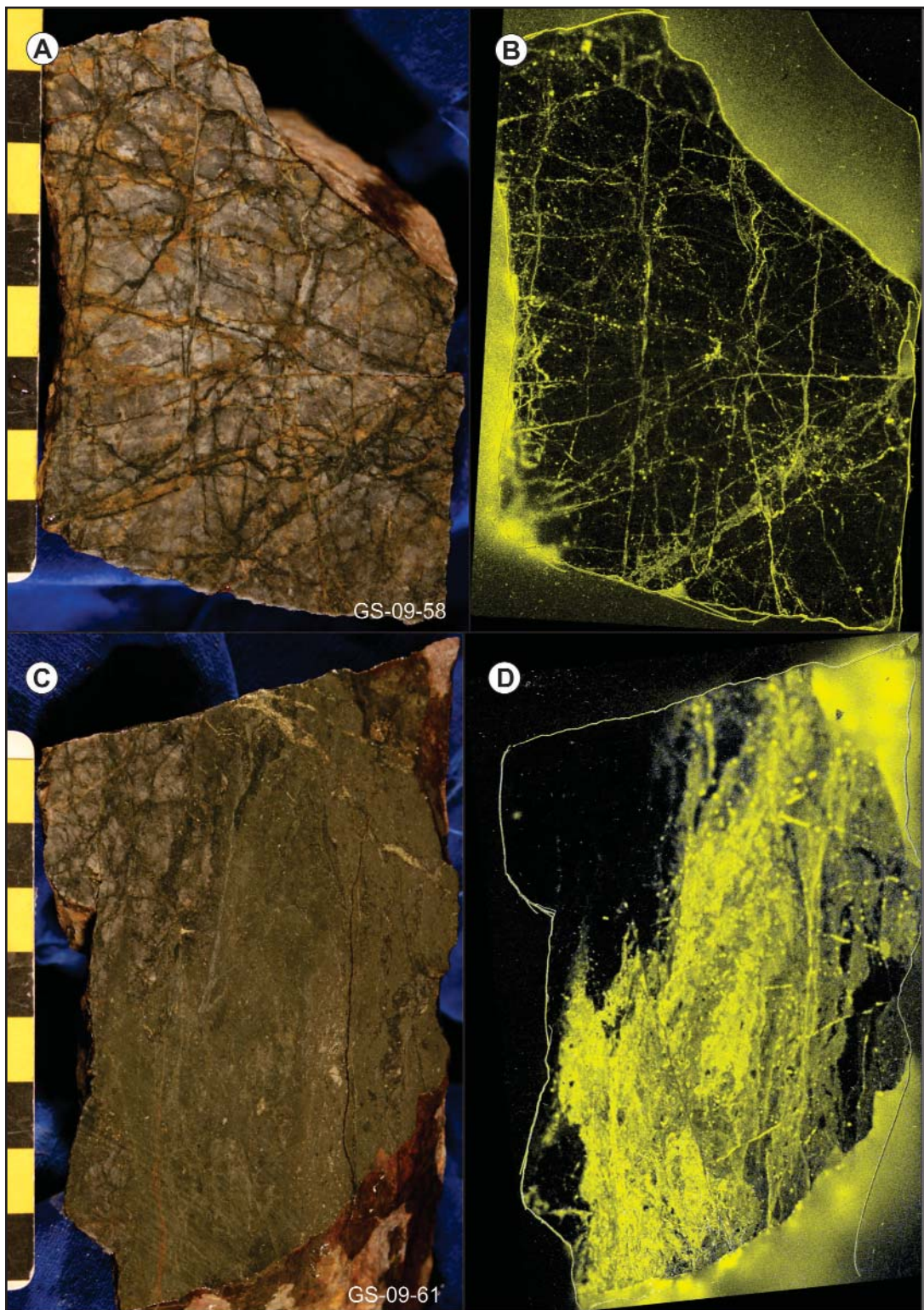


**Plate 46.** A. Hand sample of highly fractured chert containing 0.08%  $U_3O_8$  and 964 ppm Cu, crosscut by network-style fractures infilled with iron-carbonate and chlorite, B. Autoradiograph of the hand sample shown in (A) displaying fracture-hosted radioactivity (yellow), C. Hand sample of pale-green siltstone containing 0.22%  $U_3O_8$ , 2.25% Cu and 162 ppb Au; note siliceous material similar to that in (A) in upper left hand corner of the sample, D. Autoradiograph of (C) displaying finely disseminated radioactivity within the pyriteiferous siltstone; note siliceous material in upper left corner is devoid of any significant radioactivity.

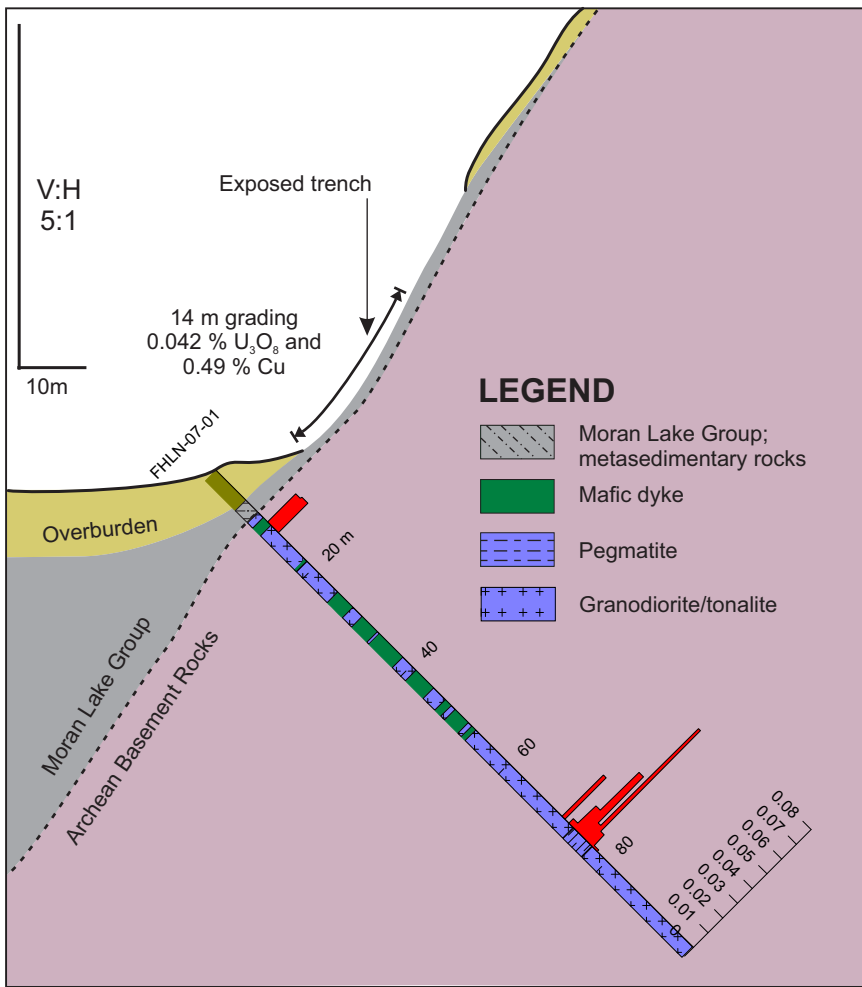


**Figure 20.** Schematic cross-section outlining the location of anomalous uranium values within rocks of the Moran Lake Group, which are juxtaposed with Archean basement rocks in the region of the Fish Hawk Lake North prospect (assay data from Willett *et al.*, 2008).

### Area 51 Prospect

Uranium mineralization within the Warren Creek Formation is also found north of Moran Lake at the Area 51 prospect (Figure 15). This zone of elevated radioactivity was explored by Crosshair Exploration and Mining in 2006 (Morgan *et al.*, 2007), but was first noted by Perry (1979) who termed it the Anomaly No. 8 prospect. In his report, Perry (*op. cit.*) noted the occurrence of a weak airborne radiometric response over the area. Follow-up ground work identified anomalous uranium mineralization within an approximate 50-m-thick dolostone unit situated immediately above Archean basement rocks; this zone was traced along strike for up to 700 m and locally produced assay values of up to 64 ppm U. The mineralized dolostone unit is, in turn, overlain by sulphidic black shale of the Warren Creek Formation, with the upper portions of the dolostone unit adjacent to the overlying shale containing the strongest radioactivity (Perry, 1979).

An airborne radiometric survey flown by Crosshair in 2005 produced a large response over the same area, measuring approximately 1.5 km in length. Subsequent trenching exposed the unconformable contact between the tonalitic rocks of the KIS and the overlying Moran Lake Group. The radioactivity within the area is confined to the dolostone unit of the Moran Lake Group, from which grab samples produced assay values of up to 0.13% U<sub>3</sub>O<sub>8</sub>. Crosshair carried out diamond drilling in the area, which intersected wide zones of low-grade uranium mineralization along a strike length of 1.2 km. The best intersection from this drilling returned 0.01% U<sub>3</sub>O<sub>8</sub> over 24.66 m (Morgan and Giroux, 2008).

Within the Area 51 prospect, the dolostone is confined to the core of a broad, southeast-plunging synclinal structure. It is commonly fractured and re-cemented, or partially replaced by quartz and locally transected by quartz and calcite veins (Ryan, 1984). The dolostone is, in turn, overlain by sulphidic black shale, and the mineralized dolostone pinches out along strike towards the southeast and at depth toward the south. No anomalous radioactivity is noted within the underlying Archean basement rocks or along the unconformable contact in the area.

The dolostone unit is typically pale grey and massive, but also contains rare thin, millimetre-scale laminations that display metre-scale slump folds. Locally, the dolostone appears to be interbedded with thin-laminated dark-grey siltstone; contacts between the two units are generally sharp. The dolostone commonly displays evidence of syn-sedimentary brecciation due to possible slumping, with the breccia matrix primarily consisting of grey siltstone and black shale along with varying amounts of pyrite. Both the brecciation and slump features are confined to the upper portions of the dolostone unit. This disrupted portion of the dolostone unit is assumed to have greater permeability, which is exploited by the uraniferous fluids, thus accounting for the higher levels of radioactivity present in this area (Plate 47).

### Canico Anomaly Nos. 15 and 16 Prospects

The Canico Anomaly Nos. 15 and 16 prospects occur at the southwestern end of a *ca.* 6.5 km long mineralized corri-



**Plate 47.** Mineralized and locally brecciated dolostone immediately overlain by sulphidic black shale hosting abundant quartz–carbonate veining; note mineralization is confined to the disrupted portions of the dolostone unit. Area 51 prospect, DDH MLA51-03, ~20 m depth.

dor within the Moran Lake Group, extending southwest from the region of the Moran Lake C Zone deposit (Figure 15). Along this trend, uranium mineralization is primarily hosted within pillow basalt of the Joe Pond Formation. At the Anomaly Nos. 15 and 16 prospects, uranium mineralization is hosted within sheared basalt that has variably developed pyrite and hematite–carbonate–albite alteration, producing rusty-weathering gossan zones at surface (Perry, 1979; Wilton, 1996). The uranium mineralization is hosted within discrete fractures that display an erratic distribution, and is inferred to be epigenetic (Perry, 1980; Wilton, 1996). This mineralization is also accompanied by minor chalcopyrite. Within the Anomaly No. 16 prospect, three subparallel zones measuring from 50 to 150 m wide and trending approximately east–west were identified, from which assay values of up to 2.02%  $U_3O_8$  were obtained (Perry, 1979). More recent mapping in the area suggests that this zone is part of the larger scale, northeast-trending mineralized corridor within the area, and likely represents the strike extension of mineralization developed in the area of the Armstrong deposit. This zone also contains locally developed hematite-rich breccias associated with uranium mineralization, which are similar to those seen in the Upper C Zone deposit.

Mineralization at the Anomaly No. 15 prospect is developed near the unconformity with basal conglomerate of the overlying Heggart Lake Formation, which locally hosts uranium mineralization in the form of narrow east–west-trending fractures filled with specularite (see Section, Uranium Mineralization within the Bruce Lake Group). The proximity of the uranium mineralization to the unconformable contact led Perry (1979) to conclude that the contact was the main control on the development of the mineralization. He interpreted the occurrences within the underlying basaltic units as the erosional remnants of unconformity related mineralization; how-

ever, drilling within the area has failed to intersect any significant uranium mineralization along the basal contact of the Heggart Lake Formation. The limited drilling carried out by Brinex in 1979 did however intersect minor hematite–carbonate–albite alteration in association with anomalous radioactivity, which assayed up to 0.27%  $U_3O_8$  over 0.20 m (Perry, 1979). This alteration is characteristic of that observed along the *ca.* 6.5 km mineralized trend and is inferred to have a primary structural control.

The development of the alteration within the basalt is associated with a decrease in the overall magnetic susceptibility of the unit proximal to uranium mineralization, suggesting the destruction of primary magnetite within the basalt by the oxidizing uraniferous fluids, as suggested by Wilton (1996). As seen elsewhere along the trend, the alteration is complex, displaying several generations of both Fe–carbonate and hematite–albite alteration, which are separated by gradational or diffuse contacts with the surrounding unaltered basalt. As in the Armstrong deposit, the host rock is overprinted by early pale-beige to pink Fe–carbonate–albite and variably developed, pale-pink hematite–albite alteration, both of which are locally observed overprinting each other suggesting a synchronous relationship (Plate 48). This mineralization is subsequently overprinted by chlorite-rich shear zones, which are common throughout the region.

### Boiteau Lake Prospect

In 2008, Bayswater Uranium discovered mineralization within the area of Boiteau Lake (see Boiteau Lake Anomaly

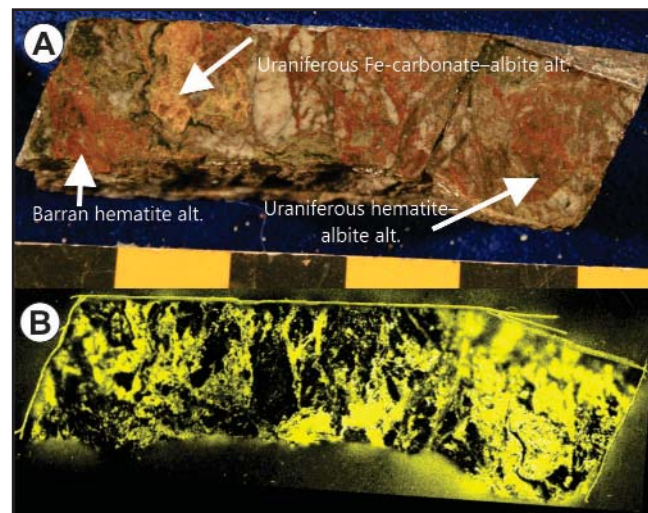


**Plate 48.** A. Sample GS-08-05; variably altered hand sample of Joe Pond basalt taken from a mineralized interval assaying up to 0.32%  $U_3O_8$ . Sample displays the complex nature of the Fe–carbonate–albite and hematite–albite alteration, B. Autoradiograph of (A) displaying the distribution of radioactivity within the sample (yellow).

1-4; Figure 15). This represents the northeastern extent of known uranium mineralization within the Moran Lake Group. Anomalous radioactivity was first noted in the region by Perry (1980b), close to minor discontinuous lenses of chert within the mafic volcanic sequence of the Joe Pond Formation. Four separate occurrences of uranium mineralization were discovered by Bayswater Uranium during follow-up work on airborne radiometric anomalies (Fraser *et al.*, 2009). The uranium mineralization is hosted within sheared mafic volcanic rocks and interbedded, or structurally interleaved, chert and siltstone units. In general, these zones seem similar to those in the southwest of the Moran Lake region. Mineralization is interpreted to be structurally controlled, and is associated with the development of carbonate alteration.

Several major northeast-trending topographic lineaments were noted within the area (*e.g.*, Ryan, 1984). The mineralization is locally sited along east-northeast-trending faults, which are interpreted to be splays off these main northeast-trending structures, which are unmineralized (Fraser, 2010). The highest levels of radioactivity are hosted in sulphidic siltstone and chert that is either interbedded or tectonically interleaved with adjacent basalt of the Joe Pond Formation. Locally, the siltstone unit is affected by pervasive Fe-carbonate alteration in association with uranium mineralization, which is also accompanied by elevated sodium values, indicating albitic alteration. This alteration is associated with finely disseminated uranium mineralization that occurs throughout the Fe-carbonate alteration (Plate 49). Samples containing elevated uranium locally have anomalous Zr (up to 3420 ppm), which is a feature common to some occurrences in the Aillik Group (*cf.* Evans, 1980; *see* Section, Uranium Mineralization within the Allik Group). The chert, which is interbedded with the siltstone unit, displays a contrasting style of mineralization in which most of the radioactivity is hosted within pyrite-rich fractures that crosscut the siliceous material (Plate 50). This style of mineralization closely resembles that seen within the rocks of the Warren Creek Formation in the vicinity of Fish Hawk Lake, with the more permeable units hosting higher grade, finely disseminated, mineralization and the more siliceous units hosting lower grade, fracture-hosted mineralization.

## GEOCHRONOLOGICAL CONSTRAINTS

The age of formation for the Moran Lake Group is not well defined by U-Pb geochronology, primarily because it contains few units suitable for dating. Basal units of the Moran Lake Group unconformably overlie the *ca.* 3000 Ma Archean basement rocks, and are not intruded by the *ca.* 2200 Ma Kikkertavak dykes (*cf.* Cadman *et al.*, 1993; Wilton, 1996). This indicates that the maximum depositional age for the Moran Lake Group is younger than 2200 Ma. The unit is

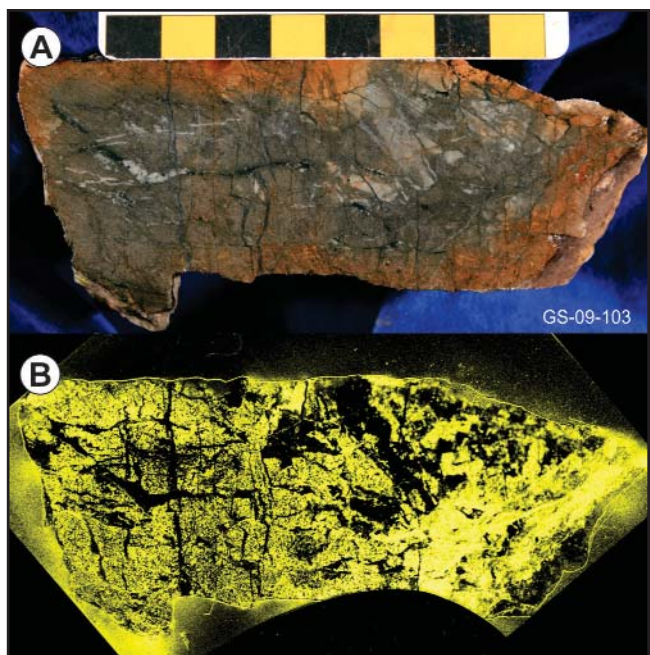


**Plate 49.** A. Hand sample displaying pervasive Fe-carbonate alteration developed within a siltstone unit subsequently overprinted by barren, white carbonate alteration and chlorite-pyrite-filled fractures; sample contains 0.31%  $U_3O_8$ . B. Autoradiograph of (A) outlining distribution of radioactivity (yellow).

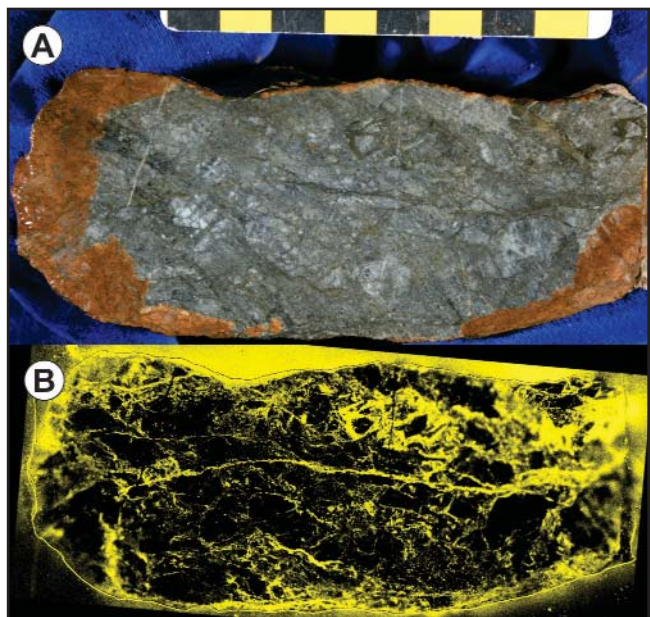


**Plate 50.** A. Hand sample containing 0.17%  $U_3O_8$  associated with extensive brittle fracturing, infilled with pyrite and minor quartz. B. Autoradiograph outlining the fracture-hosted radioactivity (yellow) in (A).

unconformably overlain by the *ca.* 1850 Ma Heggart Lake Formation (Sparkes *et al.*, 2016; *see* Section, Uranium Mineralization within the Bruce River Group), providing a possible time span of some 360 Ma for the deposition of the Moran Lake Group. However, if the time constraints obtained for the deposition of the correlative Post Hill Group are applicable, this would suggest that the Moran Lake Group formed between *ca.* 2200–2000 Ma (*see* Section, Uranium Mineralization within the Post Hill Group).

Kontak (1980) proposed an age of *ca.* 1540 Ma for the formation of the mineralization within the Upper C Zone, based on Pb–Pb uraninite ages that ranged from 1560–1470 Ma. The recognition of mineralization locally developed within the Heggart Lake Formation, immediately overlying the Upper C Zone alteration, suggests that at least some phases of this alteration postdate the deposition of the Heggart Lake Formation. Grenvillian deformation within the region further complicates the paragenesis of the mineralization by potentially remobilizing earlier uranium mineralization. An attempt was made to date a gabbroic intrusive, which crosscuts pillow basalt of the Moran Lake Group (DDH ML-A1-07, 17.10–23.50 m; Morgan *et al.*, 2007); however, the sample did not contain any suitable phases for U–Pb geochronology.

## GEOCHEMISTRY

Most of the uranium occurrences within the Moran Lake Group are hosted within the upper portions of the stratigraphic sequence, notably in pillow basalt of the Joe Pond Formation (Figure 15). This unit consists of subalkaline, tholeiitic basalt that displays a MORB-like chondrite-normalized REE pattern (Wilton, 1996). The pillow basalts of the Joe Pond Formation display minor geochemical variations

between the individual occurrences with respect to their trace-element concentrations, but, in general, the unit displays consistent major-element trends throughout the region. The host rocks to mineralization in the Moran Lake C Zone–Anomaly No. 15 area plot within the subalkaline basalt field of Winchester and Floyd (1977; Figure 21A) and display MORB-like signatures (Figure 21B); samples collected as part of this study plot in the same general area as other reported samples from the Moran Lake Group (*e.g.*, Wilton, 1996). Despite the hematite–carbonate–albite alteration developed within the rocks of the Joe Pond Formation, both the mineralized and unmineralized samples from the basaltic unit display similar trace-element concentrations.

In contrast, the associated hematite-rich breccias that are derived from the basaltic host rocks display considerable variation in SiO<sub>2</sub>, CaO, Na<sub>2</sub>O, MgO and Fe<sub>2</sub>O<sub>3</sub> (Figure 22). The breccias themselves generally display lower SiO<sub>2</sub> in association with increased CaO, Na<sub>2</sub>O and locally MgO as a result of the Fe–carbonate, albitic and hematitic alteration. Despite the extensive hematization developed within the host rocks, samples of the hematite breccia are not significantly enriched in total Fe<sub>2</sub>O<sub>3</sub> relative to the unaltered basaltic host rocks (Figure 22D). The breccia unit is enriched in V relative to the host rocks and is locally enriched in both Cu and U, although there is no obvious association between the two (Figure 22E, F). Similar geochemical relationships between hematite-rich breccias and the basaltic host rocks are also observed at the Anomaly No. 15 prospect.

Near the Upper C Zone deposit, minor argillite-hosted mineralization is exposed in trenches to the southeast of the main occurrence (Gillies *et al.*, 2009). This zone of mineralization is inferred to be structurally controlled and contains

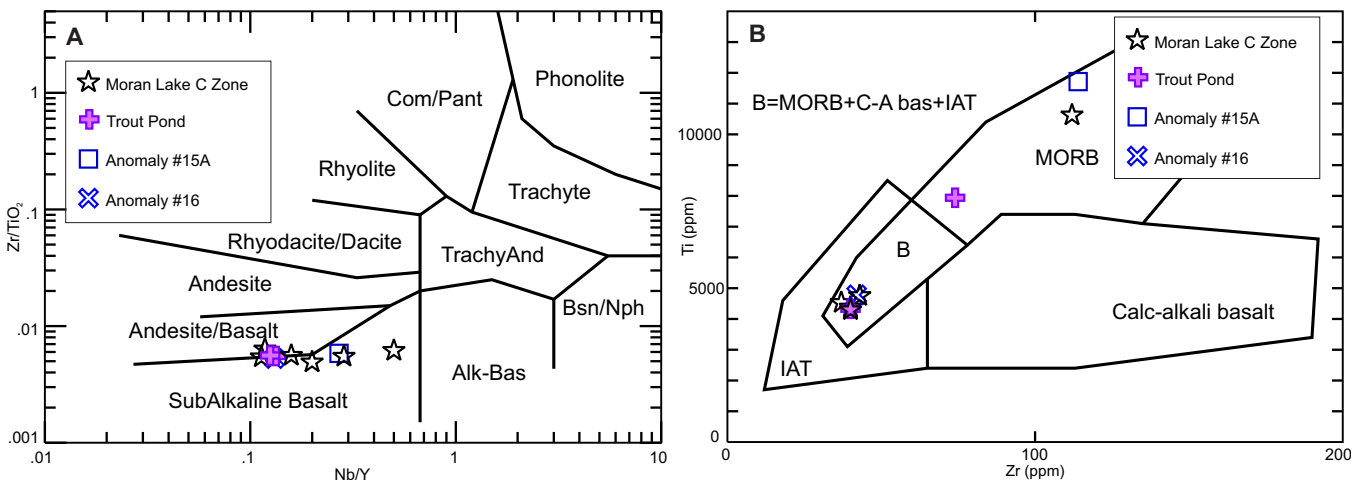


**Figure 21.** *A.* Discrimination diagram of Winchester and Floyd (1977), displaying the subalkaline basaltic nature of the host rocks to the mineralization within the Moran Lake C Zone–Anomaly No. 15 area. *B.* Discrimination diagram of Pearce and Cann (1973) displaying the dominant MORB-like signature of the basaltic host rocks. MORB – Mid-Ocean-Ridge Basalt, IAT – Island-Arc Tholeiites.

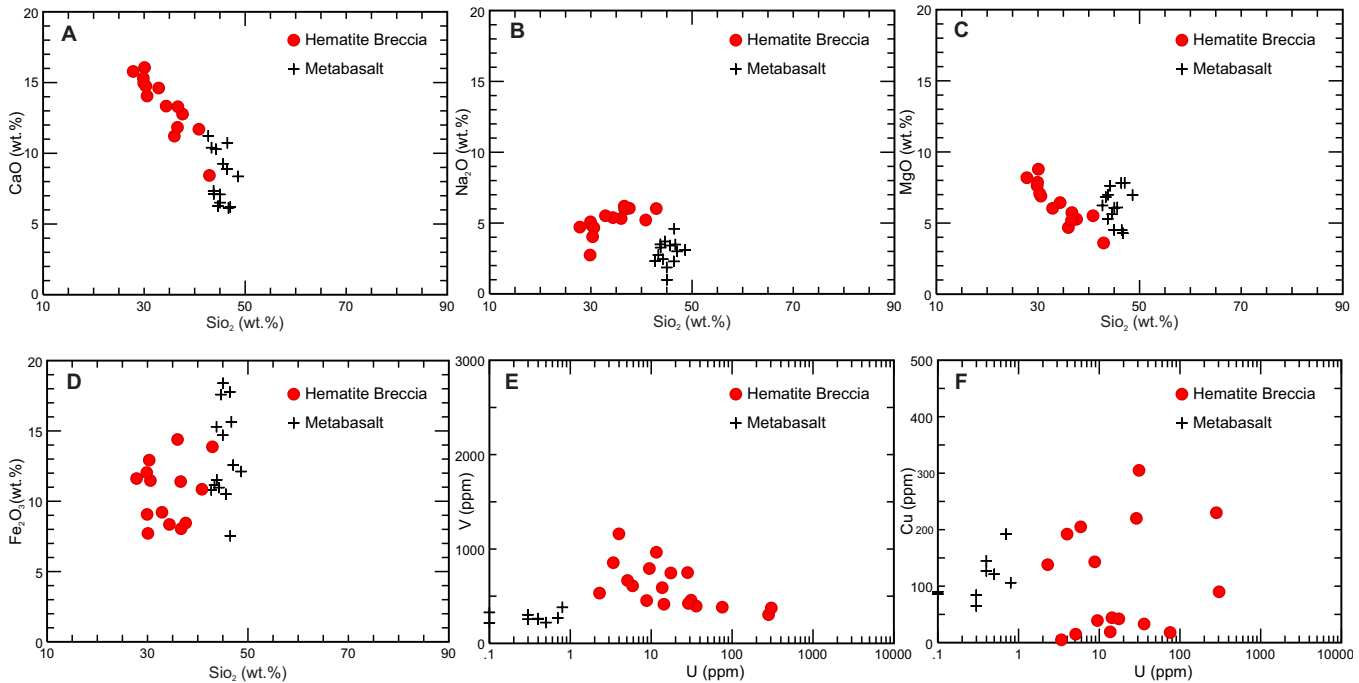


**Figure 22.** Geochemical plots displaying the increase in CaO (A), Na<sub>2</sub>O (B) and MgO (C), as well as the corresponding decrease in Fe<sub>2</sub>O<sub>3</sub> (D) within the hematite-rich breccias of the Upper C Zone in comparison to the host Joe Pond basalt. Also shown are the relative enrichment of V (E) and Cu (F) relative to U within the hematite-rich breccias.

elevated U and Pb, along with anomalous Mn, Ni, Cu, Zn, Mo, Ag and Au (Figure 23A). Mineralized chert, which is interbedded with pillow basalt of the Joe Pond Formation in the Upper C Zone deposit, shows a similar enrichment. Uranium mineralization at the Armstrong prospect is primarily hosted by Fe-carbonate–albite alteration developed within the host argillite unit. Here, samples of the unaltered argillite display elevated Ni and Cu values similar to those of the Upper C Zone deposit, along with anomalous Ag and Au (Figure 23B). Elevated values of V, Cu and Ag have also been reported from the mineralized zones within the Armstrong deposit by Gillies *et al.* (2009). Within the broader halo of Fe-carbonate–albite alteration, localized higher concentrations of uranium are associated with the development of discrete zones of hematization. These zones are associated with elevated values of Na<sub>2</sub>O, indicating the presence of albitic alteration in association with the hematization, similar to that seen at the Upper C Zone deposit.

At the Croteau Lake prospect samples from the argillite, chert and Fe-formation all display local enrichment of V, Mn, Co, Ni, Cu, Zn and Pb in association with elevated U values (Figure 23C). Grab samples from the area are reported to contain elevated V, Cu, Ag and Au (Morgan *et al.*, 2007). Similar metasedimentary rocks of the Warren Creek Formation, immediately above Archean basement rocks in the vicinity of Fish Hawk Lake, also display enrichment of Cr, Co, Ni Cu, Ag, Au and Pb in relation to elevated U (Figure 23D); these

rocks contain some of the highest uranium values obtained within the Warren Creek Formation, locally assaying up to 2.25% Cu, 23.9 ppm Ag and 162 ppb Au in association with 0.22% U<sub>3</sub>O<sub>8</sub>. The dolostone unit that hosts uranium mineralization at the Area 51 prospect displays no significant elemental enrichment other than Mn in relation to elevated Pb and U values (Figure 23E); however, the overlying argillite unit is geochemically similar to unmineralized argillite in the vicinity of the Moran Lake deposit located to the south.

Several groups of dykes crosscut units within the Moran Lake Group. Two distinct groups can be distinguished on the basis of their geochemistry. The first group of dykes (ML Group 1) display similar characteristics as the ‘Group 2’ dykes within the Archean basement rocks, which were inferred to display similarities with Harp Lake and Kikkertavak dykes of Cadman *et al.* (1993; Figure 24). As the Kikkertavak dykes are not known to intrude the Moran Lake Group, these dykes potentially represent correlatives to the younger *ca.* 1300 Ma Harp Lake dykes. The second group of dykes (ML Group 2), which are more gabbroic in composition, display lower element concentrations relative to the Group 1 dykes, except for Ba and Sr (Figure 24); the Group 2 dykes also display a more pronounced negative Nb anomaly. Both sets of dykes are located within a prominent northwest–southeast-trending airborne magnetic anomaly developed in the region separating the Upper C Zone and Trout Pond deposits.

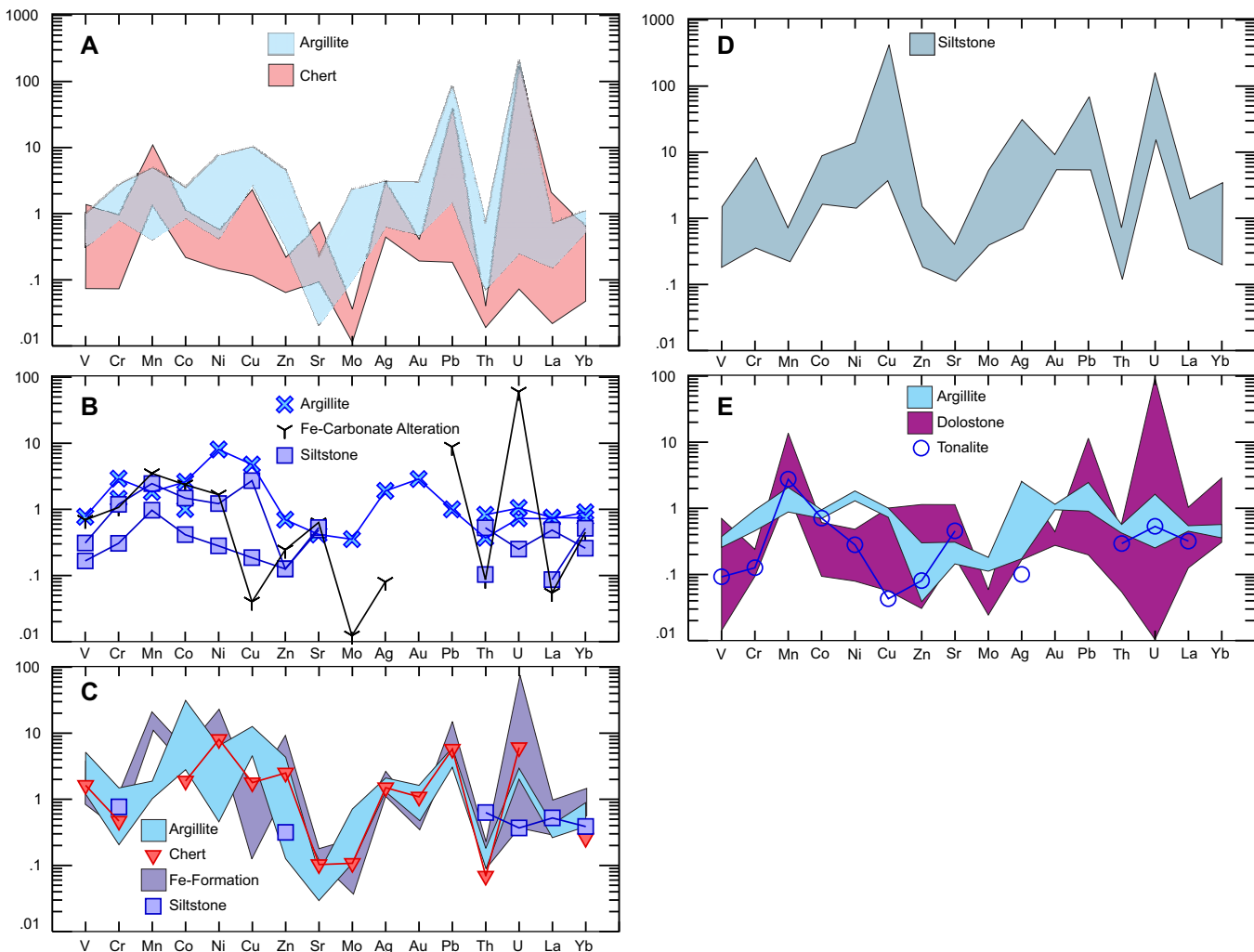


**Figure 23.** Extended trace-element diagrams for various metasedimentary units within the Moran Lake Group. (Normalizing values are from Quinby-Hunt et al., 1989, except for Cu, Ni, Pb, Ag and Mo, which are taken from Vine and Tourtelot, 1970.) A. Moran Lake Upper C Zone deposit, B. Armstrong deposit, C. Croteau Lake prospect, D. Fish Hawk Lake North area, E. Area 51 prospect.

## SUMMARY AND DISCUSSION

The resurgence in uranium exploration within the Moran Lake Group during the mid-2000s has increased the resources of previously known deposits, and identified several new prospective areas of uranium mineralization. To date, the most important host rocks to uranium mineralization are the pillow basalts of the Joe Pond Formation, with only minor mineralization identified within the underlying Warren Creek Formation. Three main styles of uranium mineralization occur within the Moran Lake Group. The first is related to hematite-rich brecciation, and is grouped under the broader classification of magmatic-related mineralization with respect to the regional classification of uranium mineralization within the CMB. The structurally controlled Fe-carbonate–albite alteration is classified as metamorphic–metasomatic-related,

and third, the localized zone of mineralization within dolostone of the Warren Creek Formation is classified as sediment-hosted mineralization.

The most distinctive alteration in the mafic volcanic rocks of the Joe Pond Formation consists of hematite-rich breccias, such as those developed within the Moran Lake Upper C Zone and the Trout Pond deposits. These breccias are characterized by initial pervasive hematite alteration of the host rock, followed by the development of calcium and sodium metasomatism. The hematite-rich breccias consist of matrix-supported, centimetre- to millimetre-scale, angular to subrounded fragments within a hematite–carbonate-rich matrix; fragments rarely display a weak alignment implying local fluidization of the breccia. These breccia units are consistently elevated in vanadium, but contain variable enrich-

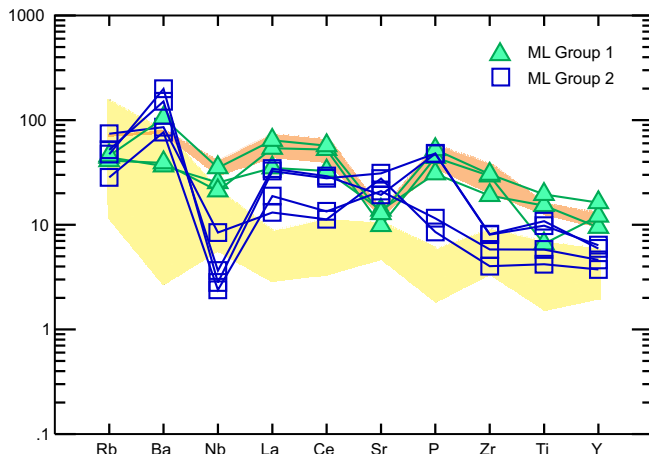


**Figure 24.** Primitive mantle normalized trace-element patterns for the two groups of dykes observed locally crosscutting rocks of the Moran Lake Group (normalizing values of Sun and McDonough, 1989). The shaded areas outline the trends defined for dykes within the Archean basement rocks shown in Figure 14.

ment of uranium and copper, which are primarily associated with late crosscutting hematite-rich fractures. These breccias are interpreted to be of magmatic-hydrothermal origin, as proposed by previous authors (e.g., Cook, 1980; Ryan 1984). This style of mineralization displays many similarities with so-called IOCG systems, however, further work is required to confirm such a relationship.

The rare occurrence of hematite-rich breccias hosting uranium mineralization, in the overlying conglomerate of the Heggart Lake Formation, within the Upper C Zone deposit implies that formation of the mineralized breccias postdate the deposition of these rocks, which have now been dated at *ca.* 1850 Ma (Sparkes *et al.*, 2016; *see* Section, Uranium Mineralization within the Bruce River Group). However, the marked decrease in the abundance of alteration and mineralization within the sedimentary rocks presently overlying the Moran Lake Upper C Zone indicates that some post-mineral structural displacement of these rocks has occurred.

Localized shear zones hosting pervasive Fe-carbonate–albite alteration are developed within the Upper C Zone deposit. One such shear zone, the Lower Shear Zone, marks the lower limit for the development of the hematite-rich hydrothermal breccias within the deposit. Similar uraniferous Fe-carbonate–albite mineralization has been identified approximately 3.5 km to the southwest of the C Zone (e.g., Armstrong deposit) and potentially represents the on-strike extension of this mineralization. The timing and development of these structures appear to postdate the development of the hematite-rich hydrothermal brecciation, and may be as young as Grenvillian in age.

Several occurrences of uranium mineralization are present within the Warren Creek Formation close to its contact with underlying Archean basement rocks; however, no true examples of unconformity-style mineralization have been identified. Uranium mineralization hosted within the Warren Creek Formation is associated with the enrichment of several other elements, which include Ag, Cu, Ni, V, Zn and locally Au. Similar geochemical associations have also been noted in relation to uranium mineralization occurring within argillite of the Post Hill Group farther to the east (e.g., Gear and Nash deposits; Cunningham-Dunlop and Lee, 2008). Within the Armstrong deposit, elevated values of V, Cu and Ag associated with uranium mineralization have been reported; such enrichment is attributed to the fact that the host rock was enriched in these elements during its deposition (Gillies *et al.*, 2009). Thus, the enriched source rocks of the Warren Creek Formation represent a plausible source for both the uranium and the accompanying metals within the western portion of the CMB. However, unaltered mafic volcanic rocks of the Joe Pond Formation also contain elevated vanadium values and could likewise be a source for the observed enrichment within the hematite-rich breccias.

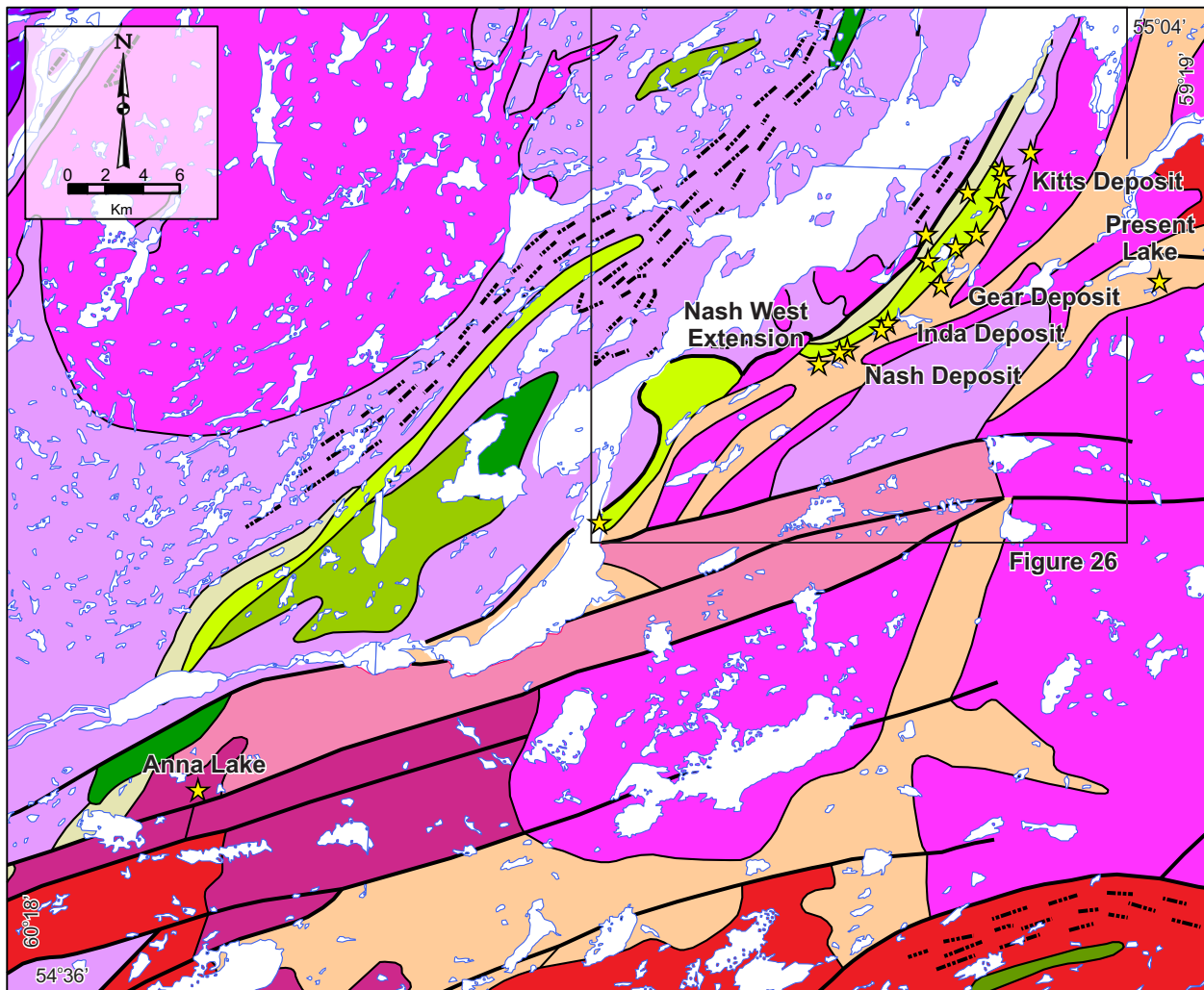
In most instances, uranium occurs as very fine-grained disseminations in association with the development of Fe–Ti oxide minerals, as indicated by autoradiographs of mineralized thin sections and SEM imaging. However, the type of alteration in which the mineralization is developed influences the style of uranium deposition. Mineralization developed within the hematite–albite alteration primarily forms within brittle network-style fractures whereas mineralization associated with Fe-carbonate–albitite-rich zones is primarily disseminated throughout the alteration.

Several groups of mafic dykes are recognized crosscutting the Moran Lake Group. Some of these dykes represent possible correlatives with the Harp Lake dykes and are obvious targets for future geochronological studies. Dykes within the Moran Lake Group locally crosscut mineralization and thus could potentially provide a minimum age on the development of uranium mineralization within the region. However, further work is required to test the suitability of these units for U–Pb geochronology.

## URANIUM MINERALIZATION WITHIN THE POST HILL GROUP

### INTRODUCTION

Some of the first discoveries of uranium within the CMB, including the highest grade deposit yet identified (*i.e.*, Kitts deposit; Figure 25), are hosted within rocks assigned to the Post Hill Group of Ketchum *et al.* (2002), which was formerly known as the Lower Aillik Group (*cf.* Marten, 1977;



### LEGEND

#### Intrusive Rocks

- Olivine gabbro and metamorphic equivalents
- Granite, quartz monzonite, granodiorite, syenite and minor quartz diorite
- High-level, locally fluorite-bearing granites
- Granite and granodiorite
- Granite
- Gabbro and leucogabbro sills

#### Aillik Group

- Rhyolite, ash-flow tuff, breccia and hypabyssal rhyolite intrusions; volcaniclastic siltstone and sandstone; minor basalt

#### Post Hill Group

- Sandstone of shallow- to deep-water origin
- Schistose amphibolite derived from mafic volcanic rocks
- Mafic volcanic and volcaniclastic rocks, lesser sedimentary and felsic volcanic rocks, and mafic-ultramafic sills; greenschist to amphibolite facies

#### ARCHEAN

- Tonalitic and other gneisses reworked and retrograded during Makkovikian orogenesis

#### SYMBOLS

- High Strain Zone.....
- Fault.....
- Geological contact.....
- Uranium occurrence.....

**Figure 25.** Regional map outlining the distribution of uranium occurrences hosted within the Post Hill Group (geological base map modified from Wardle et al., 1997). The area indicated within the black outline is detailed in Figure 26.

Evans, 1980; Gower *et al.*, 1982). The Post Hill Group consists of amphibolite-facies mafic volcanic rocks and siliciclastic metasedimentary rocks that were deposited after 2235 Ma and are locally dated at 2178 Ma (Ketchum *et al.*, 2002). These rocks have been correlated with the lithologically similar Moran Lake Group (*cf.* Wardle and Bailey, 1981; Ketchum *et al.*, 2002), described in the preceding section. However, the Post Hill Group is relatively more highly deformed and metamorphosed, so its exact stratigraphy is uncertain. It contains abundant uranium mineralization (Table 7), and has been the focus of extensive uranium exploration, which began in the mid-1950s (*cf.* Gower *et al.*, 1982; Wilton, 1996; McLean *et al.*, 2009; and *see* references therein).

Previous interpretations of the uranium mineralization within the Post Hill Group have proposed both syngenetic (*e.g.*, Gandhi, 1978) and epigenetic (*e.g.*, Marten, 1977; Gower *et al.*, 1982) mineralization. The latter model(s) generally assumed that uranium was deposited at the same time as that in the adjacent Aillik Group (*see* Section, Uranium Mineralization within the Allik Group). New geochronological data from this study demonstrate an older age for the mineralization within the Post Hill Group relative to that contained within the Aillik Group, suggesting that the mineralization represents an older mineralizing event. The higher grades of uranium mineralization found within the Post Hill Group compared to that in the likely coeval Moran Lake Group are noticeable, and the metamorphic history of the Post Hill Group maybe an important influence. The following section briefly summarizes the main lithological units within the Post Hill Group; for a more detailed description the reader is referred to Marten (1977), Gandhi (1978), Evans (1980), Gower *et al.* (1982) and Ketchum *et al.* (2002).

## REGIONAL GEOLOGY

The Post Hill Group is located in the northeastern portion of the CMB (Figure 25), within a structurally complex region that has been the focus of numerous geoscientific studies (*e.g.*, Gandhi, 1969, 1970, 1978; Marten, 1977; Gower *et al.*, 1982; Schärer *et al.*, 1988; Culshaw *et al.*, 2000, 2002; Ketchum *et al.*, 2001a, 2002). Within this region, deformed Archean basement rocks are structurally overlain by amphibolite-facies supracrustal rocks of the Post Hill Group (Ketchum *et al.*, 2002). In ascending stratigraphic order, the Post Hill Group comprises psammite, schistose mafic metavolcanic rocks and minor pelite that were deposited within a continental margin-type environment (Culshaw and Ketchum, 1995). Quartzite at the base of the Post Hill sequence contains Archean detrital zircons, and is interpreted to have been deposited after 2235 Ma, as these rocks are not observed to be cut by the Kikkertavak dyke swarm that is present within the underlying Archean basement rocks (Ketchum, *et al.*, 2002). Tuff layers contained within the over-

**Table 7.** NI 43-101 compliant resource estimates for mineralization within the Post Hill Group

Deposit	Resource Classification	Cut-off (% U <sub>3</sub> O <sub>8</sub> )	Grade (% U <sub>3</sub> O <sub>8</sub> )	Underground Tonnage (tonnes > cut-off)	Contained Resource (lbs. U <sub>3</sub> O <sub>8</sub> )	Cut-off (% U <sub>3</sub> O <sub>8</sub> )	Grade (% U <sub>3</sub> O <sub>8</sub> )	Open Pit		Contained Resource (lbs. U <sub>3</sub> O <sub>8</sub> )	Source
								Contained Resource (tonnes > cut-off)	Tonnage (tonnes > cut-off)		
Gear	Indicated	0.050%	0.080%	303,000	532,000	0.020%	0.060%	48,000	63,000	Hertel <i>et al.</i> , 2009	
	Inferred	0.050%	0.100%	273,000	596,000	0.020%	0.030%	30,000	19,000		
Inda	Indicated	0.050%	0.070%	214,000	324,000	0.020%	0.070%	985,000	1,497,000	Hertel <i>et al.</i> , 2009	
	Inferred	0.050%	0.070%	1,183,000	1,724,000	0.020%	0.070%	2,077,000	3,064,000		
Nash	Indicated	0.050%	0.060%	152,000	214,000	0.020%	0.090%	527,000	1,029,000	Hertel <i>et al.</i> , 2009	
	Inferred	0.050%	0.070%	369,000	580,000	0.020%	0.070%	138,000	228,000		
Anna Lake	Indicated					0.015%	0.037%	7,370,000	6,010,000	Fraser and Giroux, 2009	
	Inferred										

lying Post Hill Amphibolite have produced a U–Pb age of  $2178 \pm 4$  Ma, and are interpreted to be the depositional age of the protolith to the amphibolite (Ketchum *et al.*, 2001a).

The amphibolite unit is, in turn, overlain by the metasedimentary formation of Marten (1977), which includes thin-bedded psammite and minor pelite; based on mineralogy, Marten (*op. cit.*) interpreted these units to have originally been deposited as greywackes. A micaceous psammite sample collected from this sequence contains both Archean and Paleoproterozoic detrital zircons and was deposited after  $2013 \pm 3$  Ma (Ketchum *et al.*, 2001a). The Kitts Pillow Lava Formation structurally overlies the metasedimentary formation and is interpreted to form the upper most unit of the Post Hill Group stratigraphy (Marten, 1977; Evans, 1980). This unit consists of massive metavolcanic pillow basalt and minor discontinuous beds of argillite and iron formation. Also contained within the pillow basalt is a locally developed volcaniclastic sequence composed of argillite and pelitic to non-pelitic greywacke and lesser mafic tuff and chert. This unit, known as the mine volcaniclastic sequence, is the main host to the Kitts uranium deposit (Evans, 1980).

The contact separating the Post Hill Group to the west from the Aillik Group to the east has been the matter of much debate. This contact, which is recognized as a shear zone, has had several different interpretations including both unconformable (Marten, 1977; Gower *et al.*, 1982), and conformable (Evans, 1980) relationships. The recognition of pre-Aillik Group deformation within the Post Hill Group (*e.g.*, Clark, 1979; Ryan, 1984; Culshaw *et al.*, 1998; Mclean *et al.*, 2009) along with the younger age limit of the Aillik Group (*cf.* Hinckley and Rayner, 2008), provide supporting evidence for an unconformable relationship. The overlying Aillik Group is predominantly composed of an upper greenschist- to lower amphibolite-facies volcano-sedimentary sequence consisting of felsic volcanic rocks and related volcaniclastic equivalents (Clark, 1973; Gower *et al.*, 1982; Hinckley, 2007; Hinckley and LaFlamme, 2009).

Regardless of its origin, the structurally complex zone now separating the Post Hill and Aillik groups is the site of significant uranium mineralization, throughout an area referred to as the ‘Kitts–Post Hill Belt’ (Gandhi, 1978). The Kitts–Post Hill Belt includes the Kitts, Gear, Inda and Nash deposits, as well as several other significant occurrences of uranium mineralization (Gandhi, 1978; Evans, 1980; Gower *et al.*, 1982; Cunningham-Dunlop and Lee, 2008), much of which is developed at, or very near, the inferred top of the Post Hill Group stratigraphy, close to the contact with the Aillik Group. At present, the northern portion of the Kitts–Post Hill Belt, which roughly encompasses the area north of the Gear deposit, including the high-grade Kitts deposit, is classified as exempt mineral lands and has not been explored

since the mid-1980s. The portion of the belt that falls outside of the exempt minerals lands is also referred to as the ‘Inda Lake Trend’ (Cunningham-Dunlop and Lee, 2008).

Marten (1977) subdivided the deformation within the region of the Kitts–Post Hill Belt into five events. Early deformation was restricted to basement-cover interfaces with motion inferred to be largely subhorizontal. As part of his work, he identified four  $D_1$ – $D_2$  high-strain zones termed ‘tectonic slides’, which he recognized as possible shear zones associated with this subhorizontal motion ( $D_1$ ), later reactivated during  $D_2$ . These are termed the Post Hill, Fiace Lake, Nakit and Witch Lake ‘slides’. In correct structural terminology, these would be referred to simply as ‘shear zones’, and would likely be interpreted as thrust faults. This area of transpressive ductile shearing was later encompassed within the regionally extensive Kaipokok Bay Shear Zone (KBSZ; Figure 26) of Culshaw *et al.* (2000). Culshaw *et al.* (2000) subdivided the KBSZ into four components, namely the Postville, Drunken Harbour, Julies Harbour and Witch Lake shear zones.

Early amphibolite-facies metamorphism has been dated at *ca.* 1896 Ma within the Kaipokok domain northeast of the KBSZ, and it has been postulated that the Post Hill Group may have experienced some of this early deformation (Ketchum *et al.*, 1997, 2002). Thrusting associated with  $D_1$  along the KBSZ occurred prior to  $1877 \pm 5$  Ma, on the basis of a crosscutting quartz monzonite in the area of Post Hill (Figure 26; Ketchum *et al.*, 1997, 2002; Culshaw *et al.*, 2000). The KBSZ was subsequently reactivated (D4 of Culshaw *et al.*, 2000) between 1840–1784 Ma (Ketchum *et al.*, 1997, 2002), during which time regional dextral shearing was contemporaneous with amphibolite-facies metamorphism (Culshaw *et al.*, 2002). The deformational history of the region is punctuated by the intrusion of multiple felsic to mafic intrusions that include both foliated and non-foliated varieties. These magmatic pulses have been broadly subdivided into three separate events by Culshaw *et al.* (2000) utilizing the pre-existing geochronological data of Loveridge *et al.* (1987), Schärer *et al.* (1988), Kerr and Fryer (1994), Kerr *et al.* (1997), Barr *et al.* (1997), Ketchum *et al.* (1997, 2001a), and a Sinclair (1999): they are: 1) 1895–1870 Ma, 2) 1802–1784 Ma, and 3) 1720 Ma and younger plutons.

## EXPLORATION HISTORY

Uranium exploration within the eastern CMB began in 1954. The first discovery of economic significance was made along the eastern coastline of Kaipokok Bay in 1956 during regional reconnaissance prospecting by Brinex. This later became known as the Kitts deposit, after the discoverer, Walter Kitts. Initial reports on the mineralization describe a narrow zone of radioactivity occurring intermittently over a 1.5-km strike length, from which samples returned up to  $2.38\% \text{ U}_3\text{O}_8$

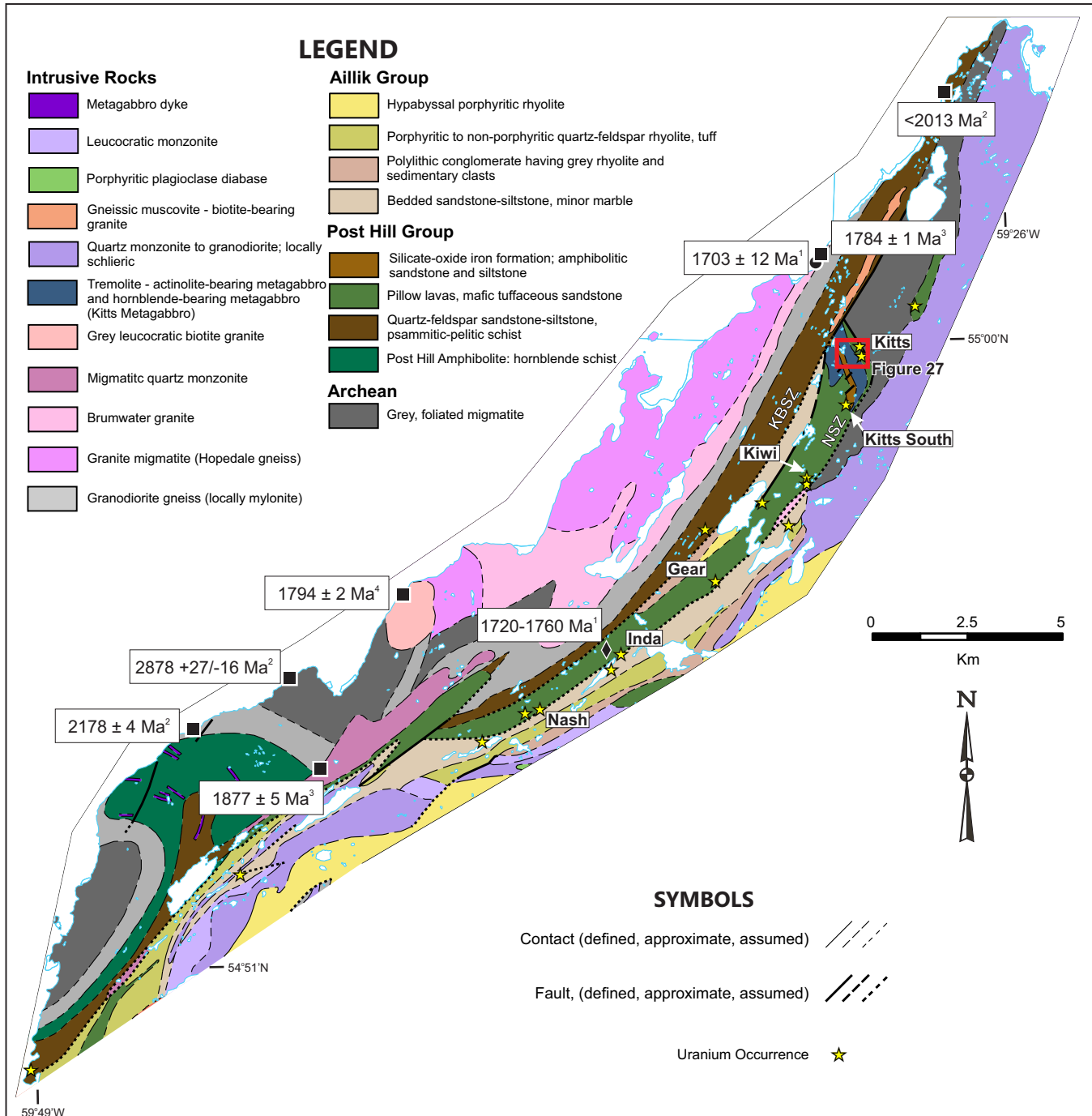


**Figure 26.** Geological map of the Kitts-Post Hill Belt, showing the location of significant uranium occurrences and the distribution of known geochronological data. Solid diamonds (amphibole) and circles (muscovite) represent Ar-Ar determinations; the solid squares represent U-Pb data. Age sources: 1) Culshaw et al., 2002; 2) Ketchum et al., 2001b; 3) Ketchum et al., 1997; 4) Schärer et al., 1988. Abbreviations KBSZ-Kaipokok Bay Shear Zone, NSZ-Nakit Shear Zone. (Modified after Marten, 1977, Gower et al., 1982 and Culshaw et al., 2002.) Red box shows location of Figure 27.

(Morrison, 1956). Most of the early uranium exploration within the area focused on the northeastern part of the Post Hill Group, and culminated with limited underground exploration and bulk sampling of the Kitts deposit. However, due to poor market conditions in the late 1950s, work on the project was suspended.

In the mid-1960s, a renewed interest in uranium led to resurgence in exploration, which included a helicopter-borne radiometric survey. This survey identified several anomalies along the belt that resulted in the discovery of the Gear, Inda and Nash deposits (Figure 26). Highlights from sampling of mineralized trenches included 0.11%  $U_3O_8$  over 18 m, and 0.09%  $U_3O_8$  over 4.6 m, from the Gear and Nash deposits, respectively (Piloski, 1968). During this time, Brinex personnel noted the preferential development of the uranium mineralization within a certain part of the stratigraphic sequence and initiated a systematic drilling campaign based on 300 m spacing along the Kitts–Post Hill Belt between the Nash and Inda Lake deposits (Piloski, 1969). Reconnaissance drilling along the favourable stratigraphic interval identified a zone of anomalous radioactivity to the southwest of the Gear deposit, known as the Inda deposit, which produced localized intersections of up to 0.36%  $U_3O_8$  over 1.5 m (Grimley, 1970).

Drilling in the vicinity of the Gear deposit also identified favourable mineralization with initial drilling defining a mineralized zone approximately 76 m in length and extending to a depth of over 45 m, from which assays of up to 0.37%  $U_3O_8$  over 2.74 m were obtained (Piloski, 1968). Follow-up drilling in 1970 extended the mineralization an additional 76 m along strike toward the southwest, and traced the zone to depths of up to 212 m (Grimley, 1970). Drilling at the Nash deposit during the same period also produced positive results, which included 0.22%  $U_3O_8$  over 2.3 m (Grimley, 1970). Subsequent drilling at the Nash deposit defined a mineralized zone measuring approximately 365 m in length with an average width of 3 m and a moderate southwest plunge, from which intersections of up to 0.32%  $U_3O_8$  over 2.1 m have been obtained from depths of up to 268 m (Piloski, 1970). During the late 1960s and early 1970s, development work was also ongoing at the Kitts deposit using both surface and underground drilling to delineate ore reserves, which in 1977 stood at 203 880 tons at a grade of 0.73%  $U_3O_8$  (Golder, 1977).

Work in the area was suspended in the early 1980s due to a downturn in market conditions, and also due to problems with environmental assessment approvals for development of the project. The Kitts–Post Hill Belt remained relatively inactive until the area was once again staked in 2003, and since that time the portion of the belt outside of exempt mineral lands has undergone numerous geophysical and geochemical surveys, along with additional diamond drilling. This exploration was largely conducted by Aurora Energy Resources

(now owned by Paladin Energy). This work has extended the mineralized zones at the Gear, Inda, and Nash deposits, both along strike and down-dip. At the Gear deposit, drilling has extended the mineralized zone to over 200 m in strike length and an additional 100 m down-dip, from which highlights include up to 0.17%  $U_3O_8$  over 10.0 m (Cunningham-Dunlop and Lee, 2008). As a result of this most recent exploration, a NI 43-101 compliant resource estimate was carried out for the Gear deposit, which defined an indicated and inferred resource of approximately 1.2 million lbs of  $U_3O_8$  at an average grade of 0.07%  $U_3O_8$  (Hertel *et al.*, 2009; Table 7). At the Inda deposit, drilling intersected local high-grade mineralization, assaying up to 2.12%  $U_3O_8$  over 3.62 m and also identified anomalous Cu, Ag and V, in close spatial association with the uranium mineralization (Cunningham-Dunlop and Lee, 2008). A NI 43-101 compliant resource estimate for this deposit has defined an indicated and inferred resource of approximately 6.6 million lbs of  $U_3O_8$  at an average grade of 0.07%  $U_3O_8$  (Hertel *et al.*, 2009; Table 7). At the nearby Nash deposit, a NI 43-101 compliant resource estimate was also carried out, which defined an indicated and inferred resource of approximately 2.1 million lbs of  $U_3O_8$  at an average grade of 0.07%  $U_3O_8$  (Hertel *et al.*, 2009; Table 7).

Along strike to the southwest of the main Kitts–Post Hill Belt, Bayswater Uranium has also outlined a NI 43-101 resource at the Anna Lake deposit (Figure 25). Mineralized boulders were first discovered in the area by Brinex in the late 1970s during regional mapping and prospecting (Darch *et al.*, 1979). Subsequent work in the early 1980s, which included diamond drilling, identified uranium and molybdenum mineralization (Wiley, 1982), but no further work was recommended. In 2007, Bayswater Uranium initiated work on the property, which included geophysical surveys, mapping and diamond drilling. From this work the company produced a NI 43-101 compliant resource estimate containing an inferred resource of approximately 6.0 million lbs of  $U_3O_8$  at an average grade of 0.04%  $U_3O_8$ , which also contains approximately 2.1 million lbs of molybdenum (Fraser and Giroux, 2009; Table 7).

## KITTS DEPOSIT

### Previous Work

The local geology of the Kitts deposit is shown in Figure 27. Mineralization in the vicinity of the Kitts deposit was first described by Morrison (1956) and Hooper (1956). The latter author noted the development of radioactivity within gossan zones in finely laminated black slate along the contact with a mafic intrusion, but also noted that not all gossan zones in the area were mineralized. He described the local occurrence of strong radioactivity in association with the hinge zones of minor folds and concluded that the mineralization was both

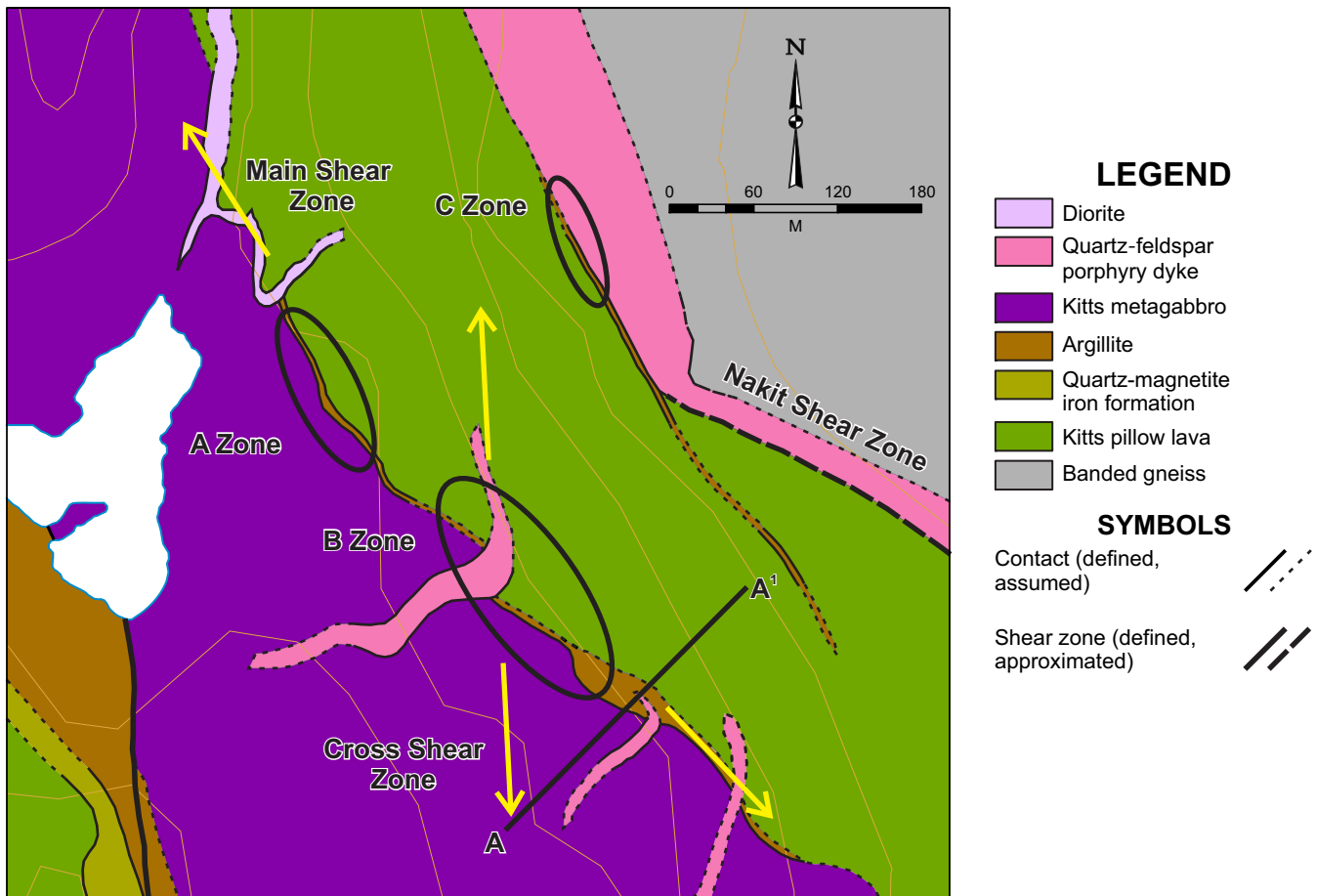


**Figure 27.** Simplified geological map of the area surrounding the Kitts deposit and the location of the A, B and C zones (modified after Marten, 1977). Schematic cross-section A-A' illustrated in Figure 29.

lithologically and structurally controlled. Beavan (1958) provided a detailed summary on the nature of the mineralization within the Kitts deposit, in which he noted the preferential concentration of the radioactivity along shear zones developed at, or very close to, the intrusive contact between the gabbro and adjacent metasedimentary rocks; these mineralized structures were interpreted to be the result of regional folding. Beavan (1958) also subdivided the mineralization into the A, B and C zones, of which the A and B zones host the bulk of the mineralization.

Gandhi (1969, 1970) conducted regional mapping in the area of the Kitts deposit and noted the strong spatial controls on the mineralization throughout the Kitts–Post Hill Belt. He noted the localized concentration of uranium within particular stratigraphic settings in the host metasedimentary sequence, as well as the localized concentration of radioactivity within the crests of minor drag folds. This led him to conclude that the uranium was of a syngenetic sedimentary origin, and was later remobilized into dilatant structures (Gandhi, 1970). He also postulated that the Kitts A, B and C zones occurred within the same stratigraphic unit that was part of a large syn-

clinal structure, noting that the fold hinge could potentially be a very prospective setting for further high-grade mineralization (Gandhi, 1976a). Gandhi (1978) extended this model by placing the other uranium occurrences along the Kitts–Post Hill Belt into a stratigraphic context, and drew parallels between the Kitts–Post Hill Belt, and the Rum Jungle district of northern Australia.

More detailed work in the area of the Kitts deposit, with a greater focus on structural details, was carried out by Marten (1977), who examined basement-cover contact relationships throughout the Kitts–Post Hill Belt. He interpreted the uranium mineralization to be remobilized into structurally dilatant zones during early syntectonic processes. In the vicinity of the Kitts deposit, Marten (1977) noted that uranium mineralization was primarily developed within the sulphidic semipelite or ‘iron formation’, which he interpreted to occur as discontinuous layers within the Kitts Pillow Lava Formation, and which formed the loci for early D<sub>1</sub>–D<sub>2</sub> shear zones (regional D<sub>1</sub> of Culshaw *et al.*, 2000). He also noted that the ‘pitchblende’ was incorporated within fine-grained metamorphic amphibole and biotite, which he inferred as evidence for

the pre- to syn- $D_2$  timing of the mineralization. The mineralization within these shear zones was noted to be concentrated along the  $S_1$ – $S_2$  schistosity planes and locally within quartz–carbonate veins (Marten, 1977). Later remobilization of the mineralization was recognized along small-scale shear zones related to  $D_3$  (regional  $D_4$  of Culshaw *et al.*, 2000); these structures also result in the remobilization of the uranium into the surrounding country rock (Marten, 1977).

Evans (1980) also conducted a detailed examination of the uranium mineralization along the Kitts–Post Hill Belt. He identified two distinct shear zones within the Kitts deposit, the first of which was essentially conformable with the schistosity in the volcaniclastic rocks ( $\sim 320^\circ$  strike/ $45$ – $90^\circ$  NE dip). This structure is termed the ‘Main Shear Zone’ and is host to most of the mineralization within the deposit (Evans, 1980). The second shear zone is developed roughly parallel to the regional schistosity ( $010$ – $020^\circ$  strike/ $55$ – $65^\circ$  SE dip) but is discordant to the lithological contacts within the deposit and is referred to as the ‘Cross Shear Zone’. The intrusion of quartz–feldspar porphyry dykes, which are generally developed subparallel to the Cross Shear Zone but are also locally transposed by this structure, are inferred to predate the main  $D_3$  event (Evans, 1980; regional  $D_4$  of Culshaw *et al.*, 2000).

### Local Geology

The Kitts uranium deposit occurs within a north–northwest-trending shear zone developed close to, and parallel to, the northern portion of the Nakit Shear Zone, where it becomes deflected to the northwest and is truncated along the Kaipokok Bay Shear Zone (Figure 26). Within this area, a large body of locally deformed and metamorphosed gabbro, known as the Kitts Metagabbro, intrudes the Kitts Pillow Lava Formation and associated interbedded iron formation (Figure 27). The metagabbro unit displays a close spatial association with the Kitts Pillow Lava Formation and is thus interpreted to represent a co-magmatic intrusion related to the mafic volcanic rocks (Marten, 1977; Evans, 1980). U–Pb dating of the metagabbro intrusive unit carried out as part of this study has produced an age of  $2018 +15/-4$  Ma (Sparkes and Dunning, 2015). Uranium mineralization is predominantly hosted within a northeasterly dipping sequence of ‘iron formation’, which is the main focus of deformation in the area. The

iron formation sequence is actually composed of sulphidic argillite, albitic greywacke and mafic tuff; these units form the ‘mine volcaniclastic sequence’ (MVS) of Evans (1980). Within the deposit, Evans (1980) subdivided the sequence into four main units: 1) a mafic tuff to argillite transition zone ( $\sim 5$  m), 2) argillite zone ( $5$ – $20$  m), 3) albitic greywacke ( $5$ – $30$  m) and 4) mafic tuff (Figure 28). A detailed description of the host rocks can be found in Gandhi (1978) and Evans (1980), and the following is a general summary from these sources.

The uranium mineralization within the deposit is primarily confined to MVS close to the northern margin of the Kitts Metagabbro (Figure 29). The metagabbro is interpreted to predate deformation as it locally contains a penetrative fabric along its margin, which is inferred to be related to  $S_1$  (Marten, 1977). As the mineralization is structurally controlled and the intrusion predates the deformation, it therefore predates the development of uranium mineralization. At surface, the mineralization is moderate to well exposed along the northeastern slope of a northerly trending ridge, and is associated with a well-developed radiometric anomaly. Occurrences of anomalously radioactive gossans are also noted within metasedimentary rocks along the southwestern margin of the

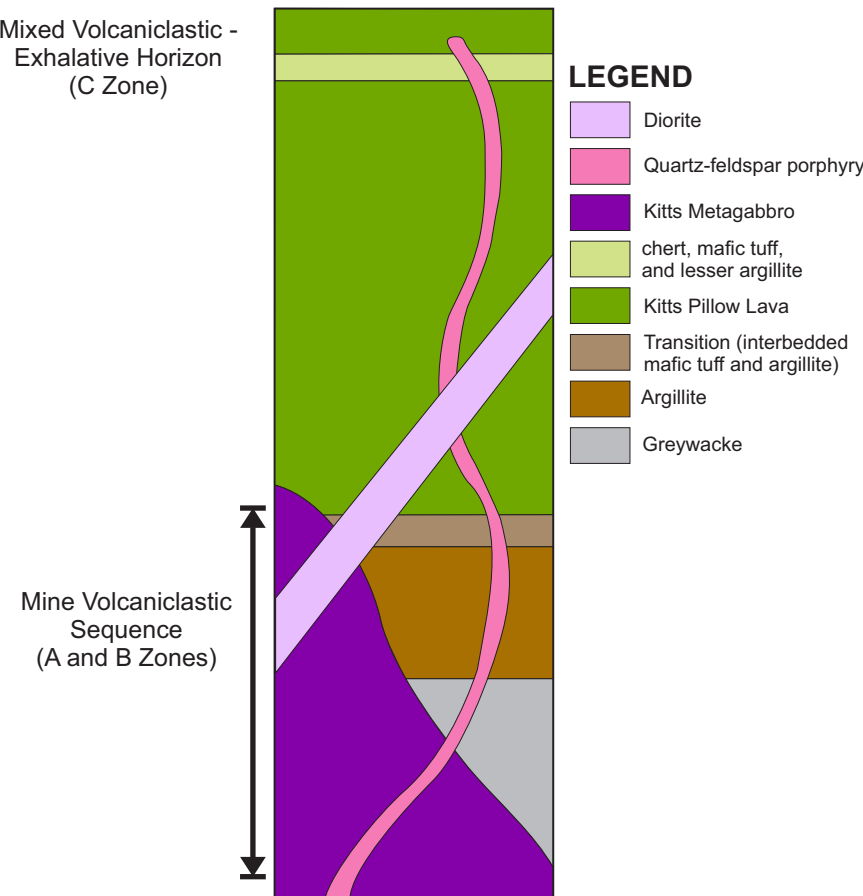


**Figure 28.** Schematic stratigraphic section of the representative rock units within the Kitts deposit (modified after Evans, 1980).

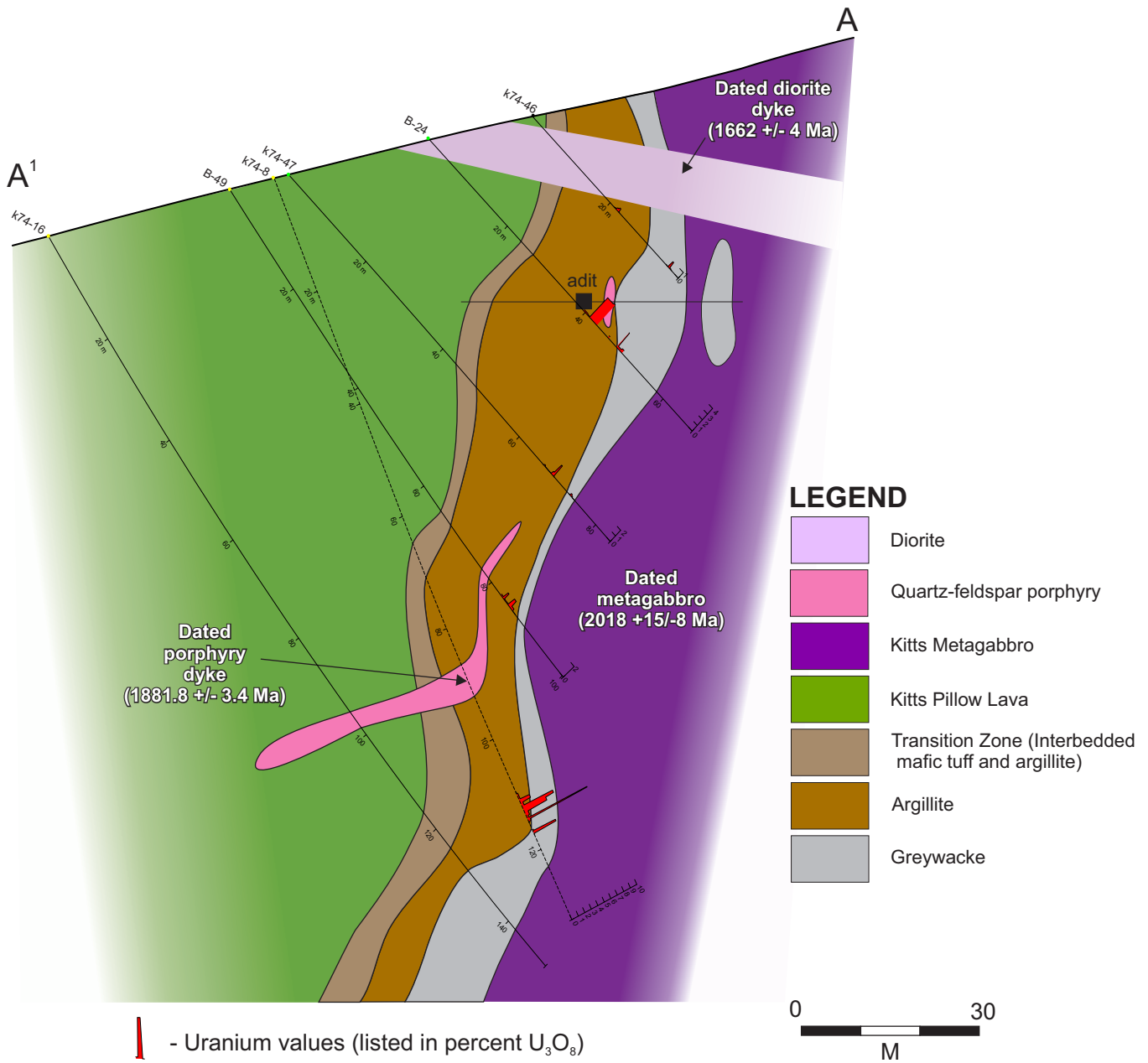


**Figure 29.** Schematic cross section through the Kitts deposit (looking southeast) displaying the distribution of the main rock units in association with uranium mineralization (modified from Evans, 1980). Note hole K74-8 is located 30 m northwest of the section and is projected onto the current plane. For location of schematic cross-section A-A', refer to Figure 27.

metagabbro; however, none of these have proven to be of economic significance (Beavan, 1958; Piloski, 1968). Evans (1980) inferred the stratigraphy of the Kitts deposit was structurally overturned, however Gandhi (1978) interpreted the stratigraphy to be right way up and part of a larger scale synclinal structure. No evidence to suggest that the sequence is overturned was observed by the author, and the younging of U-Pb ages toward the east throughout the Kitts–Post Hill Belt (Figure 26) is supportive of an overall eastward younging direction.

Mineralization is hosted within the Main Shear Zone, and is developed roughly subparallel to the margin of the metagabbro intrusion (Evans, 1980). This structure ranges from 3–50 m in width, is roughly subparallel to the regional Nakit Shear Zone, and is inferred to be related to  $D_1$ – $D_2$  (Marten 1977; Evans, 1980). The Main Shear Zone is primarily developed within units of the MVS due to the less competent nature of these rocks in comparison to the adjacent metagabbro and mafic volcanic units (Marten, 1977). A pronounced penetrative linear fabric within the MVS plunges

46° toward 135°, the trajectory of which is closely mimicked by the ore shoots within the deposit. The Main Shear Zone is affected by the younger Cross Shear Zone (Figure 27), which ranges from 60–80 m in width, and results in a dextral offset of the MVS between the A and B zones. The Cross Shear Zone trends approximately north–south and is developed roughly parallel to the regionally extensive Kaipokok Bay Shear Zone. Evans (1980) interpreted the development of the Cross Shear Zone to be related to  $D_3$  of Marten (1977; regional  $D_4$  of Culshaw *et al.*, 2000).

The region of the Cross Shear Zone is also highlighted by the intrusion of quartz–feldspar porphyry dykes, which are intruded subparallel to the structure. These dykes range from 2–8 m in width where they crosscut the MVS, but locally reach up to 20 m in width within the Cross Shear Zone. The dykes consist of mm-scale, white feldspar phenocrysts and lesser grey subrounded quartz phenocrysts, within a pale-grey, fine-grained biotite–chlorite-bearing groundmass. The porphyry dykes contain a single, well-developed, foliation that is roughly subparallel to the Cross Shear Zone. U–Pb dating of a porphyry dyke produced an age of  $1881.8 \pm 3$  Ma (Sparkes *et al.*, 2010). The quartz–feldspar porphyry dykes locally crosscut mineralization hosted within the MVS (Plate 51); however, locally uranium mineralization is also observed along discrete fractures and along the sheared margins of the porphyry dykes. The mineralization developed within the porphyry dykes is attributed to the remobilization of uranium during reactivation of the Main Shear Zone. This same deformation results in a sinistral offset of the dykes at depth within the exploration adit (Piloski, 1958). The later sinistral deformation is potentially related to the narrow, greenschist-facies, sinistral zones assigned to  $D_6$  by Culshaw *et al.* (2000).

The entire deposit is crosscut by a relatively flat-lying, to gently southwesterly dipping, undeformed diorite dyke,



**Plate 51.** Mineralized metasedimentary rock (left) containing up to 0.09%  $U_3O_8$  as well as 0.3% Mo and 1.31 ppm Re, crosscut by a quartz–feldspar porphyry dyke (right) containing up to 0.04%  $U_3O_8$  associated with fractures; Kitts deposit.

which consists of dark-green euhedral amphibole phenocrysts within a white plagioclase-rich groundmass (Plate 52). This dyke has produced a U–Pb age of  $1662 \pm 4$  Ma (Sparkes *et al.*, 2010). Petrographic examination of this dyke indicates well-developed igneous growth zoning preserved within the euhedral amphibole, and the intrusion appears to be entirely posttectonic. Thus, the intrusion represents the youngest unit within the deposit and it postdates development of the uranium mineralization and is inferred to postdate the  $D_6$  sinistral shearing of Culshaw *et al.* (2000).

The C Zone, which occurs approximately 200 m to the north-northeast of the main Kitts deposit, is predominantly hosted within mafic tuff and interbedded chert, along with lesser argillite and greywacke (Figure 27). This zone was interpreted by Evans (1980), to represent a second volcanoclastic unit within the stratigraphic sequence. However, Gandhi (1978) interpreted that the mineralization occurred within the same sequence, but was located on the opposite side of a major synclinal structure. Drilling within the C Zone has shown the mineralization to be of narrow width and limited extent (Piloski, 1968); existing drillhole data provides insufficient information to confirm whether or not this mineralization is connected with the main Kitts deposit at depth. This possibility remains intriguing in terms of potential for additional resource identification should the area become open for exploration and development.

### Mineralization and Associated Alteration

The uranium mineralization within the Kitts deposit is unequally distributed between the A, B and C zones. The bulk of the mineralization is contained within the B Zone, which is considered to be the result of folding and thickening of the mineralized MVS, along the Main and Cross shear zones (Beavan, 1958; Gandhi, 1978). The exact nature of this folding is unknown, but regional fold structures mapped by Martin (1977) are related to  $D_3$  ( $D_4$  of Culshaw *et al.*, 2000). Local embayments within the intrusive contact of the adjacent

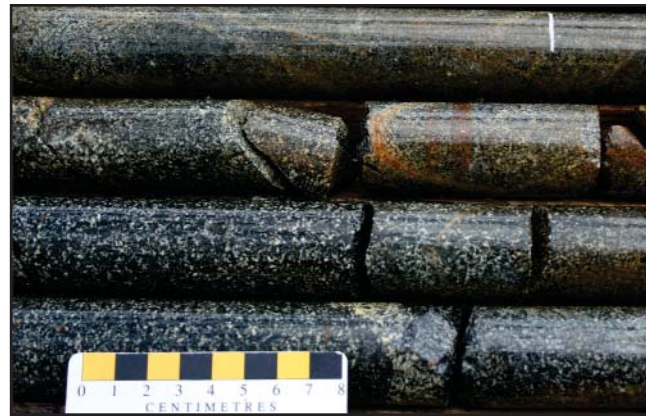


**Plate 52.** Undeformed, fine- to medium-grained amphibole-rich diorite dyke. DDH B-11, ~25 m depth; Kitts deposit.

metagabbro are also thought to contribute to the concentration of high-grade mineralization (Beavan, 1958), potentially acting as traps for mineralizing fluids.

Within the A and B zones the mineralization has been subdivided into six separate lenses, each of which displays significant variation in both dimension and grade with respect to depth. These mineralized lenses plunge toward the southeast along the Main Shear Zone (Evans, 1980). The mineralization is developed within a group of narrow shear zones ranging in width from 1–2 m and forming an *en-echelon*-like pattern within a zone 380 m long and up to 36 m wide; however the zone is more typically less than 5 m in width and extends to at least a depth of 150 m (Evans, 1980). These zones have a strike of 320°, dip moderately to steeply toward the northeast, and plunge approximately 40–50° to the southeast. Local evidence for sinistral motion exists within the Main Shear Zone; however, because this offset affects the quartz-feldspar porphyry dykes, the motion is interpreted as a later reactivation of structures in the area. The mineralization is predominantly hosted within the graphite and pyrrhotite-bearing argillite, but minor mineralization is also locally hosted within mafic tuff and quartz-feldspar porphyry. Within the A Zone, mineralization occurs within mafic tuff, argillite and mafic dykes, and also displays a close spatial association with the development of carbonate veining (Evans, 1980).

Within the mineralized lenses, uranium, in the form of uraninite and lesser coffinite, is commonly present as high-grade veins along narrow shear zones (Figure 30; Plate 53); however, lower grade, finely disseminated material is also locally developed. Gandhi (1970) highlighted that mineralization was preferentially developed along certain stratigraphic intervals within the MVS, particularly those enriched in pyrrhotite, and inferred the mineralization to have a primary stratigraphic control. Most of the high-grade vein-hosted mineralization is developed within argillite and mafic tuff and also includes rare occurrences within mafic dykes (Evans, 1980). The host rock commonly contains hornblende, sericitized plagioclase, chlorite, muscovite and minor garnet (Evans, 1980). Evans also noted that the 'pitchblende' generally occurred as 1–3 mm microcrystalline clots or veinlets and were either: 1) rimmed by Fe-rich chlorite, 2) incorporated within amphibole crystals or, 3) intergrown with calcite, graphite and pyrrhotite. The incorporation of 'pitchblende' within amphibole crystals was interpreted by Marten (1977) as supporting evidence for the development of the uranium mineralization during D<sub>1</sub>–D<sub>2</sub> deformation. Alteration surrounding the mineralization is very subtle and it is often hard to visually distinguish mineralized and unmineralized material in drillcore. Evans (1980) noted chemical evidence for a very narrow halo (generally <1 m) of sodic alteration developed within the greywacke and argillite units adjacent to mineralization, however, there is no visible evidence for this alteration.

Although the quartz-feldspar porphyry dykes crosscutting the deposit are interpreted to postdate the formation of the primary uranium mineralization, they are host to minor zones of fracture-hosted mineralization. This mineralization represents remobilization of the primary uranium mineralization. Locally, assays of up to 0.24% U<sub>3</sub>O<sub>8</sub> are obtained from within these quartz-feldspar porphyry dykes (Evans, 1980). Within these mineralized fractures, which are dominantly infilled with calcite and/or quartz, uranium mineralization is generally accompanied by hematization of the surrounding host rock. These dykes have locally undergone alteration where they crosscut the MVS, resulting in an enrichment of Ca and Na. Altered porphyries contain an average of 16.8 ppm U, whereas the unaltered equivalents contain an average of 10.2 ppm U (Evans, 1980).

### Petrography

As noted above, most of the uranium mineralization within the Kitts deposit is hosted within the MVS, where it occurs as very fine-grained disseminated material, which is locally concentrated within centimetre-scale veins. Metamorphic amphiboles hosting uranium mineralization are identified in thin section by the associated brownish haloes developed around the uraniferous minerals (Plate 54A), which in most instances is uraninite in association with lesser amounts of coffinite. In Plate 54A, the mineralization is cross-cut by a second generation of amphibole and lesser quartz,

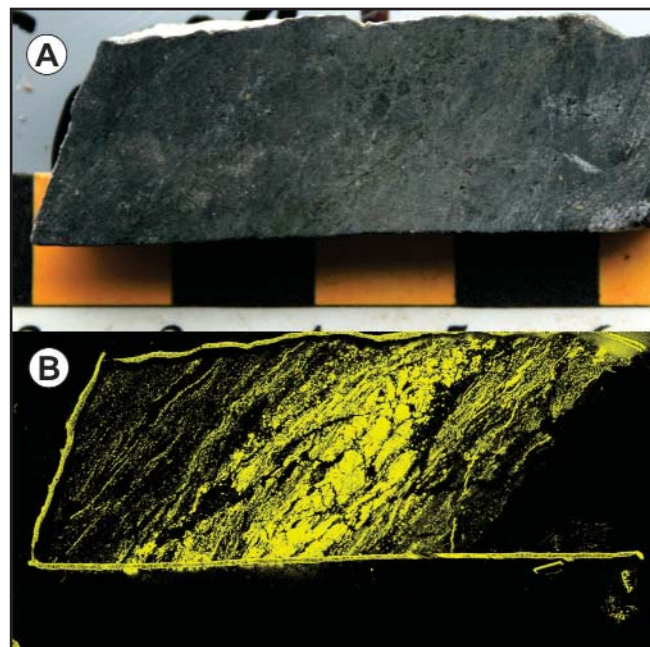


**Plate 53.** A. Hand sample of vein-hosted uranium mineralization, B. Corresponding autoradiograph of the uranium mineralization (yellow, minus the outline of the sample) within the hand sample. DDH K-74-18, Kitts deposit, ~118 m depth.

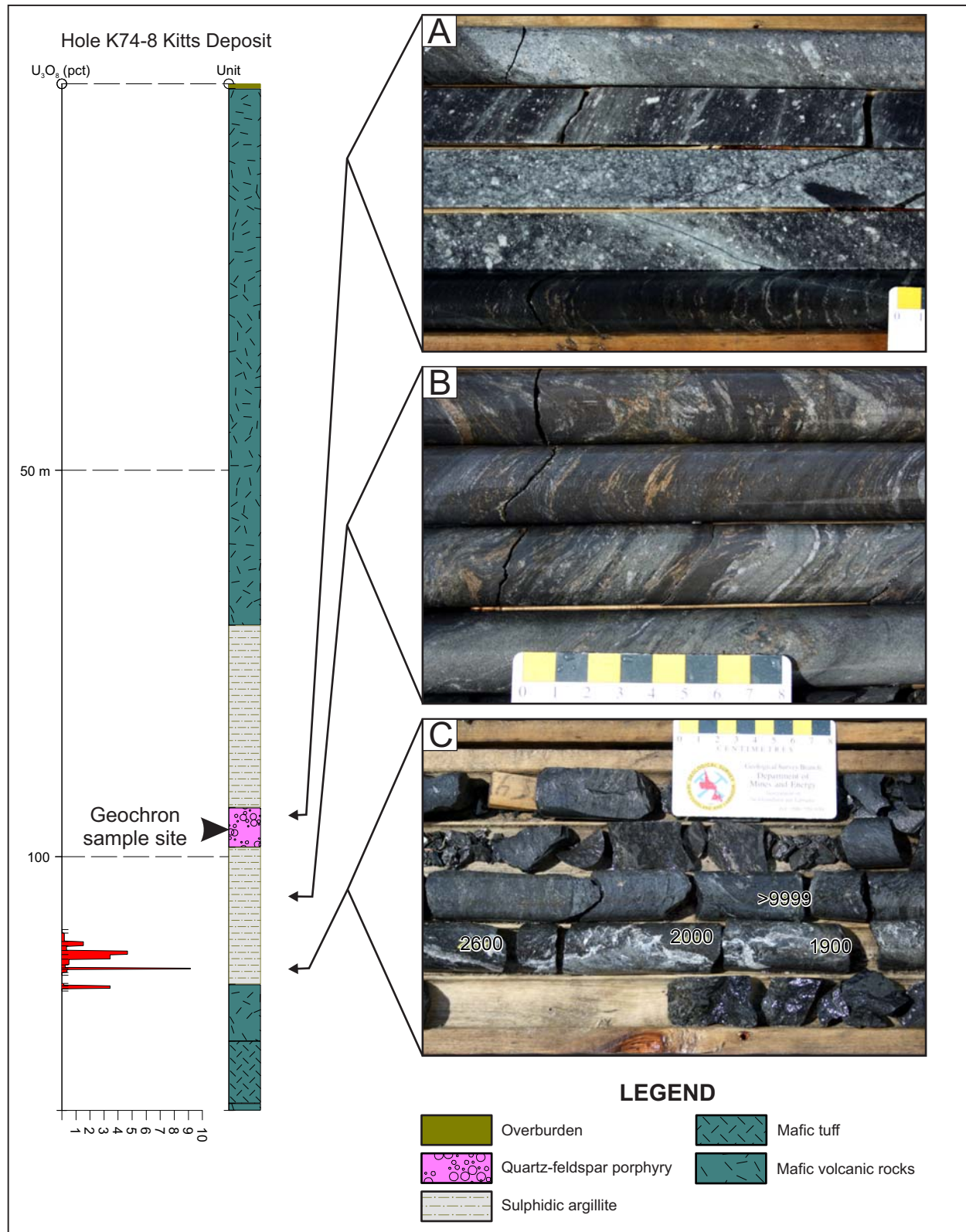


**Figure 30.** Partial drill log for hole K74-8 from the Kitts deposit, outlining the distribution of uranium mineralization and collection site of the geochronology sample from the quartz-feldspar porphyry dyke; values are listed in weight percent (data from Davidson et al., 1978). A. Dated quartz-feldspar porphyry dyke, B. Barren sulphidic argillite above mineralized zone, C. Sulphidic argillite unit hosting discrete vein-hosted uranium mineralization (note labels on the drillcore denote counts per second).

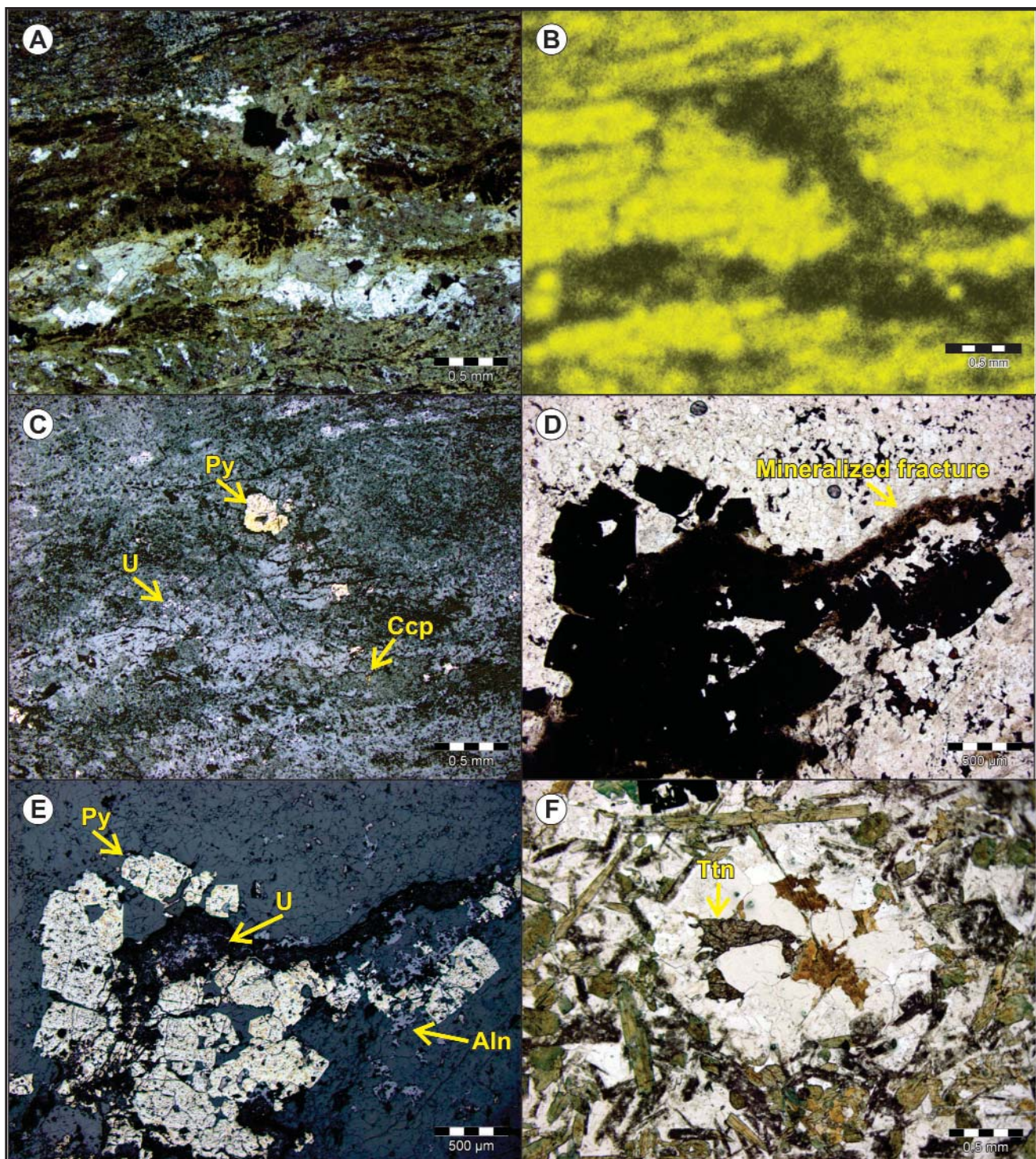


**Plate 54.** Mineralized sample shown in Plate 53 from the Kitts deposit. **A.** Uranium mineralization hosted with amphibole and rimmed by the development of brownish haloes, PPL. **B.** Autoradiograph of the thin section shown in (A) outlining the distribution of radioactivity (yellow); note the region of the second generation of amphibole (dark areas) is devoid of any significant radioactivity (refer to text). **C.** Reflected-light photomicrograph of the mineralized area shown in (A) illustrating the finely disseminated nature of the uraninite (U) in association with minor pyrite (Py) and trace chalcopyrite (Ccp). **D.** PPL photomicrograph of an uraniferous fracture crosscutting the quartz-feldspar porphyry unit. **E.** Reflected-light photomicrograph of (D), outlining the distribution of pyrite (Py), uraninite (U) and allanite (Aln) within the sample. **F.** PPL photomicrograph of titanite (Ttn) occurring within late-stage quartz-rich segregations in the diorite unit.

and is devoid of any significant radioactivity as indicated by the accompanying autoradiograph (Plate 54B); this later stage of amphibole is also locally host to trace chalcopyrite (Plate 54C).

The localized mineralization within the quartz-feldspar porphyry dykes is generally confined to discrete fractures infilled with uraninite. Locally, allanite is developed within the groundmass of the porphyry marginal to mineralized fractures (Plate 54D, E). The mineralized fractures are, in turn, overgrown by late-stage, coarse-grained, pyrite (Plate 54E).

One of the youngest units within the Kitts deposit is the diorite dyke, which contains amphibole crystals displaying well-developed growth zoning within a finer grained, quartz and plagioclase feldspar-rich groundmass. Locally, late-stage, quartz-rich segregations are observed within the groundmass; these late-stage segregations contain titanite, and are inferred to be of an igneous origin. This titanite is inferred to represent the dated titanite, which gives an age of *ca.* 1660 Ma (Sparkes *et al.*, 2010; Plate 54F).

## GEAR, INDA AND NASH DEPOSITS

### Previous Work

The Gear, Inda and Nash deposits (Figure 31), located to the southwest of the Kitts deposit, have also been the subject of several detailed exploration programs and scientific studies, but have not been studied in equivalent detail. Marten (1977) subdivided the mineralization within the area into two separate groups, namely that occurring within iron formation within the Kitts Pillow Lava Formation (*e.g.*, Gear and Inda deposits), and that occurring within the Nakit Shear Zone (*e.g.*, Nash deposit). He concluded that the mineralization within the area formed during early- to syntectonic mobilization of uranium from the overlying felsic volcanic rocks of the Aillik Group into major shear zones (*i.e.*, Nakit Shear Zone) during D<sub>1</sub>-D<sub>2</sub> deformation (Marten, 1977). Evans (1980) conducted a detailed examination of drillcore and surface trenches across mineralized zones in the area and concluded that the mineralization was primarily structurally controlled. He also noted the presence of elevated V, Cu and Zn in association with some of the uranium enriched samples; these samples were located close to altered argillite, which he inferred to be the source of the base-metal mineralization.

### Local Geology

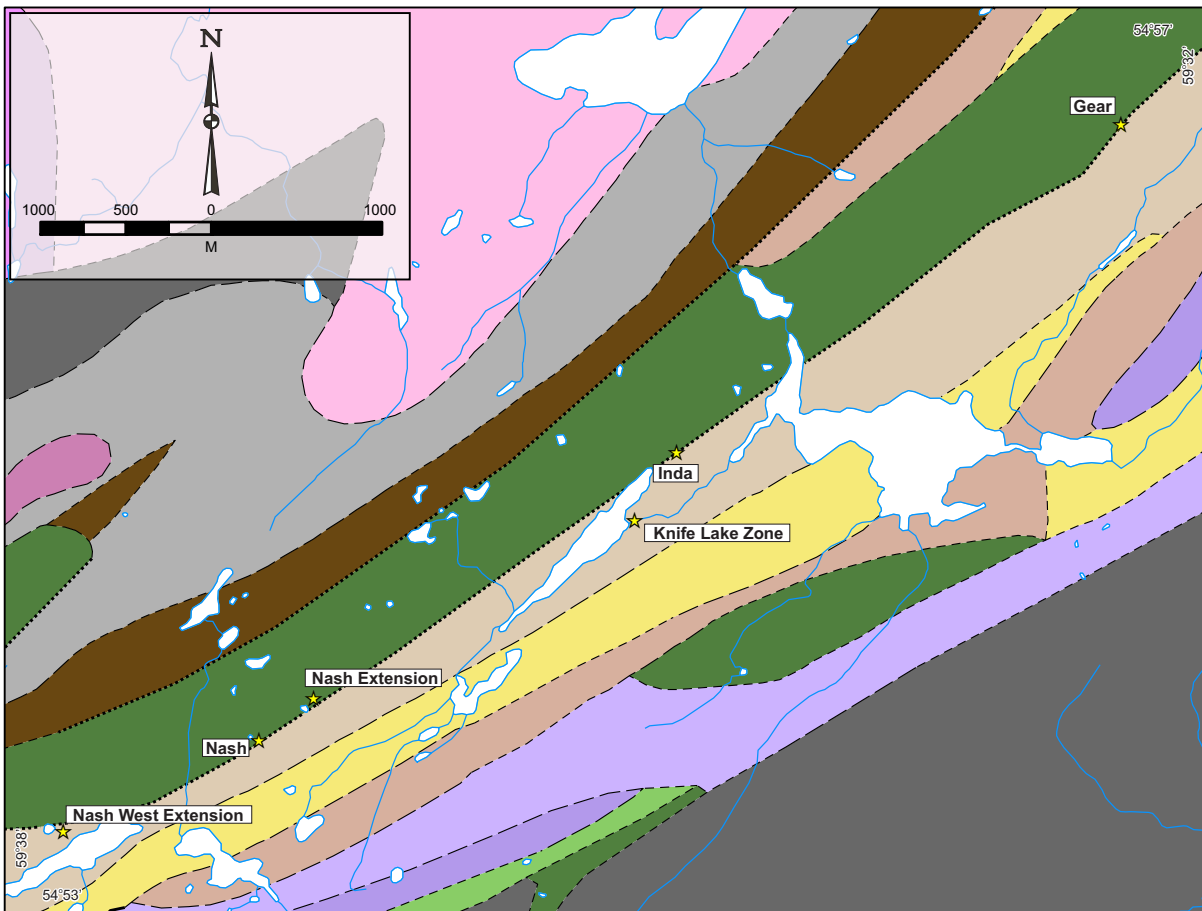
The area spanning from the Gear deposit in the north to the Nash West Extension prospect in the south, also referred to as the Inda Lake Trend (Cunningham-Dunlop and Lee, 2008), contains uranium mineralization primarily concentrated in the upper portions of the Post Hill Group, close to

the tectonic contact with the overlying Aillik Group (Figure 31). The footwall to the mineralized zones is largely dominated by mafic volcanic rocks and lesser tuffs of the Kitts Pillow Lava Formation. Mineralization is primarily developed within argillite, pelitic and non-pelitic greywacke, mafic tuff and minor chert, which are interbedded with the Kitts Pillow Lava Formation (Evans, 1980). Units correlated with the Post Hill Group are separated from the overlying Aillik Group by a strongly sheared contact (Marten, 1977; Gower *et al.*, 1982; Wardle, 1984) that has been interpreted as being both unconformable (Marten, 1977; Gower *et al.*, 1982; Cunningham-Dunlop and Lee, 2008) as well as conformable (Evans, 1980), but evidence suggests that it is largely tectonic (Ketchum *et al.*, 2001a).

Marten (1977) interpreted a regionally extensive conglomerate unit as the basal unit of the Aillik Group, which he concluded was originally disconformable upon underlying rock units of the Post Hill Group. The 'Banded Tuff Formation' of Marten (1977) lies immediately east of the Post Hill Group, and represents the first occurrence of Aillik Group rocks east of the contact; these rocks are separated from the underlying units by a major shear zone. Both Marten (*op. cit.*) and Evans (1980) had similar interpretations of Post Hill Group stratigraphy, which consists of mafic volcanic rocks overlain, and or interbedded with, minor metasedimentary rocks. Evans (1980) further subdivided these units into a conformable volcaniclastic sequence consisting of chert, argillite and greywacke, all of which were interbedded with varying amounts of mafic tuff. Based on observations from both the Gear and Inda deposits, this succession was interpreted by Evans (1980) to be right-way up and younging to the east. The metasedimentary rocks were, in turn, overlain by what he termed the 'Transition Zone', consisting of intercalated mafic and felsic volcanic tuffaceous units, which he interpreted as marking the conformable transition from the Post Hill Group into the overlying 'Banded Felsic Tuff' unit of the Aillik Group.

To the immediate west of the Post Hill Group along the Inda Lake Trend, Aillik Group rocks are dominated by massive to weakly bedded volcaniclastic sandstones and lesser rhyolite flows, felsic tuff and volcaniclastic breccia (Hinchey and LaFlamme, 2009). These rocks are generally devoid of any significant uranium mineralization; however, local geochemical evidence suggests alkali metasomatism of these rocks, which Evans (1980) suggested to be similar to that seen farther east in the vicinity of the Michelin deposit.

Mineralization within the Gear deposit is developed along the southeastern limb of a doubly plunging antiform (Cunningham-Dunlop and Lee, 2008). Within the deposit, uranium mineralization is confined to units of the Post Hill Group, with most of the mineralization hosted within argillite



## LEGEND

### Aillik Group

- Hypabyssal quartz and feldspar porphyritic rhyolite
- Porphyritic to nonporphyritic quartz-feldspar rhyolite, ash fall tuff, minor subaqueous tuff and tuffaceous sandstone
- Polyolithic conglomerate with granite, rhyolite and sedimentary clasts; volcanic breccia in part, minor monolithologic rhyolite breccia and conglomerate
- Well-bedded green, grey and pink tuffaceous sandstone and siltstone, minor marble

### Post Hill Group

- Mafic pillow lavas, mafic tuffaceous sandstone, amphibolite
- Dark-grey, quartzofeldspathic sandstone and siltstone, graphitic and pyritic siltstone, psammitic-pelitic schist

### ARCHEAN

- Banded granodioritic gneiss, granodioritic migmatite; amphibolite

### Synkinematic Intrusions

- Coarse-grained leucocratic monzonite
- Porphyritic plagioclase diabase
- Medium- to fine-grained, grey quartz monzonite to granodiorite; locally schlieric

### ARCHEAN

#### Remobilized rocks

- Migmatitic quartz monzonite, granodiorite and granite with irregularly shaped gneiss rafts
- Brumwater granite: Leucocratic biotite granite and quartz monzonite
- Granite migmatite, paleosome of Hopedale gneiss in schlieric granite neosome
- Refoliated granodioritic gneiss, grey foliated granodiorite, quartzitic mylonite

### SYMBOLS

Contact, (defined, assumed)



Fault, (defined, assumed)



Uranium Occurrence



**Figure 31.** Regional geology map outlining the main distribution of units within the area of the Gear, Inda and Nash deposits (geological base map modified from Gower et al., 1982).

rocks immediately above amphibolitized mafic volcanic rocks of the Kitts Pillow Lava Formation (Figure 32). The metasedimentary rocks hosting the uranium mineralization along the Inda Lake Trend are thickest at the Gear deposit (Evans, 1980). However, the overall thickness of these rocks does not correlate with the abundance of uranium mineralization, as the Gear deposit contains the smallest defined resource of the three deposits along the Inda Lake Trend (Table 7). Within the Gear deposit, the footwall mafic volcanic rocks are fine grained and massive; however, localized pillow structures have been reported from outcrops in the area (Evans, 1980). The overlying metasedimentary rocks are strongly deformed, making the interpretation of the original rock units and their contacts difficult to identify. These rocks locally contain garnetiferous pelite, minor psammite, and interbedded mafic tuff (Plates 55 and 56).

Due to the strong deformation, tracing the various units along strike is problematic. However, in a broad sense, uranium mineralization appears to be associated with a characteristic alteration assemblage hosted by discrete shear zones within a predominantly mafic tuffaceous metasedimentary unit. At the Gear deposit, the host rocks to the uranium mineralization appear to be more quartz-rich. Regardless of the original composition of the metasedimentary rocks, these units form the main locus of early shearing in the region, and thus are the primary host to uranium mineralization (*cf.*

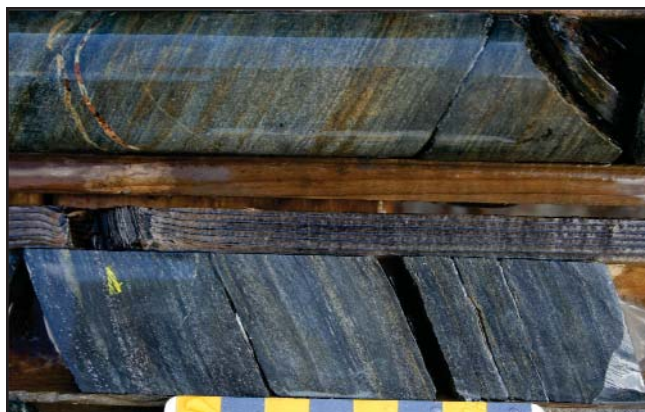


**Plate 55.** Garnetiferous metasedimentary rocks overlying amphibolite; DDH G-68-132, ~37 m depth; Gear deposit.

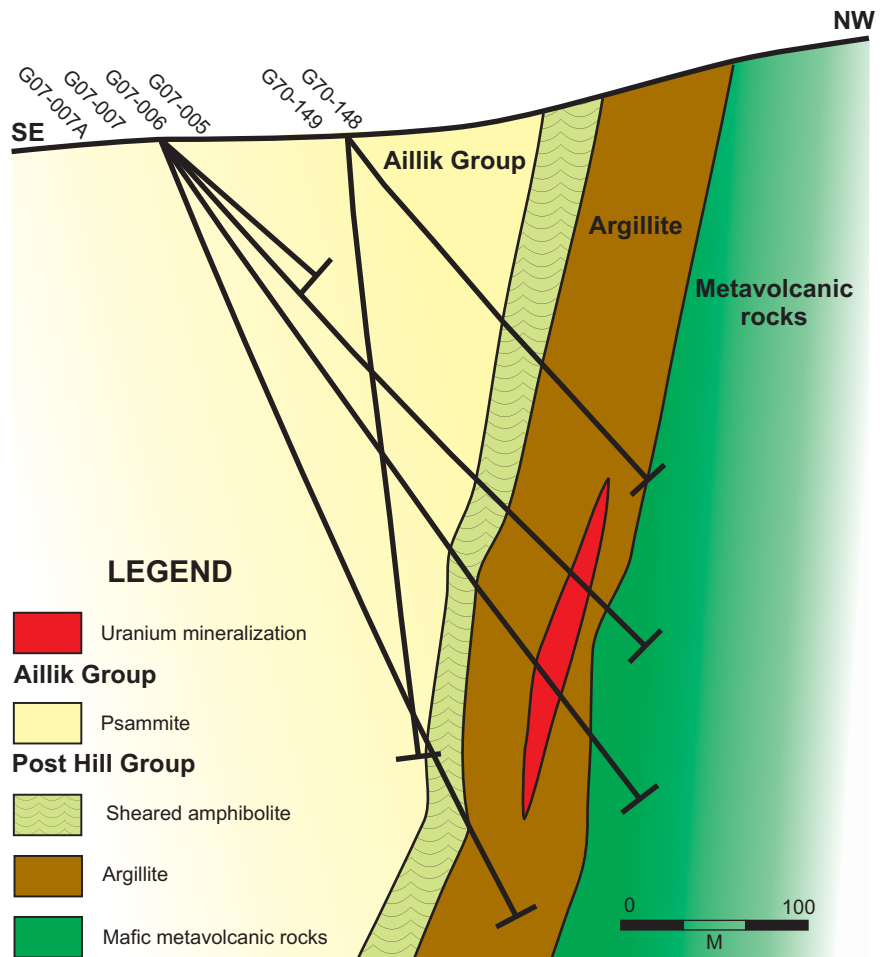


**Figure 32.** Simplified cross-section through the Gear deposit, looking southwest (modified from Cunningham-Dunlop and Lee, 2008).

Marten, 1977; Evans, 1980). Evans (1980) noted that the mineralized trend is truncated to the northeast of the Gear deposit by a structure that he termed the Watts Lake Shear Zone. To the southwest, similar lithological units along with accompanying uranium mineralization reoccur approximately 3.5 km along strike at the Inda Lake deposit (Figure 31).

Within the Inda deposit, uranium mineralization is associated with a complex zone of interleaved felsic and mafic volcanic rocks, bounded by altered and sheared Kitts Pillow Lava Formation (Evans, 1980). Rocks within this area generally strike northeast–southwest and dip between 60–85° to the southeast (Srivastava, 1976). The overall stratigraphic sequence is reportedly folded, both in plan and in section view, with at least two generations of folding identifiable in outcrop (Cunningham-Dunlop and Lee, 2008). The mineralization is interpreted to occur within the upper southeastern limb of a northeasterly trending anticline that is overturned to the northwest (Srivastava, 1976; Figure 33). However, the sequence was viewed by Evans (1980) to be right-way up and younging



**Plate 56.** Intercalated mafic and felsic tuffaceous beds within the 'Transition Zone' of Evans (1980). This unit is locally intruded by fine-grained pink aplite dykes, which are, in turn, deformed with the host rock; DDH G-68-142, ~ 20 m depth; Gear deposit.

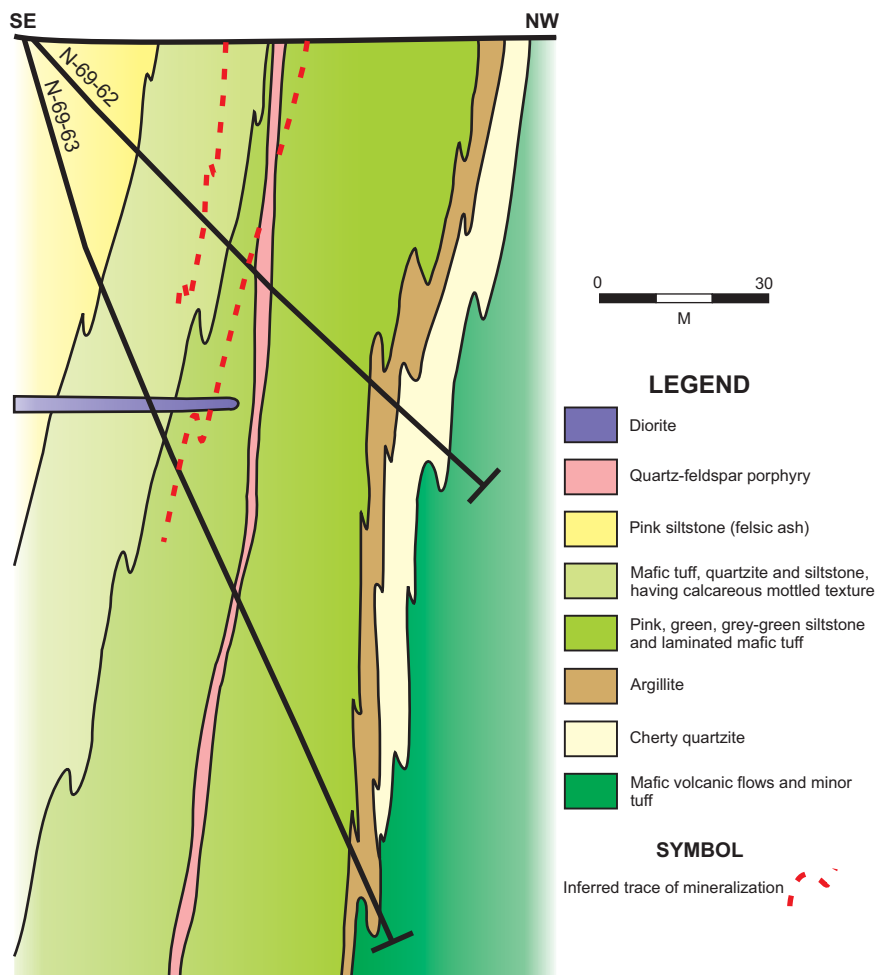


**Figure 33.** Simplified cross-section through the Inda deposit, looking southwest (modified from Srivastava, 1976).

to the east. Due to the structural complexity of the area, the exact details of the attitude and geometry have yet to be fully resolved. The northern limit to the uranium mineralization corresponds with the pinching out of a calcareous mafic tuff (Evans, 1980). In the same area, the northeast trend of the sequence is disrupted by a southeast-trending fault; this structure was inferred to represent a  $D_3$  shear zone by Marten (1977).

A small intrusion of metamorphosed gabbro close to the Inda deposit was noted by Marten (1977), and potentially represents a correlative to the Kitts Metagabbro. A quartz-feldspar porphyry unit is also noted to occur within the deposit, and is reported to crosscut the mineralization at an oblique angle (Srivastava, 1976), similar to the relationship observed at the Kitts deposit. Sills and dykes of similar quartz-feldspar porphyry span the region between the Kitts and Nash deposits, have comparable textures and geochemical characteristics, and display similar structural relationships with the older rocks. These are all inferred to be correlative (Evans, 1980).

At the Nash deposit, uranium mineralization is developed within the Nakit Shear Zone (Marten, 1977). Here, the mineralization is primarily confined to mafic-rich metasedimentary rocks that overlie and/or are interbedded with the Kitts Pillow Lava Formation (Plate 57), which occurs to the immediate north of the deposit. The mineralization is primarily focused within the footwall of the inferred structural contact that separates the Post Hill Group to the west from the overlying Aillik Group to the east (Figure 34). However, limited mineralization has also locally been intersected within rocks inferred to be correlative with the Aillik Group at the Nash West Extension prospect (Gentile *et al.*, 1977). The garnetiferous metasedimentary rocks observed at the Kitts and Gear deposits are notably absent at the Nash deposit. Here, uranium mineralization is predominantly hosted within a mafic tuffaceous unit referred to as the 'Transition Zone' by Evans (1980). This unit resembles mineralized rocks at the Gear deposit, and is locally interbedded with thin- to medium-bedded, pale-pink material, which may represent a minor felsic tuffaceous component. The transition into what is interpreted to be Aillik Group rocks is generally sharp; however, the actual contact is not exposed at

surface. The surface expression of the contact is marked by an abrupt change in the overall background radioactivity, with elevated radioactivity confined to the Post Hill Group in the footwall. Immediately adjacent to this contact zone, rocks of the Post Hill Group display a strongly developed foliation and

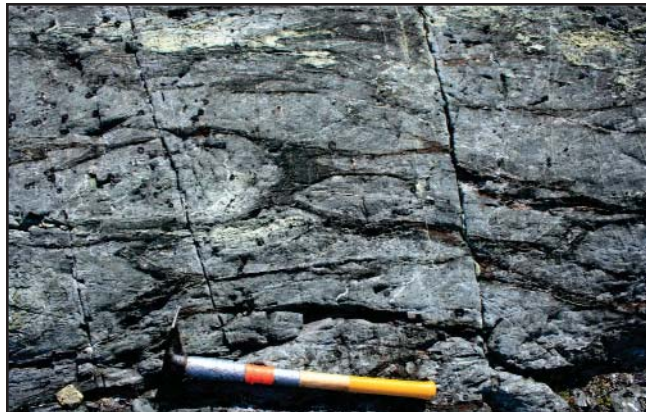


**Plate 57.** Deformed pillow basalt of the Kitts Pillow Lava Formation immediately adjacent to, and structurally below, mineralized tuffaceous rocks at the Nash deposit.

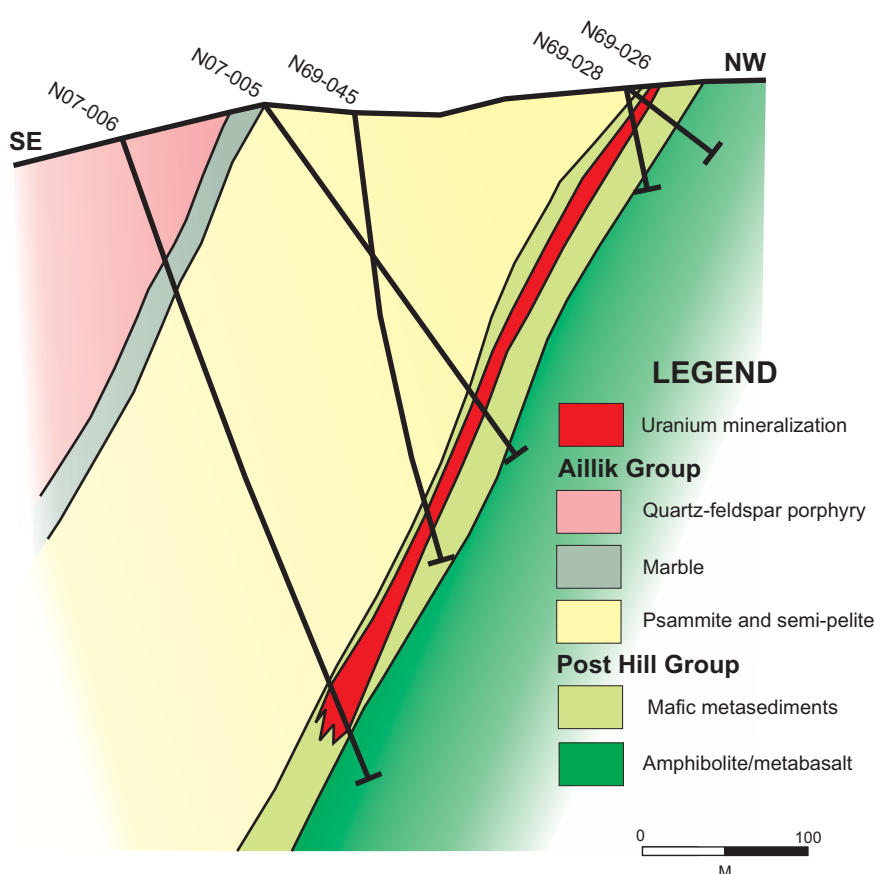


**Figure 34.** Simplified cross-section through the Nash deposit, looking southwest (modified from Cunningham-Dunlop and Lee, 2008).

tight, metre-scale folding. In contrast, no folding is evident within the strongly foliated rocks of the hanging wall (Plate 58).

### Mineralization and Associated Alteration

Within the Inda Lake Trend, most of the mineralization is inferred to be structurally controlled (e.g., Marten, 1977; Evans, 1980) and it is locally associated with hydrothermal alteration. Uranium mineralization is hosted within shear zones, up to 3 m wide, and within zones of magnetite–hornblende veining, which locally attain widths of up to 12 m (Evans, 1980). Most of the alteration zones along the Inda Lake Trend are hosted by, or developed immediately below, the ‘Transition Zone’ of Evans (1980). Within this zone, the host rocks display a well-developed foliation, which is subparallel to the compositional layering, and mineralization is developed subparallel to this main foliation.

Mineralization at the Gear deposit ranges from 0.21%  $U_3O_8$  over 0.15 m to 0.034%  $U_3O_8$  over 12.35 m, but generally averages between 0.025 to 0.073%  $U_3O_8$  over 1.7–2.44 m and is hosted within a complex set of mineralized shear

zones (Evans, 1980). These mineralized shear zones are defined over a strike length of 200 m (Cunningham-Dunlop and Lee, 2008), and pinch out along strike (Evans, 1980). Within this zone, hydrothermal alteration, defined by the development of hornblende and pyroxene, is locally developed (Plate 59) over widths of up to 55 m within the shear zones (Evans, 1980). These zones locally have anomalous Cu and Zn values in association with uranium mineralization. Evans (1980) noted the close spatial association between the base-metal enrichment and the presence of the argillite unit, and postulated that these rocks may act as the source for the base-metal enrichment. Locally, up to 0.89%  $V_2O_5$  has also been reported for selected mineralized samples from the deposit (Ruzicka, 1971). In detail, the uranium mineralization, mainly in the form of uraninite, occurs as very fine-grained disseminations contained within amphibole and biotite, which locally display a preferential concentration along early  $S_1$ – $S_2$  schistosity planes; these minerals are inferred to be developed during early metamorphism in the region (Marten, 1977). Evans (1980) also noted the association of uranium mineralization with

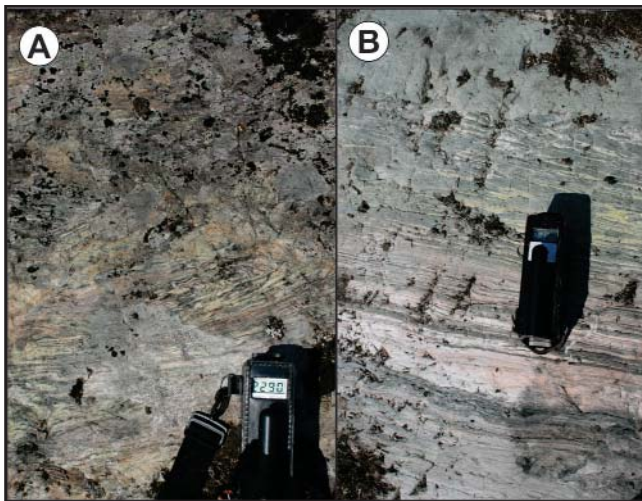


**Plate 58.** A. Predominantly mafic tuffaceous rocks of the Post Hill Group displaying a strong foliation and localized folding within the footwall of the Nash deposit, B. Interbedded pink felsic tuff with associated tuffaceous sandstone of the Aillik Group in the hanging wall of the Nash deposit.

the development of magnetite and actinolite bands occurring in altered host rocks.

Rocks hosting uranium mineralization at the Gear deposit display a pale- to light-green alteration associated with the development of pyroxene, which is locally accompanied by the development of minor sulphide veins; this alteration appears to locally overprint earlier uranium mineralization (Plate 59B, C). Evans (1980) noted the development of amphibole and lesser magnetite, in which the 'pitchblende' is often contained as fine-grained disseminations within the amphibole crystals. These mineralized zones are very discrete and are inferred to be structurally controlled (Marten, 1977; Evans, 1980). Although rocks similar to those seen at the Kitts deposit are locally present within the stratigraphy at the Gear deposit (Plate 60), these units are devoid of any significant uranium mineralization in this area.

At the Inda deposit, the mineralized zone has an approximate strike length of 945 m and ranges from 6 to 33 m in width. This zone is encompassed by a broader (100–150 m) barren alteration envelope along shear zones within the metavolcanic host rocks (Evans, 1980). The widths and grade of the mineralization vary both along strike and at depth, but typical mineralized intersections average  $\leq 0.10\% \text{ U}_3\text{O}_8$  over widths  $\leq 3$  m (Evans, 1980). Within the mineralized shear zones, Evans (1980) identified two main types of alteration; the first being plagioclase–magnetite–titanite, and the second being a less-abundant calcareous-rich alteration. Uranium mineralization occurs as very fine-grained disseminations and is subdivided into two main styles namely: 1) narrow, relatively high-grade veins, and 2) broad low-grade disseminations.

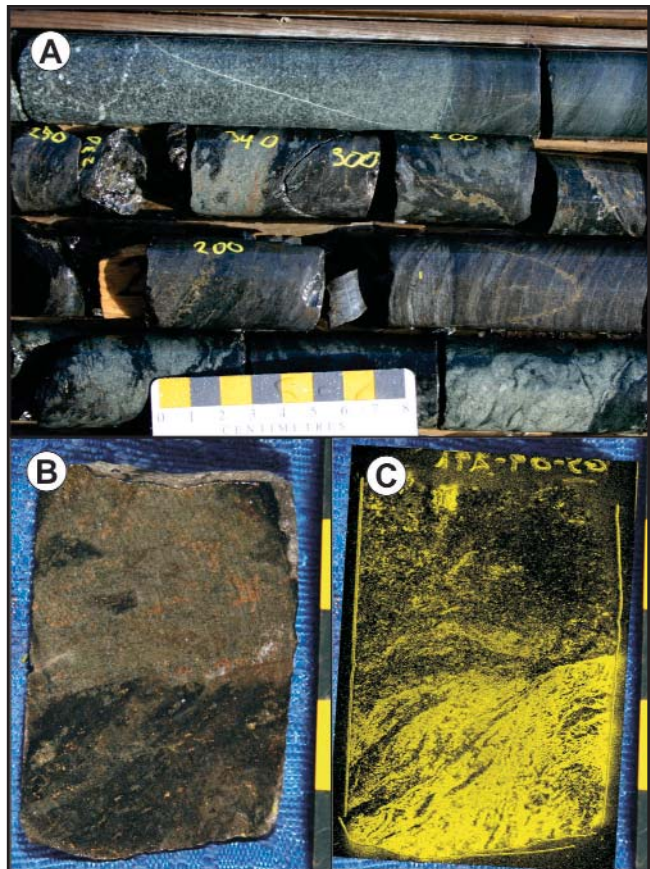


**Plate 59.** A. Hydrothermally altered metasedimentary rocks hosting anomalous radioactivity; DDH G-68-142, ~83 m depth; Gear deposit, B. Mineralized drillcore showing a late, light-green, alteration assemblage overprinting earlier uranium mineralization, C) Corresponding autoradiograph for the sample shown in (B) outlining the uranium mineralization (yellow, minus the outline of the sample) within the hand sample.



**Plate 60.** Sulphidic argillite, similar to that seen at the Kitts deposit, containing syn-sedimentary sulphides and minor porphyroblasts of garnet. DDH G-68-131, ~80 m depth; Gear deposit.

tions. The most significant portion of the mineralization occurs as discrete narrow veins, which predominantly give grades of  $\leq 0.10\%$   $\text{U}_3\text{O}_8$ ; these veins range from 0.3 to 5.2 m in width and do not show affinities with any particular rock type (Evans, 1980). The broad zones of disseminated mineralization are generally restricted to plagioclase–magnetite-rich host rocks and typically range from 10 to 45 m in width. The uranium mineralization within these zones produces grades ranging from 0.025–0.035%  $\text{U}_3\text{O}_8$  and are inferred to occur as very fine-grained disseminations within mafic silicates (Evans, 1980). Limited data from the deposit suggest that a uranium–vanadium relationship may exist in mineralized zones (Evans, 1980). Typical vanadium values range from 0.06–0.20%  $\text{V}_2\text{O}_5$ , which Evans (1980) reported to predominantly occur in association with the development of grossular–andradite. Cunningham-Dunlop *et al.* (2008a) noted a spatial association between anomalous Ag, Cu, Zn and V with uranium mineralization, in addition to anomalous Au (<100 ppb); locally values include up to 148 ppm Ag, 0.05% Cu and 0.03%  $\text{U}_3\text{O}_8$  over 6.5 m (DDH I07-007; Cunningham-Dunlop *et al.*, 2008a).

The mineralization at the Inda deposit is primarily confined to metasedimentary rocks within upper portions of the Post Hill Group, proximal to the inferred tectonic contact with overlying rocks of the Aillik Group. However, limited mineralization has also been reported in rocks inferred to be part of the Aillik Group succession (Cunningham-Dunlop *et al.*, 2008a). This mineralization occurs in association with hematite–albite and/or magnetite alteration (Cunningham-Dunlop *et al.*, 2008a), and could potentially represent subsequent remobilization of the primary uranium mineralization from the underlying Post Hill Group. The limited uranium mineralization within trenches at the Inda deposit is hosted within thinly bedded, brown-weathering siltstone interbedded with lesser mm-scale black shale laminations and mafic tuff (Plate 61A). Here the uranium mineralization displays a largely stratiform distribution, which is also parallel to the predominant foliation developed within the unit (Plate 61B, C).

Within the Nash deposit, Marten (1977) noted that mineralization occurs within interbanded amphibolite and psammitic, where ‘pitchblende’ is present as fine-grained disseminated material within hornblende. He also noted the preferential development of uranium mineralization within bands enriched in hornblende–diopside–epidote–biotite–microcline–carbonate. Evans (1980) interpreted the mineralization to be primarily hosted within the ‘Transition Zone’ unit, along with minor mineralization within the footwall metavolcanic rocks. Mineralization at the Nash deposit occurs over 490 m of strike length, trending approximately  $65^\circ$  and dipping  $55^\circ$  to the southeast, with the mineralized zone apparently decreasing in size with increasing depth (Evans, 1980). As seen in the other deposits in the region, uranium mineralization is associated with anomalous enrichment of V and Cu



**Plate 61.** *A.* Uraniferous metasedimentary rocks with minor mafic tuff, Inda deposit, *B.* Mineralized metasedimentary rock displaying a strong foliation developed parallel to compositional layering within the sample, *C.* Autoradiograph of (B) outlining the roughly stratiform uranium mineralization (shown in yellow) within the sample.

(Evans, 1980), and Tracey (2009) also noted elevated As. The mineralization within the Nash deposit occurs as two distinct styles of veining; the first of which is associated with a calc-silicate alteration assemblage consisting of diopside–grossular–andradite–epidote  $\pm$  magnetite, whereas the second consists of rare hematite–calcite  $\pm$  epidote filled fractures (Plate 62). The first style of alteration is predominantly hosted within the ‘Transition Zone’, whereas the second style of alteration is generally confined to the metavolcanic rocks (Evans, 1980).

## ANNA LAKE DEPOSIT

### Previous Work

The area surrounding Anna Lake was first highlighted as an uranium exploration target by a regional helium anomaly from a lake-water survey carried out by Brinex in 1974 (Bea-

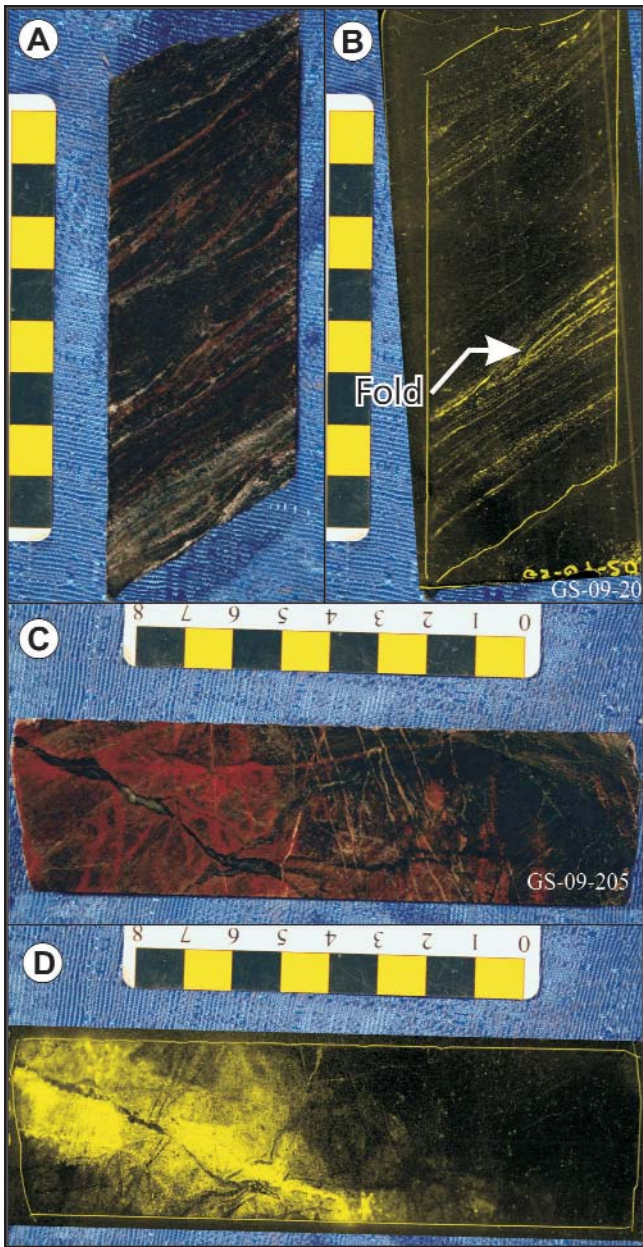


**Plate 62.** Contrasting styles of uranium mineralization developed within the area of the Nash deposit. *A.* Metavolcanic/metasedimentary host rock displaying foliation-parallel uranium mineralization as indicated by the accompanying autoradiograph. DDH NW-77-04, ~43 m; Nash West Extension prospect. *B.* Autoradiograph of the uranium mineralization (yellow, minus the outline of the sample) within the sample; note the tight isoclinal fold displayed by the uranium mineralization indicating that the mineralization has been deformed. *C.* Brittle fracture-hosted mineralization associated with hematitization of surrounding wallrock within felsic metavolcanic rocks of the Ailik Group. DDH NW-77-02, ~14 m; Nash West Extension prospect. *D.* Accompanying autoradiograph of (C) outlining the association of the radioactivity (yellow, minus the outline of the sample) with the hematite alteration.

van *et al.*, 1974). Subsequent work identified several zones of radioactive float, and limited follow-up diamond drilling was carried out by Brinex in 1981. This drilling intersected weakly mineralized schistose rocks, locally assaying up to 0.20%  $U_3O_8$  over 0.5 m (Willy *et al.*, 1982). Following these initial investigations little work was carried out until Bayswater re-examined the area in 2007. Since then, Bayswater has delineated a mineralized zone over 750 m of strike length, and down-dip to a depth of 665 m. Resource estimates in 2009 suggest a defined, NI 43-101 compliant, inferred resource of 4.91 million lbs of  $U_3O_8$  and 1.56 million lbs of Mo at a cutoff grade of 0.04%  $U_3O_8$  and 0.01% Mo (Fraser and Giroux, 2009).

### Local Geology

The regional geology of the Anna Lake area was mapped by Ryan (1984), and more detailed property mapping was carried out by Bayswater (Fraser and Giroux, 2009). Mapping is hampered by poor outcrop exposure and extensive Quaternary cover. The most recent work outlined five main lithological units within the area surrounding the Anna Lake deposit; these units are briefly summarized here; for a detailed description refer to Fraser and Giroux (2009). The most abundant supracrustal rocks consist of biotite schist and lesser mafic metavolcanic rocks that form a thin northeast-trending belt of rocks preserved between two intrusive bodies; these intrusions are grouped within the Southern Kaipokok Valley Intrusive Suite of Ryan (1984; Figure 35). Intrusive rocks in the area of the Anna Lake deposit are inferred to be intruded by the Junior Lake Granodiorite (Ryan, 1984), dated elsewhere at  $1893 \pm 2$  Ma (Kerr *et al.*, 1992). The supracrustal sequence in the area of Anna Lake has been correlated with similar rocks of the Post Hill Group located to the northeast (Fraser and Giroux, 2009).

The supracrustal sequence is intruded by several intrusive rocks that include magnetite-bearing granite, amphibolitized mafic intrusives, granite to granodiorite, and mafic dykes (Fraser and Giroux, 2009). All the mentioned units are variably deformed and are affected by folding and subsequent shearing. The supracrustal rocks are the predominant host to the uranium mineralization, similar to that observed along the Kitts–Post Hill Belt, although limited mineralization has been observed within the magnetite-bearing granite, most notably within shear zones that crosscut the unit (Fraser and Giroux, 2009). The supracrustal rocks are interpreted to have been folded by tight, northeast-trending, isoclinal folds that are overturned to the northwest (Fraser and Giroux, 2009). Within this folded sequence, the uranium mineralization forms a narrow, north–south-trending, undulating zone dipping between 50 and 70° toward the east; this zone consists of two subparallel zones of mineralization that locally coalesce to form a single body (Fraser and Giroux, 2009).

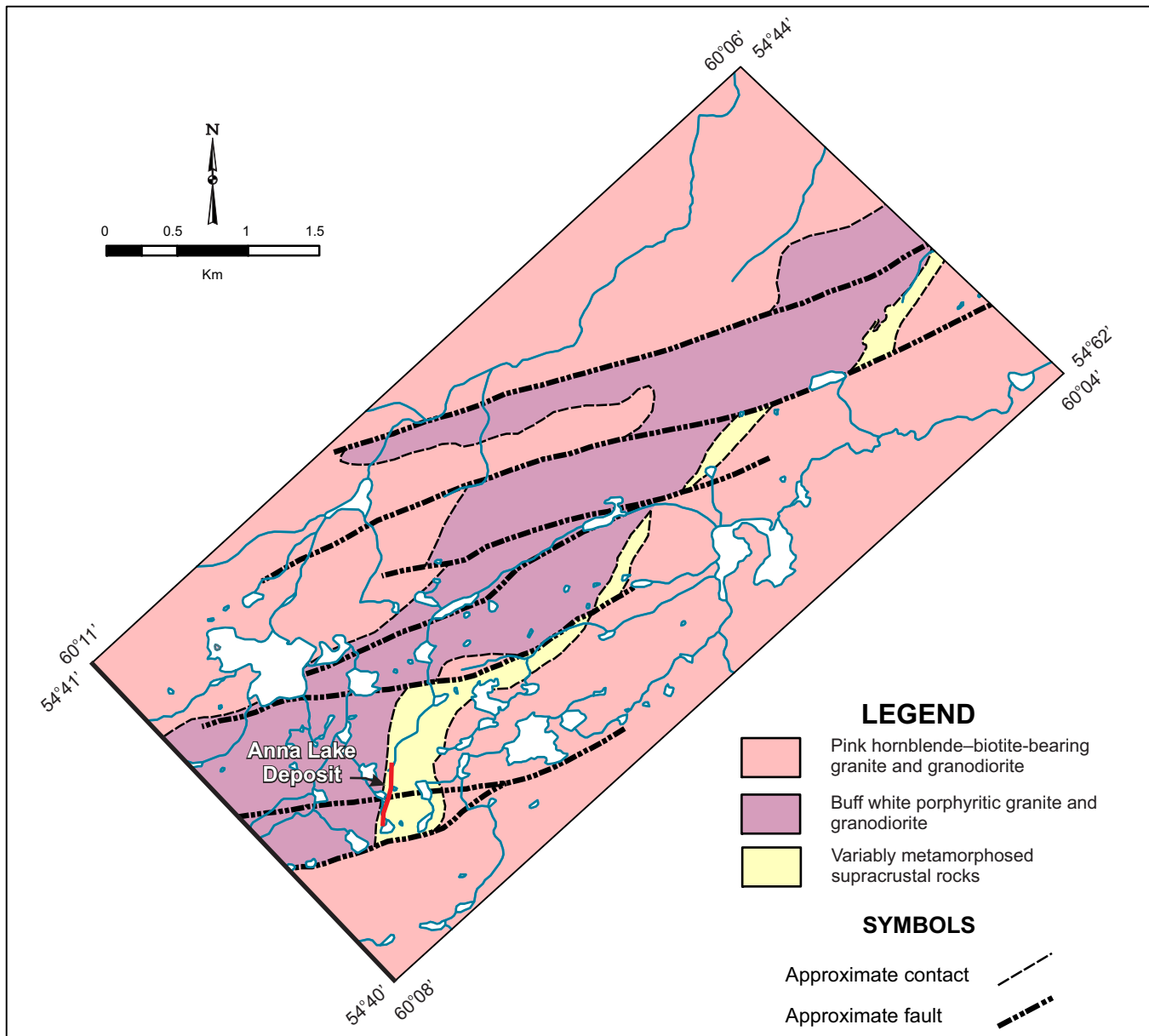


**Figure 35.** Geology map of the Anna Lake area (modified from Fraser and Giroux, 2009). For the regional location of the deposit refer to Figure 25.

#### Mineralization and Associated Alteration

Within the Anna Lake deposit, uranium mineralization occurs as uraninite and is preferentially developed within the grey, to red, to brown crenulated garnetiferous, biotite-bearing schist (Fraser and Giroux, 2009). Mineralization is accompanied by anomalous Mo and Re values, a feature that is also locally observed within the Kitts deposit. Uraninite occurs in association with finely disseminated oxide minerals, but is also locally observed as fine-grained material within pre-kinematic garnet porphyroblasts (Fraser and Giroux, 2009). The mineralization commonly displays a stratiform habit (Plate

63); however, it should be noted that due to the limited exposure, the exact relationship between compositional and primary sedimentary layering is not fully understood.

Uranium mineralization at the Anna Lake deposit is concentrated within thin amphibole-rich bands, where it occurs as finely disseminated material in association with magnetite. These bands are locally folded and overprinted by a crenulation cleavage that also affects the mineralization (Plate 63). The uranium mineralization has a predictable geometry, forming a thin zone as outlined by Fraser and Giroux (2009). Samples enriched in uranium are also noted to contain minor

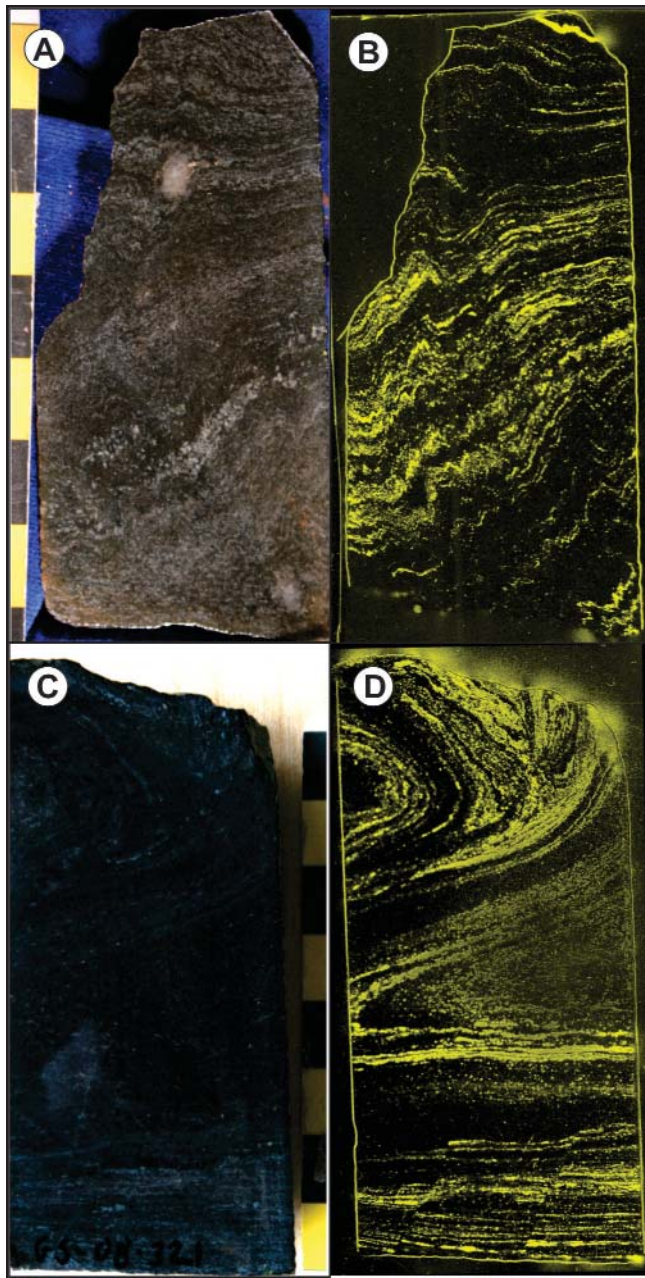


**Plate 63.** Mineralized samples from the Anna Lake deposit displaying the effects of post-mineral deformation. *A.* Amphibole–biotite schist displaying a crenulation cleavage. DDH AL-07-01, ~21 m. *B.* Autoradiograph of (A) outlining the distribution of radioactivity within the sample (yellow minus the outline of the sample); note the effect of the crenulation cleavage overprints the distribution of the radioactive material within the sample. *C.* Similar metasedimentary unit as in (A) displaying tight, cm-scale folding. DDH AL-07-01, ~117 m. *D.* Autoradiograph of (C) outlining the distribution of radioactivity within the sample (yellow minus the outline of the sample); note the effect of the folding on the distribution of the radioactive material within the sample.

Ni and Co arsenides (Fraser and Giroux, 2009), which is reminiscent of the Nash deposit, where elevated As values are also reported in association with uranium mineralization (Tracey, 2009). Highlights from some of the drilling at the Anna Lake deposit include 0.05%  $U_3O_8$  and 0.11% Mo over 25 m (Fraser and Giroux, 2009). Although localized intersections of higher grade material similar to that seen along the Kitts–Post Hill Belt have been reported, the Anna Lake deposit is generally of lower grade.

### Petrography

The uranium mineralization displays a strong spatial association with the development of sulphide minerals within the metasedimentary rocks. Specifically, uranium mineralization is hosted within amphibole–magnetite-rich layers, with the uraniferous minerals locally becoming incorporated within the amphibole crystals (Plate 64). Radioactivity within mineralized samples generally occurs in association with the complex intergrowth of magnetite, hematite, and lesser pyrrhotite. Uraninite is also present as finely disseminated material within the zones of radioactivity, where it displays a close spatial association with the formation of molybdenite (Plate 65). Barren layers intercalated with the amphibole-rich layers predominantly consist of an epidote-group mineral, possibly clinozosite, along with lesser pyrrhotite (Plate 66). Locally some of the amphibole-rich bands contain mm-scale garnet porphyroblasts that also incorporate minor amounts of radioactive material.

### OTHER URANIUM OCCURRENCES

The Post Hill Group hosts numerous minor occurrences of uranium mineralization that are not mentioned here. However, one particular area to note is a window of metasedimentary rock in the area southeast of Present Lake. This area contains uraniferous metasedimentary rocks inferred to be correlative with the Post Hill Group (Hinchey and LaFlamme, 2009), and provides supporting evidence for the broad geographical distribution of uranium mineralization within such units. Similar to the mineralization observed along the Kitts–Post Hill Belt and at Anna Lake, uranium mineralization in this area displays a patchy distribution within metasedimentary rocks, locally affected by tight isoclinal folding. A single sample collected from the area returned 0.05%  $U_3O_8$ . Mineralization is also associated with anomalous values of Cu, Zn, Ag and minor Au, further supporting the correlation of the mineralization with that seen within the Post Hill Group farther to the west.

### GEOCHRONOLOGICAL CONSTRAINTS

As part of this study, three key units within the Kitts deposit were targeted for geochronological study to constrain

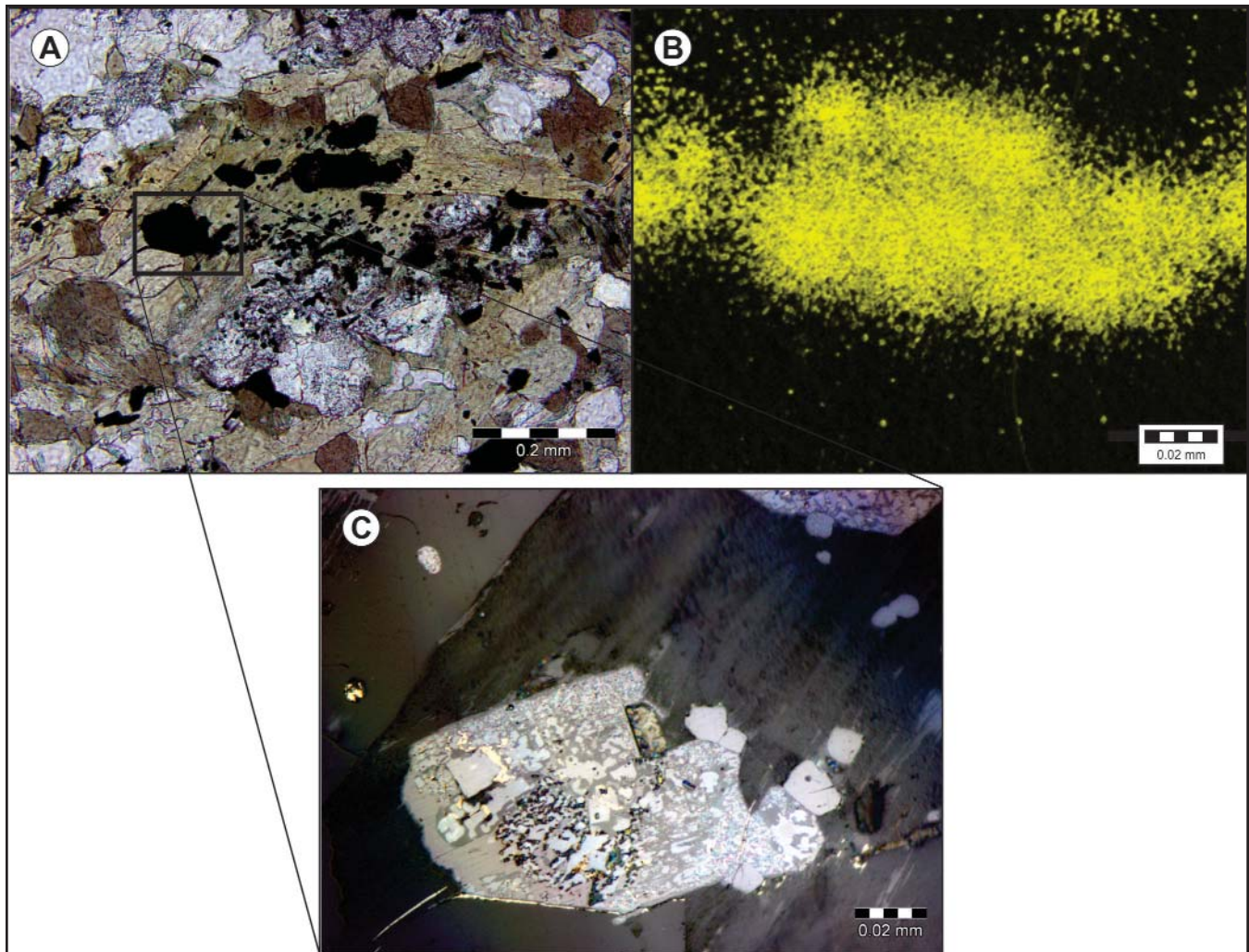


**Plate 64.** *A.* Uraniferous opaque minerals incorporated within amphibole crystals in metasedimentary rocks of the Anna Lake deposit, *B.* Corresponding autoradiograph of (A) outlining the areas of radioactivity (yellow), *C.* Complex intergrowth of magnetite–hematite–pyrrhotite within opaque minerals associated with radioactivity; shown in (A).

the age of mineralization within the Kitts–Post Hill Belt; these units were the Kitts Metagabbro, the quartz–feldspar porphyry dyke, and the diorite dyke.

Coarse-grained pegmatitic patches within the Kitts Metagabbro were sampled for U–Pb geochronology (Plate 67). The sample produced a limited number of small, strongly altered, turbid zircons, which were chemically abraded, and analysed by TIMS at Memorial University of Newfoundland. Results are reported in Appendices C and D, and presented in a concordia diagram in Figure 36A, with errors at the  $2\sigma$  level. From these analyses, four points define a line that has an upper intercept of  $2018 +15/-8$  Ma, representing the crystallization age of the unit (0.67 probability of fit; Figure 36A; Sparkes and Dunning, 2015). The Kitts Metagabbro is inferred to predate the development of uranium mineralization

and therefore provides a maximum age limit on the mineralization within the area.

Mineralized argillite at the Kitts deposit is locally cross-cut by a quartz–feldspar–porphyry dyke from which a sample was collected (drillhole K74-08) between 93.10 and 98.48 m; this was submitted to the Geological Survey of Canada for Sensitive High Resolution Ion MicroProbe (SHRIMP) dating. Results are in Appendix D and presented in a concordia diagram in Figure 36B, with errors at the  $2\sigma$  level. The sample produced an abundant population of high-quality zircon, from which a selection of grains were mounted and analyzed. Most of the analyses represent magmatic zircon. A weighted average of the  $^{207}\text{Pb}/^{206}\text{Pb}$  ages of these analyses gave an age of  $1881.8 \pm 3.4$  Ma (MSWD = 0.88; probability of fit = 0.66;  $n = 34$ ) and is assumed to represent the crystallization age of

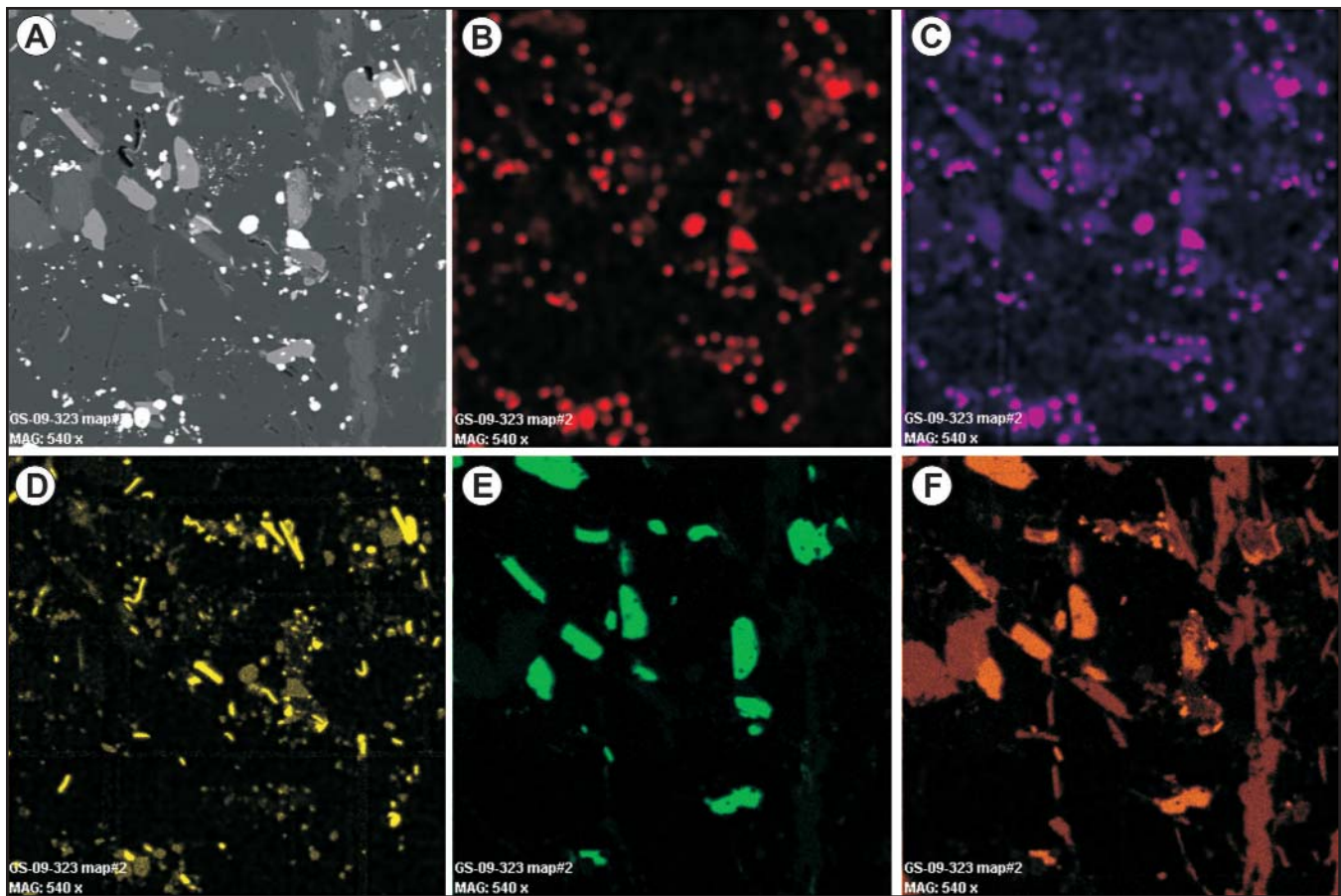


**Plate 65.** *A.* SEM image of mineralized material from the Anna Lake deposit, showing the distribution of finely disseminated uraninite (bright white). The coloured plates are element specific and include, *B.* uranium, *C.* lead, *D.* molybdenum, *E.* titanium, *F.* iron. Note, the field of view in each image is approximately 0.2 mm.

the unit (Sparkes *et al.*, 2010). Analysis of several grains also revealed the presence of inherited zircon, which had significantly older ages, ranging from *ca.* 2703 to 2835 Ma; these zircons are inferred to have been assimilated from the adjacent argillite unit that is known to contain detrital zircon from Archean basement rocks (Ketchum *et al.*, 2001a). The age provided by the quartz-feldspar porphyry is interpreted as a minimum age limit on the formation of the primary uranium mineralization within the Kitts deposit.

Finally, the entire deposit is crosscut by a gently dipping diorite dyke, which postdates all mineralization and deformation within the area. This unit was sampled to provide a minimum age limit on the timing of the deformational events that postdated the intrusion of the quartz-feldspar porphyry. A sample of coarse-grained amphibole-rich diorite was collected from drillhole B-11, between 25.21 and 30.48 m and analysed using TIMS. The sample yielded an abundant population of titanite, which based on petrographic examination, occur within late quartz-rich segregations of a predominantly quartz-amphibole-rich groundmass. Results are in Appendix

C and presented in Figure 36C. Four single-grain analyses were carried out on strongly abraded titanite. The results of these analyses produced a weighted average  $^{206}\text{Pb}/^{238}\text{U}$  age of  $1662 \pm 4$  Ma, which represents the crystallization age of the unit (95% confidence interval, MSWD = 0.50; prob. of fit = 0.68; Sparkes *et al.*, 2010). This age provides an upper limit on the deformation within the Kitts deposit and therefore provides a minimum age limit on the uranium mineralization that is remobilized subsequent to the intrusion of the quartz-feldspar porphyry dykes.

No geochronological constraints exist for the mineralization developed within the area of the Anna Lake deposit; however, intrusive rocks within the area are correlated with units dated elsewhere within the CMB. Granitic rocks occurring in the area of the Anna Lake deposit (Unit 23 of Ryan, 1984) are interpreted to be intruded by rocks correlated with the Junior Lake Granodiorite (Ryan, 1984). The Junior Lake Granodiorite has locally been dated at  $1891 \pm 5$  Ma (Kerr *et al.*, 1992), and thus potentially provides a minimum age bracket on the timing of mineralization at the Anna Lake deposit.

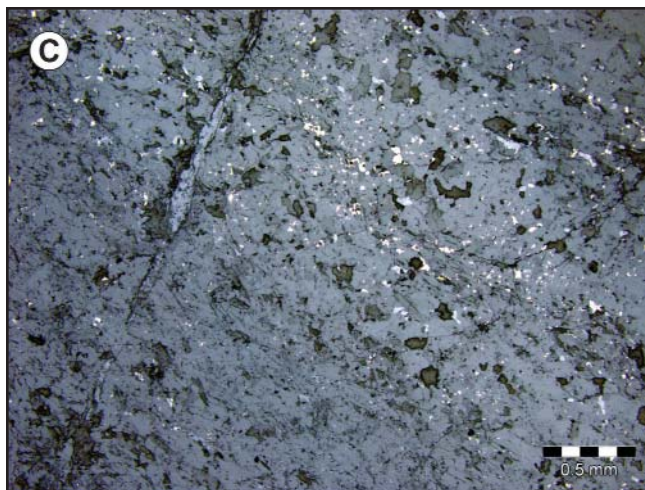
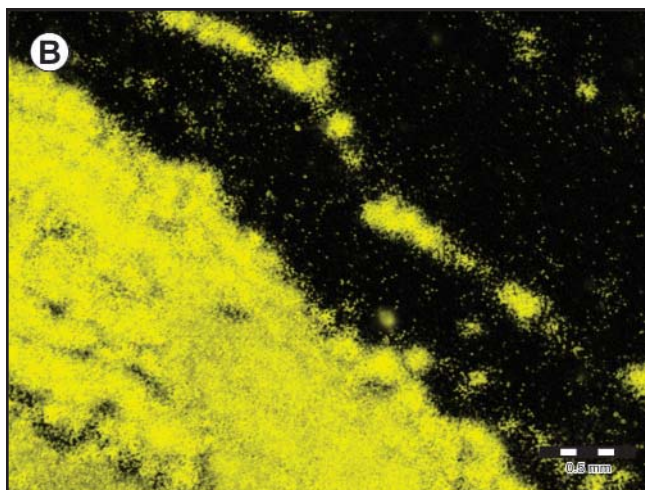


**Plate 66.** *A.* Interlayered amphibole-rich and epidote-rich bands within mineralized metasedimentary rocks of the Anna Lake deposit. *B.* Corresponding autoradiograph of (A) outlining the areas of elevated radioactivity shown in yellow. *C.* Reflected light image of (A) outlining the abundance of pyrrhotite in the non-radioactive portion of the thin section. The radioactive portion is dominated by magnetite, hematite and finely disseminated uraninite along with lesser pyrrhotite.



**Plate 67.** Coarse-grained, pegmatitic patches within the Kitts Metagabbro, sampled for U-Pb geochronology.

## GEOCHEMISTRY

The compositions of the main magmatic rocks examined within the Post Hill Group are shown in Figure 37A. These rocks include samples collected from the Kitts Pillow Lava Formation (metabasalt) and the Kitts Metagabbro, both predominantly plot within the subalkaline basalt field of Winchester and Floyd (1977; Figure 37A). The late-stage diorite dyke, which crosscuts the Kitts deposit, also plots within the same area, while the quartz-feldspar dyke spans the rhyodacite/dacite–rhyolite fields. The mafic volcanic rocks of the Kitts Pillow Lava Formation predominantly plot as MORB (Figure 37B, C), displaying similar geochemical characteristics to the mafic volcanic rocks of the Moran Lake Group (see Section, Uranium Mineralization within the Moran Lake Group). The overall trace-element pattern of the metabasalts are also similar to that of the Moran Lake Group, aside from a slight enrichment in LREE, which is similar to that noted in basalt flows of a more alkaline composition at the top of the Warren Creek Formation of the Moran Lake Group (North, 1988). The Kitts Metagabbro displays some geochemical similarities to the Kitts Pillow Lava Formation (Figures 37A–D, and 38); however, the latter generally displays more fractionated characteristics. The limited geochemical data collected are suggestive of a magmatic relationship between the Kitts Metagabbro and Kitts Pillow Lava Formation as proposed by Marten (1977).

The quartz-feldspar porphyry and late-stage diorite dykes display a more calc-alkaline trend in comparison to the mafic units discussed above (Figure 37D). Quartz-feldspar porphyry dykes are exposed, or intersected in drillcore, in a number of locations along the Kitts–Post Hill Belt, including at the Kitts and Gear deposits, as well as at the Nash West Extension prospect. These dykes are geochemically similar throughout these areas, displaying an overall LREE enrichment, along with negative Nb, Sr, P and Ti anomalies. The late-stage diorite dyke displays a similar LREE enrichment, combined with a minor negative Nb anomaly. As such, both the quartz-

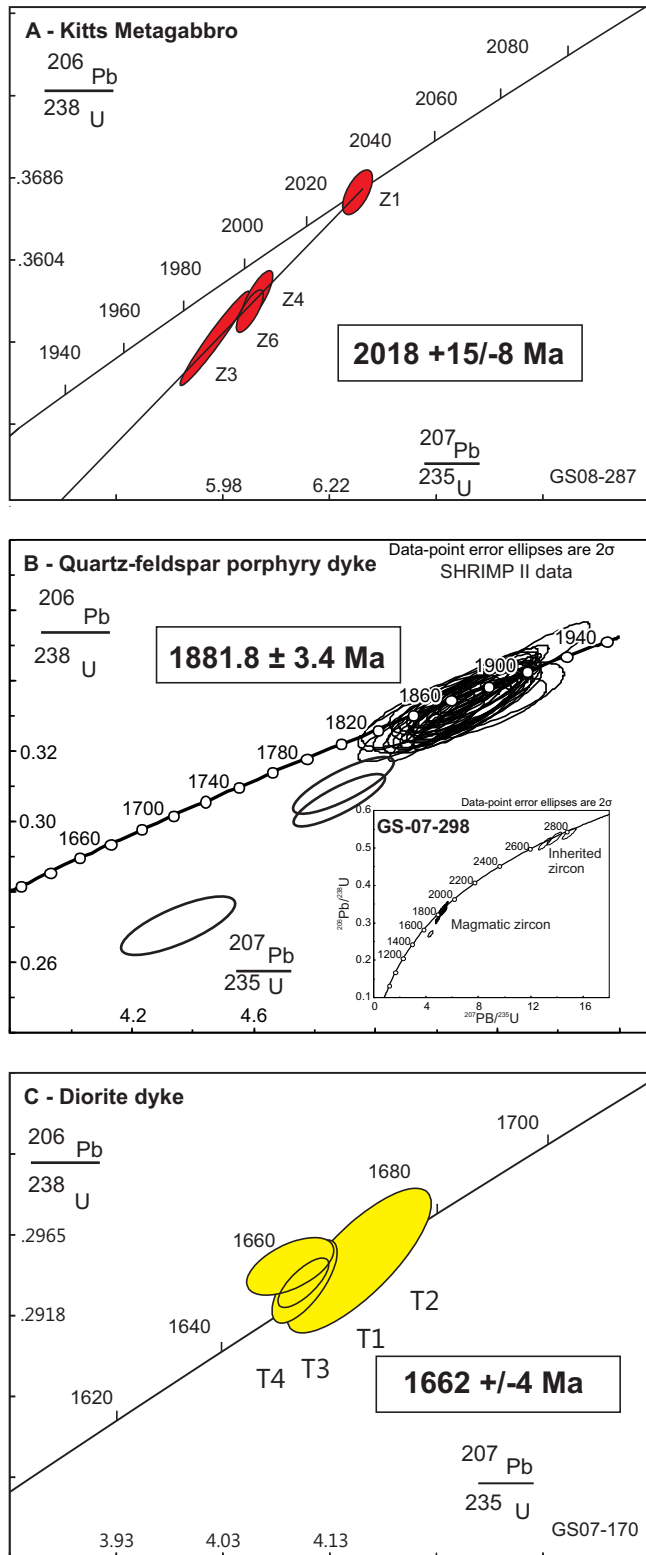


**Figure 36.** Concordia diagrams for U-Pb zircon data (A and B) as well as titanite data (C) for units sampled within the Kitts deposit. A. Kitts Metagabbro, B. Quartz-feldspar porphyry dyke, C. Diorite dyke. (Error ellipses are at the 2 $\sigma$  level; modified from Sparkes et al., 2010.)

feldspar porphyry and late-stage diorite dykes display overall arc-related signatures in contrast to the more MORB-like signatures of the Kitts Metagabbro and Kitts Pillow Lava Formation. The presence of both the quartz-feldspar porphyry and diorite dykes over a considerable strike length, and their similar geochemical compositions to the dated samples within the Kitts deposit highlights the significance of these units as potential regional markers in constraining the development of uranium mineralization and deformation throughout the Kitts–Post Hill Belt.

Mineralization throughout the Kitts–Post Hill Belt is hosted within a number of different rock units. At the Kitts deposit, uranium mineralization is primarily hosted within argillite and interbedded mafic tuff, with lesser, late remobilized mineralization locally occurring within the quartz-feldspar porphyry. Comparison of mineralized and unmineralized samples of the argillite illustrates elevated Pb and Mo with elevated U values within the Kitts deposit, along with lesser Ag and Au enrichment (Figure 39A). At both the Gear and Inda deposits, local enrichment of Ag is also associated with elevated Pb and U, while the mineralized tuff from the Gear deposit is locally associated with elevated Cu and Zn (Figure 39B). The most significant host to uranium mineralization within the area of the Nash deposit is the mafic tuff, which displays no significant enrichment of any other elements aside from Pb in association with elevated U (Figure 39C). Finally, the Present Lake mineralized metasedimentary rocks, which include minor mafic tuff, display local enrichment of Mn, and lesser Cu and Zn, in relation to elevated Pb and U values (Figure 39D).

## SUMMARY AND DISCUSSION

The Post Hill Group is host to the highest grade uranium mineralization identified so far within the CMB, and has therefore been subjected to some of the most intensive exploration in the region. Mineralization is primarily concentrated within the Kitts–Post Hill Belt, which extends for upward of 15 km from the Kitts deposit in the north to the Nash West Extension prospect in the south. Within this region, uranium mineralization is primarily concentrated within the upper portions of the Post Hill Group stratigraphy, close to its tectonic contact with the overlying Aillik Group. This mineralization is grouped with the metamorphic–metasomatic-related mineralization and is most likely linked to early, pre-1880 Ma, deformation within the region.

At the high-grade Kitts deposit, uranium mineralization is primarily developed within a shear zone, termed the Main Shear Zone, which is focused within metasedimentary rocks interbedded with the Kitts Pillow Lava Formation. Here, uranium mineralization occurs as uraninite, with lesser coffinite, in high-grade veins, but also as lesser fine-grained disseminations. The footwall of the deposit is dominated by the Kitts

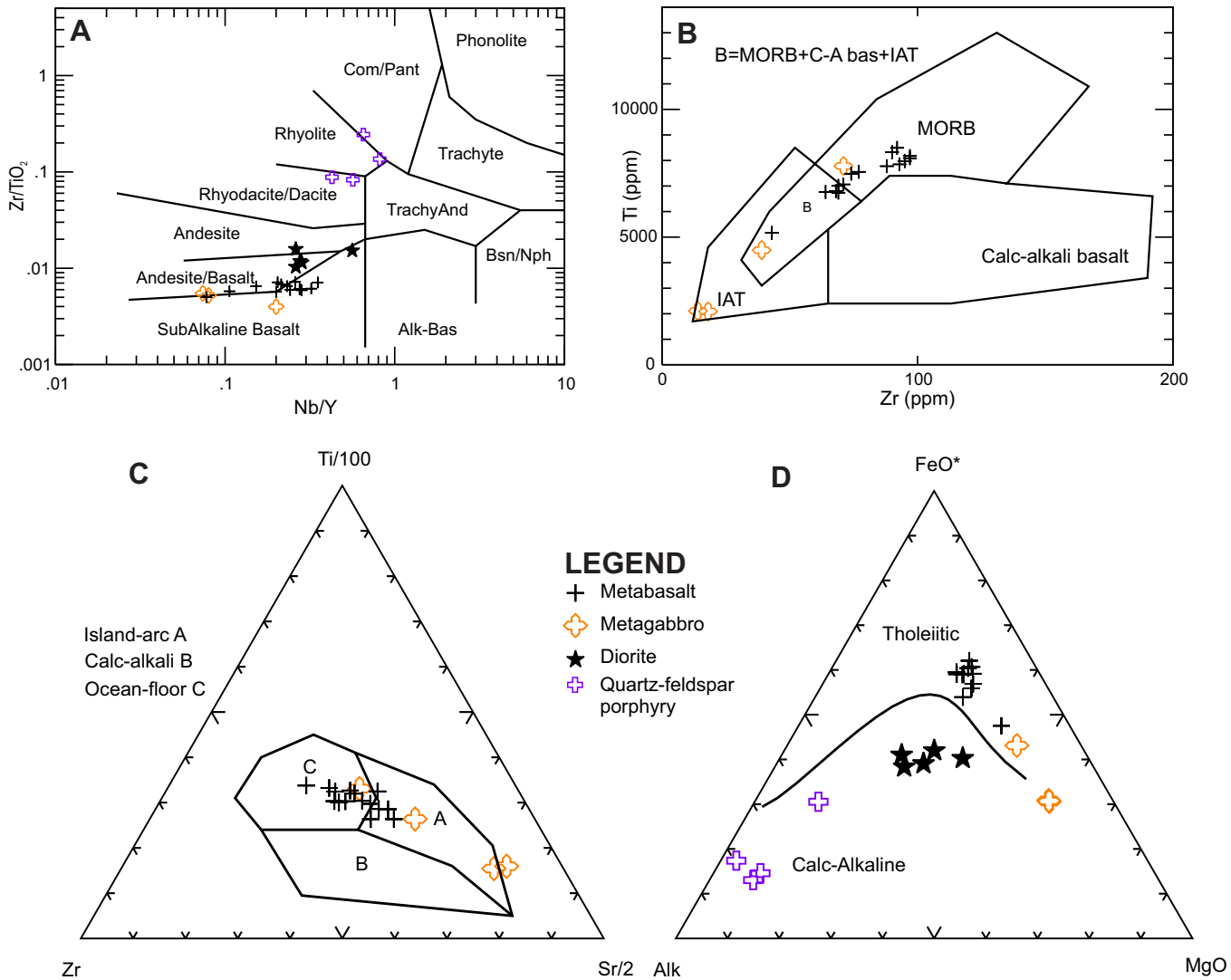


**Figure 37.** Discrimination diagrams for magmatic rocks examined in relation to uranium mineralization within the Kitts–Post Hill Belt; most samples are from the Kitts deposit, A. Discrimination diagram of Winchester and Floyd (1977) outlining the main compositions of the magmatic rocks sampled as part of this study, B. Discrimination diagram of Pearce and Cann (1973) displaying the MORB-like signature of Kitts Pillow Lava Formation and the Kitts Metagabbro; MORB–Mid-Ocean Ridge Basalt, IAT–Island-Arc Tholeiites, C. Discrimination diagram of Pearce and Cann (op. cit.) displaying predominant ocean-floor signature of the Kitts Pillow Lava Formation, D. AFM diagram illustrating the overall tholeiitic trend of the Kitts Pillow Lava Formation and Kitts Metagabbro in relation to the more calc-alkaline diorite and quartz-feldspar porphyry dykes.

Metagabbro dated at 2018 +15/-3 Ma. This age provides a potential maximum age for the development of uranium mineralization within the deposit as the metagabbro is inferred to predate the mineralization. The Main Shear Zone primarily developed along the northeastern margin of the metagabbro, is crosscut at an oblique angle by quartz-feldspar porphyry dykes interpreted to postdate mineralization. However, these dykes are locally host to fracture-hosted mineralization, inferred to represent remobilization of the uranium mineralization during later deformation. A quartz-feldspar porphyry dyke produced a U–Pb zircon age of 1881.8 ± 3.4 Ma taken

to represent the minimum age for the formation of the initial uranium mineralization, developed within the Main Shear Zone. On the basis of existing geological interpretations, the formation of uranium mineralization can be bracketed to between 2033 Ma and 1878.4 Ma, within analytical error. Finally, the entire deposit is crosscut by a late-stage, undeformed, diorite dyke that produced an U–Pb titanite age of 1662 ± 4 Ma, and thus constrains the age of the post-mineralization deformation that overprints the quartz-feldspar porphyry dykes and is inferred to have locally remobilized earlier uranium mineralization.

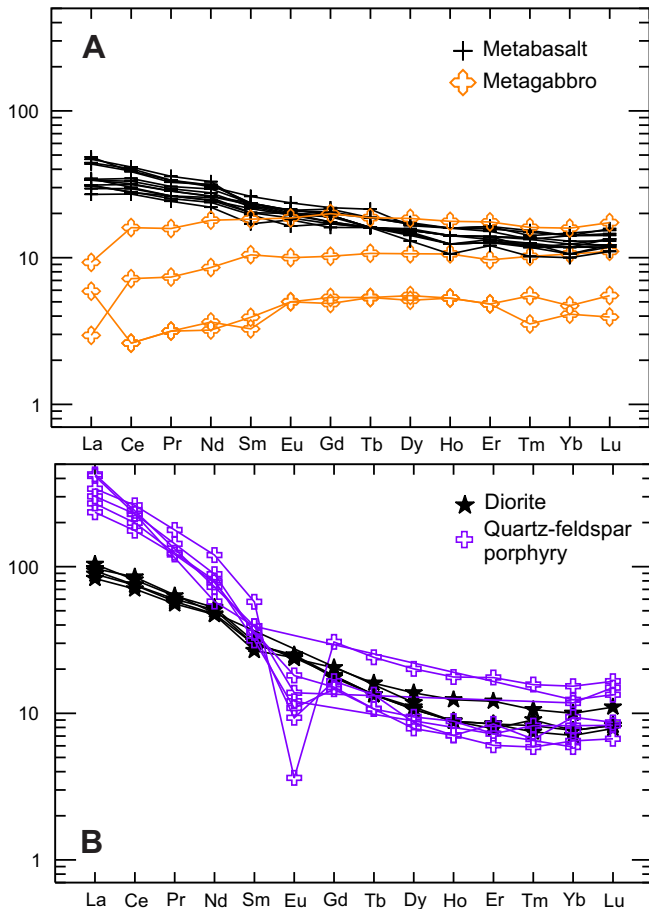


**Figure 38.** Chondrite normalized trace-element diagrams for magmatic rocks examined in relation to uranium mineralization within the Kitts–Post Hill Belt; most samples are from the Kitts deposit, A. Samples of the Kitts Pillow Lava Formation and Kitts Metagabbro; Kitts deposit, B. Samples of the quartz-feldspar porphyry and late-stage diorite dykes; the quartz-feldspar porphyry and diorite dykes include samples from Kitts, Gear and Nash West Extension occurrences. Normalizing values are from Sun and McDonough (1989).

Both, the quartz-feldspar porphyry and diorite dykes, exhibit arc-related geochemical characteristics, suggesting that they are unrelated to the overall formational environment of the Post Hill Group and share a greater affinity with rocks of the Aillik Group. U–Pb ages from quartz-feldspar–porphyritic intrusions, which overlap, within analytical error, with the quartz-feldspar porphyry dyke at the Kitts deposit, have been reported elsewhere within the Aillik Group (e.g., Hinckley and Davis, 2013), providing supporting evidence for the synvolcanic nature of these intrusion in association with the formation of Aillik Group rocks elsewhere.

South of the main Kitts deposit are the Gear, Inda and Nash deposits, which are sited near the tectonic contact sep-

arating Post Hill Group rocks to the west from Aillik Group rocks to the east. Similar to the Kitts deposit, uranium mineralization is inferred to be primarily structurally controlled and occurs as narrow, high-grade intersections that are primarily hosted within metasedimentary rocks and interbedded mafic tuffs. Autoradiographs of mineralized samples demonstrate that the mineralization is developed parallel to the main foliation, and locally displays evidence of isoclinal folding indicating a pre-deformational timing for the mineralization. Quartz–feldspar porphyry dykes locally crosscut mineralization at the Gear deposit and Nash West Extension prospect. These quartz–feldspar porphyry dykes are geochemically similar to the dated unit within the Kitts deposit and are inferred to be coeval, therefore providing a minimum age constraint on the development of uranium mineralization. Along the Inda Lake trend, most of the uranium mineralization is hosted by rocks of the Post Hill Group, but limited mineralization has been reported from the overlying Aillik Group. Where observed, this latter mineralization contrasts with that observed within the underlying Post Hill Group, and is associated with brittle fracturing and hematization of the surrounding wall rock.

Farther to the south in the area of Anna Lake, the discovery of mineralized metasedimentary rocks inferred to be part of the Post Hill Group demonstrates the regional extent of uranium mineralization within this group. Evaluation of autoradiographs of mineralized samples indicate that the mineralization is locally foliated and crenulated similar to that seen along the Kitts–Post Hill Belt. Given the similarities of the uranium mineralization in the two areas, it is inferred that these deposits are linked to the same metallogenic event. This mineralization is intruded by rocks correlated with the Junior Lake Granodiorite on the basis of geological mapping in the area, locally dated at  $1891 \pm 5$  Ma (Kerr *et al.*, 1992), and therefore potentially provides an older minimum age for uranium mineralization developed within the Post Hill Group.

The new age constraints on uranium mineralization within the Kitts–Post Hill Belt imply that the mineralization developed within this region is part of an older metallogenic event in comparison to the formation of the Michelin deposit farther to the east (see Section, Uranium Mineralization within the Aillik Group). Local enrichments of Cu, Zn, Ag and V along with anomalous Au and locally Mo are noted in association with uranium mineralization within the Post Hill Group. The source of this metal enrichment is attributed to the host metasedimentary rocks, which also represent a potential source for uranium. The structurally controlled mineralization within the Post Hill Group may have originated as some form of synmetamorphic event, indicated by the concentrations of uranium mineralization within certain metamorphic mineral assemblages along discrete shear zones. This mineralization would then have been remobilized into the

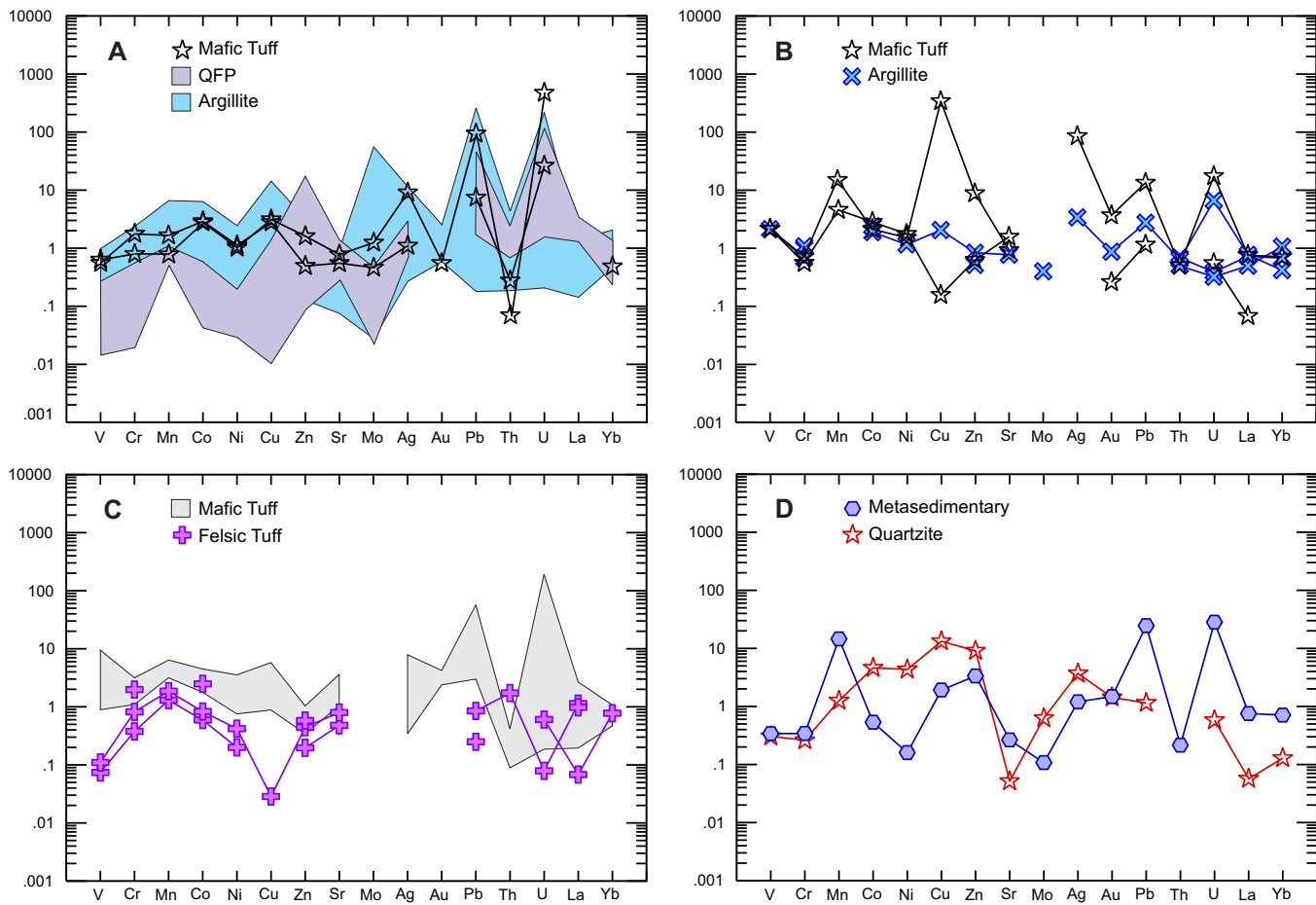


**Figure 39.** Extended trace-element diagrams for the metasedimentary and volcaniclastic units within the Post Hill Group. Normalizing values are from Quinby-Hunt *et al.* (1989) except for Cu, Ni, Pb, Ag and Mo, which are taken from Vine and Tourtelot (1970). A. Kitts deposit, B. Gear and Inda deposits; note the argillite sample containing elevated U represents mineralized argillite from the Inda deposit; all other samples are from the Gear deposit, C. Nash deposit and Nash West Extension prospect, D. Present Lake prospect.

high-grade veins during subsequent deformation, which overprinted the initial uranium mineralization.

In light of recent geochronological data from the region of the Kitts deposit, an unconformable contact between the Post Hill and Aillik groups is preferred. Supporting evidence for this conclusion is provided by the local evidence of a pre-Aillik Group deformational event, recognizable in drillcore from the Post Hill Group stratigraphy (Cunningham-Dunlop and Lee, 2008). This model is further supported by the fact that most of the known uranium mineralization occurs within the older rocks to the west of the tectonic contact separating the two groups, with only minor mineralization occurring within, what is interpreted to be, Aillik Group rocks. The latter is inferred to represent remobilization of the older uranium mineralization within the Post Hill Group. This contrasts with earlier models for the area that favour the enriched felsic volcanic rocks of the Aillik Group as the source to the uranium

within the region (e.g., Marten, 1977; Gower *et al.*, 1982). However, the new geochronological data presented here demonstrate that the mineralization within the Kitts–Post Hill Group predates most of the rocks within the Aillik Group stratigraphy (see following Section).

## URANIUM MINERALIZATION WITHIN THE AILLIK GROUP

### INTRODUCTION

The Aillik Group of Ketchum *et al.* (2002), formerly termed the Upper Aillik Group (*cf.* Gower *et al.*, 1982; Ryan, 1984), has a lengthy history of uranium exploration (*cf.* Beavan, 1958; Gandhi, 1978; Gower *et al.*, 1982; Wilton, 1996; Sparkes and Kerr, 2008). The Aillik Group, relative to other rock units within the area, contains a large concentration of uranium occurrences, including the two most significant de-

posits identified to date (*i.e.*, Michelin and Jacques Lake deposits; Table 8). Rocks assigned to the Aillik Group occur in three main geographical areas within the eastern portion of the CMB; these are: 1) from the southern shore of Kaipokok Bay to Cape Aillik, 2) from Makkovik Bay–Adlavik Bay south to the Adlavik Brook Fault, and 3) south of the Adlavik Brook Fault to Walker Lake (Figure 40). In addition, volcanic and sedimentary rocks within the Benedict Mountains region, located in the easternmost portion of the CMB, have long been inferred to be correlative with the Aillik Group (*e.g.*, Gower, 1981; Kerr *et al.*, 1996; Ketchum *et al.*, 2002). Recent U–Pb geochronology further supports this interpretation (Sparkes and Davis, 2013), and therefore the uranium mineralization hosted in these rocks is described in this section.

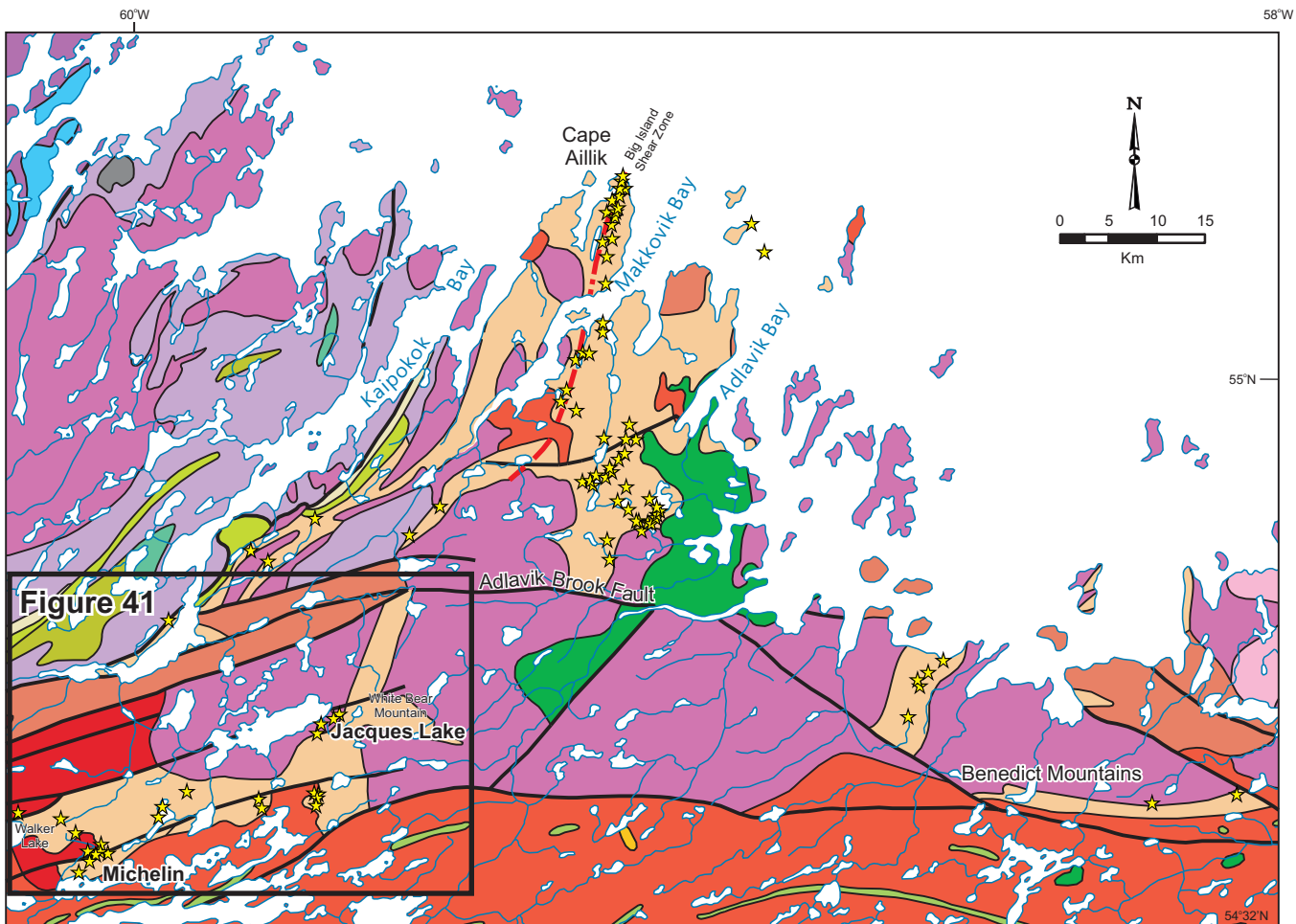
Numerous studies on the nature and genesis of the uranium mineralization within the Aillik Group have been conducted since the mid-1950s, and have led to varied conclusions concerning the style and origin of mineralization. Uranium mineralization is preferentially hosted within the upper portion of the Aillik Group, where it is developed within felsic to intermediate metavolcanic rocks in association with intense albitic and hematitic alteration. Early interpretations of the sodium metasomatism (albitization) regarded it as essentially synvolcanic (*e.g.*, Barua, 1969; Watson-White, 1976), but considered the uranium mineralization to be a separate later event. Other workers favoured a synvolcanic hydrothermal origin for the alteration and mineralization, in which uranium was sourced from the enriched felsic volcanic rocks of the Aillik Group (*e.g.*, Evans, 1980; Gower *et al.*, 1982). A third view suggested synvolcanic timing for the mineralization, but attributed the mineralizing fluids to a deeper magmatic source (*e.g.*, Gandhi, 1978). Most recently, a link with post-volcanic, metamorphic and/or metasomatic processes has been suggested for this style of mineralization (*e.g.*, Sparkes and Kerr, 2008; Wilde, 2013).

Mineralization observed within the correlative rocks of the Benedict Mountains region has a distinctly different character to that of the Aillik Group rocks farther to the west. In the Benedict Mountains, uranium is hosted within felsic volcanic rocks that lack the intense alteration and deformation typical of rocks hosting uranium mineralization within the Aillik Group. This uranium mineralization is interpreted to be essentially synvolcanic, and resembles that developed within the younger (*ca.* 1650 Ma) volcanic rocks of the Bruce River Group (Sparkes and Davis, 2013; *see* next Section).

Reports by Kerr (1994) and Wilton (1996) discuss some aspects of uranium mineralization, based on information from exploration work conducted prior to about 1990. This section of this report primarily highlights new exploration results generated since the mid-2000s, and only covers those occurrences that lie outside of exempt mineral lands. The Michelin

**Table 8.** NI 43-101 compliant resource estimates for mineralization within the Aillik Group

Deposit	Resource Classification	Underground			Open Pit			Contained Resource (lbs. U <sub>3</sub> O <sub>8</sub> )	Source
		Cut-off (% U <sub>3</sub> O <sub>8</sub> )	Grade (% U <sub>3</sub> O <sub>8</sub> )	Tonnage (tonnes > cut-off)	Contained Resource (lbs. U <sub>3</sub> O <sub>8</sub> )	Cut-off (% U <sub>3</sub> O <sub>8</sub> )	Grade (% U <sub>3</sub> O <sub>8</sub> )		
Michelin	Measured	0.050%	0.120%	1,289,000	3,310,000	0.020%	0.080%	5,783,000	Hertel <i>et al.</i> , 2009
	Indicated	0.050%	0.130%	16,170,000	44,582,000	0.020%	0.060%	6,839,000	Hertel <i>et al.</i> , 2009
	Inferred	0.050%	0.120%	12,577,000	33,647,000	0.020%	0.030%	3,393,000	Hertel <i>et al.</i> , 2009
Jacques Lake	Measured	0.050%	0.080%	103,000	176,000	0.020%	0.090%	755,000	Hertel <i>et al.</i> , 2009
	Indicated	0.050%	0.080%	1,661,000	2,809,000	0.020%	0.070%	4,374,000	Hertel <i>et al.</i> , 2009
	Inferred	0.050%	0.080%	2,149,000	3,672,000	0.020%	0.040%	5,953,000	Hertel <i>et al.</i> , 2009
Rainbow	Measured	0.050%	0.060%	26,000	34,000	0.020%	0.090%	211,000	Hertel <i>et al.</i> , 2009
	Indicated	0.050%	0.080%	365,000	624,000	0.020%	0.080%	735,000	1,409,000
	Inferred	0.050%	0.080%					546,000	1,005,000



## LEGEND

### MESOPROTEROZOIC

Olivine gabbro and metamorphic equivalents, including coronitic varieties (Shabogamo and Michael gabbros, ca. 1460 to 1425 Ma)

### PALEOPROTEROZOIC

- Granite, quartz monzonite, granodiorite, syenite and minor quartz diorite (ca. 1650 Ma)
- Rhyolitic to andesitic volcanic rocks including ash-flow tuff and agglomerate (ca. 1650 Ma)
- Mafic intrusive suites (gabbro, lesser diorite), some metamorphosed as amphibolite to granulite facies
- High-level, locally flourite-bearing granites (1776 to 1719 Ma)
- Tonalite, granodiorite and monzogranite gneiss; minor amphibolite, calc-silicate and felsic (metavolcanic?) gneiss
- Granite and granodiorite (1840 to 1795 Ma)
- Gabbro and leucogabbro sills (ca. 1884 to 1874 Ma)
- Granite plutons (ca. 2134 Ma, locally 2032 Ma in the Nain Province; 1973 to 1891 Ma in the Makkovik Province)
- Rhyolite, ash-flow tuff, breccia and hypabyssal rhyolite intrusions; volcaniclastic siltstone and sandstone; minor basalt (ca. 1860 to 1807 Ma)

Schistose amphibolite derived from mafic volcanic rocks (Moran Lake and Post Hill groups)

Pelitic schist

### ARCHEAN

- Tonalitic and other gneisses reworked and retrograded during Makkovikian orogenesis
- Granodiorite, tonalite and minor granite (Kanairiktok Intrusive Suite, ca. 2850 to 2830 Ma)
- Tonalitic to granodioritic migmatitic orthogneiss containing abundant mafic to ultramafic inclusions and relict mafic dykes
- Mafic volcanic and volcaniclastic rocks, lesser sedimentary and felsic volcanic rocks, and mafic-ultramafic sills; at greenschist to amphibolite facies (Florence Lake group, ca. 3000 Ma)

### SYMBOLS

- Geological contact .....
- Fault .....
- Significant shear zone .....
- Uranium occurrence .....

**Figure 40.** Regional geology map outlining the distribution of known uranium occurrences hosted within the Aillik Group; geological base map modified from Wardle et al. (1997). Area outlined in black box detailed in Figure 41.

and Jacques Lake deposits are discussed in detail, and supplemented by information from numerous smaller occurrences within the Aillik Group. Collectively, these localities represent key examples of typical styles of uranium mineralization developed within the Aillik Group and are considered to be regionally representative.

## REGIONAL GEOLOGY

The Makkovik Province is subdivided into three domains; from west to east they are the Kaipokok, Aillik and Cape Harrison domains (Kerr *et al.*, 1996; Ketchum *et al.*, 2002; Hinckley, 2007). The Aillik Group, forming part of the Aillik domain, represents an upper greenschist- to lower amphibolite-facies Paleoproterozoic metasedimentary and metavolcanic supracrustal sequence that was intruded by both foliated and nonfoliated intrusions ranging in age from *ca.* 1800–1630 Ma (Gower *et al.*, 1982; Kerr, 1994; Kerr *et al.*, 1996; Hinckley, 2007; Hinckley and LaFlamme, 2009). The southernmost exposure of the Aillik Group, represented by the area between White Bear Mountain and Walker Lake (Figure 40), is host to the most significant uranium deposits defined to date within the CMB. This part of the Aillik Group is separated from more northern parts by the Adlavik Brook Fault (Figure 40), which is a largely east–west-trending transtensional structure (Gower *et al.*, 1982; Kerr, 1994; Hinckley and LaFlamme, 2009). The regional geology of the Aillik Group has most recently been summarized in Hinckley (2007) and Hinckley and LaFlamme (2009).

The Aillik domain, including the Aillik Group, is a composite arc/rifted-arc sequence accreted to the Nain cratonic margin during the Makkovikian Orogeny (Kerr *et al.*, 1996, 1997; Culshaw *et al.*, 1998, 2000; Ketchum *et al.*, 2002; Hinckley, 2007; Hinckley and LaFlamme, 2009). The lower Aillik Group is dominated by metasedimentary rocks that were originally sandstone, siltstone, conglomerate, and tuffaceous sandstone. Lesser volcanic rocks include felsic tuff, rhyolite, volcanic breccia, and mafic volcanic rocks. The upper Aillik Group is dominated by metavolcanic rocks consisting of felsic to intermediate tuff, flow-banded rhyolite, quartz-feldspar porphyry rhyolite and lesser volcaniclastic material. The tectonic setting of the group is not clearly defined, but recent work suggests a shallow-marine to subaerial environment within an arc/rifted-arc to back-arc type setting (Wardle and Bailey, 1981; Gower *et al.*, 1982; Kerr *et al.*, 1996; Culshaw *et al.*, 2000; Sinclair *et al.*, 2002; Ketchum *et al.*, 2002), between *ca.* 1883–1856 Ma (Schärer *et al.*, 1988; Hinckley and Rayner, 2008).

The Aillik Group structurally overlies the Post Hill Group to the west, whereas its eastern margin is largely defined by intrusive contacts with younger plutonic rocks of both Makkovikian (*ca.* 1800 Ma) and Labradorian (*ca.* 1650

Ma) timing (Kerr *et al.*, 1996). Rocks within the Aillik Group are variably deformed, with structural overprinting dominated by large-scale, upward-facing, gently plunging folds along with intermittent steeply dipping shear zones accompanied by upper greenschist- to lower amphibolite-facies metamorphism (Clark, 1979; Gower *et al.*, 1982; Culshaw *et al.*, 2000; Ketchum *et al.*, 2002; Hinckley, 2007; Hinckley and LaFlamme, 2009). The development of the steeply dipping shear zones within the main portion of the Aillik Group is attributed to a regional  $D_3$  event representing sinistral transpression associated with the westward thrusting of the Aillik Group (Culshaw *et al.*, 2000; Hinckley and LaFlamme, 2009), and is broadly bracketed between *ca.* 1860–1800 Ma (Ketchum *et al.*, 2002). Locally, uranium mineralization displays a close spatial association with these structures, such as the Big Island shear zone of Ketchum *et al.* (2002; Figure 40). In addition, existing age constraints for uranium mineralization within the Aillik Group (*e.g.*, Sparks and Dunning, 2009, 2015; Wilton *et al.*, 2010) are broadly similar to the age bracket of the  $D_3$  deformational event (*see below*).

The Benedict Mountains are located in the easternmost Cape Harrison domain of the Makkovik Province, and is largely composed of syntectonic and posttectonic plutonic rocks, and scattered enclaves of supracrustal sequences (Figure 40; Kerr *et al.*, 1996). The contact between the Cape Harrison domain and the adjacent Aillik domain to the west is largely intrusive. Supracrustal sequences within the Cape Harrison domain are dominated by felsic volcanic rocks and related volcaniclastic units, preserved as enclaves and fault bounded blocks; these rocks are inferred to be correlatives of the Aillik Group (Gower, 1981; Gower and Ryan, 1986; Kerr *et al.*, 1996). Here, the supracrustal rocks are only locally deformed and commonly preserve primary volcanic textures (Kerr *et al.*, 1996). The plutonic rocks within the region can be broadly separated into four main intrusive events at *ca.* 1840, 1800, 1720 and 1650 Ma (Kerr, 1989; Kerr *et al.*, 1992; Kerr and Fryer, 1993, 1994).

## EXPLORATION HISTORY

Uranium exploration within the CMB first began in the mid-1950s and has continued intermittently since that time. Summaries and discussions of earlier exploration work can be found in Beavan (1958), Gandhi (1978, 1984), Gower *et al.* (1982), Ryan (1984), Kerr (1994) and Wilton (1996).

Renewed interests in uranium, within the CMB, in the mid-2000s initially consisted of re-evaluating known deposits and initiating modern airborne geophysical surveys. These surveys identified significant anomalies where only minor anomalies were generated in the past, in part, due to the higher sensitivity of the more modern equipment. One such example is the Jacques Lake deposit (formerly termed the

McLean Lake showing by Brinex). Here, follow-up work on a radiometric anomaly led to the discovery of the deposit in 2005, by drilling in an area located along the glacial transport direction from the airborne anomaly (Cunningham-Dunlop *et al.*, 2006). Subsequent work at Jacques Lake has defined a resource of approximately 20 million lbs of  $U_3O_8$ , and the deposit remains open, both down-dip and along strike (Hertel *et al.*, 2009). Aurora Energy carried out extensive drilling on the Michelin deposit, to evaluate the down-plunge extension of the mineralized zone beyond the previous limit of  $\sim 250$  m depth. This deeper exploration expanded the uranium resource, and it is currently defined at approximately 103 million lbs of  $U_3O_8$  (Hertel *et al.*, 2009).

Aurora Energy also focused on several other areas, which include the Gayle, Kathi, Burnt Brook and Aurora River prospects (Figure 41). These zones of uranium mineralization occur within an area characterized by a pronounced aeromagnetic high, a feature similar to the mineralization developed at the Jacques Lake deposit. Limited drilling at these prospects has thus far only intersected relatively narrow zones of uranium mineralization; however, petrographic studies of the mineralization indicate similarities with the Michelin and Jacques Lake deposits (Cunningham-Dunlop *et al.*, 2007b).

Approximately 10 km to the south-southwest of Jacques Lake are two large airborne radiometric anomalies that host several uranium occurrences; the two most significant being the Otter Lake (formerly known as Emben) and White Bear (formerly known as Burnt Lake) prospects (Figure 41). In the area of the White Bear prospect, initial drilling by Aurora intersected similar grades to that seen in the Michelin and Jacques Lake deposits (*e.g.*, 0.17%  $U_3O_8$  over 24.62 m; Cunningham-Dunlop *et al.*, 2007a) hosted within felsic metavolcanic rocks of the Aillik Group. Geological mapping and diamond drilling has shown the mineralization to be structurally complex and further work in the area is required (Cunningham-Dunlop *et al.*, 2007a). The Otter Lake prospect is located approximately 6 km to the east of White Bear and is also hosted within felsic metavolcanic rock of the Aillik Group; however, diamond drilling at the prospect has thus far only identified relatively narrow, 1–2-m-wide, zones of uranium mineralization (Cunningham-Dunlop *et al.*, 2006).

In the immediate area surrounding the Michelin deposit, several other prospects are located marginal to the main mineralized zone, and have been the focus of preliminary exploration. These include the Rainbow deposit as well as the Chitra, Mikey Pond and Asha Pond prospects (Figure 41). Most of these prospects were originally discovered by Brinex, but were the focus of only minimal exploration.

Although much of the recent exploration work was completed by Aurora Energy, Mega Uranium also conducted ura-

nium exploration within the Aillik Group around Mustang Lake, approximately 7 km to the northeast of the Michelin deposit (Figure 41). Mustang Lake contains highly anomalous uranium lake-sediment values (up to 154 ppm U), and several uranium prospects occur in the area, along with numerous occurrences of mineralized boulders. Diamond drilling on the property locally intersected narrow zones of uranium mineralization associated with hematitic and albitic alteration similar to that at the nearby Michelin deposit. To date, the highest grade mineralization intersected includes 0.12%  $U_3O_8$  over 9.11 m (Willett *et al.*, 2006b), but follow-up drilling failed to intersect mineralization over similar widths (Kruse, 2008).

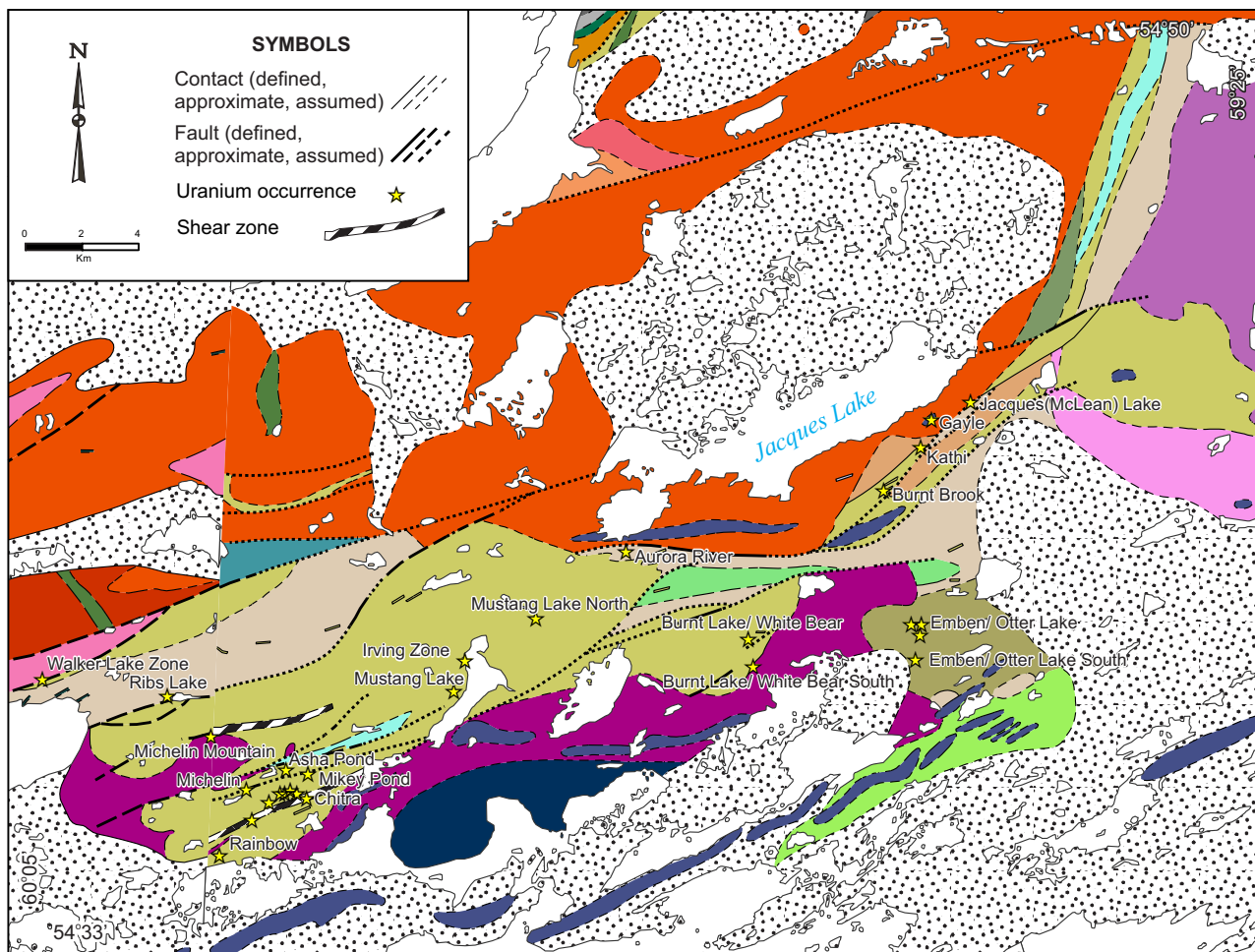
Felsic volcanic rocks in the area of the Benedict Mountains have seen much less exploration activity, although anomalies were detected in the late 1970s (Davidson and Kowalczyk, 1979). In the mid-2000s, Monster Copper discovered several new uranium occurrences within the area (Setterfield and Dyer, 2007; Setterfield *et al.*, 2008; Kruse *et al.*, 2009), which were subsequently followed-up with diamond drilling, but only intersected limited low-grade uranium mineralization (Kruse, 2012).

## MICHELIN DEPOSIT

### Previous Work

The Michelin deposit was initially discovered by Brinex in 1968, during ground follow-up of an airborne radiometric anomaly, and since that time the deposit has been the focus of several geoscience studies (*e.g.*, Gandhi, 1970, 1976b, 1978; Watson-White, 1976; Minatidis, 1976; Bailey, 1979; Evans, 1980; Gower *et al.*, 1982; Wilton and Wardle, 1987; Sparkes and Kerr, 2008). These studies have proposed several different models for the genesis of uranium mineralization. Gandhi (1976b) noted the relative narrow widths and considerable strike length of the zones hosting uranium mineralization, which could be outlined on the basis of regional structure. He noted that mineralization at the deposit was strongly controlled by stratigraphy, but also locally crosscut lithological contacts at shallow angles. Gandhi (1978) proposed a syn-volcanic, magmatic origin, for the mineralizing fluid responsible for the sodic alteration and related uranium mineralization, which he inferred predated, at least, the final stages of deformation in the region.

Watson-White (1976) focused on the volcanic origin of the rocks hosting the Michelin deposit in addition to the strong alkali (sodium) metasomatism; this alteration was derived from synvolcanic processes, but similar alteration occurred in shear zones, and was accompanied by local uranium enrichment. Minatidis (1976) carried out a comparative trace-element study of several uranium prospects throughout the CMB and noted that mineralized samples from the Michelin



## LEGEND

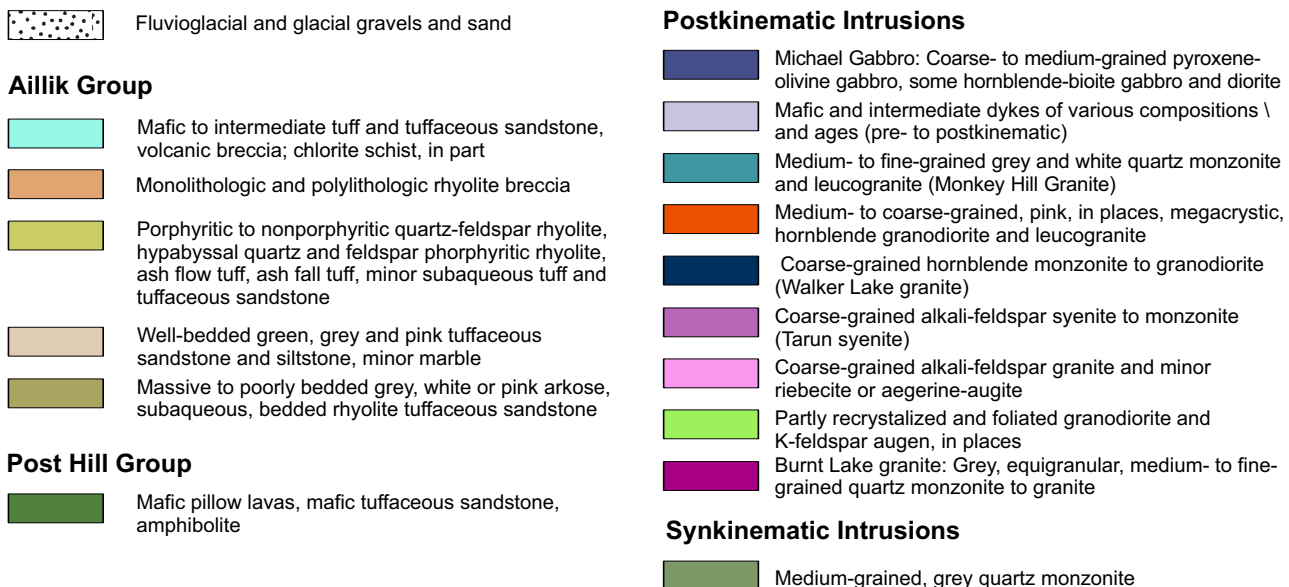


**Figure 41.** Regional geology map outlining the distribution of uranium occurrences within the White Bear Mountain–Walker Lake area (geological base map modified from Gower et al., 1982 and Ryan, 1984).

deposit contained higher concentrations of Zr, Zn and Ba as well as lower concentrations of Sr, Rb, Cu, Ni and Cr relative to unmineralized samples in the area; he interpreted this alteration to represent fenitization associated with the intrusion of carbonatites.

Bailey (1979) noted two main styles of mineralization within the western Aillik Group: 1) mineralization associated with shearing and faulting, and 2) stratigraphically controlled mineralization within felsic volcanic and sedimentary rocks. The structurally controlled style of mineralization was inferred by Bailey (1979) to represent remobilization of the uranium from the surrounding country rock during Grenvillian deformation. The stratiform style of mineralization, to which both the Michelin deposit and Burnt Lake prospect were assigned, was inferred to be indicative of volcanogenic hydrothermal processes, but it was noted that a metamorphic origin was also possible for the mineralization occurring within the Michelin deposit (Bailey, 1979).

Evans (1980) carried out a detailed study on several uranium occurrences within the eastern CMB, including Michelin. He noted that mineralization, although regionally stratabound, locally transgressed stratigraphic contacts within the metavolcanic host rocks at low angles, as also noted by Gandhi (1976b, 1978). On the basis of geochemistry, Evans (1980) outlined three main zones of alteration within the deposit, namely the transition, outer and inner alteration zones. He concluded that the U–Zr-bearing mineralizing fluid was oxidizing and sodium-enriched, and that the alteration was focused within the coarsely porphyritic units, which represented preferential zones of fluid migration within the volcanic stratigraphy. The uranium was inferred to have been leached from the surrounding volcanic host rocks by neutral to weakly alkaline, oxidizing groundwater (Evans, 1980).

Gower *et al.* (1982) reviewed the various models proposed for the genesis of the mineralization at Michelin and concluded that the mineralization was best described as an epigenetic–hydrothermal system linked to the volcanism. The most plausible source for the uranium was inferred to be the surrounding volcanic host rocks of the Aillik Group. Wilton and Wardle (1987) noted that the REE patterns for mineralized rocks from the Michelin deposit displayed similar patterns to unmineralized host rocks. They also noted differences in geochemical signatures from the Michelin deposit and uranium occurrences in the Aillik Group of the Makkovik area, which were interpreted to have been influenced by posttectonic granites.

More recently, Sparkes and Kerr (2008) provided a preliminary classification of the major uranium occurrences throughout the CMB, in which they characterized the mineralization at Michelin as being broadly metamorphic and/or

metasomatic. The mineralization was noted to display similarities to ‘albitites’ or ‘metasomatites’, most commonly known from the Baltic Shield region and Russia. The inclusion of the Michelin deposit within this classification is also discussed by Wilde (2013).

## Local Geology

The geology surrounding the Michelin deposit has been discussed in detail by Gandhi (1978, 1984), Bailey (1979), Evans (1980) and Gower *et al.* (1982). The Michelin deposit is hosted within metavolcanic rocks of the Aillik Group. The host rocks consist of interfingering coarsely feldspar porphyritic, and sub-porphyritic, felsic metavolcanic rocks (Plate 68), which represent a sequence of subaerial ash-flow tuffs (Watson-White, 1976; Bailey, 1979; Evans, 1980; Gower *et al.*, 1982). These metavolcanic host rocks contain finely disseminated magnetite throughout, which predates the development of uranium mineralization.



**Plate 68.** Metavolcanic host rock of the Michelin deposit illustrating the variably porphyritic nature of the unit. Note the inset of the stained sample outlining the primary potassio minerals within the metavolcanic rock prior to being overprinted by the sodic alteration associated with the uranium mineralization; DDH M-06-11, ~140 m depth.

Within the immediate vicinity of the deposit, the host rocks contain a moderate to strong penetrative fabric with the main foliation trending approximately 60° and dipping between 50–55° to the southeast; a prominent lineation is also developed, which plunges 65° to the southwest, and is paralleled by the main mineralized zone (Gandhi, 1978). Bailey (1979) noted that the deposit occurred within a schistose zone trending 70°, and attributed it to an anticlinal axial zone related to tight isoclinal folding in the region.

The volcanic sequence is crosscut by foliated and non-foliated mafic dykes, some of which appear to predate mineralization. These dykes have variable relationships to the

fabric, suggesting pre-, syn- and post-kinematic emplacement. The inferred oldest dykes are composed of albite–amphibole–biotite–calcite, and locally contain minor uranium mineralization; these dykes are cut by younger and more numerous amphibolite dykes that postdate uranium mineralization (Gandhi, 1978). Granitoid plutonic rocks and quartz–feldspar porphyries also form subconcordant sheets within the metavolcanic host rock (Figure 42), which are also inferred to postdate mineralization, although rare zones of anomalous radioactivity are locally noted within discrete pegmatitic zones.

Within the deposit, a mixed mafic–felsic porphyritic unit, commonly referred to as the ‘complex dyke’, is up to 10 m thick and occurs within the hanging wall of the mineralized zone (Piloski, 1976; Bailey, 1979). This unit was interpreted as a dyke by Piloski (1976), but Evans (1980) considered it to represent interlayered mafic and felsic tuff. The margins of the unit are fine-grained amphibolite, which grades inward to a porphyritic amphibolite containing centimetre-scale feldspar and quartz, and then to a quartz–feldspar porphyry core that forms the bulk of the unit (Plate 69A, B). The unit can be traced over a considerable strike length, and occurs at a predictable stratigraphic location (between 55 to 67 m) above the main mineralized zone (Piloski, 1976), and represents one of the few distinctive units that can be traced throughout the deposit.

### Mineralization and Associated Alteration

Surface exposures of mineralized rocks are limited at the Michelin deposit, and most information is obtained from drill-core, along with reports from the limited underground exploration, conducted in the 1970s (Piloski, 1976). The exploration adit is now sealed, and no longer available for examination. The deposit consists of several subparallel *en-echelon* zones of uranium mineralization, broadly concordant with the strongly deformed and recrystallized felsic metavolcanic host rock, that collectively define a northeast–southwest-trending tabular zone (Figure 42). As discussed above, mineralization is stratabound rather than stratiform (e.g., Gandhi, 1978; Evans, 1980).

The mineralization is broadly divisible into three zones, separated by lower grade or barren metavolcanic rock. The mineralized zones combine to form the ore zone, which is commonly 10–20 m thick, but locally reaches a thickness of up to 50 m (Figure 43). This zone is traceable for up to 1950 m along strike, dips steeply to the south, and has a predictable geometry that has been drilled to a depth of 1050 m (Hertel *et al.*, 2009). Within this zone, the thickest and most uranium-enriched material defines a linear zone that achieves its greatest thickness below depths of approximately 400 m.

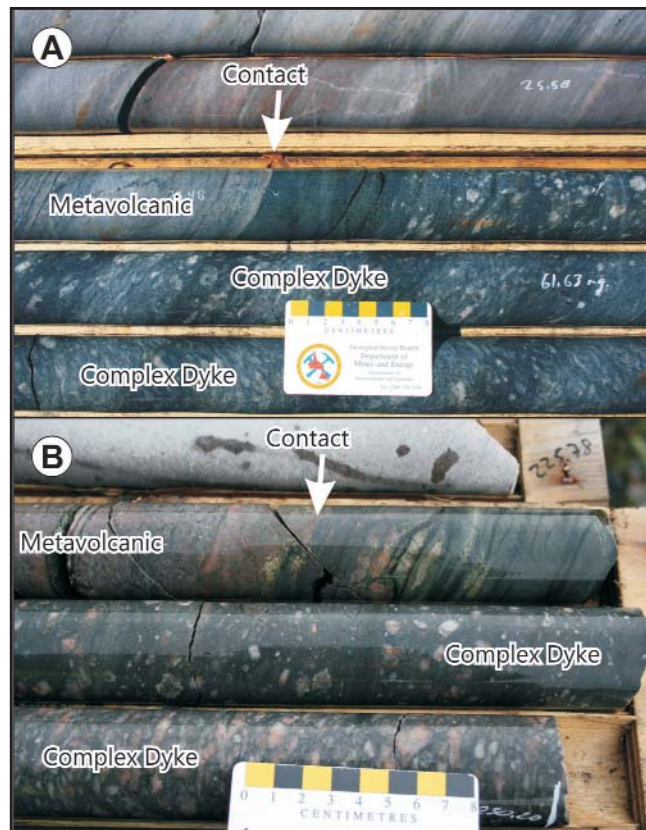
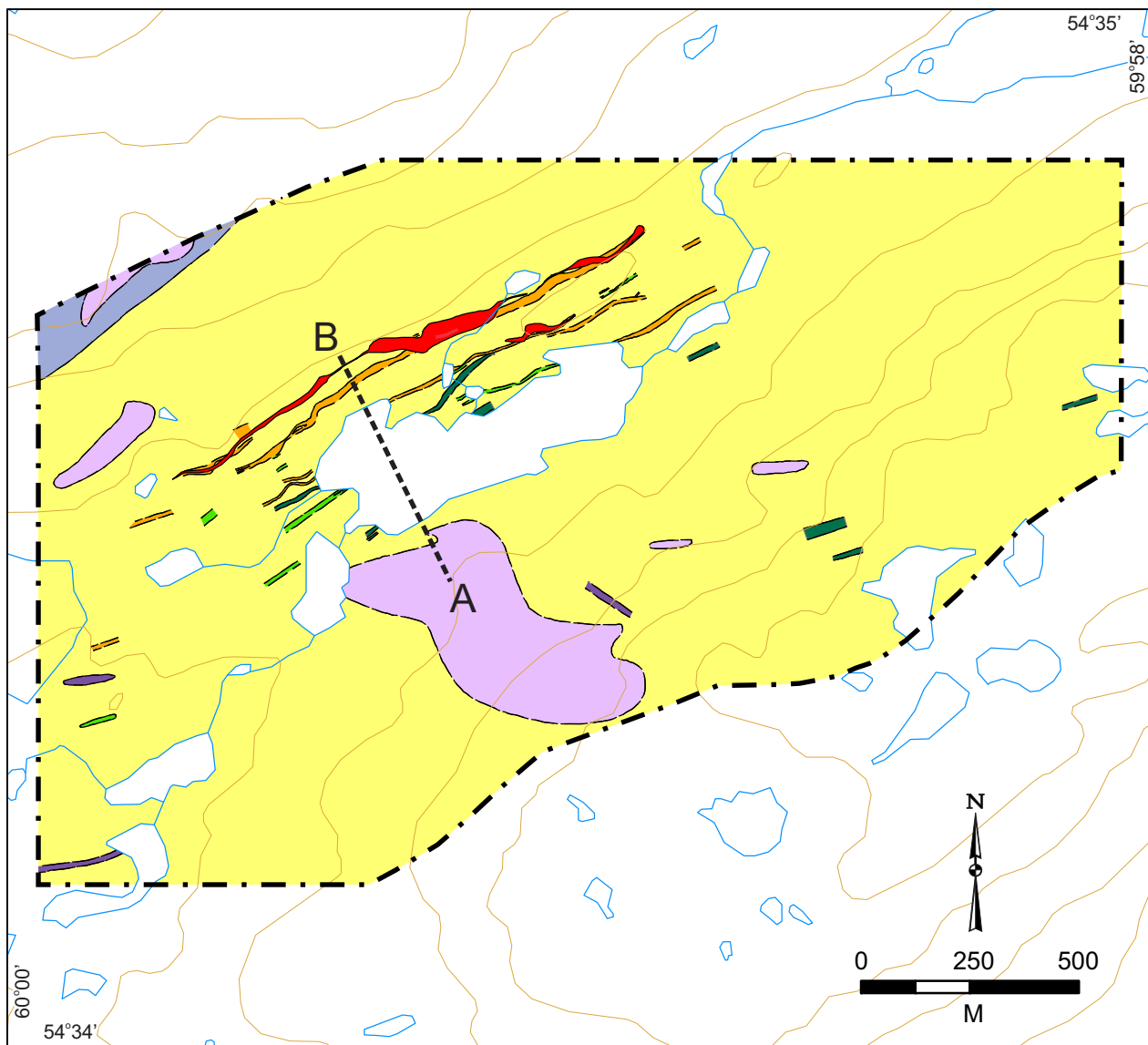


**Plate 69.** A. Photograph of the complex dyke of Piloski (1976) displaying a sharp upper contact between the adjacent metavolcanic rock and the fine-grained amphibolite margin of the dyke, which, in turn, transitions into a coarsely porphyritic felsic core; Michelin deposit, DDH M-07-75A, 792 m. B. Similar dyke as shown in (A), located approximately 900 m to the northeast; DDH M-06-11, 227 m.

Uranium mineralization within the deposit is associated with pervasive albitionization of the host rock along with variably developed hematization (Plate 70); however these alteration assemblages are not everywhere mineralized with respect to uranium (Figure 44). The development of this alteration is accompanied by an increase in actinolite, pyroxene and calcite, and a decrease in magnetite and, more locally, pyrite (Hertel *et al.*, 2009). Within the deposit, uranium occurs largely in the form of finely disseminated uraninite, much of which is associated with metamorphic or metasomatic minerals such as sodic amphibole, aegirine–augite, titanite, iron–titanium oxides, as well as along grain boundaries within the albite–quartz-rich matrix (Evans, 1980; Cunningham-Dunlop *et al.*, 2007a; Plate 71). Evans (1980) also noted the presence of allanite, as well as fluorite, in trace amounts.

Uranium mineralization is correlated with a marked increase in zirconium concentrations, coupled with depletion



### LEGEND

- Uranium mineralization
- Fine- to medium-grained, pink, weakly foliated to non-foliated granite
- Weakly to moderately foliated, fine-grained, late kinematic mafic dykes
- Fine-grained, weakly foliated gabbro to leucogabbro
- Fine-grained, strongly chloritized and foliated pre- to syn-kinematic mafic dyke
- Coarsely porphyritic felsic metavolcanic
- Finely porphyritic felsic metavolcanic
- Fine- to medium-grained pink, equigranular to feldspar porphyry
- Fine- to medium-grained, weakly to moderately foliated granodiorite to diorite

### SYMBOLS

- Approximate contact
- Limit of mapping

**Figure 42.** Local geology map outlining the distribution of the main rock units and surface projection of uranium mineralization in the area of the Michelin deposit (modified from Barrett and Ash, 2009). Cross-section A-B illustrated as Figure 43.

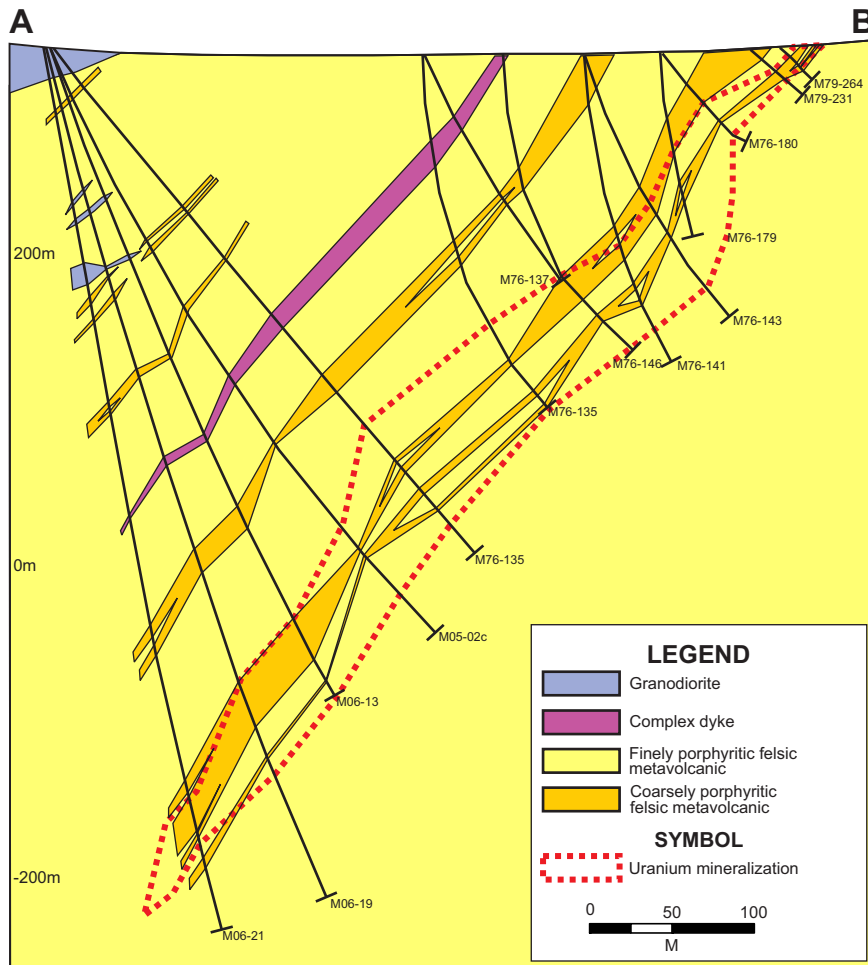


**Figure 43.** Schematic cross-section through the Michelin deposit outlining the distribution of the main rock units and uranium mineralization (modified from Cunningham-Dunlop and Lee, 2008). Location of cross-section refer to Figure 42.



**Plate 70.** Typical features of mineralized core from the Michelin deposit illustrating the light-coloured (albitized) and red (hematized) metavolcanic host rock. A. Sub-porphyritic metavolcanic host rock; M-06-13, 400 m, B. Coarsely porphyritic metavolcanic host rock, is the primary host to the mineralized zones; M-06-13, 408 m.

in potassium and de-silicification of the metavolcanic host rock (Evans, 1980; Cunningham-Dunlop *et al.*, 2007a; Hertel *et al.*, 2009). Uranium grades at Michelin typically range between 0.05 and 0.5%  $U_3O_8$ , with most intersections averaging 0.1 to 0.2%  $U_3O_8$ . The mineralization is Th-poor and contains no reported enrichment in base-metals or Mo; however, pyrite is locally present, and minor chalcopyrite has been reported by previous workers.

In drillcore, radioactivity is commonly associated with a red, hematitic alteration that generally defines a very strong banding (Plate 70A), suggesting the mineralization and alteration has been overprinted by post-mineral deformation (Gandhi, 1978). The relationships observed in drillcore, coupled with the detailed work by Evans (1980), suggest that the introduction of uranium and related metasomatism occurred pre- to syn-deformation. As illustrated in Plate 72, the locally folded and crenulated fabric within the metavolcanic host rock does not appear to exhibit significant control on the finely disseminated uraninite, implying a late- to syn-deformational timing with regards to the introduction of the mineralization relative to the formation of the strong penetrative fabric within the host rock.

**Figure 44 (opposite).** Drill log for hole M06-11 from the Michelin deposit, outlining the distribution of uranium mineralization and main rock units; uranium values are listed in ppm (data from Cunningham-Dunlop *et al.*, 2007b). A. Photograph displaying localized development of hematite alteration without associated uranium mineralization or sodium metasomatism; host rock contains approximately 4.45 wt.%  $Na_2O$  and 5.9 ppm U. B. Photograph displaying hematization and albitization with anomalous uranium enrichment; host rock contains approximately 6.12 wt.%  $Na_2O$  and 308 ppm U. C. Photograph showing a post-mineralization mafic dyke crosscutting the mineralized metavolcanic host rock (dyke contains 2.6 ppm U, whilst adjacent metavolcanic rock is host to approximately 905 ppm U).

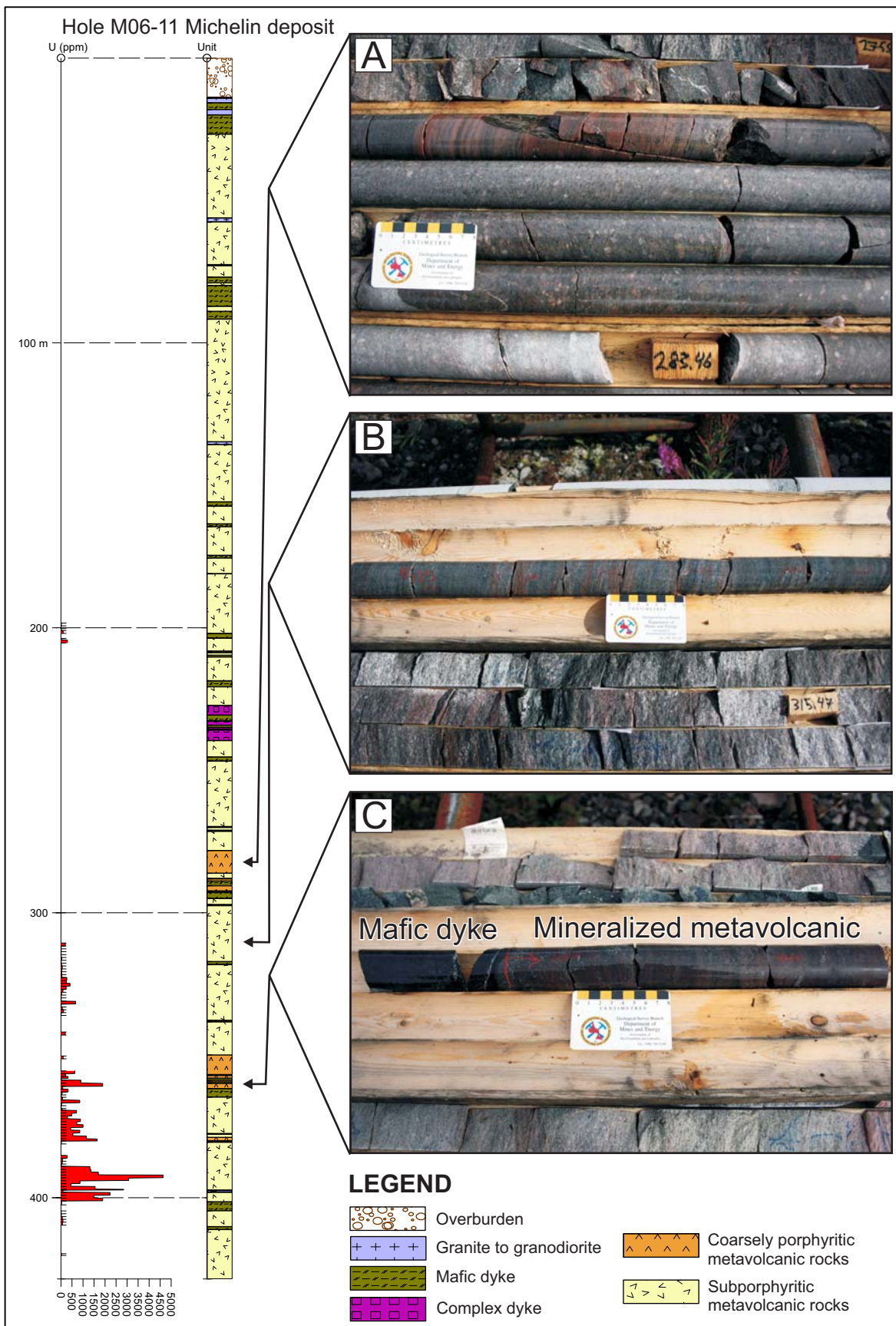
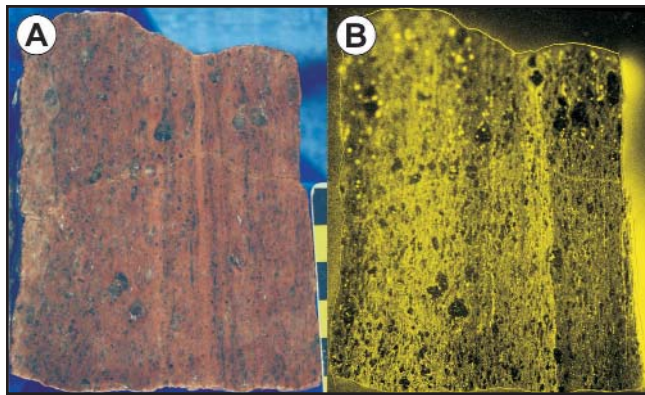


Figure 44.

## Petrography

Several industry and academic petrographic research studies summarize the alteration and mineralization related to the Michelin deposit (e.g., Ponder *et al.*, 1976; Gandhi, 1978; Evans, 1980; Cunningham-Dunlop *et al.*,



**Plate 71.** A. Representative sample of mineralized, coarsely porphyritic, metavolcanic rock obtained from material excavated during construction of the adit; note the pervasive hematite alteration and a moderate to strong penetrative fabric, B. Corresponding autoradiograph of (A) outlining the location of radioactivity (yellow, minus the outline of the sample); note the fine-grained disseminated radioactivity throughout the host rock as well as localized increases in radioactivity within more strongly foliated portions of the sample.

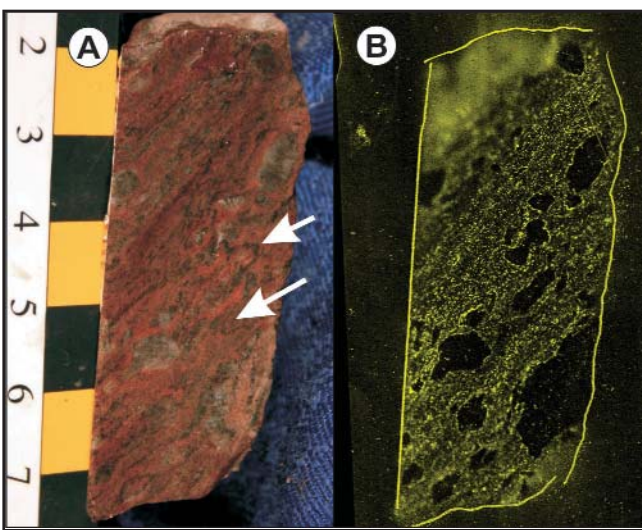


**Plate 72.** A. Pervasive hematization within a coarsely porphyritic sample of mineralized metavolcanic rock displaying a strong penetrative fabric affected by local crenulation (white arrows); DDH M-07-072, 554 m, B. Corresponding autoradiograph of (A) outlining the location of radioactivity (yellow, minus the outline of the sample); note the lack of influence on the disseminated uranium mineralization relative to the development of the crenulation.

2007a), and the reader is referred to these reports for a more detailed discussion of the alteration and related mineralization. The common alteration minerals associated with uranium mineralization are albite, amphibole, pyroxene, titanite, ilmeno-magnetite, andradite, biotite, and lesser calcite, epidote, allanite, zircon, apatite and pyrite (Evans, 1980; Cunningham-Dunlop *et al.*, 2007a).

Recent petrographic work (e.g., Cunningham-Dunlop *et al.*, 2007a) noted the presence of potassic-rich rocks marginal to the main zone of sodic alteration and related uranium mineralization. These may represent zones of potassic alteration surrounding the main zone of sodic alteration, or alternatively may represent the primary geochemical signature of the protolith. This study has identified similar potassic-rich rocks, up to 300 m from uranium mineralization. Within the metavolcanic host rocks, the potassic nature of both the phenocrysts as well as the supporting groundmass is highlighted within stained samples as shown in Plate 73. Staining the samples, hosting uranium mineralization, shows that potassium-rich minerals are absent, and as is further indicated by the geochemical data (see below).

Within mineralized zones, the most abundant minerals are albite and quartz, along with the accessory phases noted above. Autoradiographs of mineralized thin sections demonstrate the finely disseminated mineralization (Plate 74A, B). From the autoradiographs, it is evident that highest concentrations of radioactivity are developed along discrete fractures that display a pinkish hematitic alteration in hand sample. It is also evident that the more coarse-grained quartz and feldspar material in thin section, which possibly represents recrystallized phenocrysts, are devoid of any significant radioactivity (Plate 74B, D). Within zones of mineralization, finely disseminated magnetite is variably replaced by hematite. In addition, zones of localized fracturing are host to finely disseminated Fe-oxide minerals that display a spatial association with uranium mineralization (Plate 74E, F). As noted in previous studies (e.g., Ponder *et al.*, 1976; Gandhi, 1978; Evans, 1980; Cunningham-Dunlop *et al.*, 2007a), radioactive phases are also hosted within the amphibole and pyroxene minerals as well as within titanite, implying that the formation of these minerals is syn- to post-development of the uranium mineralization.

Petrographic examination of the 'complex dyke' unit illustrates that the feldspar crystals contained within the more mafic margins of the unit are visually similar to those in the more feldspar-rich core, and locally display disrupted zonation patterns that are, in turn, rimmed by more albite-rich material (Plate 75A, B). These feldspar crystals are interpreted as xenocrysts within the amphibolite margin of the dyke. Within the more feldspar-rich core of the unit, the mineralogy of the groundmass is very similar to that of the adjacent host

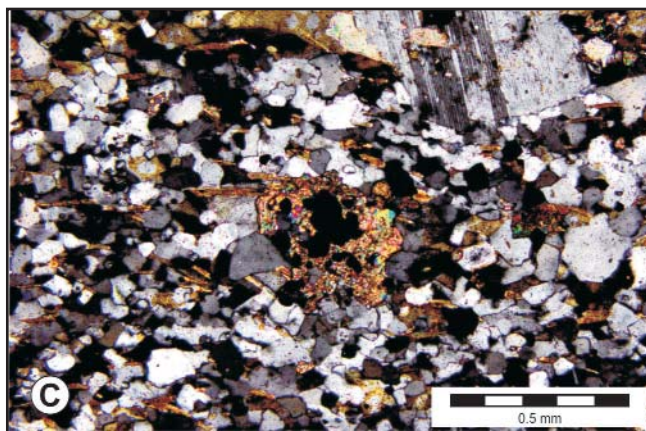
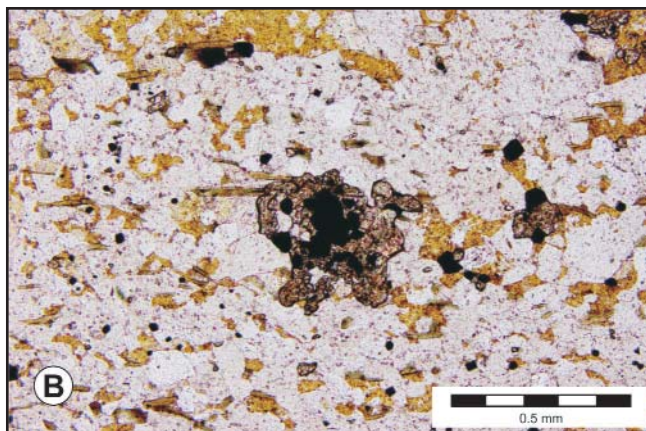


**Plate 73.** *A.* Representative sample from the Michelin deposit (DDH M-06-11 at 64 m depth) stained for potassium-bearing minerals (yellow colouration). The sample consists of a K-feldspar-phyric, fine-grained, quartz-rich metavolcanic rock illustrating the potassic nature of the metavolcanic host rock, distal to uranium mineralization. *B.* PPL photomicrograph showing the distribution of potassium (yellow) throughout the groundmass of the volcanic protolith. Also note the presence of fine-grained disseminated opaque minerals (primarily consisting of magnetite) enveloped by titanite rims within the groundmass; minor biotite is also distributed throughout. *C.* XPL photomicrograph showing the same view as in (B).

metavolcanic succession. However, the complex dyke unit is commonly much more biotite-rich, and is host to large feldspar phenocrysts that are dominated by tartan twining and display relic zonation patterns along with ragged recrystallized margins (Plate 75C, D). The feldspar-rich core of the complex dyke unit also contains titanite developed as rims around the disseminated magnetite within the groundmass (Plate 75E, F), similar to that observed within the adjacent metavolcanic rocks. In addition, the complex dyke contains a moderate to strong foliation, which is largely highlighted by the mafic minerals within the groundmass, and wraps around the feldspar phenocrysts (Plate 75C).

## JACQUES LAKE DEPOSIT

### Previous Work

The discovery of uranium mineralization in the area of Jacques Lake was made in 1956 during regional reconnaissance prospecting carried out by Brinex (Morrison, 1956). Further evaluation of the area was conducted in 1980, at which time follow-up drilling was recommended, but was never carried out (Darch, 1981). Renewed exploration in the mid-2000s included follow-up of a 4-km-long, northeast-trending, airborne radiometric anomaly, and thus, this led to the discovery of the Jacques Lake deposit (Cunningham-Dunlop *et al.*, 2006).

### Local Geology

The Jacques Lake deposit is poorly exposed at surface, consisting of sparse outcrop along the northern face of a steep northeast-southwest-trending ridge above the eastern end of Jacques Lake (Figure 41). The host rocks were originally described as quartzite due to their fine-grained, recrystallized nature (Beavan and Meyer, 1968). However, these rocks have since been reinterpreted as being volcanogenic, containing lesser interbedded volcaniclastic material (Bailey, 1979; Darch, 1981; Wilton and Cunningham-Dunlop, 2006). Within the deposit, uranium mineralization is hosted by dark-purple to grey-green, aphanitic to moderately porphyritic, magnetite-bearing intermediate rocks, interpreted as ash-flow tuff.

The mineralized tuffs are, in turn, structurally overlain to the southeast by a poorly sorted, generally matrix-supported, cobble to boulder polymictic conglomerate containing clasts of predominantly volcanic detritus (Figure 45); this unit forms the structural hanging wall to the deposit. The most intense shearing in the area is focused along the contact between the ash-flow tuff and the conglomerate, with both the contact and the penetrative fabric dipping moderately to steeply toward the southeast. The intermediate metavolcanic rocks are affected by a variably developed penetrative fabric that is locally intense and mylonitic (Plate 76). Metre-scale

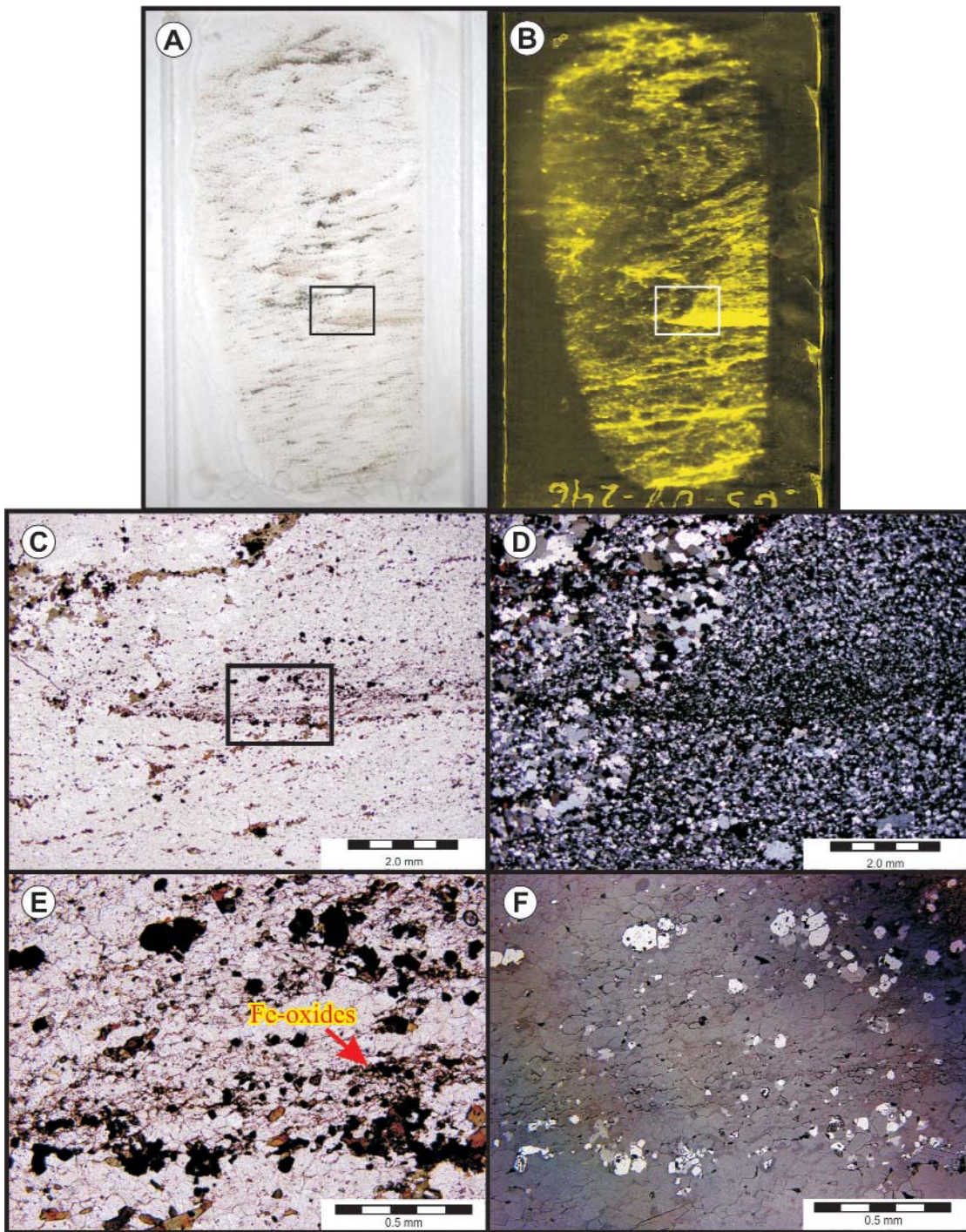


**Plate 74.** Representative sample of mineralized drillcore (Michelin deposit; DDH M-06-11, 380 m). A. Photograph of a mineralized thin section; note the inset box displays the location of (C). B. Corresponding autoradiograph of the mineralized thin section outlining the distribution of radioactivity within the sample (yellow, minus the outline of the sample). C. PPL photomicrograph covering an area of intense radioactivity. The sample contains finely disseminated magnetite throughout, but the area associated with the most intense radioactivity also contains finely disseminated hematite and Fe-Ti-oxides; note the inset box in (C) outlines the area of (E). D. XPL image of (C); note that the coarser grained quartz-albite lacks any significant radioactivity. E. PPL photomicrograph outlining the distribution of the turbid, finely disseminated Fe-oxide minerals along discrete fractures within the thin section; this area is associated with the highest radioactivity within the sample. F. Reflected light image of (E) showing the distribution of magnetite and hematite as well as highlighting the finely fractured nature of the host rock within the zone of elevated radioactivity.

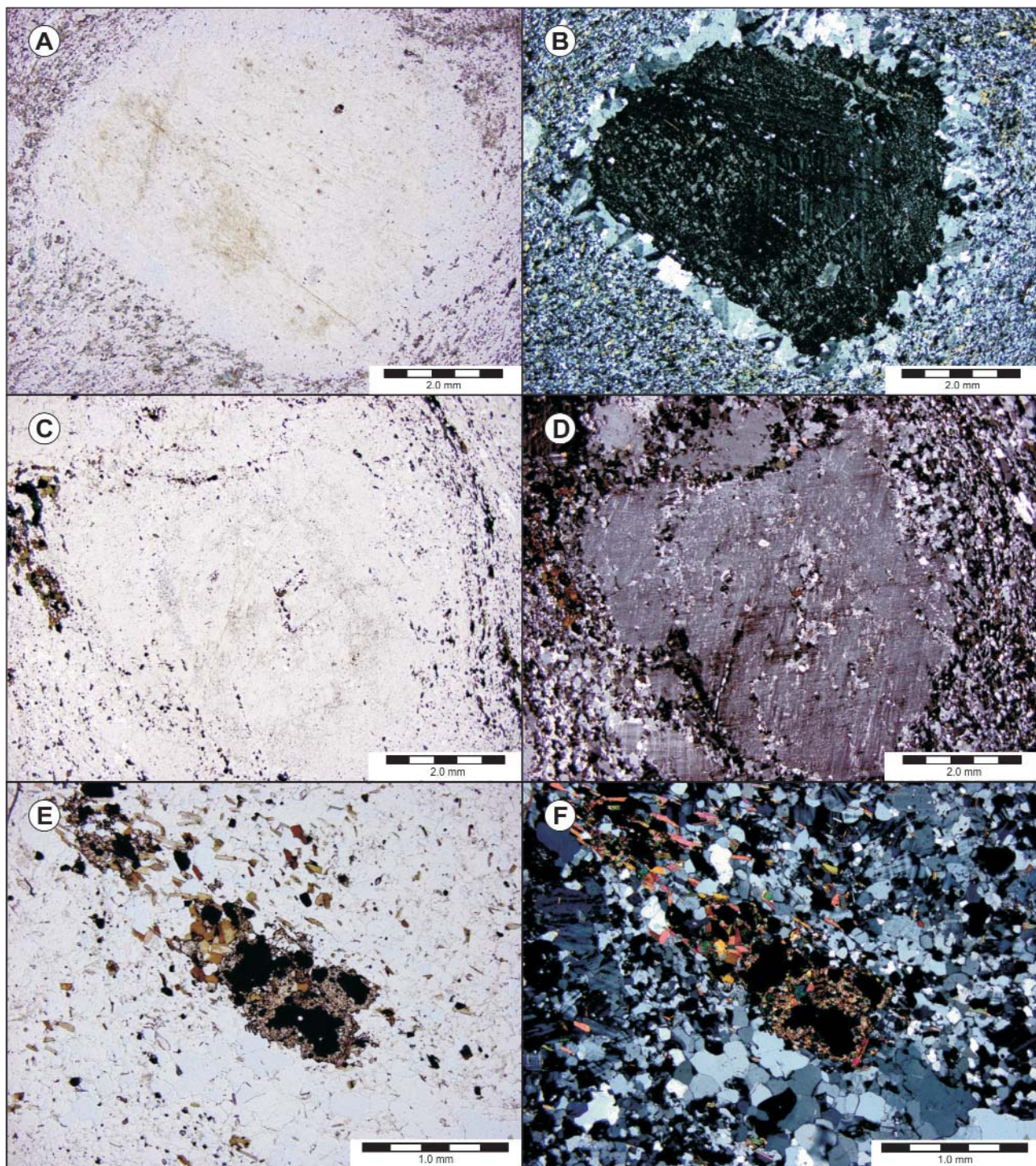


**Plate 75.** Photomicrographs of the complex dyke unit from the Michelin deposit. A. PPL image of a large feldspar crystal displaying relic compositional zoning of a more K-feldspar-rich core and albite-rich rim; the crystal is supported by a groundmass of fine-grained quartz and feldspar along with abundant blue-green amphibole and lesser biotite, pyroxene, opaque minerals and titanite; DDH M-06-11, 228 m depth, B. XPL image of (A), C. PPL image of a large feldspar phenocryst display a relic compositional zonation within a finer grained quartz-feldspar-biotite-rich groundmass; note how the foliation in the upper right hand corner of the image wraps around the feldspar phenocryst; DDH M-06-11, 230 m depth, D. XPL image of (C), E. Fine-grained, quartz-feldspar-biotite-rich groundmass, hosting disseminated magnetite rimmed by titanite; DDH M-06-11, 230 m depth, F. XPL image of (E).

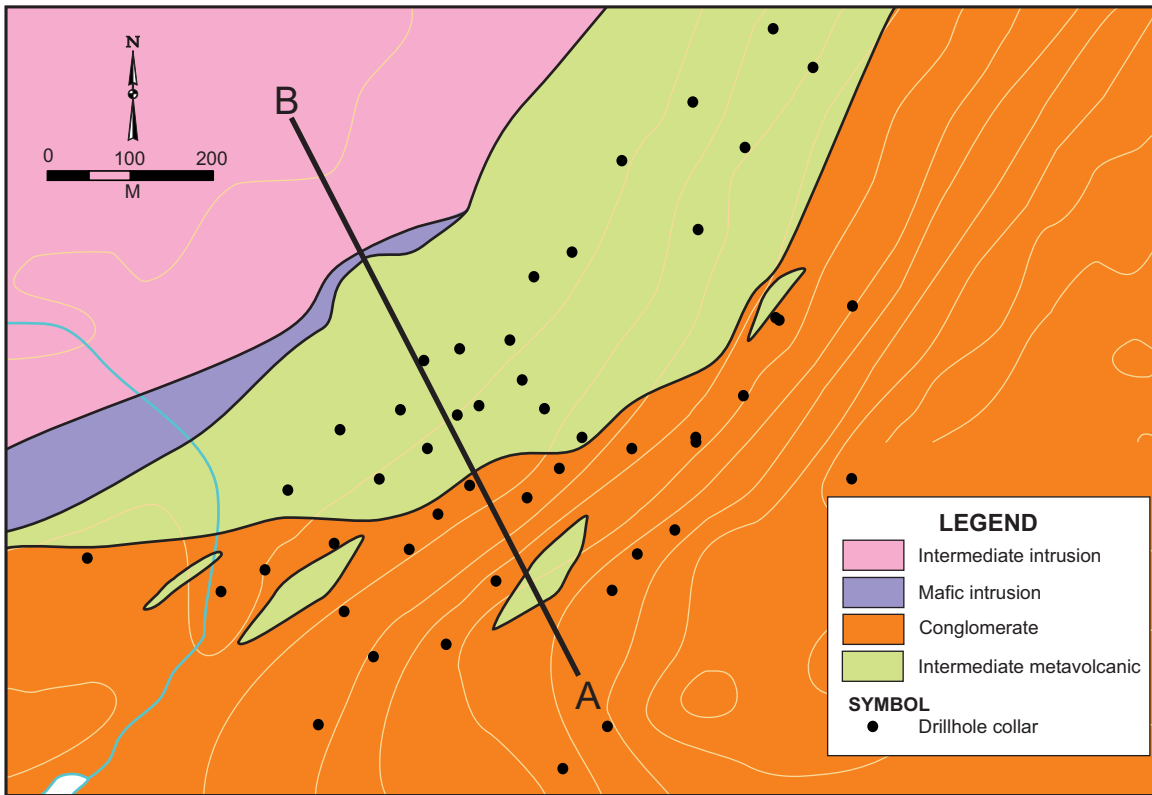


**Figure 45.** Local geology map outlining the distribution of the main rock units and diamond-drill holes in the area of the Jacques Lake deposit (modified from Cunningham-Dunlop and Lee, 2008). Cross-section A–B illustrated as Figure 46.

folding within the metavolcanic rocks has been noted on a regional scale, with fold axis locally being overturned to the southeast (Bailey, 1979). The variable orientation of the penetrative fabric in drillcore, combined with local observations of metre-scale folding, indicates that the penetrative fabric displays some rotation due to a later deformational event.



**Plate 76.** Strongly foliated intermediate metavolcanic host rock displaying a typical upper-greenschist- to lower-amphibolite-facies metamorphic assemblage consisting of chlorite, actinolite, biotite and epidote; Jacques Lake deposit, DDH JL-06-10, 142 m.

Regional metamorphism is interpreted to range from upper-greenschist to upper-amphibolite facies, with chlorite, actinolite, biotite and epidote commonly developed within the supracrustal sequence (Bailey, 1979; Cunningham-Dunlop *et al.*, 2007a). The main period of deformation that affects these rocks is the Makkovikian Orogeny, but the area was also likely affected by the subsequent Grenvillian Orogeny on at least a local scale (Bailey, 1979; Gower *et al.*, 1982).

At the base of the ridge, which hosts the deposit, the ash-flow tuff sequence and accompanying uranium mineralization is bound to the west by relatively undeformed, medium- to coarse-grained felsic to intermediate intrusive rocks that form the structural footwall to the deposit (Figure 46). These rocks display a sharp intrusive contact with the adjacent ash-flow tuff, locally displaying a well-developed chilled margin. In addition, numerous granitoid dykes are observed within the host metavolcanic rocks close to the main body of the intrusion. Within the centre of the deposit a very distinctive, post-mineralization, quartz-feldspar-porphyry dyke locally crosscuts mineralized ash-flow tuff, providing a minimum age limit on the development of uranium mineralization (see below). This unit varies from 3 to 26 m in width, and contains distinctive centimetre-scale white feldspar phenocrysts, which are commonly zoned displaying a pseudorapakivi texture; the core of

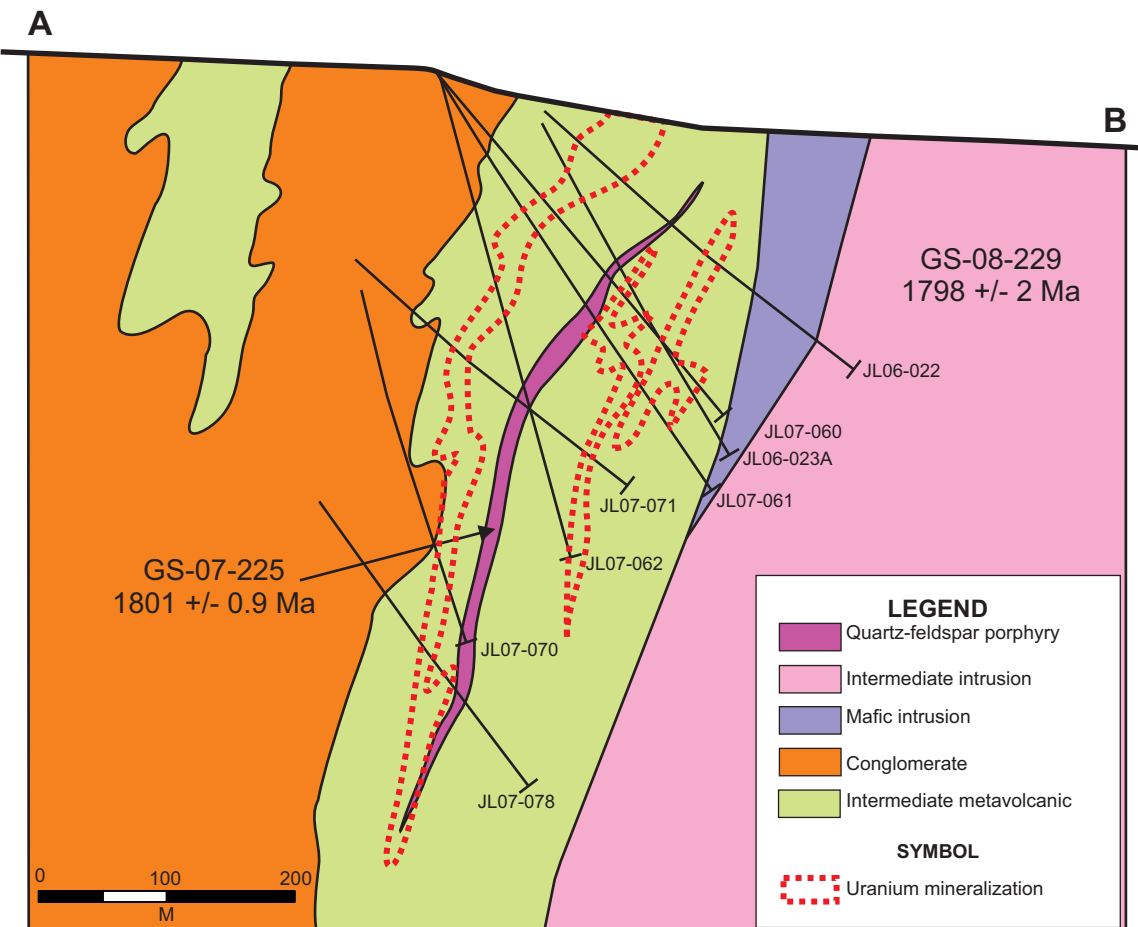


**Figure 46.** Schematic cross-section through the Jacques Lake deposit outlining the distribution of the main rock units and uranium mineralization (modified from Hertel *et al.*, 2009). Location of the cross-section refer to Figure 45. Also shown are the results from U–Pb geochronological studies carried out on samples from the deposit (refer to text).

these zoned feldspar phenocrysts also locally incorporate a small amount of mafic minerals (Plate 77). The quartz-feldspar-porphyry dyke is largely undeformed and crosscuts the main penetrative fabric developed within the metavolcanic host rock, but locally develops a weak to moderate fabric related to a younger deformational event. This unit is also spatially associated with a more mafic phase, which is generally developed along the margins of the quartz-feldspar porphyry dyke, and contains zoned feldspar crystals derived from the more feldspar-rich core (Plate 78). Several generations of mafic dykes are also observed within the mineralized zone and include both foliated and non-foliated varieties.

#### Mineralization and Associated Alteration

Within the Jacques Lake deposit, uranium mineralization and related alteration are spatially associated with a zone of relatively high strain. However, observations from drillcore indicate that the development of uranium mineralization is

not always proportional with the intensity of the penetrative fabric within the host volcanic succession. The area surrounding the Jacques Lake deposit is associated with a pronounced radiometric anomaly. Drilling carried out by Aurora Energy has shown that the *in-situ* mineralization occurs at the southwestern end of this radiometric anomaly, with the northeastern trend of the anomaly likely due to glacial dispersion (Cunningham-Dunlop and Giroux, 2007). Extensive drilling in the area has now defined the mineralization over a strike length of approximately 1100 m and to a depth of approximately 600 m (Hertel *et al.*, 2009). From this drilling it has been inferred that the uranium mineralization is overprinted by isoclinal folding similar to that developed within the host volcanic succession (Cunningham-Dunlop and Lee, 2008). This folding is related to a regional  $F_2$  event and is synchronous with the formation of the main penetrative fabric (Hinchey, 2007; Hinchey and LaFlamme, 2009), which implies a pre- to syn-deformational timing for the development of the uranium mineralization in the area.

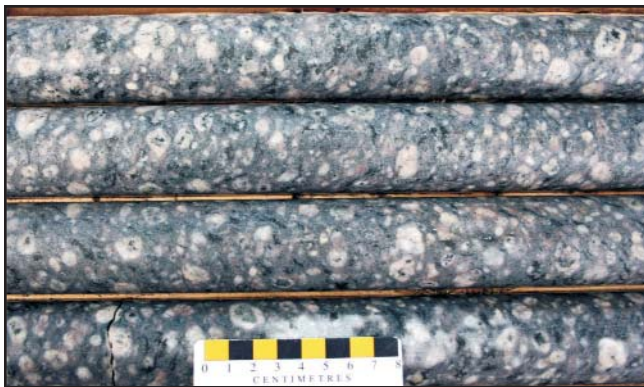


**Plate 77.** Quartz-feldspar porphyry dyke displaying a distinctive pseudorapakivi texture; Jacques Lake deposit, DDH JL-06-10, 365 m.



**Plate 78.** Feldspar crystals from the adjacent quartz-feldspar porphyry dyke hosted within a more mafic-dominated phase that intrudes along the margin of the porphyry unit; DDH JL-07-60, 205 m.

Uranium mineralization within the Jacques Lake deposit is spatially associated with the development of actinolite–magnetite–carbonate ± biotite ± pyrite veining, accompanied by variably developed hematization and sodium metasomatism (Figure 47). Mineralized rocks locally contain up to 9.5 wt.% Na<sub>2</sub>O, but the uranium mineralization is not everywhere accompanied by such high values. Within the deposit, uranium primarily occurs as fine-grained disseminations within the metavolcanic host rock, as well as along hematitic fractures that are developed roughly subparallel to the veining (Plate 79A, B). An autoradiograph from a grab sample of the exposed mineralization at surface illustrates that the mineralization is both disseminated throughout the metavolcanic wall rock as well as within the actinolite-rich veining (Plate 79C, D). Uranium grades within the deposit generally range from 0.03 to 0.66% U<sub>3</sub>O<sub>8</sub> with localized higher grade intersections.

Several styles of veining are identified on the basis of mineralogy and the relationship to the penetrative fabric within the deposit (*cf.* Sparkes and Dunning, 2009). The de-

velopment of ‘early’ hornblende–epidote ± pyrite-rich veins is evident, as these veins are locally folded and rotated, or boudinaged parallel to the penetrative fabric. These veins are generally barren and lack associated hematite alteration, but do display minor ‘bleaching’ of the adjacent wall rock. Uranium mineralization is predominantly associated with a second style of veining that is characterized by the development of wispy, discontinuous actinolite–magnetite–carbonate ± biotite ± pyrite veins. It is inferred that these veins represent a syn- to late-deformational veining event, as indicated by their parallelism with the main penetrative fabric. The hematite alteration associated with this style of veining is not everywhere developed, but where present, it locally coalesces to form regions of pervasive pale-pink hematization within the host metavolcanic rock. A third style of veining displays a more random, network-like geometry, and is inferred to postdate the development of the main penetrative fabric. These veins have actinolite–biotite–hornblende-rich margins and a more carbonate-rich core, and are generally barren with respect to uranium. A few such veins associated with anomalous radioactivity are interpreted to represent the local remobilization of uranium from earlier mineralization.

### Petrography

Compared to the Michelin deposit, the Jacques Lake deposit has received much less detailed study, but some preliminary petrographic work has been carried out (*e.g.*, Cunningham-Dunlop *et al.*, 2007a).

The volcanic host rocks at the Jacques Lake deposit are predominantly aphanitic having a fine-grained groundmass consisting of interlocking quartz and feldspar. Staining of mineralized samples indicates a lack of potassic minerals, and

**Figure 47 (opposite).** Drill log for hole JL-07-060 from the Jacques Lake deposit, outlining the distribution of uranium mineralization and main rock units; uranium values are listed in ppm (data from Cunningham-Dunlop *et al.*, 2008b). Abbreviations: Act—actinolite, Mag—magnetite, Cb—carbonate. A. Photograph illustrating zones of intermittent hematization associated with uranium mineralization (note labels on core denote counts per second (cps) as determined by a handheld scintillometer; a sample from this zone returned up to 6.23 wt.% Na<sub>2</sub>O and 1470 ppm U). B. Quartz-feldspar-porphyry dyke containing a pseudorapakivi texture; note the zoned feldspar crystals of similar composition to those within the feldspar-rich core also occur within the marginal mafic-dominated material (dyke contains background uranium values of 10.1 ppm U). C. Zone of pervasive hematization containing significant uranium enrichment (note labels on core denote cps); a sample from this zone returned up to 3.95 wt.% Na<sub>2</sub>O and 2620 ppm U).

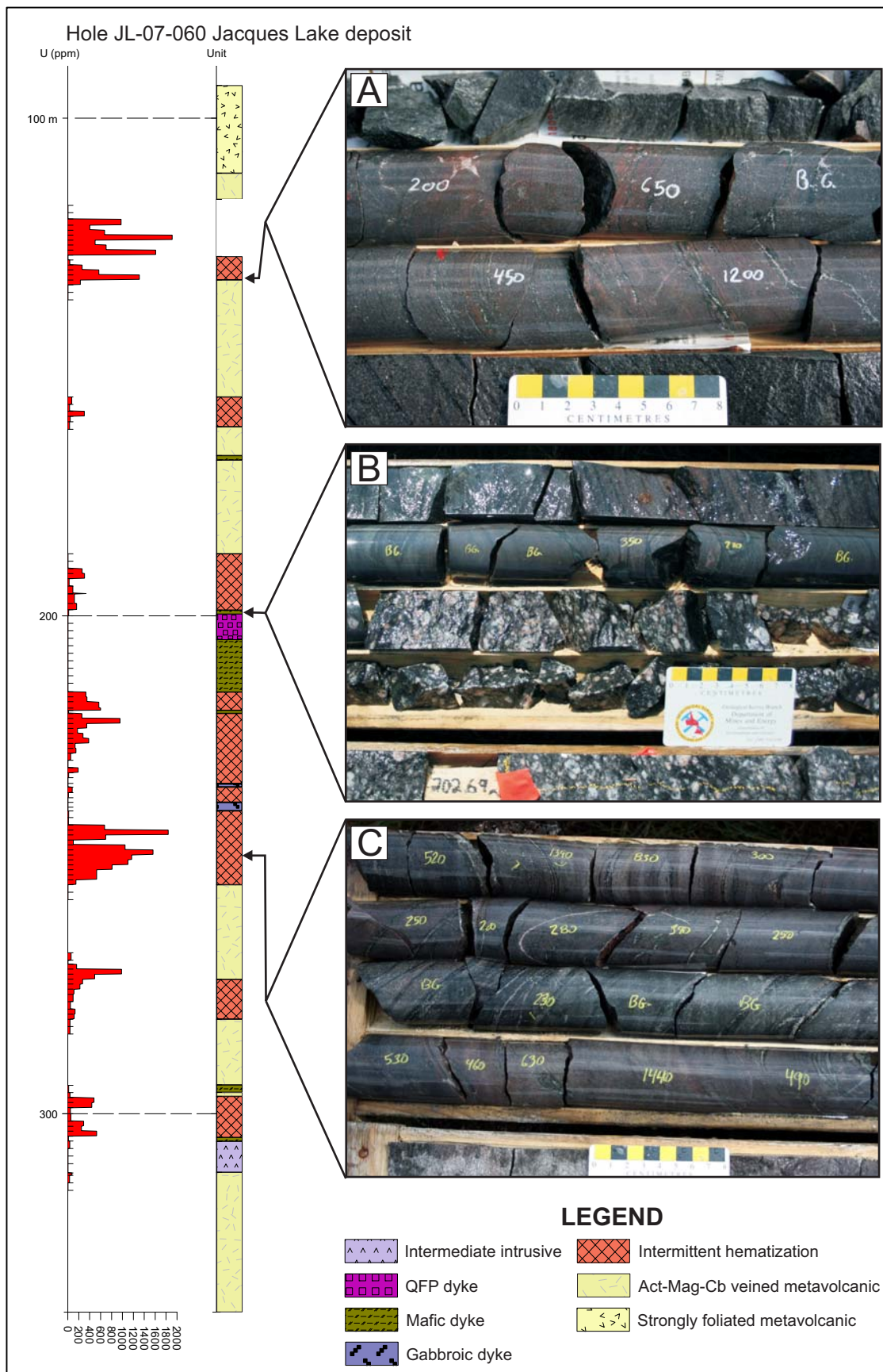
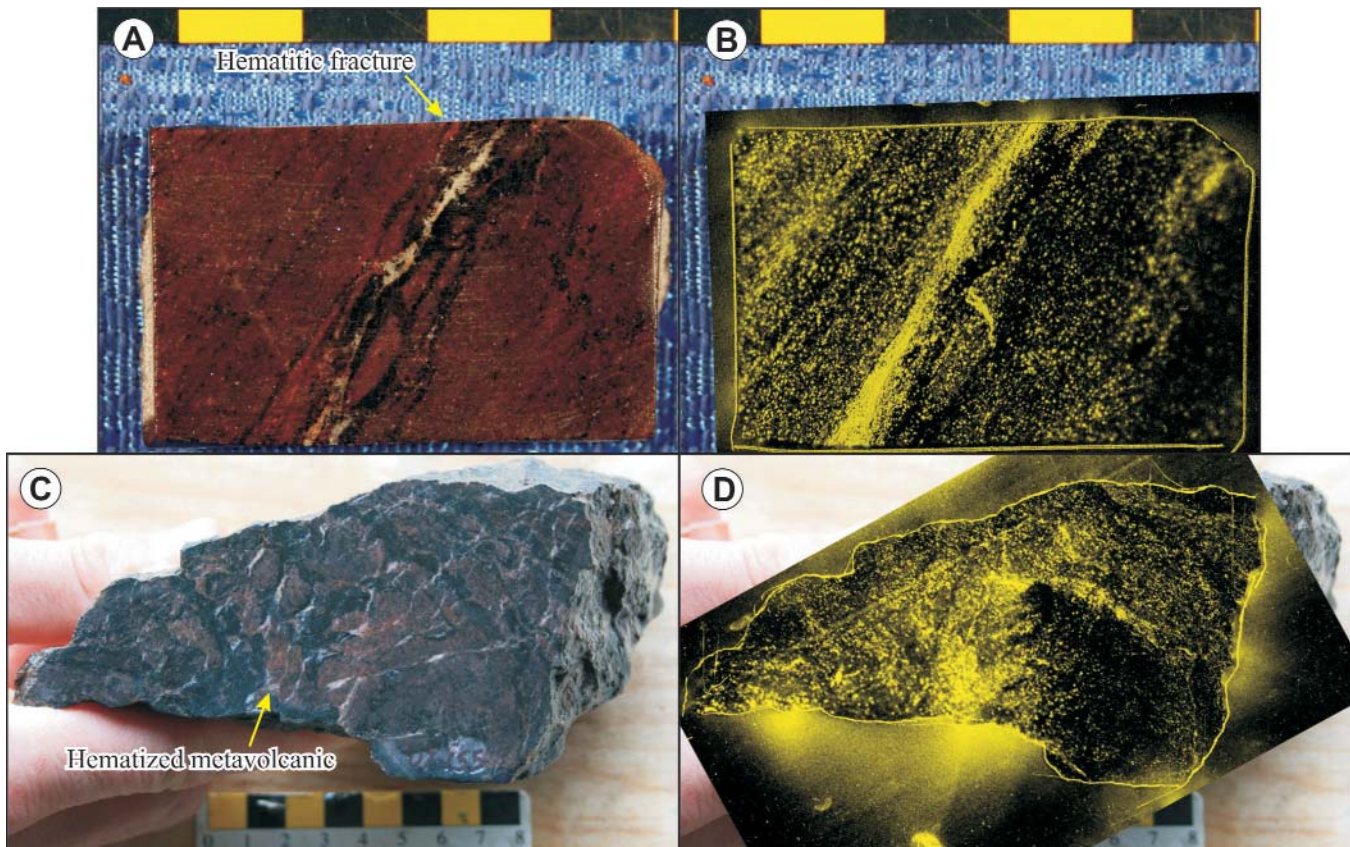


Figure 47.



**Plate 79.** *A.* Representative sample of mineralized metavolcanic host rock from the Jacques Lake deposit displaying hematization in association with uranium mineralization. Note the most intense radioactivity within the sample is developed within a hematitic fracture, roughly subparallel to the actinolite–magnetite–carbonate ± biotite ± pyrite veining; DDH JL-07-60, 132 m. *B.* Corresponding autoradiograph of (A) outlining the location of radioactivity (yellow, minus the outline of the sample). *C.* Grab sample from moderately to strongly foliated outcropping mineralization proximal to the high-strain zone within the Jacques Lake deposit. *D.* Corresponding autoradiograph of (C) outlining the location of radioactivity (yellow, minus the outline of the sample); note the radioactivity is strongest within the pinkish hematized metavolcanic marginal to the actinolite veining, which is subsequently overprinted by later carbonate veining containing notably less radioactivity.

the dominant feldspar is albite, which is further supported by geochemical data (see below). One sample of potassic-rich metavolcanic rock was noted by Cunningham-Dunlop *et al.* (2007a), which may indicate the original composition of the protolith. Within the groundmass, mafic minerals compose up to 10–20% of the unit and consist of hornblende, biotite and lesser pyroxene; fine-grained disseminated magnetite occurs throughout the metavolcanic host rock and is commonly rimmed by titanite.

Mineralized thin sections display several different styles of mineralization, highlighted by autoradiographs. Finely disseminated radioactivity is locally observed throughout the metavolcanic groundmass (Plate 80A, B); however, the most intense radioactivity occurs along discrete hematized fractures. The fracture shown in Plate 80A is developed subparallel to an actinolite–magnetite–carbonate ± biotite ± pyrite vein that contains a notable decrease in the overall abundance

of radioactivity. At least two generations of actinolite have been identified in the sample, the first displays a brownish colouration due to the development of haloes surrounding radioactive phases locally incorporated within the actinolite; the radioactive phase has been locally identified as uraninite using SEM imaging. A later light-green actinolite is associated with the carbonate veining and is relatively barren with respect to any significant radioactivity (Plate 80C, D). In contrast to the disseminated radioactivity within the groundmass, the highly radioactive hematized fracture contains abundant Fe-oxide minerals (Plate 80E, F).

In another mineralized section, the metavolcanic host rock is only mineralized immediately adjacent to the development of actinolite–magnetite–carbonate ± biotite ± pyrite veins (Plate 81). Here, the host volcanic rock in the lower left of the thin section is barren with respect to any significant radioactivity. In contrast, the wall rock immediately adjacent to

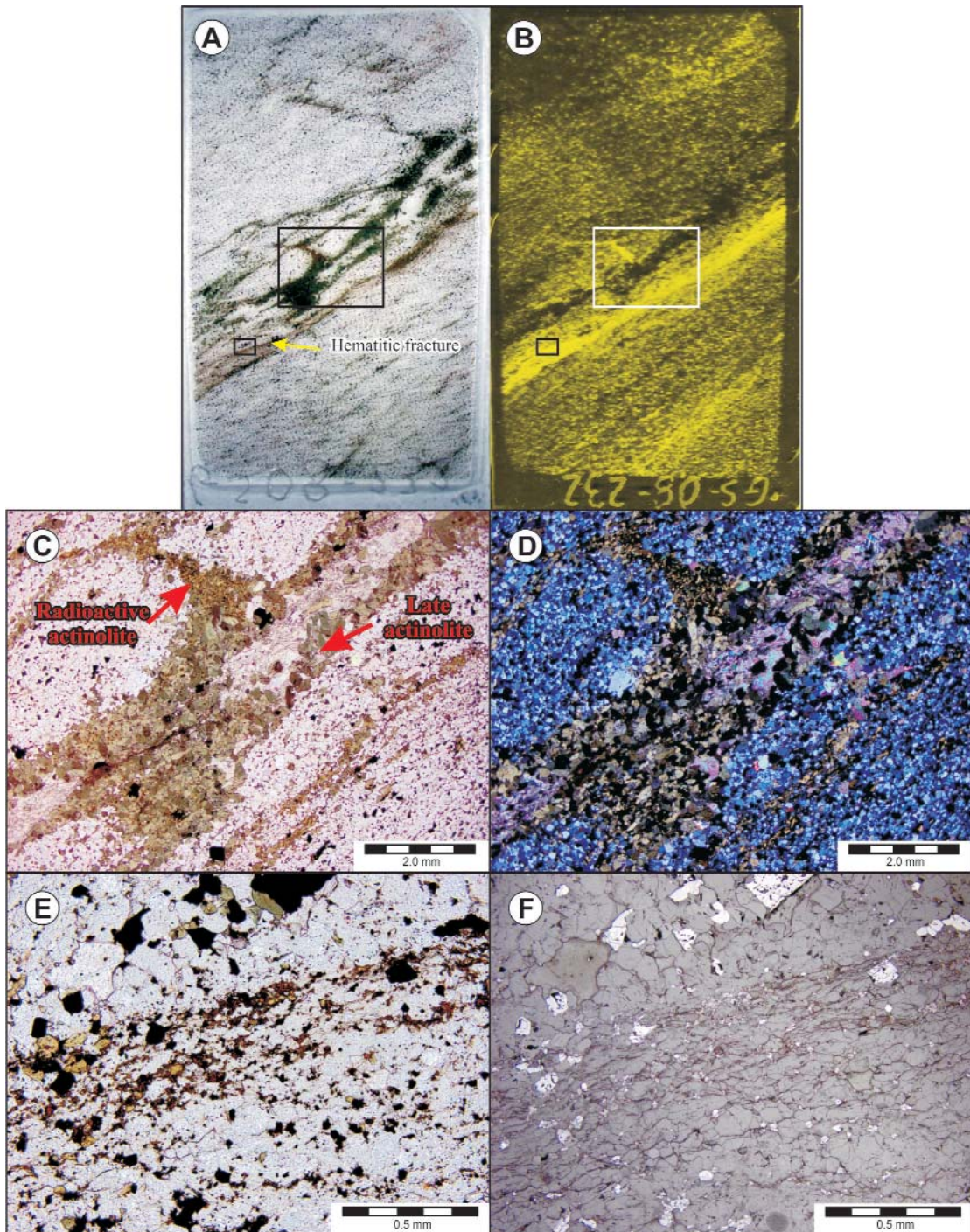


**Plate 80.** Representative sample of mineralized drillcore from the Jacques Lake deposit (DDH JL-07-60, 132 m). A. Photograph of the mineralized thin section. (The large inset box, near the centre of the section, displays the location of (C), whilst the smaller inset box to the lower left displays the location of (E)). B. Corresponding autoradiograph of the mineralized thin section outlining the distribution of radioactivity within the sample (yellow, minus the outline of the sample); note the highest concentration of radioactivity within the sample is associated with a discrete hematitic fracture. C. PPL photomicrograph showing the fine-grained metavolcanic host rock containing abundant disseminated magnetite, crosscut by actinolite–magnetite–carbonate ± biotite ± pyrite veining containing at least two generations of actinolite. D. XPL image of (C). E. PPL image of the highly radioactive hematitic fracture outlining the abundance of Fe-oxide minerals within the zone. F. Reflected light image of (E) highlighting the fractured nature of the host rock in the area of most intense radioactivity; note magnetite is more strongly altered to hematite within this zone.

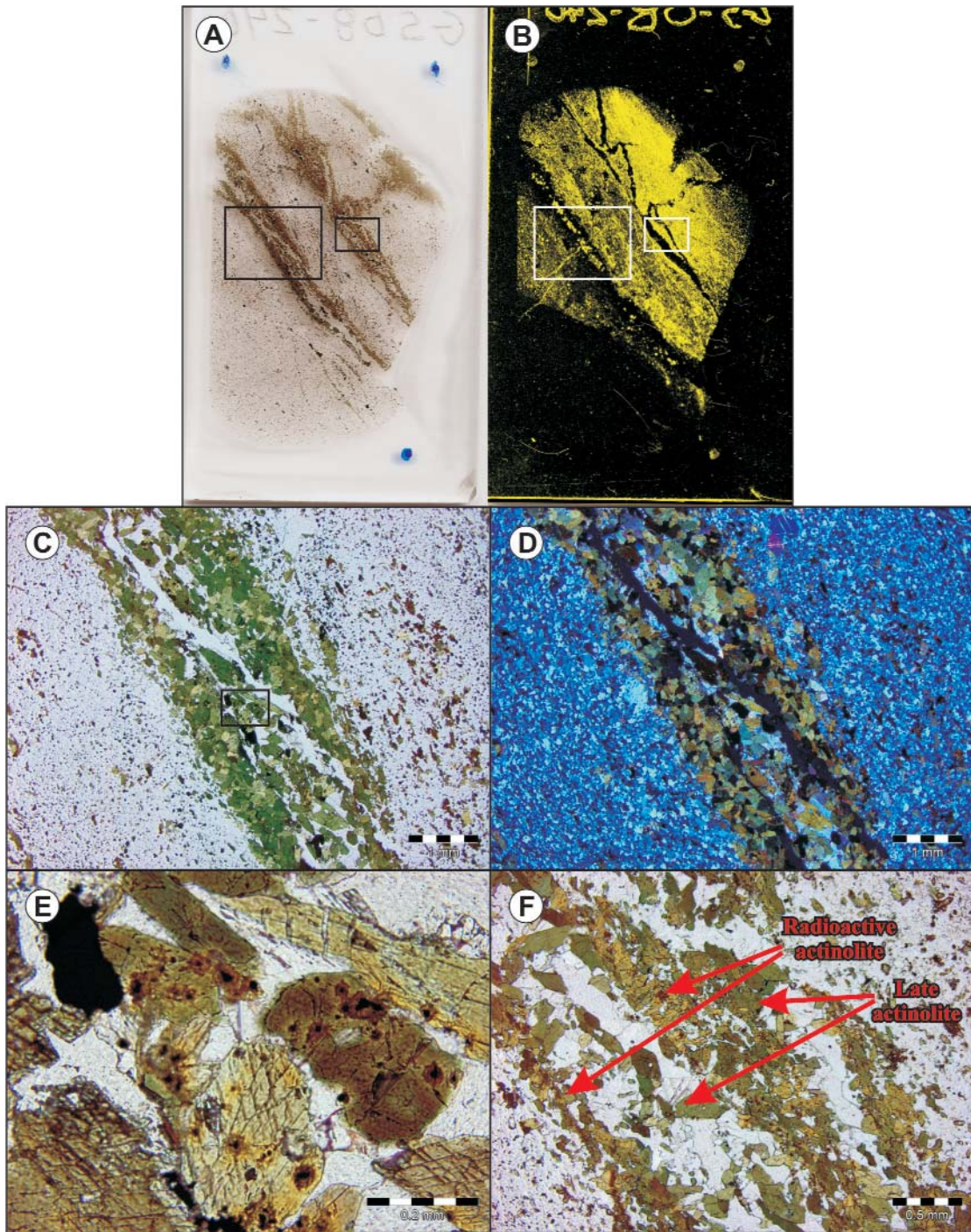


**Plate 81.** Representative sample of mineralized drillcore from the Jacques Lake deposit (DDH JL-07-60, 216 m). *A.* Photograph of the mineralized thin section. (The large inset box to the left of centre displays the location of (C), whilst the smaller inset box to the right displays the location of (F)). *B.* Corresponding autoradiograph of the mineralized thin section outlining the distribution of radioactivity within the sample (yellow, minus the outline of the sample); note the absence of radioactivity within the metavolcanic host rock in the lower left section, away from the vein margin. *C.* PPL image of the actinolite–magnetite–carbonate ± biotite ± pyrite vein. The actinolite at the margins of the vein is devoid of any significant radioactivity, but some irregularly distributed radioactivity is developed within the centre of the vein. (The small inset box outlines the location of (E)). *D.* XPL image of (C). *E.* Actinolite within the core of the vein shown in (C) hosting minor uraninite surrounded by the characteristic brown haloes. *F.* PPL image outlining two generations of actinolite, the first forms along the vein margins and occurs as ‘inclusions’ within the second phase, which is accompanied by carbonate and is barren with respect to any significant radioactivity.

the actinolite-rich veins displays abundant fine-grained disseminated radioactivity (Plate 81A, B). Within the crosscutting veins, two generations of actinolite are developed. An early phase hosts abundant finely disseminated uraninite, and a later phase is generally barren aside from minor uraninite occurring at the centre of the secondary vein (Plate 81C–F). Locally, within the mineralized zone, fine-grained uraninite is also observed as small inclusions within both the magnetite and related titanite, suggesting that both minerals are, at least, locally syn- to post-formational with respect to the uranium mineralization.

A third mineralized sample contains radioactivity that is entirely confined to the actinolite-rich veining (Plate 82A, B). In this sample, the fine-grained metavolcanic host rock is crosscut by an actinolite–magnetite–carbonate vein. The uraniferous actinolite within the vein is pale brown, whilst the barren actinolite is light green (Plate 82A, B). The contact between the relatively barren metavolcanic host rock and the mineralized vein is sharp, with little to no mineralization developed within the immediate wall rock (Plate 82B, C). Within the mineralized zone, both uraniferous and barren actinolite is developed along with minor carbonate (Plate 82D). The mineralized actinolite is host to finely disseminated uraninite as illustrated by the accompanying autoradiograph (Plate 82B, E and F). Such zones are observed in drillcore to measure up to 10–15 cm in width.

At the Jacques Lake deposit, uranium mineralization is locally crosscut by a quartz–feldspar–porphyry dyke that post-dates mineralization (Sparkes and Dunning, 2009). Staining of select samples indicates that the feldspar phenocrysts within the feldspar-rich core of the dyke are predominantly potassium-rich, and locally envelop a more sodic-rich core (Plate 83A). In thin section, local evidence for the compositional zonation within the feldspar phenocrysts is also observed (Plate 83B, C). The feldspar phenocrysts are supported within a fine-grained groundmass consisting of quartz and feldspar along with biotite and lesser actinolite and epidote. The groundmass also contains fine-grained disseminated magnetite throughout, which is commonly rimmed by titanite (Plate 83D, E). This relationship is similar to that seen in the adjacent groundmass of the intermediate metavolcanic host rock.

## OTHER URANIUM OCCURRENCES

### Mustang Lake Prospect

The Mustang Lake area is located approximately 9.5 km northeast of the Michelin deposit and is host to several uranium prospects consisting of numerous radioactive boulders, and lesser mineralized outcrop. Uranium mineralization in this area is hosted within felsic to intermediate volcanic rocks

of the Aillik Group and lesser foliated mafic dykes that cross-cut the succession. Three main prospects occur within the Mustang Lake area, they are the Mustang Lake, Irving Zone and Mustang Lake North prospects (Figure 41).

The Mustang Lake area was first identified as being prospective for hosting uranium mineralization in the late 1970s by Brinex (Busch *et al.*, 1979). Relatively little follow-up on this earlier exploration was conducted until 2003, when the area was once again staked through a joint-venture agreement between Monster Copper Resources Inc. (later acquired by Mega Uranium Ltd.) and Phelps Dodge Corporation (the joint venture later became a partnership between Mega Uranium and Santoy Resources Limited). The property was deemed prospective for uranium, as well as having potential for IOCG-styles of mineralization, due to anomalous Cu and Au values reported from the area (*cf.* Setterfield and Tykajlo, 2004; and *see* references therein). Interestingly, Mustang Lake is associated with the highest lake-sediment value for uranium (154 ppm U) within the entire Michelin–Jacques Lake region. The area was investigated from the early- to mid-2000s, during which time diamond drilling locally intersected up to 0.12%  $U_3O_8$  over 9.11 m, associated with magnetite–hematite alteration along with accompanying sodium enrichment (Willett *et al.*, 2006b). For a complete summary of the exploration work during the 2000s, the reader is referred to Kruse (2008).

Uranium mineralization within the Mustang Lake area is similar in many respects to that developed in the nearby Michelin and Jacques Lakes deposits. The mineralization is associated with magnetite–hematite alteration (Plate 84), and has an overriding structural control (Kruse, 2008). This mineralization is subsequently overprinted by later deformation as indicated by select autoradiographs of mineralized samples (Plate 85). The later deformation is believed to play an important role in the overall thickness of mineralized zones (Kruse, 2008). The mineralized zones are restricted, generally occurring on a metre-scale, relative to the much wider alteration zones observed at the Michelin and Jacques Lake deposits. Rare outcropping mineralization west of Mustang Lake displays hematized fractures and shear zones hosting uranium mineralization that is accompanied by a biotite–magnetite–amphibole alteration assemblage, along with minor calcite, and is frequently rimmed by hematite (Willett *et al.*, 2005).

Mafic dykes are common throughout the volcanic sequence, with both pre- and post-mineralization dykes developed in the area. Some of the highest grades of uranium intersected in drillcore are reported to be hosted within a mafic dyke (Willett *et al.*, 2006b). However, determination of the original protolith is somewhat difficult, given the intensity of the alteration and deformation within the mineral-

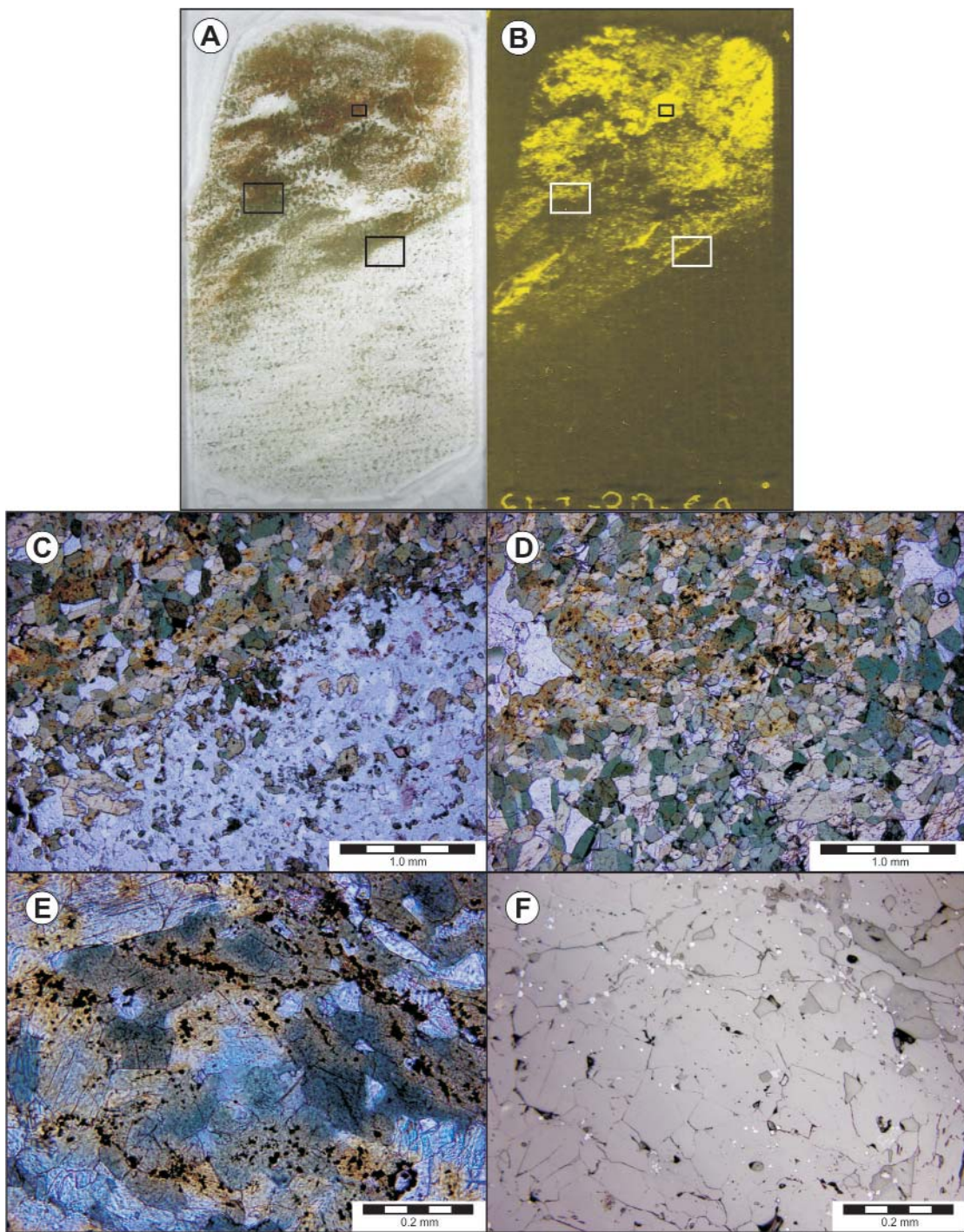


**Plate 82.** A representative sample of mineralized drillcore from the Jacques Lake deposit (DDH JL-07-60, 245 m). A. Photograph of the mineralized thin section. (The inset box to the lower right displays the location of (C), whilst the box to the left displays the location of (D); the small inset box near the centre at the top displays the location of (E)), B. Corresponding autoradiograph of the mineralized thin section outlining the distribution of radioactivity within the sample (yellow, minus the outline of the sample); note the radioactivity within the sample is entirely confined to the actinolite-rich portion of the section, C. PPL image showing the sharp contact between the metavolcanic host rock (lower right) and the uraniferous actinolite (upper left), D. PPL image of uraniferous actinolite (top) and relatively barren actinolite (bottom), E. PPL image of actinolite hosting finely disseminated uraninite throughout, F. Reflected light image of (E) showing the fine-grained nature of the uraninite.

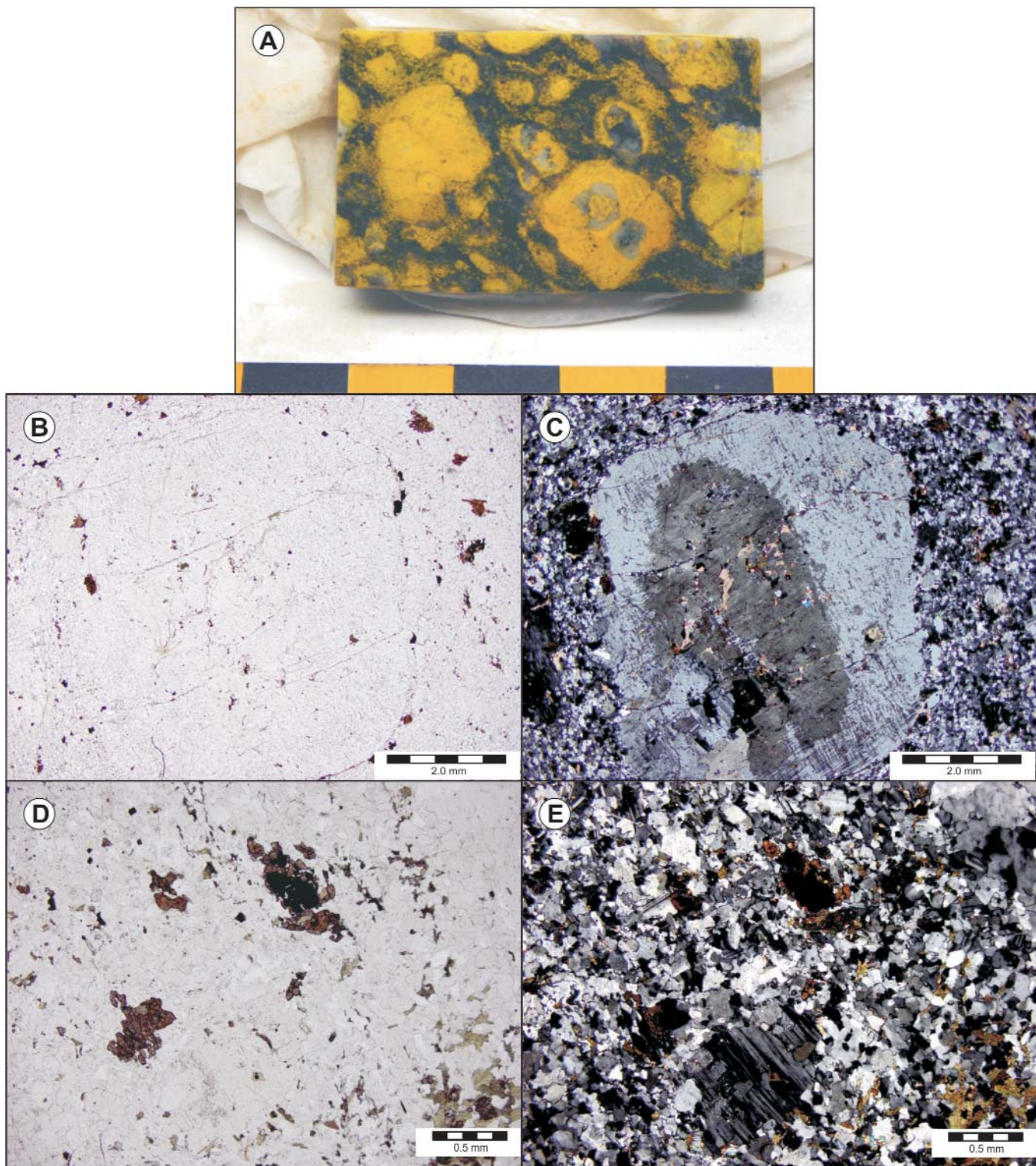


**Plate 83.** A. Representative sample of the quartz-feldspar-porphyry dyke stained for potassium-bearing minerals (yellow colouration; Jacques Lake deposit, DDH JL-06-10, 360 m), B. PPL image of a zoned feldspar phenocryst within a quartz-feldspar bearing groundmass, C. XPL image of (B) outlining the zonation within the feldspar phenocryst, D. PPL image of the groundmass of the porphyry unit, displaying the spatial association of magnetite and titanite that often occurs as rims around the oxide minerals, E. XPL image of (D).

ized zone (Plate 85A), which could alternatively represent a narrow shear zone developed within the host intermediate metavolcanic rock. Farther down hole from the mineralized intersection the host rock is less strongly deformed. Here, the protolith is an intermediate metavolcanic rock, which contains localized hematization and fracture-hosted mineralization (Plate 86).





**Plate 87.** Intermediate metavolcanic host rock displaying patchy hematization and chlorite–magnetite–actinolite–calcite veining within the mineralized zone at the Gayle prospect.

posit that has been displaced to the west by dextral motion along east–west faulting near the southern extent of the Jacques Lake deposit (Cunningham-Dunlop and Lee, 2008). Localized folding of the volcanic host rock is noted in the area of the prospect and is also interpreted to overprint mineralization (Cunningham-Dunlop and Lee, 2008). A medium-grained granitic unit occurs within the footwall of the prospect and is inferred to be correlative with similar units in the footwall of the Jacques Lake deposit. Autoradiographs of select mineralized samples indicate that zones of highest radioactivity are associated with dark-red hematization, and are inferred to predate the development of chlorite–magnetite–actinolite veining within the sample (Plate 88A, B). It is also noteworthy that the mineralization is visually similar to that locally developed at the Mustang Lake prospect (e.g., Plate 86), but displays a contrasting style of mineralization highlighting the complex, episodic nature of uranium deposition.

The Burnt Brook prospect differs from other areas in that mineralization is primarily hosted within metasedimentary rocks, in addition to albited intermediate volcanic rocks (Cunningham-Dunlop *et al.*, 2008b). The mineralization is associated with the typical hematite and magnetite alteration and biotite–chlorite–calcite ± sulphide veining. In hand specimen, the mineralized metasedimentary material appears featureless, but the associated autoradiograph illustrates the irregular distribution of radioactivity, which corresponds with patchy hematization (Plate 88C, D).

The Aurora River prospect occurs in an area where the overall northeast–southwest regional trend of geological units swings to an east–west orientation, and mineralization is associated with strongly sheared interlayered felsic and mafic metavolcanic rocks (Cunningham-Dunlop *et al.*, 2007b). This mineralization is again associated with hematite–magnetite alteration developed within the metavolcanic host rock. Select autoradiographs of mineralized samples illustrate the close

spatial association with hematite alteration and zones of elevated radioactivity (Plate 88E, F). In addition, it is also evident that the radioactivity predates the development of the later mafic mineral assemblages, which could potentially be related to the later east–west shearing.

### White Bear and Otter Lake Prospects

The White Bear (formerly known as Burnt Lake) and the Otter Lake prospects (formerly known as Emben) represent two areas located 18.5 and 24.5 km to the northeast of the Michelin deposit, respectively (Figure 41). These areas were initially identified by Brinex, and subsequently re-evaluated by Aurora Energy, and are associated with pronounced airborne radiometric anomalies. Both areas are dominated by porphyritic felsic metavolcanic rocks that are similar in both texture and alteration to those at the Michelin deposit. The White Bear and Otter Lake prospects occur on the western and eastern margins of the Burnt Lake granite, respectively. The uranium mineralization at each prospect is accompanied by albitionization and hematization of the metavolcanic host rock. In both areas, mineralization occurs as fine-grained disseminations throughout the groundmass, but with highest concentrations of radioactivity occurring along fractures or in association with aggregates of amphibole within the host metavolcanic rock (Plate 89). Samples from these prospects typically lack any strong ductile fabric associated with the mineralization; and where present it is only locally developed. This feature separates this mineralization from that observed at the Michelin and Jacques Lake deposits.

Within the White Bear prospect, discrete east–northeast-striking dextral shear zones are reported to occur roughly parallel to the long axis of a pronounced airborne radiometric anomaly. It is inferred that similar structures provide control on the development of uranium mineralization within the metavolcanic succession. Diamond drilling in the area has produced some of the best intersections outside of the Michelin deposit (e.g., 0.20%  $U_3O_8$  over 19.62 m; Cunningham-Dunlop *et al.*, 2007a). However, the mineralization is sporadic and is limited along strike. The mineralized felsic metavolcanic rocks are reported to be crosscut by early deformed mafic dykes, as well as late syn- and posttectonic mafic dykes similar to that seen elsewhere in the region. In addition, an intrusion of monzonite to the east of the main prospect crosscuts the main structural fabric developed within the host rock (Cunningham-Dunlop *et al.*, 2007a); this intrusion is inferred to represent a phase of the Burnt Lake granite.

At the Otter Lake prospect, uranium mineralization displays a strong spatial association with the development of hematitic fractures crosscutting the felsic metavolcanic host rock (Plate 89C, D). In addition, the alteration assemblages also include the development of magnetite and amphibole

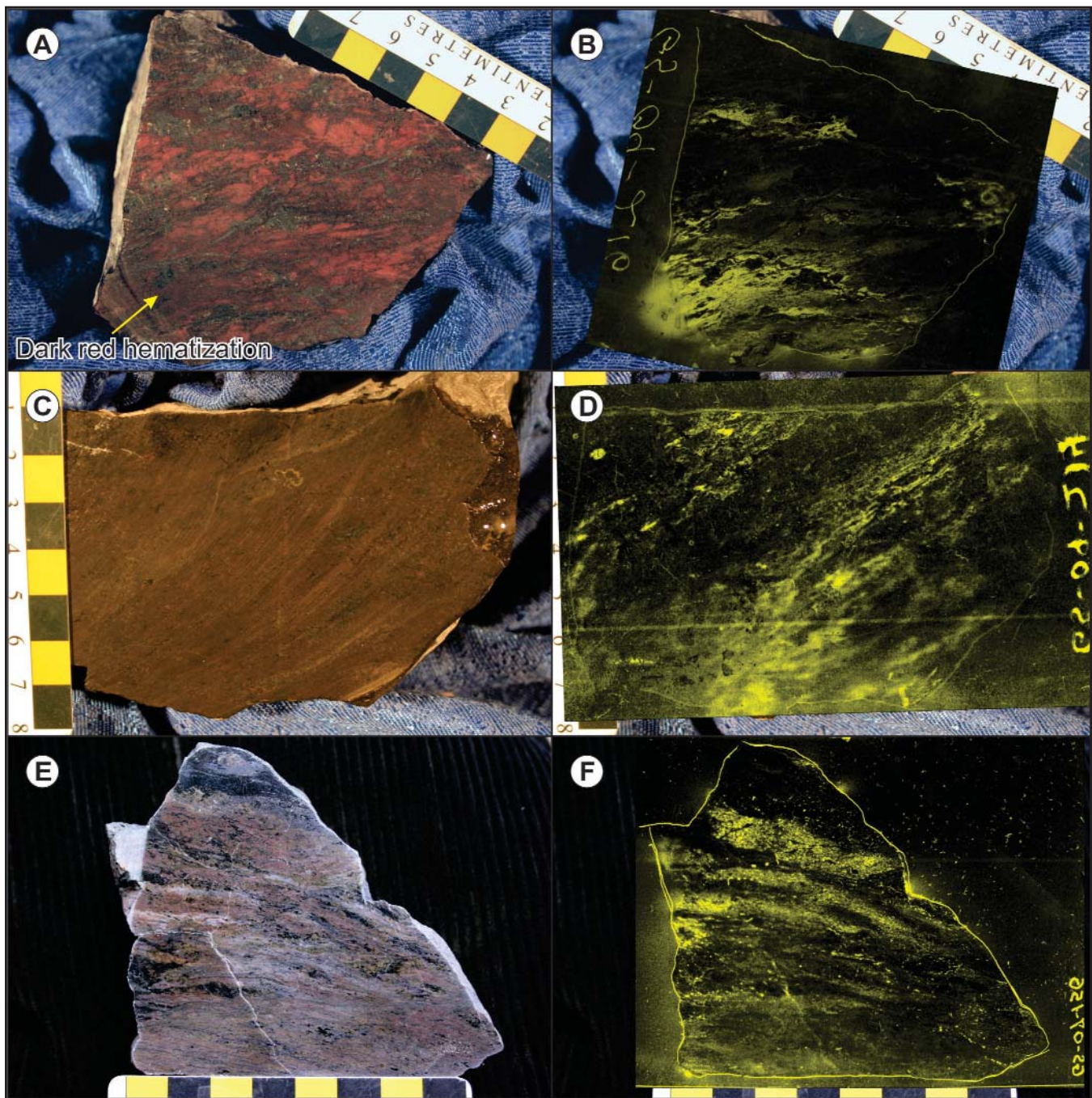


**Plate 88.** *A.* Sample of mineralized material collected from trenching at the Gayle prospect displaying hematization and chlorite–magnetite–actinolite–calcite veining in association with uranium mineralization, *B.* Corresponding autoradiograph of (*A*) outlining the location of radioactivity (yellow, minus the outline of the sample); note zones of highest radioactivity are associated with the dark-red hematized zones that appear to be overprinted by later chlorite–magnetite–actinolite–calcite veining, *C.* Representative hand specimen of mineralized metasedimentary rock exposed at the Burnt Brook prospect, *D.* Corresponding autoradiograph of (*C*) outlining the location of radioactivity (yellow, minus the outline of the sample); note the highest zones of radioactivity are associated with patchy hematization of the host rock, *E.* Highly sheared mineralized metavolcanic host rock from the Aurora River prospect, *F.* Corresponding autoradiograph of (*E*) outlining the location of radioactivity (yellow, minus the outline of the sample); note the highest levels of radioactivity within the sample are associated with hematite alteration which appears to predate the development of the mafic mineral assemblage associated with shearing.

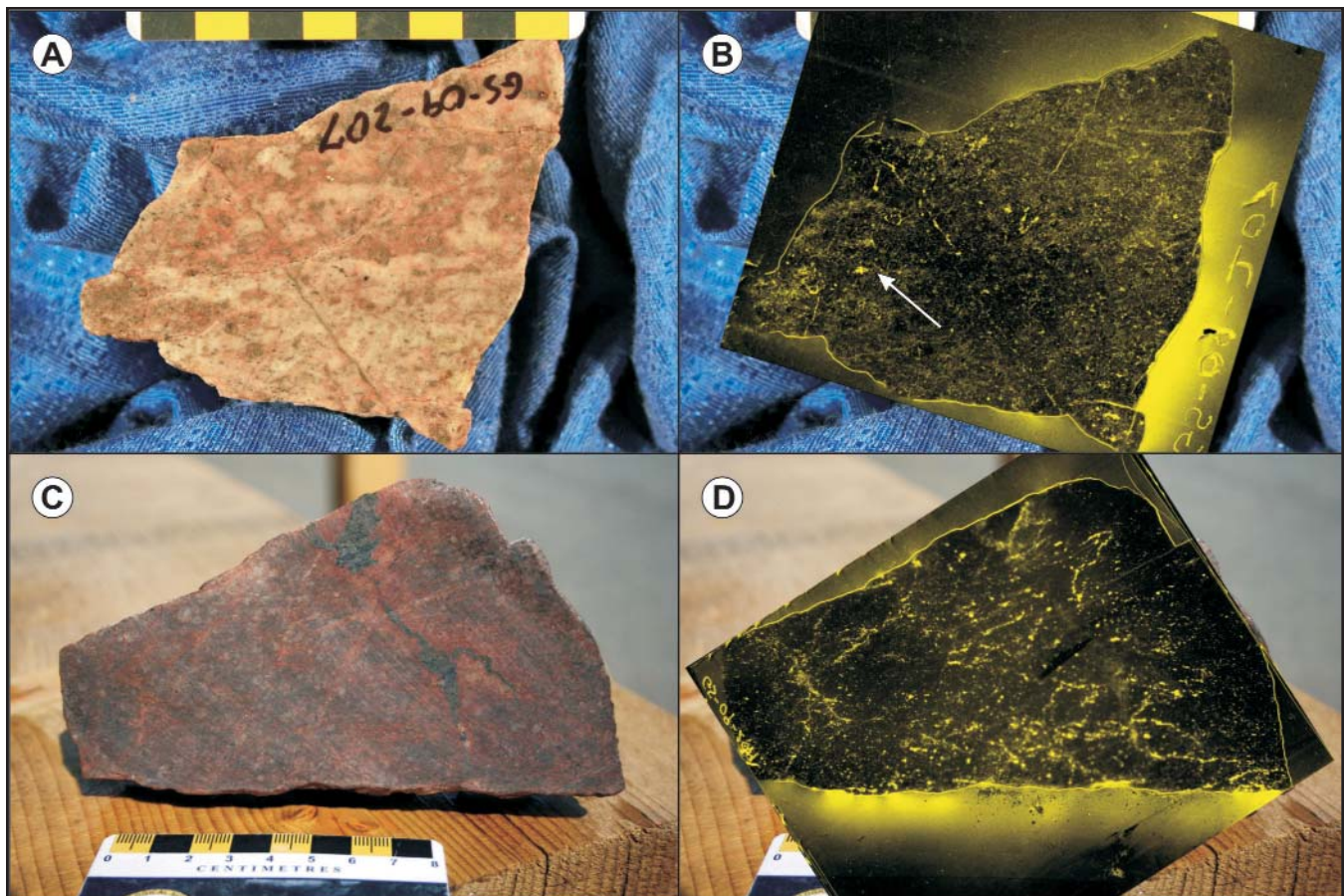


**Plate 89.** *A.* Representative sample of mineralized material from the White Bear prospect; sample contains 1300 ppm U. *B.* Corresponding autoradiograph of (A) outlining the location of radioactivity (yellow, minus the outline of the sample); note the fracture-hosted radioactivity as well as the aggregates of mafic minerals (white arrow) associated with elevated radioactivity within the groundmass. *C.* Mineralized sample from the Otter Lake prospect displaying an amphibole-rich vein in addition to abundant hairline fractures hosting hematite alteration. *D.* Corresponding autoradiograph of (C) outlining the location of radioactivity (yellow, minus the outline of the sample); note the association between the hematitic fractures and the areas of highest radioactivity within the sample. The amphibole-rich vein is also associated with weak radioactivity, but much less than the marginal hematitic fractures.

veins which crosscut, and are deformed with, the host metavolcanic rock (Smith *et al.*, 2005). These localized zones of intense albite–hematite alteration are also accompanied by magnetite, and where intersected by diamond drilling, have produced values up to 0.23%  $U_3O_8$  over 2.5 m (Cunningham-Dunlop *et al.*, 2006). However, as at the White Bear prospect, continuity of the mineralization along strike and down dip is limited. Similar to the White Bear prospect, the felsic metavolcanic host rocks at Otter Lake are crosscut by pre- and post-deformational mafic dykes (Cunningham-Dunlop *et al.*, 2006).

## BENEDICT MOUNTAINS REGION

### Local Geology

Within the Benedict Mountains there are two main belts of supracrustal rocks, a roughly north–south-trending western

belt and an east–west-trending eastern belt (Figure 40). The western belt contains most of the known uranium occurrences and is composed of felsic agglomerates, tuffs and porphyries, and lesser felsic flows and volcaniclastic sediments. These rocks range from relatively fresh and undeformed, to being effected by greenschist-facies metamorphism, and are cross-cut by numerous southeast-trending diabase and gabbroic dykes (Gower, 1981). The volcanic and plutonic rocks are relatively undeformed, and primary volcanic textures are widely preserved (Kerr *et al.*, 1996). The western belt is bound to the west and south by granitoid rocks of the *ca.* 1800 Ma Stag Bay granodiorite, and to the east by the *ca.* 1650 Ma Benedict Mountains Intrusive Suite (Kerr, 1994).

Geochronological data from volcanic rocks exposed on an island to the northeast of the western supracrustal belt are dated at  $1853 \pm 2$  Ma (Ketchum *et al.*, 2002), providing sup-

porting evidence for their correlation with the Ailik Group, which has a typical age range of 1883–1856 Ma (Schärer *et al.*, 1988; Hinckley and Rayner, 2008). This correlation is further supported by an age of  $1855.2 \pm 1.4$  Ma obtained from the felsic volcanic unit hosting uranium mineralization at the Powe prospect (Sparkes and Davis, 2013).

### Mineralization and Associated Alteration

Since the mid-2000s, several new uranium occurrences were discovered in addition to the previously known B-22 prospect (Figure 48). Uranium mineralization is predominantly fracture-hosted, and lacks widespread associated metasomatism akin to that seen at Michelin. Locally, mineralization is also developed marginal to younger mafic dykes that crosscut the volcanic sequence. In some instances, the host rocks are also crosscut by magnetite–carbonate veins, such as at the B-22 prospect (Setterfield and Dyer, 2007). This style of mineralization is similar to the ‘Type 3 - disseminated or fracture-hosted mineralization in felsic volcanic rocks without associated deformation or metasomatism’ outlined by Sparkes and Kerr (2008). As noted previously, this style is more typical of mineralization observed within the younger volcanic sequences of the Bruce River Group (see following Section).

Within the approximate 11-km-long, north–south-trending, belt of supracrustal rocks in the western Benedict Mountains, Mega Uranium has identified several occurrences of uranium mineralization; the most significant of which are shown in Figure 48. Limited diamond drilling has been carried out at four of these prospects (Kruse, 2012), which represents the first drill testing conducted in the area. The Powe prospect is host to the highest grade uranium mineralization, with assays locally returning up to 13.8%  $U_3O_8$  (Setterfield *et al.*, 2008). The main mineralization occurs within a narrow, north-northeast-trending, moderate to steep and westerly dipping shear zone, hosted within a feldspar-phyric porphyry unit. The mineralized shear zone measures 15–30 cm in width, and is flanked by magnetite and hematite alteration; channel samples from this zone have assayed up to 7.0%  $U_3O_8$  over 1 m (Kruse *et al.*, 2009). Other mineralization within the area, such as the Priority One prospect (Figure 48), is also associated with weakly anomalous Au, Ag and Cu values (Setterfield *et al.*, 2008).

At the Harbinger prospect, located approximately 1 km to the southeast of the Powe prospect, primary volcanic textures, such as spherulitic rhyolite, are preserved within the volcanic sequence, demonstrating the relatively pristine nature of the volcanic host rocks. Here, a 750-m-long, north-trending airborne radiometric anomaly is associated with variably developed fracture-hosted mineralization, from which assays of up to 0.52%  $U_3O_8$  have been obtained (Setterfield

*et al.*, 2008; Kruse *et al.*, 2009). The felsic volcanic host rocks, marginal to the fracture zones, also display local enrichment in uranium, locally assaying up to 50 ppm uranium in unaltered samples; these values are similar to the enriched volcanic rocks noted in the area of the Michelin deposit by Evans (1980).

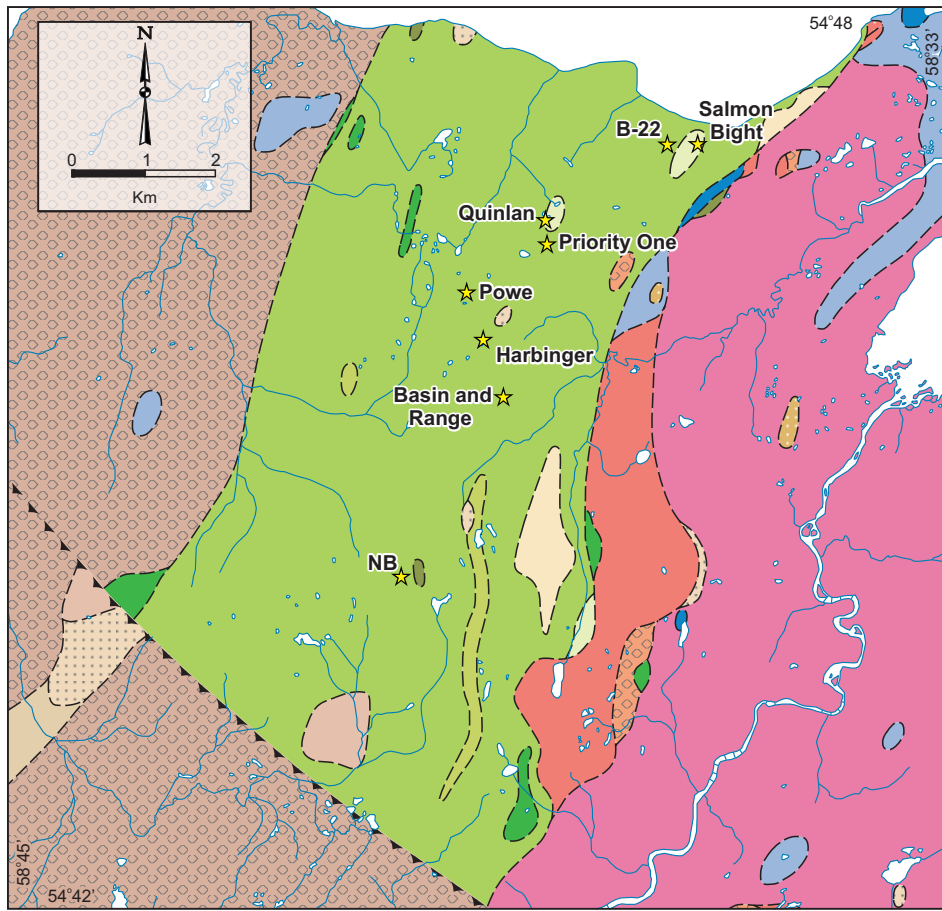
The Quinlan prospect is somewhat different than the other uranium prospects within the area, in that the uranium mineralization is developed along the margins of a younger, southwest-trending, feldspar-phyric mafic dyke. Minor uranophane-stained fractures are developed along the margin of the mafic dyke, from which grab samples of up to 2.09%  $U_3O_8$  have been obtained (Setterfield *et al.*, 2008). The fine-grained chilled margin of the dyke also contains anomalous uranium values, interpreted to represent remobilized uranium mineralization that locally assays up to 0.04%  $U_3O_8$ .

### GEOCHRONOLOGICAL CONSTRAINTS

To constrain the age of mineralization within the Ailik Group, several key geological units were sampled for U–Pb geochronological study using TIMS analysis at Memorial University (Figure 49A–E; methods and procedures in Appendix B). In addition, one sample was analyzed by isotope-dilution Thermal Ionization Mass Spectrometry (ID-TIMS) at the Geological Survey of Canada (Figure 49F). Results are reported in Appendices C and E, and presented on concordia diagrams in Figure 49, with errors at the  $2\sigma$  level.

The metavolcanic host rock at the Michelin deposit was sampled to test its age relative to the  $1856 \pm 2$  Ma age obtained from Michelin Ridge, located approximately 3.5 km to the north-northwest (Schärer *et al.*, 1988). The sample yielded a large number of euhedral, elongate, high-quality zircon prisms displaying simple zonation patterns. Three analyses, of three to four prisms each, produced tightly overlapping concordant points, which yield a weighted average  $^{207}\text{Pb}/^{206}\text{Pb}$  age of  $1858 \pm 2$  Ma (Figure 49A; Sparkes and Dunning, 2015). This age provides a maximum age limit for the formation of the uranium mineralization within the deposit. The sample also produced an abundant population of titanite, from which multiple analyses have identified a complex thermal history, identifying evidence for both Labradorian (*ca.* 1650 Ma) and Grenvillian (*ca.* 1000 Ma) events within the deposit (*cf.* Sparkes and Dunning, 2015).

A post-mineralization, fine-grained, granodiorite dyke intersected by deep drilling at the Michelin deposit was also sampled; the sample produced a population of large zircon prisms having slightly discoloured cores and minor cracks, along with a population of dark-brown titanite. Analyses of the titanite produced a number of concordant to slightly discordant points which, when combined with the zircon data,



## LEGEND

### MID-PALEOPROTEROZOIC (ca. 2100-1800 Ma)

- [Dotted Pattern] Alkali-feldspar granite, granite and quartz syenite
- [Solid Brown] Foliated to gneissic granodiorite and compositionally equivalent well-banded gneiss
- [Diamond Pattern] Foliated to gneissic megacrystic/porphyritic granitoid rocks, augen gneiss
- [Solid Tan] Foliated to gneissic granite and alkali-feldspar granite, and compositionally equivalent well-banded gneiss
- [Solid Light Tan] Quartz-feldspar psammitic schist and gneiss; medium grained and commonly rusty-weathering
- [Solid Green] Volcanic breccia, angular clasts, grading into agglomerate
- [Solid Light Green] Fine- to medium-grained, banded quartzofeldspathic rocks; locally have lensoid shapes, possibly indicating felsic volcaniclastic protolith
- [Solid Yellow-Green] Intermediate volcanic rocks
- [Solid Light Yellow-Green] Felsic volcanic porphyry interpreted to be hypabyssal

### LATE PALEOPROTEROZOIC (ca. 1800-1660)

- [Solid Green] Diorite, quartz diorite and tonalite; locally grading into leucogabbronorite
- [Solid Red] Alkali-feldspar granite, granite and quartz syenite forming discrete plutons
- [Diamond Pattern] Megacrystic/porphyritic granite to granodiorite
- [Solid Orange] Granite and minor alkali-feldspar granite
- [Solid Blue] Monzonorite and monzogabbro
- [Solid Gold] Monzonite, including minor syenite
- [Solid Pink] Syenite to quartz syenite forming discrete plutons

### LATE LABRADORIAN ANORTHOSITIC AND MAFIC INTRUSIONS (ca. 1660-1600 Ma)

- [Solid Blue] Massive to strongly foliated gabbro and norite, commonly layered, subophytic and locally coronitic

### SYMBOL

Uranium occurrence ..... ★

**Figure 48.** Regional geology map of the western belt of supracrustal rocks in the Benedict Mountains region (geological base map from Gower, 2010).

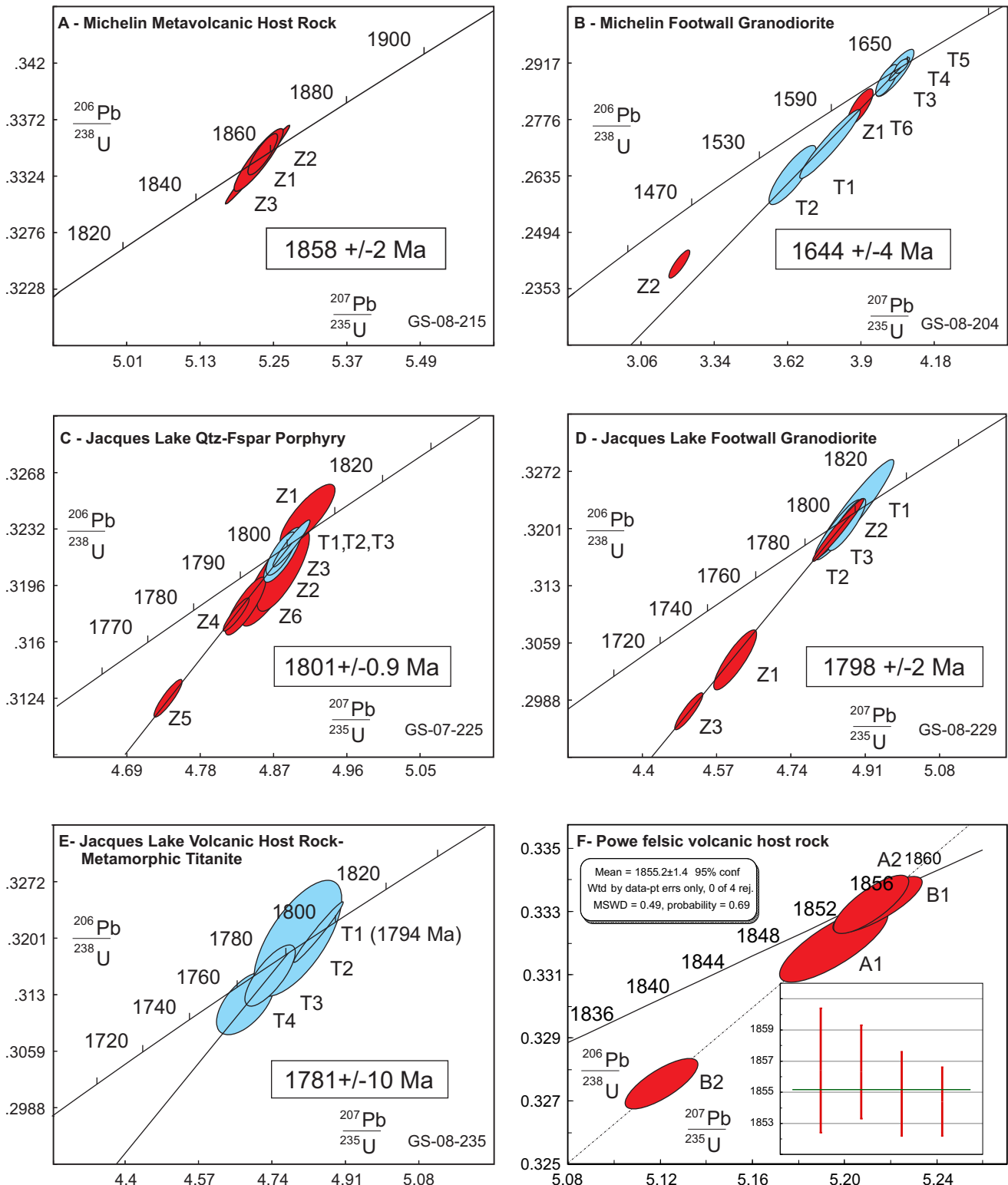


**Figure 49.** Concordia diagrams for U–Pb data from Aillik Group rocks. Red ellipses denote zircon analyses, blue ellipses are titanite analyses. A. Metavolcanic host rock hosting uranium mineralization, Michelin deposit, B. Footwall granodiorite intrusion, Michelin deposit, C. Quartz–feldspar porphyry, Jacques Lake deposit, D. Footwall granodiorite, Jacques Lake deposit, E. Metavolcanic host rock to uranium mineralization, Jacques Lake deposit; F. Felsic volcanic host rock to uranium mineralization, Powe prospect. Note error ellipses are at the  $2\sigma$  level.

produced a  $^{207}\text{Pb}/^{206}\text{Pb}$  age of  $1644 \pm 4$  Ma (Figure 49B; Sparkes and Dunning, 2015). One analysis of zircon (Z1) overlaps with the titanite data, supporting the interpretation that the titanite is of igneous origin; a second analysis (Z2) of zircon is discordant, indicating a more complex history of multi-age lead loss.

Within the Jacques Lake deposit, a distinctive quartz-feldspar porphyry unit locally crosscuts mineralization. A sample from this unit yielded a large number of high-quality zircon and titanite, from which one to two prisms of each were included in the individual analyses that produced an age of  $1801 \pm 0.9$  Ma (Figure 49C; Sparkes and Dunning, 2009). This age is similar to that obtained from the porphyry near White Bear Mountain by Schärer *et al.* (1988), and is potentially linked with this larger porphyry body. The well-defined overlap of both the zircon and titanite data suggests that the titanite is of igneous origin. In addition, an undeformed intermediate intrusion, which forms the footwall to the deposit, was also sampled. This unit yielded coarse-grained zircon and titanite from which two to four grains of each were included in individual analyses, producing an array of concordant and discordant points (Figure 49D). The well-defined overlap of both the zircon and titanite data implies the titanite is of igneous origin and the age calculation of both produce a  $^{207}\text{Pb}/^{206}\text{Pb}$  age of  $1798 \pm 2$  Ma (Figure 49D; Sparkes and Dunning, 2015).

A sample of the host intermediate metavolcanic rock at the Jacques Lake deposit was also collected, but failed to yield a significant population of zircon; however, the unit did contain anhedral to rounded grains of light- and dark-brown titanite, potentially representing two different generations. Analyses of both the light- and dark-brown titanite provide a  $^{207}\text{Pb}/^{206}\text{Pb}$  age of  $1781 \pm 10$  Ma (Figure 49E; Sparkes and Dunning, 2015). The  $ca.$  1800 Ma ages from the Jacques Lake deposit area provide an indication of a younger age limit for uranium mineralization, but the age of the host rock could not be resolved. However, preliminary LAM-ICP-MS U-Pb ages obtained from rocks in the same area are reported to have a  $^{207}\text{Pb}/^{206}\text{Pb}$  age (with large unreported errors) of 1856 Ma (Wilton *et al.*, 2010).

Finally, a felsic volcanic unit hosting uranium mineralization in the region of the Benedict Mountains was sampled to compare its age with other Aillik Group rocks. This sample produced an abundant population of euhedral prisms from which four separate analyses consisting of single and multiple grains produced a  $^{207}\text{Pb}/^{206}\text{Pb}$  age of  $1855.2 \pm 1.4$  Ma (Figure 49F; Sparkes and Davis, 2013). This age provides a maximum age limit of the formation of the uranium mineralization and also indicates that the host volcanic succession is of similar age to other Aillik Group rocks.

Preliminary LAM-ICP-MS U-Pb ages obtained from secondary zircons from both the Michelin and Jacques Lake deposits, inferred to be coincident with uranium mineralization, have reported  $^{207}\text{Pb}/^{206}\text{Pb}$  ages (with large unreported errors) of between 1828 and 1844 Ma and  $ca.$  1840 for Michelin and Jacques Lake, respectively (Wilton *et al.*, 2010). These data, although preliminary, are supportive of the main mineralizing event being coincident with the regional Makkovikian Orogeny.

## GEOCHEMISTRY

The bulk of the geochemical data obtained during this study comes from the Michelin and Jacques Lake deposits as well as the Mustang Lake area. Hence, these areas form the bulk of the following discussion. Limited geochemical data from the Benedict Mountains are also included for comparison.

Within the Michelin deposit, the primary host to uranium mineralization is a felsic, sub- to coarsely porphyritic, metavolcanic unit that plots within the rhyolite-dacite field of Pearce (1996; Figure 50A). Granitic intrusions, as well as the felsic portion of the complex dyke unit, also overlap the field of the metavolcanic host rocks. Several basaltic and dioritic dykes crosscut the volcanic sequence, and plot within the basalt field of Pearce (1996; Figure 50A). In Figure 51A, similar trace-element patterns are displayed for both the sub- and coarsely porphyritic metavolcanic host rocks. A similar trace-element pattern is also displayed by the felsic intrusions within the sequence, which include both medium-grained granite, as well as the coarsely porphyritic portion of the complex dyke (Figure 51B). With regard to the mafic dykes and more intermediate intrusions, two distinct populations are identified. Foliated mafic dykes (Mafic dyke 1) shown in Figure 51C display several distinctions relative to the trace-element profile of the non-foliated mafic dykes (Mafic dyke 2); the most significant of which is an enrichment in Sr and P. These dykes also display a greater enrichment in the LREE. Undeformed diorite intrusive rocks display a similar profile to the non-foliated mafic dyke (Mafic dyke 2; Figure 51C), lacking the enrichment in Sr and P relative to the foliated dykes (Mafic dyke 1).

At the Jacques Lake deposit, the primary host to uranium mineralization is an intermediate metavolcanic unit that primarily plots within the andesite field of Pearce (1996; Figure 50B); two outliers, which plot within the basaltic field, may represent a separate unit within the volcanic succession. Rare felsic tuff and minor felsic dykes are also observed within the volcanic sequence, both of which plot within the rhyolite-dacite field of Figure 50B, along with the quartz-feldspar porphyry intrusion that postdates mineralization. The dated

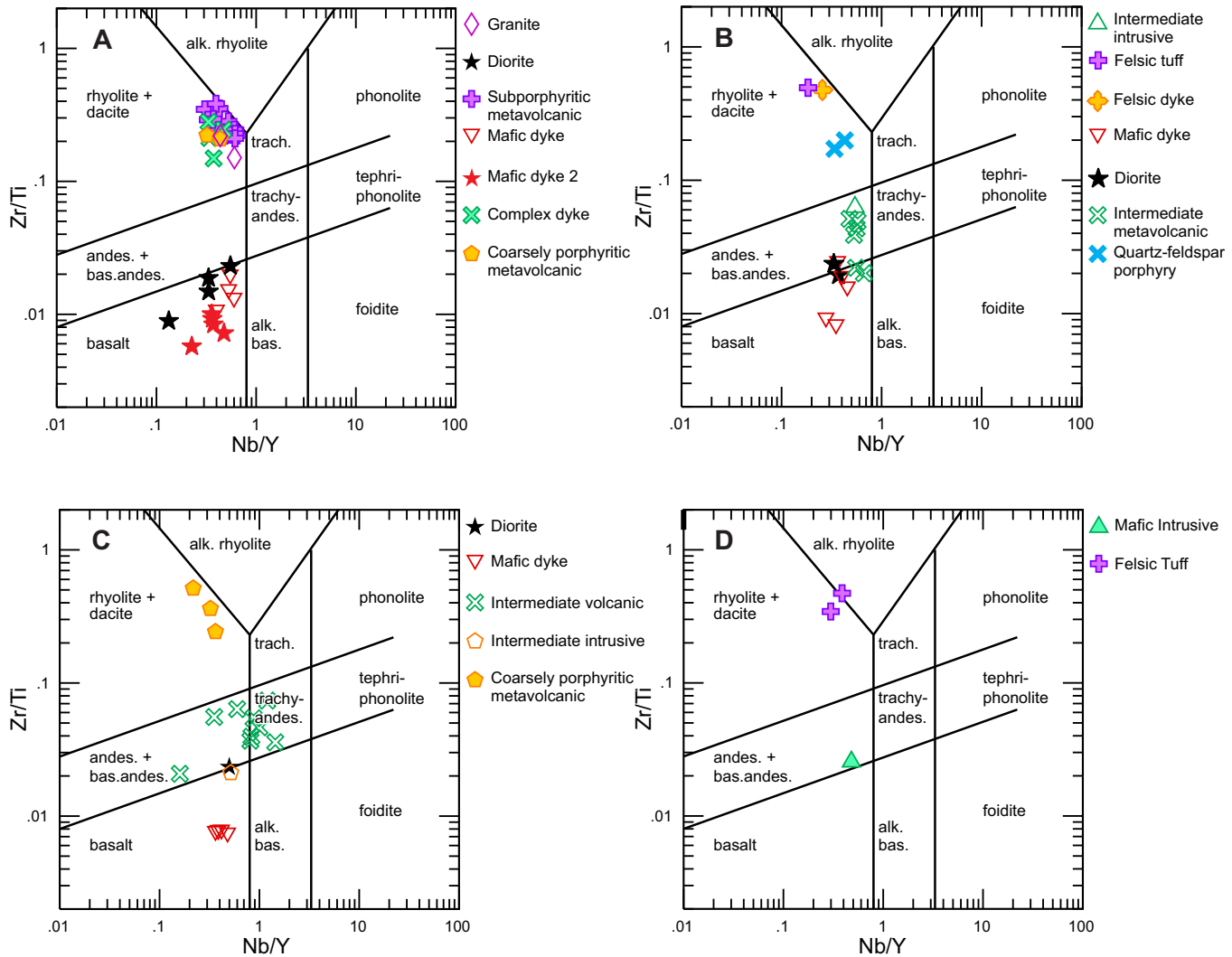


**Figure 50.** Rock classification diagrams after Pearce (1996), outlining the classification of major units at select occurrences. A. Michelin deposit, B. Jacques Lake deposit, C. Mustang Lake prospect, D. Benedict Mountains region.

footwall intermediate intrusion plots within the andesite field, and broadly overlaps with the intermediate metavolcanic rocks. Several mafic dykes crosscut the sequence, all of which appear to postdate the main deformation observed in drillcore. These non-foliated dykes fall within the basalt field, or the immediately adjacent basaltic andesite field in Figure 50B. The rare felsic units observed within the metavolcanic sequence display a distinct geochemical profile relative to the more abundant intermediate volcanic unit; these felsic units closely mimic the volcanic host rocks of the Michelin deposit (Figure 52A). The quartz-feldspar porphyry unit, as well as the footwall intermediate intrusive unit, displays a similar trace-element profile as shown in Figure 52B; both units have been dated at *ca.* 1800 Ma and display many similarities with the undated felsic intrusive units of the Michelin deposit (Figure 51B). Finally, the mafic units, which all postdate the main deformation in the area, display a similar profile to the non-foliated dykes from the Michelin deposit (Figure 52C).

Within the area of Mustang Lake, felsic volcanic rocks similar to those hosting the nearby Michelin deposit, as well as intermediate rocks similar to those hosting the Jacques Lake are observed in drillcore. The felsic volcanic rocks plot within the rhyolite-dacite field whilst the intermediate rocks plot within the andesite to trachytic-andesite fields (Figure 50C). Several mafic to intermediate dykes crosscut the volcanic succession; these dykes plot within the basalt field, whereas the more intermediate intrusions fall on the boundary between the basalt and basaltic andesite fields (Figure 50C). The trace-element profiles of the felsic and intermediate rocks are similar to those from the Michelin and Jacques Lake areas, respectively (Figure 53A). The mafic to intermediate intrusive units also display similarities with the non-foliated dykes observed at Michelin and Jacques Lake (Figure 53B).

Limited sampling of the Benedict Mountains demonstrates that the felsic volcanic rocks plot within rhyolite–

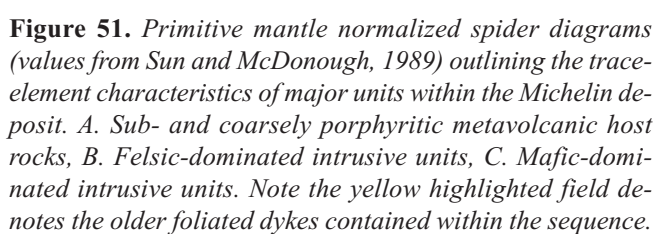
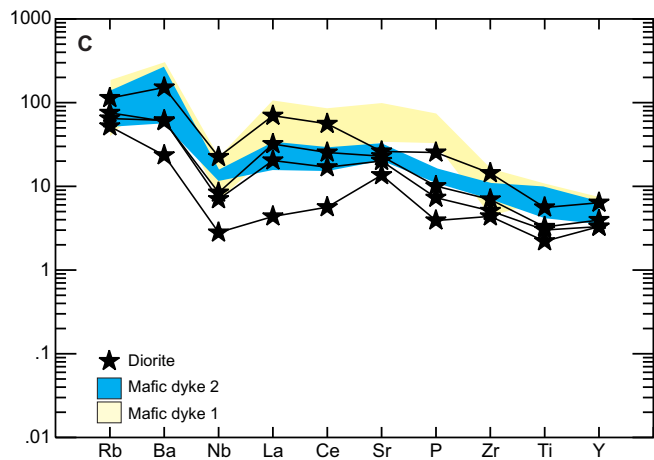
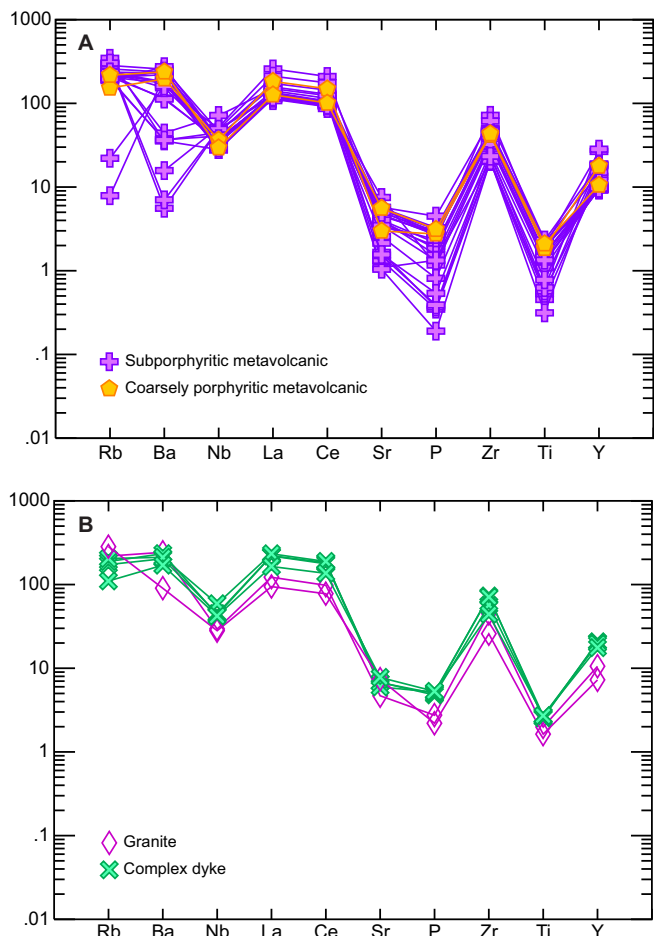


**Figure 51.** Primitive mantle normalized spider diagrams (values from Sun and McDonough, 1989) outlining the trace-element characteristics of major units within the Michelin deposit. A. Sub- and coarsely porphyritic metavolcanic host rocks, B. Felsic-dominated intrusive units, C. Mafic-dominated intrusive units. Note the yellow highlighted field denotes the older foliated dykes contained within the sequence.

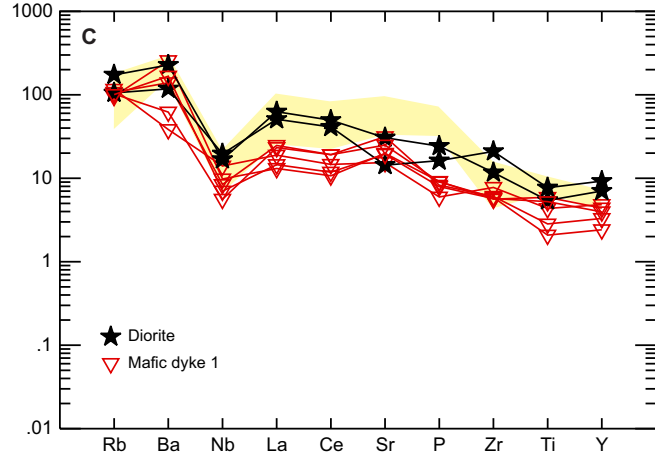
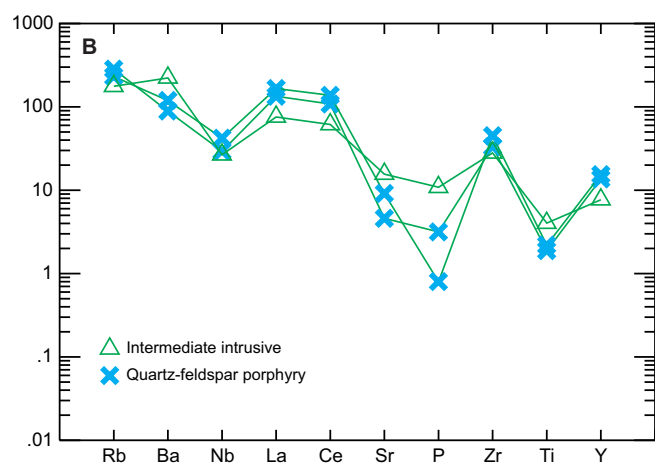
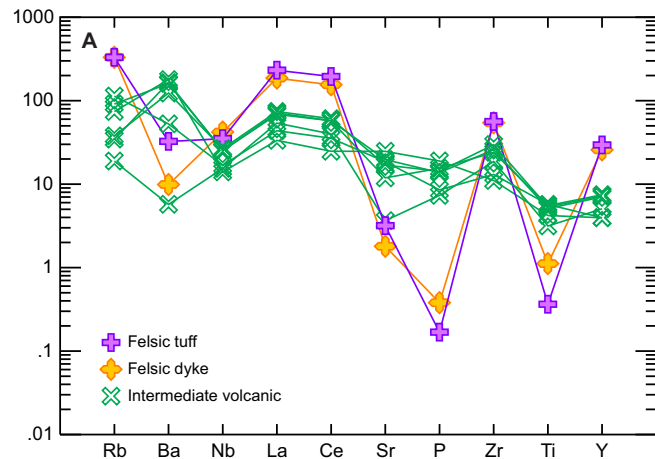


**Figure 52.** Primitive mantle normalized spider diagrams (values from Sun and McDonough, 1989) outlining the trace-element characteristics of major units within the Jacques Lake deposit. A. Felsic and intermediate metavolcanic host rocks, B. Felsic-dominated intrusive units, C. Mafic-dominated intrusive units. Note the shaded yellow area outlines the profile of the foliated dykes from the Michelin deposit for comparison.

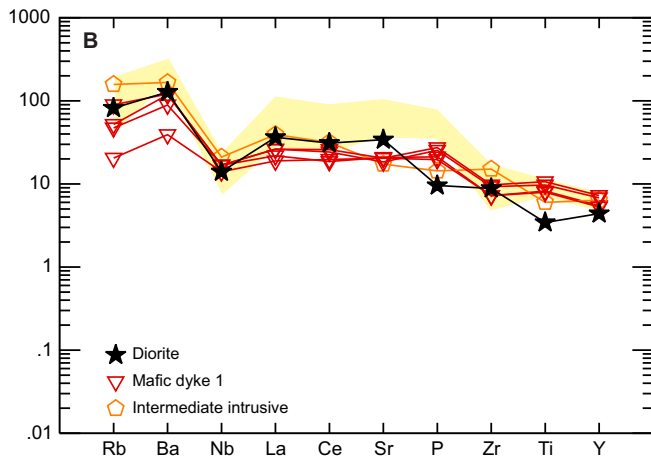
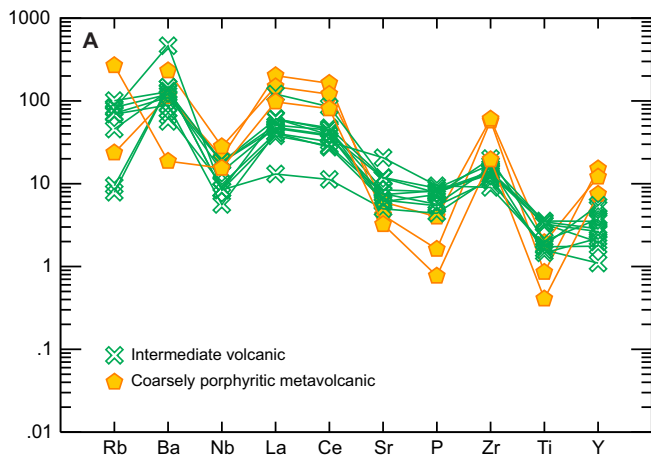


**Figure 53.** Primitive mantle normalized spider diagrams (values from Sun and McDonough, 1989) outlining the trace-element characteristics of major units within the Mustang Lake prospect. A. Felsic and intermediate metavolcanic host rocks, B. Mafic-dominated intrusive units. Note the shaded yellow area outlines the profile of the foliated dykes from the Michelin deposit for comparison.

dacite to alkali rhyolite field, whereas a mafic dyke, which crosscuts the volcanic sequence, plots within the basaltic andesite field (Figure 50D). Although the sampling from the area is restricted to select uranium occurrences, the geochemical data indicate a similar profile between the felsic volcanic host rocks in the region with those of the Michelin deposit farther to the west (Figure 54). In addition, the one mafic dyke that was sampled, which is locally associated with uranium mineralization along its margins, displays a similar profile to the younger non-foliated dykes observed within the other occurrences discussed above.

Previous studies in the region have documented the association of Na and Zr enrichment in association with uranium mineralization within the Aillik Group (e.g., Minatidis, 1976; Gandhi, 1978; Evans, 1980). Evans (1980) also noted that the stratigraphic sequence distal to the altered zone at

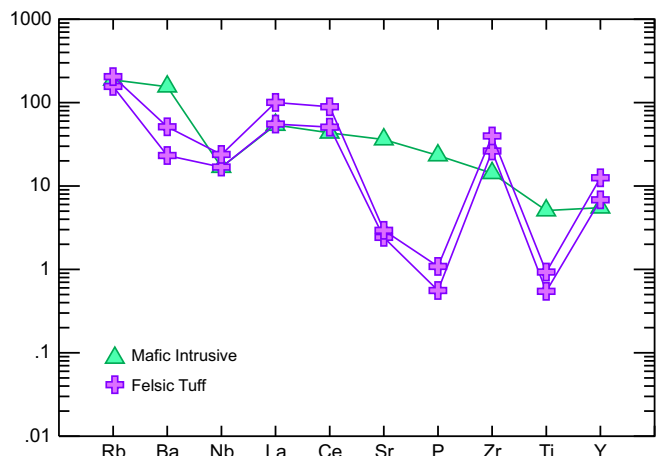


**Figure 54.** Primitive mantle normalized spider diagram (values from Sun and McDonough, 1989) outlining the trace-element characteristics of major units within the Benedict Mountains region.

Michelin displayed little geochemical variability, and contained uranium concentrations ranging from 3.9 to 56.4 ppm U, and averaging 9.7 ppm U; rocks classified as being mineralized were limited to those containing in excess of 25 ppm U. For this discussion, unmineralized rocks are taken as those samples containing less than 50 ppm U. Uranium mineralization occurrences discussed in this section rarely display significant enrichment of other elements. Therefore, mineralized and unmineralized rocks display many of the same geochemical characteristics. From Figure 55A, it is evident that the felsic sub- and coarsely porphyritic metavolcanic host rocks are primarily characterized by a Na<sub>2</sub>O content of less than 5 wt.%, whereas mineralized samples contain between 5–10 wt.% Na<sub>2</sub>O. Note that some felsic metavolcanic rocks display albitic alteration without any significant enrichment of uranium and plot above 5 wt.% Na<sub>2</sub>O, but below the 50 ppm U limit.

The unmineralized intermediate rocks from the Jacques Lake and Mustang Lake areas display Na<sub>2</sub>O contents between 5–10 wt.%, similar to the Na<sub>2</sub>O contents of the mineralized samples relative to the unmineralized ones (Figure 55A). However, the mineralized intermediate rocks do commonly display enrichment in CaO relative to unmineralized samples, as shown in Figure 55B. The mineralized samples from Jacques Lake commonly contain CaO values between 5–15 wt.%, whilst unmineralized samples typically contain less than 5 wt.%. Similarly, unmineralized samples from Mustang Lake generally contain less than 2 wt.% CaO, but locally contain values in excess of 5 wt.% in mineralized samples. One anomalous felsic volcanic sample from the Michelin deposit does display enrichment of CaO, however this sample is located immediately adjacent to a mafic dyke that may have introduced some contamination. Despite the hematite alteration

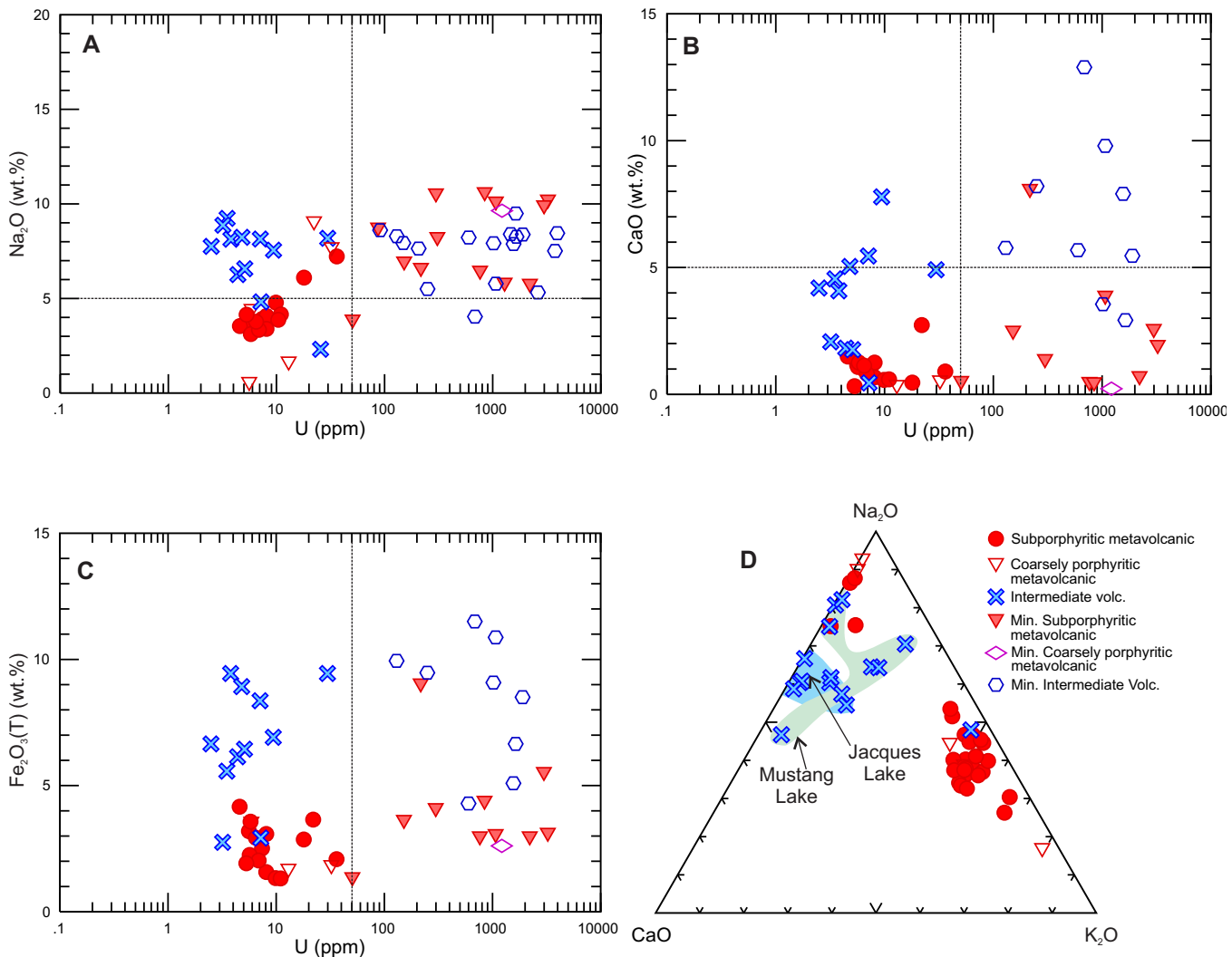


**Figure 55.** A. Relationship of U and Na<sub>2</sub>O for the metavolcanic host rocks of the Aillik Group, B. Relationship of U and CaO for the metavolcanic host rocks of the Aillik Group, C. Relationship of U and Fe<sub>2</sub>O<sub>3</sub>(T) for the metavolcanic host rocks of the Aillik Group, D. Relationship of Na<sub>2</sub>O, CaO and K<sub>2</sub>O within unmineralized (<50 ppm U) metavolcanic rocks.

associated with uranium mineralization, there is little to no overall iron enrichment within mineralized samples relative to their unmineralized equivalents as shown in Figure 55C; indicating no overall addition of iron within the mineralizing system.

The potential for potassic-style alteration has been noted outside of the identified albitic alteration, but it was also noted that this could alternatively represent the primary signature of the metavolcanic host rock (Cunningham-Dunlop *et al.*, 2007a). As shown in the Figure 55D, most of the relatively unmineralized sub- and coarsely porphyritic volcanic rocks display a roughly equal proportion of K<sub>2</sub>O and Na<sub>2</sub>O, with the K<sub>2</sub>O becoming almost completely removed during albitic alteration. As noted by Evans (1980), the host volcanic unit initially contains between 2 to 6 wt.% K<sub>2</sub>O prior to being

overprinted by the sodic alteration associated with uranium mineralization. As illustrated in Figure 55D, some of the felsic volcanic rocks plot near the Na<sub>2</sub>O apex, indicating potential albitic alteration without associated uranium mineralization. Similarly, some of the samples from the intermediate unit, Mustang Lake area, display a depletion of K<sub>2</sub>O in addition to enrichment of Na<sub>2</sub>O, which may represent possible evidence for localized albitic alteration.

## SUMMARY AND DISCUSSION

The metavolcanic rocks of the Aillik Group within the White Bear Mountain–Walker Lake region of the CMB host numerous uranium occurrences. These have several common characteristics including the development of hematization and/or albitization in association with uranium mineralization.

The mineralized zones are also commonly associated with moderately to strongly deformed host rocks. It is therefore inferred that there is a fundamental structural control on the development of uranium mineralization. The combination of this style of structurally controlled alteration, in association with the finely disseminated nature of the uranium mineralization, provides supporting evidence for its classification as albite-type mineralization as suggested by previous authors (e.g., Sparkes and Kerr, 2008; Wilde, 2013). The development of uranium mineralization is currently bracketed between *ca.* 1860–1800 Ma, using existing geochronological data that broadly overlaps the *ca.* 1900–1700 Ma Makkovikian Orogeny (Hinchey and LaFlamme, 2009, and *see references therein*). The development of steeply dipping shear zones in the region, which commonly host uranium mineralization, is inferred to be correlative with the formation of similar shear zones mapped farther to the northeast along the coast. Here, they are attributed to a regional D<sub>3</sub> event representing sinistral transpression associated with the westward thrusting of the Aillik Group (Culshaw *et al.*, 2000; Hinchey and LaFlamme, 2009).

Within the Michelin deposit, uranium mineralization mainly occurs as fine-grained disseminations throughout the metavolcanic host rock, primarily occurring as uraninite, with mineralized zones forming ore shoots that plunge parallel to the regional lineation. Within these mineralized zones, elevated uranium is accompanied by intense albitionization and hematization; however, rocks displaying this alteration are not ubiquitously uraniferous. Autoradiographs of a few samples demonstrate the finely disseminated mineralization. The common incorporation of uraniferous phases within amphibole, pyroxene, and titanite is suggestive of a syn-deformational timing for the introduction of uranium within the system. However, it remains unclear whether the association of uranium mineralization and Fe-oxide minerals within hematized fractures is related to the primary mineralizing event, or subsequent secondary remobilization. The age of 1858 ± 2 Ma for the metavolcanic host rock at the Michelin deposit provides a maximum age limit on the development of uranium mineralization in the region. The effect of the *ca.* 1650 Ma intrusive phases within the vicinity of the deposit has yet to be fully determined. Further work is required to segregate the various intrusive dykes that crosscut the volcanic succession and their relationship to deformation and uranium mineralization in the area. The complex dyke, which represents one of the few distinct traceable marker units within the deposit, is interpreted to represent a foliated intrusive unit and is an obvious target for further geochronological study.

Uranium mineralization developed within the Jacques Lake deposit is hosted within intermediate metavolcanic host rocks that display some similarities with mineralization observed at the Michelin deposit, but also contain distinct dif-

ferences. This mineralization displays a strong spatial association with intensely deformed host rocks within the area; however, the associated uranium mineralization lacks the elevated Na and Zr values as seen at Michelin. This relationship could be a function of the compositional differences between the host rocks, as opposed to differences related to the mineralizing fluids. Uranium mineralization within the Jacques Lake deposit primarily occurs as finely disseminated uraninite, which is commonly incorporated within amphibole and titanite, implying a syn-deformational timing for the development of the uranium mineralization. Autoradiographs of mineralized samples from the deposit indicate the presence of at least two different generations of amphibole within mineralized samples. However, current data suggests that only one generation of titanite is present. Mineral separates of titanite obtained from the metavolcanic host rock have produced an age of 1781 ± 10 Ma, which is supportive of a pre-1800 Ma age for the mineralization.

The Mustang Lake area contains felsic metavolcanic rocks that resemble those observed at the Michelin deposit, as well as more intermediate rocks similar to those at the Jacques Lake deposit. Locally, the styles of mineralization observed within drillcore display many similarities to mineralization observed along strike to the southwest of the Jacques Lake deposit, in the vicinity of the Gayle prospect. However, some mineralization within the area also displays the effects of intense post-mineralization deformation, which is a feature that is not observed elsewhere in the region.

Finally, the uranium mineralization observed within the Benedict Mountains may represent a precursor to that seen within the more highly deformed volcanic rocks of the Aillik Group farther to the west, or alternatively it may represent a separate style of mineralization altogether. Here, rocks of similar age to those hosting the Michelin deposit contain a distinctly different style of uranium mineralization, one that is primarily fracture-hosted within mostly undeformed and unaltered host volcanic rocks. One common feature that these rocks do share with those of the Aillik Group, farther to the west, is an overall elevated background level of uranium, and as inferred elsewhere these rocks likely represent the source to the uranium mineralization contained within.

## URANIUM MINERALIZATION WITHIN THE BRUCE RIVER GROUP

### INTRODUCTION

The Bruce River Group contains some of the youngest supracrustal rocks to host uranium mineralization within the CMB. This sequence includes siliciclastic sedimentary rocks at its base (Heggart Lake and Brown Lake formations) grading upward into a thick sequence of predominantly subaerial

bimodal volcanic rocks (Sylvia Lake Formation; Smyth *et al.*, 1978). Geochronological sampling conducted as part of this study has identified the presence of a significant unconformity between the Heggart Lake and Brown Lake formations (Sparkes *et al.*, 2016); however, all units are discussed under this section as further work is required to refine the Bruce River Group stratigraphy. The following section provides a brief summary of the regional geology and stratigraphy of the Bruce River Group as outlined by Ryan (1984).

The Bruce River Group hosts numerous occurrences of uranium mineralization (Figure 56), which can be broadly separated into two main styles, largely based on the rock hosting the uranium mineralization. Sedimentary rocks hosting uranium mineralization primarily occur within the basal Heggart Lake Formation (e.g., Moran Lake Lower C Zone deposit and Moran Heights prospect; *see below*). In some cases, uranium mineralization within the sedimentary sequence is concentrated along the margins of the intrusion of mafic to intermediate dykes, suggesting a link to their emplacement (e.g., Moran Lake B Zone and CVG prospects).

Within the upper Bruce River Group, relatively unaltered volcanic rocks contain fracture-hosted uranium mineralization (e.g., Madsen and Sylvia Lake prospects), which also commonly displays a close spatial association with the intrusion of mafic dykes within the volcanic sequence. The uranium mineralization within the Sylvia Lake Formation is the youngest example of uranium mineralization recognized within the CMB. There are reports of mineralization in basal conglomerates of the Seal Lake Group at the Stormy Lake prospect (Marten and Smyth, 1975; Kontak, 1978; Ryan, 1984); however, field observations suggest mineralization is confined to the Bruce River Group below the unconformity (Smith *et al.*, 2004; Sparkes and Kerr, 2008). Uranium mineralization is also found within deformed equivalents of the Sylvia Lake Formation along the southeastern margin of the unit (e.g., Minisinakwa prospect), where the rocks have undergone more intense deformation and recrystallization due to the emplacement of younger granites and subsequent Grenvillian deformation (Ryan and Harris, 1978).

## REGIONAL GEOLOGY

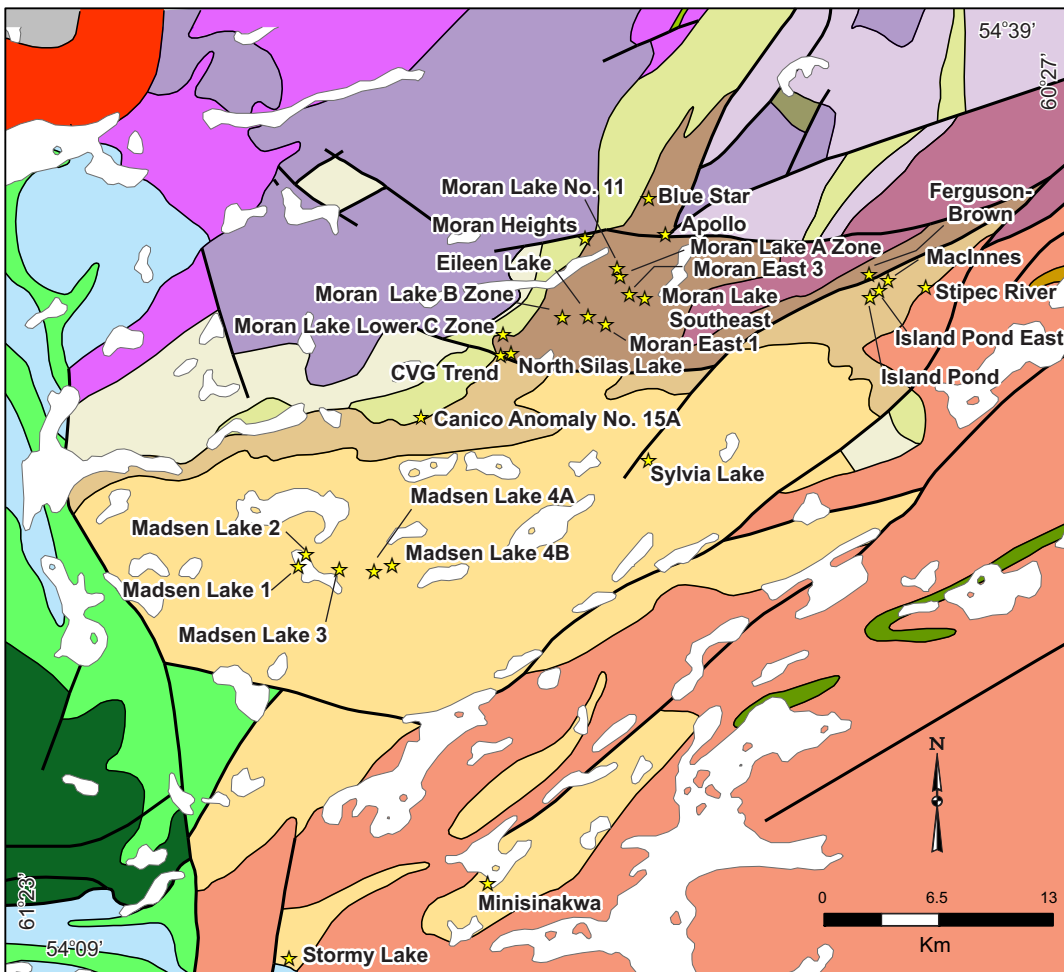
The Heggart Lake Formation unconformably overlies rocks of the Moran Lake Group and represents the lowest stratigraphic unit of the Bruce River Group. The unit also locally unconformably overlies leucocratic granite dated at  $1893 \pm 2$  Ma (Kerr *et al.*, 1992); the latter of which provides a maximum age limit for the base of the sequence. The basal contact of the formation with the Moran Lake Group occurs as an angular unconformity, as the Moran Lake Group was deformed and metamorphosed to upper greenschist facies

prior to the deposition of the overlying Bruce River Group (Ryan, 1984). The Heggart Lake Formation is dominated by grey to red conglomerate, sandstone and lesser mafic and felsic flows. Overall, it forms a coarsening-upward sedimentary succession formed within an alluvial fan–flood plain type environment (Ryan, 1981, 1984). Red and grey quartz arkose and arenite form the basal portion of the unit, passing upward into pebble to boulder conglomerates, which are subdivided into grey and red units, where the red conglomerate is inferred to be the younger of the two (Chaulk, 1979).

The Brown Lake Formation overlies the Heggart Lake Formation and consists of a discontinuous basal conglomerate that passes upward into a thick sequence of volcaniclastic sandstone containing minor interbedded conglomerate. This unit forms a fining-upward sedimentary sequence formed within a shallow lacustrine environment (Ryan, 1984). The contact between the Heggart Lake and Brown Lake formations is largely structural. However, basal conglomerate of the Brown Lake Formation locally lie disconformably upon the Heggart Lake Formation (Ryan, 1984), whereas in other areas the contact between the two formations has been described as conformable and gradational (Collins, 1958). The Brown Lake Formation also locally oversteps the Heggart Lake Formation to lie directly upon rocks of the Moran Lake Group (Ryan, 1984). The local preservation of clasts from the underlying Moran Lake Group that contain a pre-existing fabric provides additional evidence for deformational events prior to the deposition of the Brown Lake Formation (Smyth *et al.*, 1978).

The Sylvia Lake Formation is the uppermost formation within the Bruce River Group. It consists of mafic and felsic flows along with related pyroclastic deposits and lesser intercalated sedimentary and intrusive rocks. Lower portions of the formation are dominated by mafic to intermediate volcanic rocks, whereas upper portions of the formation are dominated by felsic rocks. The formation is compositionally calc-alkaline and represents volcanism within a regional subsiding depression (Ryan, 1984).

The Bruce River Group is disposed in an open, northeast-trending, upright, moderately southwest-plunging syncline, inferred to be related to the Grenvillian Orogeny, which is associated with the development of a regional northeast-trending axial-planar cleavage (Ryan, 1984). Faults of several generations, demonstrating both sinistral and dextral strike-slip movement are also common throughout the group (Ryan, 1984). The degree of metamorphism within the group is largely determined from the mineral assemblages observed within the volcanic rocks of the Sylvia Lake Formation that range from lower to upper greenschist facies (Ryan, 1984).



## LEGEND

### Seal Lake Group

Gabbro sill
Basalt
Arkose, quartzite

### Bruce River Group

Rhyolite, dacite, andesite ash-flow tuff, agglomerate - Sylvia Lake Formation
Conglomerate and volcanioclastic sandstone - Brown Lake Formation
Volcanioclastic sandstone, arkose and conglomerate; minor mafic flows and sills - Heggart Lake Formation

### Moran Lake Group

Pillow basalt, basaltic pyroclastic rocks; minor siltstone and greywacke - Joe Pond Formation
Shale and sandstone of shallow- to deep-water origin - Warren Creek Formation

### Intrusive Rocks

Olivine gabbro and metamorphic equivalents (Michael Gabbro); ca. 1460 to 1425 Ma
Granite; ca. 1650 Ma
Granite; ca. 1973 to 1891 Ma

### Archean Basement Rocks

Tonalite gneiss, granitoid gneiss
Granodiorite, tonalite and minor granite (Kanairiktok Intrusive Suite)
Tonalitic to granodioritic migmatitic orthogneiss containing abundant mafic to ultramafic inclusions and relict mafic dykes
Amphibolite gneiss, mafic granulite gneiss

## SYMBOLS

Fault.....	
Geological contact.....	
Uranium occurrence.....	

**Figure 56.** Regional geology map outlining the distribution of uranium occurrences within the Bruce River Group (geological base map modified from Wardle et al., 1997).

## EXPLORATION HISTORY

The Bruce River Group is mostly known for its large number of copper occurrences, but the group also contains several significant uranium prospects. The first uranium occurrence within the group was discovered in 1957 (Moran Lake B Zone; Mann, 1957) during early exploration by Brinex in the Moran Lake area. Subsequent exploration in the region during the late 1950s, and in the 1970s, resulted in the discovery of several more prospects, including those now known as the Moran Lake Lower C Zone, Moran Lake A and B zones, Canico Anomaly #15, Moran Heights, Madsen and Sylvia Lake prospects. Renewed uranium exploration since the early 2000s, within the Bruce River Group, has largely focused on these historical occurrences. Regional airborne and lake-sediment surveys conducted as part of this exploration identified several new anomalies, including the Moran East 1, Moran East 3 (Willett *et al.*, 2007a), CVG Trend, Blue Star and Apollo (Gillies *et al.*, 2009), Stipec River (Fraser *et al.*, 2008) and Minisinakwa prospects (Fraser *et al.*, 2009). However, most of these anomalies occur close to areas of previously known mineralization, or are of limited extent (Figure 56).

Between 2003 and 2005, most of the Bruce River Group was surveyed by modern airborne geophysical techniques. As with the underlying Moran Lake Group, the Bruce River Group was originally targeted for its potential to host IOCG-styles of mineralization, and a large gravity anomaly situated between the Moran Lake C and B zones was the focus of much exploration (*cf.* Setterfield *et al.*, 2003; Froude *et al.*, 2006). Drilling conducted within the Bruce River Group largely focused on historical uranium prospects. These included the Moran Lake Lower C Zone deposit and the Moran Lake B Zone and Moran Heights prospects, hosted within the Heggart Lake Formation, and the Madsen and Sylvia Lake prospects, hosted within the Sylvia Lake Formation (*cf.* Gilman *et al.*, 2008; Gillies *et al.*, 2009 and *see* references therein). In most instances, the uranium mineralization has been found to be limited. The main exception is the Moran Lake Lower C Zone, which now has a defined NI 43-101 resource of approximately 1.6 million pounds of  $U_3O_8$  (Table 9; Morgan and Giroux, 2008).

## MORAN LAKE LOWER C ZONE DEPOSIT

### Previous Work

The Moran Lake Lower C Zone deposit sits physically beneath the larger Moran Lake Upper C Zone deposit, for which the exploration history and previous work were summarized (*see* Section, Uranium Mineralization within the Moran Lake Group). The uranium mineralization contained within, what is now referred to as the Lower C Zone, was discovered by Shell Canada Resources in 1977, when the company carried out the first diamond drilling in the area. This drilling identified zones of quartzite-hosted uranium mineralization (McKenzie, 1978a) that displayed a close spatial association with the unconformable contact between rocks of the Heggart Lake Formation and underlying pillow basalt of the Joe Pond Formation (Moran Lake Group). The drilling carried out by Shell tested 1200 m of strike length along the unconformable contact and confirmed the presence of variable, low-grade, uranium mineralization that averaged 0.027%  $U_3O_8$  over 2.60 m (Gordanier, 1979).

In 2004, Crosshair Exploration commenced exploration of the Moran Lake C Zone area, which included the investigation of uranium mineralization contained within the Lower C Zone. During the period between 2005 and 2008, the company conducted airborne and ground geophysical surveys along with extensive diamond drilling (*cf.* Gillies *et al.*, 2009 and *see* references therein). This exploration was primarily focused on the larger Upper C Zone, but it also delineated additional uranium mineralization within the Lower C Zone deposit.

### Local Geology

Compared to the structurally complex Upper C Zone discussed earlier, the geology and related uranium mineralization contained within the Lower C Zone is much less complex (Figure 16). Within the deposit, uranium mineralization displays a close spatial association with the unconformable contact between the Moran Lake and Bruce River groups. This contact exposed in the area of Lady Lake (Figure 16) displays only minor structural modification. Examination of drillcore

**Table 9.** NI 43-101 compliant resource estimates for mineralization within the Bruce River Group

Deposit	Resource Classification	Cut-off (% $U_3O_8$ )	Grade (% $U_3O_8$ )	Tonnage (tonnes > cut-off)	Contained Resource (lbs. $U_3O_8$ )	Source
Lower C Zone	Inferred	0.035%	0.050%	1,450,000	1,600,000	Morgan and Giroux, 2008

from holes collared within the conglomerate unit, located to the southeast of the Upper C Zone, indicates that the contact between the pillow basalt and siliciclastic sediments is structural and displays an unknown degree of displacement.

At the unconformity within the Lower C Zone, the typical fine-grained, dark-green pillow basalt observed throughout the C Zone deposit develops extensive quartz carbonate veining and a variably developed dark-purple to red coloration, which extends 1–3 m below the unconformable contact and does not affect the overlying sandstone (Plate 90). The ‘reddening’ of the pillow basalt below the unconformity is inferred to be the result of paleoweathering and is unrelated to the extensive hematite alteration associated with the development of Upper C Zone mineralization. Most of the sandstone sequence above the unconformity is oxidized and red (Plate 91), but locally becomes reduced for several metres immediately above the unconformable contact as is evident in Plate 90. This zone of reduced sandstone is the site of uranium deposition within the Lower C Zone deposit; however, the reduced grey sandstone is not everywhere mineralized.

### Mineralization and Associated Alteration

Mineralization within the Lower C Zone deposit is separated from that developed within the overlying Upper C Zone by the C Zone thrust fault (Gillies *et al.*, 2009; Figure 17) and represents a distinctly different style of uranium mineralization (Sparkes and Kerr, 2008). The uranium mineralization broadly forms a moderately southeasterly dipping stratiform zone located close to the unconformity, but is generally situated several metres above the actual contact. Within the mineralized zone uranium is hosted within chloritic, fine-



**Plate 91.** Oxidized sandstone overprinted by fractures displaying an influx of reduced fluids immediately above the mineralized zone of the Lower C Zone deposit (DDH ML-34, ~310 m depth).

to medium-grained pale-green sandstone, which may record several discrete mineralizing events. The most significant event, with respect to the highest grades of uranium mineralization, occurs as patchy zones of disseminated uraniferous material. These zones display an irregular distribution, possibly representing a fluid front developed within the reduced sandstone (Plate 92); such features within the drillcore become more prevalent as the core becomes more weathered.

The Lower C Zone also displays evidence of a later mineralizing event in which the reduced sandstone is overprinted by hematite–carbonate alteration, which is, in turn, associated with the development of finely disseminated uranium mineralization. Sodium cobaltinitrite staining of the sample shown in Plate 93 identified a potassic-rich zone associated with the development of a fine-grained clay mineral; this zone is coincident with a point source of radioactivity outlined by the accompanying autoradiograph. Visible/infrared spectroscopy was used to identify the accompanying clay alteration as illite; however, this style of clay alteration is not typically abundant throughout the Lower C Zone deposit.

### Petrography

Examination of mineralized thin sections indicates that uranium mineralization contained in the reduced sandstone principally occurs as fine-grained intergrowths in association with disseminated Fe–Ti oxide minerals (Plate 94). Deposition of the oxide minerals is locally accompanied by chalcopyrite, and commonly envelopes existing pyrite within the reduced sandstone (Plate 94D). SEM imaging of the radioactive zone highlighted by the autoradiograph shown in Plate 93B, demonstrates that the resultant radioactivity is associated with brannerite, which in this case occurs in association with finely disseminated Fe–Ti oxide minerals formed within the pressure shadow of a large quartz grain (Plate 94G, H).

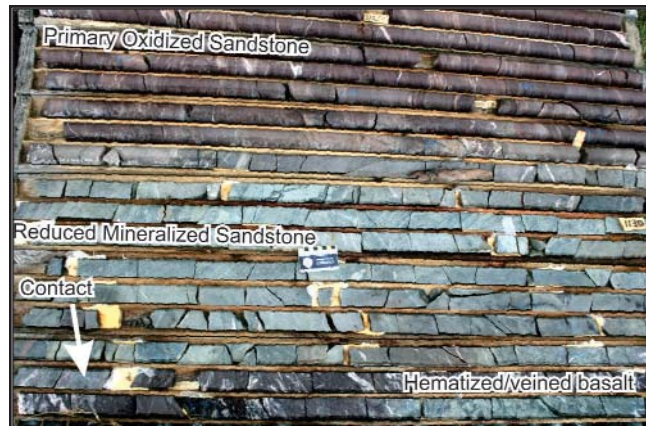


**Plate 90.** Photograph displaying the unconformable contact between basalt and overlying sandstone, Lower C Zone deposit (DDH ML-44, 340 m). The sandstone in the immediate vicinity of the contact and extending 4–5 m up-section is reduced and hosts uranium mineralization, which, in turn, grades upward into oxidized sandstone.

## MORAN HEIGHTS PROSPECT

### Previous Work

The area surrounding the Moran Heights prospect was initially highlighted as an airborne EM and IP anomaly in surveys conducted by Brinex in 1970, with subsequent work locating disseminated copper mineralization in the area (Goddard and Klein, 1971; Soonawala, 1971). In the late 1970s, Canadian Nickel Co. Ltd. discovered radioactive sandstone boulders in the same area (Perry, 1979). The company conducted the first diamond drilling on the prospect, which failed to intersect any uranium mineralization, but did identify a zone of anomalous Cu and Ag enrichment (Perry, 1980a). In 1983, Saarberg-Interplan discovered mineralization in outcrop, while conducting regional exploration for unconformity-style uranium mineralization within the CMB (Hopfengaertner *et al.*, 1984). Trenching and mapping were carried out during the following two years, after which no further work was conducted. In 2006, Crosshair Exploration conducted geological mapping and prospecting in the area of a significant airborne radiometric anomaly that highlighted the area of outcropping mineralization. This work was followed up with 25 diamond-drill holes; the most significant results from which include 0.11%  $U_3O_8$  and 0.023%  $V_2O_5$  over 5.45 m (Morgan *et al.*, 2007).

### Local Geology

The Moran Heights prospect is located some 7 km northeast of the Moran Lake C Zone deposit. Uranium mineralization is developed along the same structurally modified unconformable contact as at the Lower C Zone deposit, and displays many of the same characteristics. To the immediate northwest of the prospect, basalts of the Joe Pond Formation form a prominent northeast-trending ridge, which is unconformably overlain in the low ground to the southeast by a moderately, southeasterly dipping sequence of pebble conglomerate and coarse-grained sandstone. Near the main zone of uranium mineralization the unconformable contact is truncated by an east-northeast-trending fault (Figure



**Plate 92.** Photograph displaying the patchy distribution of disseminated uranium mineralization within reduced sandstone of the Lower C Zone deposit (DDH ML-44, ~345 m depth); the labels denote counts per second.

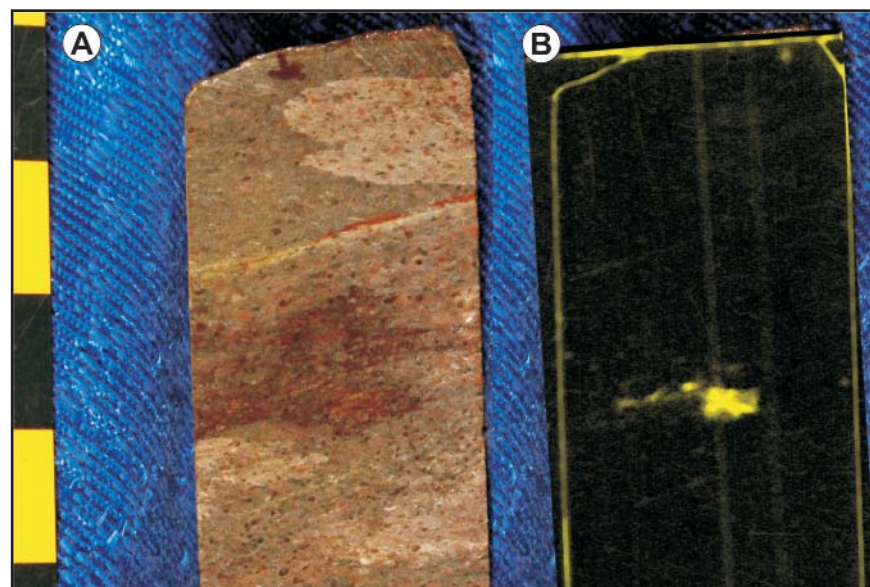


**Plate 93.** A. Sample of reduced sandstone overprinted by hematite–carbonate alteration, Lower C Zone deposit (DDH ML-55, ~330 m depth), B. Accompanying autoradiograph of (A), outlining the distribution of radioactivity within the sample (yellow; minus the outline of the sample).

57). Detailed mapping in the area of outcropping mineralization, known as the ‘Frank Trench’, has outlined several north-northeast-trending faults resulting in the dextral offset of the unconformable contact (Perry, 1979, 1980; Morgan *et al.*, 2007). In the immediate vicinity of the prospect, pebble conglomerate is the predominant rock type developed above the unconformity, which grades upward into coarse-grained sand-

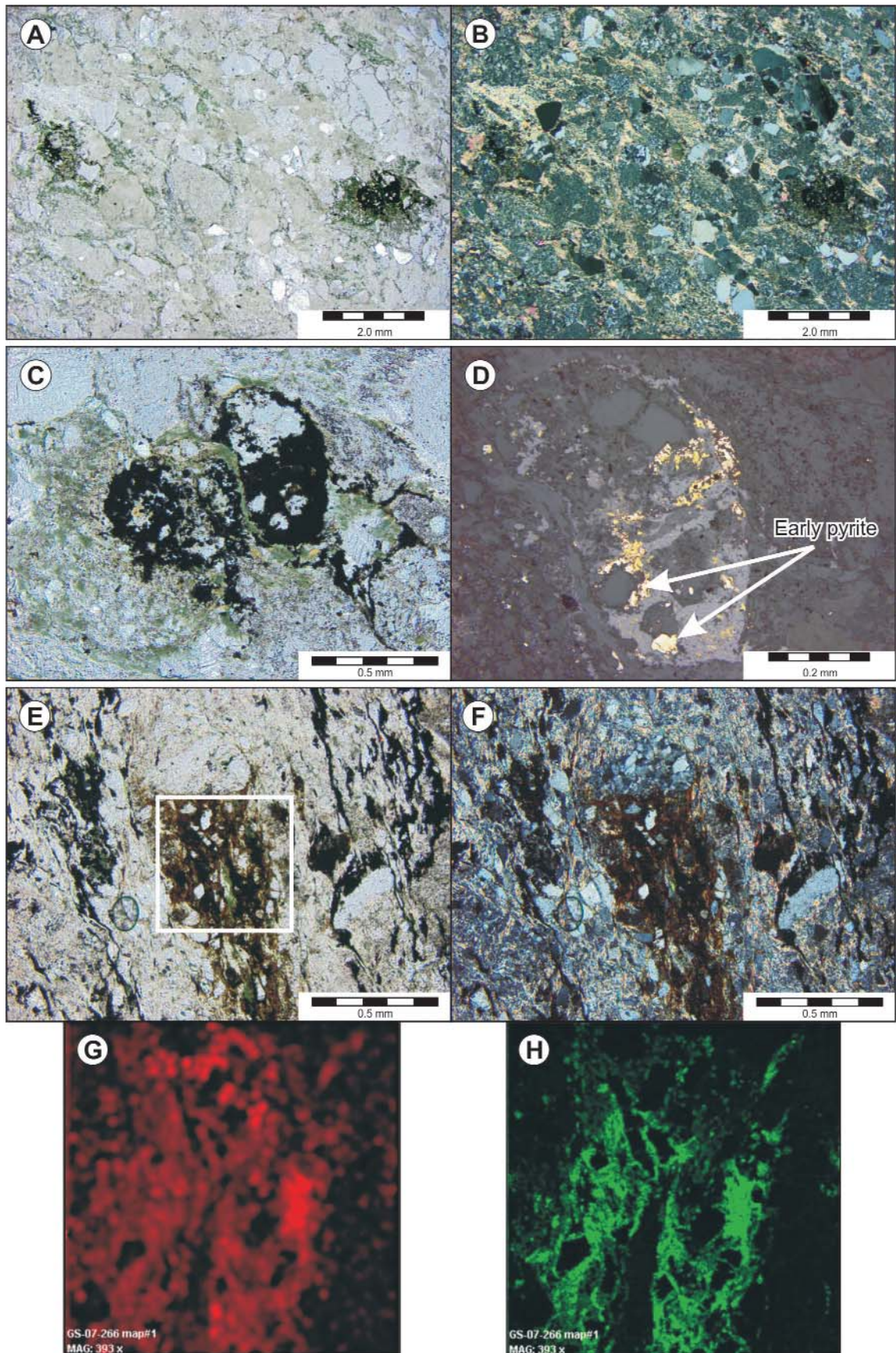


Plate 94.

stone within several metres of the contact; lesser conglomerate also occurs as interbedded material within the sandstone sequence higher in the stratigraphic succession.

The siliciclastic sedimentary rocks are inferred to have been oxidized during deposition and subsequently reduced by a later diagenetic event. The reduced zone is similar to that at the Lower C Zone and displays a distinct pale-green, chlorite-rich alteration developed immediately above the unconformable contact. However, the reduced zone at Moran Heights is more extensive than in the Lower C Zone, and extends above the unconformity for up to 10 m, where it grades into red oxidized sandstone. In addition, within the oxidized portion of the sequence, localized reduced zones are developed in association with chloritic shear zones.

### Mineralization and Associated Alteration

Two styles of uranium mineralization are evident within the siliciclastic sedimentary rocks of the Moran Heights prospect. The most significant uranium enrichment typically occurs near the upper boundary between the reduced and oxidized zones (Plate 95); this relationship is further highlighted when the location of this boundary is compared to industry acquired down-hole gamma probe data, whereby the first occurrence of anomalous radioactivity in the survey generally corresponds with the upper boundary of the reduced zone.

Within the reduced zone, uranium mineralization occurs as fine-grained disseminations in association with disseminated pyrite and chalcopyrite. Localized, narrow intersections of higher grade uranium mineralization commonly correspond with the development of hematite–carbonate alteration and veining, which overprint the reduced chlorite-rich alteration (Plate 96). However, these features are generally developed close to the oxidation-reduction boundary and may, in part, be linked to the same mineralizing event. Unlike the uranium mineralization, chalcopyrite commonly occurs throughout the reduced zone, locally producing values of up to 0.37% Cu and 1.4 g/t Ag over 5.5 m (ML-MH-02; Morgan *et al.*, 2007). The chalcopyrite occurs within the matrix of the sandstone and conglomerate units, and is also present within the carbonate veins that crosscut the stratigraphic sequence.

### Petrography

Uranium mineralization contained within the reduced sandstone and conglomerate is commonly associated with disseminated pyrite, where it occurs as fine-grained disseminations throughout the matrix of the siliciclastic sedimentary rocks in association with the development of Fe–Ti oxide minerals. The uranium phase is most likely brannerite given the U–Ti association indicated by SEM imaging. The pyrite is inferred to predate uranium mineralization as it forms coarse-grained, euhedral crystals that are locally enveloped by uranium-bearing minerals (Plate 97). SEM imaging of mineralized samples also indicate a spatial association between the formation of uraniferous Fe–Ti oxide minerals and chalcopyrite, suggesting that the two are part of the same mineralizing event. However, as indicated above, the copper mineralization is generally more widespread than the accompanying uranium mineralization.

### Other Minor Uranium Occurrences

Approximately 1 km to the east of the Moran Heights prospect, Saarberg Interplan Ltd. reported the presence of mineralized greywacke boulders locally hosting up to 5.3%  $U_3O_8$  (Hopfengaertner *et al.*, 1984). During the course of this study, several small, well-rounded boulders were located approximately 900 m east of the Moran Heights prospect, in the same general area as that reported by Saarberg (Figure 57). However, the boulders that were located consisted of coarse-grained sandstone rather than greywacke and are similar to the host rock at the Moran Heights prospect. These mineralized boulders locally produced up to 45 000 cps and are inferred to represent glacially transported material from the main Moran Heights prospect.

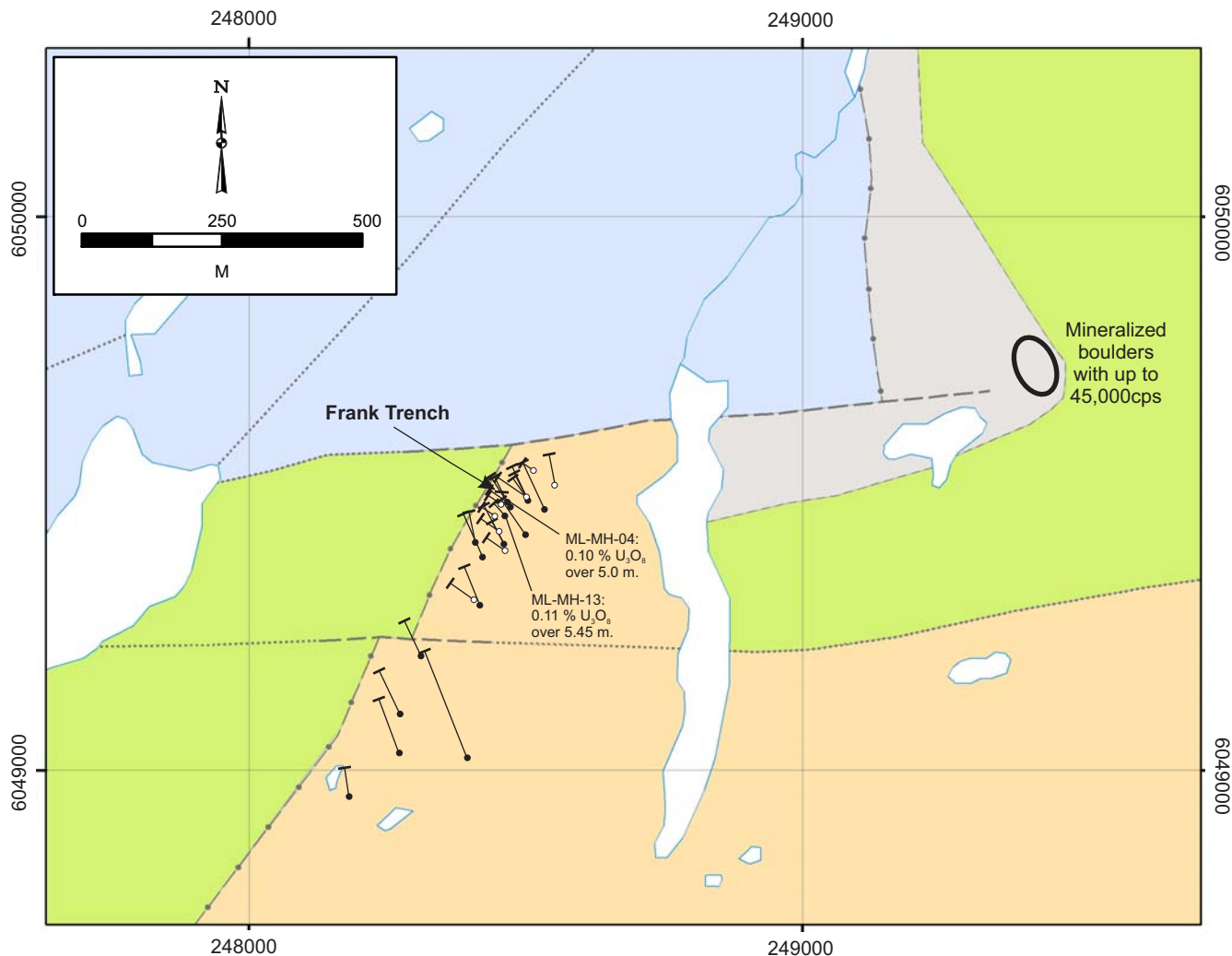
## MORAN LAKE B ZONE PROSPECT

### Previous Work

First discovered in 1957 by Brinex personnel, the Moran Lake B Zone (originally called the Montague No. 1 showing) has been the focus of several uranium exploration programs. Early investigations in the area included stripping, trenching and limited shallow drilling (*cf.* Mann, 1957; Ellingwood, 1958; Bernazeaud, 1965), and was followed up by an extensive program of trenching and diamond drilling by Shell

---

**Plate 94 (opposite).** *A. PPL photomicrograph of two areas of anomalous radioactivity associated with opaque minerals, developed in association with pervasive chlorite–carbonate alteration within reduced sandstone of the Lower C Zone (DDH ML-38, ~295 m depth), B. XPL view of (A), C. Magnified view of (A) illustrating the intergrowth of the opaque oxide minerals with the chlorite alteration, D. Reflected light magnified view of (C) showing the formation of the Fe–Ti oxide minerals along with chalcopyrite, both of which locally envelope an earlier pyrite phase, E. PPL photomicrograph of the radioactive area shown in Plate 93B (DDH ML-55, ~330 m depth); also shown is the area of the SEM image shown in (G and H), F. XPL view of (E), G. SEM image outlining the distribution of uranium (red), H. SEM image outlining the distribution of titanium (green).*



### LEGEND

#### Bruce River Group

Sandstone

#### Moran Lake Group

Pillow basalt

Siltstone

#### Kanairiktok Intrusive Suite

Granodiorite

### SYMBOLS

Unconformity (Assumed)



Contact (Approximate)



Fault (Approximate, assumed)



Drillhole Collar (Canico, Crosshair)



**Figure 57.** Plan map outlining the distribution of drillholes at the Moran Heights prospect as well as the distribution of geological units (modified from Morgan et al., 2007). Note grid coordinates are in NAD 27, Zone 21.



**Plate 95.** Photograph illustrating a zone of uranium mineralization developed at the transition zone between the reduced and oxidized siliciclastic sedimentary rocks of the Moran Heights prospect (DDH ML-MH-04, ~40 m depth); white labels denote counts per second.



**Plate 96.** Uraniferous hematite–carbonate veins crosscutting reduced sandstone, Moran Heights prospect (DDH ML-MH-13, 36.5 m depth); white labels denote counts per second.

Canada in the late 1970s (*cf.* McKenzie, 1976, 1977b). Trenching in the area has exposed mineralization that returned 0.12%  $U_3O_8$ , 0.15% Cu and 7.76 g/t Ag over 24.8 m (McKenzie, 1977b); however, drilling in the area only intersected minimal uranium mineralization and indicated it was of limited extent.

The area surrounding the B Zone prospect also formed part of a thesis study conducted by Kontak (1980). Work carried out as part of this project subdivided the intrusive dykes in the area into five types which included: 1) coarse-grained anorthosite, 2) medium-grained anorthosite exhibiting a trachytic-like texture, 3) fine-grained trachyte, 4) feldspar-porphyry and 5) feldspar-pyroxene porphyry (Kontak, 1980). He noted that the uranium mineralization was primarily confined to the coarse-grained and medium-grained anorthosite dykes as well as the feldspar-porphyry. Uranium mineralization, primarily occurring as brannerite, is associated with the development of chlorite, hematite and carbonate alteration, for which staining of the carbonate revealed the presence of dolomite, ferroan dolomite, ankerite, white calcite and red calcite (Kontak, 1980). In addition, Kontak (1980) also noted the presence of titanite, anatase, rutile and albitic plagioclase,

along with common sulphide minerals including pyrite, chalcopyrite, bornite, covellite and chalcocite with uranium mineralization.

Crosshair conducted an intensive program of mapping, prospecting and diamond drilling on the main B Zone prospect. In total 12 drillholes were completed, from which the best intersection returned 0.27%  $U_3O_8$ , 0.16%  $V_2O_5$ , 0.035% Cu and 2.4 g/t Ag over 7.56 m (DDH ML-BZ-01; Morgan *et al.*, 2007). This work confirmed earlier interpretations of the uranium mineralization, noting that the mineralization primarily occurred as brannerite, along with lesser uraninite, and was of limited extent (Eaton *et al.*, 2008).

### Local Geology

The B Zone prospect is located approximately 3 km northeast of the C Zone deposit and occurs near the edge of a large gabbroic intrusion (Figure 58). This intrusion is associated with a pronounced aeromagnetic anomaly that is much more widespread than the intrusions mapped surface expression, suggesting it is more extensive at depth. Uranium mineralization in the area is hosted within red sandstone of the Heggart Lake Formation, as well as in altered leucogabbroic dykes that intrude the sedimentary succession. Most of mineralization is concentrated along the intrusive contacts of the dykes, which develops localized brecciation within the adjacent sandstone wall rock. The main B Zone prospect is associated with an altered dyke that forms a pronounced magnetic anomaly, which can be traced over a strike length of approximately 250 m (McKenzie, 1976). Other smaller anomalies to the east of the main occurrence are also associated with dykes and plugs of the altered leucogabbroic unit, which commonly display a distinctive brownish-orange weathering due to pervasive Fe-carbonate alteration (Plate 98). The Fe-carbonate and hematite alteration developed at the B Zone prospect (Plate 99) is visually similar to that developed at the nearby Upper C Zone (*e.g.*, Plate 30), and a potential genetic link between the two areas has previously been inferred (*e.g.*, Kontak, 1978).

### Mineralization and Associated Alteration

Both the leucogabbroic dykes and the red sandstone units are locally intensely altered, highly fractured, and brecciated. The main alteration assemblages associated with the development of uranium mineralization consist of hematite, carbonate and chlorite. These assemblages are variably developed throughout the prospect, but predominantly display a close spatial association with dyke emplacement. The main zones of uranium mineralization are concentrated within fractures and localized zones of brecciation along the margins of these dykes, as shown in Plates 100 and 101; however as demonstrated by diamond drilling in the area, not all dykes are mineralized and the uranium mineralization is sporadic at depth.

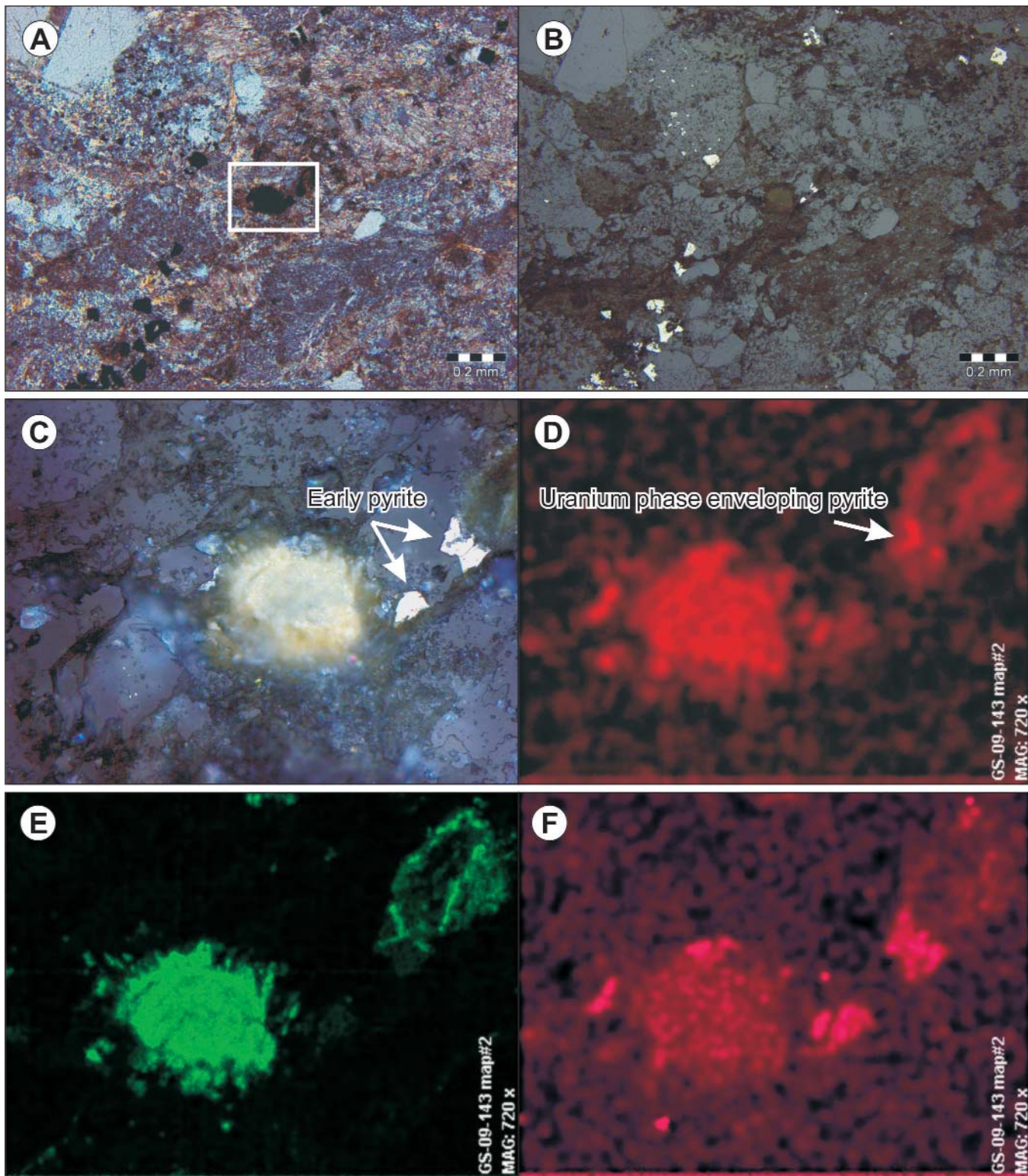
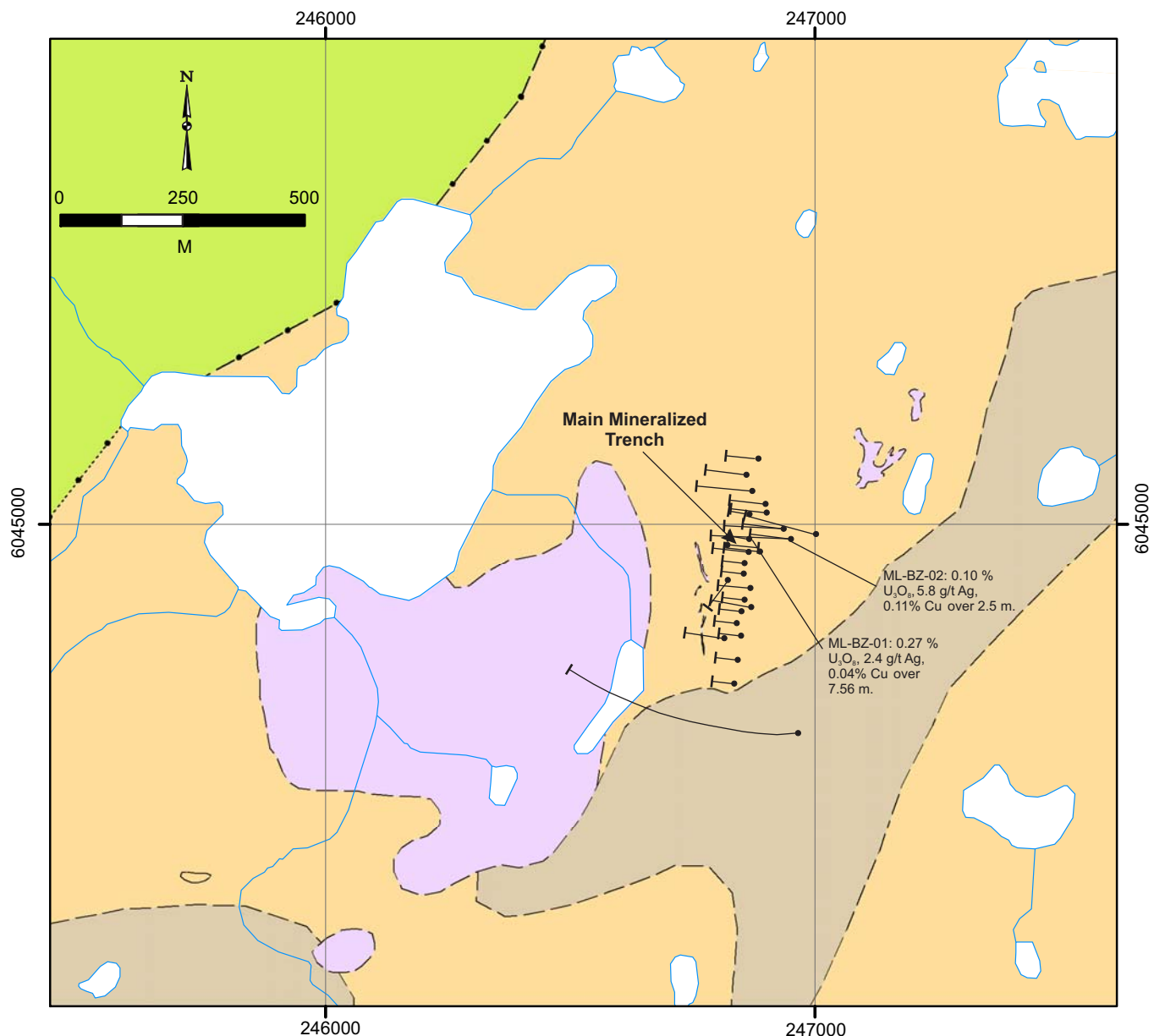


**Plate 97.** *A.* XPL view of the reduced sandstone containing euhedral disseminated pyrite and uraniferous Fe–Ti oxide minerals; inset outlines magnified view shown in (C). *B.* Reflected light view of (A) illustrating abundant coarse-grained euhedral pyrite within the sample. *C.* Magnified view of pyrite and point source of radioactivity as outlined by an autoradiograph of the thin section. *D.* SEM image outlining the distribution of uranium (shown in red); note the local presence of a uranium-rich phase enveloping pyrite. *E.* SEM image outlining the distribution of titanium (green). *F.* SEM image outlining the distribution of copper (shown in magenta); note local spatial association of uranium and copper mineralization.



## LEGEND

	Gabbro
<b>Bruce River Group</b>	
	Conglomerate
	Sandstone
<b>Moran Lake Group</b>	
	Pillow basalt

## SYMBOLS

- Unconformity (Approximated, Assumed).....
- Contact (Approximate).....
- Drillhole Collar .....

**Figure 58.** Plan map outlining the distribution of drillholes and the main geological units at the Moran Lake B Zone prospect. Note grid coordinates are in NAD 27, Zone 21.

## Petrography

Detailed examination of the mineralized breccia shown in Plate 101 indicates the breccia contains fragments of both relatively fresh anorthosite dyke material, along with fragments of Fe-carbonate alteration. The fragments of the dyke contain abundant disseminated opaque oxides, primarily consisting of magnetite, which is also present throughout the chlorite–carbonate-rich matrix of the surrounding breccia.



**Plate 98.** Uraniferous, leucogabbroic dyke displaying distinct brownish-orange weathering due to the pervasive Fe-carbonate alteration that accompanies uranium mineralization (~750 m northeast of main B Zone prospect).



**Plate 99.** Brecciated hematite and Fe-carbonate alteration overprinted by later dark-purple specularite-filled fractures, B Zone prospect. Sample contains 14.01 wt.% CaO, 4.39 wt.% Na<sub>2</sub>O and 127 ppm U.

**Plate 102 (opposite).** A. Scanned thin section of the mineralized breccia shown in Plate 101; inset shows location of (C), B. Accompanying autoradiograph outlining the distribution of radioactivity (yellow) within (A), C. PPL photomicrograph illustrating the plagioclase-rich nature of the dyke fragments within the breccia; inset shows the location of (D), D. Reflected light image of opaque oxide minerals showing magnetite and Fe–Ti oxide minerals that host uranium mineralization; inset shows the location of (E), E. Backscattered SEM image of an uraniferous zone as outlined by the autoradiograph; note finely disseminated bright spots are inferred to be uraninite, F. SEM view of (E) outlining the distribution of uranium (red), G. SEM view of (E) outlining the distribution of iron (orange), H. SEM view of (E) outlining the distribution of titanium (green).

Plate 102A represents a scanned thin section of the uraniferous breccia shown in Plate 101. The image in Plate 102B represents the corresponding autoradiograph outlining the radioactivity within the section. From this autoradiograph, it is evident that the only fragment within the breccia that does not contain radioactivity is a large angular fragment of Fe-carbonate alteration near the base of the section. The section



**Plate 100.** Fine- to medium-grained leucogabbroic dyke intruding red sandstone, and where minor fracture-hosted uranium mineralization is developed along the margin of the dyke; core of dyke contains background levels of radioactivity whilst the contact zone measures up to 300 cps (DDH ML-BZ-02, ~73 m depth); white label denotes counts per second.



**Plate 101.** Uranium-bearing breccia located along the intrusive margin of a leucogabbroic dyke; B Zone prospect. A sample from this interval returned 0.34% U<sub>3</sub>O<sub>8</sub>, 0.12% V<sub>2</sub>O<sub>5</sub>, 0.25% Cu and 14.3 g/t Ag over 0.5 m (Sample #90838; Morgan et al., 2007; DDH ML-BZ-04, ~43 m depth); white labels denote counts per second.

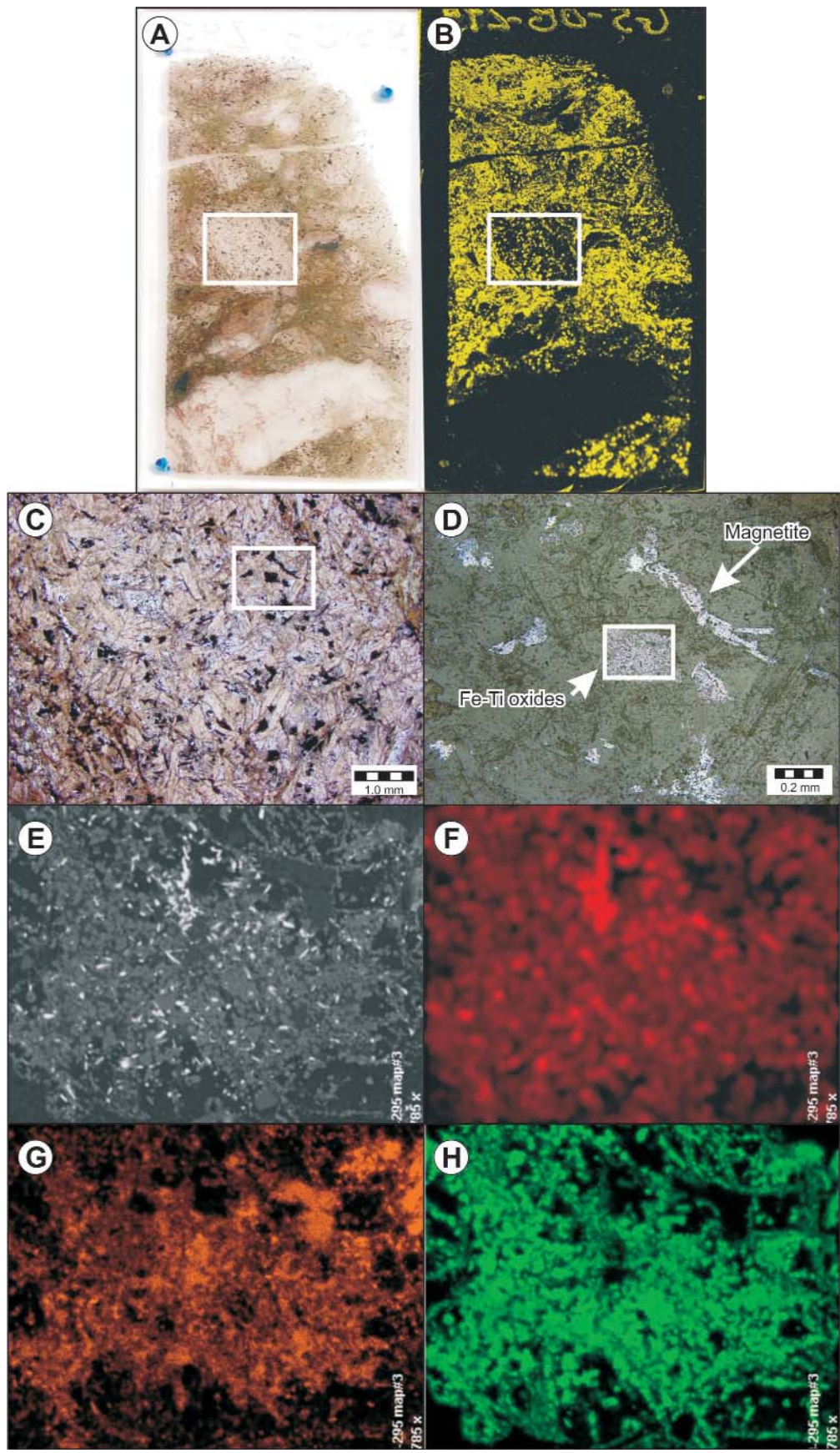


Plate 102.

contains finely disseminated radioactivity throughout, including the relatively unaltered anorthosite dyke fragments. It is also noted that the distribution of radioactivity within the sample is largely associated with the distribution of magnetite within both the fragments and the breccia matrix.

SEM imagining of the sample shown in Plate 102 indicates that the radioactivity contained within the dyke fragments is largely associated with Fe–Ti-oxide minerals, and confirms that the radioactivity is primarily the result of finely disseminated uraninite (Plate 102E, F). In contrast, imaging of uranium mineralization contained within the breccia matrix shows that uranium is dominantly present as brannerite, as indicated by the strong overlap in U and Ti in the SEM images shown in Plate 103. However, in both instances the development of uranium mineralization is spatially association with the presence of magnetite within the sample.

## OTHER URANIUM OCCURRENCES

### Moran Lake A Zone Prospect

The Moran Lake A Zone prospect (Figure 56) is one of the few anomalies developed within the Heggart Lake Formation outside of the Lower C Zone that is not located close to an aeromagnetic anomaly. This prospect appears to represent a zone of structurally controlled uranium mineralization that can be traced for approximately 800 m along strike and is locally up to 40 m wide (Willett *et al.*, 2006a). Grab samples obtained from the area have returned values of up to 0.22%  $U_3O_8$  (Willett *et al.*, 2006a); however, shallow drilling in the area indicates the mineralization pinches out at depth (*cf.* Bernazeaud, 1965).

The main zone of uranium mineralization is associated with sheared, rusty-weathering, pyritic, grey-green conglomerate, developed within an inferred, northeast-trending fault (Plate 104). A sample of uraniferous material collected from this zone, along with its corresponding autoradiograph is shown in Plate 105. Results of the autoradiograph, coupled with detailed petrographic work, demonstrate that the majority of the uranium mineralization within the sample is concentrated within clasts containing finely disseminated pyrite and also occurs as fine-grained disseminations throughout the matrix. The matrix of the conglomerate contains abundant pyrite, and white mica alteration that has been identified as muscovite by visible/infrared spectroscopy. SEM imaging of the sample indicates that the radioactivity within the sample is primarily associated with finely disseminated brannerite. In addition, autoradiographs of samples cut perpendicular to the foliation illustrate that radioactivity is also concentrated along foliation planes indicating the local structural control on the mineralization.

### CVG Prospect

This zone was discovered during exploration by Crosshair Exploration (*cf.* Gillies *et al.*, 2009 and *see references therein*) and is associated with roughly east–west-trending gabbroic dykes, which intrude conglomerate of the Heggart Lake Formation (Figure 56; Plate 106). These dykes are associated with pronounced magnetic highs as outlined by the calculated vertical gradient of airborne geophysical data (Gillies *et al.*, 2009). Four trenches were excavated along the magnetic anomaly exposing variably mineralized gabbroic dykes, which assayed up to 0.13%  $U_3O_8$  over 0.5 m; however, limited diamond drilling in the area failed to intersect any significant uranium mineralization (*cf.* Gillies *et al.*, 2009). The uranium mineralization is primarily concentrated along the margins of the dyke, and is largely concentrated within brittle to brittle-ductile fractures and vein systems associated with Fe-carbonate alteration (Gillies *et al.*, 2009). Locally the alteration and related brecciation are observed to overprint the gabbroic dykes (Plate 107).

### Madsen Prospect

Felsic volcanic rocks of the Sylvia Lake Formation are generally characterized by elevated levels of background radioactivity (250–300 cps) in comparison to the underlying sedimentary rocks (<200 cps). However, the volcanic succession is only known to host two areas of uranium mineralization, the most areally extensive of which are the Madsen Lake occurrences, and the second area being the Sylvia Lake prospect (Figure 56). At the Madsen Lake occurrences, the volcanic succession is intruded by roughly east–west-trending diabase dykes, which form prominent magnetic highs on airborne geophysical maps of the area. Four main occurrences of uranium mineralization occur along this magnetic anomaly and are termed the Madsen Lake zones 1 through 4.

Uranium mineralization is hosted within felsic volcanic rocks, primarily consisting of lapilli tuff, along with lesser tuffaceous sandstone. Crosshair conducted detailed mapping and prospecting in the area and reported that uranium mineralization occurred within narrow, carbonate-filled fractures developed along the margins of diabase dykes, and also in brittle fractures within the felsic volcanic rocks and related tuffaceous sandstone. Grab samples from the area returned values of up to 4.57%  $U_3O_8$  (Morgan *et al.*, 2007). The company also carried out diamond drilling in the area of the Madsen Lake 4B prospect in 2006, from which the highest reported intersection was 0.054%  $U_3O_8$  over 1.5 m (ML-MA-05; Morgan *et al.*, 2007). In addition, the area of the Madsen Lake 4A prospect, as well as a nearby gold in till anomaly, was also drilled in 2008, but failed to intersect any significant mineralization (Gillies *et al.*, 2009). The felsic volcanic rocks

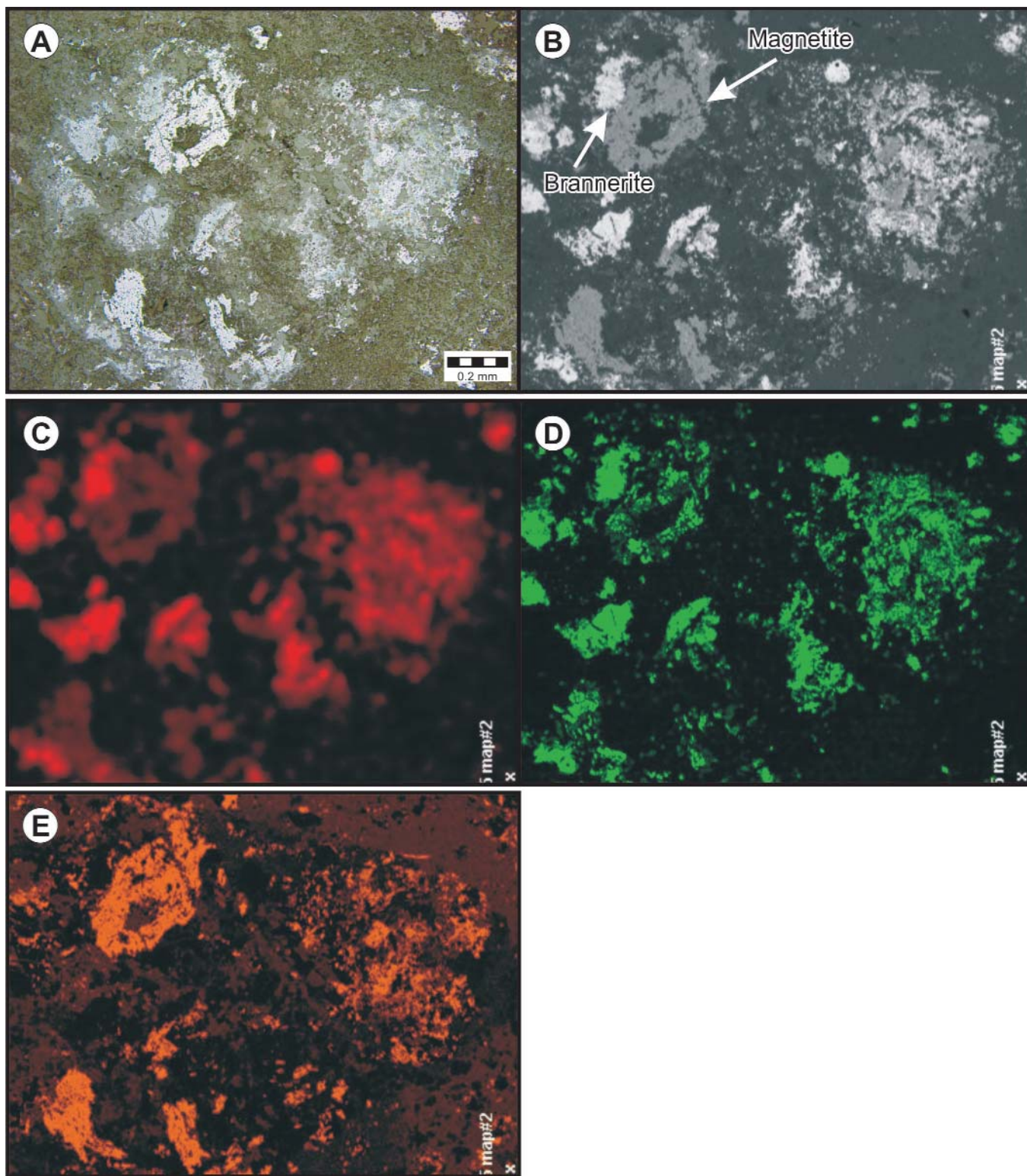


**Plate 103.** *A.* Reflected light image of opaque oxide minerals developed within the breccia matrix. *B.* Backscattered SEM image of uraniferous zone as outlined by the autoradiograph, illustrating the close spatial association of uranium mineralization and magnetite within the breccia matrix; field of view is approximately 2 mm. *C.* SEM view of (B) outlining the distribution of uranium (red). *D.* SEM view of (B) outlining the distribution of titanium (green). *E.* SEM view of (B) outlining the distribution of iron (shown in orange).



**Plate 104.** Rusty-weathering, highly sheared, uraniferous pebble conglomerate, Moran Lake A Zone prospect.

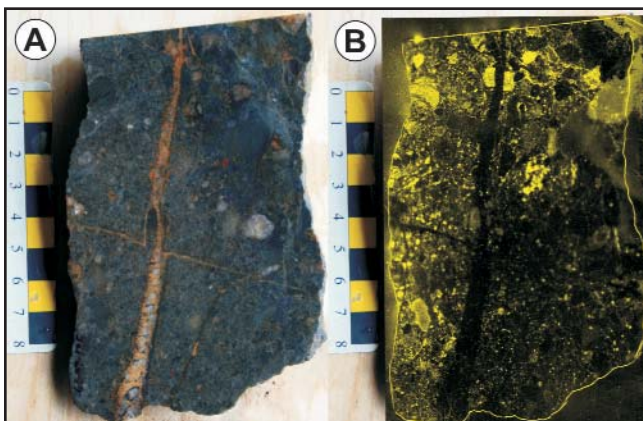


**Plate 105.** A) Uraniferous sample of pebble conglomerate from the Moran Lake A Zone prospect; sample assayed 0.15%  $U_3O_8$ . B. Corresponding autoradiograph of (A) outlining the distribution of radioactivity within the sample (yellow, minus the outline of the sample).



**Plate 106.** Large gabbroic dyke intruding siliciclastic sedimentary rocks of the Heggart Lake Formation, CVG prospect.



**Plate 107.** Uraniferous hematite and related Fe-carbonate alteration overprinting a gabbroic dyke intruding sedimentary rocks of the Heggart Lake Formation, CVG prospect.

of the Bruce River Group that are associated with uranium mineralization lack significant alteration or ductile deformation, aside from the leaching of hematite marginal to the brittle fractures hosting elevated radioactivity, which locally result in a pale-pink to orange colouration of the adjacent wall rock (Plate 108).

### Sylvia Lake Prospect

The Sylvia Lake prospect (Figure 56) is also hosted within felsic lapilli tuff of the Sylvia Lake Formation and is developed close to the intersection of two fault structures (Gilman *et al.*, 2008). Re-sampling of historical trenches at the prospect by Santoy Resources in 2005 returned values of up to 2.72%  $U_3O_8$  from chip sampling of mineralized outcrop (Willett *et al.*, 2006c). Mega Uranium drilled three diamond-drill holes at the prospect, from which the best intersection



**Plate 108.** Anomalous radioactivity developed within brittle fractures in felsic volcanic rocks of the Sylvia Lake Formation, Madsen Lake Zone 4B prospect (DDH ML-MA-02, 20 m depth); white labels denote counts per second.

assayed 0.24%  $U_3O_8$  over 0.3 m (Gilman *et al.*, 2008). Here, the mineralization was reported to be developed marginal to a sheared mafic dyke, which was logged as a chloritic phyllite (Gilman *et al.*, 2008).

The Sylvia Lake area resembles the Madsen Lake prospects, in that no significant alteration accompanies the development of uranium mineralization, which is primarily hosted within brittle fractures in the host felsic volcanic rocks (Plate 109).

#### Minisinakwa Prospect

The Minisinakwa prospect (Figure 56), which consists of highly sheared boulders of felsic metavolcanic rocks hosting hematite and magnetite alteration, was discovered in 2008 by Bayswater Uranium. The prospect consists of angular float distributed along an east-northeast-trending lineament containing several discrete magnetic anomalies, from which grab samples of up to 3.48%  $U_3O_8$  were obtained (Fraser *et al.*, 2009). The metavolcanic host rocks within the area display variable degrees of recrystallization and a strong penetrative fabric. Drilling in the area tested several magnetic anomalies and intersected localized veins of magnetite within the felsic metavolcanic rocks, but failed to intersect any significant uranium mineralization. The main unit intersected in

drillcore consisted of a fine-grained, variably recrystallized, feldspar-phyric, felsic metavolcanic rock hosting localized fractures infilled with magnetite; the unit also contains lesser fine-grained magnetite throughout the groundmass (Plate 110). A sample of this unit was collected for geochronological study to compare its age with the rest of the Sylvia Lake Formation. The sample produced an abundant population of high-quality zircon prisms, which gave a weighted average  $^{207}Pb/^{206}Pb$  age of  $1645 \pm 4$  Ma (Sparks *et al.*, 2016).

Mineralized float contains a strong penetrative fabric that overprints the magnetite alteration and related uranium mineralization (Plate 111). This mineralization displays some similarities with that developed within Aillik Group rocks farther to the northeast, such as the presence of magnetite and hematite alteration in association with uranium mineralization. However, mineralized samples contain elevated potassium values indicating potential potassic alteration in contrast to the sodic-rich alteration observed elsewhere in the Aillik Group.

#### Stormy Lake Prospect

Previous discussions of uranium mineralization at the Stormy Lake prospect (Figure 56) have interpreted the min-

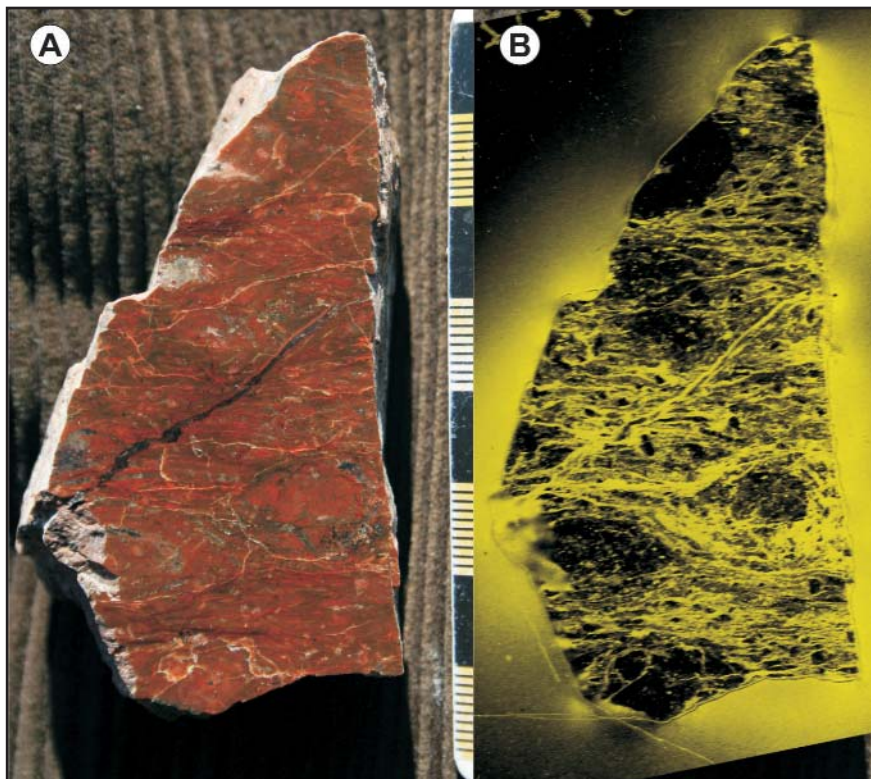


**Plate 109.** A. Uraniferous sample of a felsic volcanic rock from the Sylvia Lake prospect; sample assayed 0.69%  $U_3O_8$ . B. Corresponding autoradiograph of (A) outlining the distribution of radioactivity within the sample (yellow minus the outline of the sample); note the brittle fracture-hosted nature of the mineralization.



**Plate 110.** Quartz- and feldspar-phyric felsic metavolcanic rock displaying fracture-hosted magnetite alteration, Minisinakwa prospect.

eralization to be locally hosted within rocks of the Seal Lake Group (e.g., Marten and Smyth, 1975; Kontak, 1980; Ryan, 1984; Wilton, 1996). However, more recent examination of the mineralization indicates that it is hosted within the underlying felsic volcanic rocks of the Sylvia Lake Formation (e.g., Smith *et al.*, 2004; Sparkes and Kerr, 2008). The most significant zone of radioactivity is associated with strongly sheared, quartz-phyric, felsic metavolcanic rocks (Plate 112). This area locally produced up to 2200 cps, but assay results from the zone only returned up to 0.034%  $U_3O_8$ , in addition to anomalous values of Au (2.35 g/t) and Ag (457 g/t; Smith *et al.*, 2004).

## GEOCHRONOLOGICAL CONSTRAINTS

Age constraints on the development of uranium mineralization within the Bruce River Group are few in comparison to other areas within the CMB. The basal unit of the Bruce River Group (Heggart Lake Formation) unconformably overlies the Junior Lake granodiorite, dated at  $1893 \pm 2$  Ma (Kerr *et al.*, 1992), and the felsic volcanic rocks of the Sylvia Lake Formation are locally dated at  $1649 \pm 1$  Ma (Schärer *et al.*, 1988). The latter age was taken to represent the age of deposition for the Bruce River Group. As part of this study, four samples were submitted for U-Pb geochronological study by TIMS analysis at Memorial University (samples A-D; methods and procedures are summarized in Appendix B) in order to constrain the depositional age of the various units within the Bruce River Group. Results are reported in Appendix C and presented on concordia diagrams in Figure 59, with errors at the  $2\sigma$  level.

To constrain the age of the Heggart Lake Formation, an ash tuff, interbedded with red sandstone, located above the unconformity and within the Moran Lake Lower C Zone deposit, was sampled. The tuff produced an abundant population of euhedral zircon from which nine analyses yielded a best-fit line within an upper intercept age of  $1847 +12/-9$  Ma (Sparkes *et al.*, 2016). This age is inferred to represent the depositional age of the basal Heggart Lake Formation and demonstrates that this sedimentary sequence represents a much older unit than previously envisaged. The older age of the Heggart Lake Formation is further supported by an age obtained from intrusive rocks at the Moran Lake B Zone prospect. Here, deep drilling targeted a gravity anomaly in the area of the Henry Lake gabbro. The drillcore from this hole also intersected a granitic phase inferred to be coeval with the gabbro unit. A sample of the granitic intrusion produced many coarse zircon prisms interpreted to represent an igneous population, and produced an age of  $1772 \pm 10$  Ma (Sparkes *et al.*, 2016). This age is interpreted to represent the emplacement age of the granite, as well as the more voluminous Henry Lake gabbro. As this intrusion is emplaced into rocks of the Heggart Lake Formation, the age of the intrusion further supports the older age of the basal Heggart Lake Formation.

These new ages indicated that parts of the Bruce River Group are significantly older than previously inferred, highlighting the existence of an unrecognized unconformity within the Bruce River Group stratigraphy. To further refine the stratigraphic ages for units within the Bruce River Group,

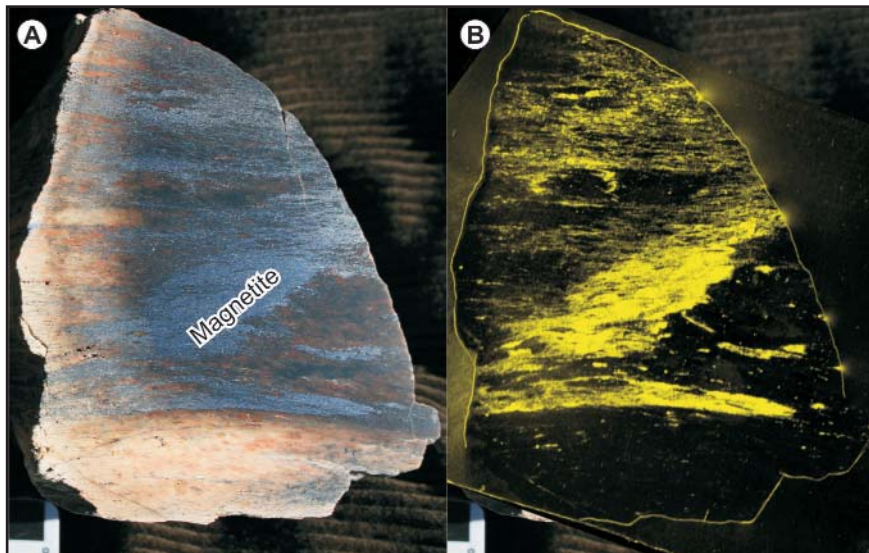


**Plate 111.** A. Uraniferous boulder of felsic metavolcanic rock from the Minisinakwa prospect; sample assayed 0.35%  $U_3O_8$ . B. Corresponding autoradiograph of (A) outlining the distribution of radioactivity within the sample (yellow, minus the outline of the sample); note spatial association between the magnetite alteration and distribution of radioactivity within the sample.



**Plate 112.** Highly sheared, metavolcanic rocks of the Sylvia Lake Formation, hosting anomalous U, Cu, Au, Ag and local fluorite, Stormy Lake prospect.

a tuff unit from the base of the Brown Lake Formation was sampled for geochronological study. This unit produced an age of  $1665 \pm 3.5$  Ma (Sparkes *et al.*, 2016), thus demonstrating the existence of an unconformity between the Heggart Lake and Brown Lake formations of the Bruce River Group.

The felsic metavolcanic rock hosting uranium mineralization at the Minisinakwa prospect was also dated to test its relationship with other volcanic rocks of the Bruce River Group. The sample produced an abundant population of euhedral zircon, which produced a U–Pb age of  $1643 \pm 5$  Ma (Sparkes *et al.*, 2016). This age is similar to the  $1649 \pm 1$  Ma age obtained by Schärer *et al.* (1988), confirming that the metavolcanic rocks in the area do indeed represent part of the Bruce River Group stratigraphy.

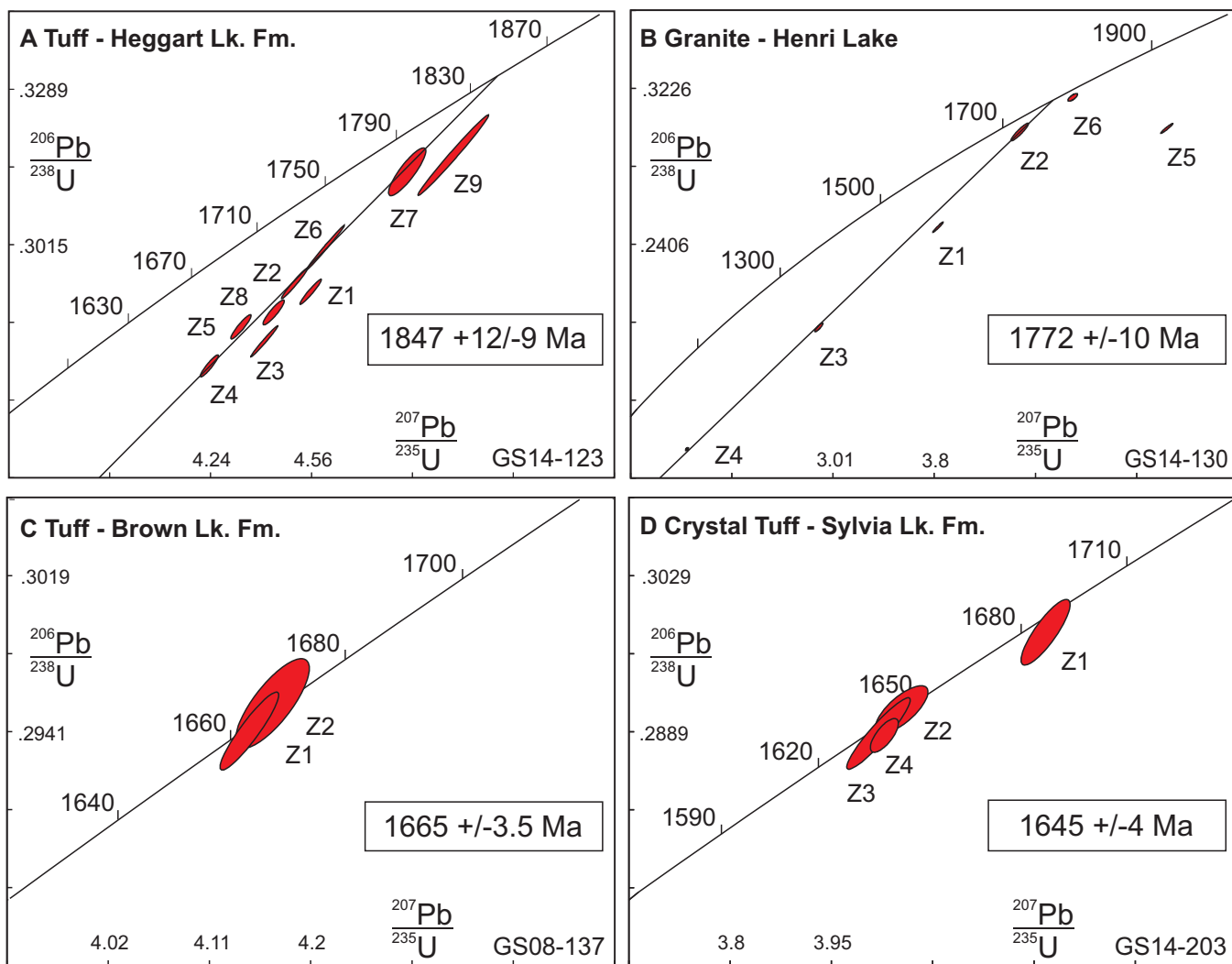


**Figure 59.** Concordia diagrams for U–Pb zircon data from rocks within the Bruce River Group. A. Tuff from the basal Heggart Lake Formation, Lower C Zone deposit, B. Granite intrusion, B Zone prospect, C. Tuff from the basal Brown Lake Formation, Croteau Lake prospect, D. Crystal tuff, Minisinakwa prospect. Note error ellipses are at the  $2\sigma$  level.

## GEOCHEMISTRY

Sandstone-hosted uranium mineralization, within the siliciclastic sedimentary rocks of the Bruce River Group, are commonly associated with the enrichment of Cu and Ag as well as displaying anomalous enrichment in V relative to unmineralized samples (Figure 60). In contrast, the Moran Lake A Zone prospect, which displays a prominent structural control, contains elevated Mo, As and weakly anomalous Au (27 ppb; Figure 60C).

The uranium mineralization developed at the Moran Lake B Zone prospect displays geochemical similarities with the sediment-hosted mineralization such as the local enrichment of Cu, V, Ag and locally Au (Figure 60D; Morgan *et al.*, 2007). The most significant enrichment is restricted to the margins of the dykes; however, the unmineralized central portions of the dykes are also locally observed to contain elevated Cu, V, Ag and Au. This enrichment of the intrusive rocks is unique to the Moran Lake B Zone prospect. In con-

trast, the gabbroic dykes developed in the area of the CVG prospect contain no anomalous enrichment of the above mentioned elements.

The volcanic-hosted mineralization, within the Sylvia Lake Formation, also display a similar enrichment of Ag, Au, and locally Cu and As, but lacks any significant Mo, or V in relation to uranium mineralization. The felsic volcanic rocks of the Bruce River Group commonly contain less than 5 ppm uranium, despite having elevated background radioactivity. Local enrichment within the host volcanic unit (up to 10 ppm) is however observed close to areas of known mineralization, such as near the Madsen Lake occurrences.

## SUMMARY AND DISCUSSION

The sedimentary and volcanic rocks of the Bruce River Group within the western CMB represent one of the youngest environments to host uranium mineralization. The lower portions of this succession host well-developed examples of sed-

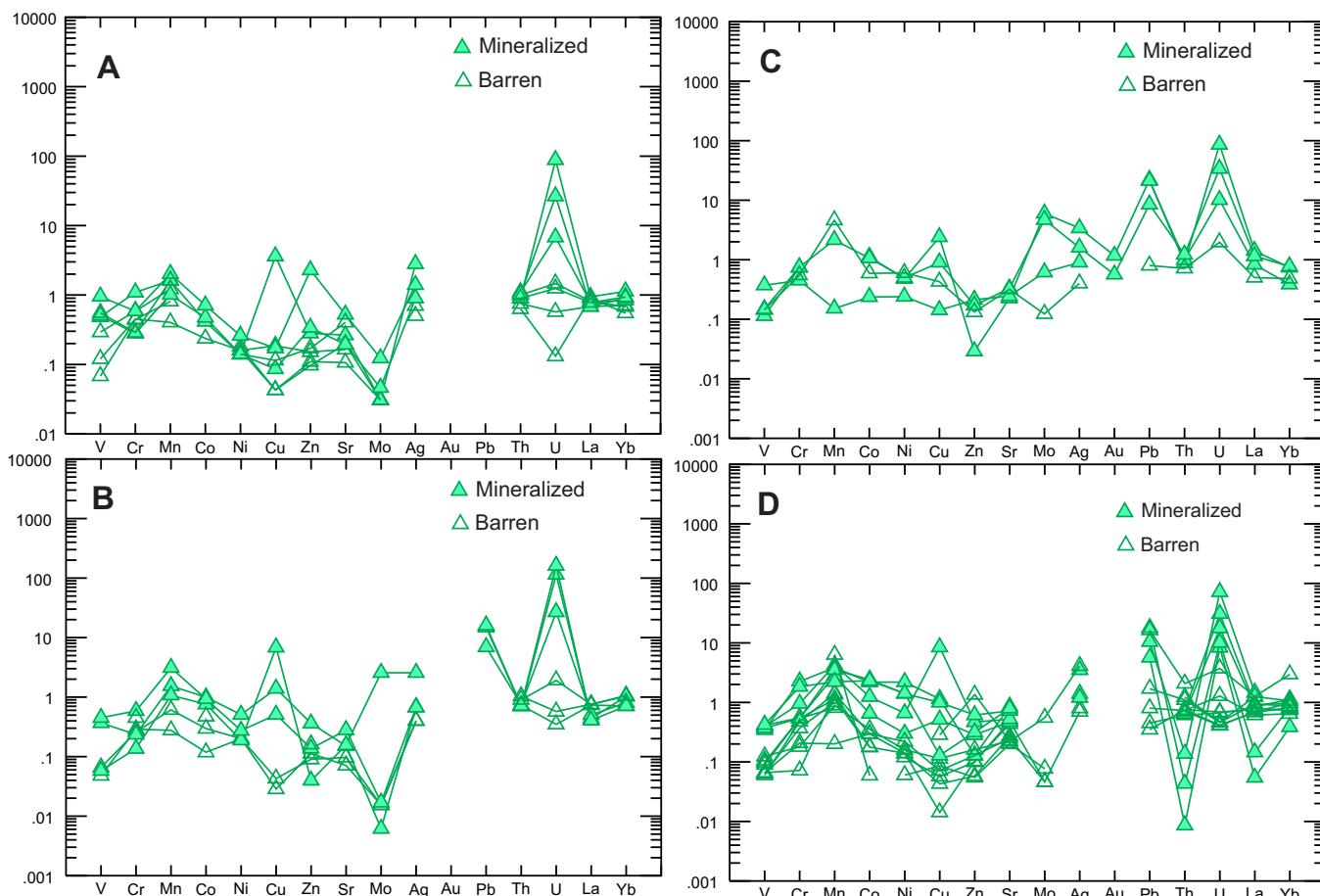


**Figure 60.** Extended trace-element diagrams for sandstone-hosted uranium mineralization within the Bruce River Group. A. Lower C Zone deposit, B. Moran Heights prospect, C. Moran A Zone prospect, D. Moran B Zone prospect. Barren samples contain less than 100 ppm U. Normalizing values are from Quinby-Hunt *et al.* (1989) except for Cu, Ni, Pb, Ag and Mo, which are taken from Vine and Tourtelot (1970).

iment-hosted uranium mineralization, which indicate the presence and circulation of uraniferous fluids within this basin environment. The examples of sediment-hosted uranium mineralization developed at the Moran Lake Lower C Zone deposit and at the Moran Heights prospect, located 7 km to the northeast, demonstrate the regional extent of this mineralizing event. In addition, these fluids, which are commonly enriched in Cu, V, and Ag as well as uranium, represent an alternative source for the enrichment of these elements within the hematite-rich breccias observed within the underlying rocks of the Moran Lake Group (*e.g.*, Moran Lake Upper C Zone).

The timing for the development and circulation of these uraniferous fluids within the Bruce River Group is poorly constrained. However, the mineralized dykes observed at the Moran Lake B Zone prospect are locally associated with the development of pervasive Fe-carbonate alteration similar to that observed in association with development of hematite-rich breccias within the underlying Moran Lake Group (*see* Section, Uranium Mineralization within the Moran Lake Group); as such these two occurrences are inferred to be related to a single mineralizing event.

Absolute age constraints on the development of uranium mineralization within the Bruce River Group are lacking. However, new data provide an older maximum age for the basal Heggart Lake Formation of *ca.* 1850 Ma; minimum age constraints have yet to be determined. For areas such as the Moran Lake C Zone, the C Zone thrust fault, and related structures such as the Lower Shear Zone, are interpreted to postdate the development of the Upper and Lower C zone deposits. These reverse structures are related to the Grenvillian Orogeny (Smyth and Ryan, 1977), and thus provide a potential minimum age constraint on the development of uranium mineralization in this area. The abundance of uranium occurrences with the Heggart Lake Formation, and the relative lack of occurrences within the Brown Lake Formation are also noteworthy, and may imply a pre *ca.* 1665 Ma age for much of the uranium mineralization, but further work is required to fully establish such a relationship. Finally, the occurrence of uranium mineralization within the volcanic rocks of the Sylvia Lake Formation implies a post 1650 Ma age for the volcanic-hosted mineralization, which represents one of the youngest uranium mineralizing events within the region.

## URANIUM MINERALIZATION WITHIN INTRUSIVE ROCKS OF UNDETERMINED AGE

Throughout the CMB, several uranium occurrences are developed within plutonic rocks of an undetermined age; however, these rocks are largely inferred to be *ca.* 1800 Ma or older based on regional mapping. Uranium mineralization

contained within these intrusive host rocks is commonly associated with highly fractured, locally brecciated, variably foliated zones accompanied by hematite  $\pm$  magnetite  $\pm$  chlorite alteration. These zones are interpreted to be largely structurally controlled and are locally associated with the deposition of relatively high-grade uranium mineralization; the most notable of which is the Melody Hill prospect (Figure 61). The prospects discussed in this section were only briefly visited and as a result, data collected for the occurrences is preliminary and subject to change with more detailed investigations.

### MELODY HILL PROSPECT

#### Previous Work

A significant amount of work has been conducted in the area of the Melody Hill prospect due to the presence of high-grade boulders hosting uranium mineralization, which locally assays up to 18.1%  $U_3O_8$  (Davidson, 1978). Rare outcropping mineralization does occur in the area; however, these exposures contain much less significant mineralization in comparison to that contained within the boulders. Exploration carried out in the area since the early 2000s by Aurora Energy has included various geochemical and geophysical techniques along with limited diamond drilling (*e.g.*, humus sampling, ground scintillometer and track etch surveys, Cunningham-Dunlop *et al.*, 2006; gravity survey, Cunningham-Dunlop *et al.*, 2007a; diamond drilling, Barrett *et al.*, 2008), but work in the area has yet to identify the source of the high-grade uraniferous boulders.

#### Local Geology

The area around Melody Lake (Figure 61) is dominated by the Melody Granite, which is composed of strongly foliated granitoid rocks consisting of K-feldspar-rich granodiorite, granite and alkali-feldspar granite, all of which are affected by a widely developed cataclastic to protomylonitic fabric (Kerr, 1994). The granitoid rocks have not been directly dated but are correlated with units farther to the west that have been dated at *ca.* 1890 Ma, and are inferred to be a part of a regional syntectonic Makkovikian magmatic event (Kerr, 1994). The exposures of outcropping mineralization at the prospect consist of albited granite, locally overprinted by structurally controlled hematite–magnetite alteration and brecciation (Smith *et al.*, 2005). In this area, altered granite is locally observed to be juxtaposed with relatively unaltered material of a similar composition, indicating the presence of post-mineral deformation in the area (Plate 113).

#### Mineralization and Associated Alteration

From the limited exposures of the alteration, it is evident that the most intense hematite–magnetite alteration is devel-

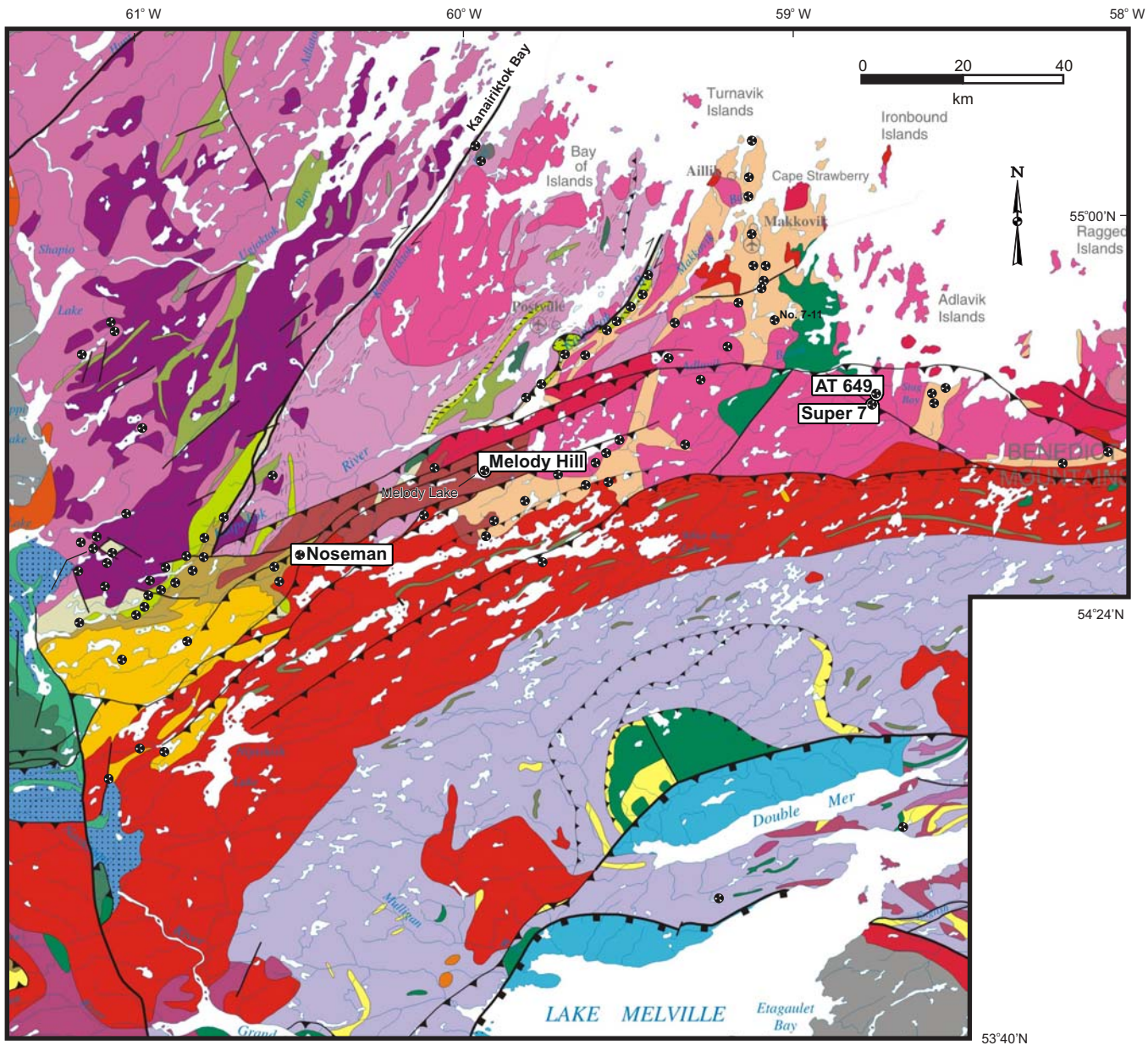


**Figure 61.** Regional geology map outlining the distribution of uranium occurrences within miscellaneous intrusive rocks within the CMB (geological base map modified from Wardle et al., 1997).

oped within the more strongly foliated portions of the host intrusion (Plate 114), indicating an overall structural control on the alteration and associated uranium mineralization. Limited sampling of these zones does not indicate the enrichment of any other elements (aside from uranium) within the hematite–magnetite alteration.

#### AT 649 AND SUPER 7 PROSPECTS

Both the AT 649 and the Super 7 prospects are located in the eastern CMB, within the Benedict Mountains region (Figure 61). This area of the CMB has received far less explo-

ration attention in comparison to the region farther to the west; also these two prospects are the first occurrences of uranium mineralization hosted within intrusive rocks in this part of the CMB.

#### Previous Work

Very limited exploration work for uranium had been carried out in this area prior to that conducted by Silver Spruce Resources in the late 2000s. Initially, the area was targeted on the basis of uranium lake-sediment anomalies, and through follow-up prospecting, two zones of uranium mineralization were

## LEGEND

### NEOPROTEROZOIC

Arkose and conglomerate

### MESOPROTEROZOIC

Gabbro sills (ca. 1250 to 1224)

Subaerial basalt flows

Arkose, grading south into quartzite

Granite plutons (ca. 1296 Ma)

Olivine gabbro and metamorphic equivalents

Granitoid rocks (1500 to 1420 Ma)

Anorthosite and other, locally layered, mafic rocks

Quartz diorite

### PALEOPROTEROZOIC

Rhyolitic to andesitic volcanic rocks including ash-flow tuff and agglomerate (ca. 1650 Ma)

Volcaniclastic sandstone, arkose and conglomerate

Granite, quartz monzonite, granodiorite, syenite and minor quartz diorite (ca. 1650)

Granitoid rocks (1645 to 1626 Ma; including some ca. 1780 to 1720 Ma rocks)

Anorthosite and other, locally layered, mafic components (1645 to 1625 Ma)

Mafic intrusive suites (gabbro, lesser diorite), some metamorphosed as amphibolite to granulite facies

Granodioritic orthogneiss (lesser quartz diorite and granitic orthogneiss (s. l.); may include Mesoproterozoic rocks

Mafic gneiss, probably of supracrustal origin, mainly at granulite facies

Quartz diorite to granodiorite plutons

K-feldspar megacrystic granite and other granitoid plutonic rocks

Pelitic, migmatitic metasedimentary gneiss and minor psammitic gneiss at amphibolite to granulite facies

High-level, locally flourite-bearing granites (1776 to 1719 Ma)

Rhyolite, ash-flow tuff, breccia and hypabyssal rhyolite intrusions; volcaniclastic siltstone and sandstone; minor basalt (ca. 1860 to 1807 Ma)

Granite and granodiorite (1840 to 1795 Ma)

Tonalite, granodiorite and monzogranite gneiss; minor amphibolite, calc-silicate and felsic (metavolcanic ?) gneiss

Gabbro and leucogabbro sills (ca. 1884 to 1874 Ma)

Pillow basalt, basaltic pyroclastic rocks; minor siltstone and greywacke

Schistose amphibolite derived from mafic volcanic rocks (Moran Lake and Post Hill groups)

Granite plutons (ca. 2134 Ma, locally 2032 Ma in the Nain Province; 1973 to 1891 Ma in the Makkovik Province)

Shale and sandstone of shallow- to deep-water origin

Pelitic schist

### ARCHEAN AND/OR PALEOPROTEROZOIC

Anorthosite, leucogabbro, leuconorite and derived gneiss

### ARCHEAN

Tonalitic and other gneisses reworked and retrograded during Makkovikian orogeny

Mafic volcanic and volcaniclastic rocks, lesser sedimentary and felsic volcanic rocks, and mafic-ultramafic sills; at greenschist to amphibolite facies

Granodiorite, tonalite and minor granite (Kanairiktok Intrusive Suite, ca. 2850 to 2830 Ma)

Tonalitic to granodioritic migmatitic orthogneiss containing abundant mafic to ultramafic inclusions and relict mafic dykes

Mafic gneisses including rocks of intrusive and extrusive origin

### SYMBOLS

Geological contact.....



Thrust or reverse fault; (major, minor)....



Thrust fault reactivated as normal fault..



Normal fault; (major, minor).....



Transcurrent fault; (major, minor).....



Fault; (major, minor).....



Ductile shear zone.....



Uranium Occurrence.....



Legend for Figure 61 opposite.



**Plate 113.** Highly fractured and hematite-altered granite juxtaposed against highly fractured, relatively unaltered granite; Melody Hill prospect.



**Plate 114.** Strongly foliated hematite–magnetite alteration developed within outcrop exposures of the Melody Hill Granite; Melody Hill prospect.

discovered, approximately 4 km apart. At the AT 649 prospect, five grab samples collected, over approximately 10 m of outcrop, exposed in a streambed, produced an average of 0.5%  $U_3O_8$ , whereas individual grab samples from the Super 7 prospect have returned values up to 1.0%  $U_3O_8$  (MacGillivray *et al.*, 2008a). Follow-up drilling at the AT 649 prospect failed to intersect any significant mineralization, but drilling at the Super 7 prospect did intersect weakly mineralized zones of uranium mineralization from which the highest assay returned 0.05%  $U_3O_8$  over 3 m (MacGillivray *et al.*, 2009).

### Local Geology

Mineralization at the AT 649 prospect is hosted within a fine- to medium-grained, biotite-bearing granodiorite, locally containing abundant fine-grained mafic xenoliths; this unit is inferred to be correlative with the *ca.* 1800 Ma Stag Bay granodiorite of Kerr (1994). The granodiorite is locally intruded by fine-grained, biotite-bearing granite that locally contain elevated background levels of uranium (up to 24 ppm).

Drilling demonstrates that both the granodiorite and biotite-bearing granite are locally deformed by discrete, moderately to strongly sheared and rarely mylonitic, fault structures. In addition, localized brecciation, developed close to outcropping mineralization, is associated with extensive chlorite and carbonate alteration along with the presence of magnetite, hematite and lesser pyrite (MacGillivray *et al.*, 2008a).

At the Super 7 prospect, the host intermediate to granitic intrusive rocks are inferred to be correlative with the Big River Granite (MacGillivray *et al.*, 2008a), which has locally been dated at  $1802 \pm 2$  Ma (Kerr *et al.*, 1992). The main host rock to the anomalous uranium mineralization is fine-grained, biotite-bearing granite similar to that observed at the AT 649 prospect. The granite is mostly undeformed, but contains localized high-strain zones that are roughly subparallel to a regionally extensive east–west-trending high-angle reverse or thrust fault located farther to the south (MacGillivray *et al.*, 2008a) known as the Benedict Fault (Gower, 1980). Detailed mapping in the area of the Super 7 prospect has identified a major northeast-trending shear structure, believed to be a splay related to the larger scale regional faults in the area, along which local uranium and base-metal mineralization is developed (MacGillivray *et al.*, 2008a). This northeast-trending shear structure is also inferred to be the same structure hosting uranium mineralization at the AT 649 prospect farther to the northeast (MacGillivray *et al.*, 2008a).

### Mineralization and Associated Alteration

The zone of uranium mineralization exposed along the stream bed at the AT 649 prospect is associated with the development of locally intense hematite–magnetite alteration (Plate 115). This alteration is not associated with the enrichment of any other elements aside from uranium, as noted at the Melody Hill prospect. From the autoradiograph shown in Plate 115, it is evident that the finely disseminated radioactivity within the sample is primarily concentrated within hairline fractures, which provides supporting evidence for the overriding structural control on mineralization. The hematite alteration associated with mineralization is locally overprinted by later epidote–chlorite veining, which represents one of the few features observed to postdate the uranium mineralization.

Drilling in the area of the Super 7 prospect intersected weak mineralization (Plate 116) associated with variably sheared, biotite-rich zones within a muscovite-rich leucogranite (MacGillivray *et al.*, 2008a). Within these zones, petrographic observations indicate that the uranium mineralization is associated with the development of brittle hairline fractures, which also hosts magnetite, biotite and allanite, along with traces of fluorite.

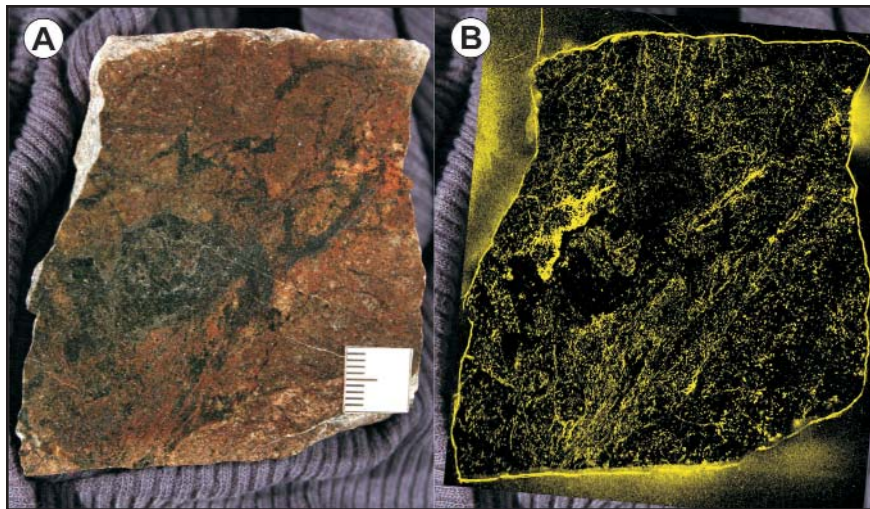


**Plate 115.** A. Hematite–magnetite-altered granodiorite containing 0.61%  $U_3O_8$ . B. Autoradiograph of (A) outlining the distribution of radioactivity within the sample (yellow, minus the outline of the sample); AT 649 prospect.

## NOSEMAN PROSPECT

The Noseman prospect was discovered in 2006 (Willett *et al.*, 2007a), and subsequently expanded upon in 2008 by Mega Uranium Ltd. (Gilman *et al.*, 2009). The mineralized zone has a predominant northeast trend, and is hosted within intrusive rock inferred to be correlative with the Junior Lake Granodiorite of Ryan (1984), dated at  $1891 \pm 5$  Ma (Kerr *et al.*, 1992). Uranium mineralization at the prospect is hosted within a cataclastic fault zone that contains subrounded to subangular fragments of the host granitoid within a chloritic matrix (Plate 117). This zone of structurally controlled mineralization forms a steep, southeasterly dipping northeasterly trending zone that has been traced along strike for up to 200 m and is locally up to 50 m in width; assays from the zone

have produced values of up to 0.29%  $U_3O_8$  (Gilman *et al.*, 2009). The best results obtained from the limited diamond drilling at the prospect include values of up to 0.13%  $U_3O_8$  over 1.0 m (Gilman *et al.*, 2012), and indicates the uranium mineralization is sporadic at depth.

## GEOCHEMISTRY

The Melody Hill Granite is noted to be a largely peraluminous, calc-alkaline unit that displays significantly lower F, Zn, high-field strength and rare-earth elements relative to other syntectonic Makkovikian granitoid rocks (Kerr, 1994); however, the limited sampling undertaken indicates that the granite in the immediate area of the prospect primarily plots within the metaluminous field. Similarly, both the granite and granodiorite in

the area of the AT 649 and Super 7 prospects are also metaluminous, calc-alkaline intrusions. Samples of relatively unaltered granite from all three of the prospects mentioned above locally contain background uranium values of between 20–40 ppm U. If these values represent the primary uranium contents of these intrusions, and have not been enriched during subsequent processes, then they would represent some of the most uranium-enriched syntectonic intrusions in the region.

## SUMMARY AND DISCUSSION

The occurrences mentioned here represent discrete zones of structurally controlled uranium mineralization hosted within intrusive rocks. Locally, *e.g.*, Melody Hill prospect, these zones have been the focus of much attention due to the presence of boulders containing very high grades of uranium mineralization; however, the drilling conducted in these areas has only discovered mineralization of limited extent. The development of hematite alteration in association with uranium mineralization is a common characteristic associated with this style of mineralization, but not all occurrences appear to contain associated magnetite alteration. Those that do contain magnetite demonstrate small-scale linear magnetite anomalies, which is inferred to highlight the overall structural control on the development of the alteration associated with the uranium mineralization. The structurally controlled nature of the mineralization is further highlighted by the fact that the mineralized zones are associated with discrete structures, and that the host intrusions display variably foliated or brecciated textures.

Limited geochemical sampling indicates the presence of intrusions containing elevated background levels of uranium;



**Plate 116.** Weakly mineralized, variably foliated, locally hematite-altered intrusive unit; Super 7 prospect (DDH MBS7-08-05, ~50 m depth); white labels denote counts per second.

these intrusions could potentially represent the source rocks for the uranium mineralization developed within the structures, however, further sampling is required. Limited investigations into the distribution of the uranium within mineralized structures indicate that the mineralization is relatively unaffected by this deformation, suggesting a late syn-to post-deformational timing. As there is limited geochronological control on the host rocks as well as the development of uranium mineralization, no firm age bracket can be placed on this style of mineralization, and it is doubtful that all three areas mentioned in this section are linked to a single mineralizing event.

## DISCUSSION AND CONCLUSION

The objective of this project was to provide a compilation of existing data for the various styles of uranium mineralization present throughout the CMB, and to incorporate the most recent developments stemming from mineral exploration

since the early 2000s. Although questions remain, this report provides new data that allows for a better understanding of the uranium mineralization. The following highlights the main outcomes of this study and some remaining issues that require further follow-up.

## SUBDIVISION AND CLASSIFICATION OF URANIUM MINERALIZATION

The division of the uranium occurrences within the CMB remains broad in scope in order to accommodate the diverse formation environments hosting uranium mineralization. Three main categories have been proposed by Sparks and Kerr (2008) and these are used to subdivide the uranium occurrences. A location table, summarizing the main host rock and the style of mineralization observed during this study is included in Appendix F. The classification system subdivides the occurrences into magmatic, metamorphic-metasomatic and sedimentary formation environments.

However, it should be noted that several of these groupings contain a broad range of uranium occurrences that in all likelihood could be further subdivided after more detailed study.

### Magmatic-related Mineralization

Magmatic-related styles of uranium mineralization within the CMB are generally minor, with the exception of the Moran Lake Upper C Zone deposit. Pegmatite-hosted mineralization developed within the Archean basement rocks represent a viable regional exploration target, most notably in areas where mineralized dykes occur within major structural zones such as the Kanairiktok Shear Zone (e.g., Dandy and Kanairiktok prospects). Pegmatite dykes hosting uranium mineralization have yet to be dated directly in the region, but in the eastern CMB, mineralized pegmatite dykes are inferred to be coeval with pegmatite dykes dated at *ca.* 1870 Ma (Sparks and Kerr, 2008), and thus potentially represent some of the earliest uranium mineralization identified in the region.

The Moran Lake Upper C Zone deposit, and the nearby B Zone prospect, display several characteristics indicative of IOCG-style mineralization, such as the development of iron oxide-rich breccias in association with extensive alkali (Ca,

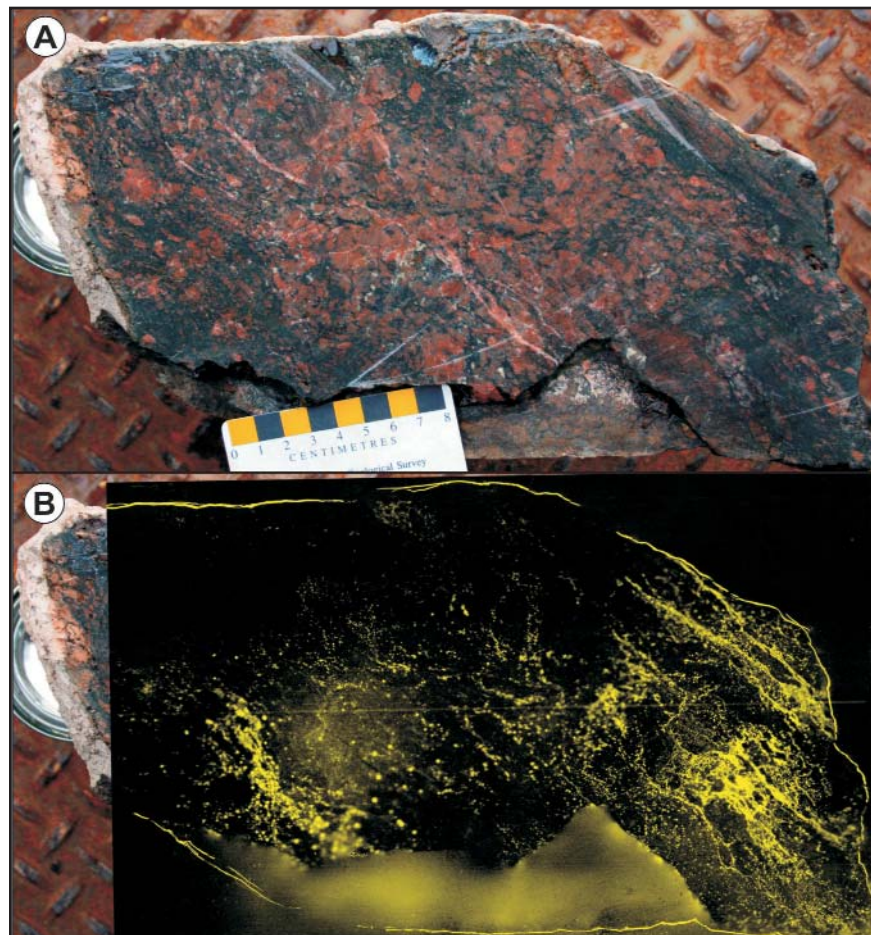


**Plate 117.** A. Cataclastic breccia developed within granodiorite, displaying moderate hematization, B. Autoradiograph of (A) outlining the distribution of radioactivity within the sample (yellow, minus the outline of the sample); Noseman prospect.

Na) metasomatism. Mineralized breccias of the Moran Lake Upper C Zone deposit are consistently elevated in V and also contain local enrichment of U, and lesser Cu and Ag. The development of similar styles of alkali metasomatism in siliciclastic sedimentary rocks adjacent to intermediate intrusive rocks in the area of the B Zone prospect suggests a genetic link with the nearby Upper C Zone deposit. The intermediate dykes associated with mineralization in the area of the B Zone prospect have yet to be dated directly and represent a possible target for future studies in the region.

Felsic volcanic rocks of the Sylvia Lake Formation, as well as those rocks correlated with the Aillik Group in the Benedict Mountains, host several occurrences of volcanic-hosted uranium mineralization, which are inferred to be largely derived from the host volcanic succession, and therefore interpreted to be magmatic in origin. This mineralization is inferred to have been remobilized from the surrounding volcanic succession into permeable fault structures as well as along the margins of mafic dykes that intrude these rocks; this mineralization generally lacks any significant alteration aside from minor hematization of the adjacent wall rock. In the Benedict Mountains, the host volcanic rocks have been dated at *ca.* 1855 Ma, whilst the host rocks of the Sylvia Lake Formation are locally dated at *ca.* 1650 Ma. Despite their distinctly different ages, these two areas display very similar styles of uranium mineralization. One exception to this is at the Minisinakwa prospect, where strongly foliated felsic volcanic rocks host hematite–magnetite alteration in association with uranium mineralization. This mineralization displays some similarities with that developed at the Stormy Lake prospect, most notably the association of mineralization with strongly deformed volcanic rocks, and may have links with Grenvillian deformation.

### Metamorphic–Metasomatic-related Mineralization

This style of mineralization encompasses the most number of occurrences within the CMB, some of which are known to be of contrasting age, and in all likelihood this group could be further subdivided after more detailed study. The mineralization contained within this group includes cataclastic-breccia-hosted mineralization within the Two-Time Trend, the Kitts deposit and related occurrences along the Post Hill Trend, as well as the Michelin and Jacques Lake deposits. In addition, the intrusive-hosted mineralization (e.g., Melody Hill prospect) is also included within this group. Most, if not all, of the examples contained within this group display an overriding structural control with respect to the development of uranium mineralization. The origin and nature of the mineralizing fluids related to the various mineralizing events are inferred to be at least partially related to metamorphic events, which in some cases can be bracketed based on existing U–Pb geochronology.

Cataclastic-breccia-hosted mineralization within Archean basement rocks has many visual similarities to breccias developed in the Moran Lake Upper C Zone deposit. However, the breccias developed within the Archean basement lack significant alkali metasomatism, and are interpreted to have a structural, rather than a hydrothermal, origin. In detail, this style of mineralization shares many similarities with the *ca.* 1800-Ma intrusion-hosted, structurally controlled mineralization, which also displays hematite and chlorite alteration in association with the local development of cataclastic brecciation. Within the Archean basement rocks, the structure hosting mineralization along the Two-Time Trend is assumed to be Paleoproterozoic or younger on the basis of field mapping. Absolute age constraints for the mineralization in this area are lacking, but local dykes crosscutting the mineralization represent obvious targets for future studies.

High-grade uranium mineralization at the Kitts deposit represents some of the oldest mineralization in the region having a minimum age of *ca.* 1880 Ma (Sparkes *et al.*, 2008). This style of mineralization is inferred to be developed within a structural corridor which, on a regional scale, defines the boundary between the Post Hill Group and the structurally overlying Aillik Group. Given the U–Pb age constraints and overriding structural control on the mineralization, its formation is inferred to be linked with the D<sub>1</sub> deformational event, locally dated at *ca.* 1896 Ma, identified by Ketchum *et al.* (1997). The mineralization within the Post Hill Group developed along this structural zone commonly displays isoclinal folding as indicated by autoradiographs, thus indicating the presence of postmineral deformation. However, to what degree this deformation has remobilized the uranium mineralization within the structural corridor has yet to be determined.

Mineralization developed along the Post Hill Trend contrasts with that developed in the Michelin–Jacques Lake area, with the former lacking of any significant alteration associated with the development of uranium mineralization. In addition, mineralization developed within the Post Hill Group locally displays enrichment of Cu, Zn, Ag, and V along with anomalous Au and locally Mo, which further distinguishes it from mineralization observed within the area of the Michelin and Jacques Lake deposits. This metal enrichment is inferred to be linked to the rocks hosting the mineralization along the Post Hill Trend, as is locally observed within mineralization developed in the Warren Creek Formation of the Moran Lake Group.

Within the Aillik Group, the development of albite-type mineralization represents one of the most economically significant styles of mineralization within the CMB. This style of metamorphic–metasomatic mineralization is currently bracketed between *ca.* 1860 and 1800 Ma, based on existing geochronological data, which broadly overlaps the *ca.*

1900–1700 Ma Makkovikian Orogeny (Hinchey and LaFlamme, 2009 and references therein). However, as seen within the Michelin deposit, subsequent remobilization of the uranium mineralization is evident based on U–Pb data from titanite, which highlight the presence of Grenvillian-related events overprinting the mineralization. This *ca.* 1000 Ma event is likely related to the extensional collapse of the Grenvillian Orogeny (Rivers *et al.*, 2002). The full effect of this deformational event, on the overall development of the deposit, is not yet fully understood and requires further study. However, mineralizing events of a similar age have been identified elsewhere in Labrador, and in adjacent Québec (Crocker, 2014; Clark, *et al.*, 2005), suggesting this period has some regional significance with respect to the development of mineralization in the region.

### Sediment-hosted Mineralization

This style of mineralization is primarily confined to units of the Bruce River Group, but minor occurrences are also locally developed within sedimentary rocks of the Moran Lake Group. The main occurrence within the Moran Lake Group is the Area 51 prospect. Here, a dolostone unit, immediately overlying Archean basement rocks, is host to anomalous radioactivity near its upper contact with overlying black shale. This mineralization is inferred to be associated with the circulation of uraniferous fluids within the sedimentary sequence; however, the timing of the mineralization remains unknown.

Sediment-hosted mineralization within the Bruce River Group is much more significant, and locally contains a defined NI 43-101 resource (*e.g.*, Moran Lake Lower C Zone). This style of mineralization is primarily restricted to the *ca.* 1850 Ma Heggart Lake Formation (Sparkes *et al.*, 2016), and displays many characteristics of typical sandstone-hosted uranium mineralization; the most notable of which is its development in association with reduced zones in an otherwise oxidized, sedimentary sequence. No true examples of unconformity-style mineralization have yet been identified in the region, and most sediment-hosted occurrences display a spatial association with regional fault structures. Minimum age constraints are lacking and represent a logical focal point for later studies in the region.

### CONCLUSIONS

The CMB of Labrador is host to several different styles of uranium mineralization. This mineralization is contained within a variety of geological environments and has developed over a long period of time. Existing U–Pb geochronological data brackets the uranium mineralization into four main events. In eastern CMB, uranium mineralization is primarily bracketed between 2030–1880 and 1860–1800 Ma. In the west, uranium mineralization is bracketed between

1860–1660, and later than 1650 Ma. In addition, U–Pb data obtained from titanite and monazite separates provide evidence for syn- to post-mineral deformational events, which include the Makkovikian (1900–1710 Ma), Labradorian (1710–1620 Ma) and Grenvillian (*ca.* 1000 Ma) orogenies. Such deformation has locally resulted in the remobilization of uranium mineralization, but the full extent of these effects remains uncertain.

The different styles of uranium mineralization display some commonalities, and can be broadly grouped, with respect to their host rock, style of mineralization, and associated alteration. The broad subdivisions of this mineralization include that associated with the magmatic, metamorphic–metasomatic and sedimentary environments. Mineralization related to the magmatic and metamorphic–metasomatic environments represent some of the most significant examples with respect to the overall areal extent of the related mineralizing systems and the contained uranium resource. Such examples include the Moran Lake Upper C Zone in the western CMB, where calcium and sodium metasomatism and related hematitic breccias can be traced intermittently along strike for upward of 10 km. In the more eastern CMB, such examples include the Kitts–Post Hill Trend, where structurally controlled mineralization can be traced intermittently for up to 15 km along strike. Furthermore, the well-known Michelin deposit is associated with the development of an extensive zone of sodic alteration related to the formation of the uranium deposit, which has yet to be fully evaluated.

The development of such systems highlights the uranium potential of the region, which remains an attractive target for future exploration. However, given the locally extensive Quaternary cover developed within the CMB, future exploration will have to move from the follow-up of airborne radiometric anomalies to more model-driven exploration techniques in order to target prospective areas of the region that are poorly exposed.

### ACKNOWLEDGMENTS

During this project I have had the pleasure of working with several field assistants. I would like to thank Justin Quinton, Ross Bowers, Matthew Spencer, Dylan Abbott and Mark Grant for enthusiastic support and hard work in the field, often in less than ideal conditions. Many fruitful discussions with various company geologists, whom there are too many to mention, during my visits to the various exploration camps throughout the CMB, greatly aided in my understanding of region. Wayne Tuttle is thanked for his efficient work and problem-solving skills in resolving logistical issues. Andy Kerr reviewed earlier versions of the manuscript and his recommendations greatly improved the content of this document, in addition a critical review by John Hinchey refined the clarity of the report.

## REFERENCES

Bailey, D.G.  
1979: Geology of the Walker-MacLean Lake area, 13K/9, 13J/12, Central Mineral Belt, Labrador. Government of Newfoundland and Labrador, Department of Mines and Energy, Mineral Development Division, Report 78-3, 17 pages.

Barua, M.C.  
1969: Geology of uranium-molybdenite bearing rocks of the Aillik-Makkovik Bay area, Labrador. Unpublished M.Sc. thesis, Queen's University, Kingston, Ontario, Canada, 76 pages.

Barr, S.M., White, C.E., Culshaw, N.G. and Ketchum, J.W.F.  
1997: Petrology, age and tectonic setting of the Island Harbour Bay Plutonic Suite, Makkovik Province, Labrador: Preliminary results. In *Eastern Canadian Shield Onshore-Offshore Transect (ECSOOT)*. Compiled by R.J. Wardle and J. Hall. Transect Meeting (April 14-15, 1997). Report 61, pages 12-24.

Barrett, S. and Ash, S.  
2009: Sixth year assessment report on diamond drilling exploration for licence 9412M on claims in the Ranjan Lake area, central Labrador. Newfoundland and Labrador Geological Survey, Assessment File LAB/1527, 441 pages.

Barrett, S., Barbour, D. and Glover, J.  
2008: Fifth year supplementary assessment report on diamond drilling exploration for licence 9482M on claims in the Melody Hill area, eastern Labrador. Newfoundland and Labrador Geological Survey, Assessment File LAB/1524, 65 pages.

Basham, I.R.  
1981: Some applications of autoradiographs in textural analysis of uranium-bearing samples—a discussion. *Economic Geology*, Volume 76, pages 974-982.

Beavan, A.P.  
1958: Report on the Kits uranium project, Labrador. Newfoundland and Labrador Geological Survey, Assessment File 13J/0025, 1958.

Beavan, A.P., Clarke, W.B. and Gandhi, S.S.  
1974: Helium survey of lake waters in the Kaipokok Bay-Big River area, Labrador. Newfoundland and Labrador Geological Survey, Assessment File 13J/0128, 28 pages.

Beavan, A.P. and Myer, W.T.  
1968: Report on exploration for the Brinex/Metallgesellschaft A G joint venture in the Kaipokok-Big River area, Labrador. Newfoundland and Labrador Geological Survey, Assessment File LAB/0211, 1968.

Bernazeaud, J.  
1965: Progress report for 1965 of the uranium project in Labrador. Newfoundland and Labrador Geological Survey, Assessment File LAB/0041.

Brummer, J.J. and Mann, E.L.  
1961: Geology of the Seal Lake area, Labrador. *Geological Society of America Bulletin*, Volume 72, pages 1361-1382.

Busch, D.J., Darch, D., Willy, A.J. and Woolham, R.W.  
1979: Annual report for 1979, comprising reports A79001-summary, G79008-Mustang-McLean Lake, G79009-Rainbow zone, G79010-Irving Zone, Mustang Lake, P79009 and P79002 Mustang Lake, for exploration in the Mustang-McLean lakes area, Labrador. Newfoundland and Labrador Geological Survey, Assessment File 13J/0195, 450 pages.

Cadman, A.C., Heaman, L., Tarney, J., Wardle, R. and Krogh, T.E.  
1993: U-Pb geochronology and geochemical variation within two Proterozoic mafic dyke swarms, Labrador. *Canadian Journal of Earth Sciences*, Volume 30, Number 7, pages 1490-1504.

Chaulk, D.  
1979: The Heggart Lake Formation, Bruce River Group, Moran Lake area [13K/7, 10], Labrador. Government of Newfoundland and Labrador, Department of Mines and Energy, Mineral Development Division, Report 79-01, pages 95-102.

Clark, A.M.S.  
1973: A reinterpretation of the stratigraphy and deformation of the Aillik Group, Makkovik, Labrador. Ph.D. thesis, Memorial University of Newfoundland, St John's, Newfoundland, 380 pages.  
1979: Proterozoic deformation and igneous intrusions in part of the Makkovik subprovince, Labrador. *Precambrian Research*, Volume 10, pages 96-114.

Clark, T., Gobeil, A. and David, J.  
2005: Iron oxide-copper-gold-type and related deposits in the Manitou Lake area, eastern Grenville Province,

Quebec: Variations in setting, composition, and style. Canadian Journal of Earth Sciences, Volume, 42, pages 1829-1847.

Collins, J.E.  
1958: Geological report on Ferguson-Brown Lakes area, Labrador. Newfoundland and Labrador Geological Survey, Assessment File 13K/0028, 37 pages.

Cook, B.J.  
1980: Re-evaluation of geology and uranium mineralization, C zone, Moran Lake property, Central Mineral Belt, Labrador. Newfoundland and Labrador Geological Survey, Assessment File 13K/07/0274, 76 pages.

Corriveau, C.R.  
1958: Report on the Montague No. 2 uranium prospect, Silas Lake area, Kaipokok Concession. Unpublished BRINEX Limited company report.

Crocker, M.  
2014: A petrographic, geochemical, and geochronological study of rare earth element mineralization in the Red Wine Intrusive Suite, Labrador, Canada. Unpublished M.Sc. thesis, Memorial University of Newfoundland, Canada, 193 pages.

Culshaw, N. and Ketchum, J.  
1995: The Kaipokok zone of the Makkovik orogen – an early Proterozoic terrane boundary? In Eastern Canada Shield Onshore-Offshore Transect (ECSOOT), Report of the 1994 Transect Meeting. Complied by R.J. Wardle and J. Hall. The University of British Columbia, Lithoprobe Secretariat, Lithoprobe Report 45, pages 7-21.

Culshaw, N., Ketchum, J. and Barr, S.  
2000: Structural evolution of the Makkovik Province, Labrador, Canada: Tectonic processes during 200 Myr at a Paleoproterozoic active margin. Tectonics, Volume 19, No. 5, pages 961-977.

Culshaw, N.G., Ketchum, J.W.F., Barr, S. and Sinclair, G.  
1998: A history of the Makkovik Province. In Eastern Canadian Shield Onshore-Offshore Transect (ECSOOT), Report of the 1998 Transect Meeting. Complied by R.J. Wardle and J. Hall. The University of British Columbia, Lithoprobe Secretariat, Lithoprobe Report 68, pages 20-37.

Culshaw, N., Reynolds, P., Sinclair, G. and Barr, S.  
2002: Amphibole and mica  $^{40}\text{Ar}/^{39}\text{Ar}$  ages from the Kaipokok and Aillik domains, Makkovik Province, Labrador; towards a characterization of back-arc processes in the Paleoproterozoic. Canadian Journal of Earth Science, Volume 39, pages 749-764.

Cunningham-Dunlop, I., Barbour, D., Buschman, A., Howson, S., King, M., Lennox-King, M., Trevors, M., Valenta, R., Wilton, D., Hannan, K., Farquhar, E. and Smith, R.  
2006: First year supplementary, second year and third year assessment report on geological, geochemical, geophysical and diamond drilling exploration for licences 9410M-9415M, 9482M, 9718M-9723M, 10022M, 10046M-10056M, 10058M-10059M, 10343M-10344M and 10726M on claims in the Kaipokok Bay area, northeastern Labrador, 5 reports. Newfoundland and Labrador Geological Survey, Assessment File LAB/1415, 906 pages.

Cunningham-Dunlop, I., Barbour, D., Buschman, A., Howson, S., Lepore, W., Lennox-King, M., Trevors, M., Woodhouse, J., Scott, W.J., Mauler, A., Thompson, A.J.B. and Ross, K.  
2007a: Second year, second year supplementary, third and fourth year assessment report on geological, geochemical, geophysical and diamond drilling exploration for licences 9410M, 9412M-9413M, 9482M, 10046M-10047M, 10050M-10051M and 10343M on claims in the Kaipokok Bay area, northeastern Labrador, 6 reports. Newfoundland and Labrador Geological Survey, Assessment File LAB/1550, 2284 pages.

Cunningham-Dunlop, I., Buschman, A., Lepore, W., Lennox-King, M. and Ross, K.  
2007b: Third year assessment report on diamond drilling exploration for licence 10343M on claims in the Aurora River area, near Postville, eastern Labrador, 2 reports. Newfoundland and Labrador Geological Survey, Assessment File 13J/12/0279, 174 pages.

Cunningham-Dunlop, I., Conaghan, E., Buschman, A., Lennox-King, M. and Savidant, S.  
2008a: Fifth year assessment report on diamond drilling exploration for licence 14457M on claims in the Inda Lake area, northeastern Labrador. Newfoundland and Labrador Geological Survey, Assessment File 13J/13/0288, 263 pages.

Cunningham-Dunlop, I., Buschman, A., Lepore, W., Lennox-King, M. and Savidant, S.  
2008b: Fourth year assessment report on diamond drilling exploration for licence 10051M on claims in the Jacques Lake area, eastern Labrador. Newfoundland and Labrador Geological Survey, Assessment File 13J/0287, 465 pages.

Cunningham-Dunlop, I.R. and Giroux, G.H.  
2007: The exploration activities of Aurora Energy Resources Inc. on the CMB uranium property, Labrador, Canada, during the period of January 2006 to January 2007. NI 43-101F1 Technical Report, 223 pages.

Cunningham-Dunlop, I.R. and Lee, C.  
 2008: An update on the exploration activities of Aurora Energy Resources Inc. on the CMB uranium property, Labrador, Canada, during the period of January 1, 2007 to December 31, 2007. NI 43-101F1 Technical Report, 216 pages.

Darch, D.  
 1979: Annual report for 1979, comprising reports A79001-summary, G79008-Mustang-Mclean Lake, G79009-Rainbow zone, G79010-Irving Zone, Mustang Lake, P79009 and P79002 Mustang Lake, for exploration in the Mustang-McLean lakes area, Labrador. Newfoundland and Labrador Geological Survey, Assessment File 13J/0195, 450 pages.  
 1981: Report on examination of new prospects in the McLean Lake and Kitts belt areas of Area A, Labrador. Newfoundland and Labrador Geological Survey, Assessment File 13J/0204, 1981.

Darch, W., Davidson, G.I. and Willy, A.J.  
 1979: Annual report for exploration in 1979 in area B, exclusive of Melody Hill area, Labrador. Newfoundland and Labrador Geological Survey, Assessment File LAB/0464, 197 pages.

Davidson, G.I.  
 1978: Summary of exploration activities for 1978 on the Melody Hill prospect Area B, Labrador. Newfoundland and Labrador Geological Survey, Assessment File LAB/0431, 1978.

Davidson, D.D. and Kowalczyk, P.  
 1979: Report of the geology of an area within the Benedict Mountains, Labrador. Newfoundland and Labrador Geological Survey, Assessment File 13J/0199, 1979, 48 pages.

Davidson, G.I., Evans, D.F. and Srivastava, P.  
 1978: Revised drill logs for the Kitts deposit, Labrador. Newfoundland and Labrador Geological Survey, Assessment File LAB/0433.

Davis, D.W.  
 1982: Optimum linear regression and error estimation applied to U-Pb data. Canadian Journal of Earth Sciences, Volume 19, pages 2141-2149.

Eaton, S.J., Morgan, J., Carriere, D., Cochrane, A., Caceres, R., Scott, W.J., McDowell, S., Wilton, D.H.C., Ross, K., Lacroix, P.A. and Cook, R.B.  
 2008: First and second year, second year supplementary and third, fourth and sixth year assessment report on geological, geochemical, geophysical and diamond drilling exploration for licences 9781M, 9783M, 10367M-10368M, 10715M-10720M, 10722M-10723M, 11395M, 11770M, 11833M-11835M, 12616M-12618M, 13427M and 13634M-13635M on claims in the Moran Lake - Otter Lake area, central Labrador, 14 reports. Newfoundland and Labrador Geological Survey, Assessment File 13K/0329, 5268 pages.

Ellingwood, S.G.  
 1958: Report on the geology of the Moran Lake area in the Kaipokok concession, Labrador. Newfoundland and Labrador Geological Survey, Assessment File 13K/0023, 24 pages.

Ermanovics, I.  
 1992: Geology, Southern Hopedale Block, Labrador, Newfoundland. Geological Survey of Canada, Map 1669A, scale 1:100,000.  
 1993: Geology of Hopedale Block, southern Nain Province, and the adjacent Proterozoic terranes, Labrador, Newfoundland. Geological Survey of Canada, Memoir No. 431, 161 pages.

Evans, D.  
 1980: Geology and petrochemistry of the Kitts and Michelin uranium deposits and related prospects, Central Mineral Belt, Labrador. Unpublished Ph.D. thesis, Queen's University, Kingston, Ontario, Canada, 311 pages.

Fox, D. and Wallis, S.  
 2012: Sixth year assessment report on prospecting and geochemical, geophysical and diamond drilling exploration for licences 16820M-16821M, 18130M-18131M and 18567M on claims in the Kanairiktok River and Jacques Lake areas, east-central Labrador. Newfoundland and Labrador Geological Survey, Assessment File LAB/1651, 483 pages.

Fraser, D.  
 2010: First and fourth year assessment report on geological, geochemical and geophysical exploration for licences 10456M, 11370M, 11374M and 16258M on claims in the Boiteau Lake area, central Labrador. Newfoundland and Labrador Geological Survey, Assessment File 13K/0331, 157 pages.

Fraser, R.D. and Giroux, G.H.  
 2009: The Anna Lake uranium project, Central Mineral Belt, Labrador, Canada. September 30, 2009. NI 43-101F1 Technical Report, 94 pages.

Fraser, D., Thomas, A., Dupre, D., Galbraith, C., Prikhodko, A., Mouge, P., D'Amours, I. and Largeaud, J.

2008: First and second year assessment report on geological, geochemical, geophysical and diamond drilling exploration for licences 10391M-10392M, 10456M, 11370M-11379M, 11394M, 11510M-11513M, 11591M, 11598M, 11605M, 11942M-11945M, 12249M-12253M, 12465M, 12517M, 12799M, 12802M, 12806M, 12811M-12812M, 12817M, 12823M, 13176M-13177M, 13321M, 13337M, 13361M, 14761M-14763M, 14766M, 14768M-14774M, 14778M, 14785M-14786M, 14788M-14793M, 14795M, 14799M and 14832M on claims in the Mistinippi Lake - Nipishish Lake - Kanairiktok Bay area, east-central Labrador, 5 reports. Newfoundland and Labrador Geological Survey, Assessment File LAB/1553, 1009 pages.

Fraser, D., Thomas, A., Galbraith, C., Charlton, J. and Owen, J.

2009: Third year assessment report on geological, geochemical, geophysical and diamond drilling exploration for licences 11370M-11371M, 11374M-11377M, 11379M, 11510M-11511M, 11598M, 12517M, 14761M-14763M, 14766M, 14789M, 14793M, and 15776M-15777M on claims in the Nipishish Lake - Kanairiktok Bay area, east-central Labrador, 3 reports. Newfoundland and Labrador Geological Survey, Assessment File LAB/1490, 945 pages.

Froude, T., Roscoe, W.E., Cook, R.B., Wilton, D., Honarvar, P., Bowslaugh, E., Scott, W.J. and Woods, D.

2006: First, second and fourth year assessment report on compilation, prospecting and geochemical and geophysical exploration for licences 9781M, 9783M, 10367M-10368M, 10562M, 10613M-10616M, 10657M-10658M, 10715M-10723M, 11383M and 11395M-11396M on claims in the Moran Lake area, Central Labrador, 5 reports. Newfoundland and Labrador Geological Survey, Assessment File 13K/0293, 332 pages.

Gandhi, S.S.

1969: Report on the geology of the Kaipokok Bay-Big River area, Labrador. Newfoundland and Labrador Geological Survey, Assessment File 13J/0042, 11 pages.

1970: Report on the geology and uranium occurrences of the Kaipokok Bay-Big River area, Labrador. Newfoundland and Labrador Geological Survey, Assessment File 13J/0061.

1976a: Summary report on 1976 exploration in Kaipokok Bay-Big River area, Labrador. Newfoundland and Labrador Geological Survey, Assessment File 13J/0163, 31 pages.

1976b: Report on geology, isotopic ages and origin of uranium occurrences in the Kaipokok Bay-Big River area, Labrador. Newfoundland and Labrador Geological Survey, Assessment File LAB/0318, 59 pages.

1978: Geological setting and genetic aspects of uranium occurrences in the Kaipokok Bay-Big River area, Labrador. Economic Geology, Volume 73, pages 1492-1522.

1984: Uranium in early Proterozoic Aillik Group, Labrador. In Proterozoic Unconformity and Stratabound Uranium Deposits. Edited by J. Ferguson. IAEA, Vienna, Technical Doc. 315, pages 35-68.

Gandhi, S.S. and Brown, A.C.

1975: Cupriferous shales of the Adeline Island Formation, Seal Lake Group, Labrador. Economic Geology, Volume 70, no. 1, 1975, pages 145-163.

Gandhi, S.S., Krogh, T.E. and Corfu, F.

1988: U-Pb zircon and titanite dates on two granitic intrusions of the Makkovik Orogen and a peralkaline granite of the Red Wine Intrusive Complex, central Labrador. Geological Association of Canada – Mineralogical Association of Canada – Canadian Society of Petroleum Geologists, Program with Abstracts, Volume 13, page A42.

Gentile, F., Srivastava, P., Bulmer, W., Krajewski, J., Turner, D., Turner, M.A. and Griep, J.L.

1977: Assessment report on geological, geochemical, geophysical, trenching and diamond drilling exploration on property in the Burnt Lake, Kitts Pond and Nash Lake areas, Labrador, 9 reports. Newfoundland and Labrador Geological Survey, Assessment File LAB/0384, 409 pages.

Gillies, S.L., Clarke, E.J. and Northcott, C.

2009: First, second, third, fourth, fifth and seventh year assessment report on geological, geochemical, geophysical, trenching and diamond drilling exploration for licences 9781M, 9783M, 10367M-10368M, 10715M-10720M, 10722M-10723M, 11395M, 11770M, 11833M-11835M, 12616M-12618M, 13427M, 13634M-13635M and 14515M on claims in the Moran Lake - Otter Lake area, central Labrador, 2 reports. Newfoundland and Labrador Geological Survey, Assessment File 13K/0313, 2723 pages.

Gilman, T.L., Kruse, S. and Jackson, R.G.

2008: Fourth year assessment report on prospecting and geochemical and diamond drilling exploration for licences 9387M-9391M on claims in the Bruce River area,

central Labrador, 2 reports. Newfoundland and Labrador Geological Survey, Assessment File 13K/0320, 497 pages.

Gilman, T.L., Loader, T. and Berube, P.  
2012: First and ninth year assessment report on prospecting and geochemical, geophysical and diamond drilling exploration for licences 9389M, 16313M, 16317M and 18576M on claims in the Bruce River area, central Labrador. Newfoundland and Labrador Geological Survey, Assessment File 13K/0337, 131 pages.

Gilman, T.L., Scott, W.J. and McGarry, T.G.  
2009: Sixth year assessment report on geological, geochemical and geophysical exploration for licences 9387M-9391M on claims in the Bruce River area, central Labrador, 2 reports. Newfoundland and Labrador Geological Survey, Assessment File 13K/0316, 121 pages.

Goddard, P. and Klein, J.  
1971: Report on an airborne electromagnetic and radio-metric survey of the Kaipokok Bay and Seal Lake area, Labrador, volumes 1-3. Newfoundland and Labrador Geological Survey, Assessment File 13K/0105, 179 pages.

Golder, H.Q.  
1977: Feasibility study volume 2-geology and reserves and volume 6 geotechnical surveys for Kitts-Michelin project, Labrador. Newfoundland and Labrador Geological Survey, Assessment File LAB/0259, 583 pages.

Gordanier, W.D.  
1979: Assessment report on diamond drilling exploration for the Moran Property in the Moran Lake area, central Labrador. Newfoundland and Labrador Geological Survey, Assessment File 13K/07/0149, 136 pages.

Gower, C.F.  
1980: Geology of the Benedict Mountains and surrounding areas (13J east and 13I), Labrador. *In Current Research*. Government of Newfoundland and Labrador, Department of Mines and Energy, Mineral Development Division, Report 80-1, pages 182-191.  
1981: The geology of the Benedict Mountains, Labrador (13J northeast and 13I northwest). Government of Newfoundland and Labrador, Department of Mines and Energy, Mineral Development Division, Report 81-3, 26 pages.  
2010: Geology of the Benedict Mountains area (NTS sheets 13J/09, 10, 15 and 16), eastern Labrador. Government of Newfoundland and Labrador, Department of Natural Resources, Geological Survey, Map 2010-03, Open File 013J/0291.

Gower, C.F., Flanagan, M.J., Kerr, A. and Bailey, D.G.  
1982: Geology of the Kaipokok Bay-Big River area, Central Mineral Belt, Labrador. Government of Newfoundland and Labrador, Department of Mines and Energy, Mineral Development Division, Report 82-7, 77 pages.

Gower, C.F. and Ryan, A.B.  
1986: Proterozoic evolution of the Grenville Province and adjacent Makkovik Province in eastern-central Labrador. *In The Grenville Province. Edited by J.M. Moore, A. Davidson and A.J. Baer. Geological Association of Canada, Special Paper 31*, pages 281-296.

Grimley, P.H.  
1970: Progress report with a geology and drilling report of the Nash Lake-Michelin area in the Kaipokok Bay area, Labrador. Newfoundland and Labrador Geological Survey, Assessment File 13J/0062, 15 pages.

Hansuld, J.A.  
1958: Report on exploration in the Block A of the Fro-bisher Concession, Labrador. Newfoundland and Labrador Geological Survey, Assessment File 13K/0037, 27 pages.

Hertel, M., Podhorski-Thomas, M., Durston, K., Edwards, C. and Allard, S.  
2009: Michelin uranium project, Labrador, Canada, NI 43-101 technical report on preliminary economic assessment. NI 43-101F1 Technical Report, 221 pages.

Hinchey, A.M.  
2007: The Paleoproterozoic metavolcanic, metasedimentary and igneous rocks of the Aillik Domain, Makkovik Province, Labrador (NTS map area 13O/03). *In Current Research*. Government of Newfoundland and Labrador, Department of Natural Resources, Geological Survey, Report 07-1, pages 25-44.

Hinchey, A.M. and Davis, W.J.  
2013: New U-Pb zircon geochronology for the Measles Point Granite, Aillik Domain, Makkovik Province, Labrador (NTS map area 13O/03). *In Current Research*. Government of Newfoundland and Labrador, Department of Natural Resources, Geological Survey, Report 13-1, pages 223-232.

Hinchey, A.M. and LaFlamme, C.  
2009: The Paleoproterozoic volcano-sedimentary rocks of the Aillik Group and associated plutonic suites of the Aillik domain, Makkovik Province, Labrador [NTS map area 13J/14]. *In Current Research*. Government of Newfoundland and Labrador, Department of Natural Resources, Geological Survey, Report 09-1, pages 159-182.

Hinchey, A.M. and Rayner, N.  
 2008: Timing constraints on the Paleoproterozoic, bimodal metavolcanic rocks of the Aillik Group, Aillik domain, Makkovik Province, Labrador. *In* Geological Association of Canada – Mineralogical Association of Canada 2008, Abstract Volume 33.

Hooper, P.L.  
 1956: Reports on geological and radiometric surveys at showings in the Luncheon Lake, Kidney Pond and Julies Harbour areas of the Kaipokok Bay area, Labrador. Newfoundland and Labrador Geological Survey, Assessment File 13O/03/0059, 20 pages.

Hopfengaertner, F., Quarch, H., Palmeter, I., Bayrock, L.A. and Tshimbalanga, S.  
 1984: First year assessment report on geological, geochemical and geophysical exploration for the Heggart Lake project for licences 100M-108M in the Moran Lake and Kaipokok River areas, Labrador, 2 parts, 3 reports. Newfoundland and Labrador Geological Survey, Assessment File 13K/0166, 276 pages.

Irvine, T.N. and Barager, W.R.A.  
 1971: A guide to the chemical classification of the common volcanic rocks. Canadian Journal of Earth Sciences, Volume 8, pages 523-548.

Jaffey, A.H., Flynn, K.F., Glendenin, L.E., Bentley, W.C. and Essling, A.M.  
 1971: Precision measurement of the half-lives and specific activities of  $^{235}\text{U}$  and  $^{238}\text{U}$ . Physical Review, Section C, Nuclear Physics, Volume 4, pages 1889-1906.

Kerr, A.  
 1989: Geochemistry of the Trans-Labrador granitoid belt, Canada: A quantitative comparative study of a Proterozoic batholith and possible Phanerozoic counterparts. Precambrian Research, Volume 45, pages 1-17.  
 1994: Early Proterozoic magmatic suites of the eastern Central Mineral Belt (Makkovik Province), Labrador: geology, geochemistry and mineral potential. Government of Newfoundland and Labrador, Department of Mines and Energy, Geological Survey Branch, Report 94-03, 167 pages.

Kerr, A. and Fryer, B.J.  
 1993: Nd isotope evidence for crust-mantle interaction in the genesis of 'A-type' granitoid suites in Labrador, Canada. Chemical Geology, Volume 104, pages 39-60.  
 1994: The importance of late- and post-orogenic crustal growth in the early Proterozoic: evidence from Sm-Nd isotopic studies of igneous rocks in the Makkovik Province, Canada. Earth and Planetary Science Letters, Volume 125, pages 71-88.

Kerr, A., Hall, J., Wardle, R.J., Gower, C.F. and Ryan, B.  
 1997: New reflections on the structure and evolution of the Makkovikian–Ketilidian orogeny in Labrador and southern Greenland. Tectonics, Volume 16, pages 942-965.

Kerr, A., Krogh, T.E., Corfu, F., Schrarer, U., Gandhi, S.S. and Kwok, Y.Y.  
 1992: Episodic Early Proterozoic granitoid plutonism in the Makkovik Province, Labrador: U–Pb geochronological data and geological implications. Canadian Journal of Earth Sciences, Volume 29, pages 1166-1179.

Kerr, A., Ryan, B., Gower, C.F. and Wardle, R.J.  
 1996: The Makkovik Province: extension of the Ketilidian Mobile Belt in mainland North America. *In* Precambrian Crustal Evolution in the North Atlantic Region. Edited by T.S. Brewer. Geological Society of London, Special Publication No. 1112, pages 155-177.

Ketchum, J.W.F., Culshaw, N.G. and Barr, S.M.  
 2002: Anatomy and orogenic history of a Paleoproterozoic accretionary belt: the Makkovik Province, Labrador, Canada. Canadian Journal of Earth Science, Volume 39, pages 711-730.

Ketchum, W.F.J., Culshaw, N.G. and Dunning, G.R.  
 1997: U–Pb geochronologic constraints on Paleoproterozoic orogenesis in the northwestern Makkovik Province, Labrador, Canada. Canadian Journal of Earth Science, Volume 34, pages 1072-1088.

Ketchum, J.W.F., Jackson, S.E., Culshaw, N.G. and Barr, S.M.  
 2001a: Depositional and tectonic setting of the Paleoproterozoic Lower Aillik Group, Makkovik Province, Canada: evolution of a passive margin-foredeep sequence based on petrochemistry and U–Pb (TIMS and LAM-ICP-MS) geochronology. Precambrian Research, Volume 105, pages 331-356.

Ketchum, J.W.F., Barr, S.M., Culshaw, N.G. and White, C.E.  
 2001b: U–Pb ages of granitoid rocks in the northwestern Makkovik Province, Labrador: evidence for 175 million years of episodic synorogenic and postorogenic plutonism. Canadian Journal of Earth Sciences, Volume 38, pages 359-372.

Kontak, D.J.  
 1978: Preliminary report on four uranium showings in the Central Mineral Belt, Labrador. *In* Report of Activities. Newfoundland Department of Mines and Energy,

Mineral Development Division, Report 78-1, pages 27-43.

1980: Geology, geochronology, and uranium mineralization in the Central Mineral Belt of Labrador, Canada. Unpublished M.Sc. thesis, University of Alberta, Edmonton, Alberta, Canada, 378 pages.

Krogh, T.E.

1973: A low-contamination method for hydrothermal decomposition of zircon and extraction of U and Pb for isotopic age determinations. *Geochimica et Cosmochimica Acta*, Volume 33, No. 3, pages 485-494.

1982: Improved accuracy of U-Pb zircon ages by the creation of more concordant systems using an air abrasion technique. *Geochimica et Cosmochimica Acta*, Volume 46, pages 637-649.

Kruse, S.

2008: Fifth year assessment report on geological, geochemical and diamond drilling exploration for licence 9702M on claims in the Mustang Lake area, central Labrador. Newfoundland and Labrador Geological Survey, Assessment File 13J/12/0266, 217 pages.

2012: Fifth and sixth year assessment report on prospecting and geochemical and diamond drilling exploration for licences 13128M and 14499M on claims in the Benedict Mountains area, east-central Labrador. Newfoundland and Labrador Geological Survey, Assessment File 13J/0304, 210 pages.

Kruse, S., Tykajlo, R. and White, R.

2009: First, second and third year assessment report on geological, geochemical and geophysical exploration for licences 11088M-11089M, 11428M, 11430M, 11538M, 13128M-13130M, 13366M-13367M, 13369M-13372M and 14499M-14502M on claims in the Benedict Mountains area, east-central Labrador, 2 reports. Newfoundland and Labrador Geological Survey, Assessment File 13J/0267, 216 pages.

Loveridge, W.D., Ermanovics, I.F. and Sullivan, R.W.

1987: U-Pb ages on zircon from the Maggo Gneiss, the Kanairiktok Plutonic Suite and the Island Harbour Plutonic Suite, coast of Labrador, Newfoundland. In *Radioactive Age and Isotopic Studies: Report 1. Geological Survey of Canada*, Paper 87-2, pages 59-65.

MacGillivray, G., Dimmell, P., Jacobs, W., Delazzer, A. and Alexander, S.

2008a: First and second year assessment report on geological, geophysical, geochemical and diamond drilling exploration for licences 12342M-12351M, 12438M-12443M, 13715M-13719M, 13736M, 13738M-13739M, 13744M-13746M, 13757M, 13759M, 13795M and 13797M on claims in the Benedict Mountains area, east-central Labrador. Newfoundland and Labrador Geological Survey, Assessment File 13J/0273, 837 pages.

MacGillivray, G., Dimmell, P., Montague, E., Delazzer, A., Baldwin, C., Jacobs, W., Charlton, J.D. and Charlton, L.

2008b: Second year assessment report on geological, geochemical, geophysical, trenching and diamond drilling exploration for licences 11384M, 11470M and 11472M-11473M on claims in the Snegamook Lake area, central Labrador, 2 reports. Newfoundland and Labrador Geological Survey, Assessment File 13K/11/0315, 460 pages.

MacGillivray, G., Dimmell, P., Montague, E., Delazzer, A., Baldwin, C., Jacobs, W., Grant, T., Selman, D., Charlton, J.D. and Charlton, L.

2008c: First and second year assessment report on geological, geochemical, geophysical, trenching and diamond drilling exploration for licences 11274M, 11298M, 11385M-11386M, 11389M-11392M, 11475M-11477M, 11521M, 11525M, 11559M-11560M, 11648M-11649M, 12538M-12539M, 12588M, 12601M, 13292M-13296M and 13686M on claims in the Kanairiktok River, Otter Lake, and Portage Lake areas, central Labrador, 4 reports. Newfoundland and Labrador Geological Survey, Assessment File 13K/0317, 1193 pages.

MacGillivray, G., Dimmell, P., Jacobs, W., Delazzer, A. and Alexander, S.

2009: First and third year assessment report on geological, geophysical, geochemical and diamond drilling exploration for licences 11650M-11651M, 11654M, 11712M-11715M, 14927M and 14945M on claims in the Benedict Mountains area, east-central Labrador. Newfoundland and Labrador Geological Survey, Assessment File 13J/0274, 311 pages.

Maniar, P.D. and Piccoli, P.M.

1989: Tectonic discrimination of granitoids. *Geological Society of America Bulletin*, Volume 101, pages 635-643.

Mann, E.L.

1957: Report on Moran Lake area of the Kaipokok concession, Labrador. Newfoundland and Labrador Geological Survey, Assessment File 13K/0032, 17 pages.

Marten, B.E.

1977: The relationship between the Aillik Group and the Hopedale gneiss, Kaipokok Bay, Labrador. Unpublished Ph.D. thesis, Memorial University, St. John's, 389 pages.

Marten, B.E. and Smyth, W.R.  
 1975: Uranium potential of the basal unconformity of the Seal Lake Group, Labrador. *In Report of Activities. Government of Newfoundland and Labrador, Department of Mines and Energy, Mineral Development Division, Report 75-1*, pages 106-115.

Mattinson, J.M.  
 2005: Zircon U-Pb chemical abrasion (CA-TIMS) method; combined annealing and multi-step partial dissolution analysis for improved precision and accuracy of zircon ages. *Chemical Geology*, Volume 220, pages 47-66.

McKenzie, W.L.  
 1976: Report on exploration including geological and geophysical surveys for the Central Mineral Belt project, Labrador. *Newfoundland and Labrador Geological Survey, Assessment File 13K/07/0131*, 65 pages.

1977a: Central Mineral Belt Project, report on exploration, 1977. *Newfoundland and Labrador Geological Survey, Assessment File 13K/0155*, 158 pages.

1977b: Report on geology, geophysics and diamond drilling in the Central Mineral Belt project B1 zone on the Moran property, Labrador. *Newfoundland and Labrador Geological Survey, Assessment File 13K/07/0132*, 82 pages.

1978a: Report on 1978 drilling program on the Moran property in the Central Mineral Belt, Labrador. *Newfoundland and Labrador Geological Survey, Assessment File 13K/07/0148*, 193 pages.

1978b: Report on 1978 exploration of the Central Mineral Belt, Labrador. *Newfoundland and Labrador Geological Survey, Assessment File 13K/07/0156*.

McLean, C., Boyer, L., Hansen, L., Savidant, S., Sarioglu, K., Taiani, M., McCuaig, S., Thompson, G.M. and Wilton, D.  
 2009: Second year, second year supplementary, third year, third year supplementary, and fourth, fifth and sixth year assessment report on geological, geochemical and geophysical exploration for licences 9411M-9414M, 9482M, 9719M, 9722M-9723M, 10022M, 10047M-10048M, 10050M-10052M, 10054M-10056M, 10059M, 10343M-10344M and 14457M on claims in the Kaipokok Bay area, northeastern Labrador, 3 reports. *Newfoundland and Labrador Geological Survey, Assessment File LAB/1545*, 424 pages.

Minatidis, D.G.  
 1976: A comparative study of trace element geochemistry and mineralogy of some uranium deposits of Labrador and evaluation of some uranium exploration techniques in a glacial terrain. *Memorial University of Newfoundland, M.Sc., St John's, Newfoundland*, 239 pages.

Morgan, J.A., Froude, T., Farquhar, E., Penney, G. and Scott, W.J.  
 2007: First, second, third and fifth year assessment report on geological, geochemical, geophysical, trenching and diamond drilling exploration for licences 9781M, 9783M, 10367M-10368M, 10715M-10720M, 10722M-10723M, 11395M, 11770M, 11833M-11835M and 12616M-12618M on claims in the Moran Lake - Otter Lake area, central Labrador. *Newfoundland and Labrador Geological Survey, Assessment File 13K/0296*, 3368 pages.

Morgan, J.A. and Giroux, G.H.  
 2008: Form 43-101 Technical Report on The Central Mineral Belt (CMB) Uranium Project, Labrador, Canada. NI 43-101 Technical report, 237 pages.

Morrison, E.R.  
 1956: Report on prospecting in area D, Labrador. *Newfoundland and Labrador Geological Survey, Assessment File LAB/0182*.

North, J.W. and Wilton, D.H.C.  
 1988: Stratigraphy of the Warren Creek Formation, Moran Lake Group, Central Mineral Belt of Labrador. *In Current Research, Part C. Geological Survey of Canada, Paper 88-01C*, pages 123-128.

Parrish, R.R., Roddick, J.C., Loveridge, W.D. and Sullivan, R.W.  
 1987: Uranium-lead analytical techniques at the Geochronology Laboratory, Geological Survey of Canada. *In Radiogenic Age and Isotopic Studies, Report 1. Geological Survey of Canada, Paper 87-2*, pages 3-7.

Pearce, J.A.  
 1996: A user's guide to basalt discrimination diagrams. *In Trace Element Geochemistry of Volcanic Rocks: Applications for Massive Sulphide Exploration. Edited by D.A. Wyman. Geological Association of Canada, Short Course Notes, Volume 12*, pages 79-113.

Pearce, J.A. and Cann, J.R.  
 1973: Tectonic setting of basic volcanic rocks determined using trace element analyses. *Earth and Planetary Science Letters*, No. 12, pages 290-300.

Perry, J.  
 1979: Annual exploration report for 1978 with appendix 5-9 on the Moran and Seal Lake areas, Labrador. New-

foundland and Labrador Geological Survey, Assessment File LAB/0437, 282 pages.

1980a: Assessment report on geological, geochemical, geophysical and diamond drilling exploration for 1979 submission for British Newfoundland Exploration Limited Statutory Agreement in the Moran Lake-Seal Lake area, Labrador. Newfoundland and Labrador Geological Survey, Assessment File LAB/0463, 205 pages.

1980b: Annual exploration report for 1980 on the Canico-Brinex joint venture in the Makkovik area, Labrador. Newfoundland and Labrador Geological Survey, Assessment File LAB/0592, 121 pages.

Piloski, M.J.

1958: Adit level plan for the Kitts Pond area in the Kaipokok Bay area, Labrador. Newfoundland and Labrador Geological Survey, Assessment File 13O/03/0065.

1968: Report on operations in 1968 in Kaipokok-Big River joint venture area, Labrador. Newfoundland and Labrador Geological Survey, Assessment File 13J/0003.

1969: Summary report for work done in 1969 on the uranium belt in the Kaipokok-Big River joint venture area, Labrador. Newfoundland and Labrador Geological Survey, Assessment File 13J/0008.

1970: Preliminary appraisal on grade and tonnage potential of the Nash Lake and Michelin showings, Labrador. Newfoundland and Labrador Geological Survey, Assessment File 13J/13/0037.

1976: Annual report for 1975 on exploration at the Michelin prospect, Labrador, Part 1. Newfoundland and Labrador Geological Survey, Assessment File 13J/12/0155, 61 pages.

Ponder, H., Hounslow, A.W. and Link, J.M.

1976: Mineralogy of ore specimens from the Kaipokok area, Labrador. Newfoundland and Labrador Geological Survey, Assessment File 013J/0176, 31 pages.

Quinby-Hunt, M.S., Wilde, P., Orth, C.J. and Berry, W.B.N.

1989: Elemental geochemistry of black shales – statistical comparison of low-calcic shales with other shales. In *Metalliferous Black Shales and Related Ore Deposits; Program and Abstracts*. Edited by R.I. Grauch and J.S. Leventhal. US Geological Survey Circular: 1037, pages 8-15.

Rivers, T., Ketchum, J., Indares, A. and Hynes, A.

2002: The high pressure belt in the Grenville Province: architecture, timing and exhumation. *Canadian Journal of Earth Sciences*, Volume 39, pages 867-893.

Romer, R.L., Schärer, U., Wardle, R.J. and Wilton, D.H.C.

1995: U-Pb age of the Seal Lake Group, Labrador: relationship to Mesoproterozoic extension-related magmatism of Laurasia. *Canadian Journal of Earth Sciences*, Volume 32, Number 9, pages 1401-1410.

Ross, D.A.

2008: Technical report on the CMBNW property, Labrador, Canada. NI 43-101F1 Technical Report, 103 pages.

2009: Technical report on the CMBNW property, Newfoundland and Labrador, Canada. NI 43-101 Technical Report, 101 pages.

Ruzicka, V.

1971: Geological comparison between east European and Canadian uranium deposits. *Geological Survey of Canada, Paper 70-48*.

Ryan, A.B.

1981: Volcanism, sedimentation, plutonism and Grenvillian deformation in the Helikian basins of central Labrador. In *Proterozoic Basins in Canada*. Edited by F.H.A. Campbell. Geological Survey of Canada. Paper 81-10, pages 361-378.

1984: Regional geology of the central part of the Central Mineral Belt, Labrador. Government of Newfoundland and Labrador, Department of Mines and Energy, Mineral Development Division, Memoir 3, 185 pages.

Ryan, A.B. and Harris, A.G.

1978: Geology of the Otter-Nipishish-Stipec lakes area, Labrador [NTS 13K/2, 3, 6, 7]. In *Report of Activities*. Government of Newfoundland and Labrador, Department of Mines and Energy, Mineral Development Division, Report 78-01, pages 51-58.

Ryan, A.B., Kay, A. and Ermanovics, I.

1983: The geology of the Makkovik Subprovince between Kaipokok Bay and Bay of Islands, Labrador. Government of Newfoundland and Labrador, Department of Mines and Energy, Mineral Development Division, Maps 83-38 to 83-41, with descriptive notes (21 pages).

Schärer, U., Krogh, T.E., Wardle, R.J., Ryan, B. and Gandhi, S.S.

1988: U-Pb ages of early to middle Proterozoic volcanism and metamorphism in the Makkovik Orogen, Labrador. *Canadian Journal of Earth Sciences*, Volume 25, pages 1098-1107.

Setterfield, T. and Dyer, R.  
 2007: First and second year assessment report on geological and geochemical exploration for licences 11088M-11089M, 11428M, 11430M, 11538M and 12147M-12148M on claims in the Benedict Mountains area, east-central Labrador, 2 reports. Newfoundland and Labrador Geological Survey, Assessment File 13J/0260, 99 pages.

Setterfield, T., McNeill, P. and Tykajlo, R.  
 2008: First year, second year and second year supplementary assessment report on prospecting and geochemical and geophysical exploration for licences 11088M-11089M, 11428M, 11538M, 13128M-13130M, 13366M-13367M, 13369M-13372M and 14499M-14502M on claims in the Benedict Mountains area, east-central Labrador. Newfoundland and Labrador Geological Survey, Assessment File 13J/0280, 97 pages.

Setterfield, T. and Tykajlo, R.  
 2004: First year assessment report on geological, geochemical and geophysical exploration for licence 9702M on claims in the Mustang Lake area, central Labrador, 2 reports. Newfoundland and Labrador Geological Survey, Assessment File 13J/12/0255, 57 pages.

Setterfield, T., Tykajlo, R. and Elieff, S.  
 2003: First year assessment report on geophysical exploration for licences 9387M-9391M on claims in the Bruce River area, central Labrador, 2 reports. Newfoundland and Labrador Geological Survey, Assessment File 13K/0276, 91 pages.

Sibson, R.H.  
 1977: Fault rocks and fault mechanisms. *Journal of the Geological Society of London*, Volume 133, pages 191-213.

Sinclair, G.S.  
 1999: Geochemistry and argon thermochronology of the Upper Aillik Group and associated granitoid rocks in the Makkovik Bay area, Aillik Domain, Makkovik Province, Labrador. M.Sc. thesis, Dalhousie University, Halifax, Nova Scotia, Canada, 328 pages.

Sinclair, G.S., Barr, S.M., Culshaw, N.G. and Ketchum, J.W.F.  
 2002: Geochemistry and age of the Aillik Group and associated plutonic rocks, Makkovik Bay area, Labrador: implications for tectonic development of the Makkovik Province. *Canadian Journal of Earth Sciences*, Volume 39, pages 731-748.

Smith, R.L., Marshall, L., Butler, R., Wilton, D.H.C., Madore, C., Annesley, I.R. and Elieff, S.  
 2004: First year assessment report on geological, geochemical and geophysical exploration for licences 9410M-9417M, 9441M and 9482M on claims in the Post Hill, Burnt Lake, Melody Lake, Michinappi Lake, Croteau Lake, Stormy Lake and Letitia Lake areas, central Labrador, 3 reports. Newfoundland and Labrador Geological Survey, Assessment File LAB/1393, 280 pages.

Smith, R.L., Valenta, R., Butler, R., Hall, R., Wilton, D.H.C. and St-Hilaire, C.  
 2005: First and second year assessment report on geological, geochemical and geophysical exploration for licences 9410M-9414M, 9482M, 9718M-9723M, 10022M, 10046M-10059M and 10343M-10344M on claims in the Kaipokok Bay - Jacques Lake - Walker Lake area, northeastern Labrador, 3 reports. Newfoundland and Labrador Geological Survey, Assessment File LAB/1404, 422 pages.

Smyth, W.R. and Ryan, B.  
 1977: Geologic setting of the Moran Lake uranium showings, Central Mineral Belt, Labrador. *In Report of Activities*. Newfoundland Department of Mines and Energy, Mineral Development Division, Report 77-1, pages 57-62.

Smyth, W.R., Marten, B.E. and Ryan, A.B.  
 1978: A major Apebian-Helekan unconformity within the Central Mineral Belt of Labrador: Definition of new groups and metallogenic implications. *Canadian Journal of Earth Sciences*, Volume 15, pages 1954-1966

Soonawala, N.M.  
 1971: Report on ground magnetic electromagnetic and IP surveys in the Moran Lake area, Labrador. Newfoundland and Labrador Geological Survey, Assessment File 13K/10/0100, 23 pages.

Sparkes, G.W.  
 2013: A re-evaluation of the application of CR-39 autoradiographs in the textural analysis of uranium-bearing samples and thin sections. *Exploration and Mining Geology*, Volume 21, pages 79-83.

Sparkes, G.W. and Davis, W.J.  
 2013: Volcanic-hosted uranium mineralization in the eastern Central Mineral Belt of Labrador: Benedict Mountains Region. *In Current Research*. Government of Newfoundland and Labrador, Department of Natural Resources, Geological Survey, Report 13-1, pages 189-198.

Sparkes, G.W. and Dunning, G.R.  
 2009: Preliminary investigations into the style, setting and timing of uranium mineralization, Jacques Lake deposit, Central Mineral Belt, Labrador. *In Current Research. Government of Newfoundland and Labrador, Department of Natural Resources, Geological Survey, Report 09-1*, pages 81-93.

2015: New U-Pb age constraints on the development of uranium mineralization within the Central Mineral Belt of Labrador. *In Current Research. Government of Newfoundland and Labrador, Department of Natural Resources, Geological Survey, Report 15-1*, pages 105-123.

Sparkes, G.W., Dunning, G.R., Fonkew, M. and Langille, A.  
 2016: Age constraints on the formation of iron oxide-rich hydrothermal breccias of the Moran Lake area: evidence for potential IOCG-style mineralization within the Central Mineral Belt of Labrador. *In Current Research. Government of Newfoundland and Labrador, Department of Natural Resources, Geological Survey, Report 16-1*, pages 71-90.

Sparkes, G.W., Dunning, G.R. and McNicoll, V.J.  
 2010: New U-Pb age constraints and potential implications for the genesis of the Kitts uranium deposit, Central Mineral Belt, Labrador. *In Current Research. Government of Newfoundland and Labrador, Department of Natural Resources, Geological Survey, Report 10-1*, pages 93-109.

Sparkes, G.W. and Kerr, A.  
 2008: Diverse styles of uranium mineralization in the Central Mineral Belt of Labrador: an overview and preliminary discussion. *In Current Research. Government of Newfoundland and Labrador, Department of Natural Resources, Geological Survey, Report 08-1*, pages 193-227.

Srivastava, P.  
 1976: Geological evaluation of the Inda Lake prospect, Labrador. Newfoundland and Labrador Geological Survey, Assessment File 13J/13/0165, 48 pages.

Stacey, J.S. and Kramers, J.D.  
 1975: Approximation of terrestrial lead isotope evolution by a two stage model. *Earth and Planetary Science Letters*, Volume 26, pages 207-221.

Stern, R.A.  
 1997: The GSC Sensitive High Resolution Ion Microprobe (SHRIMP): analytical techniques of zircon U-Th-Pb age determinations and performance evaluation. *In Radiogenic Age and Isotopic Studies, Report 10. Geological Survey of Canada, Current Research 1997-F*, pages 1-31.

Stern, R.A. and Amelin, Y.  
 2003: Assessment of errors in SIMS zircon U-Pb geochronology using a natural zircon standard and NIST SRM 610 glass. *Chemical Geology*, Volume 197, pages 111-142.

Sun, S.S. and McDonough, W.F.  
 1989: Chemical and isotopic systematics of oceanic basalts: Implications for mantle composition and processes. *In Magmatism in the Ocean Basins. Geological Society, Special Publication 42*, pages 313-345.

Thomas, A.  
 1981: Geology along the southwestern margin of the Central Mineral Belt, Labrador. *Government of Newfoundland and Labrador, Department of Mines and Energy, Mineral Development Division, Report 81-4*, 40 pages.

Tracey, M.  
 2009: A study of volcanic and sediment-hosted uranium with the Post Hill Group, Central Mineral Belt Region, Labrador. Unpublished B.Sc. thesis, Memorial University of Newfoundland, St. John's, Newfoundland, 137 pages.

van Nostrand, T.S. and Lowe, D.  
 2010: Geology of the Seal Lake area, central Labrador (parts of NTS map areas 13K/3, 4, 5 and 6). *In Current Research. Government of Newfoundland and Labrador, Department of Natural Resources, Geological Survey, Report 10-1*, pages 351-371.

Vine, J.D. and Tourlelot, E.B.  
 1970: Geochemistry of black shale deposits – A summary report. *Economic Geology*, Volume 65, pages 253-272.

Wallis, C.S., Sparkes, B.A. and Giroux, G.H.  
 2011: Technical report on the Central Mineral Belt (CMB) uranium-vanadium project, Labrador, Canada. NI 43-101 Technical Report, 94 pages.

Wardle, R.J.  
 1984: Geological fieldwork in the Lower Proterozoic Aillik Group, eastern Labrador. *In Report of Activities. Government of Newfoundland and Labrador, Department of Mines and Energy, Mineral Development Division*, pages 14-16.

Wardle, R.J. and Bailey, D.G.  
 1981: Early Proterozoic sequences in Labrador. *In Proterozoic Basins of Canada. Geological Survey of Canada, Paper 81-10*, pages 331-359.

Wardle, R.J., Gower, C.F., Ryan, B., Nunn, G.A.G., James, D.T. and Kerr, A.

1997: Geological map of Labrador; 1:1 million scale. Government of Newfoundland and Labrador, Department of Mines and Energy, Geological Survey, Map 97-07.

Watson-White, M.V.

1976: A petrological study of acid volcanic rocks in part of the Aillik Series, Labrador. M.Sc. thesis, McGill University, Montreal, Quebec, 132 pages.

Wilde, A.

2013: Towards a model for albitite-type uranium. Minerals, Volume 3, pages 36-48.

Willett, B., Nichols, R. and Morse, R.H

2008: Third year assessment report on geological, geochemical, geophysical, trenching and diamond drilling exploration for licences 13379M-13380M on claims in the Fish Hawk Lake area, central Labrador, 2 reports. Newfoundland and Labrador Geological Survey, Assessment File 13K/0330, 431 pages.

Willett, B., Nichols, R. and Tykajlo, R.

2007a: Second year supplementary assessment report on geological, geochemical and trenching exploration for licences 9387M-9391M on claims in the Bruce River area, central Labrador. Newfoundland and Labrador Geological Survey, Assessment File 13K/0301, 116 pages.

Willett, B., Tykajlo, R. and Setterfield, T.

2005: Second year assessment report on geological, geochemical and geophysical exploration for licence 9702M on claims in the Mustang Lake area, central Labrador, 3 reports. Newfoundland and Labrador Geological Survey, Assessment File 13J/12/0256, 72 pages.

Willett, B., Nichols, R., Tykajlo, R. and Jackson, R.

2007b: Second year assessment report on geological, geochemical and trenching exploration for licences 10348M, 10355M-10358M and 11219M on claims in the Croteau Lake area, central Labrador, 2 reports. Newfoundland and Labrador Geological Survey, Assessment File 13K/0300, 98 pages.

Willett, B., Nichols, R., Setterfield, T. and Tykajlo, R.

2006a: First year supplementary assessment report on geological, geochemical, geophysical, trenching and diamond drilling exploration for licences 10348M, 10355M-10358M and 11219M on claims in the Croteau Lake area, central Labrador, 2 reports. Newfoundland and Labrador Geological Survey, Assessment File 13K/0295, 117 pages.

2006b: Third year assessment report on geophysical and diamond drilling exploration for licence 9702M on claims in the Mustang Lake area, central Labrador. Newfoundland and Labrador Geological Survey, Assessment File 13J/12/0259, 370 pages.

2006c: Second year supplementary assessment report on prospecting and geochemical exploration for licences 9387M-9391M on claims in the Bruce River area, central Labrador. Newfoundland and Labrador Geological Survey, Assessment File LAB/1430, 65 pages.

Wiley, A.J.

1982: Summary of exploration activities for extended licences 1524bx and 1525bx in Area B, Labrador. Newfoundland and Labrador Geological Survey, Assessment File LAB/0601, 52 pages.

Willy, A.J., Vanderveer, D., van der Heyden, P., Nelson, J. and Payne, J.

1982: Assessment report on geological, geochemical, geophysical and diamond drilling exploration for the Labrador uranium project for 1981 submission for licence 1524bx on claim blocks 2927bx-2928bx in the Anna Lake areas, Labrador. Newfoundland and Labrador Geological Survey, Assessment File 13K/09/0157, 150 pages.

Wilton, D.H.C.

1996: Metallogeny of the Central Mineral Belt and adjacent Archean basement, Labrador. Government of Newfoundland and Labrador, Department of Mines and Energy, Geological Survey, Mineral Resources Report 8, 178 pages.

Wilton, D.H.C. and Cunningham-Dunlop, I.

2006: The exploration activities of Aurora Energy Inc. on the CMB uranium property, Labrador, Canada during the period of June 2005 to December 2005. Prepared for Aurora Energy Inc. NI 43-101F1 Technical Report, 137 pages.

Wilton, D.H.C. and Longerich, H.P.

1993: Metallogenic significance of ICP-MS-derived trace element and Pb isotope data on uraninite separates from the Labrador Central Mineral Belt. Canadian Journal of Earth Sciences, Volume 30, pages 2352-2365.

Wilton, D.H.C. and Wardle, R.J.

1987: Two contrasting granophile and non-granophile metallogenic styles in the Early Proterozoic Upper Aillik Group, Central Mineral Belt, Labrador, Canada. Mineralium Deposita, Volume 22, pages 198-206.

Wilton, D.H.C., McNeil, P., Hicks, C., Tracey, M., Cunningham-Dunlop, I., Lee, C., Thompson, G.M. and Piercy, S.

2010: The nature of uranium mineralization in the Paleoproterozoic Aillik and Post Hill Groups, Labrador, Central Mineral Belt. *In* Geological Association of Canada – Mineralogical Association of Canada 2010. Abstract Volume, GeoCanada 2010-Working with the Earth.

Winchester, J.A. and Floyd, P.A.

1977: Geochemical discrimination of different magma series and their differentiation products using immobile elements. *Chemical Geology*, Volume 20, pages 325-343.

## APPENDIX A

### A summary of the procedure used in the generation of CR-39 autoradiographs

The following summary provides a brief description for the autoradiograph technique used in this study as outlined in Sparkes (2013). This technique utilizes a special plastic polymer known as “CR-39” to produce images capable of displaying the distribution of radioactivity with a given geological sample. Several distributors of CR-39 do business on the internet; the material can be easily ordered over the phone from distributors such as Homalite, who sell the material under the trade name H-911 ([www.homalite.com](http://www.homalite.com)). The CR-39 was obtained in approximately 46 cm (18 in) by 66 cm (26 in) sheets with a thickness of 1 mm (0.031 in). Two surface finishes can be chosen for the material; however, the best results obtained by the author were from the LR92 finish, which provided the best optical resolution. In 2009, one sheet cost approximately \$150, from which fifteen to twenty samples around 10 cm in size could be imaged.

Basham (1981) briefly outlined the procedures for the production of radiographic images. Sparkes (2013) provided information on the effects of exposure time and various levels of radioactivity with respect to the generation of the autoradiographs. The geological samples were cut using a standard rock saw to produce a flat surface; this surface can be polished if very fine detailed images of the radioactivity are required. The resultant flat surface was then placed in contact with a piece of the CR-39 material, which was cut to fit the individual geological samples, and left for approximately 6 days.

Once in place, a rough outline of the sample was scratched into the CR-39 sheet using a pointed instrument such as a scribe; this was done to ensure proper positioning of the autoradiograph when comparing it with the corresponding sample at the end of the process. After the samples were exposed, the CR-39 sheet was removed from the sample and placed in a heated bath of a 6N NaOH solution. It was found that a temperature between 60–70°C was the desirable range, and avoided possible damage of the material when processing several autoradiographs at once. After approximately 2½ hours a white precipitate begins to form within the solution and adheres to the material, corroding the quality of the image. After the etching the CR-39 material was removed from the bath, rinsed with water and allowed to air dry.

The CR-39 images were converted to digital images for further analysis. Scanning was carried out using a standard desktop scanner, and was completed at a resolution of 1200 dpi for hand samples and up to 2400 dpi for thin section autoradiographs. The scanned images were then overlain upon a digital photograph of the corresponding sample using standard photo processing software to enable a detailed visual comparison. For the purpose of this study, areas of radioactivity were given a yellow colour to highlight features. Note that as a result of this colour conversion the sample outline also becomes yellow, although it is not related to radioactivity.

## APPENDIX B

### A summary of the geochronological techniques utilized and corresponding procedures

Due to the time span of this project several different geochronological techniques were utilized over the course of the study. The majority of the samples were analyzed at Memorial University, utilizing Thermal Ionization Mass Spectrometry (TIMS) technique. The zircon, titanite and monazite grains analyzed were selected from mineral concentrates under a microscope according to criteria of clarity, euhedral crystal form and lack of inclusions. For earlier analyses, grains were physically abraded as per the procedure outlined by Krogh (1982), while for more recent analyses, grains were chemically abraded (CA-TIMS) following the procedure of Mattinson (2005).

For each sample, a small number of zircon grains were grouped into fractions of like morphology, and analyzed by TIMS. The selected mineral fractions were washed in distilled nitric acid, then double-distilled water, prior to loading in Krogh-type TEFILON dissolution bombs. A mixed  $^{205}\text{Pb}/^{235}\text{U}$  tracer was added in proportion to the sample weight, along with approximately 15 drops of distilled hydrofluoric acid, then the bomb was sealed and placed in an oven at 210°C for 5 days. Ion exchange was carried out according to the procedure of Krogh (1973), with modified columns and reagent volumes scaled down to one tenth of those reported in 1973. The purified Pb and U were collected in a clean beaker in a single drop of ultrapure phosphoric acid.

Lead and uranium are loaded together on outgassed single Re filaments with silica gel and dilute phosphoric acid. Mass spectrometry is carried out using a multi-collector MAT 262. The faraday cups are calibrated with NBS 981 lead standard and the ion-counting secondary electron multiplier (SEM) detector is calibrated against the faraday cups by

measurement of known lead isotopic ratios. The small amounts of Pb were measured by peak jumping on the SEM, with measurement times weighted according to the amounts of each mass present. The U was measured by peak jumping on the SEM. A series of sets of data are measured in the temperature range 1400 to 1550°C for Pb and 1550 to 1640°C for U, and the best sets are combined to produce a mean value for each ratio. The measured ratios are corrected for Pb and U fractionation of 0.1%/amu and 0.03%/amu, respectively, as determined from repeat measurements of NBS standards. The ratios are also corrected for laboratory procedure blanks (1-2 picograms - Pb, 0.3 picogram - U) and for common lead above the laboratory blank with lead of the composition predicted by the two-stage model of Stacey and Kramers (1975) for the age of the sample. Ages are calculated using the decay constants recommended by Jaffey *et al.* (1971). The uncertainties on the isotopic ratios are calculated and are reported as two sigma. The age of each rock is reported as the weighted average of the  $^{206}\text{Pb}/^{238}\text{U}$  ages calculated using ISOPLOT for weighted averages or following the procedure outlined by Davis (1982) for linear regressions. Uncertainties on all ages are reported at the 95% confidence interval.

Several samples were also analyzed at the Geological Survey of Canada by Sensitive High Resolution Ion Microprobe (SHRIMP) technique (GS-07-298; Appendix D) as well as Isotope-Dilution Thermal Ionization Mass Spectrometry (ID-TIMS) technique (GS-08-288; Appendix E). For the SHRIMP dating, the analytical procedures described in Stern (1997) and Stern and Amelin (2003) were followed. For the ID-TIMS analysis, the analytical techniques used are described in Parrish *et al.* (1987).

## APPENDIX C

Compilation table of U–Pb data for analyses conducted at Memorial University; UTM's for each sample are provided in NAD 27, Zone 21 coordinates

Fraction	Concentration			Measured			Corrected Atomic Ratios*						Age [Ma]			
	Weight [mg]	U [ppm]	Pb rad [ppm]	total			common Pb [pg]	$^{206}\text{Pb}$ $^{204}\text{Pb}$	$^{208}\text{Pb}$ $^{206}\text{Pb}$	$^{206}\text{Pb}$ $^{238}\text{U}$	$^{207}\text{Pb}$ $^{235}\text{U}$	$^{207}\text{Pb}$ $^{206}\text{Pb}$	$^{206}\text{Pb}$ $^{238}\text{U}$	$^{207}\text{Pb}$ $^{235}\text{U}$	$^{207}\text{Pb}$ $^{206}\text{Pb}$	
				common Pb [pg]	$^{206}\text{Pb}$ $^{204}\text{Pb}$	$^{208}\text{Pb}$ $^{206}\text{Pb}$										
<b><sup>2</sup>GS-07-170 Diorite Dyke (340900, 6097160)</b>																
T1 1 lrg dk xtal	0.003	281	90.2	22	720	0.1678	0.2937	12	4.105	19	0.10138	32	1660	1655	1649	
T2 1 lrg dk xtal	0.003	266	95.5	20	770	0.3090	0.2950	34	4.158	55	0.10222	84	1666	1666	1665	
T3 1 lrg dk xtal	0.003	316	117.3	29	614	0.3624	0.2947	14	4.093	33	0.10075	68	1665	1653	1638	
T4 1 lrg dk brn	0.003	108	42.4	5	1239	0.4456	0.2938	20	4.107	25	0.10138	50	1660	1656	1650	
<b><sup>1</sup>GS-07-225 Quartz-feldspar Porphyry Dyke (333233, 6066065)</b>																
Z1 1 lrg equ euh abr	0.004	213	72.2	19	954	0.1048	0.32408	162	4.9118	276	0.10992	36	1810	1804	1798	
Z2 2 lrg euh equ abr	0.008	145	48.2	7.7	3051	0.0972	0.32008	252	4.8709	332	0.11037	46	1790	1797	1805	
Z3 2 lrg euh equ abr	0.008	99	33.4	2.7	5946	0.1139	0.32058	214	4.8819	264	0.11045	46	1793	1799	1807	
Z4 7 lrg euh abr	0.021	179	59.9	22	3457	0.1160	0.31774	86	4.8242	130	0.11012	12	1779	1789	1801	
Z5 9 lrg euh abr	0.027	129	42.2	1.7	40870	0.1064	0.31240	98	4.7405	142	0.11005	16	1753	1774	1800	
Z6 7 lrg euh abr	0.021	127	42.3	3.5	15347	0.1039	0.31828	150	4.8356	202	0.11019	28	1781	1791	1803	
T1 1 lrg brn abr	0.005	729	264.8	37	2008	0.1994	0.32228	122	4.8921	186	0.11009	14	1801	1801	1801	
T2 2 sml clr dk brn abr	0.006	317	113.8	30	1306	0.1870	0.32155	142	4.8812	190	0.11010	28	1797	1799	1801	
T3 2 sml clr brn abr	0.006	259	94.2	24	1300	0.2054	0.32163	112	4.8793	152	0.11003	24	1798	1799	1800	
<b><sup>3</sup>GS-08-204 Michelin Footwall Granodiorite (306492, 6051177)</b>																
Z1 1 lrg prm A	0.003	574	163.6	2.0	15415	0.0795	0.28079	366	3.8979	398	0.10068	82	1595	1613	1637	
Z2 1 lrg prm A	0.003	907	232.8	2.4	16910	0.1394	0.24147	286	3.2066	326	0.09631	58	1394	1459	1554	
T1 1 lrg dk brn A	0.005	1087	500.7	71	1316	0.8648	0.27146	706	3.7821	944	0.10105	82	1548	1589	1643	
T2 1 clr dk brn A	0.005	969	422.2	70	1165	0.8139	0.26372	604	3.6387	736	0.10007	122	1509	1558	1625	
T3 1 clr dk brn A	0.005	823	444.6	50	1515	1.0612	0.28923	482	4.0303	592	0.10106	84	1638	1640	1644	
T4 1 dk brn clr A	0.002	1141	596.3	29	1449	0.9808	0.29091	146	4.0553	210	0.10110	42	1646	1645	1644	
T5 1 clr dk brn A	0.002	822	410.8	19	1601	0.8944	0.29018	236	4.0467	320	0.10114	34	1642	1644	1645	
T6 1 equant dk brn A	0.002	1361	522.6	20	2431	0.4489	0.28738	322	3.9988	348	0.10092	74	1628	1634	1641	
<b><sup>3</sup>GS-08-215 Michelin Host Volcanic Rock (307146, 6051898)</b>																
Z1 3 clr sharp euh E	0.004	287	102.8	2.5	11060	0.1308	0.33426	144	5.2326	198	0.11354	26	1859	1858	1857	
Z2 4 clr sharp euh E	0.006	96	34.0	2.2	5466	0.1271	0.33378	218	5.2259	328	0.11355	32	1857	1857	1857	
Z3 3 clr sharp euh E	0.004	163	57.9	1.6	9673	0.1257	0.33338	274	5.2241	430	0.11365	16	1855	1857	1859	
T1 1 best clr dk A	0.002	167	46.7	13	335	0.1510	0.26066	180	3.4371	326	0.09564	80	1493	1513	1541	
T2 1 clr euh crystal	0.002	162	46.4	27	213	0.2040	0.25593	130	3.3467	266	0.09484	56	1469	1492	1525	
T3 1 rasp overgrowth	0.002	270	47.4	22	221	0.0550	0.18032	114	1.9025	192	0.07652	60	1069	1082	1109	
T4 1 clr euh pale brn	0.002	91	14.9	12	178	0.0170	0.17469	116	1.7709	328	0.07353	118	1038	1035	1028	
T5 1 sml clr A	0.002	63	10.5	34	57	0.0437	0.17374	108	1.7633	294	0.07361	116	1033	1032	1031	
T6 1 sml clr A	0.001	121	19.0	33	57	0.0121	0.16889	142	1.6654	760	0.07152	300	1006	995	972	
T7 1 clr pale brn	0.002	137	21.5	18	175	0.0134	0.16832	92	1.6704	296	0.07198	114	1003	997	985	
T8 1 clr dk brn A	0.002	193	30.1	45	85	0.0117	0.16808	114	1.5923	432	0.06871	168	1002	967	890	
T9 2 best clr dk A	0.002	231	35.2	14	271	0.0009	0.16484	118	1.6193	242	0.07125	94	984	978	965	
T10 1 grain	0.002	157	23.8	12	278	0.0001	0.16446	72	1.6148	166	0.07121	68	982	976	964	
T11 1 rasp overgrowth	0.002	1186	70.1	32	223	0.0985	0.05852	86	0.6128	98	0.07595	76	367	485	1094	
<b><sup>3</sup>GS-08-229 Jacques Lake Footwall Granodiorite (332769, 6065965)</b>																
Z1 4 3:1 prm melt icl	0.006	253	82.0	2.1	13757	0.1280	0.30380	304	4.6125	402	0.11012	56	1710	1752	1801	
Z2 2 3:1 prm	0.003	224	73.3	2.3	5867	0.0743	0.32060	264	4.8681	352	0.11013	44	1793	1797	1802	
Z3 4 sml 3:1 prm	0.006	247	79.8	6.4	4310	0.1536	0.29743	188	4.5064	262	0.10989	30	1679	1732	1798	
T1 2 lrg dk brn clr	0.006	555	205.5	47	1447	0.2242	0.32245	508	4.8854	736	0.10988	56	1802	1800	1797	
T2 3 lrg dk brn clr	0.009	480	175.4	55	1587	0.2174	0.31992	320	4.8480	478	0.10991	24	1789	1793	1798	
T3 6 lrg dk brn clr	0.018	274	115.9	55	1814	0.4258	0.32007	294	4.8464	422	0.10982	38	1790	1793	1796	

## APPENDIX C (continued)

Fraction	Concentration			Measured			Corrected Atomic Ratios*						Age [Ma]		
	Weight [mg]	U [ppm]	Pb rad [ppm]	total common Pb [pg]	$^{206}\text{Pb}$ $^{204}\text{Pb}$	$^{208}\text{Pb}$ $^{206}\text{Pb}$	$^{206}\text{Pb}$ $^{238}\text{U}$	±	$^{207}\text{Pb}$ $^{235}\text{U}$	±	$^{207}\text{Pb}$ $^{206}\text{Pb}$	±	$^{206}\text{Pb}$ $^{238}\text{U}$	$^{207}\text{Pb}$ $^{235}\text{U}$	$^{207}\text{Pb}$ $^{206}\text{Pb}$
<b><sup>3</sup>GS-08-235 Jacques Lake Host Volcanic Rock (332815, 6065831)</b>															
T1 4 med clr dk brn	0.008	353	123.0	85	688	0.1512	0.32086	312	4.8477	468	0.10958	22	1794	1793	1792
T2 3 med clr dk brn	0.006	299	104.5	121	313	0.1588	0.32008	594	4.7999	830	0.10876	156	1790	1785	1779
T3 3 med clr lt brn	0.006	46	15.5	23	255	0.1337	0.31540	314	4.7357	476	0.10890	74	1767	1774	1781
T4 4 med lt brn	0.008	75	26.6	51	247	0.2180	0.31193	324	4.6788	548	0.10879	110	1750	1763	1779
<b><sup>3</sup>GS-08-287 Kitts Metagabbro (340475, 6097407)</b>															
Z1 3 prm E	0.002	92	39.1	2.1	1519	0.2253	0.36715	182	6.2829	274	0.12411	50	2016	2016	2016
Z2 2 clr euh E	0.002	333	144.4	3.6	4067	0.3051	0.35257	386	5.9615	634	0.12263	32	1947	1970	1995
Z3 1 euh prm E	0.001	853	383.0	3.5	5424	0.3376	0.35677	210	6.0566	290	0.12312	44	1967	1984	2002
Z4 1 poor euh prm E	0.001	180	77.1	4.4	935	0.2779	0.35529	174	6.0406	248	0.12331	38	1960	1982	2005
<b><sup>3</sup>GS-09-44 Two Time Quartz Monzodioite (230994, 6052981)</b>															
Z1 2 sml prm E	0.002	59	44.8	4.5	1001	0.2273	0.60240	632	18.99971840	0.22875	124	3039	3042	3043	
Z2 2 sml prm E	0.002	33	25.9	4.1	637	0.2649	0.60331	362	19.00721160	0.22849	74	3043	3042	3042	
Z3 3 sml prm E	0.003	81	59.6	4.1	2248	0.1786	0.60369	398	19.03961242	0.22874	44	3045	3044	3043	
M1 2 lrg pale yel A	0.003	2711	5995.6	13	19559	3.7518	0.51760	270	13.1348690	0.18404	14	2689	2689	2690	
M2 1 lrg pale yel A	0.002	1906	4392.4	14	6404	4.1746	0.49699	324	12.4168810	0.18120	18	2601	2636	2664	
M3 1 lrg pale yel A	0.002	2306	5885.6	25	4477	4.6153	0.50844	210	12.7831540	0.18235	12	2650	2664	2674	
<b><sup>4</sup>GS-14-123 Tuff–Heggart Lake Formation (244157, 6043818)</b>															
Z1 1 prm	0.002	533	163.2	6.7	2220	0.1009	0.29319	180	4.5575	278	0.11274	20	1657	1742	1844
Z2 2 prm	0.003	1071	328.9	48	1239	0.1004	0.29466	220	4.5061	336	0.11091	18	1665	1732	1814
Z3 2 prm	0.003	801	241.6	29	1496	0.1198	0.28448	224	4.4107	352	0.11245	14	1614	1714	1839
Z4 2 prm	0.003	614	178.0	32	1010	0.0941	0.28013	158	4.2361	232	0.10967	24	1592	1681	1794
Z5 1 prm	0.002	1213	363.3	34	981	0.1031	0.28702	174	4.3365	262	0.10958	26	1627	1700	1792
Z6 1 prm	0.002	2075	646.6	35	1704	0.0926	0.30097	322	4.6041	494	0.11095	14	1696	1750	1815
Z7 1 clr euh prm	0.001	286	94.2	5.1	1131	0.1049	0.31434	344	4.8635	482	0.11221	60	1762	1796	1836
Z8 2 clr euh prm	0.002	527	159.3	13	1461	0.1018	0.28956	178	4.4400	274	0.11121	30	1639	1720	1819
Z9 1 clr euh prm	0.001	524	177.2	7.4	1417	0.1246	0.31728	580	5.0099	914	0.11452	30	1776	1821	1872
<b><sup>4</sup>GS-14-130 Granite–Henri Lake (246963, 6044570)</b>															
Z1 1 prm	0.002	1818	497.4	58	749	0.1628	0.24956	220	3.8290	334	0.11128	24	1436	1599	1820
Z2 1 prm	0.002	529	160.0	16	945	0.0659	0.29964	376	4.4674	556	0.10813	50	1690	1725	1768
Z3 2 prm	0.003	435	90.1	18	893	0.1151	0.19689	188	2.8994	262	0.10680	46	1159	1382	1746
Z4 2 simple prm	0.003	383	56.7	15	637	0.1920	0.13284	60	1.8706	96	0.10213	42	804	1071	1663
Z5 3 prm	0.004	470	155.0	18	2220	0.1370	0.30151	210	5.6150	386	0.13506	26	1699	1918	2165
Z6 1 clr prm	0.001	267	89.8	6	834	0.1199	0.31781	162	4.8803	304	0.11137	46	1779	1799	1822
<b><sup>4</sup>GS-08-137 Tuff–Brown Lake Formation (226840, 6037730)</b>															
Z1 1 clr med prm	0.001	643	223.6	2.6	4662	0.2714	0.29413	160	4.1451	214	0.10221	22	1662	1663	1665
Z2 1 clr euh prm	0.001	242	84.7	2.7	1697	0.2757	0.29552	184	4.1658	270	0.10224	42	1669	1667	1665
Z3 2 clr euh prm	0.002	68	30.7	1.9	1771	0.1573	0.39627	210	8.8244	526	0.16151	50	2152	2320	2472
<b><sup>4</sup>GS-14-203 Crystal Tuff–Sylvia Lake Formation (242807, 6012434)</b>															
Z1 1 lrg euh clr prm	0.002	506	173.3	4.7	3010	0.2326	0.29782	240	4.2671	296	0.10391	44	1680	1687	1695
Z2 2 lrg clr euh prm	0.003	288	97.5	80	214	0.2534	0.29089	174	4.0541	318	0.10108	54	1646	1645	1644
Z3 4 lrg clr euh prm	0.006	333	114.0	64	583	0.2754	0.28874	262	4.0197	384	0.10097	34	1635	1638	1642
Z4 2 lrg clr euh prm	0.003	128	41.9	2.8	2510	0.2145	0.28857	124	4.0285	170	0.10125	32	1634	1640	1647

**Notes:**

Z=zircon, T=titanite, abr=abraded, brn=brown, clr=clear, dk=dark, equ=equant, euh=euohedral, lrg=large, pg=pictogram, sml=small, all fractions were strongly abraded (Krogh, 1982).

\* Atomic ratios corrected for spike, lab blank of 1-2 picograms, isotopic fractionation. Common lead above the lab blank was subtracted according to the model of Stacey and Kramers (1975) for the age of the sample. Two sigma uncertainties are reported after the isotopic ratios and refer to the final digits.

Original Source: 1 – Sparkes and Dunning (2009); 2 – Sparkes *et al.* (2010); 3 – Sparkes and Dunning (2015); 4 – Sparkes *et al.* (2016).

## APPENDIX D

$\text{U-Pb}$  SHRIMP analytical data for sample number GS-07-298; Quartz-feldspar porphyry, Kitts deposit, Labrador (z937); from Sparkes *et al.* (2010)

### Notes:

Uncertainties reported at one sigma and are calculated by numerical propagation of all known sources of error (Stern, 1997).  $\text{f}206$  refers to mole fraction of total  $206\text{Pb}$  that is due to common  $206\text{Pb}$  based on  $204\text{Pb}$ ; data have been corrected for common  $\text{Pb}$  according to procedures outlined in Stern (1997). GSC mount IP470. Spot size for analysis =  $16 \times 23 \mu\text{m}$ . GSC laboratory zircon standard z2666 zircon, with  $^{206}\text{Pb}/^{238}\text{U}$  age = 559 Ma. Common- $\text{Pb}$  corrected ratios and ages are reported with  $1\sigma$  analytical errors, which incorporate an external uncertainty of 1.0% in calibrating the standard zircon (see Stern and Anselin, 2003). Sample collected from drill hole number K74-08 (UTM coordinates; NAD 27, Zone 21; 340829/6097189) between 93.10 and 98.48 m.

## APPENDIX E

U-Pb ID-TIMS analytical data for sample number GS-08-288; crystal lapilli tuff, Powe prospect, Benedict Mountains region; from Sparks and Davis, 2013

Fraction	Description	# gr	Size	Wt. <sup>1</sup> ( $\mu$ g)	U (ppm)	Pbr <sup>2</sup> (ppm)	$\frac{206\text{Pb}}{204\text{Pb}}$	$\frac{206\text{Pb}}{235\text{U}}$	$\frac{208\text{Pb}}{206\text{Pb}}$	$\frac{207\text{Pb}}{238\text{U}}$	Atomic Ratios <sup>3</sup> ( $\pm$ 1 sigma error absolute)		Correlation Coefficient <sup>4</sup>	$\frac{207\text{Pb}}{206\text{Pb}}$	$\pm$	Age (Ma) $\pm$			
											$\frac{206\text{Pb}}{238\text{U}}$	$\pm$	$\frac{207\text{Pb}}{206\text{Pb}}$	$\pm$	$\frac{207\text{Pb}}{206\text{Pb}}$	$\pm$			
<b>GS-08-288 Allik Group (Z9690)<sup>6</sup></b>																			
A1 (Z)	Z,Co,Cl,ff,Fr,Eu, Pr,Abf,	1	80	1	43	15	1243	0.59	0.09	5.19525	0.00942	0.333195	0.00048	0.78667935	0.11351	0.00013	1856.4	4	0.53
A2 (Z)	Z,Co,Cl,ff,Fr,Eu, Pr,Abf,	8	100	3.1	66	23	1306.9	3.31	0.1	5.21434	0.00786	0.333317	0.00035	0.85175422	0.11351	0.00009	1856.3	3	0.16
B1 (Z)	Z,Co,Cl,Fr,Eu, Pr,Abf,	1	75	0.9	113	39	3596.1	0.44	0.11	5.21136	0.00675	0.333324	0.00037	0.81094172	0.11342	0.00009	1854.9	2.7	0.06
B2 (Z)	Z,Co,Cl,Fr,Eu Pr,Abf,	8	75	2.6	100	34	2800.9	1.9	0.1	5.12085	0.00643	0.322754	0.00031	0.88938409	0.11339	0.00007	1854.4	2.2	1.73

**Description Legend:** Z=Zircon, Co=Colourless, Cl=Clear, ff=Fractures, Eu=Euclidean, P=Prismatic, Abf=Abraded

<sup>1</sup> Concentration uncertainty varies with sample weight: >10% for sample weights <10  $\mu$ g, <10% for sample weights above 10  $\mu$ g

<sup>2</sup> Pbr = radiogenic Pb; Pbc = total common Pb in analysis corrected for spike and fractionation

<sup>3</sup> Atomic ratios corrected for spike, fractionation, blank and initial common Pb, except  $^{206}\text{Pb}/^{204}\text{Pb}$  ratio corrected for spike and fractionation only. Errors are one sigma absolute. Pb blank: <1 pg for Zr-con; blank composition in atomic proportions = 51.966:21.356:25.288:1.3895 (208:207:206:204)

<sup>4</sup> Correlation coefficient of errors in isotopic ratios

<sup>5</sup> Discordance of the analysis

<sup>6</sup> UTM coordinates; NAD 27, Zone 21; 393366/6070271

## APPENDIX F

Summary table outlining the location and main host rock for prospects visited as part of this study, along with the corresponding classification of the style of mineralization. Note UTM's are provided in NAD 27, Zone 21

ID	Easting	Northing	Prospect Name	Main Host Rock	Style of Mineralization
1	382610	6072221	AT 649	Plutonic	Metamorphic-Metasomatic
2	295053	6054601	Active Pond	Plutonic	Metamorphic-Metasomatic
3	297292	6063448	Anna Lake	Sedimentary	Metamorphic-Metasomatic
4	238986	6039226	Anomaly #15	Volcanic	Magmatic-related
5	239779	6040792	Anomaly #16	Volcanic	Magmatic-related
6	227647	6049621	Anomaly #17	Plutonic	Metamorphic-Metasomatic
7	233095	6047161	Anomaly #7	Plutonic	Metamorphic-Metasomatic
8	253117	6049744	Apollo Zone	Sedimentary	Sediment-hosted
9	244661	6048734	Area 51	Sedimentary	Sediment-hosted
10	240792	6041450	Armstrong	Sedimentary	Magmatic-related
11	321125	6060647	Aurora River	Volcanic	Metamorphic-Metasomatic
12	417494	6057553	Benedict Mt. #1	Plutonic	Magmatic-related
13	426645	6058467	Benedict Mt. #2	Volcanic	Magmatic-related
14	252999	6052583	Blue Star	Sedimentary	Sediment-hosted
15	257213	6060520	Boiteau Lake	Volcanic	Metamorphic-Metasomatic
16	238081	6014192	Boundary Lake	Plutonic	Magmatic-related
17	329611	6063042	Burnt Brook	Sedimentary	Metamorphic-Metasomatic
18	325484	6058120	Burnt Lake/White Bear	Volcanic	Metamorphic-Metasomatic
19	227088	6037879	Croteau Lake	Sedimentary	Metamorphic-Metasomatic
20	310199	6125433	Dandy	Plutonic	Magmatic-related
21	240134	6014636	East Otter Lake	Plutonic	Magmatic-related
22	331272	6058367	Emben/Otter Lake	Volcanic	Metamorphic-Metasomatic
23	264755	6047515	Ferguson-Brown	Sedimentary	Metamorphic-Metasomatic
24	238541	6050939	Fire Stone	Plutonic	Metamorphic-Metasomatic
25	234828	6050703	Fish Hawk Lake North Zone	Plutonic	Metamorphic-Metasomatic
26	234497	6049153	Fish Hawk Lake South Zone	Plutonic	Metamorphic-Metasomatic
27	237997	6051450	Ford	Plutonic	Metamorphic-Metasomatic
28	331600	6065651	Gayle	Volcanic	Metamorphic-Metasomatic
29	337125	6091231	Gear	Sedimentary	Metamorphic-Metasomatic
30	393624	6069672	Harbinger	Volcanic	Magmatic-related
31	334500	6089220	Inda	Sedimentary	Metamorphic-Metasomatic
32	333119	6066053	Jacques Lake	Volcanic	Metamorphic-Metasomatic
33	310871	6122627	Kanairiktok	Plutonic	Magmatic-related
34	340571	6097332	Kitts	Sedimentary	Metamorphic-Metasomatic
35	237735	6030994	Madsen	Volcanic	Magmatic-related
36	307702	6062780	Melody Hill	Plutonic	Metamorphic-Metasomatic
37	307350	6052571	Michelin	Volcanic	Metamorphic-Metasomatic
38	243092	6012520	Minisinakwa	Volcanic	Metamorphic-Metasomatic
39	248449	6049512	Moran Heights	Sedimentary	Sediment-hosted
40	250907	6047565	Moran Lake A Zone	Sedimentary	Metamorphic-Metasomatic
41	246822	6044912	Moran Lake B Zone	Sedimentary	Magmatic-related
42	243646	6044136	Moran Lake Lower C Zone	Sedimentary	Sediment-hosted
43	243610	6043614	Moran Lake Upper C Zone	Volcanic	Magmatic-related
44	314745	6056010	Mustang South	Volcanic	Metamorphic-Metasomatic
45	317647	6058601	Mustang East	Volcanic	Magmatic-related

## APPENDIX F (continued)

ID	Easting	Northing	Prospect Name	Main Host Rock	Style of Mineralization
46	331802	6087492	Nash	Sedimentary	Metamorphic-Metasomatic
47	330458	6087013	Nash West	Volcanic	Metamorphic-Metasomatic
48	392474	6066433	NB	Volcanic	Magmatic-related
49	226722	6050876	Near Miss	Plutonic	Metamorphic-Metasomatic
50	267586	6050293	Noseman	Plutonic	Metamorphic-Metasomatic
51	358696	6090856	Pitch Lake	Plutonic	Metamorphic-Metasomatic
52	393363	6070258	Powe	Volcanic	Magmatic-related
53	242623	6042904	Poz Pond	Volcanic	Magmatic-related
54	349430	6091737	Present Lake	Sedimentary	Metamorphic-Metasomatic
55	394421	6070987	Priority One	Volcanic	Magmatic-related
56	339032	6093232	Punch Lake South	Plutonic	Metamorphic-Metasomatic
57	394405	6071317	Quinlan	Volcanic	Magmatic-related
58	306236	6050125	Rainbow	Volcanic	Metamorphic-Metasomatic
59	359019	6105008	Retreat Lake No. 1	Volcanic	Metamorphic-Metasomatic
60	304312	6055726	Ribs Lake	Volcanic	Metamorphic-Metasomatic
61	396415	6072363	Salmon Bight/B 22	Volcanic	Magmatic-related
62	231060	6053109	Snegamook	Plutonic	Metamorphic-Metasomatic
63	242784	6098785	Stomach Lake	Plutonic	Magmatic-related
64	231695	6008519	Stormy Lake	Volcanic	Magmatic-related
65	361278	6113904	Sunil	Volcanic	Metamorphic-Metasomatic
66	378697	6069937	Super 7	Plutonic	Metamorphic-Metasomatic
67	252197	6037270	Sylvia Lake	Volcanic	Magmatic-related
68	241421	6042574	Trout Pond	Volcanic	Magmatic-related
69	230387	6054396	Two Time	Plutonic	Metamorphic-Metasomatic
70	235628	6050956	Wisky Jack	Sedimentary	Metamorphic-Metasomatic